

Yellapu V. Murty  
Mary Anne Alvin  
Jack P. Lifton  
*Editors*

# Rare Earth Metals and Minerals Industries

Status and Prospects



Springer

# Rare Earth Metals and Minerals Industries

Yellapu V. Murty • Mary Anne Alvin  
Jack P. Lifton  
Editors

# Rare Earth Metals and Minerals Industries

Status and Prospects

 Springer

*Editors*

Yellapu V. Murty  
MC Technologies LLC  
Charlottesville, VA, USA

Mary Anne Alvin  
DOE Office of Fossil Energy  
and Carbon Management  
Washington, DC, USA

Jack P. Lifton  
Technology Metals Research, LLC  
Farmington Hills, MI, USA

ISBN 978-3-031-31866-5      ISBN 978-3-031-31867-2 (eBook)  
<https://doi.org/10.1007/978-3-031-31867-2>

© The Editor(s) (if applicable) and The Author(s), under exclusive license to Springer Nature Switzerland AG 2024

All rights are reserved by the Publisher, whether the whole or part of the material is concerned, specifically the rights of translation, reprinting, reuse of illustrations, recitation, broadcasting, reproduction on microfilms or in any other physical way, and transmission or information storage and retrieval, electronic adaptation, computer software, or by similar or dissimilar methodology now known or hereafter developed.

The use of general descriptive names, registered names, trademarks, service marks, etc. in this publication does not imply, even in the absence of a specific statement, that such names are exempt from the relevant protective laws and regulations and therefore free for general use.

The publisher, the authors, and the editors are safe to assume that the advice and information in this book are believed to be true and accurate at the date of publication. Neither the publisher nor the authors or the editors give a warranty, expressed or implied, with respect to the material contained herein or for any errors or omissions that may have been made. The publisher remains neutral with regard to jurisdictional claims in published maps and institutional affiliations.

Cover caption: Shown on the cover is a secondary electron scanning electron microscopic image of calcined mixed rare earth oxides produced from coal ash, a byproduct of coal fired power generation plant and is provided as a courtesy by Physical Sciences Inc. and Winner Water Services Inc. through their efforts conducted under the US Department of Energy project, DE-FE0027167

This Springer imprint is published by the registered company Springer Nature Switzerland AG  
The registered company address is: Gewerbestrasse 11, 6330 Cham, Switzerland

Paper in this product is recyclable.

# Preface

This publication, born out of curiosity and the desire to spread knowledge, sponsored by ASM programming committee through two consecutive symposia in 2017 and 2018, encouraged by friends and colleagues from government, industry, and academia, finally culminating into the current book format *Rare Earth Metals and Minerals Industry – Status and Prospects*. The editorial team likes to express their gratitude and appreciation to the contributors of individual chapters and to many others who provided guidance and continued encouragement to this effort. Finally, many thanks for the assistance received from the Springer Nature book publishing and production team for making this effort a reality.

Yellapu V. Murty  
Mary Anne Alvin  
Jack P. Lifton

# Contents

<b>1</b>	<b>Introduction</b> .....	<b>1</b>
	Yellapu V. Murty	
<b>Part I Upstream Primary Operations</b>		
<b>2</b>	<b>Conventional Rare Earth Element Mineral Deposits—The Global Landscape</b> .....	<b>17</b>
	Nora K. Foley and Robert A. Ayuso	
<b>3</b>	<b>Energy-Related Rare Earth Element Sources</b> .....	<b>57</b>
	Allan Kolker, Liliana Lefticariu, and Steven T. Anderson	
<b>4</b>	<b>Rare Earth Ore Flotation Principles and Kinetics: Significance of Collectors and Application of Novel Depressants</b> .....	<b>103</b>
	Courtney A. Young, Peter A. Amelunxen, and Richard LaDouceur	
<b>5</b>	<b>Rare Earth Extraction from Ion-Adsorption Clays in U.S. Coal By-Products</b> .....	<b>123</b>
	Roe-Hoan Yoon	
<b>6</b>	<b>Solvent Extraction</b> .....	<b>149</b>
	Alain Rollat	
<b>7</b>	<b>Continuous Ion Chromatography</b> .....	<b>179</b>
	Richard Shaw and David Dreisinger	
<b>8</b>	<b>Ionic Liquids for the Processing of Rare Earth Elements</b> .....	<b>195</b>
	Tommee Larochele	
<b>Part II Metal Refining</b>		
<b>9</b>	<b>Reduction of Rare Earth Elements Through Electrochemical and Metallothermic Methods</b> .....	<b>235</b>
	Patrick R. Taylor, Matthew Earlam, and Sridhar Seetharaman	

<b>10 Rare Earth Element Reduction to Metals</b> . . . . .	257
Tommeé Larochelle	
<b>Part III Applications – Product Manufacturing</b>	
<b>11 Rare Earth Markets and Their Industrial Applications</b> . . . . .	273
Gaétan Lefebvre and Nicolas Charles	
<b>12 Rare Earth Magnets: Manufacturing and Applications</b> . . . . .	295
James Bell	
<b>13 Role of Rare Earths as Catalysts in the Chemical, Petroleum and Transportation Industries</b> . . . . .	319
Aaron Akah	
<b>14 High-Performance Aluminum Castings Containing Rare Earth Elements</b> . . . . .	343
David Weiss	
<b>15 Scandium in Commercial Wrought Aluminum Alloys</b> . . . . .	359
Timothy J. Langan and Thomas Dorin	
<b>16 Rare Earth Oxide Applications in Ceramic Coatings for Turbine Engines</b> . . . . .	391
David L. Poerschke and Jessica A. Krogstad	
<b>Part IV Recycling</b>	
<b>17 Value Recovery Pathways for Rare Earth Elements and Nd-Fe-B Magnets from End-of-Life Products</b> . . . . .	423
Nighat Afroz Chowdhury, Ikenna C. Nlebedim, Daniel M. Ginosar, Carol Handwerker, and Hongyue Jin	
<b>18 Recovery of Rare Earth Metals from Waste Fluorescent Lights</b> . . . . .	447
Brajendra Mishra, Mark Strauss, and Manish Kumar Sinha	
<b>Part V Economics and Regulatory Issues</b>	
<b>19 Fundamental Perspectives on the Economic Analysis of Rare Earth Processing from Various Feedstocks</b> . . . . .	457
Aaron Noble	
<b>20 Rare Earth Element Mining and Recovery: A Regulatory Overview</b> . . . . .	485
Larry Long	
<b>Index</b> . . . . .	505

# About the Editors

**Yellapu V. Murty, Ph.D, FASM**, a Fellow of ASM and currently the President of MC Technologies LLC., provides materials consulting services. He is also an adjunct faculty staff member in the University of Virginia's Mechanical and Aerospace Engineering Department. Dr. Murty, with about half a century of industrial exposure, has been active in the RD&E aspects of engineered materials, their manufacturing, and final applications. His main interests through the years focused on multifunctionality packaging optimum properties such as conductivity (electrical and thermal), corrosion/oxidation, light weight, magnetic, strength and toughness (ambient and harsh environments), super elastic, superplastic, shape-memory, and resistance to high velocity penetration/shock waves, to meet final product's functional features. His industry exposure spans across electronics, energy, transportation, and industrial sectors. He has worked for fortune 100 companies such as Carpenter Technologies, NGK Insulators, Tyco Electronics, as well as leveraging academia and government laboratories such as MIT, University of Illinois, and Sandia and Oak Ridge National Laboratories where he was instrumental in identifying key materials technologies and transitioning them into successful commercial products.

**Mary Anne Alvin** currently serves as the Critical Minerals Processing Program Manager at the Department of Energy's Office of Fossil Energy and Carbon Management. She previously served as the Rare Earth Element Technology Manager at the National Energy Technology Laboratory. Prior to joining NETL, Ms. Alvin was employed at the Westinghouse Electric Corporation and at Siemens Westinghouse Power Generation, working in the area of advanced energy systems. As a Fellow Scientist, she was internationally recognized for her contributions in the area of high temperature porous ceramic materials, ceramic matrix composites, intermetallics, advanced alloys, and metal media for hot gas filtration use in the electric power generation industry. She holds 28 patents in these areas.



**Jack P. Lifton** is currently an industrial consultant providing evaluation and due diligence studies of business operations in mining, refining, fabrication, and manufacturing in the metals and materials area. As a research scientist, technical operations/sales manager, a plant manager, and the CEO in the OEM automotive electronics and minor metals industries with over four decades of direct experience, he gained worldwide reputation as an expert in this area. He has been a respected member of this community with a distinction among his peers.

# Chapter 1

## Introduction



**Yellapu V. Murty**

Minerals, metals, and materials are essential for manufacturing products that are vital to the global economy, creating advanced technological innovations and raising the standards of our daily way of life. The advent of electricity, telephones, locomotives, internal combustion engines, the radio, television, air, and space travel are some of the cornerstones of modern society that were propelled into many day-to-day consumer products. While the discovery and mass production of iron (Fe), copper (Cu), aluminum (Al), and their alloys became the pillars of these underlying innovations, the readers of this book will realize that rare earth elements (REEs) have played a critical role in advancing the manufacturing of numerous commodity, energy, and defense products and their derivatives. These and other critical or advanced metals are needed to improve the functional features and unique characteristics of these components or devices. Now, we are well into the modern data-driven information age, having an abundance of Internet-connected devices that use components that are manufactured with specialty, critical, and/or engineered materials.

This publication focuses on one class of those materials—the rare earth elements which are also referred to as the lanthanides. Our objectives for this publication were to provide a comprehensive review of the past, the current, and the expected future of REEs, spanning their entire lifecycle. A detailed understanding of the minerals containing REEs, the extraction and production of rare earth oxides (REOs), and refining to high-purity rare earth metals (REMs), their applications, and the challenges facing the industry are covered emphasizing the progress in research, development, and manufacturing, highlighting future needs and potential opportunities.

---

Y. V. Murty (✉)  
MC Technologies LLC, Charlottesville, VA, USA  
e-mail: [ymurty@mctechnologies.us](mailto:ymurty@mctechnologies.us)

The content of this book is divided into five sections, with each section addressing a specific REE topic area as follows: (1) upstream primary operations; (2) metal refining; (3) applications and product manufacturing; (4) recycling; and (5) economics and regulatory issues. It is our hope that this publication will provide a better understanding of the origin of rare earth minerals and materials (REMMs), their extraction and separation into respective oxides and/or metals, their applications and recycle recovery potential, and the economic, regulatory, and sociopolitical impact. This publication also attempts to provide the reader with a better appreciation of REE contributions to the energy, medical, industrial, consumer, and defense sectors. Based on the content assembled by experts in these fields, it is clear that the future for REEs is astonishingly bright and is expanding at sonic speed.

Over 1500 references capture information pertinent to the REE resource landscape, their concentration in mineral deposits, production yields, consumption volumes, commodity pricing, cost of goods, supply chain inequalities, and so on. Infrequently, there are differing statistics presented within the chapters which resulted from citing various reference sources or occurred due to the manner in which data were collected or to the technology advancements that have been made over time. Similarly, acronyms are used interchangeably by the authors for REE complexes. The reader is asked to reserve judgment, and view what is presented in this book as information that is currently known and which can be open for further interpretation and discussion. The fact that several figures are duplicatively presented underpins their technical importance to the chapter's narrative and illustrates the interdependence of the mining, geology, metallurgy, chemical engineering, and materials science disciplines for successful recovery of REEs and their utilization.

## 1.1 What Are Rare Earth Elements?

Fifteen lanthanides with atomic numbers ranging from 57 to 71 on the periodic table and scandium (Sc) with atomic number 21 and yttrium (Y) with atomic number 39 form what is commonly known as the assemblage of REEs. The lanthanides are further grouped into *light REEs (LREEs)* which include lanthanum (La), cerium (Ce), praseodymium (Pr), neodymium (Nd), and promethium (Pm); *medium REEs (MREEs)* which include samarium (Sm), europium (Eu), gadolinium (Gd), terbium (Tb), and dysprosium (Dy); and *heavy REEs (HREEs)* which include holmium (Ho), erbium (Er), thulium (Tm), ytterbium (Yb), and lutetium (Lu). Alternately, it has been the practice to simply classify REEs as LREEs and HREEs in which case LREEs include elements with atomic numbers 57–64 (La, Ce, Pr, Nd, Pm, Sm, Eu, and Gd) and HREEs include elements with atomic numbers 65–71 (Tb, Dy, Ho, Er, Tm, Yb, and Lu). Scandium (Sc) is usually considered as a LREE, while Y has been designated as a HREE primarily due to their elemental association with the corresponding REE group.

As the lanthanide elements have extraordinary similarities in atomic, electronic, ionic, and chemical structure, they typically occur as a single group of elements that are present in the earth's upper continental crust (UCC). Rare earth elements are found either in a crystalline mineral form as complex carbonates, phosphates, oxides and silicates, and so on, and in adsorbed states as ion exchangeable clays in the soil regolith. Rare earth elements are more easily extracted from clays in comparison to their crystalline counterparts where the REEs are more tightly bonded within complex crystalline mineral structures.

As a group of disproportionately distributed elements, REEs are often associated with other metallic species as a result of their natural formation over millions of years, being exposed to myriads of geological, physical, and environmental conditions. Therefore, identifying an individual element for extraction becomes a challenging task which is often governed by process economics and the economic value or demand of the specific element of interest. As a result of extraction and use of select elements as Nd and Pr for magnet production, undervalued REEs remain in tailings that are possibly stockpiled for future reclamation, or even more unfortunately, shipped to landfill sites.

## 1.2 The Origin of Rare Earth Elements

Rare earth elements have been known for over 200 years. They were first discovered in 1778 in Sweden and later studied in Finland, where the REE mineral was named *gadolinite* after the scientist J. Gadolin. With time, the nomenclature shifted to *rare earth*, then *black earth*, and then to *lanthanides* when the fifteen elements were finally recognized as individual elements, each with an elemental name and chemical symbol.

Despite the acronym, REEs are not rare. What makes them rare is the difficulty of extracting and separating them efficiently and economically, without creating environmental issues. Cerium is the most abundant REE element with a total estimated availability equal to that of copper (Cu) in the earth's UCC. Lanthanum and Y are next in line in terms of REE abundance in ore bodies. The next industrially important REE is neodymium (Nd) which has a resource availability comparing well with known cobalt (Co) reserves. The least abundant REE is lutetium (Lu) with reserves estimated at slightly exceeding that of gold (Au) (Chap. 2).

The use of REEs in various applications is discussed in Chaps. 11–16. As REEs are finding their use in more applications, such as solar panels, medical diagnostics, batteries, and others, their demand continues to grow, attracting new investments and interests by both public and private sectors, which is a hallmark of a growing industry.

### 1.3 How Rare Earths Are Extracted

In general, REEs exist in two types of natural resources deposits—a crystalline state within the ore deposit mineral structure and an adsorbed state within ion exchangeable or adsorption clays (IACs). While hundreds of REE ore deposits have been identified (Chaps. 2 and 3), only a limited number of these deposits have been commercially exploited.

As crystalline minerals, REEs are present as fluorocarbonates (e.g., bastnaesite), as phosphates (e.g., monazite and xenotime), or as complex mixtures of oxides (e.g., loparite). The concentration of REOs in the heterogeneous crystalline mineral ores can be as high as or greater than 30%, while within the clays (IACs), the REO concentration may be limited somewhat greater than 10%. However, IACs contain rich concentration of commercially significant REEs like Nd, Pr, Sm, Gd, and Dy. To emphasize this point, the distribution of the relative REO concentration in popular bastnasite mineral bodies averaged at 28% La, 50% Ce, 5% Pr, 15% Nd, and 1% Sm oxide equivalent. In contrast, IACs averaged at 37% Y, 5% Pr, 17% Nd, 3% Sm, 5% Gd, 3% Dy, 2.5 Er, 1.0% Y, and 1.5% Ce. Notably, the Ce-rich crystalline mineral-based ore bodies contain predominantly LREEs, while IACs are enriched with Y tend to contain higher HREE continents.

Conventional hard rock ore bodies as monazite and bastnaesite are obtained by ground blasting followed by crushing and then dry/wet grinding to form a slurry. The final slurry size is generally optimized to maximize the yield of REE minerals. Processes as gravity and magnetic separation are employed in handling and grading these ore bodies. These operations are followed by hydrometallurgical operations as flotation, roasting, leaching, and molten salt electrolysis (also known as electrowinning) to obtain REO concentrates and REE mixtures. These primary upstream processes, including extensive details on hydrometallurgical flotation operations, are reviewed in Chap. 4. The hydrometallurgical operation of flotation, which is sometimes referred to as froth flotation, is a complex process that uses many inorganic solvents and organic surface-active reagents including collectors, activators, depressants, modifiers, and frothers to maximize extraction of critical REEs for generation of valuable mixed RE concentrates.

The clay minerals have been selective adsorbents (or collectors) of HREEs over geological time. As ion-adsorbed clays (IAC), these materials are leached with acids generating heavy mixed rare earth oxide (HREO) concentrates. The leached solution can then be reacted with oxalic acid, precipitating RE oxalate solids, which when roasted at 900 °C yields REO solid concentrates (Chap. 5). In contrast to monazite and bastnaesite, minimal to no thorium (Th) or uranium (U) is present in the IAC leach liquors or REO solid concentrates.

Unconventional and secondary sources have recently been considered for extraction and recovery of REEs. These include abandoned tailings from coal preparation site (e.g., fine coal wastes, partings, underburden/overburden clays, waste rocks), fly ash and/or bottom ash from power generation facilities, legacy ash ponds, coal and mineral mine acid drainage (AMD), iron metal production scrap/dross, recycled

fluorescent lamp phosphor dust, and electronic scrap. The REE content in these materials are often substantially lower in comparison to the REE concentration in monazite and bastnaesite ore bodies (Chaps. 3 and 5). Economic and sustainable processing of these unconventional resources remains to be determined. Efforts have additionally focused on recovering REE from electronic waste material as end-of-life (EOL) hard drives and spent fluorescent lamp phosphors (Chaps. 17 and 18).

## 1.4 How Rare Earth Elements are Separated and Refined

The performance and cost of intermediate and/or consumer end products are critically dependent on the unique physical and chemical properties and purity of their contained REEs. As previously noted, separation of the mixed REEs into individual or binary high-purity elements is challenging as this series of elements is atomically, electronically, and chemically closely aligned. The most widely used method for elemental separation and purification is solvent extraction (SX) (Chap. 6). Typically, hundreds of mixer–settler separator stages and large volumes of organic solvents are needed to separate MREO concentrates into individual high-purity materials. Consequentially, SX is capital (CAPEX) and operating (OPEX) cost-intensive. Irrespective of these issues, SX remains as today’s industry standard for REE separation.

To overcome these issues, other processes as continuous ion exchange (CIX) or continuous ion chromatography (CIC), ionic liquid separation, and other molecular methods are being developed, but to date, no industrial scale operation using these separation processes has been reported (Chap. 7). Continuous ion exchange chromatography is used as an analytical chemistry tool and to a limited extent used in high-purity REE refining operations. It is claimed to have a smaller operational footprint in comparison to SX, using less harsh chemicals, and has the hallmark of being a cheaper operation. Alternately, molecular recognition technology (MRT) is being developed that is based on solid-phase extraction using ligands grafted onto nanoparticle surfaces, thus eliminating the extensive use of solvents. Details of MRT’s process have yet to be published and are kept as proprietary (Chap. 6).

Ionic liquids (ILs), another newcomer to the field of REO separation, is receiving significant academic attention. Most ILs, due to their ionic nature, tend to be more soluble in aqueous phases than their molecular organic counterparts. Other advantages of ILs as an alternative to organic solvents are their versatility with respect to manipulating solution viscosity, polarity, solubility, and coordination ability allowing for their optimization regarding specific REE cation/anion extraction through IL molecule design and engineering. The status of ILs and their applicability in the widely accepted SX process and in other hydrometallurgical operations as leaching are presented in Chap. 8.

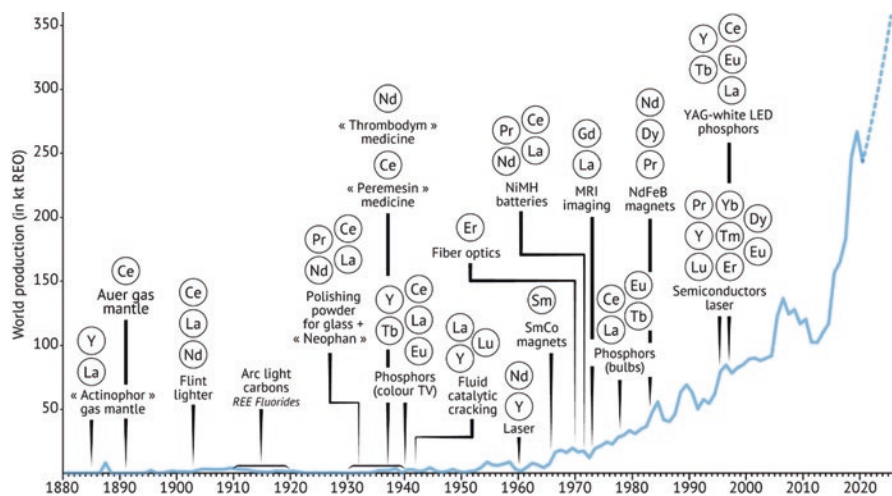
The next step of REE refinement is reduction to their respective metallic state for downstream alloying. Reduction to metals has conventionally been achieved by high-temperature electrolytic methods using molten salt electrolytes and by

metallothermic reduction methods using thermodynamically favorable reductants as calcium (Ca), lithium (Li), La, and zinc (Zn). Rare earth oxides, fluorides, and chlorides are used as precursors in these processes with each contributing both positive and negative environmental, energy, and cost benefits (Chaps. 9 and 10). Other RE metal production efforts as the FFC Cambridge process, Infinium’s fueled anode molten salt electrolysis process, and the carboxylate reduction process (CRP) developed by Hela Novel Metals are under active consideration as future viable candidates for refining to metals (Chap. 10).

## 1.5 How Rare Earth Elements Came to Light

The first known application for REEs can be traced back to 1885 when Ce was used in urban lighting in Vienna, Austria—a millennium after their discovery in 1778. As the REE journey slowly continued, the unseparated mixture of lanthanide metals or *mischmetal* was produced in Germany, the United States, and China, which was used in the production of many metallurgical products (Chap. 11), Fig. 1.1.

Progress continued during the first half of the nineteenth century which saw the use of REEs not only in lighting, but also in glass and ceramics manufacturing. Synthesis and processing of high-purity chemical compounds as REE color phosphors, catalysts for cracking hydrocarbons, glass dopants, isotopes for medical diagnosing, and nuclear fuel rod applications further accelerated interest in REEs. The development of samarium–cobalt (SmCo) permanent magnets in the United States in 1966 is yet another cornerstone in the use of REEs leading to further accelerate REE market growth and production volumes and to expand mineral resource availability.



**Fig. 1.1** Major historical technological innovations that have driven REE consumption over the past 150 years. (Reproduced from Chap. 11)

## 1.6 The Rare Earth Landscape

The landscape of known global mine deposits, their estimated reserves, and current mining volumes along with their historical perspectives including forecasts for the future are discussed in Chap. 2. According to a 2020 estimate, China has the highest known number REE deposits, followed by Brazil and Vietnam, Russia, and then the rest of the world including the United States, India, Australia, and Greenland.

In 1970, the United States was the largest global producer of REOs, using bastnaesite from its Molycorp mine in Mountain Pass, California. By 1990, China became the largest producer of REOs, similarly using bastnaesite ore, but additionally used ionic clays. In 2020, China's strong REO market share had dropped to an estimated 60%. In 2021, mine production worldwide reached an estimated 280,000 metric tons of REO equivalent, with production of final products derived from REEs being disproportionately distributed in Asia. This highlights the existing global supply chain disparities.

Revitalization efforts started in the beginning of this century and have continued during the past two decades to restore the RE production capability in the United States. Besides the United States and its allied countries France, Germany, the United Kingdom, Brazil, and Japan, Australia maintains partial capability to process certain REEs and finished products in a limited capacity. Australia is also renewing its efforts to build its REE infrastructure. To date, no single nation has fully integrated facilities for mine-to-metal production operations other than China. During 2014–2020, the United States, Australia, Brazil, Burma, Vietnam, and Russia have been increasing processing capacity of REO mineral concentrate; however, they have not yet reached a significant production scale to meet the current market or forecasted future demand.

## 1.7 Rare Earth Element Applications

Rare earth elements are essential alloying/trace elements that can be found in intermediate components and manufactured end-products in the agriculture, chemical, electronics, clean energy, defense, medical, industrial, and transportation markets, with their demand projected to significantly increase as the world moves toward electrification. The physical and chemical properties of the REEs provide vast improvement in magnetic, catalytic, optical, chemical, nuclear, and structural performance. As integral to today's products, with no known near-future substitution, weight reduction, miniaturization, high-temperature stability, corrosion and oxidation resistance, optical wavelength and light intensity control, magnetic strength, abrasion resistance, and microstructure control are some of the key features making REEs unique. Listed below, covered in this book, are four major application areas where REEs play a significant role in the manufacture of consumer, energy, and defense industry products.



## 1.8 Magnets

Permanent magnet applications are numerous as they are utilized in a broad spectrum of market sectors. The RE magnet industry may account for the largest consumption of REEs today. Their penetration into the electronics, automotive, defense, blue tooth connectivity, and energy markets is a clear testimony to this fact. Rare earth elements have not only enhanced component and end-product performance features as switching, wireless connectivity, and linear motion control (Chaps. 11 and 12), but also paved a revolutionary pathway for miniaturization and significant weight savings when compared to traditional magnet architectures (Fig. 1.2).

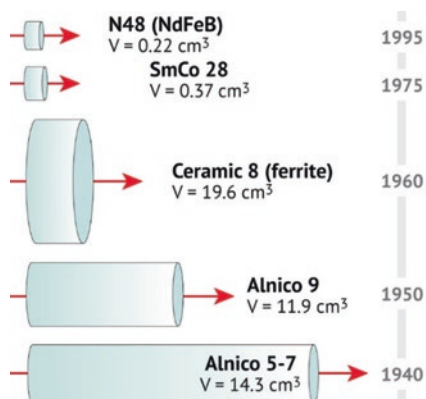
In contrast to traditional ferrite magnets, REEs in permanent magnets provided substantially improved high remanence (field strength), very high coercivity (resistance to demagnetization), stability at high temperatures with respect to magnetic properties, and environmental stability—all of which propelled the explosive growth of magnet applications.

As a major hallmark in technology development, samarium–cobalt (SmCo) magnets that were manufactured in 1975 were thirty-two times smaller in volume than the same 1940’s performance level *Alnico 9* magnets. Notably, the SmCo magnets retain their stable performance capability at high temperature (e.g., 550 °C).

While the cost of SmCo magnets is relatively high, research in the United States in the 1980s led to the development of the lower cost neodymium–iron–boron (NdFeB) family of magnets. With enhanced design flexibility, the addition of small amounts of dysprosium (Dy) and praseodymium (Pr) increased coercivity and corrosion resistance, while terbium (Tb) increased the operating temperature of the NdFeB magnets.

With growing interests in renewable energy and decarbonization technologies since 2012, the market for electric vehicles (EVs) using traction motors and offshore wind turbines requiring permanent magnet generators became apparent, which in turn increased the need for REE permanent magnets. All together, the demand for Nd, Pr, Dy, Tm, and Sm is projected to far exceed resource availability in the 2025–2030 timeframe.

**Fig. 1.2** Magnet development. (Reproduced from Chap. 11)



## 1.9 Catalysts

The second largest product sector for REEs is catalysts. Rare earth elements are used to support and enhance catalytic reactions and their kinetics. Attributed to their unique ability to influence the chemical and surface properties of the catalyst substrate, REEs have become essential in petroleum refining, in pollution control, in chemical industry, and are as critical fuel additives (Chap. 13). Notably, fluid catalytic cracking (FCC) is a process in petroleum refining to produce high-octane gasoline, light fuel oils, and olefin-rich gases, using La-impregnated porous zeolite catalysts in fluidized-bed reactors to remove hydrocarbons (HCs) or coke and to trap vanadium (V) and nickel (Ni) impurities.

Rare earth elements are critically essential in the transportation industry. Catalysts in automotive catalytic converters contain precious metals (platinum (Pt), palladium (Pd), and rhodium (Rh)—also known as platinum group metals (PGMs), alumina ( $\text{Al}_2\text{O}_3$ ) substrates, and RE-based materials that enhance PGMs catalytic activity. Rare earths promote noble metal dispersion, increase the thermal stability of the alumina support, and offer excellent completion of redox conversion reactions. Cerium in combination with Pt/Pd enhances the efficiency for conversion of fuel-based HCs and greenhouse gas emissions (e.g., carbon monoxide (CO) and nitrogen oxides ( $\text{NO}_x$ )) to ecosystem-friendly carbon dioxide ( $\text{CO}_2$ ), water vapor ( $\text{H}_2\text{O}$ ), oxygen ( $\text{O}_2$ ), and nitrogen ( $\text{N}_2$ ).

Another area that is beginning to see the emergence of catalysts containing REEs is chemical processing where REEs enhance catalytic performance, as, for example, in the production of methanol ( $\text{CH}_3\text{OH}$ ). Methanol is an important industrial chemical that is used to produce organic raw materials. Methanol derivatives are found in products as paints, solvents, engineered wood, plastics, polyethylene terephthalate (PET) bottles, safety glass, carpets, mattress foam, fertilizer, and furniture resins.

Rare earth elements are also being studied for incorporation into metal–organic frameworks (MOFs) for a wide variety of potential applications including sensing, gas adsorption, chemical separations, catalysis, drug delivery, near-infrared emission, proton conductivity, single-molecule magnets, and lighting (Chap. 13).

## 1.10 Metallurgy and High-Temperature Coatings

In contrast to the anticipated high-volume demand for REEs in the future magnet and electric vehicle (EV) industries, the use of minor quantities of REEs as alloying elements that modify the structure and properties of metals and ceramics is another major growth area for REEs.

The use of pyrophoric mischmetal in flint lighters was one of the earliest REE applications in metallurgy (Chap. 11). Subsequently, research efforts demonstrated the beneficial use of minor additions of mischmetal to iron (Fe), steel, and other metals production. Modification of graphite flakes to a spherical morphology

resulted when Ce and magnesium (Mg) were added to molten cast Fe, which enhanced the cast iron overall ductility. Mischmetal had also been shown to remove unwanted alloy impurities such as sulfur (S) and controlled the size and shape of manganese sulfide (MnS) inclusions which resulted in higher metal strength, fracture toughness, and fatigue properties.

Similar to mischmetal, REEs were used to remove arsenic (As) and lead (Pb) impurities in molten metals and to have deoxidation characteristics that are critical for removal of O<sub>2</sub> during steel solidification. The reactive ionic/atomic affinity of REEs to other alloying elements leads to the formation of stable compounds with improved bulk material properties. This feature has been used extensively in developing commercial alloys and ceramic coatings (Chaps. 14–16).

Alloy design concepts using REEs fostered the development of light metal Al and Mg alloys and a new series of Al-Sc alloys that were developed for the aerospace industry. A remarkable improvement of strength, corrosion resistance, weldability, and formability had been demonstrated in a select number of Sc-containing alloys (Chap. 15). Significant barriers for implementing the use of these advanced alloy systems are the apparent price of Sc, its current limited availability, and the lack of a potential, long-term, and future sustainable supply.

Cerium as an alloying element in Al alloys was studied extensively due to its abundant availability along with La as a co-product during the separation of LREEs from ore body concentrates. Currently, the Al-Ce family of alloys is targeted for automotive castings and other wrought alloy applications (Chap. 14). Addressing new applications where Ce and/or La could be beneficially utilized would ultimately support an improvement to the overall REE processing economics.

Magnesium alloys containing Y, Nd, and Gd have been studied for use in aerospace applications. As certified by the U.S. Federal Aviation Administration (FAA), these alloys have ideal strength-to-weight ratios and flame-retardant properties and are incorporated as commercial material systems into today's aircraft passenger seats.

Additionally, optimized nickel-based superalloys and ceramic thermal barrier coatings (TBCs) have expanded the operational space of both jet and gas turbine engines. The Y-stabilized zirconia (ZrO<sub>2</sub>) (YSZ) TBCs are known to improve the high-temperature thermal shock resistance of ceramic coatings due to their inherent ability to undergo phase transformation at temperatures around 1500 °C. High-temperature TBCs and environmental barrier coatings (EBCs) are routinely used in most aero and ground-based power generation turbine engines (Fig. 1.3). Details of current coating applications, relevant RE-containing coating material families, coating development trends, and anticipated impact on REO utilization are discussed in Chap. 16.

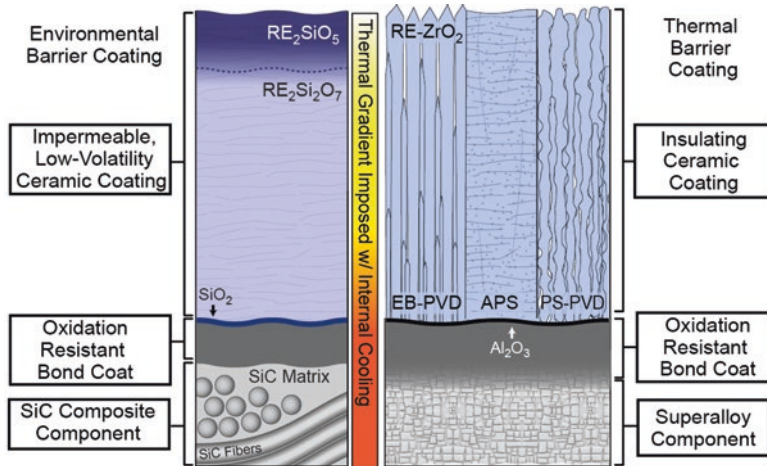


Fig. 1.3 TBC and EBC coating architecture. (Reproduced from Chap. 16)

### 1.11 Rare Earth Element Recycling and End-of-Life Products

Rare earth elements are incorporated into many of today’s consumer electronics, household appliances, transportation vehicles, and industrial machinery, as well as in utility and electric power generation systems. Typical products as laptops, cell phones, televisions, light bulbs, batteries, headphones, earbuds, audio sound bars, washing machines, automobiles including EV, wind turbines, airplanes, and robots have life cycles that range from two to twenty years. Notably, most consumer products are portable and/or are disposable. At the end-of-life (EOL), these products are destined for landfills, junk yards, or other designated collection points or entities.

There is a robust infrastructure in place to recover bulk commodity product materials as Fe, Al, Cu, and plastics. Many of these commodity products are recycled and serve as the primary base metal resource used by industry for subsequent alloy production. There is, however, no such infrastructure in place for REE recovery. Critical minerals projections indicate that the demand for Dy, Tb, Eu, and other rare earths is destined to exceed their availability by 2025. Also known is that the reserves of the most value-added HREEs are much lower than the LREEs reserves as these elements occur disproportionately in nature. For these reasons, significant efforts are underway globally to recycle EOL components from nickel–metal hydride (Ni-MH) batteries as those used in EVs, fluorescent lamp phosphors, magnet swarf, and neodymium–iron–boron (NdFeB) magnets. Chapters 17 and 18, respectively, discuss REE separation and recovery pathways for NdFeB magnets extracted from EOL electronics (e.g., computer hard drives) and spent fluorescent lamp (FL) phosphors.

For EOL NdFeB magnets, the advantages and disadvantages of magnet assembly reuse, magnet recycling, and REE recovery were explored with respect to the quality and performance of the recycled component. Clearly industry has yet to establish compliance standards and practices that lead to a successful resolution of the recycle/reuse paradigm. With environmentally benign and economically profitable recycling practices, precious raw material REE resources would be preserved for future use.

Recovery of REEs from spent lamp phosphors is perhaps the most advanced recycling process available to date. This has been catalyzed by the increased use of color phosphors in light-emitting diode (LED) devices, flat panel displays, and cell phones. These phosphors use expensive high-purity Eu, Tb, and Y which exist globally in limited quantities. The high cost of these elements coupled with supply chain disruptions have motivated REE recovery from spent waste phosphors. Novel, high recovery rate, and reduction–precipitation processes are being developed to produce high-purity Eu from waste phosphor powders.

## 1.12 Economics and Regulatory Issues

The fundamental perspectives on the economic evaluation of both conventional and unconventional REE resources as viable commercial operations are discussed as a benchmark study in Chap. 19. The economic viability or lack thereof is estimated for unconventional coal-based resources, sea-floor sediment, and monazite sands and compared to other REE projects using an alternate basket or contained value approach akin to the ones used in evaluating conventional hard rock mines. A realistic economic evaluation of REE sources is often complicated by the lack of transparency of commodity pricing history, lack of clarity with respect to the destined process streams (e.g., whether they are limited to mixed oxides or individually separated oxides), and to the purity of the final REE end-products. The most interesting historically proven production and manufacturing data remain with the offshore private sector. In general, REE extraction involves several co-products and by-products that further complicate cost estimates, as not all REEs processed from a single mining source carry the same pricing weight due to supply–demand scenarios. Generally, the value of any REE operation is strictly a function of the yield of its high value-added commodities. The economic analysis is highly sensitive to the operational stream which may be limited to processing and refining, with some processes ending at the production of mineral concentrates, mixed rare earth oxides (MREOs) or mixed rare earth salts (MRESs), partial elemental separation of target elements, or full elemental separation of all REEs.

The benchmark study used publicly available data from published sources and metadata was compiled to assess different REE mine/ore starting resources, Chap. 19. The economic viability of prior REE projects used in this study varied by a wide margin. It was shown that process operations using ore deposits that contain a

0.5–2% total REO content can be economically viable if sufficient ore reserves are known or projected. Analysis of unconventional resources showed that while the REE resource is vast in most cases, the contained values of REOs in some cases were estimated to be quite low (around <500 ppm), but still were within the range of economic viability. Coal-based materials typically contain a higher concentration of HREEs and are generally considered as waste materials (i.e., coal prep plant refuse, fly ash, ash ponds, acid mine drainage). There are virtually no mining costs associated for REE recovery from coal-based wastes. These materials contain low to negligible concentrations of radionuclides, and there is the potential to mitigate or eliminate legacy environmental issues.

To mitigate supply chain interruptions and price volatility, the industrialized countries are taking steps to strengthen and/or re-establish REE operations including mining, processing and production, manufacturing, and recycling to levelize the playing field. Significant investments have been made both by private and public sectors in the past two decades. The regulating bodies controlling the underlying processes to produce critical materials including REEs have been engaged in establishing the guidelines that prevent global REE monopolies and protect the environment (Chap. 20). The overseeing governing bodies including the Chinese Government, European Commission (EC), Australian Governing agencies, and the U.S. Administrative Procedure Act (APA) along with the United Nations Environmental Agency (UNEA) are taking steps in their own way to establish regulating policies. While the individual regulatory perspective differs greatly from country to country, most programs share common goals and objectives for the protection of human health and the environment. The U.S. Presidential Executive Order (EO) 13817 was issued in 2017 to ensure secure and reliable supplies of critical materials that extend beyond REEs. Similarly, a charter-based United Nations Convention on the Law of the Sea (UNCLOS) was issued to cover many issues that focused on deep-sea mining of RE minerals in ocean basins.

Regulations for new construction or expansion of current REE recovery facilities are no different from regulations that govern other typical mine-to-metal operations. They are based on the source materials, the recovery process (i.e., chemical, physical or biological), the surrounding geographical landscape and the type of ground and air discharges, and the storage of hazardous materials located on or at the REE recovery facility. The facilities must satisfy federal, state, and local environmental regulatory agency guidelines along with tribal and local governances.

### 1.13 Future Prospects

Throughout this book, the importance and unique features of REEs in making devices smaller, lighter, and cost-effective are emphasized. The critical importance of REEs in magnets, catalysts, color phosphors, dopants, and other metallurgical products in energy, medical, electronics, and industrial products is discussed with

an emphasis on resource availability, manufacturing, future growth drivers, and needs. Historical supply chain issues and the lack of a global levelized field for industry participation are obvious, leaving an immediate opportunity to develop a comprehensive global strategy supported by local policies and plans. Resource conservation, resource recoveries through recycling and the use of unconventional resources, development of suitable REE alternatives, cost-effective processing, and manufacturing methods to extract and refine REEs are necessary critical elements of this strategy, so that a healthy and prosperous REE market base can be realized indefinitely.

**Part I**  
**Upstream Primary Operations**



# Chapter 2

## Conventional Rare Earth Element Mineral Deposits—The Global Landscape



Nora K. Foley and Robert A. Ayuso

### 2.1 Introduction

The unique properties of rare earth elements (REEs) (Fig. 2.1) make them useful in a wide variety of applications, such as alloys, batteries, catalysts, magnets, phosphors, and polishing compounds. The REEs and their primary uses by manufacturing sector are covered in Table 2.1. Four main geologic types of REE resources supply REEs and rare earth oxides (REOs) that are vital to modern life. These are (1) carbonatite and (2) alkaline igneous deposits; (3) heavy mineral placer/paleoplacer (mineral sand) deposits; and (4) regolith-hosted ion-adsorption clay (IAC) deposits. Carbonatite is generally defined as an igneous rock composed of greater than 50% by volume of primary carbonate minerals (mainly calcite and/or dolomite). Alkaline and peralkaline igneous deposits are hosted by igneous rocks of nepheline syenite (a silica (Si)-poor, sodium (Na)–potassium (K) feldspar-rich rock) and peralkaline granitic (a rock with Na+K in excess of aluminum (Al), so that other Na-K minerals are present in addition to Na-K-feldspar) and, more rarely, trachytic (a low Si volcanic rock with abundant Na-K feldspar) compositions. Mineral sand deposits form from dispersal and sorting of refractory minerals that are derived from weathering diverse types of igneous and metamorphic rock debris; the mineralogy reflects the source rock. Ion-adsorption clay deposits form when high concentrations of REEs are adsorbed to newly formed clay minerals in regolith derived from intense weathering of REE-enriched granitic rocks. Carbonatite, alkaline igneous, and mineral sand deposits typically contain enrichments of the lighter REEs, for example, lanthanum (La), cerium (Ce), praseodymium (Pr), and

---

N. K. Foley (✉) · R. A. Ayuso  
United States Geological Survey, MS 954 National Center, Reston, VA, USA  
e-mail: [nfoley@usgs.gov](mailto:nfoley@usgs.gov)

© This is a U.S. government work and not under copyright protection in the U.S.; foreign copyright protection may apply 2024  
Y. V. Murty et al. (eds.), *Rare Earth Metals and Minerals Industries*,  
[https://doi.org/10.1007/978-3-031-31867-2\\_2](https://doi.org/10.1007/978-3-031-31867-2_2)

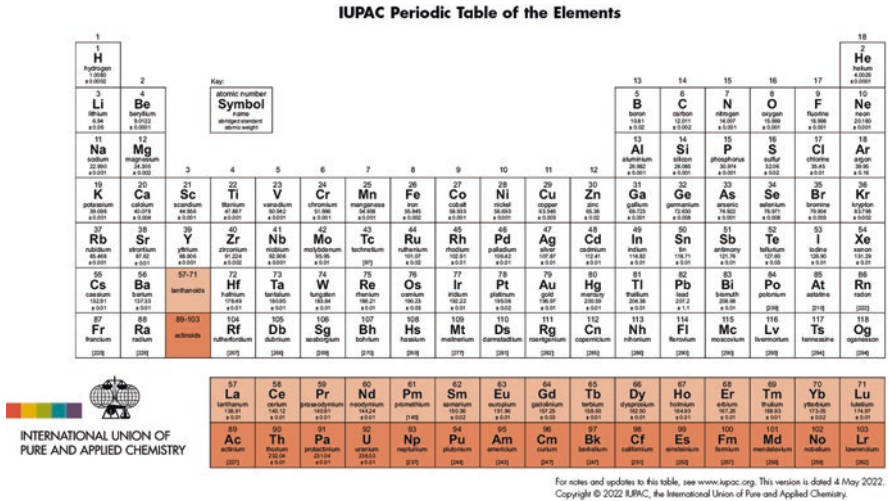


Fig. 2.1 Periodic table [1]

Table 2.1 Rare earth elements and their primary applications

Element	Symbol	Primary uses by market sectors and application
Lanthanum	La	Catalysts, ceramics, glass, polishing compounds, metallurgy, and batteries
Cerium	Ce	Catalytic converters, ceramics, glass, metallurgy, and polishing compounds
Praseodymium	Pr	Permanent magnets, batteries, aerospace alloys, ceramics, and colorants
Neodymium	Nd	Permanent magnets rubber catalysts and in medical and industrial lasers
Samarium	Sm	Permanent magnets as an absorber in nuclear reactors and in cancer treatments
Europium	Eu	Phosphors and nuclear control rods
Gadolinium	Gd	Medical imaging, permanent magnets, and steelmaking
Terbium	Tb	Permanent magnets, fiber optics, lasers, and solid-state devices
Dysprosium	Dy	Permanent magnets, data storage devices, and lasers
Holmium	Ho	Permanent magnets, nuclear control rods, and lasers
Erbrium	Er	Fiber optics, optical amplifiers, lasers, and glass colorants
Thulium	Tm	Various metal alloys and in lasers
Ytterbium	Yb	Catalysts, scintillometers, lasers, and metallurgy
Lutetium	Lu	Scintillators for medical imaging, electronics, and some cancer therapies
Scandium	Sc	Alloys, ceramics, and fuel cells
Yttrium	Yb	Ceramic, catalysts, lasers, metallurgy, and phosphors

neodymium (Nd), whereas regolith-hosted IAC deposits are the primary source of the scarcer heavy REEs, such as dysprosium (Dy) and terbium (Tb).

This chapter provides an overview of the geochemical behavior and mineralogy of REEs for the most important geologic REE sources, a summary of estimated global resources and production data, and an analysis of the geochemical and geological attributes of conventional deposit types. Other mineral deposit types that may have future economic potential to be exploited for REEs as a principal commodity, by-product, or co-product commodity are also briefly examined. The main goal of the chapter is to provide a conceptual scheme for REE mineral systems and to provide information on the primary conventional sources of the REEs and REE compounds used in various applications, in comparison with unconventional-type REE resources (Chap. 3). Readers are also referred to comprehensive reviews of individual REE deposit types and mines referenced in this chapter. These reviews provide extensive information on historic mining activity, detailed deposit descriptions, and summaries of past and current exploration and extraction activities for the diverse REE mineral deposits currently under study. From our examination, we

**Table 2.2** Minerals commonly associated with conventional REE resources

Mineral name	General chemical formula
Alkali feldspar	(K, Na) AlSi <sub>3</sub> O <sub>8</sub>
Allanite	(Ce, Ca, Y) <sub>2</sub> (Al, Fe <sup>3+</sup> ) <sub>3</sub> (SiO <sub>4</sub> ) <sub>3</sub> (OH); up to 20% of REE by weight
Ancylite-(Ce)	CeSr(CO <sub>3</sub> ) <sub>2</sub> (OH) · H <sub>2</sub> O
Ancylite	Sr(REE)(CO <sub>3</sub> ) <sub>2</sub> (OH) · H <sub>2</sub> O
Apatite	Ca <sub>5</sub> (PO <sub>4</sub> ) <sub>3</sub> (OH)(F, Cl)
Bastnäsite	(M)(CO <sub>3</sub> ) <sub>2</sub> F; M=LREE, Ca
Biotite	K(Mg, Fe <sup>2+</sup> ) <sub>3</sub> [AlSi <sub>3</sub> O <sub>10</sub> (OH, F) <sub>2</sub>
Brannerite	(U, Ca, Y, REE) (Ti, Fe) <sub>2</sub> O <sub>6</sub>
Britholite	(REE, Ca, Th) <sub>5</sub> (SiO <sub>4</sub> , PO <sub>4</sub> ) <sub>3</sub> (OH, F)
Burbankite	(Na, Ca) <sub>3</sub> (Sr, Ba, Ce) <sub>3</sub> (CO <sub>3</sub> ) <sub>5</sub>
Cerianite-(Ce)	(Ce <sup>4+</sup> , Th)O <sub>2</sub>
Chevkinite	(Ce, La, Ca, Th) <sub>4</sub> (Fe <sup>2+</sup> , Mg) <sub>2</sub> (Ti, Fe <sub>3+</sub> ) <sub>3</sub> Si <sub>4</sub> O <sub>22</sub>
Diamond	C
Doverite	(Y, Ca, HREE)F(CO <sub>3</sub> ) <sub>2</sub>
Eudialyte	Na <sub>4</sub> (Ca, REE) <sub>2</sub> (Fe <sup>2+</sup> , Mn, Y)ZrSi <sub>8</sub> O <sub>22</sub> (OH, Cl) <sub>2</sub>
Euxenite	(Y, HREE, Ca, Ce, U, Th)(Nb, Ta, Ti) <sub>2</sub> O <sub>6</sub>
Fergusonite	(Nd, Ce)(Nb, Ti)O <sub>4</sub>
Fergusonite-(Y)	YNbO <sub>4</sub>
Florencite	CeAl <sub>3</sub> (PO <sub>4</sub> ) <sub>2</sub> (OH) <sub>6</sub>
Fluorapatite	(Ca, REE, Na) <sub>5</sub> (PO <sub>4</sub> ) <sub>3</sub> (F, OH)
Francolite	Ca <sub>5</sub> (PO <sub>4</sub> , CO <sub>3</sub> ) <sub>3</sub> F
Gadolinite	(REE, Y) <sub>2</sub> Fe <sup>2+</sup> Be <sub>2</sub> Si <sub>2</sub> O <sub>10</sub>
Garnet	(Fe, Ca, Mg, Mn, REE) <sub>3</sub> (Fe, Al, Cr) <sub>2</sub> Si <sub>3</sub> O <sub>12</sub>
Gittinsite	CaZrSi <sub>2</sub> O <sub>7</sub>
Gorceixite	(Ba, REE)Al <sub>3</sub> (PO <sub>4</sub> ) <sub>2</sub> (OH <sub>5</sub> , H <sub>2</sub> O)

(continued)

**Table 2.2** (continued)

Mineral name	General chemical formula
Goyazite	$(\text{Sr, REE})\text{Al}_3(\text{PO}_4)_2(\text{OH}_3, \text{H}_2\text{O})$
Halloysite	$\text{Al}_2\text{Si}_2\text{O}_5(\text{OH})_4$
Iimoriite-(Y)	$\text{Y}_2\text{SiO}_4\text{CO}_3$
Ilmenite	$\text{Fe}^{2+}\text{TiO}_3$
Kainosite	$\text{Ca}_2(\text{Y, REE})_2\text{Si}_4\text{O}_{12}\text{CO}_3 \cdot \text{H}_2\text{O}$
Kaolinite	$\text{Al}_2\text{Si}_2\text{O}_5(\text{OH})_4$
Leucoxene	Variable, a mixture of Fe-Ti oxides
Loparite-(Ce)	$(\text{Na, Ce, La, Ca, Sr})(\text{Ti, Nb})\text{O}_3$
Magnetite	$\text{Fe}^{2+}\text{Fe}^{3+}_2\text{O}_4$
Monazite	$(\text{M})\text{PO}_4$ ; M= Ce, La, Nd, Th
Montmorillonite	$(\text{Na, Ca})_{0.33}(\text{Al, Mg})_2(\text{Si}_4\text{O}_{10})(\text{OH})_2 \cdot n\text{H}_2\text{O}$
Mosandrite	$(\text{Ca, Na, REE})_{12}(\text{Ti, Zr})_2\text{Si}_7\text{O}_{31}\text{H}_6\text{F}_4$
Niobite	$\text{Nb}_2\text{O}_6$
Nontronite	$\text{Na}_{0.3}\text{Fe}_2((\text{Si, Al})_4\text{O}_{10})(\text{OH})_2 \cdot n\text{H}_2\text{O}$
Parisite	$\text{Ca}(\text{REE})_2(\text{CO}_3)_3\text{F}_2$
Rhabdophane	$(\text{REE})\text{PO}_4 \cdot \text{H}_2\text{O}$
Rutile	$\text{TiO}_2$
Saponite	$\text{Ca}_{0.25}(\text{Mg, Fe})_3((\text{Si, Al})_4\text{O}_{10})(\text{OH})_2 \cdot n\text{H}_2\text{O}$
Sapphire	$\text{Al}_2\text{O}_3$
Staurolite	$\text{Fe}^{2+}_2\text{Al}_9\text{O}_6(\text{SiO}_4)_4(\text{O, OH})_2$
Synchysite	$\text{Ca}(\text{REE})(\text{CO}_3)_2\text{F}$
Thalenite-(Y)	$\text{Y}_3\text{Si}_3\text{O}_{10}\text{OH}$
Xenotime	$\text{YPO}_4$
Zircon	$(\text{Zr, REE})\text{SiO}_4$ ; rarely up to a few % REE by weight

conclude that the need for both conventional and unconventional REE mineral sources will continue to expand to meet the demands of modern society. Readers are referred to Table 2.2 for REE mineral formulae.

## 2.2 Lanthanide Behavior in Natural Systems

### 2.2.1 General Concepts

The lanthanide series of REEs consists of fifteen elements that range in atomic number from 57 to 71 and include La to lutetium (Lu) (Fig. 2.1). The series is named after the first and lightest element—La [1]. All elements of the lanthanide series are chemically like La, which was named after the Greek word *lanthanein* meaning “to escape detection.” Like most of the light rare earth elements (LREEs), La was first discovered in mixtures with Ce. The metals scandium (Sc, atomic

number 21) and yttrium (Y, atomic number 39) are often included in the group because they can occur together with the lanthanides in minerals due to similarities in ionic size and other geochemical properties. The REEs are relatively abundant in nature [2]. Cerium, at 60 ppm (or  $\text{mg}\cdot\text{kg}^{-1}$ ), has the highest abundance in the earth's crust, comparable to that of copper (Cu), while Nd at about 28 ppm has a crustal abundance like that of cobalt (Co). Thulium (Tm) and Lu, the least abundant lanthanides at 0.5 ppm, have a crustal abundance that exceeds that of gold (Au). For the REEs, similar attributes such as ionic radii and their typical trivalent (+3) charge result in an overall geochemical affinity among the lanthanide series. In natural systems deviations from the typical trivalent charge are best documented for europium ( $\text{Eu}^{2+}$ ) and  $\text{Ce}^{4+}$  depending on the availability of oxygen in igneous and mineralized systems; however, valences of +2 (Nd, Dy, Tm, ytterbium (Yb), Eu, and samarium (Sm)) and +4 (Ce, Pr, and Tb) have been reported to occur in some minerals. These charge differences can result in anomalies in some types of geochemical plots when the contents of these elements deviate from the overall regular distribution typically shown by the trivalent lanthanides.

For descriptive purposes, the lanthanides can be discussed as belonging to three geochemically coherent groups: The light REE (LREE) generally includes La through Nd (atomic numbers 57 through 60), the middle REE (MREE) includes Sm through Dy (atomic numbers 62 through 66), and the heavy REE (HREE) includes holmium (Ho) through Lu (atomic numbers 67 through 71) [2]. There are alternative ways that the REEs are subdivided. For example, La to Sm can be classified as LREE and elements from Eu to Lu and Y grouped as the HREEs. A subdivision between LREE and MREE is used in a variety of applications (Table 2.2), most notably in the manufacture of permanent magnets. The HREE group is particularly important to emerging technologic requirements of the green energy, defense, and electronic industries [3]. Locating new HREE deposits and expanding their availability are critical to the economies of modern societies.

### 2.2.2 Mineralogy

Rare earth elements share many geochemical and physical properties under natural conditions [4]. This geochemical similarity depends on the electronic configuration of elements in the lanthanide series and on a small but consistent decrease in ionic radius with increasing atomic number for a given coordination number (number of atoms or ions around an atom in a mineral). Lanthanum, the lightest of the REEs, has an ionic radius of  $\sim 1.061 \text{ \AA}$ , and Lu, the heaviest of the lanthanides, has an ionic radius of  $\sim 0.848 \text{ \AA}$ . Most importantly, the ionic radius of lanthanide elements is similar to that of many elements that are widely distributed in the earth's crust (e.g., calcium (Ca), strontium (Sr)), which allows them to substitute in various minerals.

The lanthanide series is particularly important in understanding geologic processes because depending on the type, size, and electronic requirements of various minerals, lanthanides are fractionated by mechanisms that result in relative

enrichments and depletions of LREEs, MREEs, and HREEs in bulk rocks. Rarely do minerals contain a single REE. The main exception is Ce which can be fractionated from other REEs at the earth's surface as the mineral cerianite ( $\text{CeO}_2$ ) due to the ability of Ce to be oxidized to a stable  $3^+$  quadrivalent state. Scandium (ionic radius 0.745 Å) is another example that exists in major amounts in only a few minerals. The main Sc ore mineral is thortveitite, a Sc-Y silicate. Scandium also occurs in minor amounts in euxenite and gadolinite and in trace amounts in many minerals. Yttrium (ionic radius of 0.9 Å) is typically found with the HREEs in various minerals, and it is also the main component of xenotime ( $\text{YPO}_4$ ) which is widely disseminated in many rock types.

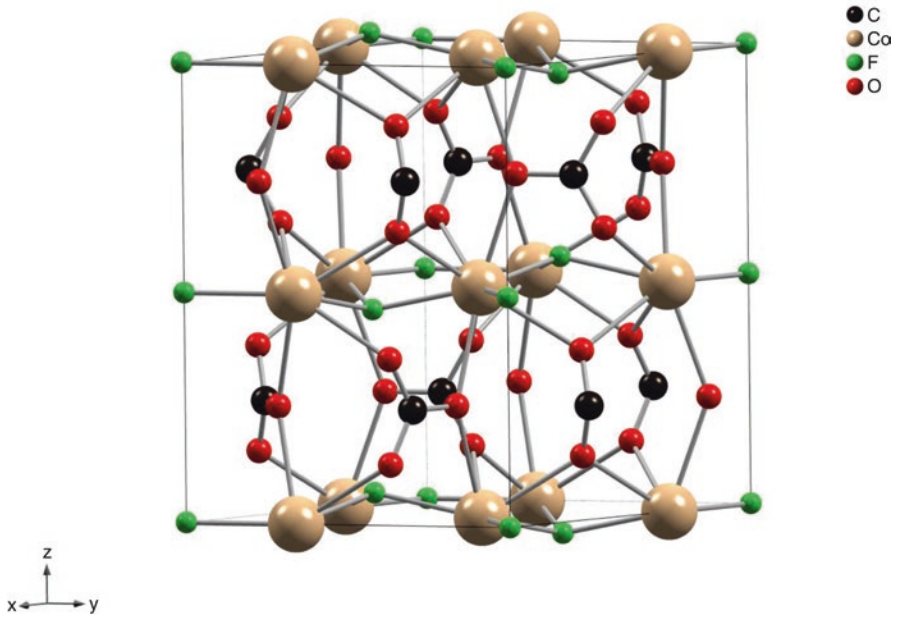
Hundreds of minerals containing REEs are known to occur in nature [5]. Most REE minerals contain mainly LREEs (the larger ions), a mixture of all the REEs, or only heavy REEs (the smaller ions). These differences reflect the site requirement with the crystal structure of the mineral. The REEs can substitute for a similar-sized element within a mineral's crystal structure or occur as adsorbed ions on a suitable mineral substrate such as clays or iron oxides. The majority of REE minerals contain LREEs (La, Ce, Pr, and Nd), while the remaining minerals, most notably the HREE-enriched minerals, typically contain one or more lanthanides [6]. In general, fluorocarbonate/carbonate, complex oxide, phosphate, and silicate mineral groups (Table 2.2) contain the minerals of most interest to mining geology because of current knowledge of discovered deposits, advances in exploitation and beneficiation processes, and overall economic and environmental constraints.

Out of the hundreds of minerals that contain REEs, only a limited number are commercially exploitable under current economic and sociopolitical conditions. These include bastnäsite, monazite, loparite, and the ion-adsorption clays described below. Some potentially important sources of REE cannot be currently utilized because extraction technologies are lacking. In the following sections, we will discuss in more detail the occurrence of such minerals in economic ore deposits exploited today.

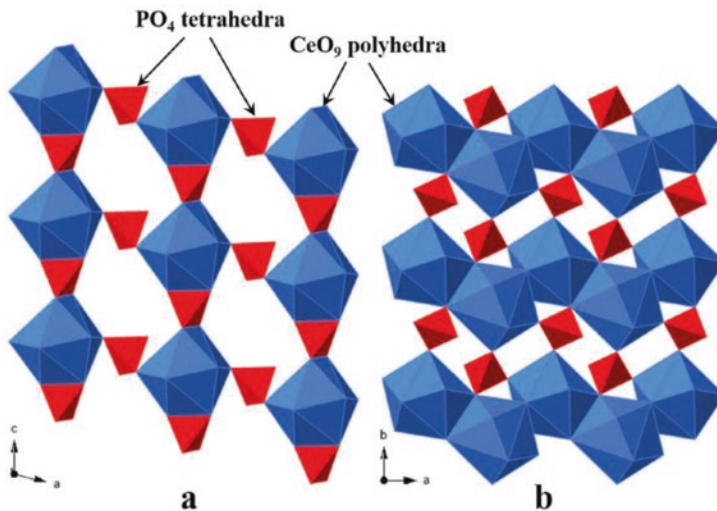
Bastnäsite ( $\text{MCO}_3\text{F}$ ) is a fluorocarbonate mineral group that contains Ca and up to approximately 65% LREEs (La-Nd) in the M site of the mineral structure. There are three main variations of bastnäsite-(M), where La, Ce, or Nd dominates the M site. Figure 2.2 shows the arrangement of atoms for bastnäsite-(Ce).

Monazite [ $\text{MTO}_4$ -(M)] belongs to a group of phosphates and arsenates where LREEs and thorium (Th) fill the M site, and phosphorous (P) or arsenic (As) and less commonly Si fill the T mineralogical structural site. Varieties of phosphate have either La, Ce, Nd, or Sm as the dominant cation in the M site (Fig. 2.3). In deposits hosted by carbonatite igneous rocks, bastnäsite-(Ce) and monazite-(Ce) are the most typical compositions [8]. In heavy mineral sand placer deposits, detrital monazite sourced from weathered igneous rocks is also generally LREE-enriched (La, Ce, Pr, Nd) as well as Th-bearing [9].

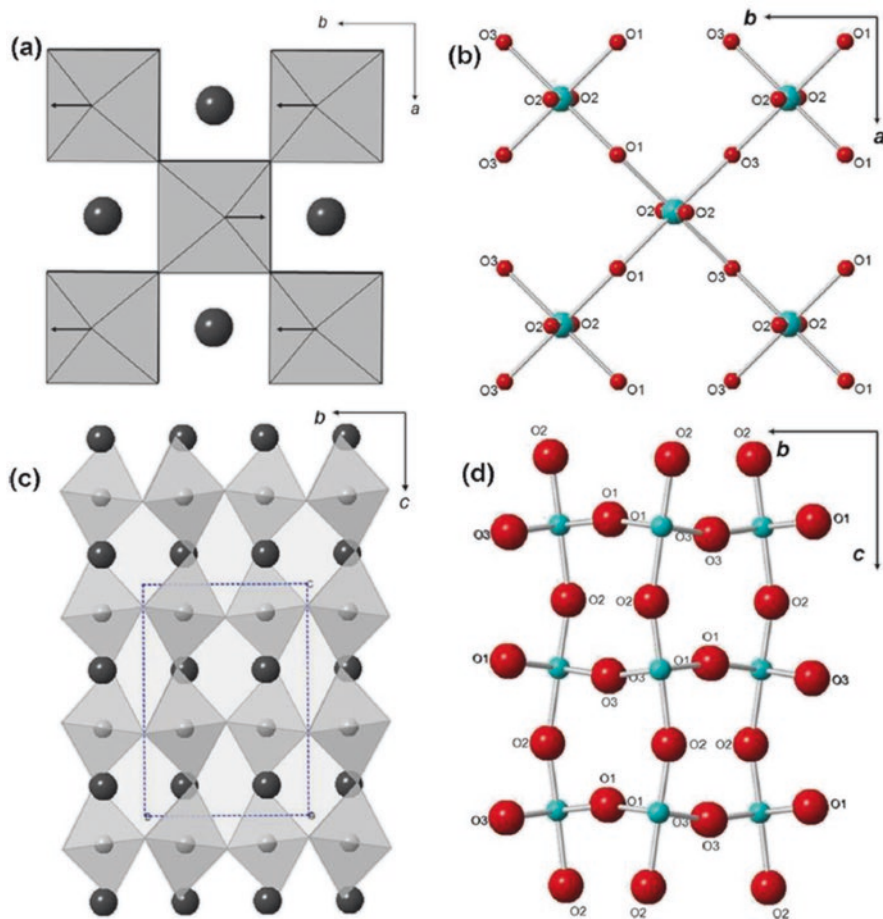
Loparite ( $\text{ABO}_3$ ) is a complex oxide in which LREEs, Na, and Ca generally occupy the A-site, and titanium (Ti), niobium (Nb), or iron ( $\text{Fe}^{+3}$ ) occupy the B site. Loparite occurs as a primary mineral in differentiated nepheline syenite massifs which are silica-poor igneous rocks composed of the minerals nepheline and alkali



**Fig. 2.2** Ball-and-stick representation of bastnäsite-(Ce). (This figure is modified from A.G. Christy (unpubl., 2022), created using CrystalMaker software based on the atomic coordinates of Ni et al. [7]. Bastnäsite consists of REE-F sheets separated by carbonate ions and is characterized by a hexagonal crystal structure. In this example, the Ce atom (beige) is coordinated by three F atoms (green) within Ce-F sheets and six O atoms (black) in  $\text{CO}_3$  sheets; the Ce-F sheets are bonded to adjacent  $\text{CO}_3$  (C shown in red) sheets by Ce-O bonds)



**Fig. 2.3** A polyhedral representation of the monazite structure [10]. (a) Isolated  $\text{PO}_4$  tetrahedra and  $\text{CeO}_9$  polyhedra that share edges or corners to form chains parallel to the c-axis; (b)  $\text{CeO}_9$  polyhedra share common edges along the a-axis, whereas  $\text{PO}_4$  tetrahedra and  $\text{CeO}_9$  polyhedra share corners along the b-axis. This study investigated the crystal chemistry of detrital monazite from two beach placer sand samples collected from Cox's Bazar, Bangladesh [10]. The elements Th and U commonly substitute in the Ce site in the crystal structure



**Fig. 2.4** A new structural variety of loparite—acentric loparite from the Khibiny alkaline massif, Kola Peninsula, Russia [12]. The crystal structure of loparite is shown in polyhedral and ball-and-stick representations projected onto the *ab* (**a**, **b**) and *bc* (**c**, **d**) planes. The polyhedral view shows the  $\text{BO}_6$  ( $\text{TiO}_6$  and  $\text{NbO}_6$ ) octahedra in gray and the A cations (the REEs) as black spheres. The acentric behavior is due to the rotation and tilting of chains of octahedra with respect to the *c*-axis (compare Figure (**a**) and (**b**) with (**c**) and (**d**), respectively). As seen in Figure (**d**), the  $-\text{O}_2\text{-B-O}_2\text{-B-}$  bond chains running along the *c*-axis form a zigzag chain within the *bc* projection

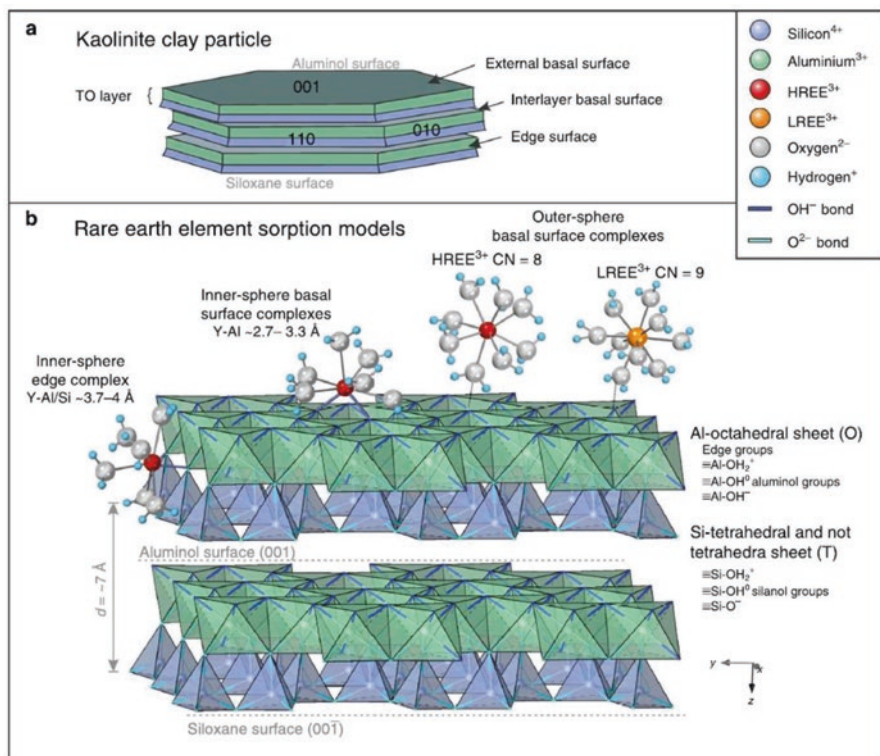
feldspar. It also occurs in some pegmatites, in particular those that are silica-poor and contain alkali (Na-K) feldspar and as a replacement of perovskite ( $\text{CaTiO}_3$ ) in carbonatites. Studies show that loparite composition is highly variable due to coupled element substitutions, polymorphism, and defects in element distribution in the mineral and from radioactive decay of incorporated uranium (U) and Th [11]. The different structural models for loparite likely result from the dependency of mineral structure on composition. A new “acentric” structural variety of loparite from the Kola Peninsula (Fig. 2.4) has been recently described [12]. This type of loparite is thought to be the result of higher contents of Ti compared to other loparites.



Variations such as these in crystal structures can impact strategies for extracting REEs from loparites.

During formation of IAC deposits from source bedrock, REE ions or hydroxides can be adsorbed onto suitable substrates in a developing soil profile within a regolith. Typical substrates consist of clay minerals, iron-manganese oxyhydroxides, and organic material (such as humic acid). Precipitation of new, secondary REE minerals also commonly occurs under these geologic conditions. Local differences in pH, redox state, and complexing agents within the soil profile control whether separation of REEs occurs by adsorption on to substrates or precipitation of new REE minerals such as phosphates (e.g., monazite) or fluorocarbonates (e.g., synchysite, doverite). Weathering of igneous rocks converts constituents such as volcanic glass, feldspars, and other common rock-forming minerals (e.g., amphiboles, epidotes, micas, and pyroxenes) to clay minerals. These mainly include kaolins (kaolinite and halloysite) and smectite-group (montmorillonite, nontronite, and saponite) minerals (Table 2.2). Kaolinitic layers typically form within the middle part of a soil profile (“B and C” layers), whereas smectites which are chemically more complex than kaolins are typically found in lowermost parts of weathering profiles, nearer the source bedrock where availability of Fe and magnesium (Mg) exerts strong control on mineralogy. Thus, adsorption of REEs to newly forming clay minerals in a regolith deposit can be an intricate function of particle size (surface area) and reactivity of the substrate, pH, redox state, and presence or absence of complexing agents in the aqueous fluid, in addition to the original REE and silicate mineralogy of the source rock [13]. Two main types of IAC deposits are identified in China: (1) enriched in LREE with  $Y_2O_3 < 50\%$  of the total REE+Y resource and (2) enriched in HREE with  $Y_2O_3 > 50\%$  of the total REE+Y resource [14].

The crystal structure of clays results in two distinct types of surfaces capable of binding ions—basal surfaces and edge surfaces (Fig. 2.5a). Basal (and interlayer) surfaces have generally been thought to be independent of changes in pH, while edge surfaces which result from broken bonds are pH dependent [15]. A recent study [16] employed high-energy synchrotron radiation to address the distribution and local bonding environment of REEs on kaolinite (Fig. 2.5b). They used Y and Nd as proxies for HREE and LREE adsorption to investigate possible mineralogical analogs to deposits currently mined in China. This study provides a significant advance in understanding REE adsorption onto clays in regolith. The authors [15] showed that REEs in Malagasy clays (Madagascar), which formed from regolith developed on peralkaline rocks, occur as leachable hydrated complexes adsorbed onto kaolinite. The study confirms that the adsorption process operates globally in lateritic weathering profiles and encourages the search for IAC REE deposits in supergene environments.



**Fig. 2.5** A schematic adsorption model for REE onto kaolinite [16]. (a) The 1:1 stacking of Al-octahedral (O) and Si-tetrahedral (T) sheets, forming TO layers with aluminol and siloxane external basal surfaces, edge, and interlayer surfaces; (b) an REE sorption model indicating that LREE and HREE complexes can occur as eight- to nine-coordinated inner-sphere (basal surface or edge) complexes or loosely adsorbed as eightfold or ninefold hydrated outer-sphere complexes [16]. <https://creativecommons.org/licenses/by/4.0/> [16]

### 2.3 Global Resources, Production, and Consumption

Rare earth elements are relatively abundant in the earth's crust, but minable concentrations are less common than those for many other mineral commodities [17–19]. Global resource estimates of REEs (and other mineral commodities) typically include both discovered and undiscovered deposits, and these resource types are generally categorized with increasing geologic confidence as *inferred*, *indicated*, or *measured*. Geologic classification for reserves of REEs includes those deposits that are either *probable* or *proven* [18]. The guidelines listed are set out by the Society for Mining, Metallurgy, and Exploration (SME) in the United States. Mineral reporting codes and guidelines for most parts of the world (Australia, Asia, Canada, Chile, Europe, South Africa, and the United States) are set by the Committee for Mineral Reserves International Reporting Standards (CRIRSCO). China, Russia,

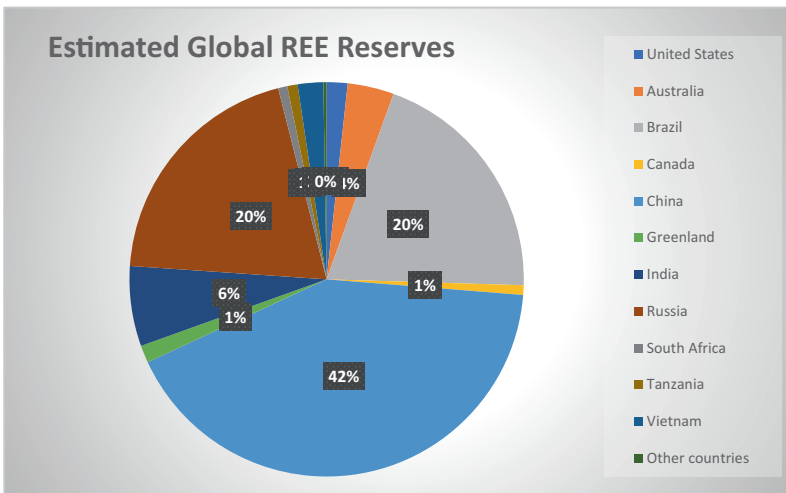
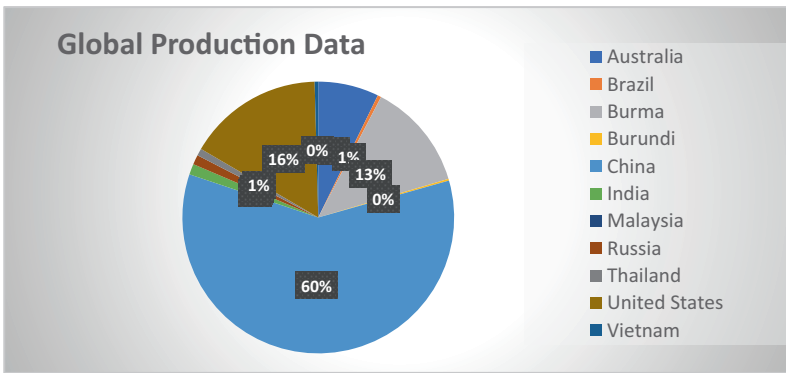
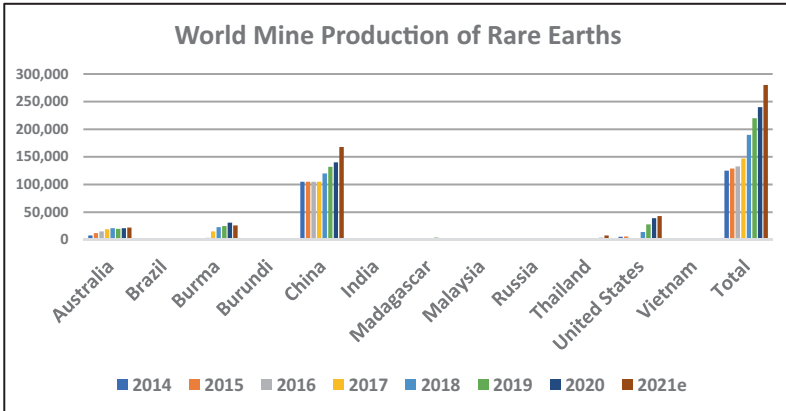


**Fig. 2.6** Global distribution of active REE deposits and advanced projects by deposit type. (Compiled for 2017 [20])

and India use similar classification schemes. In general, global resource estimates offer a view to the future, whereas reserve estimates provide a snapshot of the current global picture. Figure 2.6 shows a snapshot of the global distribution of conventional REE deposits by type and status around 2017.

Bastnäsite deposits in alkaline rocks and carbonatites of China and the United States [3, 14, 21, 22] constitute the largest percentage of the world’s economic resources. Monazite-bearing mineral sands in Australia, Brazil, China, India, Malaysia, South Africa, Sri Lanka, Thailand, and the United States make up the second largest segment [23–25]. These two deposit types primarily produce LREEs. Loparite which is also a source for LREEs is mined from a small number of deposits in layered alkaline rocks of the Kola Peninsula, Russia [12, 26]. Most of the remaining economic resources of REEs are contained in regolith-hosted ion-adsorption clays which are mainly kaolinite and halloysites [27]. Regolith-hosted REE resources of the IAC type found in China and Southeast Asia are especially important because they currently are the source of virtually all HREEs, Y, and a large proportion of LREEs reaching global markets [14, 21, 28]. World reserves of most REEs are thought to be sufficient to meet forecasts of world consumption well into the twenty-first century (Fig. 2.7); however, their global distribution varies widely.

Prior to the discovery and exploitation of the REE ion-adsorption clay deposits of China in the 1970s, essentially all REEs were produced from either bastnäsite mined from carbonatite at Mountain Pass, California, or derived from monazite from heavy mineral sand deposits primarily located in Australia. The production of REEs from bastnäsite, monazite, and loparite ores by conventional methods is energy intensive and involves multiple chemical processing steps tailored to the



**Fig. 2.7** World mine production of REEs (in metric tons REO) from 2014 to 2021 (estimated) by country. Global production and reserve data, by country for 2020 [17–19]

mineral composition. These include electrochemical extraction (heating the mineral to its melting point) and leaching the resulting glass with sulfuric acid ( $\text{H}_2\text{SO}_4$ ) or sodium hydroxide ( $\text{NaOH}$ ) [29]. Recent advances in separation and extraction technologies for bastnäsite [30, 31], monazite [32], and loparite [33] have led to more environmentally sustainable approaches to recovery of REE from bulk ore having more complex mineral compositions. The production of REEs from low-grade ores containing ion-adsorbed clay minerals employs bulk mining of clay deposits from open pits and extraction of REEs by ion exchange using a dilute electrolyte solution [34, 35]. Previous approaches focused mainly on REE adsorbed to kaolins. The knowledge that REEs can have multiple modes of occurrence such as soluble fluorocarbonate minerals has led to newly developed approaches aimed at liberating encapsulated REE-bearing minerals through expansion of kaolinite aggregates and converting REE-bearing minerals into more soluble forms [36].

The global production status has changed drastically since the 1970s when the main supplier was the United States. By 1990, China had become the main global supplier of REEs. China continues to hold that position today mainly by producing REEs both from bastnäsite mineral deposits and REE-adsorbed clays. Global mine production [18] has almost doubled since 2014 to an estimated 280,000 metric tons of rare earth oxide (REO) equivalent in 2021. Data for recent years show changing production of REEs in many countries (Fig. 2.7). For example, the production of REO derived from concentrates mined in Australia, Burma, and the United States increased by about 60% from 2014 to 2020. In comparison, China supplied about 60% of the total global REO production in 2020, a drop of about 25% since 2014. China continues to dominate REE production by balancing excess global supply with changing mining production quotas. China's Ministry of Industry and Information Technology [18] reports the mine production quota for 2020 was 140,000 metric tons (an increase of 16% over 2019) with 120,850 metric tons allocated to LREEs and 19,150 metric tons allocated to ion-adsorption clays. Overall, these data emphasize the continued dominance of China in supplying global needs for REEs. Global efforts are underway to expand exploration, discovery, economic assessment, and feasibility studies and novel extraction procedures applied to both conventional and unconventional rare earth resources. For example, the Critical Minerals Mapping Initiative (CMMI) is a joint effort by Australia, Canada, and the United States to identify and ensure the supply of critical minerals [37]. The resulting geochemistry database—along with basic query, statistical analysis, and display tools—will be served to the public through a Web-based portal managed by Geoscience Australia. A searchable database on critical mineral resources of the world is currently under development by the CMMI [37].

Magnets, catalysts, polishing, and metallurgical applications consumed the bulk of global REE production, while other uses included ceramics, glass, phosphors, and pigments [19]. These distinct market sectors and applications differ significantly in the amount and type of REEs used (Table 2.1). For example, consumption in the magnet sector includes light, middle, and HREEs with the REEs varying depending on the type of permanent magnet. Neodymium–iron–boron (NdFeB) magnet technologies currently use primarily Nd and Pr with lesser amounts of Dy,

Gd, and Tb. Samarium–cobalt (Sm-Co) magnets use Sm and lesser amounts of gadolinium (Gd). Lanthanum has limited use in certain ferrite-type magnets. Ferrite is a ferrimagnetic ceramic compound derived from iron oxides. These types of strong permanent magnets are used in missile guidance and control systems, disk drive motors installed in aircraft and tanks, satellite communications, and radar and sonar systems. Certain types of high-unit-value applications impact consumption of HREE. For example, laser crystals based on Nd and Y are doped with HREE (e.g., Dy, Er, Tm, and Yb), and positron emission tomography and scintillometers for medical imaging and cancer therapies use Lu.

Demand for REEs is expected to continue to grow due, in large part, to the expanding market needs for permanent magnets, electric vehicles, and materials used in energy-related sectors such as energy-efficient lighting and wind turbines and other products related to cutting carbon emissions. Industry estimates of the global consumption of REEs, as summarized by the U.S. Geological Survey [17, 18], have varied significantly in recent years from about 140,000 to 170,000 metric tons of REO equivalent. Consumption varies widely on a global scale primarily as a function of REE needs based on individual countries' manufacturing requirements and production capabilities in distinct REE market sectors and required applications. For example, apparent consumption of REEs in the United States was estimated to be 9100 metric tons of REO equivalents in 2017 [19]. The United States as reported in 2020 for 2017 [18] has limited capabilities to produce battery alloys, magnet alloys, and phosphors. As a result, most current LREE consumption is in the form of Ce and La compounds used to produce catalysts, ceramics, glass and polishing compounds, and ferrocenium and rare earth metals used for alloys and other metallurgical applications. Moreover, consumption of HREE (Tb, Dy, Ho, erbium (Er), Tm, Yb, and Lu) has been estimated to contribute less than 2% to the total U.S. consumption.

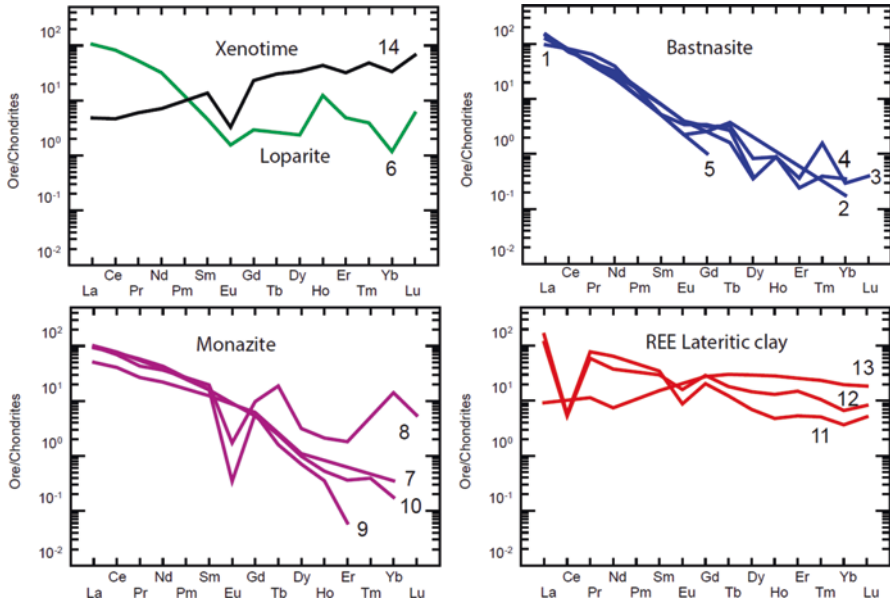
## **2.4 Rare Earth Element Deposit Types and Their Geochemical Characteristics**

### ***2.4.1 Rare Earth Mineral Systems***

Rare earth deposits are found in specific rock or deposit types that occur in certain geological settings. The growing demand for critical minerals such as the REEs has resulted in advances in understanding and predicting how, why, and where economic mineral systems might occur [37]. One ongoing effort by the CMMI to advance knowledge about the abundance of critical minerals, such as REEs, has resulted in a revised classification of ore-forming settings based on certain essential characteristics that include the larger-scale geologic environment in which deposits form (i.e., the deposit environment (Table 2.3)). A “deposit environment” is akin to a geologic setting having a distinctive set of physical and chemical attributes and crustal processes, such as magmatism, metamorphism, and weathering. The

**Table 2.3** Mineral systems for conventional rare earth element deposits

Depositional environment	Deposit group	Deposit type	Examples	References
Magmatic	Carbonatite	Carbonatite REE	Mountain Pass, California, United States	[3, 20]
			Bayan Obo, Inner Mongolia, China	[14, 44, 47, 49]
			Khanneshin, Helmand Province, Afghanistan	[50, 51]
	Alkaline/peralkaline igneous	Layered alkaline igneous	Lovozero and Khibiny, Kola Peninsula, Russia	[55, 56]
			Norra Kärr, Sweden	[56]
		Peralkaline igneous high field strength element (HFSE)—REE	Toongi, Dubbo, New South Wales, and Brockman/Hastings, New South Wales, Australia	[56, 57]
Pegmatite	Abyssal pegmatite REE	Bokan Mountain, Alaska, United States	[20, 56]	
		Fraser Lakes, Saskatchewan, Canada	[76, 93]	
		Apatite intrusion REE/apatite vein	Nolans Bore, Northwest Territories, Australia	[45, 77]
Magmatic–hydrothermal	Breccia pipe	Breccia pipe REE	Pea Ridge REE, Missouri, United States	[78–80]
	Skarn	Skarn uranium-REE	Mary Kathleen REE-U, Queensland, Australia	[93]
Erosional	Placer	Heavy mineral sands/mineral sands/placers	WIM150, Victoria, Australia	[9, 25, 60, 61]
			Boise REE-Th-Ti-Nb-Ta, Idaho, United States	[9]
			Carolina Piedmont, Southeastern United States	[9]
Supergene	Clay	Ion-adsorption clay REE/regolith-hosted REE	Grande-Vallée, Quebec, Canada	[27]
			Jiangxi, Guangdong, Fujian, and Guangxi provinces, China	[14]
			Stewartville IAC, Virginia, United States	[70]
			Liberty Hill IAC, South Carolina, United States	[74]
	Laterite	Carbonatite laterite REE	Mt. Weld laterite, Western Australia, Australia	[8, 64, 67]
Basin hydrothermal	Unconformity-Related	Unconformity-related REE	Browns Range, Western Australia, Australia; Maw zone, Saskatchewan, Canada	[89]
Basin chemical	Phosphorite	Phosphate (REE in carbonate–fluorapatite)	Athabasca Basin, Saskatchewan Canada; Phosphoria Fm., Montana-Idaho-Wyoming, United States	[83–85]



**Fig. 2.8** Chondrite-normalized REE patterns showing published compositions of bulk REE from conventional REE deposits and occurrences [19] normalized to chondrite values [38]. Note: These patterns differ from typical REE patterns for minerals. The sharp inflections (e.g., shown for Yb for monazite (line 8), loparite (line 6), xenotime (line 14); Tm in bastnaesite (line 4) may result from analytical error or impure mixtures. Normalization removes the Oddo–Harkins effect which reflects the greater abundance of even-numbered versus odd-numbered REE and results in generally smooth patterns. Only Ce (e.g., REE clay, lines 11, 12) and Eu (monazite, lines 8, 9) are expected to show enrichment or depletion anomalies. (Location number and data source [19])

conventional types of REE deposits currently being mined occur in a small number of deposit environments as exemplified by (1) magmatic (igneous) settings, such as the deposits associated with carbonatites and alkaline and peralkaline igneous rocks; (2) supergene (or chemical weathering) settings where enrichment of mineral deposits by solutions can lead to formation of regolith-hosted IAC and carbonatite laterite deposits; and (3) erosional environments which involve a combination of chemical and physical weathering processes and can produce different placer-type mineral sand deposits (Table 2.3).

Within a given deposit environment, mineral deposits can be grouped by key attributes. For REE deposits, mineralogy is perhaps most important attribute because REE availability and cost of extraction are mineral-dependent. Moreover, mineralogy controls the specific groups of REEs—light, middle, or HREEs, which likely can be produced from a deposit type. Where REE distributions are normalized to those in chondritic meteorites which is a common approach used by geochemists, mineralogically controlled differences in deposit types can be seen (Fig. 2.8). The mineralogy of each of these deposit types illustrates the range of light, middle, and heavy REEs that can be recovered depending on the mineral hosts of REEs in the



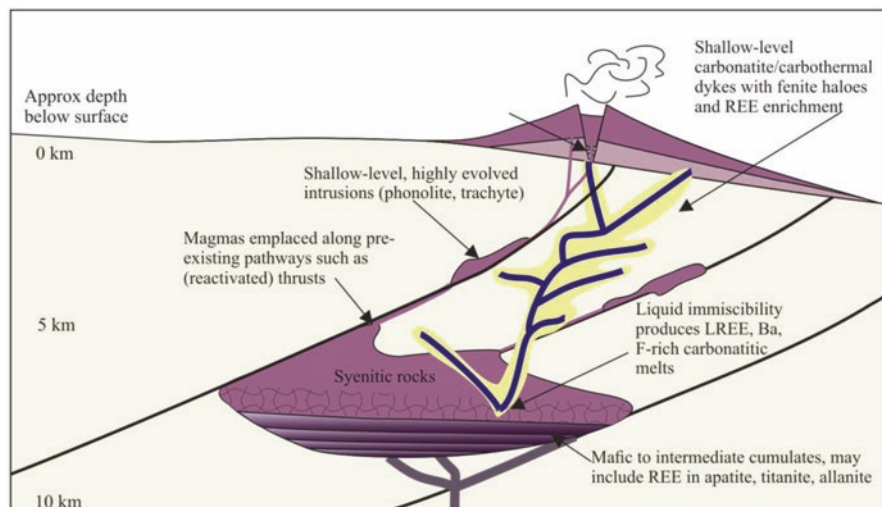
different deposit types. These REE minerals are part of distinctive mineral assemblages that are characteristic of specific deposit types. Mineral assemblages include all of the minerals that compose a given rock type and their relative abundances. Assemblages consist of the major rock-forming minerals, such as quartz, calcite, and feldspars, and minor, accessory-type, minerals that are present in small quantities.

#### ***2.4.2 Deposits Associated with Igneous Rocks—Magmatic REE Deposits***

##### **Carbonatite**

Carbonatite is generally defined as an igneous rock composed of greater than 50% by volume of primary carbonate minerals (mainly calcite and/or dolomite) [39]. Rare earth-enriched deposits hosted by carbonatites (Table 2.3) are a major global source of LREEs. Bastnäsite-Ce and monazite-Ce are the dominant REE minerals in most carbonatite deposits, and they can occur as both coarse-grained euhedral grains (showing a crystal outline) and as interstitial grains that fill in around other minerals. Bastnäsite typically contains approximately 75% REE oxides. Other REE phases include light rare earth-enriched carbonate and fluorocarbonate minerals (e.g., burbankite, parisite, and synchysite), hydrated carbonates (e.g., ancylite group), and phosphates (Table 2.2). Carbonatites can also host significant amounts of other economically important mineral resource commodities, including Cu, Fe, Nb, Th, Ti, U, calcium carbonate, fluorite, phlogopite, sodalite, vermiculite, baddeleyite, Zr-Nb minerals, and pyrochlore group minerals [40, 41].

Carbonatites from more than 600 localities are currently known, occurring mostly on cratons (ancient, stable areas of continental crust) and varying widely in age over a large portion of earth's history [40–44]. Currently, only a small number of carbonatites are being mined for REEs; these include Bayan Obo, China (REE-Nb-Fe), the Maoniuping and Dalucao deposits, China, and Mountain Pass in the United States. The origin of carbonatites is currently thought to be closely linked to melting of the earth's mantle or evolution of mantle-derived materials. Carbonatites are found associated with various tectonic settings [45]. These settings include intracontinental, the old, and stable parts of continents (e.g., Mt. Weld carbonatite, Australia); collisional where episodes of magmatism and mountain building are related to colliding continental plates; post-collisional or the “relaxation phase” following collision (Miaoya carbonatite, Mianning–Dechang belt, China) and during active continental rifting (Bayan Obo REE-Nb-Fe deposit). For example, a recent review of syn- to post-collisional alkaline igneous and carbonatite complexes worldwide [46] used trace and rare earth element data for carbonatite and associated alkaline igneous rocks to construct a broadly based model for REE mineral systems expected to develop in such environments (Fig. 2.9).



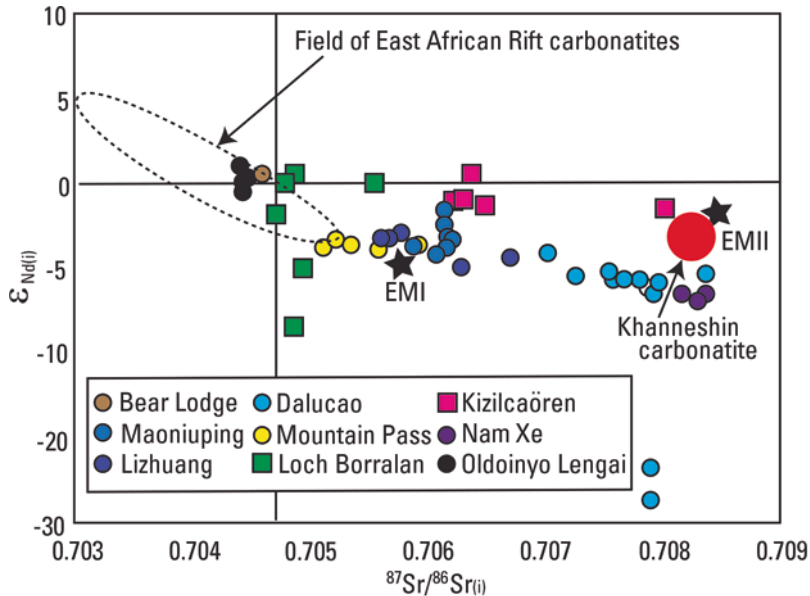
**Fig. 2.9** Schematic illustration—A postulated structure for an upper crustal, post-collisional alkaline-carbonatite system capable of producing LREE, barium (Ba)-, and fluorine (F)-rich carbonatitic melts. <https://creativecommons.org/licenses/by/4.0/> [46]

Magmatic processes responsible for REE enrichment include fractional crystallization (removal and segregation of crystals from a melt, changing the composition of a magma) which enriches the carbonatitic magma in REEs, and later hydrothermal processes that lead to precipitation of REEs. These processes have important roles in upgrading carbonatite REE resources. For example, a study of the Bachu carbonatites, NW China [47], showed that fractional crystallization of carbonates resulted in elevated REE concentrations in the residual magma. The late REE-enriched veins resulted from hydrothermal processes. Thus, like most carbonatite-related deposits, the Bachu REE deposit formed by a multistage model involving fractional crystallization and hydrothermal fluids. Modeling the evolution of chemical characteristics of carbonatite systems will be fundamental to further understanding how REEs are partitioned in these complex magmatic-to-hydrothermal systems. Comparative studies of the metallogeny of fertile and barren carbonatites may lead to advances in identifying factors controlling the fertility of carbonatite mineral systems [47, 48]. For post-collisional carbonatite complexes (Fig. 2.9), immiscibility (separation of immiscible liquids) of carbonate-rich magmas and fluids in generating mineralization partitions REE, Ba, and F into the carbonate-rich phase. This partitioning leads to the potential for by-products such as barite, fluorite, and manganese oxides. In post-collisional settings, shallow-level carbonatite intrusions have been identified as most significant for REE deposits, but deeper carbonatite bodies and associated alteration zones may also have REE enrichment [46].

Of relevance to exploration geologists interested in REEs associated with carbonatite genesis and mineralization are two published papers identifying ~527 known global occurrences of carbonatite with detailed attributes for 477 of these in a searchable and updatable database [42, 44]. A recent review of the definition and classification of carbonatites and a summary of information germane to exploration efforts such as resource characterization, exploration methods, and prospectivity [40] suggests that intracratonic rift (extensional) settings are most favorable exploration areas for carbonatite and related deposits. Intense exploration efforts in such settings, however, have likely identified most shallow or exposed intrusive carbonatites and alkaline-carbonatite complexes. Thus, most new carbonatite discoveries will probably be in the collisional-type settings. Examples of carbonatite complex mineral systems include such diverse deposits as Bayan Obo [14, 47–49], Mountain Pass [3, 20] and Khanneshin, Afghanistan [50, 51].

The genesis of Bayan Obo, the world's largest known REE-Fe-Nb deposit, has been the subject of study for decades [49], and the deposit is reported to contain 118 million metric tons of ore having 6% total REO [14]. Past models to explain its genesis have varied widely [52]. A recent model has proposed that the Bayan Obo Fe-REE-Nb ore deposits and the barren host, a dolomite, were generated when fluids expelled from a mantle-derived carbonatite magma interacted with sedimentary carbonates [52]. The genetic complexity and extended timescale of the Bayan Obo carbonatite deposit were likely important factors in its large size and significant REE content.

The Sulfide Queen carbonatite in California hosts Mountain Pass which is the largest known REE deposit in the United States [3]. Other smaller REE-rich carbonatites in the United States include the Bear Lodge deposit in northeastern Wyoming and the Elk Creek deposit in southeastern Nebraska [3]. Prior to 1995, the Mountain Pass deposit was the world's leading source of REEs. After operating intermittently in the 2000s and 2010s, the Mountain Pass mine reopened in 2018, with proven and probable reserves totaling 18.4 million metric tons of carbonatite ore averaging 7.98% REE oxide (REO) using a cutoff grade of 5% REO [53]. The geologic setting of the Mountain Pass carbonatite and related alkaline silicate rocks represents a classic carbonatite model related to a mantle source [54]. Evidence of primary magmatic textures includes euhedral bastnäsite in association with calcite, barite, and dolomite [8]. The mine currently produces a bastnäsite concentrate. Other REE-bearing minerals include parisite, synchysite, and monazite, and many less abundant REE phases. Alkaline intrusions are associated in time and space with the carbonatite rock that hosts REE ore at Mountain Pass. A recent age-dating study of zircon in associated alkaline igneous rocks at Mountain Pass [55] supports a model in which alkaline and carbonatite magmatism occurred over tens of millions of years. Repeated tapping of a mantle source altered by fluids and assimilation of older igneous, metaigneous, and metasedimentary crust to the magma endowed the magmas with high contents of REEs and other elements (e.g., F, Ba).



**Fig. 2.10** Epsilon Nd versus  $^{87}\text{Sr}/^{86}\text{Sr}_{(i)}$ —base diagram for post-collisional settings [46] showing data for Mountain Pass, with the addition of a data field for the Khanneshin carbonatite, Afghanistan, shown in red [50]. This figure shows the relatively tight coherence between Sr and Nd isotopic systems and mantle source for Khanneshin, an example of a young carbonatite derived from enriched mantle (EM) sources which may also be post-collisional in nature [50]. In comparison, Maoniuping–Dalucao carbonatites (blue dots), which are part of the Mianing–Dechang belt of China, a type locality for post-collisional alkaline-carbonatite systems, show a widespread in EM sources (EMI and EMII type mantle end members). <https://creativecommons.org/licenses/by/4.0/4> [6]

An example of a geologically young carbonatite is Khanneshin in Afghanistan [51]. Geological studies have suggested that mineralized rocks of the Khanneshin carbonatite, a LREE-enriched carbonatite complex of Quaternary age (formed within the last 2.6 million years), may be comparable in grade to Bayan Obo, China, and Mountain Pass [51]. Based on radiogenic isotopes of Nd, Sr, and lead (Pb) in the Khanneshin carbonatite, a mantle source was established for the deposit [50]. The study [50] also demonstrated that isotopic signatures of carbonatite can aid regional exploration efforts to identify other mineralized systems that share the same source reservoirs, origins, and evolution (Fig. 2.10).

### Alkaline/Peralkaline Igneous

Alkaline/peralkaline igneous complexes (Table 2.3) that host REE deposits are generally thought to form within continental plate tectonic settings that are associated with rifts, faults, or hotspot magmatism [56, 57]. The REE ores occur in layered alkaline complexes of nepheline syenite, peralkaline granitic stocks and late-stage

dikes, and more rarely, trachytic, peralkaline volcanic and volcanoclastic deposits. The mineralization is thought to be the result of extensive fractional crystallization. Typically, late-stage fluorine-rich fluids are thought to increase the rare metal concentrations by overprinting primary ore minerals with additional REE minerals. This is consistent with suggestions by Goodenough and others [48] who note that the most significant REE grades in alkaline igneous complexes are typically found in the “agpaitic” peralkaline lithologies. Agpaitic rocks represent the most evolved and latest stages of peralkaline systems and can also contain potentially economic concentrations of U, Be, and other rare elements. These complexes typically are relatively small compared to other types of alkaline complexes and can have extremely complex mineralogy and geometallurgy [58].

Deposits associated with layered alkaline igneous suites that include nepheline syenites (alkaline igneous rocks that lack quartz) are important exploration targets because they are known to contain REE deposits enriched in HREE and Y [56, 57]. The host rocks and ore layers typically show cumulate (layered) textures which form by crystal settling within a magma chamber. The REE minerals accumulate in portions of the magma chamber that have undergone fractional crystallization to a great extent. Ore layers are often enriched in eudialyte, loparite, and apatite and contain Y, Zr, Nb, tantalum (Ta), and P. Examples of these deposits include Ilimaussaq (Greenland), Lovozero, and Khibiny (Kola Peninsula, Russia), and Norra Kärr (Sweden). The only REE deposit of this type currently being mined is Lovozero. Loparite has been mined for about 50 years at Lovozero, with a reported annual production in 2012 of approximately 6000 metric tons of loparite concentrate that contained about 30–35% REE<sub>2</sub>O<sub>3</sub> [26].

Peralkaline igneous deposits containing both high field strength elements (HFSE—those elements whose ions have a small radius and high charge, such as Hf, zirconium (Zr), Ti, Nb, and Ta) and REEs occur in pegmatites (in two types: Li-Ce-Ta and Nb-Y-F) hosted by peralkaline granites, e.g., Strange Lake, Quebec-Labrador, Canada [56], or as hydrothermal disseminations and/or structurally controlled late-magmatic-to-hydrothermal quartz-feldspar dikes related to small, highly evolved peralkaline granitic stocks, e.g., Bokan Mountain, southeastern Alaska [20, 56]. Neither the deposit type nor its host rocks show features of crystal accumulation. Strange Lake is hosted by a circular ring complex composed of peralkaline granite with mineralization occurring both as low-grade disseminations in granite and as high-grade ore in pegmatites. Hydrothermal overprinting played a significant role during the formation of ore minerals which are of primary magmatic and secondary hydrothermal origin. The dominant REE-bearing mineral is gittinsite which is likely an alteration product of eudialyte. Other important minerals include bastnäsite, monazite, kainosite, thorite, pyrochlore, and gadolinite (Table 2.2). At Bokan Mountain, the Dotson vein system has a combined inferred resource of 5.275 million metric tons of rock averaging 0.262% HREE oxides and 0.392% LREE oxides [59].

Rarely, peralkaline felsic volcanic rocks (mainly trachytes) with HFSE and REE contain disseminations of fine-grained REE-bearing minerals (as well as a high abundance of HFSE) [57]. Examples of these mineralized peralkaline felsic

volcanic rocks are Toongi (Dubbo Zirconia) and Brockman/Hastings, both located in Australia. At Toongi, the mineralization includes ores of eudialyte, niobite, and bastnäsite. Primary interstitial REE phases were enriched by late-magmatic-to-hydrothermal fluids. The Brockman/Hastings deposit is hosted by fluorite-bearing felsic volcanoclastic rocks that form the lowermost unit of the early Proterozoic Brockman volcanic suite, a sequence of trachytic and rhyolitic volcanic rocks, and shallowly emplaced intrusive rocks. The fluorite-bearing volcanic rocks are distinctly enriched in HFSE and HREE and include fine-grained disseminated ore (e.g., zircon, bastnäsite, parasite, and synchysite).

### ***2.4.3 Deposits Associated with Physical Weathering Environments***

#### **Heavy Mineral Sands/Mineral Sands**

Placer deposits are a subset of supergene deposits that undergo processes of physical erosion in addition to chemical weathering. Ancient (paleoplacer) and modern sedimentary placer deposits can be significant sources of REEs [9]. The terms heavy mineral sands and minerals sands are used interchangeably to describe placer deposits that contain abundant minerals that have high densities and are resistant to chemical and physical erosion. These minerals include ilmenite, zircon, leucoxene, rutile, the REE minerals monazite and xenotime, and less commonly, garnet, magnetite, sapphire, diamond, and staurolite (Table 2.2). Placers form from mechanical concentration of minerals from weathered rock debris. Because these minerals are strongly resistant to chemical weathering due to their low solubility in surface waters, they endure transport by wind or water and subsequent deposition in modern sedimentary environments and persist in ancient (paleo) deposits.

In fluvial (transported by surface waters) settings, slope is an important factor for the concentration of heavy minerals from material transported in riverbeds. In areas of high topographic relief, the action of erosional processes (such as mineral abrasion and transport) on exposed bedrock transports resistant minerals downslope through networks of natural drainage channels to depositional sites in topographically low-lying settings. These include deltas, the beach face, the near shore, barrier islands or dunes and tidal lagoons, as well as channels and floodplains of streams and rivers. In near-coastal settings, waves, currents, tides, and the wind sort and concentrate mineral particles based on size and density. So, monazite, xenotime, and other heavy mineral placers typically are found in zones where minerals that survive the weathering process are concentrated, such as beaches, rivers and streams, dunes, and offshore areas. Bedrock terranes containing abundant high-grade metamorphic rocks or igneous rocks are suitable source rocks for primary monazite-bearing placer deposits. Recovery of monazite or

xenotime as a low-cost co-product of heavy mineral sands may accompany production of other industrial minerals (e.g., ilmenite, rutile, zircon, sillimanite, garnet, and staurolite) [9]. The high density of monazite and xenotime makes them relatively easy to separate from other minerals in placers by low-cost mechanical techniques.

Monazite-bearing placers occur widely across the globe. Australia, Brazil, China, Indonesia, Korea, New Zealand, the United States, and Zaire have produced monazite from placers in the past with significant amounts remaining in place [9, 25]. For example, the WIM150 mineral sands deposit in Australia within the Murray basin of western Victoria contains substantial resources of monazite (580,000 metric tons) and xenotime (170,000 metric tons) which are associated with economic amounts of Ti minerals and zircon in the heavy mineral suite [60]. The high concentrations of heavy minerals in placers in the Murray Basin are linked to the formation of barrier sand complexes during the Pliocene (from about 5.4 to 2.4 million years ago) as the shoreline grew seaward [61]. Thus, the heavy mineral sand deposits formed by reworking of older underlying heavy mineral-rich sands. More recently, monazite has been recovered from coastal and alluvial placers in India, Malaysia, Sri Lanka, Thailand, and Brazil [9]. Only India and Brazil currently produce monazite from mineral sands. Major monazite placer concentrations of India are located along both the southwestern and southeastern coasts of India, where heavy mineral sand beach deposits are undergoing renewed exploration and development. The exploration plan for these deposits is to recover monazite for REEs as well as its Th, which can be stored for later use as a nuclear fuel source [9].

Monazite in heavy mineral placer deposits typically has high Th content. Both Th and U substitute readily into the crystal structure of monazite (Fig. 2.3). Only the most refractory and least metamict minerals (high Th, low U) are sufficiently robust to survive transport. The abundance of Th in some monazite can make the mineral concentrate too radioactive for storage, shipping, or processing in many countries [62]. For example, the radioactivity of monazite concentrates from heavy mineral placers limits further development of this resource in the United States.

Some of the mineral sand districts in India and Brazil are areas of high background radiation with potential dose exposure, primarily due to the Th and U in detrital grains of monazite and zircon [9]. Several recent studies of heavy mineral sand deposits have clarified the environmental issues that can be associated with monazite-bearing placer deposits. High background radiation from U occurs in groundwater sampled near monazite placer deposits in the Kanniyakumari District, Tamil Nadu, India [63]. The spatial variations in U content are seasonal and related to pre- and post-monsoon weather patterns.

Coastal belts of Kollam District, Kerala, India, are also enriched in naturally occurring radionuclides ( $^{40}\text{K}$ ,  $^{226}\text{Ra}$ , and  $^{232}\text{Th}$ ) in sand samples [64]. This study compared local variations in radiological parameters with Indian and world average values. By using geospatial techniques, the local variations of radionuclide enrichment were then connected to local lithology, drainage conditions, and sea wave

directions in order to establish the source and paths of distribution. The study of the Kollam District provided details on source and locations of the parent material for the heavy mineral sands.

Another study [65] investigated radon (Rn) in residential indoor spaces in households surrounding the Ban Gie monazite mine in the Quy Hop District, Nghe An Province, Vietnam. The study focused on  $^{222}\text{Rn}$  because of its impact on human health and environment. They identified high levels of  $^{222}\text{Rn}$  indoor concentration in households and showed that residents in the survey area may be exposed to an average dose of radon nearly 3.5 times the world average.

#### ***2.4.4 Deposits Associated with Chemical Weathering Environments***

##### **Carbonatite Laterite Deposits**

Surficial chemical weathering processes acting on carbonatite intrusive complexes can result in significant enrichment in REEs in shallow laterite-type deposits. Weathering can also enhance the prospectivity of otherwise low-grade carbonatite deposits. Supergene enrichment in REEs in weathered horizons reflects breakdown of primary minerals in the carbonatite by chemical weathering and sequestration of REEs in either secondary rare earth minerals or in association with clays or organics. Carbonatite-derived laterite deposits are known to have significant amounts of REEs, Nb, and a variety of other elements and minerals of economic interest including phosphate, Fe, fluorite, Cu, V, Ti, U, and calcite. Examples of carbonatite-derived laterite deposits include Mount Weld in Western Australia, which currently produces REEs, and the Araxá deposit, Minas Gerais state, Brazil, which currently produces Nb, but is also enriched in REEs [8].

The Mount Weld deposit is a world-class carbonatite-derived lateritic REE deposit and has been an important source of REE since the mine opened in 2011 [66]. The deposit has an average REE grade of 9.8% total  $\text{REE}_2\text{O}_3$  with locally concentrations reaching 45% total  $\text{REE}_2\text{O}_3$  [23]. The laterite deposit is fully contained within the weathered cap of an intrusive carbonatite plug within the Mount Weld carbonatite complex that is a part of the alkaline Eastern Goldfield Province of the Yilgarn Craton of Western Australia [66, 67]. New data on bulk geochemistry, mineralogy, and geochronology of the deposit [67] have established the role of magmatic and supergene processes in the genesis of the REE deposit. For example, monazite-(Ce) and apatite in the regolith is chemically identical to monazite and apatite in the carbonatite, thus establishing a strong genetic link. High-REE regolith (with 51.8% total  $\text{REE}_2\text{O}_3$ ) has a negative Ce anomaly (interpreted as indicative of intense weathering) and contains monazite within a cement matrix of florencite-(Ce) and rhabdophane-(Nd) (Table 2.2). The rhabdophane has textures resembling casts of plant material suggesting that bio-assisted processes contributed to the extreme fractionation of LREEs. Bacteria- and plant-mediated processes likely



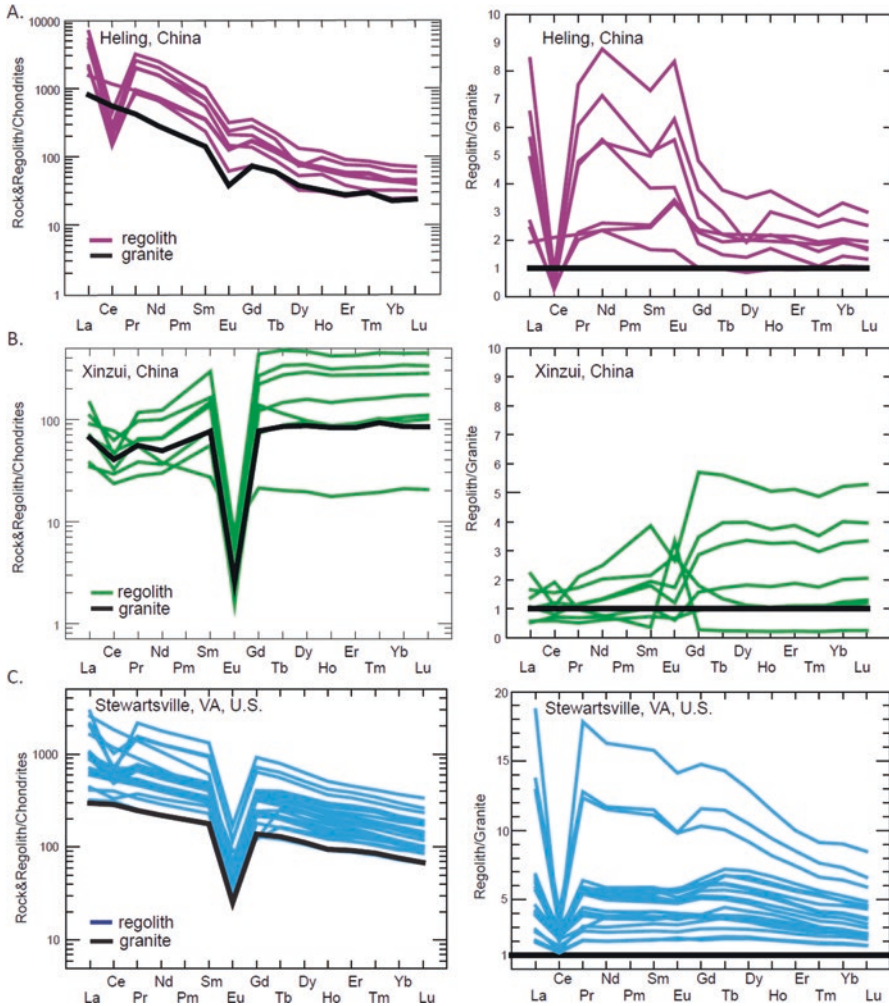
played a significant role in REE redistribution during supergene stages of development of regolith-hosted carbonatite-related laterite deposits [67].

### **2.4.5 *Regolith-Hosted Ion-Adsorption Clay (IAC) REE Deposits***

Regolith-hosted IAC deposits are of global importance because they currently provide virtually all HREEs, Y, and a significant portion of LREE to global markets. General stages of formation of IAC deposits [28] include (1) emplacement of granites containing precursor source minerals (e.g., apatite, allanite and REE fluorocarbonates); (2) development of thick overlying in-situ regolith with adsorption of liberated REEs onto newly formed kaolinites in clay-rich zones; and (3) preservation of the ore bodies. The IAC deposits generally are thought to occur in temperate and tropical regions of the globe where regions afford high temperatures and precipitation rates that induce chemical weathering in granitic rocks [27]. Engineering and environmental considerations associated with developing IAC deposits include a large stripping ratio, large leach residue, overexploitation, and environmental restoration [68]. The best-known deposits and occurrences of this type occur in parts of Brazil, China, Madagascar, Malawi, and Southeast Asia [27]. Currently, virtually all mined deposits [14] are in southern China in the Jiangxi, Hunan, Guangdong, Guangxi, and Fujian provinces and a few in Guizhou and Yunnan provinces. Minor deposits are reported in Inner Mongolia, Shandong, and the Shanxi provinces of northern China. Exploration for deposits and occurrences of this type continues globally due to their high economic importance.

Economic deposits typically occur as small, disseminated ore bodies that when combined make large tonnage, low-grade deposits. Available data on ore reserves of IAC deposits indicate they range in size from greater than >0.5 million metric tons to less than 0.01 million metric tons [69]. The ore bodies generally have over 50% ion-exchangeable REEs+Y occurring as adsorbed ions on clay surfaces (mainly kaolinite and halloysite [28]). The REE+Y contents in parent source rocks of China range from 110 to 590 ppm. The highest REE+Y contents are found in alkali granite and alkali granite porphyry [14, 28]. The total REE+Y contents of mined IAC deposits of China range from 140 to 6500 ppm, and thus, the deposit can contain up to six times the amount in the parent rock [28]. Due to deep weathering of the precursor rock, IAC deposits typically contain relatively low amounts of Th and U compared to many other REE deposit types, making IACs an attractive exploration target.

The IAC deposits of China are genetically linked to weathering of granitic rocks and less commonly to weathering of volcanic rocks and some low-Si, high-K igneous rocks [14]. The most important age of parent rocks in China is early to late Mesozoic (younger than approximately 250 million years), although mineralized regolith is also known from older granites. Although all weathered igneous rocks can contain some exchangeable REEs, weathering of REE-enriched granitic rocks

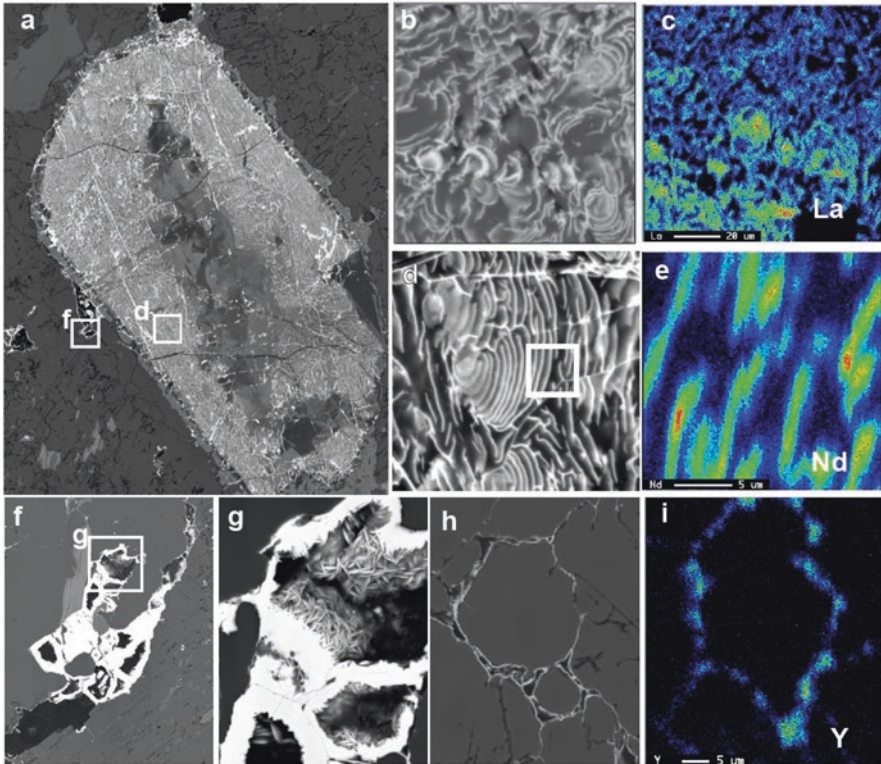


**Fig. 2.11** Chondrite-normalized granite–regolith patterns (left panel) and granite-normalized patterns for regolith (right panel). (a) the LREE-enriched Heling IAC deposit, Xunwu County, Jiangxi Province, China (in purple), and (b) the HREE-enriched Longnan REE+Y deposit, which occurs in the weathering profile of the Xinxu Granite, Longnan County, Jiangxi Province, China (in green). (Data from Bao et al. [28]). The left panel show showing increases in REE concentrations in saprolite and overlying soils compared to granite (black), normalized to chondrite values [38]. The tetrad behavior is shown by the subtle convex upward curves corresponding to quarter (Nd/Pm), half (Gd), three-quarter (Ho/Er), and complete (Lu) filling of the 4f electron shell. The right panel shows clay-bearing regolith samples from bedrock soil profile over the granitic precursors, normalized to average REE values for granitic bedrock at the sites. Also shown for comparison are (c) chondrite- and bedrock-normalized REE patterns for Stewartville, VA, site [70]

(originally enriched by magmatic processes) best provides a source for further accumulating REEs in regolith during weathering [70]. Moreover, alkaline and peralkaline-type granites with primary middle and heavy REE enrichment are key targets for exploration [14]. One prominent feature recognized in many granites and related IAC deposits [70] is tetrad behavior of the lanthanides. This is displayed in REE patterns as distinct discontinuities (Fig. 2.11) corresponding to quarter (Nd/Pm), half (Gd), three-quarter (Ho/Er), and complete (Lu) filling of the 4f electron shell [71]. Tetrad patterns in granite and regolith are thought to result from processes that promote the redistribution, enrichment, and fractionation of REE, such as alteration of granite in the regolith. Thus, REE patterns identify source rocks and regolith that are good candidates for IAC deposits. Tetrad behavior is well documented for rare metal granites of South China [72].

Two main types of IAC deposits are identified in China (see examples shown in Fig. 2.11). These include HREE-enriched material containing >50%  $Y_2O_3$  and LREE-enriched material containing <50%  $Y_2O_3$  [14]. Parent granites of HREE-rich deposits are typically highly evolved by fractional crystallization and have abundant alkali feldspars with  $SiO_2$  contents of approximately 75% and low contents of  $P_2O_5$  (<0.02%) which limit sequestration of REEs in phosphates like monazite [28]. The first recognized IAC deposit in China was the Zudong HREE deposit which was discovered in South Jiangxi Province in the 1960s [14]. The ore occurs in the weathering profile of the Zudong granite, a medium-grained, muscovite-, K feldspar-, and alkali feldspar-bearing granite. The parent granite was enriched initially in HREEs where hydrothermal alteration converted the original minerals to F-bearing, HREE-rich carbonate minerals. The deposit contained a total REE+Y resource of 131,000 metric tons at an average grade of 0.048 wt.% of  $Y_2O_3$ , with Y estimated to be 35.8% to 62.5% of the total resource. Parent rocks of LREE-enriched deposits typically consist of peralkaline biotite granite having high contents of REEs and HFSE. In 1972, the LREE-enriched Heling deposit also was identified in South Jiangxi Province. Accessory minerals in the granite porphyry include apatite, bastnaesite, and Ce-apatite, while those in the volcanic rocks include monazite, bastnaesite, chevkinite, and minor apatite. The deposit has a total REO resource of 239,000 metric tons and REE-Y grade averaging 1350 ppm with >60% recovery of exchangeable REE+Y [14].

Regolith-hosted IAC REE deposits form by the chemical weathering of a source rock containing a relative high abundance of REEs in minerals that are not resistant to weathering. In granitic rocks, fluorine-bearing biotite or muscovite can foster formation of soluble REE fluorocarbonates (Table 2.2) in the overlying regolith. Decomposition and dissolution of magmatic REE-bearing minerals (e.g., allanite, soluble fluorocarbonates, titanite, garnet, apatite) during regolith formation release REEs from the original mineralogical sites, enrich aqueous fluids, and through fluid–mineral reactions the REE are subsequently adsorbed to receptive surfaces in available secondary minerals within the residual profile. Kaolinite, halloysite, and other clay minerals formed by weathering of silicate minerals (e.g., biotite, feldspars, and allanite) are thought to be the most receptive substrates in this process. Whole rock REE patterns of both regolith-hosted ion-adsorption deposits and



**Fig. 2.12** Stewartville regolith samples. (a) Intensely weathered allanite crystal from granitic regolith profile. Paired backscatter electron SEM and electron microprobe images of areas marked in (a): (b) and (d) Fe-Al clays (dark layers) decorated with REE (La, Nd, Sm, Gd, Dy) oxides (bright areas) showing distributions of (c) La and (e) Nd. Areas (f) and (g) show synchysite infilling open spaces and (h) and (i) show doverite cementing quartz grains within the regolith

occurrences commonly show negative Ce anomalies due to oxidation within the developing regolith [27, 70].

Many studies have shown that a significant portion of the REEs within a regolith can also precipitate as either soluble or insoluble minerals, typically carbonate or phosphates. This association between amorphous phosphates and kaolin group minerals has been identified in deeply weathered metavolcanic rocks of the Carolina Slate belt, United States, where clay layers in a kaolin pit were found to contain secondary amorphous phosphates of monazite in addition to leachable REEs [73]. Chemical environments favoring formation of soluble HREE fluorocarbonate minerals, like doverite, can result in regolith deposits that have higher amounts of ion-exchangeable HREEs. Figure 2.12 illustrates mineral weathering in a granite-derived regolith overlying peraluminous-to-peralkaline granite, Stewartville regolith, Virginia, United States.

Exploration for regolith-hosted IAC REE deposits continues in many regions of the globe, particularly in areas identified as having paleogeography akin to that of southeast China. For example, occurrences of IAC REEs have been identified in belts of weathered peralkaline granite and highly fractionated igneous rocks in the Southeast United States [73, 74]. The granitic rocks have highly silicic compositions and high contents of HFSE, Ga, F, Nb, Sn, Ta, Y, and Zr, and high total REEs. Granite outcrops in the Piedmont region of Virginia are commonly intensely weathered and overlain with thick layers of saprolite regolith of extending to depths of tens of meters. Geochemical and mineralogical comparisons of regolith formed on the Stewartville and Striped Rock plutons and the Robertson River batholith [73] demonstrate REE grades comparable to some IAC REE deposits mined in China. For example, the Stewartville pluton is a biotite granite containing abundant allanite and fluorite, inclusions of synchysite-(Nd) and fergusonite in feldspar, and gadolinite. The fraction of readily extractable REE in the bedrock soil profile varied from 30 to 70%, with an average yield of 900 ppm REE. A negative Eu anomaly present in the granite is retained in weathered alluvium where the uppermost soil samples show a pronounced negative Ce anomaly (Fig. 2.11c). Normalized to average values for bedrock, the deposits show increases in REE (La-Dy) relative to bedrock.

These results compare favorably with LREE-enriched deposits of China (e.g., Heling (Fig. 2.11a)) and highlight the importance of paleoclimate in global exploration models for deposits of this type. Granites of the southeastern United States were emplaced during crustal extension related to opening of an ancient ocean that existed before the Atlantic Ocean. Later, assembly of the supercontinent Pangaea positioned the Appalachians at tropical to subtropical latitudes. The Appalachians remained under tropical to subtropical conditions until the opening of the Atlantic Oceans which began about 200 million years ago. This provided moisture adjacent to the Appalachians and promoted high rainfall conditions which led to weathering under subtropical conditions. Geologic evidence for the warm and humid conditions is present in the extensive kaolin and bauxite deposits of the southeastern United States, which match the distribution of bauxite and kaolins in China [73]. Thus, globally distributed granitic rocks of any age that have undergone a history of weathering under subtropical to temperate conditions comparable to those of China can be highly prospective for regolith-hosted IAC REE deposits.

#### ***2.4.6 Other Magmatic-Related Deposit Types***

##### **Abyssal Pegmatite REE**

Abyssal pegmatites typically have relatively simple major mineral assemblages (e.g., quartz, mica and feldspar) and highly variable accessory mineral assemblages which contain the rare metals. Most abyssal pegmatites are thought to have formed through partial melting of surrounding metamorphic rocks [75]. The Fraser Lakes

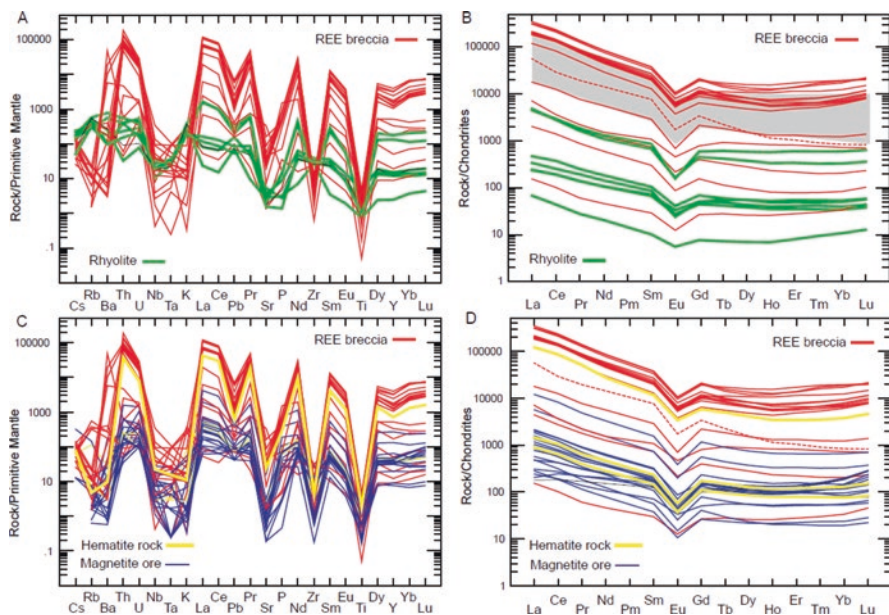
area in the Wollaston Domain hosts several U- and Th-REE-bearing granitic pegmatites and associated rocks containing Li, rubidium (Rb), cesium (Cs), beryllium (Be), tin (Sn), Nb, Ta, Zr, Y, REE, and U. They are NYF-type (Nb–Y–fluorine (F)) pegmatites and are interpreted to have formed in a late syn- to post-collisional tectonic setting [76]. The pegmatitic melts were generated by partial melting of metasedimentary rocks with slightly elevated U and Th concentrations. The melts entrained Th and REE-bearing accessory minerals from the metasedimentary rocks. Subsequently, the melts underwent fractional crystallization processes during transport to the crystallization site. The U, Th, REE, Zr, Y, and Nb contents of the residual magma were high enough to enable thorite, allanite, xenotime, monazite, apatite, rutile, garnet, and zircon (Table 2.2) to form. Pegmatites of this type have been mined for REE in the past, and they also have potential for Zr, Nb, and U production.

### **Apatite Intrusion REE/Apatite Vein Deposits**

Apatite intrusion REE and apatite vein deposits consist primarily of fluorapatite and alteration products that fill veins and structures in high-grade metamorphic rocks. A classic example is the 1525 Ma old REE–P–Th apatite vein deposit at Nolans Bore in the Aileron Province, Northern Territory, Australia [77]. The ore grade ranges up to 5% REO. Recent studies [45] suggest that the vein structures formed by a complex process involving carbonatite magma intruding into silica-rich rocks (e.g., granites). The magma assimilated silica from the granite to form REE- and F-enriched apatite. The studies at Nolans Bore demonstrate that carbonatites can undergo modification and in turn modify the composition of the silicate rocks with which they interact. In effect, Nolans Bore and similar deposits are likely remnants of chemical alteration caused by carbonatitic magma traversing silicate-dominated rocks. The resulting mineral assemblage (other than fluorapatite) consists of minerals commonly associated with granulite-facies rock. Evidence for carbonatite can be overlooked if distinctively carbonatitic minerals are not present. Thus, exploration models for carbonatite and related deposit types incorporate models for apatite vein deposits to provide a more complete understanding of the behavior of carbonatite melts in the crust.

### **Breccia Pipe REE**

Iron oxide apatite (IOA) constitutes an important REE resource. The deposits are characterized by large bodies of generally Ti-poor iron oxides that are hosted in volcanic and intrusive subalkaline to alkaline rocks. They have extensive marginal breccia zones and pervasive Na–K alteration, which can be identified at regional scales [78]. The type locality for the IOA group is Kiruna, Sweden. The IOA deposits often occur with iron oxide–copper–gold (IOCG) deposits. For example, IOA and IOCG deposits at Pea Ridge, Missouri, United States, occur within 1.48 to 1.47-billion-year-old alkaline volcanic rocks of the St. Francois Mountains terrane



**Fig. 2.13** Pea Ridge IOA-type deposit, Missouri [82]. Trace element (a, c) and rare earth element (b, d) abundances for felsic and mafic to intermediate composition rocks, breccia, and ore. (a) and (b) Pea Ridge rhyolite and REE-rich breccia. The majority of REE breccia samples are monazite-rich. Data for one molybdenite-rich breccia sample are shown as dotted line. (c) and (d) show data for REE breccia, magnetite ore, and specular hematite rocks. Normalized to primitive mantle and chondrite [38]

[79] near a regional boundary separating crustal blocks [80]. The IOA group contain monazite, xenotime, allanite, apatite, and minor amounts of fluorocarbonate minerals in a REE breccia. Pea Ridge has high concentrations of REE in breccia pipes that crosscut the IOA deposit. The breccia pipes average 12% REO [78]. The tonnage of known REE-rich breccia pipes is on the order of 200,000 metric tons [78].

Major trace element and Nd-Pb-Sr isotopic compositions suggest that the deposit reflects a magmatic–hydrothermal origin [80]. The deposit likely formed because of extensional tectonics occurring in a rift setting where mafic magmas added to the base of the continental crust remelted rocks and enriched the Pea Ridge magmas in distinctive geochemical features (Fig. 2.13) [80] with very high chlorine (Cl) in the least evolved and most alkaline magmas [81]. Magmatic fluids leached metals from Si-rich volcanics, which provided the metal source reflected in the REE-rich breccias and mineralized rocks (Fig. 2.13). Ore fluids derived from the Cl-rich melts transported Fe and REEs in a long-lived hybrid, magmatic–hydrothermal system. A study of F-rich apatite from Pea Ridge identified many shared geochemical features and also showed that ore-stage apatite likely crystallized from mixed magmatic–hydrothermal fluids [82]. These authors concluded that apatite chemistry is not able to distinguish IOA from related IOCG-type deposits but can be useful to distinguish IOA and IOCG deposits from other types of mineral deposits (e.g., gold, base metal).

### ***2.4.7 Deposits Associated with Basin Hydrothermal and Basinal Chemoclines***

#### **Phosphorite Deposits**

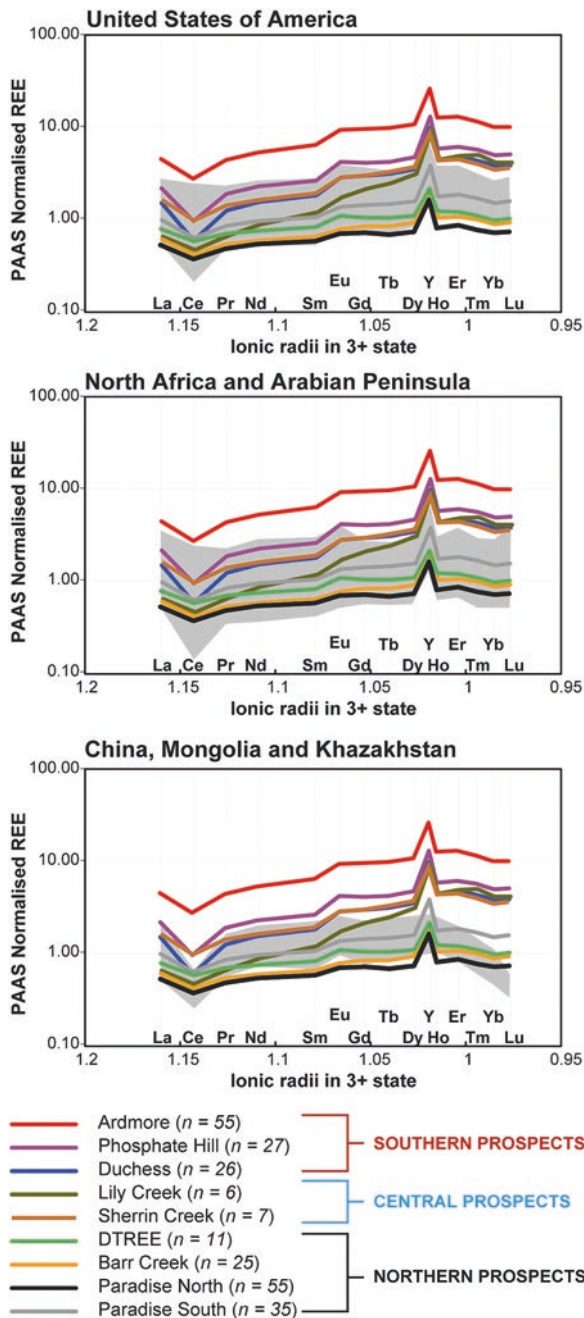
Phosphate-rich sedimentary rocks (phosphorites) can host significant concentrations of REE and Y in the carbonate–fluorapatite mineral francolite. Enrichments of REE in phosphorites have been found in the United States and globally [83–85]. Phosphorite formation occurs in a variety of marine settings, including continental shelves and slopes, oceanic islands, atop seamounts, and shallow sea environments. The processes linked to phosphorite formation include direct precipitation from seawater; degradation of organic matter; desorption of phosphate from Fe-Mn hydroxides minerals in bottom sediments; conversion of pre-existing carbonate grains and muds to phosphate during diagenesis; and direct precipitation of francolite from pore waters [86]. Extraction issues and obstacles to exploiting these potentially significant sources of REE include scalability of the process and insufficient knowledge of the chemical behavior of REEs within phosphoric acid-producing plants [84, 87].

An inventory of REE hosted in global phosphorites, based in part on the assumption that horizons of the same age are relatively uniform in their REE content [83, 84], has suggested that the world’s major phosphate-producing districts contain on the order of 70 million metric tons total REE, including 30 million metric tons HREE. Phosphorite deposits of Upper Mississippian, Devonian, Ordovician, and lower Silurian age were identified as being particularly prospective, in contrast to Cambrian and Proterozoic phosphorites. A more recent study [86] found that global secular changes of seawater chemistry through time are unlikely to be the dominant control on the REE content of phosphorites in the Georgina Basin, Australia (Fig. 2.14). Higher concentrations of REE in some prospects could be explained by surface and groundwater interaction with granite and mica-bearing metamorphosed sedimentary basement rocks. Thus, they concluded that REE prospectivity of phosphatic sedimentary rocks is not primarily controlled by age or temporal variations in global seawater chemistry, but rather by local sedimentological and source region factors. Further research to identify sources and processes leading to the accumulation of high concentrations of REE, especially HREEs, in phosphorites will help to inform exploration strategies for this global resource.

### ***2.4.8 Unconformity-Related REE***

Unconformity-related REE deposits represent a new type of HREE mineralization that is entirely hydrothermal in origin with no demonstrable links to magmatism or weathering processes [89]. The mineralization is associated with a regional unconformity (i.e., a surface separating rock strata of different ages, indicating that sediment deposition was not continuous) between Archean (approximately 2–2.5 billion years old) metamorphosed sedimentary rocks of the Browns Range and overlying Proterozoic (approximately 250–550 million years old) sandstones of the Birrindudu





**Fig. 2.14** Comparison of the means for the Cambrian Georgina Basin phosphorites with means from younger and older phosphorites from across the globe [86]. Additional data and references compiled in Emsbo et al. [83]. Shaded fields encompassing average values of deposits: (upper left) Miocene to Ordovician phosphorites of the United States; (lower left) Eocene to Upper Cretaceous phosphorites of the North Africa and Arabian Peninsula (Togo, Tunisia, Algeria, and Morocco, Egypt); (upper right) Cambrian phosphorites of China, Mongolia, and Kazakhstan. Normalized to Post-Archean Australian Shale (PAAS [88]). <https://creativecommons.org/licenses/by-nc-nd/4.0/> [83]

Group in Australia. The deposits formed 1.65–1.61 billion years ago along steeply dipping faults and are spread across a large area of northern Australia. Ore consists primarily of HREE-enriched xenotime (Table 2.2) in vein and breccia ore bodies. The genetic model proposed for the veins and breccia fill involves mixing of two fluids: (1) a fluid that leached HREE from rocks of the Browns Range and (2) an acidic P-bearing fluid that was generated from the overlying sandstones. The xenotime ore precipitated from the mixed fluids in extensively distributed fault zones near the unconformity by coupling of P and HREEs. Chondrite-normalized plots for bulk ore show distinct enrichment in MREE and HREE (Gd-Lu) in xenotime [89]. The HREE deposit type is likely an analog of unconformity-related U deposits of northern Australia and the Athabasca basin, Canada, and as such, can be expected to occur near regional unconformities within Proterozoic intracontinental sedimentary basins across the globe.

## 2.5 Outlook

The outlook for expanding accessible reserves of REE in the future is decidedly positive considering the forward-thinking research and exploration efforts described here that have come to fruition in recent years. Global resource estimates of mineable REE are large. For example, North America alone is estimated to contain measured and indicated resources of REE exceeding 17 million metric tons [19]. The global production picture has changed significantly since the 1970s, and more recently since 2017, with a significant increase in the number of countries producing REEs (Fig. 2.7). Although China remains the dominant supplier of REE, continued research, exploration, and development efforts across the globe will likely result in better defined REE reserves and increased production of REE from a more diverse group of conventional and unconventional mineral deposit types, including energy-related sources. The United States currently produces under 50,000 metric tons of REO [18, 19]. However, expectations are that this will increase in future years. Exploration activities aimed at identifying additional deposits of HREE resources (e.g., IAC deposits and the promise of new deposit types, such as Unconformity HREE) are critical to meeting growing global demands. Mineral deposit types that have the economic potential to be exploited for REEs as a by-product or co-product commodity [9, 78, 83], and burgeoning efforts to extract REE from waste [90], offer additional avenues leading to global expansion of REE production.

## 2.6 Summary

Four conventional REE mineral deposit types—carbonatite, alkaline igneous, heavy mineral sand, and regolith-hosted IACs—currently supply global markets with the REE and RE oxides necessary to meet technological requirements that sustain

modern economic communities. REE production is currently limited by host mineralogy of the known deposits, geometallurgy constraints, environmental considerations, and overall economic conditions associated with REE exploration and exploitation. Modern economies require that REE production supply the full range of light, middle, and heavy REEs. Predicted technological advances will require even higher availability of REEs than possible now. In order to meet these needs, REE production from both conventional REE mineral deposit types and other alternate REE sources such as unconventional resources (Chap. 3) is likely required.

Processes that promote redistribution, enrichment, and fractionation of REEs such as hydrothermal alteration, supergene or lateritic weathering, and physical transport of REE-rich minerals aid in developing mineable deposits. Alteration of granitic rocks originally enriched in REE by magmatic processes best provides a source for further accumulating REEs in these settings. Because of this, alkaline and peralkaline-type granites represent significant potential source rocks for deposits formed by post-magmatic alteration processes. Consequently, the knowledge of tectonic setting, typical rock associations, deposit morphology, and deposit genesis has led to the discovery of many conventional REE deposit types. Recent developments on this front are expected to result in further discoveries. Advances in exploitation and beneficiation processes are necessary for ensuring a wider availability of all REEs, especially for the HREE. Recent efforts to improve separation and extraction technologies are also leading to more environmentally sustainable approaches to recovery of REE from traditional types of bulk ore and from ores having complex mineral compositions. Underlying this are advances in understanding how REEs are incorporated in crystal structures and how variations in compositions impact the potential of a REE deposit [91]. Technological advances can improve access to significant known, but not-yet-utilized resources of REE because extraction technologies are lacking for some exceptionally complex minerals and previously unmineable resources of REE. Underlying these efforts is a need for fundamental studies, both experimental [92] and field-based [93] types, aimed at quantifying the geochemical processes that redistribute REEs in surface environments and advancing knowledge of the behavior of REEs in both natural and anthropogenically modified surficial system.

## References

1. International Union of Pure and Applied Chemistry, Periodic table of elements (2016). Accessed 17 Aug 2023, <https://iupac.org/what-we-do/periodic-table-of-elements/>
2. S.R. Taylor, S.M. McLennan, *The Continental Crust its Composition and Evolution* (Blackwell, Oxford, 1985), pp. 1–312
3. K.R. Long, B.S. Van Gosen, N.K. Foley, D. Cordier, The principal rare earth elements deposits of the United States: A summary of domestic deposits and a global perspective, in *Non-Renewable Resource Issues. International Year of Planet Earth*, ed. by R. Sinding-Larsen, F.W. Wellmer, (Springer, Dordrecht, 2012). [https://doi.org/10.1007/978-90-481-8679-2\\_7](https://doi.org/10.1007/978-90-481-8679-2_7)
4. P. Henderson, The rare earth elements: Introduction and review, in *Rare Earth Minerals: Chemistry, Origin, and Ore Deposits. The Mineralogical Society 7*, ed. by A.P. Jones, W. Frances, C.T. Williams, (Chapman & Hall., 372 p, Chap. 1, 1996), pp. 1–17

5. A.P. Jones, F. Wall, C.T. Williams (eds.), *Rare Earth Minerals-Chemistry, Origin and Ore Deposits. The Mineralogical Society*, vol 7 (Chapman & Hall, 1996), 372p
6. A.R. Chakhmouradian, F. Wall, Rare earth elements: Minerals, mines, magnets (and more). *Elements* **8**, 333–340 (2012). <https://doi.org/10.2113/gselements.8.5.333>
7. Y. Ni, J.M. Hughes, A.N. Mariano, The atomic arrangement of Bastnasite-(Ce), Ce(CO<sub>3</sub>)F, and structural elements of Synchysite-(Ce), Rontgenite-(Ce) and Parisite-(Ce). *Am. Mineral.* **78**, 415–418 (1993)
8. A.N. Mariano, Nature of economic mineralization in carbonatites and related rocks, in *Carbonatites — Genesis and Evolution*, ed. by K. Bell, (Unwin Hyman, London, 1989), pp. 149–176
9. D. Sengupta, B.S. Van Gosen, Placer-type rare earth element deposits. *Rev. Econ. Geol.* **18**, 81–100 (2016). <https://doi.org/10.5382/Rev.18.04>
10. M.M. Zuman, S.M. Antoa, Crystal structure refinements of four monazite samples from different localities. *Fortschr. Mineral.* **10**, 1028 (2020). <https://doi.org/10.3390/min10111028>
11. R.H. Mitchell, M.D. Welch, A.R. Chakhmouradian, Nomenclature of the Perovskite Supergroup: A hierarchical system of classification based on crystal structure and composition. *Mineral. Mag.* **81**(3), 411–461 (2017). <https://doi.org/10.1180/minmag.2016.080.156>
12. E.A. Popova, S.G. Lushnikov, V.N. Yakovenchuk, S.V. Krivovichev, The crystal structure of Loparite: A new acentric variety. *Miner. Petrol* **111**, 827–832 (2017). <https://doi.org/10.1007/s00710-017-0498-y>
13. N.K. Foley, Rare earth elements in clays: A resource for the future? 16th international clay conference, Granada, Spain, 2017. <https://www.scientevents.com/16icc/granada-2/>
14. Y. Xie, Z. Hou, R.J. Goldfarb, X. Guo, L. Wang, Rare earth element deposits in China. *Rev. Econ. Geol.* **18**, 115–136 (2016). <https://doi.org/10.5382/Rev.18.0>
15. X. Liu, X. Lu, M. Sprik, J. Cheng, E.J. Meijer, R. Wang, Acidity of edge surface sites of Montmorillonite and Kaolinite. *Geochim. Cosmochim. Acta* **117**, 180–190 (2013). <https://doi.org/10.1016/j.gca.2013.04.008>
16. A.M. Borst, M.P. Smith, A.A. Finch, G. Estrade, C. Villanova-de-Benavent, P. Nason, E. Marquis, K.M. Goodenough, C. Xu, J. Kynický, K. Geraki, Adsorption of rare earth elements in Regolith-hosted clay deposits. *Nat. Commun.* **11**, 4386 (2020). <https://doi.org/10.1038/s41467-020-17801-5>
17. U.S. Geological Survey, Minerals yearbook rare earths [ADVANCED RELEASE] 2017: U.S. Geological Survey, 202 p., myb1–2017-raree.pdf (2020). <https://doi.org/10.3133/mcs2022>
18. U.S. Geological Survey, Minerals yearbook rare earths [ADVANCED Date Release of the 2018 Annual Tables] 2017: U.S. Geological Survey, myb1–2018-raree-adv.xlsx (2021). <https://doi.org/10.3133/mcs2022>
19. U.S. Geological Survey, Mineral commodity summaries 2022: U.S. Geological Survey, 202 p., (2022). <https://doi.org/10.3133/mcs2022>
20. B.S. Van Gosen, P.L. Verplanck, R.R. Seal II, K.R. Long, J. Gambogi, Rare earth elements, in *Critical Mineral Resources of the United States — Economic and Environmental Geology and Prospects for Future Supply: U.S. Geological Survey Professional Paper 1802*, ed. by K.J. Schulz, J.H. DeYoung Jr., R.R. Seal II, D.C. Bradley, (2017), pp. O1–O31. <https://doi.org/10.3133/pp1802O>
21. J. Kynický, M.P. Smith, C. Xu, Diversity of rare earth deposits: The key example of China. *Elements* **8**, 361–367 (2013). <https://doi.org/10.2113/gselements.8.5.36>
22. C. Xu, L. Wang, W. Song, M. Wu, Carbonatites in China: A review of genesis and mineralization. *Geosci. Front.* **1**, 105–114 (2010). <https://doi.org/10.1016/j.gsf.2010.09.001>
23. S. Jaireth, D.M. Hoatson, Y. Miezitis, Geological setting and resources of the major rare-earth element deposits in Australia. *Ore Geol. Rev.* **62**, 72–128 (2014). <https://doi.org/10.1016/j.oregeorev.2014.02.008>
24. V.M. Levson, Marine placers, in *Selected British Columbia Mineral Deposit Profiles, Volume 1 — Metallics and Coal*, ed. by D.V. Lefebure, G.E. Ray, (British Columbia Ministry of Energy of Employment and Investment, Open File 1995–20, 1995), pp. 29–31
25. B.S. Van Gosen, D.L. Fey, A.K. Shah, P.L. Verplanck, T.M. Hoefen, Deposit model for heavy mineral sands in coastal environments. U.S. Geological Survey Scientific Investigations Report 2010–5070–L, 51 p (2014). <https://doi.org/10.3133/sir20105070L>

26. V. Zaitsev, L. Kogarko, Sources and perspectives of REE in the Lovozero Massif (Kola Peninsula, Russia). European Mineralogical Conference 2012, Universität in Frankfurt, Germany EMC2012–290.pdf, 2012
27. K. Sanematsu, Y. Watanabe, Characteristics and genesis of ion adsorption-type rare earth element deposits. *Rev. Econ. Geol.* **18**, 55–79 (2016). <https://doi.org/10.5382/Rev.18.03>
28. Z. Bao, Z. Zhao, Geochemistry of mineralization with exchangeable REY in the weathering crusts of granitic rocks in South China. *OGR* **33**(3–4), 519–535 (2008). <https://doi.org/10.1016/j.oregeorev.2007.03.005>
29. T. Cheisson, E.J. Schelter, Rare earth elements: Mendeleev's Bane, modern Marvels. *Science* **363**(6426), 489–493 (2019). <https://doi.org/10.1126/science.aau7628>. Epub 2019 Jan 31 PMID: 30705185
30. P. Cen, X. Bian, Z. Liu, M. Gu, W. Wu, B. Li, Extraction of rare earths from Bastnaesite concentrates: A critical review and perspective for the future. *Miner. Eng.* **171**, 107081 (2021a). <https://doi.org/10.1016/j.mineng.2021.107081>
31. P. Cen, X. Bian, W. Wu, B. Li, A sustainable green technology for separation and simultaneous recovery of rare earth elements and fluorine in Bastnaesite concentrates. *Sep. Purif. Technol.* **274**, 118380., ISSN 1383-5866 (2021b). <https://doi.org/10.1016/j.seppur.2021.118380>
32. L. Teixeira, R. Silva, D. Majuste, V. Ciminelli, Selective extraction of rare earth elements from Complex Monazite Ores. Proceedings of the first global conference on extractive metallurgy, 2018. [https://doi.org/10.1007/978-3-319-95022-8\\_200](https://doi.org/10.1007/978-3-319-95022-8_200)
33. D.A. Elatontsev, A.P. Mukhachev, Investigation of methods for separating thorium and rare earth elements in nitric-acid leaching solutions for Loparite concentrate. *Atom. Energy* **130**, 82–87 (2021). <https://doi.org/10.1007/s10512-021-00778-9>
34. G.A. Moldoveanu, V.G. Papangelakis, Recovery of rare earth elements adsorbed on clay minerals: I. Desorption mechanism. *Hydrometallurgy* **117–118**, 71–78 (2012). <https://doi.org/10.1016/j.hydromet.2012.02.007>
35. G.A. Moldoveanu, V.G. Papangelakis, Recovery of rare earth elements adsorbed on clay minerals: II. Leaching with ammonium sulfate. *Hydrometallurgy* **131–132**, 158–166 (2013a). <https://doi.org/10.1016/j.hydromet.2012.10.011>
36. B. Ji, Q. Li, R. Honaker, W. Zhang, Acid leaching recovery and occurrence modes of rare earth elements (REEs) from natural Kaolinities. *Miner. Eng.* **175**, 107278 (2022). <https://doi.org/10.1016/j.mineng.2021.107278>
37. A. Hofstra, V. Lisitsin, L. Corribeau, S. Paradis, J. Peter, K. Lauzière, C. Lawley, M. Gadd, J.-L. Pilote, I. Honsberger, E. Bastrakov, D. Champion, K. Czarnota, M. Doublier, D. Huston, O. Raymond, S. VanDerWielen, P. Emsbo, M. Granitto, D. Kreiner, Deposit classification scheme for the critical minerals mapping initiative global geochemical database. U.S. Geological Survey Open-File Report 2021–1049 60 p (2021). <https://doi.org/10.3133/ofr20211049>
38. S. Sun, W.F. McDonough, Chemical and isotopic systematics of Oceanic Basalts: Implications for mantle composition and processes, in *Magmatism in the Ocean Basins*, ed. by A.D. Saunders, M.J. Norry, vol. 42, (Special Publication, Geological Society of London, 1989), pp. 313–345
39. A.R. Chakhmouradian, E.P. Reguir, A.N. Zaitsev, Calcite and Dolomite in intrusive carbonatites. I. Textural variations. *Mineral. Petrol.* **110**, 333–360 (2016). <https://doi.org/10.1007/s00710-015-0390-6>
40. G.J. Simandl, S. Paradis, Carbonatites: Related ore deposits, resources, footprint and exploration methods. *Appl. Earth Sci.* **127**(4), 123–152 (2018). <https://doi.org/10.1080/25726838.2018.1516935>
41. V.S. Kamenetsky, A.G. Doroshkevich, H.A.L. Elliott, A.N. Zaitsev, Carbonatites: Contrasting, complex and controversial. *Elements* **17**, 307–314 (2021). <https://doi.org/10.2138/gselements.17.5.307>
42. A. Woolley, B. Kjarsgaard, Paragenetic types of carbonatite as indicated by the diversity and relative abundances of associated silicate rocks: Evidence from a global database. *Canadian Mineralogist - CAN MINERALOG.* **46**, 741–752 (2008). <https://doi.org/10.3749/canmin.46.4.741>
43. A.P. Jones, M. Genge, L. Carmody, Carbonate melts and carbonatites. *Rev. Miner. Geochem* **75**, 289–322 (2013)

44. A. Woolley, A. Kjarsgaard, Carbonatite occurrences of the world: Map and database. Geological Survey of Canada. Open File 5796, 2008, 28 pages; 1 CD-ROM (2008). <https://doi.org/10.4095/225115>
45. M. Anenburg, S. Broom-Fendley, W. Chen, Formation of rare earth deposits in carbonatites. *Elements* **17**, 327–332 (2022). <https://doi.org/10.2138/gselements.17.5.327>
46. K.M. Goodenough, E.A. Deady, C.D. Beard, S. Broom-Fendley, H.A.L. Elliott, F. van den Berg, H. Öztürk, Carbonatites and alkaline igneous rocks in post-collisional settings: Storehouses of rare earth elements. *J. Earth Sci.* **32**, 1332–1358 (2021). <https://doi.org/10.1007/s12583-021-1500-5>
47. Z. Cheng, Z. Zhang, A. Aibai, W. Kong, F. Holtz, The role of magmatic and post-magmatic hydrothermal processes on rare earth element mineralization: A study of the Bachu Carbonatites from the Tarim Large Igneous Province, NW China. *Lithos* **314–315**, 71–87 (2018). <https://doi.org/10.1016/j.lithos.2018.05.023>
48. Z.-Y. Wang, H.-R. Fan, L. Zhou, K.-F. Yang, H.-D. She, Carbonatite-related REE deposits: An overview. *Fortschr. Mineral.* **10**, 965 (2020). <https://doi.org/10.3390/min10110965>
49. H.-D. She, H. Fan, K.-F. Yang, X.-C. Li, Z.-F. Yang, Q.-W. Wang, L.-F. Zhang, Z.-J. Wang, Complex, multi-stage mineralization processes in the Giant Bayan Obo REE-Nb-Fe deposit, China. *Ore Geol. Rev.* **139**, 104461 (2021). <https://doi.org/10.1016/j.oregeorev.2021.104461>
50. R.A. Ayuso, R. Tucker, S. Peters, N.K. Foley, J.A. Jackson, S. Robinson, M. Bove, Preliminary radiogenic isotope study on the origin of the Khanneshin Carbonatite Complex, Helmand Province, Afghanistan. *J. Geochem. Explor.* **133**, 6–14 (2013). <https://doi.org/10.1016/j.gexplo.2013.06.012>
51. R.D. Tucker, H.E. Belkin, K.J. Schulz, S.G. Peters, F. Horton, K. Kim Buttleman, E.R. Scott, A major Light Rare Earth Element (LREE) resources in the Khanneshin Carbonatite Complex, Southern Afghanistan. *Econ. Geol.* **107**, 197–208 (2012). <https://doi.org/10.2113/econgeo.107.2.197>
52. X.Y. Yang, X.D. Lai, F. Pirajno, Y.L. Liu, M.X. Ling, W.D. Sun, Genesis of the Bayan Obo Fe-REE-Nb formation in Inner Mongolia, North China Craton: A perspective review. *Precambrian Res.* **288**, 39–71 (2017). <https://doi.org/10.1016/j.precamres.2016.11.008>
53. Molycorp, Inc., Molycorp's rare earth reserves at mountain pass increase by 36%: Molycorp Press Release, April 9, 2012 (2012). Accessed 19 March 2019, at <https://us1.campaign-archive.com/?u=a9e8676e87fad805702b98564&id=8bad5e9295&e=%5BUNIQID%5D>
54. J.E. Poletti, J.M. Cottle, G.A. Hagen-Peter, J.S. Lackey, Petrochronological constraints on the origin of the Mountain Pass Ultra-Potassic and Carbonatite Intrusive Suite, California. *J. Petrol.* **57**, 1555–1598 (2016). <https://doi.org/10.1093/petrology/egw05>
55. K.E. Watts, G.B. Haxel, D.M. Miller, Temporal and Petrogenetic links between Mesoproterozoic alkaline and carbonatite magmas at Mountain Pass, California. *Econ. Geol.* **117**(1), 1–23 ISSN 0361-0128 (2022). <https://doi.org/10.5382/econgeo.4848>. 23 p
56. J. Dostal, Rare metal deposits associated with alkaline/peralkaline igneous rocks, in *Reviews in Economic Geology 18 — Rare Earth and Critical Elements in Ore Deposits*, ed. by P. Verplanck, M. Hitzman, (Society of Economic Geologists, Inc., Littleton, 2016), pp. 33–54. <https://doi.org/10.5382/Rev.18.02>
57. J. Dostal, Rare earth element deposits of alkaline igneous rocks. *Resources* **6**(3), 34 (2017). <https://doi.org/10.3390/resources6030034>
58. M.A.W. Marks, G. Markl, A global review on Agpaitic rocks. *Earth Sci. Rev.* **173**, 229–258 (2017). <https://doi.org/10.1016/j.earscirev.2017.06.0>
59. R.J. Robinson, M.A. Power, J.C. Barker, Technical report on the exploration Program and mineral resource estimate for the Bokan Mountain Property, Prince of Wales Island, Alaska. NI 43–101 Report, 190 p (2011) <http://ucore.com/projects/bokan-mountain-alaska/43-101>
60. M. O'Driscoll, Rare earths — Enter the dragon. *Ind. Miner* **254**, 21–55 (1988)
61. P.S. Roy, J. Whitehouse, Changing Pliocene Sea levels and formation of heavy Mineral Beach placers in the Murray Basin, Southeastern Australia. *Econ. Geol.* **98**, 975–983 (2003). <https://doi.org/10.2113/gsecongeo.98.5.975>

62. F. Wall, A. Rollat, R.S. Pell, Responsible sourcing of critical minerals. *Elements* **13**, 313–318 (2017). <https://doi.org/10.2138/gselements.13.5.313>
63. V. Raja, S.K. Sahoo, K. Sreekumar, M.A. Neelakantan, High background radiation places and spatial distribution of uranium in groundwater of monazite placer deposit in Kanniyakumari District, Tamil Nadu, India. *J. Radioanal. Nucl. Chem.* **328**, 925–939 (2021). <https://doi.org/10.1007/s10967-021-07727-7>
64. V. Vineethkumar, R. Akhil, K.P. Shimod, V. Prakash, Sources of monazite patches and dynamics of radionuclides concentration in the high background radiation areas of Kollam District, Kerala. *J. Radioanal. Nucl. Chem.* **327**, 189–198 (2021). <https://doi.org/10.1007/s10967-020-07520-y>
65. N. Van Dung, V.T.L. Anh, Radon, thoron gas concentration and level living in Ban Gie monazite mineral sand mine area, Quy Hop District, Nghe An Province, Vietnam, in *Proceedings of the 2nd Annual International Conference on Material, Machines and Methods for Sustainable Development (MMMS2020)*. *MMMS 2020. Lecture Notes in Mechanical Engineering*, ed. by B.T. Long, Y.H. Kim, K. Ishizaki, N.D. Toan, I.A. Parinov, N.P. Vu, (Springer, Cham, 2021). [https://doi.org/10.1007/978-3-030-69610-8\\_83](https://doi.org/10.1007/978-3-030-69610-8_83)
66. B.G. Lottermoser, Rare earth element mineralization within the Mt. Weld Carbonatite Laterite, Western Australia. *Lithos* **24**, 151–167 (1990). [https://doi.org/10.1016/0024-4937\(90\)90022-S](https://doi.org/10.1016/0024-4937(90)90022-S)
67. I.A. Zhukova, A.S. Stepanov, S.-Y. Jiang, D. Murphy, J. Mavrogenes, C. Allen, W. Chen, R. Bottrill, Complex REE systematics of carbonatites and weathering products from Uniquely Rich Mount Weld REE Deposit, Western Australia. *Ore Geol. Rev.* **139**, 539 (2021). <https://doi.org/10.1016/j.oregeorev.2021.104539>
68. J. Tian, X.K. Tang, J.Q. Yin, X.P. Luo, G.H. Rao, M.T. Jiang, Process optimization on leaching of a lean weathered crust elution-deposited rare earth ores. *Int. J. Miner. Process.* **119**, 83–88 (2013). <https://doi.org/10.1016/j.minpro.2013.01.004>
69. F. Wall, Rare earth elements, in *Critical Metals Handbook*, ed. by G. Gunn, (Wiley, 2014), pp. 312–339. <https://doi.org/10.1002/9781118755341.ch13>
70. N.K. Foley, R.A. Ayuso, REE enrichment in granite-derived Regolith Deposits of the Southeastern United States — Prospective source rocks and accumulation processes, in *Symposium on Critical and Strategic Materials Proceedings. British Columbia Geological Survey Paper 2015–3*, ed. by G. Simandl, M. Neetz, (2015), pp. 131–138. [http://cmscontent.nrs.gov.bc.ca/geoscience/PublicationCatalogue/Paper/BCGS\\_P2015-03-16\\_Foley.pdf](http://cmscontent.nrs.gov.bc.ca/geoscience/PublicationCatalogue/Paper/BCGS_P2015-03-16_Foley.pdf)
71. S.M. McLennan, Rare earth element geochemistry and the “Tetrad” effect. *Geochim. Cosmochim. Acta* **58**, 2025–2033 (1994). [https://doi.org/10.1016/0016-7037\(94\)90282-8](https://doi.org/10.1016/0016-7037(94)90282-8)
72. Z.H. Zhao, X. Xiong, X.D. Han, Y. Wang, Q. Wang, Z.W. Bao, B.M. Jahn, Controls on the REE Tetrad Effect in Granites: Evidence from the Qianlishan and Baerzhe Granites, China. *Geochem. J.* **36**, 527–543 (2002). <https://doi.org/10.2343/geochemj.36.527>
73. N.K. Foley, R.A. Ayuso, Rare earth element mobility in High-Alumina Altered Metavolcanic Deposits, South Carolina, USA. *J. Geochem. Explor.* **133**, 50–67 (2013). <https://doi.org/10.1016/j.gexplo.2013.03.008>
74. C.R. Bern, T. Yesavage, N.K. Foley, Ion adsorption REEs in regolith of the Liberty Hill Pluton, South Carolina, USA: An effect of hydrothermal alteration. *J. Geochem. Explor.* **172**, 29–40 (2017). <https://doi.org/10.1016/j.gexplo.2016.09.009>
75. P. Černý, T.S. Ercit, The classification of granitic Pegmatites revisited. *Can. Mineral.* **43**, 2005–2026 (2005). <https://doi.org/10.2113/gscanmin.43.6.2005>
76. M.A. McKeough, D.R. Lentz, C.R.M. McFarlane, J. Brown, Geology and evolution of pegmatite-hosted U-Th ± REE-Y-Nb mineralization, Kulyk, Eagle, and Karin Lakes region, Wollaston Domain, Northern Saskatchewan, Canada: Examples of the dual role of extreme fractionation and hybridization processes. *J. Geosci.* **58**(4), 321–346 (2013). <https://doi.org/10.3190/jgeosci.133>
77. D.L. Huston, R. Maas, A. Cross, K.J. Hussey, T.P. Mernagh, G. Fraser, D.C. Champion, The Nolans Bore rare earth element-phosphorus-uranium mineral system — Geology, origin and post-depositional modifications. *Mineral. Deposita* **51**(6), 797–822 (2016). <https://doi.org/10.1007/s00126-015-0631-y>

78. W.C. Day, J.F. Slack, R.A. Ayuso, C.M. Seeger, Regional geologic and petrologic framework for iron oxide  $\pm$  Apatite  $\pm$  rare earth element and iron oxide copper-gold deposits of the Mesoproterozoic St. Francois Mountains Terrane, Southeast Missouri, USA. *Econ. Geol.* **111**, 1825–1858 (2016). <https://doi.org/10.2113/econgeo.111.8.1825>
79. J.N. Aleinikoff, D. Selby, J.F. Slack, W.C. Day, R.M. Pillers, M.A. Cosca, C.M. Seeger, C.M. Fanning, I.M. Samson, U-Pb, Re-Os, and Ar/Ar geochronology of rare earth element (REE)-rich Breccia pipes and associated host rocks from the Mesoproterozoic Pea Ridge Fe-REE-Au deposit, St. Francois Mountains, Missouri. *Econ. Geol.* **111**, 1883–1914 (2016). <https://doi.org/10.2113/econgeo.111.8.1883>
80. R.A. Ayuso, J.F. Slack, W.C. Day, A.E. McCafferty, Geochemistry, Nd-Pb isotopes, and Pb-Pb ages of Mesoproterozoic Pea Ridge iron oxide-Apatite-rare earth element deposit, Southeast Missouri. *Econ. Geol.* **111**, 1935–1962 (2016). <https://doi.org/10.2113/econgeo.111.8.1935>
81. K.E. Watts, C.N. Mercer, Zircon-hosted melt inclusion record of silicic magmatism in the Mesoproterozoic St. Francois Mountains Terrane, Missouri: Origin of the Pea Ridge iron oxide-Apatite-rare earth element deposit and implications for regional crustal pathways of mineralization. *Geochim. Cosmochim. Acta* **272**, 54–77 (2020). <https://doi.org/10.1016/j.gca.2019.12.032>
82. C.N. Mercer, K.E. Watts, J. Gross, Apatite trace element geochemistry and cathodoluminescent textures — A comparison between regional magmatism and the Pea Ridge IOAREE and Boss IOCG Deposits, Southeastern Missouri Iron Metallogenic Province, USA. *OGR* **116**, 103129 (2020). <https://doi.org/10.1016/j.oregeorev.2019.103129>
83. P. Emsbo, P.I. McLaughlin, G.N. Breit, E.A. du Bray, A.E. Koenig, Rare earth elements in sedimentary phosphate deposits: Solution to the global REE crisis? *Gondwana Res.* **27**, 776–785 (2015). <https://doi.org/10.1016/j.gr.2014.10.008>
84. P. Emsbo, P.I. McLaughlin, E.A. du Bray, E.D. Anderson, T.R.A. Vandembroucke, R.A. Zielinski, Rare earth elements in sedimentary phosphorite deposits: A global assessment. *Rev. Econ. Geol.* **18**, 101–113 (2016). <https://doi.org/10.5382/Rev.18.05>
85. R. Buccione, R. Kechiched, G. Mongelli, R. Sinisi, REEs in the North Africa P-Bearing Deposits, Paleoenvironments and economic perspectives: A review. *Fortschr. Mineral.* **11**(2), 214 (2021). <https://doi.org/10.3390/min11020214>
86. M. Valetich, D. Zivak, C. Spandler, H. Degeling, M. Grigorescu, REE enrichment of phosphorites: An example of the Cambrian Georgina Basin of Australia. *Chem. Geol.* **588**, 120654 (2022). <https://doi.org/10.1016/j.chemgeo.2021.120654>
87. S. Wu, L. Wang, L. Zhao, P. Zhang, H. El-Shall, B. Moudgil, X. Huang, L. Zhang, Recovery of rare earth elements from phosphate rock by hydrometallurgical processes – A critical review. *Chem. Eng. J.* **335**, 774–800 (2018). <https://doi.org/10.1016/j.cej.2017.10.143>
88. A. Pourmand, N. Dauphas, T.J. Ireland, A novel extraction chromatography and MC-ICP-MS technique for rapid analysis of REE, Sc and Y: Revising CI-Chondrite and Post-Archean Australian Shale (PAAS) abundances. *Chem. Geol.* **291**, 38–54 (2012). <https://doi.org/10.1016/j.chemgeo.2011.08.011>
89. T. Nazari-Dehkordi, C. Spandler, N.H.S. Oliver, R. Wilson, Unconformity-related rare earth element deposits: A regional-scale hydrothermal mineralization type of Northern Australia. *Econ. Geol.* **113**(6), 1297–1305 (2018). <https://doi.org/10.5382/econgeo.2018.4592>
90. S. Costis, K.K. Mueller, L. Couder, M.N. Carmen, N. Reynier, J.-F. Blais, Recovery potential of rare earth elements from mining and industrial residues: A review and cases studies. *J. Geochem. Explor.* **221**, 106699 (2020). <https://doi.org/10.1016/j.gexplo.2020.106699>
91. S.A. Wood, The aqueous geochemistry of the rare earth elements and yttrium. 1. Review of available low-temperature data for inorganic complexes and the inorganic REE speciation of natural waters. *Chem. Geol.* **82**, 159–186 (1990). [https://doi.org/10.1016/0009-2541\(90\)90080-Q](https://doi.org/10.1016/0009-2541(90)90080-Q)
92. L.D. Meinert, G.M. Dipple, S. Nicolescu, World Skarn deposits, in *Economic Geology — One Hundredth Anniversary v. 1905–2005*, ed. by J.W. Hedenquist, J.F.H. Thompson, R.J. Goldfarb, J.P. Richards, (Society of Economic Geologists, Inc., Littleton, 2005), pp. 299–336
93. D. London, Rare Element Granitic Pegmatites, in *Reviews in Economic Geology, volume 18 — Rare Earth and Critical Elements in Ore Deposits*, (Society of Economic Geologists, Inc., Littleton, 2016), pp. 165–194. <https://doi.org/10.5382/Rev.18.08>



# Chapter 3

## Energy-Related Rare Earth Element Sources



Allan Kolker, Liliana Lefticariu, and Steven T. Anderson

### 3.1 Introduction

Rare earth elements (REEs) are needed globally in a wide range of applications, including electronics, communications, medical science, manufacturing, and transportation [1–6]. Increasingly, REEs are required in clean energy applications, for example, through use of neodymium (Nd) magnets in wind power generation [7]. In the transportation sector, projected conversion to a fleet of non-polluting vehicles will also require REEs, as well as elements such as lithium (Li), manganese (Mn), cobalt (Co), and nickel (Ni), in batteries to power these vehicles [8]. In 2020, China accounted for approximately 60% of global REE production and while the most recent compilation [9] indicates that this proportion has decreased slightly in recent years, China still exerts considerable control over REE markets. Given this dependence, the United States continues to seek greater domestic production of REEs, including development of unconventional sources such as coal and coal combustion products [10]. While development of coal-related REE sources is primarily a domestic effort, technologies introduced to extract REEs from these materials have the potential to be applicable globally, wherever coal is mined and used for power generation.

Coal is a complex natural material, derived from peat, which consists of loosely consolidated layers of mixed plant material and mineral matter [11, 12]. Accumulation of peat in landforms known as mires, bogs, or swamps is favored by a persistent wet climate, stable to slowly sinking land surface, and protection from erosion by rivers and ocean waves. Over millions of years, burial, compression by

---

A. Kolker (✉) · S. T. Anderson  
U.S. Geological Survey, Geology, Energy & Minerals Science Center, Reston, VA, USA  
e-mail: [akolker@usgs.gov](mailto:akolker@usgs.gov)

L. Lefticariu  
Southern Illinois University, Department of Geology, Carbondale, IL, USA

overlying sediments, and the effects of heat within the Earth cause peat to transform to coal, a layered organic-rich sedimentary rock. Chemical constituents of coal, including REEs, reflect constituents inherited from peat-derived plant material, together with those present in mineral matter deposited in the mire by wind or water. Within a given coal bed, organic-rich horizons are commonly separated by clay-rich zones called partings, and the entire bed is typically underlain by a clay-rich horizon known as an underclay. Partings and underclays are recognized as zones of REE enrichment and therefore have attracted interest as exploration targets.

When coal is burned for electric power generation, inorganic portions that do not burn are retained as solid coal combustion products, of which fly ash is the largest fraction. Recovery of valuable constituents from fly ash, including REEs, has been considered since the 1930s [13]. As of 2019, coal use accounted for approximately 21% of electric power generating capacity in the United States, a proportion that has been steadily declining as gas-fired generation and renewables make up an increasing share of the U.S. energy market [14]. Despite this trend, fly ash currently generated and not already used in other beneficial applications remains a vast resource of potentially recoverable REEs, supplemented by fly ash already in storage [15–18]. Globally, coal accounts for more than one-third of electric power generation [19]. In the short term, global coal use is expected to remain relatively flat, with reductions in the United States, the European Union, and Japan being offset by continued reliance on coal in China, and increased usage in India and South Asian countries [19].

In projects supported by the U.S. Department of Energy [10], four coal-related sources showed promise at or reaching the pilot scale for recovery of REEs. These are (1) coal combustion fly ash; (2) waste coal from coal mining and preparation facilities; (3) coal in place, including delineation of specific REE-enriched horizons; and (4) coal-based acid-mine drainage (AMD). Each of these four sources will be discussed in detail in this chapter. Rare earth elements in materials 1–3 are primarily in solid form, whereas in AMD, REEs are dissolved or in colloidal form. De-watering of AMD leaves behind solids from which REEs can be recovered. In addition to these coal-related sources, oil shales [20] and geologic formation waters extracted during oil and gas production (produced waters [21]) are other potential energy-related REE sources, but these have not been developed to the pilot scale and are not considered further here.

The goal of this chapter is to present an overview of energy-related materials that could substantially augment domestic REE resources. In addition to providing a detailed review of the characteristics of these materials, this chapter highlights key factors influencing recovery, including REE enrichment and extractability, as well as economic concerns and implications for each material. Readers are referred to the summary by Zhang et al. [22] for a more detailed discussion of extraction approaches. As discussed in this chapter, each coal-related source has advantages and disadvantages. Which among them proves to be the most economically advantageous remains to be determined, as the landscape for unconventional REE sources is rapidly evolving. In this effort, coal-related materials have the potential to benefit society by providing critical resources from energy waste products.

## 3.2 REE Distribution in Coal-Related Sources

Rare earth element ores, discussed in the Chap. 2 [23], reflect the concentration of REE-bearing minerals by geologic processes, and hence, considerable enrichment relative to overall REE concentrations found in the Earth's crust. Distribution of REEs present in these ores is strongly controlled by the ore minerals present, such as bastnäsite ((REE)(CO<sub>3</sub>)F), monazite ((REE)PO<sub>4</sub>), or xenotime (YPO<sub>4</sub>), the three most commonly extracted REE minerals [23, 24]. In coal-related sources such as fly ash, waste coal, and sludge from AMD, overall REE concentrations are much lower, posing challenges for their economic recovery. Additionally, the distribution of REEs in these energy-sourced materials is similar to the average reported values for the Earth's upper continental crust (UCC) [25–28], rather than those of REE ores. Relative to the Earth as a whole, UCC is enriched in light rare earths (LREE). Coal and coal-related REE sources also show this predominant LREE enrichment, but REE contents and LREE proportions are much less than those of ores containing REE minerals such as bastnäsite [23] (Table 3.1).

**Table 3.1** Characteristics of coal-related REE source materials

	1	2	3	4	5	
Material	REEs total (ppm)	Percent HREE	Percent LREE	Percent critical REE	Ce/Yb <sub>N</sub>	Reference
MREE-enriched coal Xian'an Coalfield, China (average of 4 samples)	1020	19.6	80.4	32.7	1.39 <sup>a</sup>	[29]
HREE-enriched coal Xian'an Coalfield, China (average of 4 samples)	198.7	41.8	58.2	42.7	0.35	[29]
World average fly ash	426.5	29.3	70.7	33.3	0.72	[30]
"300 ppm" reference	300.0	27.2	72.8	30.4	1.0	[27] ×1.65 Table 3.2
Upper continental crust	182.0	27.2	72.8	30.4	1.0	[27] Table 3.2
World average hard coal	72.1	27.8	72.2	33.3	0.79	[30]
U.S. average coal	66.3	29.1	70.9	32.6	0.76	[31] Table 3.2

(1) Includes lanthanide series plus Y and Sc; (2) HREE include scandium (Sc), yttrium (Y), gadolinium (Gd), terbium (Tb), dysprosium (Dy), holmium (Ho), erbium (Er), thulium (Tm), ytterbium (Yb), lutetium (Lu); (3) LREE include lanthanum (La), cerium (Ce), praseodymium (Pr), neodymium (Nd), samarium (Sm), europium (Eu); (4) critical REEs include Y, Nd, Eu, Tb, Dy, and Er; (5) Ce/Yb normalized to UCC of Taylor and McLennan [25, 26] and McLennan [27]

<sup>a</sup>MREE-enriched samples show a slight positive Ce anomaly. Ce anomalies occur rarely where Ce is fractionated from the trivalent REEs due to formation of Ce<sup>4+</sup> from interaction of coals with fluids in highly oxidizing environments [32]. Yb is not subject to this anomalous behavior or to non-redox sensitive anomalies recognized in some other REE (La, Gd, Y) [32]

REEs, as defined by the International Union of Pure and Applied Chemistry (IUPAC) [33], consist of the lanthanide series, plus yttrium (Y) and scandium (Sc), which have chemical properties in common with the lanthanides, but are lighter. Yttrium occurs together with the lanthanides whereas Sc generally does not [34]. Scandium is, nonetheless, very important due to its high economic value among the REEs [35, 36]. In this chapter, unless otherwise designated, total REEs include Y, Sc, and the lanthanides, whereas REY, or REE + Y refer to the lanthanides and yttrium only. As the lanthanides are a continuous series from lanthanum (La, atomic number 57) to lutetium (Lu, atomic number 71), geochemists have traditionally divided the series into light rare earths (LREE: La, Ce, Pr, Nd), middle rare earths (MREE: Sm, Eu, Gd, Tb, Dy), and heavy rare earths (HREE: Ho, Er, Tm, Yb, Lu), or similar divisions [25, 32, 37–40]. Among the lanthanides, a simple way to indicate relative HREE enrichment is to consider the ratio of cerium (Ce, a LREE) vs. ytterbium (Yb, a HREE), either in absolute, or relative to a reference such as UCC (normalized) [41–43] (Table 3.1). Despite overall LREE enrichment, many coals have a Ce/Yb less than UCC (i.e., less LREE-enriched), due to a partial organic association of HREEs, which is especially apparent in low-rank coals [41, 44–50] (Table 3.1).

An alternative classification is to consider the REEs only as LREE (La to Eu) and HREE (Gd to Lu plus Y and, if available, Sc [22, 51], or similar groupings [2, 52]). In this approach, some elements that would alternately be considered MREE (Sm, Eu) are included with the LREE and others (Gd, Tb, Dy) are included with the HREE. Yttrium, which is not part of the lanthanide series, is sometimes considered separately as REE + Y or REY and placed between the MREE dysprosium (Dy) and the HREE holmium (Ho) [38, 53, 54]. Alternately, Y is grouped with the HREE [2, 22, 51]. Inclusion of Y with the HREEs gives the largest proportion of heavy rare earths, as Y is more abundant in crustal materials, including coal, than the lanthanide HREEs combined [25, 38, 55]. Counting Y as an HREE can be somewhat misleading, as HREE enrichment becomes strongly dependent on this one element. Beyond this, equating a high proportion of HREEs with high economic value is an oversimplification, as not all HREE are equally valuable. For example, the price per kg of yttrium oxide (\$3/kg for 99.999% purity) is only marginally above that for lower-valued oxides of the LREE, such as La and Ce (each \$2/kg for 99.5%+ purity), whereas higher-valued HREE oxides such as Dy and terbium (Tb) have values in the \$100s per kg [9, 56]. Despite these complexities, classifying all REEs as either LREE or HREE and considering their relative proportions is gaining acceptance as a reference for comparing samples with different REE distributions.

As an alternative to the above approaches, Seredin and Dai [38] introduced a classification of the rare earths in coal-related materials based on their economic prospects, rather than their atomic weight. In this approach, Nd, Eu, Tb, Dy, Y, and Er are considered critical rare earths; La, Pr, Sm, and Gd are considered uncritical; and Ce, Ho, Tm, Yb, and Lu are excessive. Although this classification is based on economic considerations at the time of its introduction, and Sc is omitted, critical designations are largely applicable using present valuations [9, 35, 56]. Importantly, this classification recognizes that not all HREE are critical (e.g., Ho, Tm, Yb, and

Lu are excluded), and not all LREE are uncritical or excessive (e.g., Nd is critical). This classification has been adopted together with REE distribution by atomic weight in many subsequent studies of coal and coal ash [3, 16, 39, 40, 57]. Because La and Ce, the two most abundant LREEs, are excluded, except in unusual circumstances, the proportion of critical rare earths in energy-derived materials is no greater than about 40% on a weight concentration basis, with Y and Nd being the two most abundant critical rare earths (Table 3.1).

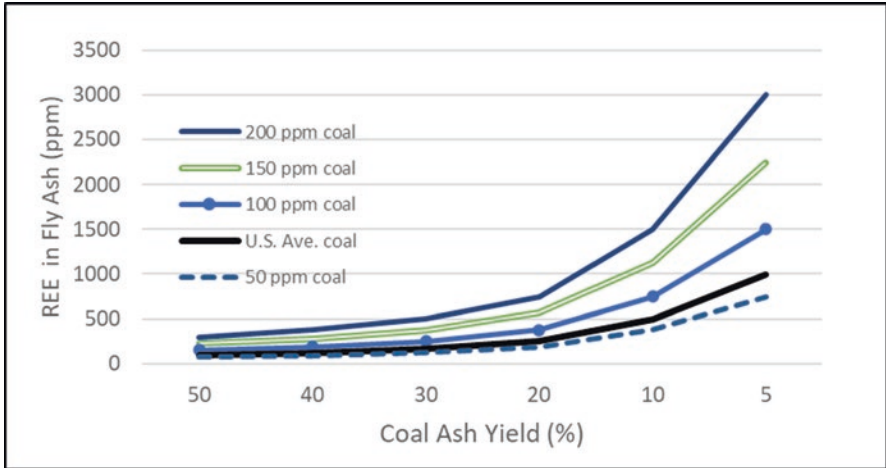
### 3.3 Coal Combustion Fly Ash

Among materials derived from coal use, fly ash is consistently the most REE-enriched and therefore has attracted considerable attention as an unconventional REE source [3, 8, 16, 18, 38, 58–64]. When coal is burned, relative REE distributions are carried over into corresponding coal combustion products at higher concentrations [16, 39, 65, 66]. Rare earth elements are highly refractory (resistant to decomposition by heat) and are therefore strongly retained in solid coal combustion products, unlike volatile elements such as mercury (Hg) and selenium (Se) which are carried in power station flue gas when coal is burned [67, 68]. These solids, including fly ash and bottom ash, are primarily derived from non-combustible mineral matter in coal.

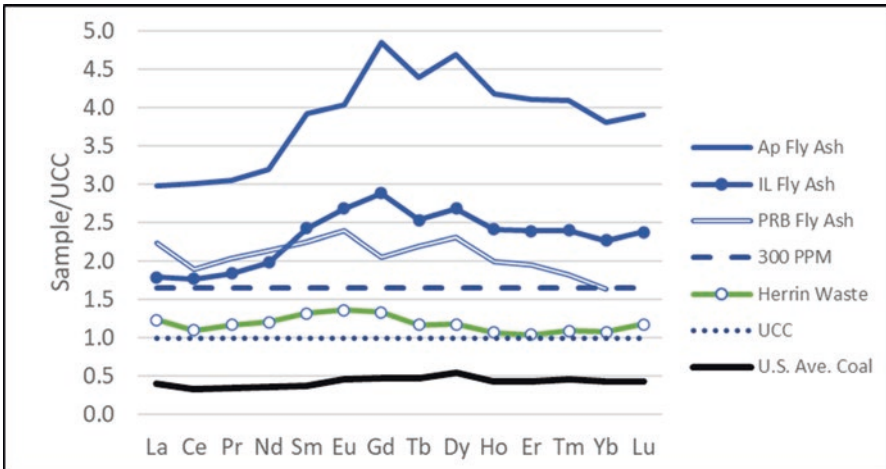
#### 3.3.1 REE Variation in Fly Ash

Key factors in determining the REE content of fly ash are the REE content of the coal burned and its ash yield, which is the proportion of mineral matter present in coal (Fig. 3.1). Due to their refractory behavior, large proportions of the REEs originally present in coal are retained in a smaller mass fraction, leading to REE enrichment of solid coal combustion products. In general, coals used for power generation have REE abundances below those of UCC, but concentration of REEs by combustion leads to REE enrichment in fly ash to values above UCC, typically in the 200–600 ppm range [30, 57, 58, 63, 69–71]. As such, many fly ash samples meet the minimum interest level for total REEs ( $\geq 300$  ppm) set by the U.S. Department of Energy (DOE) [72] in their initial evaluation of U.S. energy-related REE sources (Fig. 3.2). Higher REE values in coal combustion products may result where the coal combusted is unusually REE-enriched [38, 43, 52, 73, 74], has a low ash yield [38, 75], or both. The inverse relation between ash yield of the feed coal and REE content of the fly ash results because a high proportion of REEs originally present is retained in a much smaller mass, thereby concentrating the REEs (Fig. 3.1).

Enrichment factors in fly ash of approximately 3–8 times whole-coal values are common, as would be predicted for commercial or export coals having ash yields of approximately 25–10%, respectively, assuming REEs are nearly or entirely retained



**Fig. 3.1** Calculated enrichment of REEs in coal fly ash assuming 100% retention from coals having 50 to 200 ppm total REEs and ash yields ranging from 50% to 5%. Calculations further assume a 75:25 proportion of fly ash to bottom ash such that 75% of total REEs from coal are retained in the fly ash. This figure shows that fly ashes typical of commercial coals (ash yield 10–20%) have total REEs in the hundreds of ppm and that low ash coals with average to below average REE contents can produce fly ash approaching or exceeding 1000 ppm REEs. U.S. Average Coal (66.3 ppm, including Y and Sc) from Finkelman [31]



**Fig. 3.2** UCC-normalized lanthanide distributions. (1) U.S. Average Coal (Finkelman [31]); (2) Upper Continental Crust Reference (UCC; Taylor and McLennan [25, 26] and McLennan [27]); (3) average of 8 samples of Herrin #6 waste coal from the U.S. Illinois Basin (Herrin Waste; Kolker et al. [40]); (4) calculated DOE 300 ppm interest level (300 ppm; this study); (5) Powder River Basin fly ash (PRB Fly Ash; Deonarine et al. [81], Kolker et al. [39], Lu not determined); (6) Illinois Basin fly ash (IL Fly Ash; Taggart et al. [60]); and (7) Appalachian Basin fly ash (Ap Fly Ash; Taggart et al. [60])

(Fig. 3.1). But in coals of poorer quality, having higher ash yields, REE enrichment in the fly ash, relative to the feed coal, will be lower because REEs from the feed coal are distributed over a larger mass fraction (Fig. 3.1). Using global averages for hard coal (anthracite, bituminous, and subbituminous A, B) and hard coal ash [30], an enrichment factor of 6.5 is indicated for total REEs in the ash. Patterns in the distribution of lanthanides have been noted where plots for coals and fly ashes deviate from a crustal distribution, showing preferred enrichments in MREEs (M-type), LREEs (L-type), or HREEs (H-type) with respect to the UCC distribution [32, 38, 58, 61, 62, 76]. These characteristics are especially common in highly REE-enriched coal-derived materials [29, 32] and have begun to be used to distinguish ashes from specific coal basins [61, 62, 77, 78], or derived from coals containing REEs bound to specific mineral assemblages [79, 80].

Within coal-burning power stations, factors that influence trace element content of fly ash captured by air pollution control devices such as electrostatic precipitators (ESPs) and fabric filters include temperature of the flue gas and size of particles captured. Both parameters decrease in successive rows of ESPs downstream of the boiler [76, 82, 83]. In general, this distribution leads to an increase in the content of volatile and partially volatile trace elements in fly ash captured by successive ESPs [75, 84, 85]. Mercury, capture by ESPs, is also determined by the amount of unburned carbon in the ash [82, 83, 86, 87]. Unlike the more volatile elements, refractory elements such as REEs and associated elements with similar behavior, including scandium (Sc), rubidium (Rb), zirconium (Zr), hafnium (Hf), and thorium (Th), are not strongly partitioned, either between fly ash and bottom ash, or within successive rows of ESPs [67, 68, 76, 83, 87]. However, in some cases, decreases in the proportion of LREEs were found in finer ash fractions collected in the most downstream hoppers [76, 87].

### 3.3.2 Occurrence of REEs in Fly Ash

Understanding how REEs in fly ash occur is essential to developing suitable approaches for their extraction. The host of REEs in fly ash has been somewhat of a puzzle. Despite having lower bulk REE contents, in many commercial coals, common REE-bearing minerals such as monazite or its hydrated equivalent, rhabdophane  $(\text{REE})\text{PO}_4 \cdot \text{H}_2\text{O}$ , xenotime, other REE-bearing phosphates, apatite  $(\text{Ca}_5(\text{PO}_4)_3(\text{OH}, \text{F}, \text{Cl}))$ , and crandallite  $(\text{CaAl}_3(\text{PO}_{3.5}(\text{OH})_{0.5})_2(\text{OH})_6)$  and the silicates, allanite  $(\text{Ca}(\text{REE}, \text{REE})\text{Al}_2\text{Fe}^{2+}[\text{Si}_2\text{O}_7][\text{SiO}_4]\text{O}(\text{OH}))$ , and zircon  $(\text{ZrSiO}_4)$  are observable as trace phases by optical and scanning electron microscopy [32, 48, 88]. These REE minerals are less apparent in fly ash, and where present, tend to occur as smaller particles than those in the corresponding feed coal [18, 39, 89].

To help resolve this apparent contradiction, recent investigations have used a range of modern analytical approaches to show the distribution of REE in fly ash at the micrometer (micron or  $\mu\text{m}$ ) and (or) even the nanometer (nm) scale. At boiler

temperatures (1400–1500 °C), major clay minerals present in coal such as kaolinite ( $\text{Al}_2\text{Si}_2\text{O}_5(\text{OH})_4$ ) and illite-smectite (a series of potassium (K), sodium (Na), iron (Fe), magnesium (Mg) aluminosilicates) are melted. Upon rapid cooling in combustion systems, this melt quenches to form aluminosilicate glasses that comprise the largest portion of fly ash. Analysis of these glasses at the scale of individual grains [39] showed that lanthanide REEs are present at a range of concentrations which overlaps that of the bulk fly ash. In addition, Kolker et al. [39] found that calcium (Ca)- and Fe-bearing glasses had higher lanthanide contents than those of pure aluminosilicates lacking other major elements. And, as also noted by Yang et al. [90], co-occurring Fe-oxide magnetospheres are REE-bearing. Quartz, which survives combustion but is transformed to a high-temperature Beta form, contains little or no REE and is essentially a diluent [39]. Extracting REEs from fly ash glasses poses a particular challenge because their digestion on a commercial scale is difficult.

Whereas partitioning of REEs into aluminosilicate glasses helps explain the paucity of observable REE minerals in fly ash, it is not the whole story. Using scanning electron microscopy [63, 91, 92], synchrotron-based approaches [63, 65] or high-resolution transmission microscopy [18, 92], discrete REE-enriched domains (mineralogical host uncertain or undetermined) or phases (with a specific mineralogical host) have been shown to persist as inclusions within fly ash glasses, or separately, at the micron to sub-micron scale. REE-bearing trace minerals such as monazite (approximately 2000 °C) [93] and zircon (1690 °C) [94] have melting temperatures for pure phases that are above normal combustion temperatures. As such, these and other refractory phases are expected to persist in fly ash [18, 91]. But upon heating, monazite will shatter at approximately 1400 °C, that is, below its melting temperature, due to thermal expansion of helium (He), present from radioactive decay of Th [87, 95, 96]. This phenomenon may explain the apparent size reduction of monazite in fly ash. A similar process, or simply shock from rapid heating, could apply to other He-diffusing REE trace phases, such as apatite and zircon [18, 97]. Recognition that fine-scale REE-enriched domains or mineral inclusions persist in fly ash is an important advance, and these forms must be considered in determining the overall distribution of REEs in fly ash. But the finding that REE distributions for specific glass compositions are relatively constant throughout a fly ash sample argues against randomly distributed finer-scale REE-bearing domains or inclusions as the primary REE host. These forms are therefore considered additional to REEs contained in fly ash glasses [39, 65].

### 3.4 Coal Resources

Rare earth element data for U.S. and international coals are available in a growing number of sources and databases, in response to international demand for REEs, and widespread interest in their extraction from energy-related sources. The largest sources, in terms of number of samples determined, are for world coals [30], U.S. coals [31, 51, 55, 98], and Chinese coals [32, 99, 100]. Mean total REE



contents of world hard coals (72.1 ppm) [30] and U.S. coals (66.3 ppm) [31] are similar. Each of these REE totals is less than half that of UCC [27] and less than a quarter of the 300 ppm DOE interest level (Table 3.2). Compilations for Chinese coals indicate a somewhat higher overall REE content, on average approaching that of UCC [32, 99, 100]. REE enrichment in Chinese coals is likely explained by inclusion of coals that have become relatively REE-enriched by one or more of the processes discussed below, together with coals having more typical REE contents. Recent publications highlight the REE potential of various international coals, including those in Australia [101], Colombia [102], India [103], Indonesia [104], and South Africa [57]. Overall, these studies are consistent with trends shown for U.S. and world coals in which REE contents of coals produced for commercial power generation are generally lower than crustal abundances and much lower than 300 ppm DOE interest levels (Table 3.2 and Fig. 3.2).

A primary source of REE data for U.S. coals is the U.S. Geological Survey (USGS) COALQUAL database, an inclusive compilation containing records for more than 7500 samples [98]. Sample distribution in COALQUAL is weighted toward U.S. Eastern bituminous coals from the Appalachian Basin, reflecting

**Table 3.2** Reference REE distributions relative to the upper continental crust (UCC) Values in parts per million (ppm)

	1	2	3	4	5	6
REEs	U.S. coal	World coal	UCC [25, 26]	UCC [27]	UCC [28]	“300 ppm”
Sc	4.2	3.7	11	13.6	14.0	22.42
Y	8.5	8.2	22	22	21	36.27
La	12	11	30	30	31	49.46
Ce	21	23	64	64	63	105.51
Pr	(2.4)	3.4	7.1	7.1	7.1	11.71
Nd	[9.5]	12	26	26	27	42.86
Sm	1.7	2.2	4.5	4.5	4.7	7.42
Eu	0.40	0.43	0.88	0.88	1.0	1.45
Gd	[1.8]	2.7	3.8	3.8	4.0	6.26
Tb	0.30	0.31	0.64	0.64	0.7	1.06
Dy	1.9	2.1	3.5	3.5	3.9	5.77
Ho	[0.35]	0.57	0.80	0.80	0.83	1.32
Er	1.0	1.00	2.3	2.3	2.3	3.79
Tm	[0.15]	0.30	0.33	0.33	0.30	0.54
Yb	[0.95]	1.0	2.2	2.2	2.0	3.63
Lu	0.14	0.20	0.32	0.32	0.31	0.53
SUM	66.3	72.1	179.37	181.97	183.14	300.00
% UCC	36.4	39.6		100.00		164.86

(1) U.S. Average Coal (Finkelman [31]). Bracketed values are calculated, and those in parentheses are estimated (see text); (2) World Hard Coal (Ketris and Yudovich [30]); (3) Upper Continental Crust (UCC) of Taylor and McLennan [25, 26]; (4) UCC of McLennan [27]; (5) UCC of Rudnick and Gao [28]; (6) Calculated 300 ppm enrichment having UCC proportions of McLennan [27]. To convert to REE oxides, multiply by 1.53 (Sc), 1.27 (Y), and 1.17–1.14 (La to Lu)

U.S. coal production at the time this compilation began. Characteristics of the COALQUAL database and its limitations are discussed in detail by Lin et al. [55] In short, results for REE concentrations vary in quality depending on the analytical method used, and in many cases, censored values (less than a stated value) are given. Lin et al. [55] devised an approach to adjust for censored values and compared it to the approach used by Finkelman [31], who in determining a U.S. average from these data, assumed a crustal distribution or otherwise estimated values for elements having the greatest proportion of censored values (e.g., Pr, Tb, Ho, and Tm). Results for “*U.S. average coal*” obtained by these differing approaches are similar. Despite its shortcomings, COALQUAL is a useful starting point for characterizing REE distribution in U.S. coals. Data from COALQUAL, together with other recent compilations, indicate that among U.S. coals, Eastern bituminous coals in the Appalachian Basin have somewhat higher overall REE contents than lower rank Western coals [55, 60, 78], reflecting an Appalachian regional sediment source terrain that is relatively REE-enriched [105, 106]. This apparent advantage is offset by the fact that, in general, REEs from Eastern bituminous coals and their ashes are less readily extractable than those from Western coals having lower REE contents [47, 60] (Sect. 3.4.2 on Low-Rank Coals).

### 3.4.1 REE-Enriched Coals, Coal Zones

While overall REE contents of many commercial coals are below crustal averages, in certain cases, coals can become unusually REE-enriched. Geologic processes by which coal beds become REE-enriched are summarized by Seredin and Dai [38]. These include: (1) deposition of sediment-derived REE minerals, with sediment carried primarily by surface waters (terrigenous type); (2) REEs derived from air fall and leaching of volcanic ash (tuffaceous type); (3) enrichment associated with thermal waters or deep fluids (hydrothermal type); and (4) REEs from ground water that infiltrates coals (infiltrational type). One or more of these enrichment types may be operative at a given location [3, 38, 43, 51, 52, 107, 108]. Furthermore, variations within coal beds have been noted and these REE-enriched zones are recognized as areas for exploration.

#### **Terrigenous REE Enrichment**

REE distribution in coal can reflect characteristics of sediment contributed to the mire during coal formation. REE minerals such as zircon, monazite, and allanite are very stable in the sedimentary environment, persisting during sediment transport. Terrigenous REE enrichment can result where REE-enriched source areas contribute sediment to a coal basin or where stable REE minerals are concentrated by reworking of these sediments prior to deposition. In Appalachian Basin coals, relative REE enrichment of coals occurs over a wide geographic and stratigraphic interval

suggesting REE-enriched source rocks were exposed regionally and for an extended period [105, 106]. While development of the Appalachian Basin reflects a complex series of tectonic events, the adjacent Grenville Province, in which monazite- and zircon-bearing granitic source rocks are common, is indicated in studies of the origin (provenance) of Appalachian Basin sediments [109–112]. Terrigenous REE enrichment is also recognized in the Jungar coalfield, Ordos Basin, China, where the No. 6 coal shows enrichment in REEs (193.3 ppm) and Zr (234 ppm) due in part to zircon derived from adjacent sediment source areas [38, 99, 113].

### **Tuffaceous REE Enrichment**

Air fall deposition of volcanic ash concurrently with coal formation is recognized as the source in some of the most REE-enriched coals, contributed both from the ash itself and from leaching of the ash in portions of coal that immediately underly these horizons [16, 43, 73, 77, 104, 114–116]. Where continuous volcanic ash beds are recognized within coal, these are termed tonsteins. Evidence for tuffaceous deposition is given by the presence of volcanic-derived high-temperature mineral phases and horizons enriched in aluminosilicate clay minerals such as kaolinite that is derived from decomposition of volcanic glasses [73, 116–121]. The most extreme REE enrichment is generally limited to the immediate vicinity of tonstein-bearing horizons and this localization may limit commercial scale development [16]. Apart from their role as a source of REE enrichment, tonsteins are also very useful to geologists to correlate coal-bearing sequences separated over broad geographic areas [117, 120, 122].

Input of volcanic ash contributed to REE enrichment seen in the Fire Clay coal of Eastern Kentucky and adjacent parts of Tennessee and West Virginia, making it one of the most promising U.S. sources of REE-enriched coal [43, 73, 74, 77, 123]. The Fire Clay coal is notable for containing a prominent tonstein either within it or in close association with the coal [73–75]. Elsewhere, dispersion of volcanic-derived material contributed to mineral matter within the coal. A recent study gives mean total REEs of  $797 \pm 27.2$  ppm for eight samples of fly ash derived from Fire Clay coal, compared to a mean of  $564 \pm 28.8$  ppm for nine samples of fly ash from other Central Appalachian Basin coal sources [61].

Other examples of tuffaceous REE enrichment include the Banko coalfield, South Sumatra Basin, Indonesia, where at least six tonsteins are recognized, and coals beneath the tonsteins show REE enrichment to as much as 118 ppm [104]. In the Azeisk deposit of the Irkutsk Coal Basin of Siberian Russia [113], enrichment of REEs and associated trace elements occurs in narrow zones both above and below tonstein layers. This occurrence is one of a large number of cases where volcanic input influenced REE distribution of coals in the North Asian region [115]. As tonsteins occur widely, and interest in coal-related REE sources remains high, new sources of coal with tuffaceous REE enrichment and other REE-enriched modes continue to be demonstrated.

## Hydrothermal REE Enrichment

Hydrothermal enrichment of REEs in coal is analogous to processes by which hydrothermal ore deposits are formed, as discussed in the Chap. 2 [23]. In this process, REE enrichment results from interaction of coal with hydrothermal fluids such as thermal waters emanating from heat sources regionally or in the immediate proximity of coals [38, 43, 52, 124–126]. As is the case with coals influenced by input of volcanic ash, mineralized coals are restricted to regions where the appropriate geologic conditions for this enrichment existed. Hydrothermal REE enrichment may be concurrent with coal formation (syngenetic) or postdate it (epigenetic). A well-known example of hydrothermal element enrichment described by Seredin [52] is in thinly bedded Cenozoic coals of the Russian Far East, (Kuznetsk Basin and vicinity) in which hydrothermal alteration (as well as volcanic input) were simultaneous with coal accumulation, giving rise to coals having REY contents in the 300–1200 ppm range. Similar hydrothermal (or mixed hydrothermal-tuffaceous) mineralization styles have been recognized in other REE-enriched East Asian mineralized coal occurrences including the South Primorye area of Russia and analogous occurrences in southwestern China [29, 126]. In addition to the REEs, a range of other valuable metals may be enriched in these deposits, including germanium (Ge) which is present at economic levels in some mineralized coals of the Russian Far East and in Inner Mongolia, China [32, 124, 126–129].

## Infiltrational REE Enrichment

Trace elements, including REEs, may be carried in solution in groundwater where these waters have passed through REE-bearing sources prior to interacting with coal. This phenomenon may cause REEs and other constituents carried in solution to become incorporated in the coal [38, 53, 124]. This process primarily occurs after coal formation; however, influx of seawater earlier on, during coal formation can similarly impact the distribution of REEs. This is shown by an association of REEs with portions of the coal having the greatest marine influence and correspondence of REEs with other marine-derived elements, such as sulfur (S), Na, and Mg [130]. In addition, redistribution of REEs having a tuffaceous source, such as in REE-enriched zones beneath tonsteins, is an example of infiltrational REE redistribution within a coal bed [43].

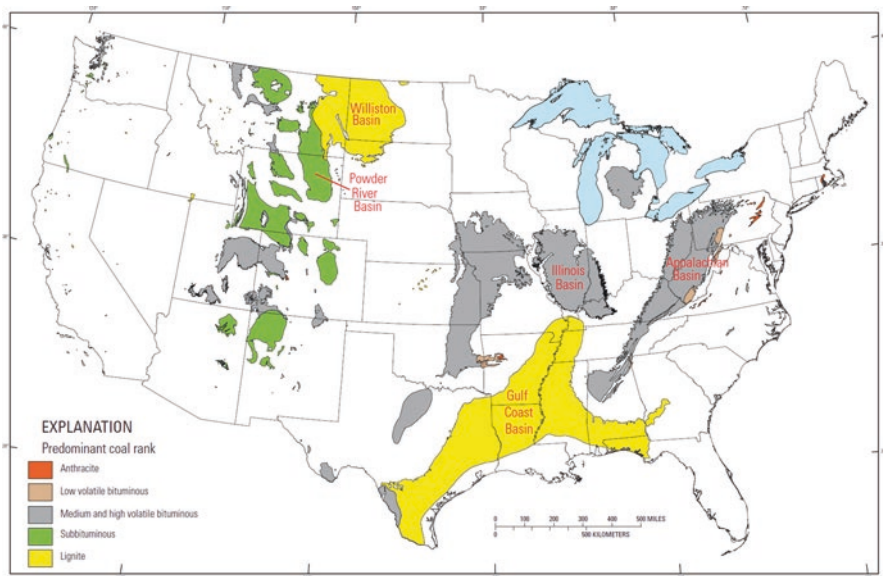
## Within-Bed REE Variation

Localized REE enrichment within coal beds is an area of active research. Where coal beds have been sampled in detail, certain zones show preferential REE enrichment. Examples of such enrichment noted in recent studies include underclays [131–133], coal partings [134, 135], and roof zones [132, 135]. In general, these zones show higher contents of mineral matter which are correlated with increased

REE contents [48, 135]. Underclays and, to some extent, roof material, are of further interest because of their potential for easily recoverable REEs that are ion-adsorbed on clays that are enriched in these zones [136]. Yang et al. [133] reported total REE contents ranging from 235 to 399 ppm for fourteen samples of U.S. Appalachian Basin coalbed underclays from commercial coals. Detailed site-specific characterization of coal beds is needed to take advantage of within-bed REE variation, with selective mining required for the most promising zones.

### 3.4.2 Low-Rank Coals

In the United States, vast low-rank (lignite or subbituminous) coal resources are present in the Powder River Basin of Wyoming and Montana [137], in the Williston Basin of North Dakota [47, 51] and along the Texas Gulf Coast [138] (Fig. 3.3). These low-rank coals generally have lower REE contents than bituminous coals of the Appalachian Basin and the Illinois Basin, which together, are considered Eastern bituminous coals [98]. Despite having lower REE contents, U.S. low-rank coals have raised interest as potential REE resources due to the relative extractability of their REEs compared to Eastern bituminous coals, resulting from a greater proportion of REEs as organic complexes, and for LREEs in acid-soluble mineral forms such as carbonates, sulfates, and some oxides [47, 139].



**Fig. 3.3** Map showing conterminous U.S. coal basins, including location of Appalachian Basin, Illinois Basin, Power River Basin, Williston Basin, and Gulf Coast Basin. (Map is modified after East [140], USGS)

In a nationwide survey comprising 609 samples of U.S. coal and coal combustion products, Zygarlicke et al. [51] sought to identify coal-related materials containing greater than the 300 ppm U.S. DOE interest level for REEs, and compare analytical approaches used in REE determination. The sampling emphasizes Western U.S. coals which are underrepresented in COALQUAL. The study shows that coals containing more than 300 ppm total REE are uncommon but present locally at the top or bottom of coalbeds, even in coals having relatively low REE contents. This study also noted a significantly higher concentration of Y in the Williston Basin of North Dakota compared to other U.S. sample regions. Enrichment in Ge, which associates with organic constituents of coal, has also been reported in some low-rank coals of this region [141, 142]. In some low-rank coals, there is no clear correspondence between ash yield and REE-enriched zones seen in higher rank coals, further indicating organic association of the REEs [51].

Importantly, recent studies have determined that while lower relative REE enrichment found for Powder River Basin coals extends to fly ash derived from these coals [61, 143], so too does greater REE extractability from these ashes [60, 144, 145]. Given the widespread use of Powder River Basin coals in North America and increasingly for export, fly ash from these coals could be a significant resource requiring less pretreatment to release REEs compared to ashes from U.S. Eastern bituminous coals.

### 3.5 Coal Mining and Coal Preparation Wastes

Among solid waste products from coal use, waste from coal mining and coal preparation (waste coal) is second only to coal combustion products in terms of REE enrichment. During coal preparation, major mineral constituents, such as clays, are concentrated in waste coal together with REE-bearing trace minerals such as monazite, xenotime, zircon, and allanite. Concentrating these major and trace constituents in waste coal leads to REE enrichment at or above UCC levels, exceeding that in corresponding raw and prepared coals [40] (Fig. 3.2).

#### 3.5.1 *Pyrite in Coal, Waste Coal*

During coal preparation, sulfide minerals, primarily pyrite ( $\text{FeS}_2$ ), are concentrated in waste coal together with more abundant waste constituents such as clays [40, 146]. Removal of  $\text{FeS}_2$  before it reaches the boiler has beneficial effects in plant operation, as well as reducing the load of sulfur and harmful trace elements captured to meet emissions regulatory standards. A downside of waste coal is that harmful minor constituents in  $\text{FeS}_2$ , such as arsenic (As), Hg and Se, are also concentrated in these wastes [40, 147]. Based on its crystal chemistry,  $\text{FeS}_2$  is not expected to contribute significantly to the proportion of REEs in coal or waste coal

[40, 48, 147, 148]. And while direct determinations of REEs in coal  $\text{FeS}_2$  are limited, several studies have shown that REE contents of  $\text{FeS}_2$  are negligible or less than that of the host coal [149–151], consistent with expected exclusion of REEs from the  $\text{FeS}_2$  structure.

### 3.5.2 *Other Elements of Interest*

Just as REEs are concentrated in waste coal, so are a suite of elements having similar lithophile characteristics, including Li, aluminum (Al), phosphorous (P), titanium (Ti), Sc, rubidium (Rb), zirconium (Zr), niobium (Nb), cesium (Cs), barium (Ba), Hf, Th, and uranium (U), which are present in aluminosilicate mineral matter concentrated in waste coal [40, 48]. Of these, all but P, Th, and U are currently included as U.S. critical minerals [152–154]. Barium is included as the mineral barite. Therefore, if any other critical minerals could be extracted together with the REEs, they may contribute to the economic success of the extraction operation. Kolker et al. [40] found that lithophile elements Rb, Cs (and U) all showed enrichments of five times or greater in the mean of twelve Illinois Basin waste coal samples, relative to the averages for these elements in hard coals [30]. Similar enrichments were found for chromium (Cr) and vanadium (V), which have mixed organic-inorganic associations. There are currently no U.S. mines for Rb or Cs, and they are among the most valued non-REE mineral commodities [155, 156].

## 3.6 Coal-Based Acid-Mine Drainage

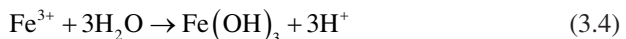
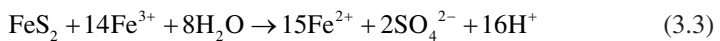
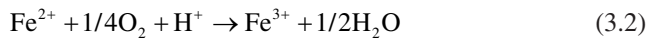
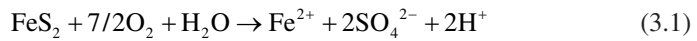
Coal-based acid-mine drainage (AMD) includes waters associated with inactive and abandoned coal mining operations, often characterized by high acidity ( $\text{pH} < 5$ ) and elevated concentrations of sulfate ( $\text{SO}_4$ ) and metals—primarily Fe, but also Al, manganese (Mn), Ca and trace metal(loid)s (e.g., zinc (Zn), nickel (Ni), cobalt (Co), copper (Cu), cadmium (Cd), Hg, As, Se, antimony (Sb), and REE) [149, 157–164]. Due to its acidity and high concentrations of harmful dissolved constituents, AMD is known to cause substantial environmental damage in coal mining regions of the United States [165, 166] and throughout the world [167–170]. There are many commonalities between coal-based AMD and AMD generated at metal mining operations in terms of their generation, geochemical characteristics, and REE contents [157, 171, 172]. Therefore, the discussion presented in this section is highly relevant not only to coal-based AMD but also extends to AMD sourced from mining of massive sulfide deposits [173–175] and other mineralization types such as porphyry Cu-Mo [167], tungsten (W) [176], and oxide-apatite mineralization [177].

Coal-based AMD is generated during weathering of coal mining waste (waste coal or CMW) deposited at operation sites during mining and processing of coal [157, 161, 178, 179]. These materials typically include overburden and underlying

rocks, coal partings, and other high-ash materials that do not meet coal quality specifications for power generation [16, 54]. Additional CMW is generated at coal-mine sites where beneficiation (coal cleaning) approaches such as froth flotation and density separation are used to produce clean coal with higher caloric value and lower contents of S, Hg, and other potentially toxic elements [180].

### 3.6.1 AMD Generation

The most relevant mineral to AMD generation is FeS<sub>2</sub> which is the main sulfide mineral both in coal and in CMW [3, 38, 40]. Other metal sulfides (i.e., sphalerite (ZnS); galena (PbS)) may be present, but in much smaller amounts and their weathering does not contribute to production of acidity [181, 182]. Pyrite, when exposed to water and oxygen at the Earth's surface, produces acidity and dissolved SO<sub>4</sub><sup>2-</sup> and ferrous iron (Fe<sup>2+</sup>), through a series of weathering reactions shown below (3.1–3.3), catalyzed by microorganisms [171, 183, 184]. Microorganisms can further oxidize Fe<sup>2+</sup> to ferric iron (Fe<sup>3+</sup>) which in turn acts as an effective oxidant back-reacting with any residual FeS<sub>2</sub> to produce even more acidity, further increasing Fe and SO<sub>4</sub> in solution [185]. This reinforcing positive feedback mechanism depicted in reactions (3.1–3.3) greatly increases the rate and degree of FeS<sub>2</sub> weathering, thus promoting the formation of acidic drainage [168]. Additional acidity is produced when aqueous Fe<sup>3+</sup> hydrolyzes to ferric hydroxide Fe(OH)<sub>3</sub> (reaction 3.4, [186, 187]) which occurs at higher rates at pH >4 [188–190].



The resulting acidic solutions interact with and increase the weathering of organic and inorganic matter of CMW producing drainage that contains not only high levels of acidity, SO<sub>4</sub> and Fe but also various dissolved metals leached from CMW constituents, including Al, Si, Ca, Mn, Zn, Ni, and the REEs [157, 163]. Once the weathering of FeS<sub>2</sub> mine wastes starts, it is very difficult to control the generation of acidic AMD [151, 178, 191], which can continue for decades and even centuries after mining operations have ceased, degrading water quality, impacting aquatic ecosystems and corroding infrastructure [168, 171]. AMD is generated throughout the world including the U.S. Appalachian Basin [159, 192] and Illinois Basin [163, 193] as well as Canada [194, 195], China [149, 151, 158, 164], Brazil [196], Iran [197], and India [160]. The main control parameters on the forms and the amount of



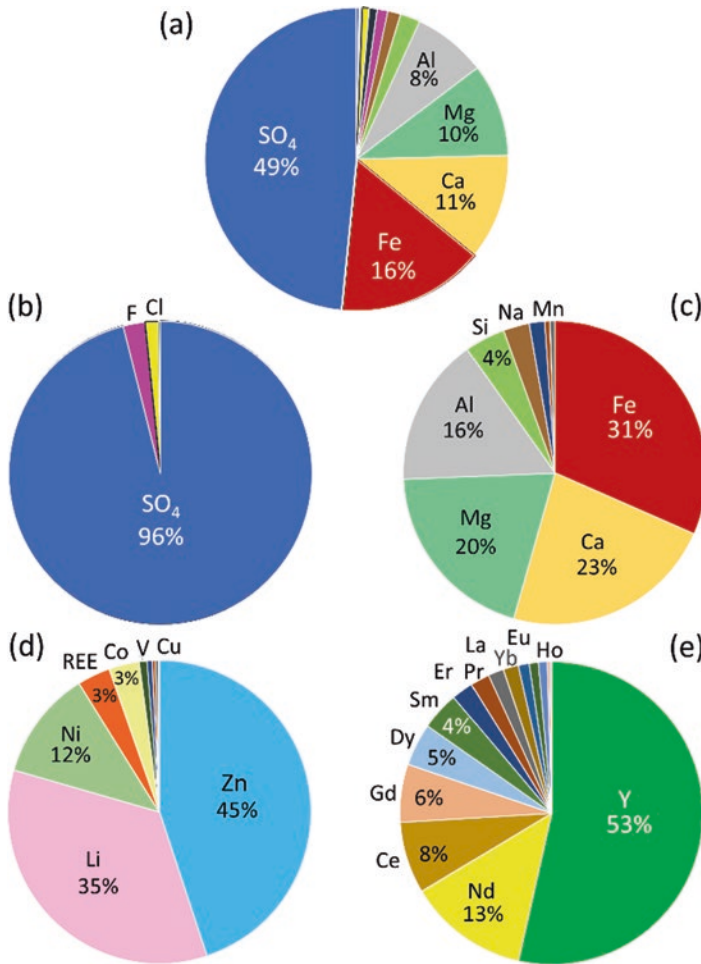
total REEs transported by AMD include the following: (1) hydrologic (i.e., water supply, flow rate), (2) physical (i.e., temperature), and (3) chemical (i.e., pH, redox conditions, chemical composition of AMD), as well as (4) biogeochemical processes. All these parameters interact in a dynamic, complex manner which can vary on daily, seasonal, or annual/multi-annual timescales [168]. Therefore, the concentration patterns of REEs and other metals can exhibit significant changes in space and time within any AMD system [163, 172].

### **3.6.2 Advantages of REE Recovery from AMD**

Although the contents of many economically relevant constituents (i.e., REEs) in AMD are relatively low compared to commercial ores [2] and solids from coal use (described in Sects. 3.3, 3.3.1, 3.3.2, 3.4, 3.4.1, “[Terrigenous REE Enrichment](#)”, “[Tuffaceous REE Enrichment](#)”, “[Hydrothermal REE Enrichment](#)”, “[Infiltrational REE Enrichment](#)”, “[Within-Bed REE Variation](#)”, 3.4.2, and 3.5), there are several advantages to recovering REEs from AMD including: (1) AMD are enriched in critical REEs (Nd, Eu, Tb, Dy, Er, and Y) and other energy relevant elements such as Li, Zn, Ni, Cr, Co, V, and Cd [159, 161, 192, 193] compared to natural water types (ground, ocean, river, and lake water [198]); (2) AMD has very low contents of radionuclides (i.e., U and Th [157, 193]) when compared to traditional REE ore deposits [199, 200]; (3) the elements of economic interest in AMD are already in solution and thus their extraction does not involve additional mining costs [201]; and (4) the extraction and commercialization of these by-products could help cover the cost of AMD treatment [162, 202–204]. Despite the above-mentioned advantages, there are many technical, economic, and environmental problems left to be resolved to fully validate existing extraction technologies [201, 205].

### **3.6.3 Major Constituents of AMD**

AMD geochemistry is exceedingly diverse ranging from highly acidic (pH <3) to circumneutral (pH ~7) and even alkaline (pH >8). Sustained FeS<sub>2</sub> weathering is a common characteristic producing SO<sub>4</sub> and Fe as the two major components of all mine drainages, including coal-based AMD [168] (Fig. 3.4a). Sulfate is the dominant negatively charged ion (anion), typically >90%, followed by chloride (Cl<sup>-</sup>), fluoride (F<sup>-</sup>), phosphate (PO<sub>4</sub><sup>3-</sup>), and, potentially, bicarbonate (HCO<sub>3</sub><sup>-</sup>) in AMD with pH >4.5 (Fig. 3.4b). Iron is the prevalent positively charged ion (cation) followed by other major cations (i.e., Al, Ca, Mn, silicon (Si) and trace metals) (Fig. 3.4c). The identity and concentrations of trace metals (i.e., Zn, Li, As, Cu, Ni, Co, lead (Pb), Cd, Se, Hg) (Fig. 3.4d), including REEs (Fig. 3.4e), vary widely and are mostly controlled by the chemical and mineralogical constituents of weathering CMW [172].



**Fig. 3.4** Molal fraction distribution of (a) total ions, (b) major anion, (c) major cation, (d) trace metals, and (e) REEs in a typical AMD drainage sample from Tab Simco (main seep; sample SIU 5 in Lefticariu et al. [193] U.S. Illinois Basin). The molal fraction is defined here as the amount of a constituent (expressed in moles) divided by the total amount of all constituents (expressed in moles) in solution

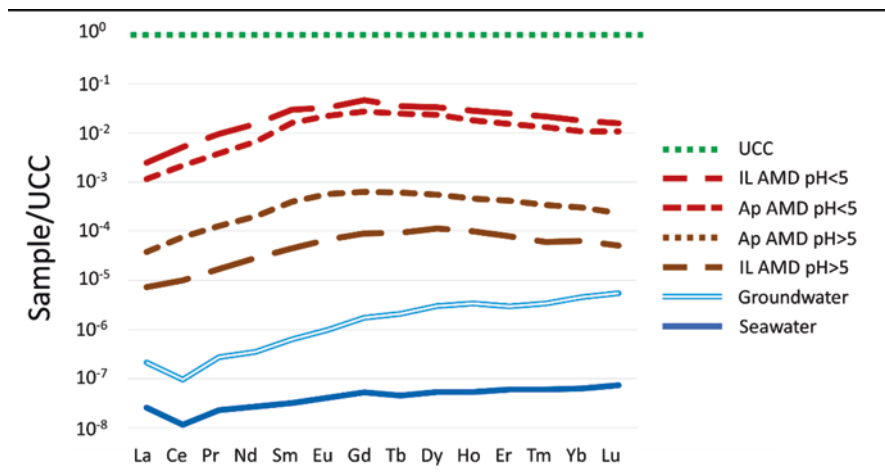
In general, the most highly acidic AMD ( $\text{pH} < 5$ ) has a substantially higher load of dissolved constituents than less acidic AMD ( $\text{pH} > 5$ ) [159, 164, 172, 193, 205], indicating that acidic waters react more vigorously with CMW materials producing more ions in solution [185]. Conversely, as  $\text{pH}$  increases to values  $> 5$ , precipitation of solid phases from solution significantly decreases the AMD ion load [188, 194, 195]. Beyond this, the proportions of dissolved constituents in AMD depend on many parameters that do not correlate with  $\text{pH}$ , but rather with the overall composition of the weathering bedrock and/or CMW materials, as well as the treatment approaches applied to an AMD system such as addition of alkalinity producing

materials, bioreactors, etc. [172, 193]. Notably, geochemical surveys of AMD in the Appalachian Basin [157, 159, 161, 162], Illinois Basin [163, 193], or Guizhou Province of China [151, 164] have shown that basin-wide, AMD exhibits diverse geochemical attributes in terms of total load and the contents of major and trace elements, including REEs. The inherently wide range and site-specific geochemical attributes of AMD can significantly impact the type and efficiency of technologies designed for both AMD remediation [159, 163, 166, 206] or secondary resource recovery [175, 192, 201, 205, 207]. While many of the main AMD constituents are major contaminants in the environment [157, 208], some of these potentially have economic value and new technologies are being developed for their recovery and commercialization [192, 201].

### 3.6.4 Rare Earth Elements in AMD

Knowledge of the behavior of REEs in solution is needed to understand the REE distribution in AMD and geochemical processes for their extraction. This topic is primarily covered elsewhere [209–216]. And while REEs are defined to include Y and Sc, few AMD studies measure Y and almost none have determined Sc, so the subsequent discussion applies mostly to the lanthanides. Nonetheless, recent work suggests Y is the chief REE in AMD, comprising 20–50% of total REE content, followed by Nd, Ce, Gd, Dy, and Sm (Fig. 3.4e). Critical REEs, with Y and Nd being the two most abundant, are also enriched in AMD as they account on average for >50% of total REEs, with reported values up to 70% [159, 164, 179, 193]. This enrichment is a remarkable feature of AMD as the fraction of critical REEs in most AMD is substantially higher than that reported in coal (typically <30%) and CMW materials (typically <40%) [179] or conventional REE ores, such as those dominated by bastnäsite (typically <15%) [2, 199].

Concentrations of lanthanide REEs in AMD, expressed in moles per liter (mol/L), span over four orders of magnitude ( $10^{-3}$ – $10^{-7}$  mol/L) reflecting the geochemical diversity of AMD [149, 151, 157, 159–161, 164, 193, 217]. These values are several orders of magnitude higher than those for most continental waters (i.e., rivers, lakes, and groundwaters) and seawater ( $10^{-6}$ – $10^{-9}$  mol/L) [198] due to the low solubility of REEs in neutral and alkaline waters [218]. Rainwater is the primary carrier of the AMD dissolved load. The average REE concentration in rainwater ( $<10^{-10}$  mol/L) is substantially lower than that of a typical AMD [219, 220], making its contribution to the AMD ion load trivial. Acidity is the key controlling parameter on the REE load, such as the acidic (pH  $\leq 5$ ) drainages have the highest REE contents (Fig. 3.5). The main source of REEs in AMD is REE-bearing parts of the weathering CMW, including organic matter (i.e., coal macerals) and REE-bearing minerals [3, 16, 48, 49, 73, 116, 217, 221]. Weathering of REE-enriched CMW materials [16, 78] can also contribute to higher REE contents in AMD, regardless of the solution pH [159, 193]. The contents of total REEs and many trace metals (i.e., Zn, Ni, Co, Li) are often correlated, supporting the idea that acidic, metal-rich AMD holds potential for recovering multiple constituents.



**Fig. 3.5** Rare earth element patterns of coal-mine drainage (AMD) from the U.S. Appalachian Basin (Ap) and Illinois Basin (IL) normalized to UCC. Average REE concentration values in AMD with low (pH <5) and high (pH >5) values from Lefticariu et al. [193] for the U.S. Illinois Basin, and Stewart et al. [159] and Hedin et al. [205] for the U.S. Appalachian Basin. Except for the lowest concentration samples, most AMD exhibits MREE enrichment. Low-pH samples tend to have higher total REE concentrations than high pH samples. Median total REE concentrations of seawater and groundwater samples are from Noack et al. [198] These waters display a characteristic Ce and LREE depletion and a distinct HREE enrichment. Upper Continental Crust Reference (UCC; Taylor and McLennan [25, 26] and McLennan [27])

A compilation from several AMD sites shows that total REE contents in AMD with pH  $\leq 5$  range from 23.4 to 9879.2 micrograms per liter ( $\mu\text{g/L}$ ; equivalent to parts per billion in solids), with a median value of 750  $\mu\text{g/L}$  [151, 159, 161, 164, 193, 197, 217]. In contrast, the aforementioned studies also found that in circum-neutral and alkaline AMD, total REE contents were consistently less than 50  $\mu\text{g/L}$ . This bimodal distribution of REE contents in AMD is due to: (1) pH-dependent weathering capacity of AMD [159, 193] and (2) limited REE mobility in solutions with neutral or alkaline pH values, where REEs are often sequestered in solids by sorption on or coprecipitation with Fe, Al, Ca, and Mn phases and clay minerals [170, 194, 195, 222, 223].

### Dissolved Versus Particulate REEs

A significant fraction of the total REEs carried in AMD is in fine suspended particles including colloids that can partition the REEs between a truly dissolved fraction and the solid phases [224–226]. The suspended or colloidal phases may include common REE-bearing minerals of the weathering CMW (i.e., apatite, monazite, clay minerals, zircon) as well as the newly formed Fe-, Al- and/or Mn-colloidal phases onto which REE can adsorb or coprecipitate [162, 205, 213, 217].

## MREE Enrichment

Aside from their total amount, REE patterns in mine drainages often exhibit a distinctive convex curvature (on a plot of lanthanide REE vs. abundance) indicative of an enrichment in MREE (including Nd) with respect to both LREE and HREE, in relation to crustal averages, such as UCC (Fig. 3.5) [218, 223, 224, 227, 228]. The distinctive MREE enrichment of AMD [149, 159, 160, 164, 193, 229] is still not fully explained and may be related to multiple processes in the aquatic environment [167, 218, 230, 231]. Even though MREE enrichment has been described in many low-pH settings [200, 223, 232], it is not exclusive to acidic environments, having also been noted in some river systems [233].

### 3.6.5 AMD Treatment Approaches

Effective treatment approaches are required to address the environmental impacts of AMD, often at high costs [166, 234–236]. Recently, it has been suggested that AMD as well as precipitates and treatment waste produced in AMD systems represent a promising secondary economic resource for metals, especially for certain critical elements such as REEs [174, 192, 204, 205, 222, 229]. In terms of remediation approaches, two main categories have been widely utilized to treat AMD, namely (1) active and (2) passive treatment technologies [234, 237].

#### Active Treatment Approaches

Active treatment technologies are often employed where large amounts of AMD are generated. These technologies involve the addition of chemicals (i.e., soda ash or sodium carbonate ( $\text{Na}_2\text{CO}_3$ ), hydrated lime or calcium hydroxide ( $\text{Ca}(\text{OH})_2$ ), quicklime or calcium oxide ( $\text{CaO}$ ), caustic soda or sodium hydroxide ( $\text{NaOH}$ ), and hydrogen peroxide ( $\text{H}_2\text{O}_2$ ) [238]), in conjunction with other approaches such as reverse osmosis, evaporation, ion exchange, and magnetic separation [239]. During treatment, as AMD acidity is neutralized, the dissolved metals are oxidized and/or hydrolyzed promoting precipitation of Fe, Al, and Mn minerals such as gypsum, calcite, and dolomite. The resulting sludge accumulates in settling ponds containing a mixture of metal precipitates and unreacted caustic agents or mechanical clarifiers. To limit sludge build-up, the ponds need to be cleaned regularly. Active systems are expensive to set up and operate and require safe disposal of treatment sludge which contain large quantities of toxic metals [237]. Due to the large volume of AMD precipitates and added chemicals, the overall REE concentration in the final sludge is inconsequential.

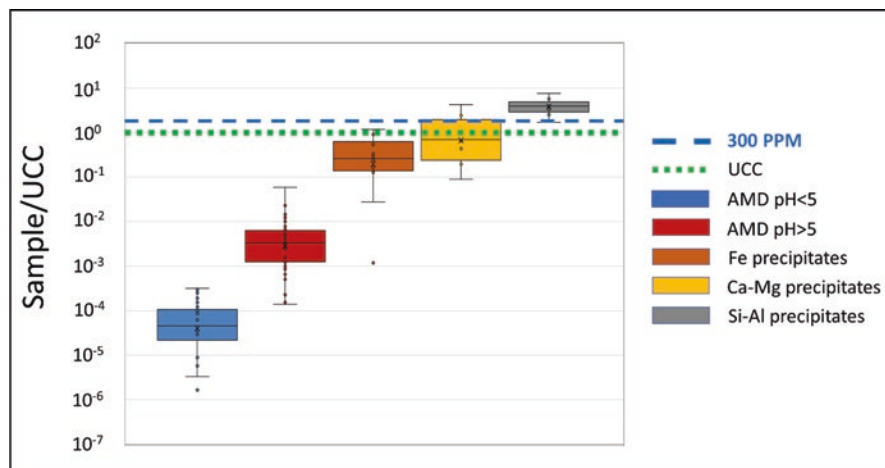
## Passive Treatment Approaches

Passive remediation technologies rely on gravity flow and biogeochemical processes for AMD treatment [163, 237, 240]. Their distinguishing feature is the use of biological treatments based on enhancing the activity of selected microbial communities in order to generate alkalinity and promote reduction of sulfate and ferric iron with subsequent precipitation of sulfide minerals. Most of the anaerobic reductive metabolisms are alkali-generating and thus promote precipitation of solids [163]. Such systems have been applied both *ex situ* (i.e., passive compost bioreactors, active sulfidogenic reactors) and *in situ* (i.e., permeable reactive barriers, anaerobic wetlands) [171, 236, 238]. In the United States, due to a wide range of AMD chemistry and local conditions, various site-specific passive remediation systems have been built and operated [205, 235, 236]. Even though the current passive remediation systems are low-cost alternatives to active systems, they have lower removal efficiency and limited metal recovery potential and are unable to provide long-term treatment of drainage with high acidity (>1000 mg/L) and elevated Al contents (>200 mg/L) [163, 206, 241]. Nonetheless, the passive remediation technologies are intrinsically flexible and can be optimized for enhanced metal recovery by including selective precipitation steps using chemical controls designed to separate precipitates based on their uptake capacity for REEs and other metals of economic interest [201].

### 3.6.6 REE in AMD Precipitates

The mobility of REEs and other chemical constituents in AMD, AMD-impacted environments, and AMD treatment systems is strongly affected by the precipitation of solid phases [162, 205, 206]. By comparison, the REE contents of AMD precipitates are orders of magnitude higher than those of AMD (Fig. 3.6), with reported enrichments in total REEs up to ~1000 mg/kg (~1000 ppm) [159, 162]. Moreover, a USGS database comprising REE contents of sludge from 233 U.S. AMD sites revealed that at 46% of the surveyed AMD sites, the sludge contained >300 mg/kg of REEs (corresponding to 0.036% REO), while 31% contained >1 g/kg (corresponding to 0.12% REO) [192]. Existing technologies can sequester >90% of REEs from AMD and concentrate them by a factor of  $10^3$ – $10^4$  in the solid precipitates [179, 201]. Furthermore, estimates indicate that up to  $5 \times 10^5$  kg of REEs could be recovered annually from Appalachian AMD alone [159]. Together these data strongly support the idea that AMD precipitates can become a promising secondary source of REEs [159, 174, 192, 242].

While precipitation of solids occurs naturally in any AMD system as a result of pH adjustments either due to mixing or neutralization [172, 188], extensive precipitation is restricted to AMD treatment when decreased acidity promotes partitioning of the dissolved load into solid precipitates [234]. Detailed knowledge of the minerals present in AMD precipitates is central to understanding REE uptake



**Fig. 3.6** UCC-normalized ranges of total REE concentration values in AMD and AMD precipitates. Upper Continental Crust reference (UCC; Taylor and McLennan [25, 26] and McLennan [27]); REE concentration values in AMD from Leticariu et al. [193], U.S. Illinois Basin; and Stewart et al. [159] and Hedin et al. [205], U.S. Appalachian Basin; REE concentration values in Fe, Ca-Mg, and Si-Al precipitates from Hedin et al. [205]

mechanisms and in designing technologies that maximize REE recovery. Modern laboratory characterization techniques (i.e., X-ray diffraction (XRD), scanning electron microscopy (SEM), transmission electron microscopy (TEM), and synchrotron X-ray absorption spectroscopy (XAS)) provide valuable information on the structure and composition of AMD precipitates, as well as the mechanisms by which REEs can become attached to mineral surfaces [222, 243]. In all cases, precipitates from AMD are complex mixtures of nanophases (materials at the nanometer scale) of diverse mineralogy and variable crystallinity, ranging from amorphous (having no ordered atomic structure), to short-range atomic order and crystalline (fully ordered) phases [206]. Based on their main element chemistry, the AMD precipitates can be subdivided into Fe, Al, Ca, and Mn groups [205], as discussed below.

The Fe<sup>3+</sup>-rich phases which in coal mining-impacted areas form yellow-red-brown ferruginous deposits, include sulfates and oxyhydroxides with various degrees of crystallinity. The most common forms are schwertmannite (ideal formula Fe<sub>8</sub>O<sub>8</sub>(OH)<sub>6</sub>SO<sub>4</sub>) [244], goethite ( $\alpha$ -FeOOH), lepidocrocite ( $\gamma$ -FeOOH), ferrihydrite, Fe(OH)<sub>3</sub>·0.5H<sub>2</sub>O, and jarosite (e.g., KFe<sub>3</sub>(SO<sub>4</sub>)<sub>2</sub>(OH)<sub>6</sub> [188, 206]). The formation of Fe precipitates occurs over a wide range of pH values from highly acidic (i.e., jarosite) to circumneutral (i.e., ferrihydrite) and their mineralogy and/or crystallinity often changes over time [245]. Fe<sup>3+</sup>-rich phases dominate the mineralogy of any AMD system, with schwertmannite and goethite being the prevalent solid precipitates in limestone drains, settling ponds, and neutralization sludge in AMD treatment systems [206].

Aluminum-rich AMD typically produces a milky-white precipitate comprised of a mixture of poorly crystalline basaluminite (Al<sub>4</sub>(SO<sub>4</sub>)(OH)<sub>10</sub>·5H<sub>2</sub>O) [188, 222] and

amorphous  $\text{Al}(\text{OH})_3$  [208], which can easily recrystallize to gibbsite ( $\gamma\text{-Al}(\text{OH})_3$ ) or boehmite ( $\gamma\text{-AlO}(\text{OH})$ ) depending on pH and/or temperature [246]. Precipitation of Al-rich phases can occur only in AMD systems with  $\text{pH} \geq 5$ , as in solutions with a  $\text{pH} < 5$ , the dissolved Al remains in solution [188].

Calcium and magnesium sulfates and carbonates are less common in untreated AMD systems because low-pH conditions are less favorable for their precipitation [247]. Commonly, these precipitates are found in both passive and active remediation systems and are generated where pH is adjusted to higher values by addition of lime and/or carbonates producing neutral to alkaline solutions from which Ca- and Mg-rich sludge/slurries and/or Ca- and Mg-rich sulfate minerals (i.e., gypsum ( $\text{CaSO}_4 \cdot 2\text{H}_2\text{O}$ ); hexahydrate ( $\text{MgSO}_4 \cdot 6\text{H}_2\text{O}$ )) are precipitated [205, 234].

Manganese-rich AMD is a significant environmental problem for both operating and abandoned coal mines across the United States and globally [248]. Removal of Mn from acidic AMD is challenging and special treatments are required for successful Mn removal which include: (1) active remediation systems where NaOH is added to raise the pH to  $\sim 8\text{--}10$  and promote the abiotic (without microbial) oxidation of  $\text{Mn}^{2+}$  in solution in AMD to precipitate Mn as  $\text{Mn}^{3+}/\text{Mn}^{4+}$  (oxyhydr)oxides or (2) passive remediation systems under circumneutral pH conditions, where  $\text{Mn}^{2+}$  can be oxidized by microbes, or by a catalyst that promotes oxidation on surfaces, followed by precipitation of phyllophanates (e.g., birnessite ( $(\text{Na},\text{Ca})\text{Mn}_7\text{O}_{14}$ ); and todorokite ( $(\text{Ca},\text{Na},\text{K})\cdot\text{Mn}_6\text{O}_{12}$ )) [248, 249].

Laboratory experiments of sorption (the process by which REEs become attached to) and coprecipitation of REEs onto solid precipitates associated with mine drainage systems have demonstrated that: (1) these precipitates (i.e., ferric and manganese oxides/hydroxides, schwertmannite, and basaluminite) have a high capacity for sequestering REEs from solution: [170, 216, 222–224]; (2) pH strongly controls the mobility of REEs such that at  $\text{pH} < 4$ , REEs preferentially remain in solution, but at  $\text{pH} > 4$  become sequestered by solid precipitates, with significant REE uptake occurring at pH values between 5 and 7 [170, 216, 222]; (3) higher sulfate concentrations in solution were noted to increase the REE sequestration in basaluminite [170, 222]; and (4) HREEs were preferentially partitioned into the solid phase compared to LREEs [170, 222]. These results are encouraging as they demonstrate that under laboratory-controlled conditions, REEs could be entirely recovered from AMD by selective precipitation in treatment plants [179, 201].

Field studies have largely confirmed the results of laboratory experiments emphasizing the high capacity of AMD precipitates to sequester REEs. However, under field conditions the REE sequestration capacity was found to be controlled by mineralogy, with field studies reporting a direct correlation between the REE and Al contents in mine drainage precipitates [175, 205]. Specifically, recent field studies of passive remediation systems in the Appalachian Basin have highlighted the wide range of REE contents of AMD precipitates (Fig. 3.6) with average concentration values of 50 mg/kg for Fe precipitates, 120 mg/kg for Ca-Mg precipitates, and 670 mg/kg for Al-Si precipitates [159, 161, 205]. These results suggest that under field conditions, REE sequestration capacity of AMD precipitates might exclusively depend on their mineralogy and less so on local environmental conditions.



Aside from these observations, there is little research on the mineralogy of AMD precipitates at the nanometer scale, or on the specific uptake mechanisms of REEs by various types of precipitates. Consequently, the ability to forecast REE uptake to optimize technological processes for cost-effective recovery is limited. Research in the last several decades has shown that a range of chemical, physical, hydrologic, and mineralogical controls govern the partitioning of the AMD chemical load between solution and solid precipitates [161, 223, 224, 248, 250]. Sorting out the relative importance of these processes under environmentally relevant conditions remains a challenge in optimizing REE uptake from AMD [188, 205, 222].

### 3.7 Economic Implications

For economic analysis of the potential production of REEs, classifications that account for market conditions and trends are preferred to classifications based on physical criteria. But as market conditions change over time, these classifications can also change while classifications based on physical criteria are more likely to remain constant. Based on market conditions at the time, Seredin and Dai [38] classified REEs as either critical (CREEs), non-critical or in excessive supply, and their scheme resulted in Nd, Eu, Tb, Dy, Y, and Er being classified as critical. The DOE Critical Materials strategy [251], Luttrell et al. [252] and Zhang et al. [22] have considered just the first five of these (Nd, Eu, Tb, Dy, and Y) to be CREEs. Owing to its high price relative to other REEs [31, 253], Sc could also be considered a CREE. The total rare earth oxide (REO) content of coal could be less than 0.1% [254]. However, Franus et al. [59] found the average percentage of CREEs in the total estimated REE content of coal samples from nine coal mines in Poland to be about 30% and others have estimated that the proportion of CREEs in the total REE content of coal could be as high as 40%. Thus, despite the very low overall concentration of REEs in coal, there is still economic interest in coal and coal combustion products because the distribution of REEs in coal could be more heavily oriented toward higher-value CREEs (including Sc) than in many conventional REE deposits [254, 255].

#### 3.7.1 *Critical Rare Earths Versus Critical Minerals*

Readers are reminded here that designation of certain REEs as “critical” in the classification of Seredin and Dai [38] is not the same as the U.S. Government designation of rare earths as Critical Minerals (CMs) under Executive Order No. 13817 [152]. The CM list identifies mineral commodities that are essential to the economy or national security of the United States and serve essential functions but are vulnerable to disruption in supply. In the initial draft list of thirty-three individual CMs, REEs are one of two additional included mineral groups (platinum group metals being the other group). In recent updates to the CMs list [153, 154], the rare earths are included individually, with Nd, Dy, Pr, Ce, La, and Y, among the highest in overall supply risk.

### 3.7.2 Coal Ash

Existing sources of coal fly ash could provide a total volume of REEs that is at least comparable to U.S. demand [252]. The processing cost of extracting REEs from coal ash could be significantly greater than the value of the REOs (a marketable form of rare earth mineral commodities) produced. Still, reprocessing of coal ash just to produce REEs might be considered economic in some cases where the distribution of REEs is heavily oriented toward critical and high-value minerals. Das et al. [253] found that Sc could account for up to 90% of the total value of the REEs produced from coal ash.

The Ellen MacArthur Foundation [256] has defined the circular economy as “*an industrial system that is restorative or regenerative by intention and design.*” With respect to (coal) mining, consideration of the circular economy would include evaluating the full costs and benefits of mine waste reprocessing activities [257]. In many cases, the circular economy will need to be evaluated to assess the full potential feasibility of the secondary REE production project, and the project owner–operator may need to have a reasonable expectation regarding the feasibility of monetizing the benefits of any land reclamation, restoration of ecosystem services, and other public benefits of remediating surface piles and other repositories of coal ash before deciding to invest in the project (Table 3.3).

Post-combustion coal ash can have as much as 10 times the concentration of REEs as in the source coal [258] and well above the 300 ppm REE content suggested by the U.S. Department of Energy [72] as necessary to be of interest. The enriched content of REEs overall combined with the potentially higher proportion of CREEs could imply that the value of production of REOs from coal ash could be significantly higher per volume than that from conventional REE deposits. In addition, at least partially owing to high energy and grinding costs, processing of mine output of conventional REE mines to produce REOs can be extremely expensive, but coal fly ash is already in a fine powder form that could allow REE extraction and processing at substantially lower cost [258, 259]. Finally, the particles from the residual ash material after extraction of the REEs could still be used to produce a value-added product salable to industry, including for utilization in the manufacture of cement [258].

### 3.7.3 Waste Coal

Waste coal is not as enriched in REE content as post-combustion coal ash, and its level of enrichment may not be likely to meet the U.S. Department of Energy’s minimum 300 ppm level to be of interest [72]. Thus, the economic feasibility of producing REEs from waste coal could depend more on the feasibility of production of other mineral commodities (including critical minerals such as Li) as by-products. As with coal ash, the potential owner–operator may need to be able to monetize

**Table 3.3** Summary of potential economic considerations associated with producing rare earth elements (REEs) from coal ash or coal-based acid-mine drainage (AMD)

Revenue considerations	Cost considerations	Circular economic considerations
<i>Coal combustion fly ash</i>		
<ul style="list-style-type: none"> <li>• 270–1500 ppm REE in fly ash [253]</li> <li>• Could be about 10 times higher concentration of REEs in fly ash than in coal</li> <li>• Higher proportion of critical REEs (including Nd and Sc) in total REE content than in many conventional REE deposits [253]</li> <li>• 20 coal preparation plants could produce &gt;10,000 t/yr of REE, which is about equal to U.S. demand [242]</li> <li>• Residual ash (post-REE extraction) still marketable to industry (e.g., cement)</li> <li>• Carbon dioxide (CO<sub>2</sub>) mineralization could enhance recovery of REEs from leachate of coal ash</li> </ul>	<ul style="list-style-type: none"> <li>• No costs for in situ characterization of REEs</li> <li>• In fine powder form, eliminating grinding costs and reducing energy costs relative to typical REE processing</li> <li>• Lower concentrations of radionuclides mean lower costs of separation and disposal than for processing conventional REE mine output</li> <li>• CO<sub>2</sub> mineralization could reduce chemical costs compared with just using hydroxides (NaOH) in REE precipitation processes</li> <li>• If captured CO<sub>2</sub> is used, the REE recovery project could possibly qualify for 45Q income tax credits</li> <li>• The processing costs could be independent of the distribution of contained REEs, and the profitability is almost entirely dependent on the proportion of critical (high value) relative to non-critical REEs</li> </ul>	<ul style="list-style-type: none"> <li>• Reclamation of land</li> <li>• Possible restoration of ecosystem services</li> <li>• Mitigation and potential elimination of legacy environmental issues</li> <li>• Valuation of the environmental benefits may rely on public perception of risks, but it could also help gain public acceptance</li> <li>• If captured CO<sub>2</sub> is used to increase precipitation of REE from coal ash leachate, then mitigation of CO<sub>2</sub> emissions to the atmosphere and associated risks is an additional (unaccounted for) benefit</li> </ul>

(continued)

**Table 3.3** (continued)

Revenue considerations	Cost considerations	Circular economic considerations
<i>Acid-mine drainage (AMD)</i>		
<ul style="list-style-type: none"> <li>• Conventional treatment of AMD can enrich the REE concentration in the residual sludge several thousand times</li> <li>• Vass et al. [162] found an average REE concentration of about 700 ppm in residual sludge left after treatment of AMD in the Appalachian Basin</li> <li>• Productivity of treatment of AMD in the Appalachian Basin could range from 771 to 3400 t/yr REE [161]</li> <li>• Distribution of REEs in AMD is toward a greater proportion of critical REEs than in conventional REE ore deposits [22]</li> <li>• Adding CO<sub>2</sub> mineralization to the process could increase recovery of REEs to 85% compared with 70% if just using NaOH and other hydroxides [260]</li> </ul>	<ul style="list-style-type: none"> <li>• Capital costs for AMD treatment systems at scale could range up into the millions of dollars [159]</li> <li>• Even if not profitable to just produce REEs, public funding to remediate AMD could be used to offset the costs</li> <li>• The Clean Water Act requires treatment, and state reclamation funds could be available to remediate AMD</li> <li>• Incorporating CO<sub>2</sub> could reduce total chemical cost compared with just using hydroxide to precipitate REEs [260]</li> <li>• If captured CO<sub>2</sub> is used, project costs could be offset by any 45Q income tax credits that the owner operator might qualify for</li> <li>• AMD treatment cost could be independent of the distribution of contained REEs, and the profitability is almost entirely dependent on the proportion of critical (high value) relative to non-critical REEs</li> </ul>	<ul style="list-style-type: none"> <li>• Natural processes can perpetually produce AMD and associated environmental damage. Treating AMD may limit environmental damage but not eliminate it.</li> <li>• Non-market valuation techniques could be used to assess any mitigation of the environmental hazard associated with REE extraction from AMD. However, these valuation techniques are not consistent with the (market-based) valuation of the REE output, and such estimates of the potential remediation value cannot be simply added to the value of REE production to obtain a total value of the project.</li> <li>• Valuation of the environmental benefits could help gain public acceptance of the project</li> <li>• If captured CO<sub>2</sub> is used to increase AMD precipitation of REE, then mitigation of CO<sub>2</sub> emissions to the atmosphere could be an additional (unaccounted for) benefit</li> </ul>

*t* metric ton, *CO*<sub>2</sub> carbon dioxide, *yr* year, *ppm* parts per million, *NaOH* sodium hydroxide, *REE* rare earth element, *REO* rare earth oxide

public benefits associated with the circular economy before considering that there could be sufficient incentives to invest in a project to remediate waste coal piles and extract the REE content. Nonetheless, recovery of REEs from waste coal has shown promise at the pilot scale [22, 179, 261–263]. While REE contents could be below DOE interest levels, advantages of waste coal include: (1) the most REE-enriched portions of coal beds are removed and concentrated in waste coal; (2) detailed characterization and selective mining of the most REE-enriched portions of coals in situ are not required.

### 3.7.4 *Acid-Mine Drainage*

In general, REEs are not as concentrated in AMD as in fly ash or waste coal, and the AMD processing costs could be prohibitive if the only purpose is to produce REOs [159]. However, treatment of AMD is required under section 402 of the U.S. Clean Water Act [161, 264], and there are already-existing programs and public funding to treat AMD to mitigate the environmental impacts even without considering the potential REE recovery. Treatment of AMD to address the environmental liability could increase the overall concentration of REEs in the post-treatment sludge to around 700 ppm or possibly far higher in some cases [162]. Based on sampling from twenty-two sites in Pennsylvania, Stewart et al. [159] estimated that about 540 t/yr REEs could be contained in flows of coal-mine AMD, and Vass et al. [161] estimated that about 800 t/yr (or even greater annual tonnages) of REEs could be contained in the flow of over 1100 AMD sources in the Appalachian Basin. Similar to recovery of REEs from coal ash, the production of REOs from coal-mine AMD could be of higher value per ton produced than that from conventional REE deposits owing to the potentially higher proportion of CREEs in the total REE content (Table 3.3). Although water produced because of (legally required) treatment of AMD would be produced whether REEs are extracted from the residual sludge or not, the revenue from any sales of this water for industrial or possibly agricultural use could be considered as value added to the production of the REEs [260].

### 3.7.5 *REE Recovery and CO<sub>2</sub> Capture and Utilization*

Hassas et al. [260] found that utilization of CO<sub>2</sub> in a multi-stage precipitation process could increase the recovery of REEs in AMD to 85% from about 70% if sodium hydroxide (NaOH) or other hydroxide-based chemicals were used to control pH. In addition, they found that utilization of CO<sub>2</sub> in the process would likely reduce chemical costs. If this potential utilization of CO<sub>2</sub> were able to meet the criteria to qualify for the U.S. 45Q income tax credit, this could add significant value to a project to recover REEs from AMD. However, the CO<sub>2</sub> used in this REE production process would have to be captured from the process emissions, a minimum of 100,000 t/yr of captured CO<sub>2</sub> would have to be utilized, and all the CO<sub>2</sub> would have to meet stringent criteria to be considered permanently “sequestered” [265]. Studies of the potential utilization of the CO<sub>2</sub> mineralization process to enhance the recovery of REEs from the leachate of solid forms of coal-related waste (such as fly ash or waste coal) are not available. If the CO<sub>2</sub> mineralization process could be integrated into REE recovery from the leachate of other coal waste materials in a manner analogous to that proposed by Hassas et al. [260] for AMD, then similar production efficiency and cost considerations could apply.

### ***3.7.6 Benefit from Remediation of Coal-Related Liabilities***

In addition to producing valuable mineral commodities (possibly including several critical minerals and water) as by-products of the production of REEs from coal-mine waste streams, it could be necessary to account for the benefits of remediation of these coal-related environmental liabilities in order to accurately assess the total net value of such projects and whether they are economic. Owing to the lower REE enrichment level in waste coal than in coal ash, and possibly to less public interest and available funding to remediate waste coal repositories than AMD, a project to produce REEs from waste coal may not appear as beneficial in comparison. However, accounting for the circular economic benefits of remediating coal and coal combustion wastes would add value to any of these secondary REE recovery projects, and this could help incentivize investment if the project owner/operator can monetize those benefits.

### ***3.7.7 Role in a Circular Economy***

Approaches to quantifying the circular economy of mineral and energy resources have been applied almost entirely to post-consumption recycling and not to reprocessing of primary mineral and energy waste streams and repositories, such as mine waste piles, tailings, and produced waters [257]. Non-market methods to quantify the value of remediating these primary waste streams are inconsistent with the market-based valuation of the expected production of REEs and other expected benefits and costs of these projects, and the environmental benefits could be ignored in any investment decision. Despite this difficulty, some comparisons could be made regarding the circular economy of recovery of REEs from different coal-related waste streams. As waste coal and coal ash take up space on the surface, the value of any land reclaimed and possible restoration of ecosystem services during the reprocessing of these waste piles to recover REEs could potentially be added to the value of the project. These circular economic benefits might not be as applicable to production of REEs from AMD, because there might not be as much reclamation of land or restoration of ecosystem services during that process. On the other hand, treatment of AMD will convert some contaminated water into a resource that could be used in some industrial or agricultural applications. In addition, quantification of the circular economic benefits could be helpful in gaining public acceptance for a project to recover REEs from coal-related waste materials [6].

## **3.8 Summary**

Four coal-related sources show promise for recovery of REEs and associated elements, including fly ash, waste coal, coal itself, and coal acid-mine drainage. Of these, fly ash, especially that derived from combustion of bituminous coals, shows

the greatest REE enrichment. However, extraction of REEs from bituminous coal fly ash generally requires initial chemical or physical treatment to improve REE recovery, which can add to the cost of producing REEs from this material [22]. Fly ash from lower rank (lignite and subbituminous) coals is generally less REE-enriched, but more extractable, potentially allowing REE recovery without pretreatment. The same (less enriched, more extractable) applies to low-rank coals from which these ashes are derived. Among solids from coal use, waste coal is the next-most REE-enriched source, after fly ash, as the most REE-enriched horizons from coals being mined are concentrated in waste coal. REE recovery from waste coal has shown promise at the pilot scale in multistep procedures. Compared to waste coals, recovery of REEs from coal resources requires more extensive characterization to delineate the most REE-enriched horizons prior to mining.

In coal-based AMD, REEs are present in a dissolved or colloidal form, at lower concentrations than in any of the coal-associated solids. But REEs from AMD become concentrated to levels of interest in precipitates from AMD solutions. Which of these sources proves to be most favorable for REE recovery depends on a wide range of factors, including not only REE concentration, extractability, and primary costs, but also associated benefits such as remediation of coal-related environmental liabilities and possible co-recovery of non-REE critical elements. The landscape of resource recovery from these sources is rapidly evolving as the need to support current and projected use of REEs grows.

## References

1. U.S. Geological Survey, The rare earth elements – vital to modern technologies and lifestyles: U.S. Geological Survey Fact Sheet 2014–3078 (2014), 4 p. <https://pubs.usgs.gov/fs/2014/3078/>
2. B.S. Van Gosen, P.L. Verplanck, R.R. Seal II, K.R. Long, J. Gambogi, Rare earth elements, Chapter O, in *Critical Mineral Resources of the United States—Economic and Environmental Geology and Prospects for Future Supply: U.S. Geological Survey Professional Paper 1802*, ed. by K.J. Schulz, J.H. DeYoung Jr., R.R. Seal II, D.C. Bradley, (2017), pp. O1–O31. <https://doi.org/10.3133/pp1802O>
3. S. Dai, R.B. Finkelman, Coal as a promising source of critical elements: progress and future prospects. *Int. J. Coal Geol.* **186**, 155–164 (2018). <https://doi.org/10.1016/j.coal.2017.06.005>
4. Stanford University, Critical minerals scarcity could threaten renewable energy future, Stanford earth matters magazine (2018). <https://earth.stanford.edu/news/critical-minerals-scarcity-could-threaten-renewable-energy-future#gs.hnmriv>. Accessed 11/26/21
5. V. Balaram, Rare earth elements: a review of applications, occurrence, exploration, analysis, recycling and environmental impact. *Geosci. Front.* **10**, 1285–1303 (2019). <https://doi.org/10.1016/j.gsf.2018.12.005>
6. D.H. Dang, K.A. Thompson, L. Ma, H.Q. Nguyen, S.T. Luu, M.T. Nguyen Duong, A. Kernaghan, Toward the circular economy of rare earth elements: a review of abundance, extraction, applications and environmental impacts. *Arch. Environ. Contam. Toxicol.* **81**(p), 521–530 (2021). <https://doi.org/10.1007/s00244-021-00867-7>
7. T. Fishman, T.E. Graedel, Impact of the establishment of U.S. offshore wind power on neodymium flows. *Nat. Sustain.* **2**, 332–338 (2019). <https://doi.org/10.1038/s41893-019-0252-z>

8. C. Xu, Q. Dai, L. Gaines, M. Hu, A. Tukker, B. Steubing, Future material demand for automotive lithium-based batteries. *Commun. Mater.* **1**, 99 (2020). <https://doi.org/10.1038/s43246-020-00095-x>. [www.nature.com/commsmat](http://www.nature.com/commsmat)
9. U.S. Geological Survey, Mineral commodity summaries, rare earths (2021). <https://pubs.usgs.gov/periodicals/mcs2021/mcs2021-rare-earth.pdf>
10. U.S. Department of Energy, National Energy Technology Laboratory, Rare earth elements, 2019 project portfolio (2019), 36 p. <https://netl.doe.gov/sites/default/files/2019-04/2019-REE-Project-Portfolio.pdf>. Accessed 12/6/2021
11. S.P. Schweinfurth, Coal — a complex natural resource: An overview of factors affecting coal quality and use in the United States. *U.S. Geol. Surv. Cir.* **1143**, 39 p (2003). <https://doi.org/10.3133/cir1143>
12. S. Dai, A. Bechtel, C.F. Eble, R.M. Flores, D. French, I.T. Graham, M.M. Hood, J.C. Hower, V.A. Korasidis, T.A. Moore, W. Püttmann, Q. Wei, J.M.K. O’Keefe, Recognition of peat depositional environments in coal: a review. *Int. J. Coal Geol.* **219**, 103383 (2020). <https://doi.org/10.1016/j.coal.2019.103383>
13. V.M. Goldschmidt, Rare elements in coal ashes. *Ind. Eng. Chem.* **27**, 1100–1102 (1935). <https://doi.org/10.1021/ie50309a032>
14. U.S. Energy Information Administration, Energy explained: coal data and statistics (2021). <https://www.eia.gov/energyexplained/coal/data-and-statistics.php>. Accessed 11/23/2021
15. American Coal Ash Association, Beneficial use of coal combustion products – an American recycling success story (2021). <https://aca-usa.org/wp-content/uploads/coal-combustion-products-use/ACAA-Brochure-Web.pdf>. Accessed 4/8/22
16. J.C. Hower, E.J. Granite, D.B. Mayfield, A.S. Lewis, R.B. Finkelman, Notes on contributions to the science of rare earth element enrichment in coal and coal combustion byproducts. *Fortschr. Mineral.* **6**, 32 (2016). <https://doi.org/10.3390/min6020032>
17. J.C. Hower, J.G. Groppo, K.R. Henke, U.M. Graham, M.M. Hood, P. Joshi, D.V. Preda, Pondered and landfilled fly ash as a source of rare earth elements from a Kentucky power plant. *Coal Combust Gasif Prod* **9**, 1–21 (2017). <https://doi.org/10.4177/CCGP-D-17-00003.1>
18. J.C. Hower, A. Kolker, H. Hsu-Kim, D. Plata, Rare earth elements in coal and coal ash and their potential extraction, in *Rare Earth Elements and Their Sustainable Extraction from Secondary Sources*, ed. by A. Karamalidis, R. Eggert, (American Geophysical Union, Geophysical Monograph Series, 2023)
19. International Energy Agency, Key World Energy Statistics (2021). <https://www.iea.org/reports/key-world-energy-statistics-2021>. Accessed 11/23/2021
20. J.E. Birdwell, Review of rare earth element concentrations in oil shales of the Eocene Green River Formation: U.S. Geological Survey Open-File Report 2012–1016 (2012), 20 p. <https://pubs.usgs.gov/of/2012/1016/>
21. M.S. Blondes, K.D. Gans, M.A. Engle, Y.K. Kharaka, M.E. Reidy, V. Saraswathula, J.J. Thordsen, E.L. Rowan, E.A. Morrissey, *U.S. Geological Survey National Produced Waters Geochemical Database (ver. 2.3, January 2018)* (U.S. Geological Survey Data Release, 2018). <https://doi.org/10.5066/F7J964W8>
22. W. Zhang, A. Noble, X. Yang, R. Honaker, A comprehensive review of rare earth elements recovery from coal-related materials. *Fortschr. Mineral.* **10**, 451 (2020). <https://doi.org/10.3390/min10050451>
23. N.K. Foley, R.A. Ayuso, Conventional rare earth element mineral deposits—the global landscape, in *Rare Earth Metals and Minerals Industries: Status and Prospects*, ed. by Y.V. Murty, M.A. Alvin, J.P. Lifton, (Springer Nature, Cham, 2023)
24. A. Jordens, Y.P. Cheng, K.E. Waters, A review of the beneficiation of rare earth element bearing minerals. *Miner. Eng.* **41**, 97–114 (2013). <https://doi.org/10.1016/j.mineng.2012.10.017>
25. S.R. Taylor, S.M. McLennan, *The Continental Crust — Its Composition and Evolution* (Blackwell Scientific Publishers, Boston, 1985), 312 p
26. S.R. Taylor, S.M. McLennan, The geochemical evolution of the continental crust. *Rev. Geophys.* **33**, 241–265 (1995). <https://doi.org/10.1029/95RG00262>



27. S.M. McLennan, Relationships between the trace element composition of sedimentary rocks and the upper continental crust. *Geochem Geophys Geosyst* **2**, 2000GC000109 (2001). <https://doi.org/10.1029/2000GC000109>
28. R.L. Rudnick, S. Gao, The composition of the continental crust, in *Treatise on Geochemistry, Vol. 3, The Crust*, ed. by H.D. Holland, K.K. Turekian, (Elsevier-Pergamon, Oxford, 2003), pp. 1–64. <https://doi.org/10.1016/b0-08-043751-6/03016-4>
29. F. Zhang, B. Li, X. Zhuang, X. Querol, N. Moreno, Y. Shanguan, J. Zhou, J. Liao, Geological controls on enrichment of rare earth elements and yttrium (REY) in late Permian coals and non-coal rocks in the Xian'an Coalfield, Guangxi Province. *Fortschr. Mineral.* **11**, 301 (2021). <https://doi.org/10.3390/min11030301>
30. M.P. Ketris, Y.E. Yudovich, Estimations of Clarkes for carbonaceous biolithes: world averages for trace element contents in black shales and coals. *Int. J. Coal Geol.* **78**, 135–148 (2009). <https://doi.org/10.1016/j.coal.2009.01.002>
31. R.B. Finkelman, Trace and minor elements in coal, in *Organic Geochemistry: Principles and Applications*, ed. by M.H. Engel, S.A. Macko, (Springer, 1993), pp. 593–607
32. S. Dai, I.T. Graham, C.R. Ward, A review of anomalous rare earth elements and yttrium in coal. *Int. J. Coal Geol.* **159**, 82–95 (2016). <https://doi.org/10.1016/j.coal.2016.04.005>
33. International Union of Pure and Applied Chemistry (IUPAC), Nomenclature of inorganic chemistry, in *IUPAC Recommendations, 2005*, (RSC Publishing, Cambridge, 2005), p. 51
34. C. Scott, A. Kolker, Rare earth elements in coal and coal fly ash: U.S. Geological Survey Fact Sheet 2019–3048 (2019), 4 p. <https://doi.org/10.3133/fs20193048>
35. U.S. Geological Survey, Mineral commodity summaries, scandium (2021). <https://pubs.usgs.gov/periodicals/mcs2021/mcs2021-scandium.pdf>
36. A. Noble, Fundamental Perspectives on Economic Analysis of Rare Earth Processing from Various Feedstocks, in *Rare Earth Metals and Minerals Industries: Status and Prospects*, ed. by Y.V. Murty, M.A. Alvin, J.P. Lifton, (Springer Nature, Cham, 2023)
37. G.N. Hanson, Rare earth elements in petrogenetic studies of igneous systems. *Annu. Rev. Earth Planet. Sci.* **8**, 371–406 (1980)
38. V.V. Seredin, S. Dai, Coal deposits as potential alternative sources for lanthanides and yttrium. *Int. J. Coal Geol.* **94**, 67–93 (2012). <https://doi.org/10.1016/j.coal.2011.11.001>
39. A. Kolker, C. Scott, J.C. Hower, J.A. Vazquez, C.L. Lopano, S. Dai, Distribution of rare elements in coal combustion fly ash, determined by SHRIMP-RG ion microprobe. *Int. J. Coal Geol.* **184**, 1–10 (2017). <https://doi.org/10.1016/j.coal.2017.10.002>
40. A. Kolker, C. Scott, L. Lefticariu, M. Mastalerz, A. Drobniak, A.M. Scott, Trace element partitioning during coal preparation: insights from U.S. Illinois Basin coals. *Int. J. Coal Geol.* **243**, 103781 (2021). <https://doi.org/10.1016/j.coal.2021.103781>
41. G.M. Eskenazy, Rare earth elements and yttrium in lithotypes of Bulgarian coals. *Org. Geochem.* **11**, 83–89 (1987). [https://doi.org/10.1016/0146-6380\(87\)90030-1](https://doi.org/10.1016/0146-6380(87)90030-1)
42. G.M. Eskenazy, Aspects of the geochemistry of rare earth elements in coal: an experimental approach. *Int. J. Coal Geol.* **38**, 285–295 (1999). [https://doi.org/10.1016/S0166-5162\(98\)00027-5](https://doi.org/10.1016/S0166-5162(98)00027-5)
43. J.C. Hower, C.F. Eble, S. Dai, H.E. Belkin, Distribution of rare earth elements in eastern Kentucky coals: indicators of multiple modes of enrichment. *Int. J. Coal Geol.* **160–161**, 73–81 (2016). <https://doi.org/10.1016/j.coal.2016.04.009>
44. G.M. Eskenazy, Rare earth elements in a sampled coal from the Pirin deposit, Bulgaria. *Int. J. Coal Geol.* **7**, 301–314 (1987). [https://doi.org/10.1016/0166-5162\(87\)90041-3](https://doi.org/10.1016/0166-5162(87)90041-3)
45. R.B. Finkelman, The origin, occurrence, and distribution of the inorganic constituents in low-rank coals, in *Proceedings of the Basic Coal Science Workshop. H.H. Schobert, Compiler*, (Grand Forks Energy Tech, Center, Grand Forks, ND, 1981), pp. 70–90
46. R. Lin, T.L. Bank, E.A. Roth, E.J. Granite, Y. Soong, Organic and inorganic associations of rare earth elements in central Appalachian coal. *Int. J. Coal Geol.* **179**, 295–301 (2017). <https://doi.org/10.1016/j.coal.2017.07.002>

47. D.A. Laudal, S.A. Benson, R.S. Addleman, D. Palo, Leaching behavior of rare earth elements in Fort Union lignite coals of North America. *Int. J. Coal Geol.* **191**, 112–124 (2018). <https://doi.org/10.1016/j.coal.2018.03.010>
48. R.B. Finkelman, S. Dai, D. French, The importance of minerals in coal as the hosts of chemical elements: a review. *Int. J. Coal Geol.* **212**, 103251 (2019). <https://doi.org/10.1016/j.coal.2019.103251>
49. S. Dai, J.C. Hower, R.B. Finkelman, I.T. Graham, D. French, C.R. Ward, G. Eskanazy, Q. Wei, L. Zhao, Organic associations of non-mineral elements in coal: a review. *Int. J. Coal Geol.* **218** (2020). <https://doi.org/10.1016/j.coal.2019.103347>
50. S. Dai, R.B. Finkelman, D. French, J.C. Hower, I.T. Graham, F. Zhao, Modes of occurrence of elements in coal: a critical evaluation. *Earth Sci. Rev.* **222** (2021). <https://doi.org/10.1016/j.earscirev.2021.103815>
51. C.J. Zygarić, B.C. Folkedahl, C.M. Nyberg, I.K. Feole, B.A. Kurz, N.L. Theakar, S.A. Benson, J.C. Hower, C.F. Eble, Rare earth elements (REEs) in U.S. coal based resources: sampling, characterization and round-Robin Interlaboratory Study (2019). <https://edx.netl.doe.gov/dataset/rare-earth-elements-in-u-s-coal-based-resources,rfp-10982-fe0029007-final-report-RRIS-UND.pdf>. Accessed 17 Nov 2021
52. V.V. Seredin, Rare earth element-bearing coals from the Russian Far East deposits. *Int. J. Coal Geol.* **30**, 101–129 (1996). [https://doi.org/10.1016/0166-5162\(95\)00039-9](https://doi.org/10.1016/0166-5162(95)00039-9)
53. V.V. Seredin, S. Dai, Y. Sun, I.Y. Chekryzhov, Coal deposits as promising sources of rare metals for alternative power and energy-efficient technologies. *Appl. Geochem.* **31**, 1–11 (2013). <https://doi.org/10.1016/j.apgeochem.2013.01.009>
54. M. Mastalerz, A. Drobniak, C. Eble, P. Ames, P. McLaughlin, Rare earth elements and yttrium in Pennsylvanian coals and shales in the eastern part of the Illinois Basin. *Int. J. Coal Geol.* **231** (2020). <https://doi.org/10.1016/j.coal.2020.103620>
55. R. Lin, Y. Soong, E.J. Granite, REE in U.S. Coal. Evaluation of trace elements in U.S. coals using the USGS COALQUAL database version 3.0. Part I: rare earth elements and yttrium (REY). *Int. J. Coal Geol.* **192**, 1–13 (2018). <https://doi.org/10.1016/j.coal.2018.04.004>
56. U.S. Geological Survey, Mineral commodity summaries, yttrium (2021). <https://pubs.usgs.gov/periodicals/mcs2021/mcs2021-yttrium.pdf>
57. N.J. Wagner, A. Matiane, Rare earth elements in select Main Karoo Basin (South Africa) coal and coal ash samples. *Int. J. Coal Geol.* **196**, 82–92 (2018). <https://doi.org/10.1016/j.coal.2018.06.020>
58. R.S. Blissett, N. Smalley, N.A. Rowson, An investigation into six coal fly ashes from the United Kingdom and Poland to evaluate rare earth element content. *Fuel* **199**, 236–239 (2014). <https://doi.org/10.1016/j.fuel.2013.11.053>
59. W. Franus, M.M. Wiatros-Motyka, M. Wdowin, Coal fly ash as a resource for rare earth elements. *Environ. Sci. Pollut. Res.* **22**, 9464–9474 (2015). <https://doi.org/10.1007/s11356-015-4111-9>
60. R.K. Taggart, J.C. Hower, G.S. Dwyer, H. Hsu-Kim, Trends in rare earth element content of U.S.-based coal combustion fly ashes. *Environ. Sci. Technol.* **50**(11), 5919–5926 (2016). <https://doi.org/10.1021/acs.est.6b00085>
61. J.C. Hower, J.G. Groppo, H. Hsu-Kim, R.K. Taggart, Signatures of rare earth element distributions in fly ash derived from the combustion of central Appalachian, Illinois, and Powder River Basin coals. *Fuel* **301** (2021). <https://doi.org/10.1016/j.fuel.2021.121048>
62. J.C. Hower, J.G. Groppo, H. Hsu-Kim, R.K. Taggart, Distribution of rare earth elements in fly ash derived from the combustion of Illinois Basin coals. *Fuel* **289** (2021). <https://doi.org/10.1016/j.fuel.2020.119990>
63. P. Liu, R. Huang, Y. Tang, Comprehensive understandings of rare earth element (REE) speciation in coal fly ashes and implication for REE extractability. *Environ. Sci. Technol.* **53**, 5369–5377 (2019). <https://doi.org/10.1021/acs.est.9b00005>
64. N. Couto, A.R. Ferreira, V. Lopes, S.C. Peters, E.P. Mateus, A.B. Ribeiro, S. Pamukcu, Electrodialytic recovery of rare earth elements from coal ashes. *Electrochim. Acta* **359** (2020). <https://doi.org/10.1016/j.electacta.2020.136934>

65. M.Y. Stuckman, C.L. Lopano, E.J. Granite, Distribution and speciation of rare earth elements in coal combustion by-products via synchrotron microscopy and spectroscopy. *Int. J. Coal Geol.* **195**, 125–138 (2018). <https://doi.org/10.1016/j.coal.2018.06.001>
66. Z. Wang, S. Dai, J. Zou, D. French, I.T. Graham, Rare earth elements and yttrium in coal ash from the Luzhou Power Plant in Sichuan, Southwest China: concentration, characterization and optimized extraction. *Int. J. Coal Geol.* **203**, 1–14 (2019). <https://doi.org/10.1016/j.coal.2019.01.001>
67. L.B. Clarke, L.L. Sloss, *Trace Elements – Emissions from Coal Combustion and Gasification* (IEA Coal Research, IEACR/49, 1992), 111 p
68. J.A. Ratafia-Brown, Overview of trace element partitioning in flames and furnaces of utility coal-fired boilers. *Fuel Process. Technol.* **39**, 139–157 (1994)
69. J.C. Hower, J.G. Groppo, K.R. Henke, M.M. Hood, C.F. Eble, R.Q. Honaker, W. Zhang, D. Qian, Notes on the potential for the concentration of rare earth elements and yttrium in coal combustion fly ash. *Fortschr. Mineral.* **5**, 356–366 (2015). <https://doi.org/10.3390/min5020356>
70. C. Lanzerstorfer, Pre-processing of coal combustion fly ash by classification for enrichment of rare earth elements. *Energy Rep.* **4**, 660–663 (2018). <https://doi.org/10.1016/j.egy.2018.10.010>
71. A. Valian, J.G. Groppo, C.F. Eble, J.C. Hower, R.Q. Honaker, S.F. Greb, Distribution of rare earth elements in the Illinois Basin coals. *Min. Metall. Explor.* **38**, 1645–1663 (2021). <https://doi.org/10.1007/s42461-020-00257-y>
72. U.S. Department of Energy, National Energy Technology Laboratory (2017). <https://www.energy.gov/articles/high-concentrations-rare-earth-elements-found-american-coal-basins>
73. J.C. Hower, L.F. Ruppert, C.F. Eble, Lanthanide, yttrium and zirconium anomalies in the Fire Clay coal bed, Eastern Kentucky. *Int. J. Coal Geol.* **39**, 141–153 (1999)
74. J.C. Hower, D. Berti, M.F. Hochella Jr., S.M. Mardon, Rare earth minerals in a “no tonstein” section of the Dean (Fire Clay) coal, Knox County, Kentucky. *Int. J. Coal Geol.* **193**, 73–86 (2018). <https://doi.org/10.1016/j.coal.2018.05.001>
75. S.M. Mardon, J.C. Hower, Impact of coal properties on coal combustion by-product quality: examples from a Kentucky Power Plant. *Int. J. Coal Geol.* **59**, 153–169 (2004). <https://doi.org/10.1016/j.coal.2004.01.004>
76. J. Liu, S. Dai, X. He, J.C. Hower, T. Sakulpitakphon, Size-dependent variations in fly ash trace-element chemistry: a case study from a Kentucky Power Plant and with emphasis on rare earth elements. *Energy Fuel* **31**, 438–447 (2017). <https://doi.org/10.1021/acs.energyfuels.6b02644>
77. J.C. Hower, C.F. Eble, J.S. Backus, P. Xie, J. Liu, B. Fu, M.M. Hood, Aspects of rare earth element enrichment in Central Appalachian coals. *Appl Geochem* **120** (2020). <https://doi.org/10.1016/j.apgeochem.2020.104676>
78. J.C. Hower, C.F. Eble, P. Xie, J. Liu, B. Fu, M.M. Hood, Aspects of rare earth element enrichment in Allegheny Plateau coals, Pennsylvania, USA. *Appl. Geochem.* **136**, 105150 (2022). <https://doi.org/10.1016/j.coal.2020.103610>
79. S. Dai, L. Zhao, S. Peng, C.L. Chou, X. Wang, Y. Zhang, D. Li, Y. Sun, Abundances and distribution of minerals and elements in high-alumina coal fly ash from the Jungar Power Plant, Inner Mongolia, China. *Int. J. Coal Geol.* **81**, 320–332 (2010). <https://doi.org/10.1016/j.coal.2009.03.005>
80. S. Dai, Y. Jiang, C.R. Ward, L. Gu, V.V. Seredin, H. Liu, D. Zhou, X. Wang, Y. Sun, J. Zou, D. Ren, Mineralogical and geochemical compositions of the coal in the Guanbanwusu Mine, Inner Mongolia, China: further evidence for the existence of an Al (Ga and REE) ore deposit in the Jungar Coalfield. *Int. J. Coal Geol.* **98**, 10–40 (2012). <https://doi.org/10.1016/j.coal.2012.03.003>
81. A. Deonarine, A. Kolker, M. Doughten, Trace elements in coal ash: U.S. Geological Survey Fact Sheet 2015–3037 (2015), 6 p. <https://doi.org/10.3133/fs20153037>
82. C. Senior, Mercury behavior in coal combustion systems, in *Mercury Emissions Control for Coal-Derived Gas Streams*, ed. by E. Granite, C. Senior, H. Pennline, (Wiley-VCH, 2014), pp. 109–132. <https://doi.org/10.1002/9783527658787.ch7>

83. C. Senior, E. Granite, W. Linak, W. Seames, Chemistry of trace inorganic elements in coal: a century of discovery. *Energy Fuels* **34**(12), 15141–15168 (2020). <https://doi.org/10.1021/acs.energyfuels.0c02375>
84. J.C. Hower, T. Sakulpitakphon, A.S. Trimble, G.A. Thomas, W.H. Schram, Major and minor element distribution in fly ash from a coal-fired utility boiler in Kentucky. *Energy Sources Part A Recover Util. Environ. Eff.* **28**(1), 79–95 (2006). <https://doi.org/10.1080/009083190889753>
85. R. Świetlik, M. Trojanowska, M.A. Józwiak, Evaluation of the distribution of heavy metals and their chemical forms in ESP-fractions of fly ash. *Fuel Process. Technol.* **95**, 109–118 (2012). <https://doi.org/10.1016/j.fuproc.2011.11.019>
86. J.C. Hower, C.L. Senior, E.M. Suuberg, R.H. Hurt, J.L. Wilcox, E.S. Olson, Mercury capture by native fly ash carbons in coal-fired power plants. *Prog. Energy Combust. Sci.* **36**, 510–529 (2010). <https://doi.org/10.1016/j.peccs.2009.12.003>
87. M.M. Hood, R.K. Taggart, R.C. Smith, H. Hsu-Kim, K.R. Henke, U.M. Graham, J.G. Groppo, J.M. Unrine, J.C. Hower, Rare earth element distribution in Fly ash derived from the fire clay coal, Kentucky. *Coal Combust. Gasif. Prod.* **9**, 22–33 (2017). <https://doi.org/10.4177/CCGP-D-17-00002.1>
88. C.R. Ward, Analysis, origin and significance of mineral matter in coal: an updated review. *Int. J. Coal Geol.* **165**, 1–27 (2016). <https://doi.org/10.1016/j.coal.2016.07.014>
89. W. Zhang, J.G. Groppo, R.Q. Honaker, Ash beneficiation for REE recovery. *World of Coal Ash*, 5–7 May 2015, Nashville, TN, Paper 194-Groppo-2015 (2015). <http://www.flyash.info/2015/194-Groppo-2015.pdf>. Accessed 29 Nov 2021
90. J. Yang, Y. Zhao, V. Zyryanov, J. Zhang, C. Zheng, Physical-chemical characteristics and elements enrichment of magnetospheres from coal fly ashes. *Fuel* **135**, 15–26 (2014). <https://doi.org/10.1016/j.fuel.2014.06.033>
91. S.N. Montross, C.A. Verba, H.L. Chan, C. Lopano, Advanced characterization of rare earth element minerals in coal utilization by-products using multimodal image analysis. *Int. J. Coal Geol.* **195**, 362–372 (2018). <https://doi.org/10.1016/j.coal.2018.06.018>
92. J.C. Hower, D. Qian, N.J. Briot, E. Santillan-Jimenez, M.M. Hood, R.K. Taggart, H. Hsu-Kim, Nano-scale rare earth distribution in fly ash derived from the combustion of the fire clay coal, Kentucky. *Fortschr. Mineral.* **9**, 10 (2019). <https://doi.org/10.3390/min9040206>
93. Y. Hikichi, T. Nomura, Melting temperatures of monazite and xenotime. *J. Am. Ceram. Soc.* **70**, C252–C253 (1987). <https://doi.org/10.1111/j.1151-2916.1987.tb04890.x>
94. R.J. Finch, J.M. Hanchar, Structure and chemistry of zircon and zircon group minerals, in *Zircon. Reviews in Mineralogy and Geochemistry*, ed. by J.M. Hanchar, P.W.O. Hoskin, vol. 53, (Mineralogical Society of America, 2003), pp. 1–25. <https://doi.org/10.2113/0530001>
95. K.A. Farley, He diffusion systematics in minerals: evidence from synthetic monazite and zircon structure phosphates. *Geochim. Cosmochim. Acta* **71**, 4015–4024 (2007). <https://doi.org/10.1016/j.gca.2007.05.022>
96. D.J. Cherniak, E.B. Watson, Diffusion of helium in natural monazite, and preliminary results on He diffusion in synthetic light rare earth phosphates. *Am. Mineral.* **98**, 1407–1420 (2013)
97. D.J. Cherniak, E.B. Watson, J.B. Thomas, Diffusion of helium in zircon and apatite. *Chem. Geol.* **268**, 155–166 (2009). <https://doi.org/10.1016/j.chemgeo.2009.08.011>
98. C.A. Palmer, C.L. Oman, A.J. Park, J.A. Luppens, The U.S. geological survey coal quality (COALQUAL) database version 3.0: U.S. Geological Survey Data Series 975 (2015), 43 p with appendices. <https://doi.org/10.3133/ds975>
99. S. Dai, D. Li, C.-L. Chou, L. Zhao, Y. Zhang, D. Ren, Y. Ma, Y. Sun, Mineralogy and geochemistry of boehmite-rich coals: new insights from the Haerwusu Surface Mine, Jungar Coalfield, Inner Mongolia, China. *Int. J. Coal Geol.* **74**, 185–202 (2008). <https://doi.org/10.1016/j.coal.2008.01.001>
100. S. Dai, X. Yan, C.R. Ward, J.C. Hower, L. Zhao, X. Wang, L. Zhao, D. Ren, R.B. Finkelman, Valuable elements in Chinese coals: a review. *Int. Geol. Rev.* **60**(5–6), 590–620 (2018). <https://doi.org/10.1080/00206814.2016.1197802>

101. J.H. Hodgkinson, M. Grigorescu, Strategic elements in the fort Cooper coal measures: potential rare earth elements and other multi-product targets. *Aust. J. Earth Sci.* **67**(3), 305–319 (2020). <https://doi.org/10.1080/08120099.2019.1660712>
102. Q. Huang, D. Talan, J.H. Restrepo, O.J. Restrepo Baena, V. Kecojevic, A. Noble, Characterization study of rare earths, yttrium and scandium from various Colombian coal samples and non-coal lithologies. *Int. J. Coal Geol.* **209**, 14–26 (2019). <https://doi.org/10.1016/j.coal.2019.04.008>
103. V. Mishra, S. Chakravarty, R.B. Finkelman, A.K. Atul Kumar Varma, Geochemistry of rare earth elements in lower Gondwana coals of the Talchir Coal Basin, India. *J. Geochem. Explor.* **204**, 43–56 (2019). <https://doi.org/10.1016/j.gexplo.2019.04.006>
104. F. Anggara, D.H. Amijaya, A. Harijoko, T.N. Tambaria, A.A. Sahri, Z.A. Zain Andrian Nur Asa, Rare earth element and yttrium content of coal in the Banko Coalfield, South Sumatra Basin, Indonesia: contributions from tonstein layers. *Int. J. Coal Geol.* **196**, 159–172. <https://doi.org/10.1016/j.coal.2018.07.006>
105. S.J. Schatzel, B.W. Stewart, Rare earth element sources and modification in the Lower Kittanning coal bed, Pennsylvania: implications for the origin of coal mineral matter and rare earth element exposure in underground mines. *Int. J. Coal Geol.* **54**, 223–251 (2003). [https://doi.org/10.1016/S0166-5162\(03\)00038-7](https://doi.org/10.1016/S0166-5162(03)00038-7)
106. S.J. Schatzel, B.W. Stewart, A provenance study of mineral matter in coal from Appalachian Basin coal mining regions and implications regarding the respirable health of underground coal workers: a geochemical and Nd isotope investigation. *Int. J. Coal Geol.* **94**, 123–136 (2012). <https://doi.org/10.1016/j.coal.2012.01.011>
107. C. Zhao, B. Liu, L. Xiao, Y. Li, S. Liu, Z. Li, B. Zhao, J. Ma, G. Chu, P. Gao, Y. Sun, Significant enrichment of Ga, Rb, Cs, REEs and Y in the Jurassic No. 6 coal in the Iqe Coalfield, Northern Qaidam Basin, China — a hidden gem. *Ore Geol. Rev.* **83**, 1–13 (2017). <https://doi.org/10.1016/j.oregeorev.2016.12.012>
108. B. Fu, J.C. Hower, W. Zhang, G. Luo, H. Hu, H. Yao, A review of rare earth elements and yttrium in coal ash: content, modes of occurrence, combustion behavior and extraction methods. *Prog. Energy Combust. Sci.* **88**, 100954 (2022). <https://doi.org/10.1016/j.peccs.2021.100954>
109. K.A. Eriksson, I.H. Campbell, J.M. Palin, C.M. Allen, Predominance of Grenvillian magmatism recorded in detrital zircons from modern Appalachian rivers. *J. Geol.* **111**, 707–717 (2003). <https://doi.org/10.1086/378338>
110. K.A. Eriksson, I.H. Campbell, J.M. Palin, C.M. Allen, B. Bock, Evidence for multiple recycling in neoproterozoic through Pennsylvanian sedimentary rocks of the central Appalachian basin. *J. Geol.* **112**, 261–276 (2004). <https://doi.org/10.1086/382758>
111. W.A. Thomas, G.E. Gehrels, S.F. Greb, G.C. Nadon, A.M. Satkoski, M.C. Romero, Detrital zircons and sediment dispersal in the Appalachian foreland. *Geosphere* **13**(6), 2206–2230 (2017). <https://doi.org/10.1130/GES01525.1>
112. T.A. Johnson, J.D. Vervoort, M.J. Ramsey, S. Southworth, S.R. Mulcahy, Tectonic evolution of the Grenville Orogen in the central Appalachians. *Precambrian Res.* **346**, 105740 (2020). <https://doi.org/10.1016/j.precamres.2020.105740>
113. S. Dai, D. Ren, C.-L. Chou, S. Li, Y. Jiang, Mineralogy and geochemistry of the No. 6 coal (Pennsylvanian) in the Junger Coalfield, Ordos Basin, China. *Int. J. Coal Geol.* **66**, 253–270 (2006). <https://doi.org/10.1016/j.coal.2005.08.003>
114. S.I. Arbuzov, A.M. Mezhibor, D.A. Spears, S.S. Ilenok, M.V. Shal'dybin, E.V. Belaya, Nature of tonsteins in the Azeisk deposit of the Irkutsk Coal Basin (Siberia, Russia). *Int. J. Coal Geol.* **153**, 99–111 (2016). <https://doi.org/10.1016/j.coal.2015.12.001>
115. S.I. Arbuzov, I.Y. Chekryzhov, R.B. Finkelman, Y.Z. Sun, C.L. Zhao, S.S. Il'enok, M.G. Blokhin, N.V. Zarubina, Comments on the geochemistry of rare earth elements (La, Ce, Sm, Eu, Tb, Yb, Lu) with examples from coals of North Asia (Siberia, Russian far East, North China, Mongolia, and Kazakhstan). *Int. J. Coal Geol.* **206**, 106–120 (2019). <https://doi.org/10.1016/j.coal.2018.10.013>

116. S. Dai, C.R. Ward, I.T. Graham, D. French, J.C. Hower, L. Zhao, X. Wang, Altered volcanic ashes in coal and coal-bearing sequences: a review of their nature and significance. *Earth Sci. Rev.* **175**, 44–74 (2017). <https://doi.org/10.1016/j.earscirev.2017.10.005>
117. B.F. Bohor, D.M. Triplehorn, Tonsteins: altered volcanic-ash layers in coal-bearing sequences. *Geol. Soc. Am. Spec. Pap.* **285**, 44 p (1993)
118. S. Dai, D. Ren, X. Hou, L. Shao, Geochemical and mineralogical anomalies of the late Permian coal in the Zhijin Coalfield of Southwest China and their volcanic origin. *Int. J. Coal Geol.* **55**, 117–138 (2003). [https://doi.org/10.1016/S0166-5162\(03\)00083-1](https://doi.org/10.1016/S0166-5162(03)00083-1)
119. S. Dai, X. Wang, Y. Zhou, J.C. Hower, D. Li, W. Chen, X. Zhu, J. Zou, Chemical and mineralogical compositions of silicic, mafic and alkali tonsteins in the late Permian coals from the Songzao Coalfield, Chongqing, Southwest China. *Chem. Geol.* **282**, 29–44 (2011). <https://doi.org/10.1016/j.chemgeo.2011.01.006>
120. P.C. Lyons, T.E. Krogh, Y.Y. Kwok, D.W. Davis, W.F. Outerbridge, H.T. Evans Jr., Radiometric ages of the fire clay tonstein [Pennsylvanian (upper carboniferous), Westphalian, Duckmantian]: a comparison of U–Pb zircon single-crystal ages and <sup>40</sup>Ar/<sup>39</sup>Ar sanidine single-crystal plateau ages. *Int. J. Coal Geol.* **67**, 259–266 (2006). <https://doi.org/10.1016/j.coal.2005.12.002>
121. D.A. Spears, The origin of tonsteins, an overview and links with seatearths, fireclays and fragmental clay rocks. *Int. J. Coal Geol.* **94**, 22–31 (2012). <https://doi.org/10.1016/j.coal.2011.09.008>
122. M. Guerra-Sommer, M. Cazzulo-Klepzig, J.O.S. Santos, L.A. Hartmann, J.M. Ketzer, M.L.L. Formoso, Radiometric age determination of tonsteins and stratigraphic constraints for the lower Permian coal succession in Southern Paraná Basin, Brazil. *Int. J. Coal Geol.* **74**, 13–27 (2008). <https://doi.org/10.1016/j.coal.2007.09.005>
123. X. Yang, R.Q. Honaker, Leaching kinetics of rare earth elements from fire clay seam coal. *Fortschr. Mineral.* **10**, 491 (2020). <https://doi.org/10.3390/min10060491>
124. V.V. Seredin, R.B. Finkelman, Metalliferous coals: a review of the main genetic and geochemical types. *Int. J. Coal Geol.* **76**, 253–289 (2008). <https://doi.org/10.1016/j.coal.2008.07.016>
125. S. Dai, D. Ren, C.-L. Chou, R.B. Finkelman, V.V. Seredin, Y. Zhou, Geochemistry of trace elements in Chinese coals: a review of abundances, genetic types, impacts on human health and industrial utilization. *Int. J. Coal Geol.* **94**, 3–21 (2012a). <https://doi.org/10.1016/j.coal.2011.02.003>
126. S. Dai, I.Y. Chekryzhov, V.V. Seredin, V.P. Nechaev, I.T. Graham, J.C. Hower, C.R. Ward, D. Ren, X. Wang, Metalliferous coal deposits in East Asia (Primorye of Russia and South China): a review of geodynamic controls and styles of mineralization. *Gondwana Res.* **29**, 60–82 (2016). <https://doi.org/10.1016/j.gr.2015.07.001>
127. Q. Wei, S.M. Rimmer, Acid solubility and affinities of trace elements in the high-Ge coals from Wulantuga (Inner Mongolia) and Lincang (Yunnan Province), China. *Int. J. Coal Geol.* **178**, 39–55 (2017). <https://doi.org/10.1016/j.coal.2017.04.011>
128. S.I. Arbutov, I.Y. Chekryzhov, D.A. Spears, S.S. Ilenok, B.R. Soktoev, N.Y. Popov, Geology, geochemistry, mineralogy and genesis of the Spetsugli high-germanium coal deposit in the Pavlovsk Coalfield, Russian Far East. *Ore Geol. Rev.* **139** (2021). <https://doi.org/10.1016/j.oregeorev.2021.104537>
129. B. Jiu, W. Huang, Y. Li, The origin, migration, and accumulation mechanism of germanium and the metallogenic model of coal-hosted Ge ore deposits in Wulantuga, Erlan Basin, China. *J. Geochem. Explor.* **226** (2021). <https://doi.org/10.1016/j.gexplo.2021.106779>
130. W. Wang, Y. Qin, S. Sang, Y. Zhu, C. Wang, D.J. Weiss, Geochemistry of rare earth elements in a marine influenced coal and its organic solvent extracts from the Antaibao Mining District, Shanxi, China. *Int. J. Coal Geol.* **76**, 309–317 (2008). <https://doi.org/10.1016/j.coal.2008.08.012>
131. S.N. Montross, J. Yang, J. Britton, M. McKoy, C. Verba, Leaching of rare earth elements from central Appalachian coal seam underclays. *Fortschr. Mineral.* **10**, 577 (2020). <https://doi.org/10.3390/min10060577>

132. W. Zhang, A. Noble, Mineralogy characterization and recovery of rare earth elements from the roof and floor materials of the Guxu Coalfield. *Fuel* **270** (2020). <https://doi.org/10.1016/j.fuel.2020.117533>
133. J. Yang, S. Montross, J. Britton, M. Stuckman, C. Lopano, C. Verba, Microanalytical approaches to characterizing REE in Appalachian basin underclays. *Fortschr. Mineral.* **10**, 546 (2020). <https://doi.org/10.3390/min10060546>
134. L. Zheng, G. Liu, C.-L. Chou, C. Qi, Y. Zhan, Geochemistry of rare earth elements in Permian coals from the Huaibei Coalfield, China. *J. Asian Earth Sci.* **31**, 167–176 (2007). <https://doi.org/10.1016/j.jseaeas.2007.06.001>
135. X. Yang, J. Werner, R.Q. Honaker, Leaching of rare earth elements from an Illinois Basin coal source. *J. Rare Earths* **37**, 312–321 (2019). <https://doi.org/10.1016/j.jre.2018.07.003>
136. P. Rozelle, A. Khadikar, N. Pulati, N. Soundarrajan, M. Klima, M. Mosser, C. Miller, S. Pisupati, A study on removal of rare earth elements from U.S. coal by-products by ion exchange. *Metall. Mater. Trans. E* **3**, 6–17 (2016). <https://link.springer.com/journal/40553>
137. J.A. Luppens, D.C. Scott, J.E. Haacke, L.M. Osmonson, P.E. Pierce, Coal geology and assessment of coal resources and reserves in the Powder River Basin, Wyoming and Montana: U.S. Geological Survey Professional Paper 1809 (2015), 218 p. <https://doi.org/10.3133/pp1809>
138. P.D. Warwick, C.E. Aubourg, S.E. Suitt, S.M. Podwysocki, A.C. Schultz, Coal resources for part of the Wilcox Group (Paleocene through Eocene), Central Texas, in *Geologic Assessment of Coal in the Gulf of Mexico Coastal Plain, U.S.A.: AAPG Discovery Series No. 14/AAPG Studies in Geology No. 62*, ed. by P.D. Warwick, A.K. Karlsten, M. Merrill, B.J. Valentine, (2011), pp. 192–259
139. M.D. Mann, N.L. Theaker, B.J. Rew, S.A. Benson, A. Benson, D. Palo, C. Haugen, D. Laudal, Investigation of rare earth element extraction from North Dakota coal-related feedstocks: phase 2 final technical report, U.S. Department of Energy DE-FOA 0001202 (2021), 287 p. <https://doi.org/10.2172/1785352>
140. J.A. East, Coal fields of the conterminous United States – National Coal Resource Assessment Updated Version: U.S. Geological Survey, Open-File Report 2012–1205 (2013). <https://doi.org/10.3133/ofr20121205>
141. L.D. Moxness, E.C. Murphy, N.W. Kruger, Rare earth and other critical element concentrations in the sentinel Butte formation, Tracy Mountain, North Dakota, North Dakota Geological Survey Report of Investigation no. 128 (2021), 65 p
142. E.C. Murphy, Germanium in North Dakota Lignites. *North Dakota Depart. Miner. Resources Newslett.* **36**(1), 14–15 (2009)
143. Z. Huang, M. Fan, H. Tian, Rare earth elements of fly ash from Wyoming’s Powder River Basin coal. *J. Rare Earths* **38**, 219–226 (2020). <https://doi.org/10.1016/j.jre.2019.05.004>
144. R.K. Taggart, J.C. Hower, H. Hsu-Kim, Effects of roasting additives and leaching parameters on the extraction of rare earth elements from coal fly ash. *Int. J. Coal Geol.* **196**, 106–114 (2018). <https://doi.org/10.1016/j.coal.2018.06.021>
145. J.F. King, R.K. Taggart, R.C. Smith, J.C. Hower, H. Hsu-Kim, Aqueous acid and alkaline extraction of rare earth elements from coal combustion ash. *Int. J. Coal Geol.* **195**, 75–83 (2018). <https://doi.org/10.1016/j.coal.2018.05.009>
146. C.M. Oliveira, C.M. Machado, G.W. Duarte, M. Peterson, Beneficiation of pyrite from coal mining. *J. Clean. Prod.* **139**, 821–827 (2016). <https://doi.org/10.1016/j.jclepro.2016.08.124>
147. A. Kolker, Minor element distribution in iron-disulfides in coal: a geochemical review. *Int. J. Coal Geol.* **94**, 32–43 (2012). <https://doi.org/10.1016/j.coal.2011.10.011>
148. A.P. Deditius, S. Utsunomiya, M. Reich, S.E. Kesler, R.C. Ewing, R. Hough, J. Walshe, Trace metal nanoparticles in pyrite. *Ore Geol. Rev.* **42**, 32–46 (2011). <https://doi.org/10.1016/j.oregeorev.2011.03.003>
149. H. Sun, F. Zhao, M. Zhang, J. Li, Behavior of rare earth elements in acid coal mine drainage in Shanxi Province, China. *Environ. Earth Sci.* **67**, 205–213 (2012). <https://doi.org/10.1007/s12665-011-1497-7>

150. A.L. Wolfe, B.W. Stewart, R.C. Capo, R. Liu, D.A. Dzombak, G.W. Gordon, A.D. Anbar, Iron isotope investigation of hydrothermal and sedimentary pyrite and their aqueous dissolution products. *Chem. Geol.* **427**, 73–82 (2016). <https://doi.org/10.1016/j.chemgeo.2016.02.015>
151. X. Li, P. Wu, Geochemical characteristics of dissolved rare earth elements in acid mine drainage from abandoned high-ash coal mining area, southwestern China. *Environ. Sci. Pollut. Res.* **24**, 20540–20555 (2017). <https://doi.org/10.1007/s11356-017-9670-5>
152. S.M. Fortier, N.T. Nassar, G.W. Lederer, J. Brainard, J. Gambogi, E.A. McCullough, Draft critical mineral list — summary of methodology and background information—U.S. geological survey technical input document in response to secretarial order no. 3359: U.S. Geological Survey Open-File Report 2018–1021 (2018), 15 p. <https://doi.org/10.3133/ofr20181021>
153. N.T. Nassar, S.M. Fortier, Methodology and technical input for the 2021 review and revision of the U.S. critical minerals list: U.S. Geological Survey Open-File Report 2021–1045 (2021), 31 p. <https://doi.org/10.3133/ofr20211045>
154. U.S. Geological Survey, News Release, U.S. geological survey releases 2022 list of critical minerals | U.S. Geological Survey (usgs.gov) (2022). Accessed 7/13/2022
155. U.S. Geological Survey, Mineral commodity summaries, cesium (2021). <https://pubs.usgs.gov/periodicals/mcs2021/mcs2021-cesium.pdf>
156. U.S. Geological Survey, Mineral commodity summaries, rubidium (2021). <https://pubs.usgs.gov/periodicals/mcs2021/mcs2021-rubidium.pdf>
157. C.A. Cravotta III, Dissolved metals and associated constituents in abandoned coal mine discharges, Pennsylvania, USA. Part 1: constituent quantities and correlations. *Appl. Geochem.* **23**, 166–202 (2008). <https://doi.org/10.1016/j.apgeochem.2007.10.011>
158. F. Zhao, Z. Cong, H. Sun, D. Ren, The geochemistry of rare earth elements (REE) in acid mine drainage from the Sitai Coal Mine, Shanxi Province, North China. *Int. J. Coal Geol.* **70**(1), 184–192 (2007). <https://doi.org/10.1016/j.coal.2006.01.009>
159. B.W. Stewart, R.C. Capo, B.C. Hedin, R.S. Hedin, Rare earth element resources in coalmine drainage and treatment precipitates in the Appalachian basin, USA. *Int. J. Coal Geol.* **169**, 28–39 (2017). <https://doi.org/10.1016/j.coal.2016.11.002>
160. P.K. Sahoo, S. Tripathy, S.M. Equeenuddin, M.K. Panigrahi, Geochemical characteristics of coal mine discharge vis-à-vis behavior of rare earth elements at Jaintia Hills Coalfield, Northeastern India. *J. Geochem. Explor.* **112**, 235–243 (2012). <https://doi.org/10.1016/j.gexplo.2011.09.001>
161. C.R. Vass, A. Noble, P.F. Ziemkiewicz, The occurrence and concentration of rare earth elements in acid mine drainage and treatment by-products: part 1 — initial survey of the northern Appalachian coal basin. *Min. Metall. Explor.* **36**(5), 903–916 (2019). <https://doi.org/10.1007/s42461-019-0097-z>
162. C.R. Vass, A. Noble, P.F. Ziemkiewicz, The occurrence and concentration of rare earth elements in acid mine drainage and treatment by-products. Part 2: regional survey of northern and central Appalachian coal basins. *Min. Metall. Explor.* **36**(5), 917–929 (2019). <https://doi.org/10.1007/s42461-019-00112-9>
163. L. Lefticariu, E.R. Walters, C.W. Pugh, K.S. Bender, Sulfate reducing bioreactor dependence on organic substrates for remediation of coal-generated acid mine drainage: field experiments. *Appl. Geochem.* **63**, 70–82 (2015). <https://doi.org/10.1016/j.apgeochem.2015.08.002>
164. X. Li, R. Zhang, Q. Li, P. Wu, H. Ye, Rare earth elements and yttrium (REY) in coal mine drainage from Southwest China: geochemical distribution and resource evaluation. *Sci. Total Environ.* **782**, 146904 (2021). <https://doi.org/10.1016/j.scitotenv.2021.146904>
165. U.S. Environmental Protection Agency (U.S. EPA), 303(d) list impaired waters NHDPlus indexed dataset with program attributes. May 1, 2015 (2015). Retrieved from <https://www.epa.gov/waterdata/waters-geospatial-data-downloads>
166. C.A. Cravotta III, K.B. Brady, Priority pollutants and associated constituents in untreated and treated discharges from coal mining or processing facilities in Pennsylvania, USA. *Appl. Geochem.* **62**, 108–130 (2015). <https://doi.org/10.1016/j.apgeochem.2015.03.001>



167. C.H. Gammons, S.A. Wood, J.P. Jonas, J.P. Madison, Geochemistry of rare earth elements and uranium in the acidic Berkeley Pit Lake, Butte, Montana. *Chem. Geol.* **198**, 269–288 (2003). [https://doi.org/10.1016/S0009-2541\(03\)00034-2](https://doi.org/10.1016/S0009-2541(03)00034-2)
168. D.K. Nordstrom, D.W. Blowes, C.J. Ptacek, Hydrogeochemistry and microbiology of mine drainage: an update. *Appl. Geochem.* **57**, 3–16 (2015). <https://doi.org/10.1016/j.apgeochem.2015.02.008>
169. K.A. Hudson-Edwards, H.E. Jamieson, B.G. Lottermoser, Mine wastes: past, present, future. *Elements* **7**(6), 375–380 (2011). <https://doi.org/10.2113/gselements.7.6.375>
170. A. Lozano, C. Ayora, A. Fernández-Martínez, Sorption of rare earth elements on schwertmannite and their mobility in acid mine drainage treatments. *Appl. Geochem.* **113**, 104499 (2020). <https://doi.org/10.1016/j.apgeochem.2019.104499>
171. D.W. Blowes, C.J. Ptacek, J.L. Jambor, C.G. Weisener, D. Paktunc, W.D. Gould, D.B. Johnson, The geochemistry of acid mine drainage, in *Environmental Geochemistry. Treatise on Geochemistry*, ed. by B.S. Lollar, H.D. Holland, K.K. Turekian, vol. 11, 2nd edn., (Elsevier-Perigamon, Oxford, 2014), pp. 131–190. <https://doi.org/10.1016/B978-0-08-095975-7.00905-0>
172. C.A. Cravotta III, Dissolved metals and associated constituents in abandoned coalmine discharges, Pennsylvania, USA. Part 2: geochemical controls on constituent concentrations. *Appl. Geochem.* **23**, 203–226 (2008). <https://doi.org/10.1016/j.apgeochem.2007.10.003>
173. R.R. Seal II, J.M. Hammarstrom, A.N. Johnson, N.M. Piatak, G.A. Wandless, Environmental geochemistry of a Kuroko-type massive sulfide deposit at the abandoned Valzinco Mine, Virginia, USA. *Appl. Geochem.* **23**(2), 320–342 (2008). <https://doi.org/10.1016/j.apgeochem.2007.10.001>
174. C. Ayora, F. Macías, E. Torres, A. Lozano, S. Carrero, J.M. Nieto, R. Pérez-López, A. Fernández-Martínez, H. Castillo-Michel, Recovery of rare earth elements and yttrium from passive-remediation systems of acid mine drainage. *Environ. Sci. Technol.* **50**, 8255–8262 (2016). <https://doi.org/10.1021/acs.est.6b02084>
175. A. Lozano, C. Ayora, F. Macías, R. León, M.J. Gimeno, L. Auqué, Geochemical behavior of rare earth elements in acid drainages: modeling achievements and limitations. *J. Geochem. Explor.* **216**, 106577 (2020). <https://doi.org/10.1016/j.gexplo.2020.106577>
176. S.A. Wood, W.M. Shannon, L. Baker, The aqueous geochemistry of the rare earth elements and yttrium. Part 13: REE geochemistry of mine drainage from the Pine Creek Area, Coeur d'Alene River valley, Idaho, USA, in *Rare Earth Elements in Groundwater Flow Systems*, (Springer, Dordrecht, 2005), pp. 89–110
177. R.D. Taylor, A.K. Shah, G.J. Walsh, C.D. Taylor, Geochemistry and geophysics of iron oxide-apatite deposits and associated waste piles with implications for potential rare earth element resources from ore and historical mine waste in the Eastern Adirondack Highlands, New York, USA. *Econ. Geol.* **114**, 1569–1598 (2019). <https://doi.org/10.5382/econgeo.4689>
178. P.T. Behum, Y.P. Chugh, L. Lefticariu, Management of coal processing wastes: studies on an alternate technology for control of sulfate and chloride discharge. *Int. J. Coal Sci. Technol.* **5**(1), 54–63 (2018). <https://doi.org/10.1007/s40789-017-0185-y>
179. W. Zhang, R.Q. Honaker, Rare earth elements recovery using staged precipitation from a leachate generated from coarse coal refuse. *Int. J. Coal Geol.* **195**, 189–199 (2018). <https://doi.org/10.1016/j.coal.2018.06.008>
180. S.F. Greb, W.J. Nelson, S.D. Elrick, Mining geology of the principal resource coals of the Illinois Basin. *Int. J. Coal Geol.*, 103589 (2020). <https://doi.org/10.1016/j.coal.2020.103589>
181. P. Acero, J. Cama, C. Ayora, Sphalerite dissolution kinetics in acidic environment. *Appl. Geochem.* **22**(9), 1872–1883 (2007). <https://doi.org/10.1016/j.apgeochem.2007.03.051>
182. J. Liu, D.M. Aruguete, J.R. Jinschek, J.D. Rimstidt, M.F. Hochella Jr., The non-oxidative dissolution of galena nanocrystals: insights into mineral dissolution rates as a function of grain size, shape and aggregation state. *Geochim. Cosmochim. Acta* **72**(24), 5984–5996 (2008). <https://doi.org/10.1016/j.gca.2008.10.010>

183. J.D. Rimstidt, D.J. Vaughan, Pyrite oxidation: a state-of-the-art assessment of the reaction mechanism. *Geochim. Cosmochim. Acta* **67**(5), 873–880 (2003). [https://doi.org/10.1016/S0016-7037\(02\)01165-1](https://doi.org/10.1016/S0016-7037(02)01165-1)
184. L. Lefticariu, L.M. Pratt, E.M. Ripley, Mineralogic and sulfur isotopic effects accompanying oxidation of pyrite in millimolar solutions of hydrogen peroxide at temperatures from 4 to 150°C. *Geochim. Cosmochim. Acta* **70**(19), 4889–4905 (2006). <https://doi.org/10.1016/j.gca.2006.07.026>
185. D.K. Nordstrom, Effects of microbiological and geochemical interactions in mine drainage, in *Environmental Aspects of Mine Wastes, Short Course Series*, ed. by J.L. Jambor, D.W. Blowes, A.I.M. Ritchie, vol. 31, (Mineralogical Association of Canada, Ottawa, 2003), pp. 227–238
186. J.P. Jolivet, C. Chanéac, E. Tronc, Iron oxide chemistry. From molecular clusters to extended solid networks. *Chem. Commun.* **5**, 481–483 (2004). <https://doi.org/10.1039/B304532N>
187. J. Majzlan, S.C.B. Myneni, Speciation of iron and sulfate in acid waters: aqueous clusters to mineral precipitates. *Environ. Sci. Technol.* **39**(1), 188–194 (2004). <https://doi.org/10.1021/es049664p>
188. J.M. Bigham, D.K. Nordstrom, Iron and aluminum hydroxysulfates from acid sulfate waters. *Rev. Mineral. Geochem.* **40**, 351–403 (2000). <https://doi.org/10.2138/rmg.2000.40.7>
189. D.B. Johnson, T. Kanao, S. Hedrich, Redox transformations of iron at extremely low pH: fundamental and applied aspects. *Front. Microbiol.* **3**, 96 (2012). <https://doi.org/10.3389/fmicb.2012.00096>
190. M.A. Caraballo, J.D. Rimstidt, F. Macías, J.M. Nieto, M.F. Hochella, Metastability, nanocrystallinity and pseudo-solid solution constraints to schwertmannite solubility. *Chem. Geol.* **360/361**, 22–31 (2013). <https://doi.org/10.1016/j.chemgeo.2013.09.023>
191. R. Fan, G. Qian, Y. Li, M.D. Short, R.C. Schumann, M. Chen, R.S.C. Smart, A.R. Gerson, Evolution of pyrite oxidation from a 10-year kinetic leach study: implications for secondary mineralization in acid mine drainage control. *Chem. Geol.*, 120653 (2021). <https://doi.org/10.1016/j.chemgeo.2021.120653>
192. P. Ziemkiewicz, T. He, A. Noble, X. Liu, Recovery of rare earth elements (REEs) from coal mine drainage, in *West Virginia Mine Drainage Task Force Symposium*, (Morgantown, WV, USA, 2016)
193. L. Lefticariu, K.L. Klitzing, A. Kolker, Rare earth elements and yttrium (REY) in coal mine drainage from the Illinois Basin, USA. *Int. J. Coal Geol.* **217**, 103327 (2020). <https://doi.org/10.1016/j.coal.2019.103327>
194. A. Biswas, M.J. Hendry, J. Essilfie-Dughan, S. Day, S.A. Villeneuve, S.L. Barbour, Geochemistry of zinc and cadmium in coal waste rock, Elk Valley, British Columbia, Canada. *Appl. Geochem.*, 105148 (2021). <https://doi.org/10.1016/j.apgeochem.2021.105148>
195. J. Essilfie-Dughan, M.J. Hendry, J.J. Dynes, Y. Hu, A. Biswas, S.L. Barbour, S. Day, Geochemical and mineralogical characterization of sulfur and iron in coal waste rock, Elk Valley, British Columbia, Canada. *Sci. Total Environ.* **586**, 753–769 (2017). <https://doi.org/10.1016/j.scitotenv.2017.02.053>
196. J.A. Galhardi, D. Bonotto, Hydrogeochemical features of surface water and groundwater contaminated with acid mine drainage (AMD) in coal mining areas: a case study in southern Brazil. *Environ. Sci. Pollut. Res.* **23**, 18911–18189 (2016). <https://doi.org/10.1007/s11356-016-7077-3>
197. M. Shahhosseini, F.D. Ardejani, B. Ernest, Geochemistry of rare earth elements in a neutral mine drainage environment, Anjir Tangeh, Northern Iran. *Int. J. Coal Geol.* **183**, 120–135 (2017). <https://doi.org/10.1016/j.coal.2017.10.004>
198. C.W. Noack, D.A. Dzombak, A.K. Karamalidis, Rare earth element distributions and trends in natural waters with a focus on groundwater. *Environ. Sci. Technol.* **48**, 4317–4326 (2014). <https://doi.org/10.1021/es4053895>
199. A.E. Williams-Jones, A.A. Migdisov, I.M. Samson, Hydrothermal mobilization of the rare earth elements: a tale of “ceria” and “yttria”. *Elements* **8**, 355–360 (2012). <https://doi.org/10.2113/gselements.8.5.355>

200. Z.M. Migaszewski, A. Gałuszka, The characteristics, occurrence and geochemical behavior of rare earth elements in the environment: a review. *Crit. Rev. Environ. Sci. Technol.* **45**(5), 429–471 (2015). <https://doi.org/10.1080/10643389.2013.866622>
201. W. Zhang, R. Honaker, Process development for the recovery of rare earth elements and critical metals from an acid mine leachate. *Miner. Eng.* **153**, 106382 (2020). <https://doi.org/10.1016/j.mineng.2020.106382>
202. B.C. Hedin, R.S. Hedin, R.C. Capo, B.W. Stewart, Critical metal recovery potential of Appalachian acid mine drainage treatment solids. *Int. J. Coal Geol.* **231**, 103610 (2020). <https://doi.org/10.1016/j.coal.2020.103610>
203. A. Royer-Lavallee, C.M. Neculita, L. Coudert, Removal and potential recovery of rare earth elements from mine water. *J. Ind. Eng. Chem.* **89**, 47–57 (2020). <https://doi.org/10.1016/j.jiec.2020.06.010>
204. R. León, F. Macías, C.R. Cánovas, R. Pérez-López, C. Ayora, J.M. Nieto, M. Olías, Mine waters as a secondary source of rare earth elements worldwide: the case of the Iberian Pyrite Belt. *J. Geochem. Explor.* **224**, 106742 (2021). <https://doi.org/10.1016/j.gexplo.2021.106742>
205. B.C. Hedin, R.C. Capo, B.W. Stewart, R.S. Hedin, C.L. Lopano, M.Y. Stuckman, The evaluation of critical rare earth element (REE) enriched treatment solids from coalmine drainage passive treatment systems. *Int. J. Coal Geol.* **208**, 54–64 (2019). <https://doi.org/10.1016/j.coal.2019.04.007>
206. L. Lefticariu, S.R. Sutton, K.S. Bender, M. Lefticariu, M. Pentrak, J.W. Stucki, Impacts of detrital nano- and micro-scale particles ( $d_{NP}$ ) on contaminant dynamics in a coal mine AMD treatment system. *Sci. Total Environ.* **575**, 941–955 (2017). <https://doi.org/10.1016/j.scitotenv.2016.09.154>
207. M. Micari, A. Cipollina, A. Tamburini, M. Moser, V. Bertsch, G. Micale, Techno-economic analysis of integrated processes for the treatment and valorisation of neutral coal mine effluents. *J. Clean. Prod.* **270**, 122472 (2020). <https://doi.org/10.1016/j.jclepro.2020.122472>
208. A.M. Jones, R.N. Collins, T.D. Waite, Mineral species control of aluminum solubility in sulfate-rich acidic waters. *Geochim. Cosmochim. Acta* **75**, 965–977 (2011). <https://doi.org/10.1016/j.gca.2010.12.001>
209. D.G. Brookins, Aqueous geochemistry of rare earth elements. *Rev. Mineral. Geochem.* **21**(1), 201–225 (1989). <https://doi.org/10.1515/9781501509032-011>
210. S.A. Wood, The aqueous geochemistry of the rare earth elements and yttrium. 1. Review of available low-temperature data for inorganic complexes and the inorganic REE speciation of natural waters. *Chem. Geol.* **82**, 159–186 (1990). [https://doi.org/10.1016/0009-2541\(90\)90080-Q](https://doi.org/10.1016/0009-2541(90)90080-Q)
211. E.N. Rizkalla, G.R. Choppin, Lanthanides and actinides hydration and hydrolysis, in *Handbook on the Physics and Chemistry of Rare Earths. Lanthanides/Actinides: Chemistry*, ed. by K.A. Gschneider, L. Eyring, G.R. Choppin, G.H. Lander, vol. 18, (Elsevier Science B.V., Amsterdam, 1994). [https://doi.org/10.1016/S0168-1273\(05\)80050-9](https://doi.org/10.1016/S0168-1273(05)80050-9)
212. Y. Takahashi, H. Yoshida, N. Sato, K. Hama, Y. Yusa, H. Shimizu, W- and M-type tetrad effects in REE patterns for water-rock systems in the tonon uranium deposit, Central Japan. *Chem. Geol.* **184**, 311–335 (2002). [https://doi.org/10.1016/S0009-2541\(01\)00388-6](https://doi.org/10.1016/S0009-2541(01)00388-6)
213. M.I. Leybourne, K.H. Johannesson, Rare earth elements (REE) and yttrium in stream waters, stream sediments and Fe-Mn oxyhydroxides: fractionation, speciation and controls over REE + Y patterns in the surface environment. *Geochim. Cosmochim. Acta* **72**, 5962–5983 (2008). <https://doi.org/10.1016/j.gca.2008.09.022>
214. A. Thompson, M.K. Amistadi, O.A. Chadwick, J. Chorover, Fractionation of yttrium and holmium during basaltic soil weathering. *Geochim. Cosmochim. Acta* **119**, 18–30 (2013). <https://doi.org/10.1016/j.gca.2013.06.003>
215. J. Schijf, R.H. Byrne, Speciation of yttrium and the rare earth elements in seawater: review of a 20-year analytical journey. *Chem. Geol.* **584**, 120479 (2021). <https://doi.org/10.1016/j.chemgeo.2021.120479>
216. M. Bau, Scavenging of dissolved yttrium and rare earths by precipitating iron oxyhydroxide: experimental evidence for Ce oxidation, Y–Ho fractionation and lanthanide tetrad effect. *Geochim. Cosmochim. Acta* **63**, 67–77 (1999). [https://doi.org/10.1016/S0016-7037\(99\)00014-9](https://doi.org/10.1016/S0016-7037(99)00014-9)

217. I.L. Wallrich, B.W. Stewart, R.C. Capo, B.C. Hedin, T.T. Phan, Neodymium isotopes track sources of rare earth elements in acidic mine waters. *Geochim. Cosmochim. Acta* **269**, 465–483 (2020). <https://doi.org/10.1016/j.gca.2019.10.044>
218. K.H. Johannesson, W.B. Lyons, M.A. Yelken, H.E. Gaudette, K.J. Stetzenbach, Geochemistry of the rare earth elements in hypersaline and dilute acidic natural terrestrial waters: complexation behavior and middle rare earth element enrichments. *Chem. Geol.* **133**(1–4), 125–144 (1996). [https://doi.org/10.1016/S0009-2541\(96\)00072-1](https://doi.org/10.1016/S0009-2541(96)00072-1)
219. E.R. Sholkovitz, T.M. Church, R. Arimoto, Rare earth element composition of precipitation, precipitation particles and aerosols. *J. Geophys. Res. Atmos.* **98**(D11), 20587–20599 (1993). <https://doi.org/10.1029/93JD01926>
220. M. Iwashita, A. Saito, M. Arai, Y. Furusho, T. Shimamura, Determination of rare earth elements in rainwater collected in suburban Tokyo. *Geochem. J.* **45**(3), 187–197 (2011). <https://doi.org/10.2343/geochemj.1.0121>
221. O. Eterigho-Ikelegbe, H. Harrar, S. Bada, Rare earth elements from coal and coal discard – a review. *Miner. Eng.* **173**, 107187 (2021). <https://doi.org/10.1016/j.mineng.2021.107187>
222. A. Lozano, C. Ayora, A. Fernandez-Martinez, Sorption of rare earth elements onto Basaluminite: the role of sulfate and pH. *Geochim. Cosmochim. Acta* **258**, 50–62 (2019). <https://doi.org/10.1016/j.gca.2019.05.016>
223. P.L. Verplanck, D.K. Nordstrom, H.E. Taylor, B.A. Kimball, Rare earth element partitioning between hydrous ferric oxides and acid mine water during iron oxidation. *Appl. Geochem.* **19**, 1339–1354 (2004). <https://doi.org/10.1016/j.apgeochem.2004.01.016>
224. C.H. Gammons, S.A. Wood, D.A. Nimick, Diel behavior of rare earth elements in a mountain stream with acidic to neutral pH. *Geochim. Cosmochim. Acta* **69**(15), 3747–3758 (2005). <https://doi.org/10.1016/j.gca.2005.03.019>
225. S.A. Wood, C.H. Gammons, S.R. Parker, The behavior of rare earth elements in naturally and anthropogenically acidified waters. *J. Alloys Compd.* **418**(1–2), 161–165 (2006). <https://doi.org/10.1016/j.jallcom.2005.07.082>
226. M.L.B. Moraes, A. Murciego, E. Lvarez-Ayuso, A.C.Q. Ladeira, The role of Al13-polymers in the recovery of rare earth elements from acid mine drainage through pH neutralization. *Appl. Geochem.* **113**, 104466 (2019). <https://doi.org/10.1016/j.apgeochem.2019.104466>
227. S.A. Welch, A.G. Christy, L. Isaacson, D. Kirste, Mineralogical control of rare earth elements in acid sulfate soils. *Geochim. Cosmochim. Acta* **73**, 44–64 (2009). <https://doi.org/10.1016/j.gca.2008.10.017>
228. R. Pérez-López, J. Delgado, J.M. Nieto, B. Márquez-García, Rare earth element geochemistry of sulphide weathering in the São Domingos Mine Area (Iberian Pyrite Belt): a proxy for fluid-rock interaction and ancient mining pollution. *Chem. Geol.* **276**, 29–40 (2010). <https://doi.org/10.1016/j.chemgeo.2010.05.018>
229. A. Grawunder, D. Merten, G. Büchel, Origin of middle rare earth element enrichment in acid mine drainage-impacted areas. *Environ. Sci. Pollut. Res.* **21**, 6812–6823 (2014). <https://doi.org/10.1007/s11356-013-2107-x>
230. E.R. Sholkovitz, The aquatic chemistry of rare earth elements in rivers and estuaries. *Aquat. Geochem.* **1**(1), 1–34 (1995). <https://doi.org/10.1007/BF01025229>
231. R.E. Hannigan, E.R. Sholkovitz, The development of middle rare earth element enrichments in freshwaters: weathering of phosphate minerals. *Chem. Geol.* **175**(3–4), 495–508 (2001). [https://doi.org/10.1016/S0009-2541\(00\)00355-7](https://doi.org/10.1016/S0009-2541(00)00355-7)
232. E. Da Silva, E. Ferreira, I. Bobos, J. Matos, C. Patinha, A.P. Reis, E.C. Fonseca, Mineralogy and geochemistry of trace metals and REE in massive volcanic sulphide host rocks, stream sediments, stream waters and acid mine drainage from the Lousal Mine Area (Iberian Pyrite Belt, Portugal). *Appl. Geochem.* **24**, 383–401 (2009). <https://doi.org/10.1016/j.apgeochem.2008.12.001>
233. K.A. Quinn, R.H. Byrne, J. Schijf, Sorption of yttrium and rare earth elements by amorphous ferric hydroxide: influence of pH and ionic strength. *Mar. Chem.* **99**, 128–150 (2006). <https://doi.org/10.1016/j.marchem.2005.05.011>

234. D.B. Johnson, K.B. Hallberg, Acid mine drainage remediation options: a review. *Sci. Total Environ.* **338**, 3–14 (2005). <https://doi.org/10.1016/j.scitotenv.2004.09.002>
235. J.G. Skousen, C.E. Zipper, A. Rose, P.F. Ziemkiewicz, R.W. Nairn, L.M. McDonald, R.L. Kleinmann, Review of passive systems for acid mine drainage treatment. *Mine Water Environ.* **36**, 133–153 (2017). <https://doi.org/10.1007/s10230-016-0417-1>
236. P.T. Behum, L. Lefticariu, K.S. Bender, Y.T. Segid, A.S. Burns, C.W. Pugh, Remediation of coal-mine drainage by a sulfate-reducing bioreactor: a case study from the Illinois Coal Basin, USA. *Appl. Geochem.* **26**, S162–S166 (2011). <https://doi.org/10.1016/j.apgeochem.2011.03.093>
237. P.L. Younger, S.A. Banwart, R.S. Hedin, *Mine Water – Hydrology, Pollution, Remediation* (Kluwer Academic Publishers, Dordrecht, 2002)
238. J.G. Skousen, A. Sexstone, P.F. Ziemkiewicz, Acid mine drainage control and treatment, in *Reclamation of Drastically Disturbed Lands*, ed. by R.I. Barnhisel, R.G. Darmody, W.L. Daniels, (American Society of Agronomy Monograph 41, Madison, 2000), pp. 131–168. <https://doi.org/10.2134/agronmonogr41.c6>
239. J. Weijma, C. Copini, C. Buisman, C. Schultz, Biological recovery of metals, sulfur and water in the mining and metallurgical industry, in *Water Recycling and Recovery in Industry*, ed. by P.N.L. Lens, L.W. Hulshoff Pol, P. Wilderer, T. Asano, (IWA Publishing, London, 2002)
240. R. Hedin, T. Weaver, N. Wolfe, K. Weaver, Passive treatment of acidic coal mine drainage: the Anna’s mine passive treatment complex. *Mine Water Environ.* **29**(3), 165–175 (2010). <https://doi.org/10.1007/s10230-010-0117-1>
241. Hedin Environmental, Optimizing the design and operation of self-flushing limestone systems for mine drainage treatment (2008). Retrieved from: <http://files.dep.state.pa.us/Mining/Abandoned%20Mine%20Reclamation/AbandonedMinePortalFiles/InnovativeTechnologyGrantFinalReports/Flushing.pdf>
242. B. Erickson, Rare earth recovery. *Chem. Eng. News* **96**(28), 28–33 (2018). <https://asset-pdf.scinapse.io/prod/2871462933/2871462933.pdf>
243. S.R. Sutton, A. Lanzirotti, M. Newville, M.L. Rivers, P. Eng, L. Lefticariu, Spatially resolved elemental analysis, spectroscopy and diffraction at the GSECARS sector at the advanced photon source. *J. Environ. Qual.* **46**(6), 1158–1165 (2017). <https://doi.org/10.2134/jeq2016.10.0401>
244. J.M. Bigham, U. Schwertmann, S.J. Traina, R.L. Winland, M. Wolf, Schwertmannite and the chemical modeling of iron in acid sulfate waters. *Geochim. Cosmochim. Acta* **60**, 2111–2121 (1996). [https://doi.org/10.1016/0016-7037\(96\)00091-9](https://doi.org/10.1016/0016-7037(96)00091-9)
245. U. Schwertmann, L. Carlson, The pH-dependent transformation of schwertmannite to goethite at 25°C. *Clay Mineral.* **40**, 63–66 (2005). <https://doi.org/10.1180/0009855054010155>
246. J.P. Jolivet, C. Chanéac, D. Chiche, S. Cassignon, O. Durupthy, J. Hernandez, Basic concepts of the crystallization from aqueous solutions: the example of aluminum oxy(hydroxi)des and aluminosilicates. *Compt. Rendus Geosci.* **343**, 113–122 (2011). <https://doi.org/10.1016/j.crte.2010.12.006>
247. A.E. Van Driessche, T.M. Stawski, L.G. Benning, M. Kellermeier, Chapter 12: Calcium sulfate precipitation throughout its phase diagram, in *New Perspectives on Mineral Nucleation and Growth*, (Springer, 2017), pp. 227–256. [https://doi.org/10.1007/978-3-319-45669-0\\_12](https://doi.org/10.1007/978-3-319-45669-0_12)
248. H. Tan, G. Zhang, P.J. Heaney, S.M. Webb, W.D. Burgos, Characterization of manganese oxide precipitates from Appalachian coal mine drainage treatment systems. *Appl. Geochem.* **25**(3), 389–399 (2010). <https://doi.org/10.1016/j.apgeochem.2009.12.006>
249. F. Luan, C.M. Santelli, C.M. Hansel, W.D. Burgos, Defining manganese(II) removal processes in passive coal mine drainage treatment systems through laboratory incubation experiments. *Appl. Geochem.* **27**(8), 1567–1578 (2012). <https://doi.org/10.1016/j.apgeochem.2012.03.010>
250. J. Sánchez-España, I. Yusta, W.D. Burgos, Geochemistry of dissolved aluminum at low pH: hydrobasaluminite formation and interaction with trace metals, silica and microbial cells under anoxic conditions. *Chem. Geol.* **441**, 124–137 (2016). <https://doi.org/10.1016/j.chemgeo.2016.08.004>

251. U.S. Department of Energy (U.S. DOE), Critical materials strategy. Darby, Pennsylvania, U.S. Department of Energy report, DOE/PI-0009 (2011), 190 p. [https://www.energy.gov/sites/prod/files/DOE\\_CMS2011\\_FINAL\\_Full.pdf](https://www.energy.gov/sites/prod/files/DOE_CMS2011_FINAL_Full.pdf)
252. G.H. Luttrell, M.J. Kiser, R.-H. Yoon, A. Noble, M. Rezaee, A. Bhagavatula, R.Q. Honaker, Field Survey of rare earth element concentrations in process streams produced by coal preparation plants in the eastern USA. *Min. Metall. Explor.* **36**, 889–902 (2019). <https://doi.org/10.1007/s42461-019-00124-5>
253. S. Das, G. Gaustad, A. Sekar, E. Williams, Techno-economic analysis of supercritical extraction of rare earth elements from coal ash. *J. Clean. Prod.* **189**, 539–551 (2018). <https://doi.org/10.1016/j.jclepro.2018.03.252>
254. M. Summers, The path to commercialization through techno-economics: presentation. U.S. Department of Energy, National Energy Technology Laboratory Project Review Meeting for Rare Earth Elements (REE) Program, April 10 (2018). [https://netl.doe.gov/sites/default/files/netl-file/20180410\\_1030C\\_Presentation\\_Summers\\_NETL.pdf](https://netl.doe.gov/sites/default/files/netl-file/20180410_1030C_Presentation_Summers_NETL.pdf)
255. W. Sutterlin, Recovery of rare earth elements from coal mining waste materials: presentation. U.S. Department of Energy, National Energy Technology Laboratory Project Review Meeting for Rare Earth Elements (REE) Program, April 10 (2018). [https://netl.doe.gov/sites/default/files/netl-file/20180410\\_0900C\\_Presentation\\_FE0030146\\_InventureRenewables.pdf](https://netl.doe.gov/sites/default/files/netl-file/20180410_0900C_Presentation_FE0030146_InventureRenewables.pdf)
256. Ellen MacArthur Foundation, Towards the circular economy 3 — accelerating the scale-up across global supply chains. Cowes, Isle of Wight, United Kingdom, Ellen MacArthur Foundation report, January (2014), 76 p. <https://ellenmacarthurfoundation.org/towards-the-circular-economy-vol-3-accelerating-the-scale-up-across-global>
257. É. Lèbre, G. Corder, A. Golev, The role of the mining industry in a circular economy: a framework for resource management at the mine site level. *J. Ind. Ecol.* **21**(3), 662–672 (2017)
258. B. Folkedahl, Economic extraction and recovery of REEs and production of clean value-added products from low-rank coal fly ash. Poster, U.S. Department of Energy, National Energy Technology Laboratory Project Review Meeting for Rare Earth Elements (REE) Program, April 10 (2018). [https://netl.doe.gov/sites/default/files/netl-file/2018\\_Poster-04\\_FE0031490\\_UNDEERC.pdf](https://netl.doe.gov/sites/default/files/netl-file/2018_Poster-04_FE0031490_UNDEERC.pdf)
259. R.Q. Honaker, W. Zhang, J. Werner, A. Noble, G.H. Luttrell, R.H. Yoon, Enhancement of a process flowsheet for recovering and concentrating critical materials from bituminous coal sources. *Min. Metall. Explor.* **37**(1), 3–20 (2020)
260. B.V. Hassas, M. Rezaee, S.V. Pisupati, Precipitation of rare earth elements from acid mine drainage by CO<sub>2</sub> mineralization process. *Chem. Eng. J.* **399** (2020). <https://doi.org/10.1016/j.cej.2020.125716>
261. R.Q. Honaker, W. Zhang, X. Yang, M. Rezaee, Conception of an integrated flowsheet for rare earth elements recovery from coal coarse refuse. *Miner. Eng.* **122**, 233–240 (2018). <https://doi.org/10.1016/j.mineng.2018.04.005>
262. W. Zhang, R.Q. Honaker, Calcination pretreatment effects on acid leaching characteristics of rare earth elements from middlings and coarse refuse material associated with a bituminous coal source. *Fuel* **249**, 130–145 (2019). <https://doi.org/10.1016/j.fuel.2019.03.063>
263. P.K. Sarswat, Z. Zhang, M.L. Free, Rare earth elements extraction from coal waste using a biooxidation approach, in *Rare Metal Technology*, ed. by G. Azimi, T. Ouchi, K. Forsberg, H. Kim, S. Alam, A. Abdullahi Baba, N.R. Neelamegah, (Springer, 2021), pp. 210–216. <https://link.springer.com/book/10.1007%2F978-3-030-65489-4>
264. U.S. Environmental Protection Agency (U.S. EPA), Section 404 of the Clean Water Act—Clean Water Act, Section 402: National Pollutant Discharge Elimination System (2021). <https://www.epa.gov/cwa-404/clean-water-act-section-402-national-pollutant-discharge-elimination-system>
265. Internal Revenue Service, 26 CFR Part 1 [TD9944] RIN 1545–BP42 credit for carbon oxide sequestration. *Fed. Regist.* **86**(10), 4728–4773 (2021)

# Chapter 4

## Rare Earth Ore Flotation Principles and Kinetics: Significance of Collectors and Application of Novel Depressants



Courtney A. Young, Peter A. Amelunxen, and Richard LaDouceur

### 4.1 Introduction

#### 4.1.1 Rare Earth Minerals

Rare earth elements (REEs) are comprised of the 15 lanthanides as well as scandium (Sc) and yttrium (Y) due to similarities in their physical and chemical properties. Because of these similarities, REEs are often sub-grouped into light (LREEs), middle (MREEs), and heavy (HREEs) categories. Properties within each subgroup are practically the same. In fact, property differences within each subgroup are so subtle that making separations among them is very difficult. Consequently, initial processing usually correlates to the REEs being separated from associated waste and perhaps later into these subgroups as opposed to individual REEs. Normally, LREEs include lanthanum (La), cerium (Ce), praseodymium (Pr), neodymium (Nd), and promethium (Pm); MREEs are samarium (Sm), europium (Eu), gadolinium (Gd), terbium (Tb), and dysprosium (Dy); and HREEs constitute holmium (Ho), erbium (Er), thulium (Tm), ytterbium (Yb), and lutetium (Lu). Furthermore, Sc is usually considered to be an LREE and Y as an HREE due to elemental associations with the corresponding REEs. It is understood that promethium (Pm) is essentially nonexistent because all of its isotopes are radioactive with half-lives too short for them to accumulate appreciably in nature.

---

C. A. Young (✉)

Montana Tech, Metallurgical and Materials Engineering, Butte, MT, USA

e-mail: [cyoung@mtech.edu](mailto:cyoung@mtech.edu)

P. A. Amelunxen

Hudbay Minerals, Toronto, ON, Canada

R. LaDouceur

Montana Tech, Mechanical Engineering, Butte, MT, USA

In general, REEs exist in natural resources in two forms of deposits, either in an adsorbed state on ion-exchangeable clays or in a crystalline state within mineral structures. Most primary production of HREEs comes from Southern China with most reportedly involving kaolinite and halloysite clays. Both clays have the same chemical composition of  $\text{Al}_2\text{Si}_2\text{O}_5(\text{OH})_4$ . On the other hand, so-called rare earth minerals (REMs) occur in one of six types of deposits: carbonatites, peralkaline igneous systems, magmatic magnetite-hematite bodies, iron oxide-copper-gold deposits, xenotime-monazite accumulations in mafic gneiss, and monazite-xenotime-bearing placer deposits [1]. REMs themselves generally exist as four kinds depending on which anions the corresponding REE cations are bound to, namely oxides (REOs), phosphates (REPs), carbonates (RECs), and silicates (RESSs). Because carbonatites are the most prevalent deposits, RECs are the most common REMs. Most carbonatite deposits are associated with LREEs and include the orebodies at Bayan Obo in China and Mountain Pass in California [2].

However, most non-clay mineral deposits contain more than one kind of REM. They particularly change with location due to depth, aeration, hydration, and, of course, time (i.e., age). Furthermore, REMs are usually comprised of at least two REEs and often with other elements, forming solid solutions of variable content and purity due to nonstoichiometric substitutions in the crystal lattice. There are nearly 250 known REMs, but the most prevalent appear to be knopite and loparite as REOs, xenotime and monazite as REPs, bastnaesite and parasite as RECs, and allanite and gadolinite as RESSs [3]. Most REMs are LREE-dominant but those containing Y tend to contain the most HREEs. Monazites can also be HREE-rich. It is important to note that an ore is, by definition, a deposit that can be mined and processed economically.

### ***4.1.2 Flotation***

In order to prepare ores for separation, the minerals must first be comminuted from run-of-mine (ROM) feed that can be as large as three-foot boulders into products with the size-consistency no larger than sand. Comminution generally consists of blasting followed by dry crushing and then wet grinding to yield a slurry. The final product size depends on many factors. Generally, it is optimized to maximize liberation of the valuable minerals from the invaluable gangue, subject to downstream processing, and cost constraints. Ultimately, the separation process is used to maximize recovery and grade of the valuable minerals being selectively separated to produce the concentrate. In the past, dry processing by electrostatic separation was used but required either dry grinding or slurries be dried. Today, all REM ores tend to be wet processed by froth flotation, also known simply as flotation, to produce a final concentrate. However, depending on the type of deposit, preconcentration by either magnetic or gravity separation may be done.

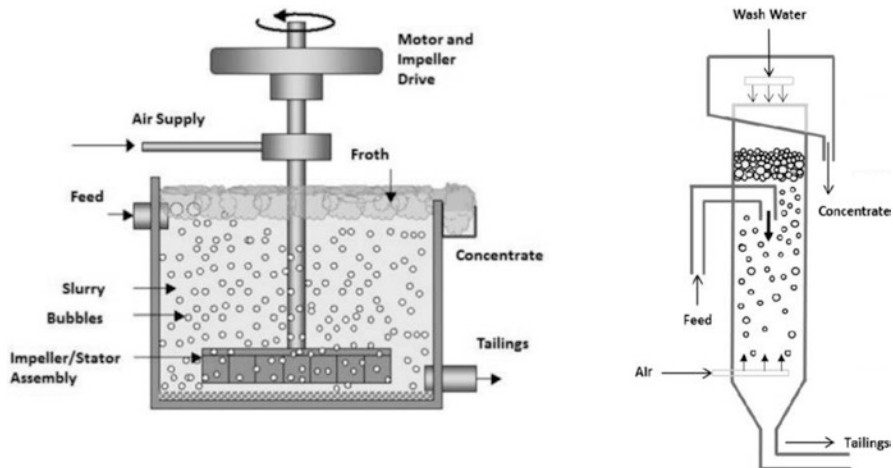
Flotation, when applied to REM ores, is used to separate hydrophobic REM particles from hydrophilic gangue particles in a slurry. When air is injected into the slurry, bubbles are generated and attach to the hydrophobic REM particles which



then float to the slurry surface, thereby forming a froth that is removed by mechanical or hydraulic means into a REM concentrate. The hydrophilic gangue particles exit out the slurry bottom as tailings. Although there are several types of flotation devices, the two most common types are the mechanical agitation cell and column (Fig. 4.1). Typically, each are used under different circumstances. Generally speaking, the agitation cells are used to keep coarse sizes (i.e., sand) pulped with turbulent mixing which allows them to be used on ores at high capacity yielding rougher concentrates. By comparison, columns are used on fine sizes (i.e., powders) in predominantly quiescent conditions at low capacity to process the rougher concentrates into cleaner concentrates.

Flotation can be enhanced using various surface-active reagents including but not limited to collectors, activators, depressants, modifiers, and frothers:

- Collectors are heteropolar molecules that have a reactive inorganic head group and inert organic tail. The head group bonds preferentially with REEs so adsorption occurs selectively at REM surfaces, causing the organic tail to protrude into solution and make the surface hydrophobic. Common REM collectors include hydroxamates, carboxylates, and phosphoric acids with organic tails of various lengths. The most prevalent include octyl hydroxamate (=  $C_8$ ) and fatty acid (e.g., oleic =  $C_{18}$ ).
- Activators are used to increase collector adsorption at the REM surfaces so they can become more hydrophobic and thereby float better into the froth. Common activators include oxalate ( $C_2O_4^{2-}$ ) as well as metal cations of, for example,  $Pb^{2+}$ ,  $Fe^{2+}$ , and  $Co^{2+}$ .
- Depressants are used to prevent collector adsorption on gangue so they remain hydrophilic and therefore report to the tailings. Numerous depressants have been used and depend greatly on what REMs and gangue are present. Common examples include inorganics like sodium silicate ( $Na_2SiO_3$ ) and sodium fluoride ( $NaF$ ) and organics like starch and quebracho.



**Fig. 4.1** Basic schematics of a conventional agitation flotation cell at left and flotation column at right [4]

- Modifiers can act simultaneously as both activators and depressants and are exemplified by pH reagents such as hydrochloric acid (HCl), soda ash ( $\text{Na}_2\text{CO}_3$ ), and caustic (NaOH). For basic pH control, soda ash is favored because it can also serve as a depressant for gangue like calcite and barite. Lime, as either CaO or  $\text{Ca}(\text{OH})_2$ , is avoided because  $\text{Ca}^{2+}$  can act as an activator for gangue, particularly silicates.
- Frothers stabilize the froth so that it does not break until after it reports to the launder as concentrate. Frothers are often categorized according to the stability of their respective froths. The two most commonly used frothers are methyl isobutyl carbinol (MIBC) and Dow Froth 250 which is a polypropylene glycol methyl ether. Although there is no correlation established yet, Jordens et al. [3] illustrated MIBC, a weak frother, yielded poor flotation recoveries, opposite that obtained with Flottec 150, a strong frother containing a proprietary mixture of polyglycols.

These and other reagents are explored in detail in general reviews [3, 5, 6] as well as specific REM applications [7, 8].

Studies have revealed that collectors may work well for floating some, but not all, REMs due to which REEs are present and which anions they are bound to [9–11]. This phenomenon has been attributed to a combination of lanthanide contraction and coordination number (CN). For example, REOs have CNs of 6–7 so REE atomic diameters range from 2.460 Å for La to 2.002 Å for Lu. Likewise, REPs have CNs of 8–9 so REE atomic diameters are larger ranging from 2.700 Å for La to 2.234 Å for Lu, and RECs have CNs of 10 so atomic diameters are even larger ranging from 2.800 Å for La to 2.460 Å for Lu. Thus, if flotation is conducted with a single collector that targets a particular REE diameter, it may preferentially float. Thus, for example, LREOs, MREPs, and HRECs may float well but HREOs and LRECs may not [12]. Hence, blends of at least two collectors should be used to float all REMs. As an example, Greenland Minerals [13] has noted they have so far been using a single collector for their studies but have different recoveries of 87% for LREOs and 68% for HREOs [13]. Clearly, both recoveries could increase upon using collector blends as has been the case for several successful studies [6, 14–19].

### 4.1.3 Flowsheets

Flotation flowsheets can vary significantly from one operation to another. A typical flowsheet will have a series of flotation cells known as roughers to produce an initial rougher concentrate. The rougher tailings may be processed further in another series of cells called scavengers to produce a scavenger concentrate as well as final tailings. The rougher concentrate may then be refloat in another series of flotation cells referred to as cleaners. The cleaner concentrate is usually the final concentrate but can be processed further with additional cleaning. Scavenger concentrates and cleaner tailings are usually fed back to the roughers and may be reground for liberation and sizing purposes.

An example industrial flowsheet is simplified and shown in Fig. 4.2 for the Bayan Obo operation. The flowsheet illustrates how Bayan Obo utilizes a classical comminution circuit to size the ore to less than 74 microns. That is followed by both

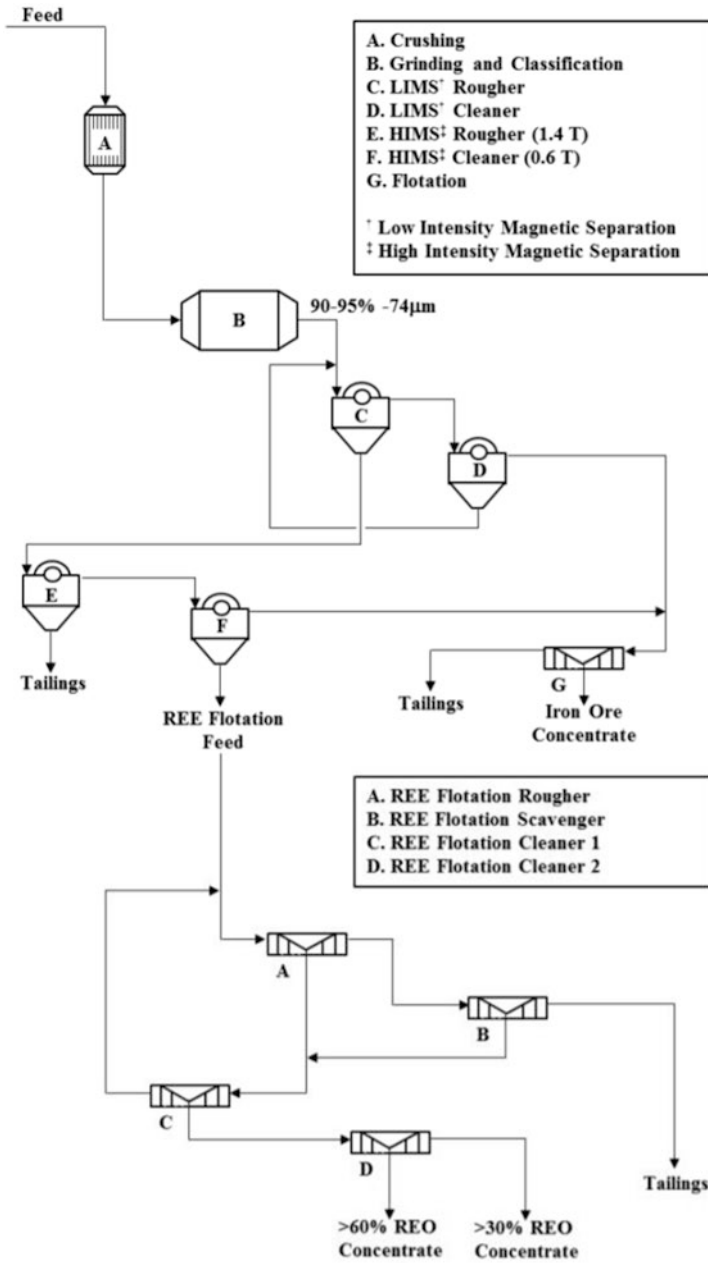


Fig. 4.2 Bayan Obo flowsheet for processing REE-bearing iron ore [20, 21]

low- and high-intensity magnetic separation (LIMS and HIMS) to not only remove iron minerals (mostly hematite,  $\text{Fe}_2\text{O}_3$ ) for feeding to the iron flotation cells but, more importantly, to preconcentrate the REMs (mostly bastnaesite and monazite) as feed to the REE flotation circuit and produce a rougher REM concentrate. The rougher concentrate is cleaned to yield a final concentrate; however, the concentrate is further cleaned to separate the bastnaesite and monazite. The bastnaesite concentrate exceeds 60% equivalent REO and the monazite concentrate exceeds 30% equivalent REO. All flotation is conducted using soda ash (pH 9) and J10 frother which is believed to be MIBC. For rougher and first cleaner flotation, naphthyl hydroxamate is used as the collector and sodium silicate as the silicate mineral depressant. The final cleaner cells use either phthalic acid or benzoic acid as the collector for the bastnaesite and alum, presumably  $\text{KAl}(\text{SO}_4)_2$ , as the depressant for monazite. Thus, the final cleaner cell appears to use a collector blend.

Another example of industrial REM flotation is at Mountain Pass per Fig. 4.3. In this case, after comminuting the ore to a size initially below 150 microns, resulting slurries are heated to 180 °F and conditioned for approximately 10 minutes with three main reagents: soda ash as pH modifier, lignin sulfonate as depressant, and fatty acid as collector. Roughers are employed to produce a concentrate which is then cleaned four times. Furthermore, the first cleaner tailings are scavenged to assure maximum recovery of REMs which is mostly bastnaesite. In addition, the scavenger tailings and the rougher tailings are combined as final tailings and the scavenger concentrate is reground below 44 microns for liberation purposes and combined with rougher feed. Recently, Mountain Pass started using a second collector in their flotation circuit. This collector blend is proprietary but appears to include octyl hydroxamate.

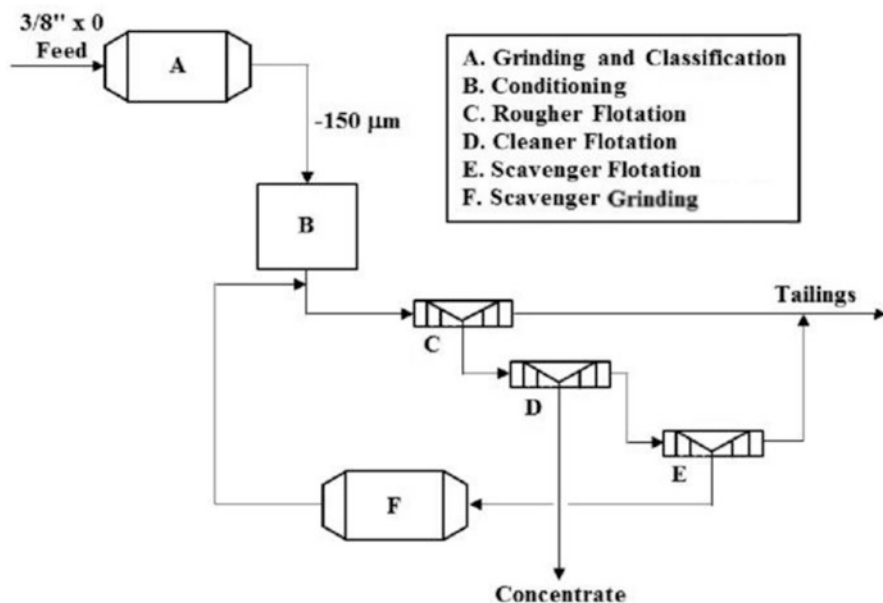


Fig. 4.3 Mountain Pass flotation flowsheet for processing REE ore [21, 22]

#### 4.1.4 Modeling

Flotation is used to separate and concentrate approximately 50% of the world's mineral commodities and is often viewed as a simple process. This is a misconception. Like most separation processes, the primary goals are to maximize both recovery and grade of valuable mineral to the concentrate. However, these responses are inversely related such that increasing one usually comes at the sacrifice of the other. Furthermore, the flotation process is controlled by at least 30 variables, albeit some variables have more dramatic impacts than others and they are not always straightforward because of variable interaction. For example, soda ash is dual purpose; it is a pH modifier because it serves as a depressant for some minerals and as an activator for other minerals. If it is added in excess, it can cause all minerals to depress but, if it is added insufficiently, the minerals needing activation may not float well. In this regard, the design or optimization goals can be difficult to achieve. Often, they must be realized via optimization (i.e., developing an appropriate model that simultaneously accounts for as many variables as possible).

Empirical modeling methods are the most common in industry, due to their simplicity. Unfortunately, there are many disadvantages associated with these methods. One of the most significant disadvantages is that they often employ scale-up or correction factors that are based on the operator's experience and skill in properly assessing the process. Due to this user dependence, empirical models are often not reliable.

So-called compartmental kinetic models are perhaps the most widely accepted phenomenological model of flotation [23]. These models are "compartmental" because they divide the flotation system into two or more distinct "compartments," each with their own unique characteristics and sub-models. For example, the two-compartment model incorporates separate models for the pulp or collection zone and the froth zone. There are some limitations associated with a two-compartment kinetic model, including over-simplification of the froth recovery, water recovery, and collection zone. The degree of hydraulic entrainment must also be considered to properly account for the kinetics of fast floating versus slow-floating minerals.

The mineral flotation kinetics will depend on the hydrophobicity of the particle. The flotation kinetics in a particular flotation cell are affected by many different variables including those that are hydrodynamic, chemical and mechanical. The entrainment is also affected by the amount of froth lost back into the cell. In laboratory tests, at slower scraping rates, the froth has a higher chance of being lost back into the cell. This reduces the mineral recovery across the froth zone; yet, this is often ignored when interpreting laboratory kinetics data [24]. The use of a high-fidelity kinetic model with three compartments accounts for the entrainment phase while avoiding the drawbacks of the methods described above. It has been shown that the scraping frequency needs to be quick at the beginning of a laboratory flotation test to properly model the flotation kinetics in an industrial setting. This method can be used for scaling up and models most minerals well. Currently, the shape of the particles is assumed to be spherical in the model.

To emphasize this modeling philosophy in the ensuing case study, computational fluid dynamics (CFD) was incorporated to apply the phenomenological processes that occur in a traditional, mechanically agitated flotation cell using a comprehensive three-compartment kinetic model with consideration for mass transport. This was accomplished by examining the effect of depressants on grade and recovery as responses from a parametric design of experiments conducted to determine first-order rate constants by varying the parameters which included collector dosage and four novel depressant types. Resulting models were found to be statistically significant.

## 4.2 Methods

A rare earth containing ore (approximately 1.5–2% REE) was obtained from the Bear Lodge Project operated by Rare Element Resources (RER) for this study [25]. The ore was chosen as it contained only trace amounts of uranium and thorium (<0.05%). The ore sample was homogenized and split into approximately 1.2 kg samples which would be used for the flotation experiments. A 60%-solid by mass slurry was prepared using deionized water and placed into a rod mill under varying conditions depending upon the experiment matrix.

A cylindrical six-liter flotation cell designed by FLSmidth was used for the flotation testing. The flotation experiments were performed by varying the flotation cell energy input parameters of volumetric air input flow rate and flotation cell rotor speed depending upon the experiment matrix. Level in the flotation cell was maintained using a 20-liter conditioning tank. Frother and pH modifiers were added into the conditioning tank. Methyl isobutyl carbinol was used as the frother at a dosage of 125 grams per ton. Hydrochloric acid (1 M HCl) or sodium hydroxide (1 M NaOH) was used as pH modifiers depending on the desired flotation pH. The flotation cell is shown in Fig. 4.4.

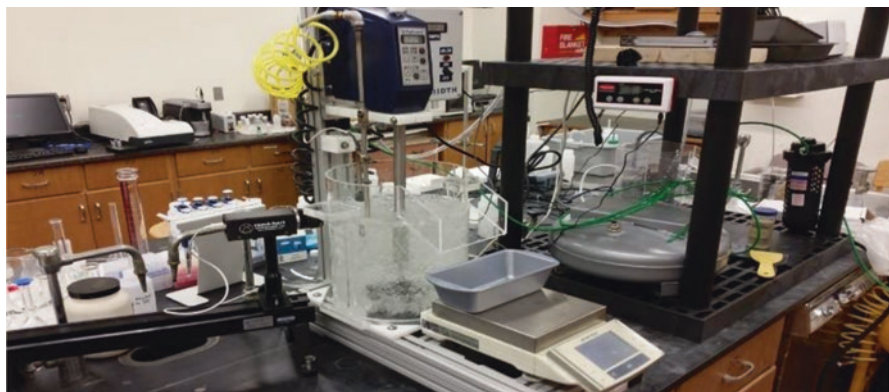


Fig. 4.4 FLSmidth laboratory flotation cell

Prior to the beginning of the experiment, an approximately 0.4 L feed sample of the slurry was taken and wet-sieved. Flotation experimentation for the REM tests was performed based on the simple kinetics test (SKT) designed by Aminpro [24] for all collectors and depressants. SKT is performed for 30 minutes with samples collected at predetermined times. In the case of these experiments, concentration samples were collected at 45 seconds (Con 1), 2 minutes (Con 2), 8 minutes (Con 3), and 30 minutes (Con 4). The collection times allow for the separation of fast floating and slow-floating minerals.

The sized feed, timed concentrate, and tailings samples were prepared and then analyzed using a LEO 14.30VP scanning electron microscope (SEM) equipped with an Ametek Apollo 40 electron dispersive X-ray analysis (EDAX) detector for all collectors and depressants. SEM imaging as well as spectroscopy was conducted at an electron beam accelerating potential of 25 kV. Samples were prepared for the SEM using a cross mount procedure. Cross mounting procedure involves mixing the flotation samples with carbon and then epoxy resulting in a sample block. The block is then cut in half through the thickness to ensure a sample face with both light and heavy or small and large particles. A puck is formed by mounting the block face side down in epoxy. The puck was then coarse polished from 400 to 180 microns and fine polished from 15 to 0.3 microns. Afterward, the surface was carbon coated. EDAX spectra from the SEM were analyzed using mineral liberation analysis (MLA) software by FEI to semi-quantitatively determine the weight fraction of REMs present in feed, concentrate, and tailings samples as well as REM liberation and association.

A design of experiment matrix was created using Design-Expert 10 by Stat-Ease Inc. for the depressants with salicyl hydroxamic acid (SHA) as the chosen collector. The matrix set flotation cell energy input parameters, impeller rotor speed, and air flow rate, to 2200 rpm and 20 lpm, respectively. Type of depressant, collector dosage, and whether the depressant was added were varied. The matrix was set using a two-factorial design with three parameters and three midpoints for curvature, which resulted in 12 tests. Each depressant (Huntsman Polymax T10, T12, and K55) would be tested with a dosage of 417 g/ton (0.83 lb/ton) and dosages of SHA at 417 g/ton (0.83 lb/ton), 750 g/ton (1.5 lb/ton), and 1083 g/ton (2.17 lb/ton). Polymax T10 and T12 are different concentrations of diethylene glycol monobutyl ether (DGME), a nonionic polymer and Polymax K55 is a sodium sulfate-based ionic comb-graft copolymer. The matrix for the design of experiments is shown in Table 4.1.

### 4.3 Results and Discussions

Twelve flotation experiments were performed based on the design of experiments matrix (Table 4.1) and the simple kinetics test parameters. The REMs present in the ore in major quantities were monazite and parisite. A typical feed grade for the REMs and select gangue is shown in Table 4.2. Mineral grade or weight percent of REMs tends to the smaller particle sizes along with calcite while potassium feldspar

**Table 4.1** Parametric design of experiments for REM flotation using depressants

Experiment	Collector dosage (g/ton)	Depressant
1	417	None
2	417	K55
3	417	T10
4	1083	None
5	1083	K55
6	1083	T10
7	750	None
8	750	K55
9	750	T10
10	417	T12
11	750	T12
12	1083	T12

**Table 4.2** Select flotation experiment feed of minerals of interest for depressants design of experiments

Mineral	Feed +150 $\mu\text{m}$ (Wt%)	Feed -150/+75 $\mu\text{m}$ (Wt%)	Feed -75/+37 $\mu\text{m}$ (Wt%)	Feed -38 $\mu\text{m}$ (Wt%)	Feed composite (Wt%)
Monazite	0.13	0.26	0.56	1.57	0.97
Parisite	0.36	0.74	1.37	2.36	1.66
RE Minerals	0.57	1.22	2.21	5.83	3.69
Calcite	4.02	8.03	11.09	10.97	10.04
K-Feldspar	82.01	72.89	63.99	48.55	59.21

has a higher weight percent in the larger particle sizes. The simple kinetics test had four concentrate collection times. Similar particle size distributions are observed for all experiments, with the REMs reporting to the finer size fractions in greater quantities than the coarse particle sizes. An example of concentrate mineral grade for T10 as determined from MLA is shown in Table 4.3, T12 in Table 4.4, and K55 in Table 4.5.

The concentrate composite is a mass-weighted average of the four concentrate collection time frames. Representative gangue such as calcite and K-feldspar are shown as they constitute roughly 70% of the ore. A higher grade is observed during the second-time period (from 45 seconds to 2 minutes) for the REMs for two of the three depressants, T12 has a higher grade in the first-time period. Gangue grade increases as the experiment is performed with lowest grades observed for the first-time period and highest grade for the fourth-time period, except for calcite with K55 as a depressant. Calcite grade is significantly larger, 121% higher, for the fourth concentrate sample compared to the second concentrate. A typical particle size distribution for the REM concentrate grade is shown in Fig. 4.5.



**Table 4.3** Select flotation experiment concentrate sample of minerals of interest for T10

Mineral	Con 1 (0–45 s) (Wt%)	Con 2 (45 s–2 min) (Wt%)	Con 3 (2–8 min) (Wt%)	Con 4 (8–30 min) (Wt%)	Con composite (Wt%)
Monazite	1.33	2.03	1.29	0.60	1.28
Parisite	2.43	3.11	1.55	0.79	1.99
RE Minerals	5.38	6.69	3.54	1.72	4.40
Calcite	9.58	10.85	14.07	13.69	11.70
K-Feldspar	46.29	44.62	56.75	66.94	52.81

**Table 4.4** Select flotation experiment concentrate sample of minerals of interest for T12

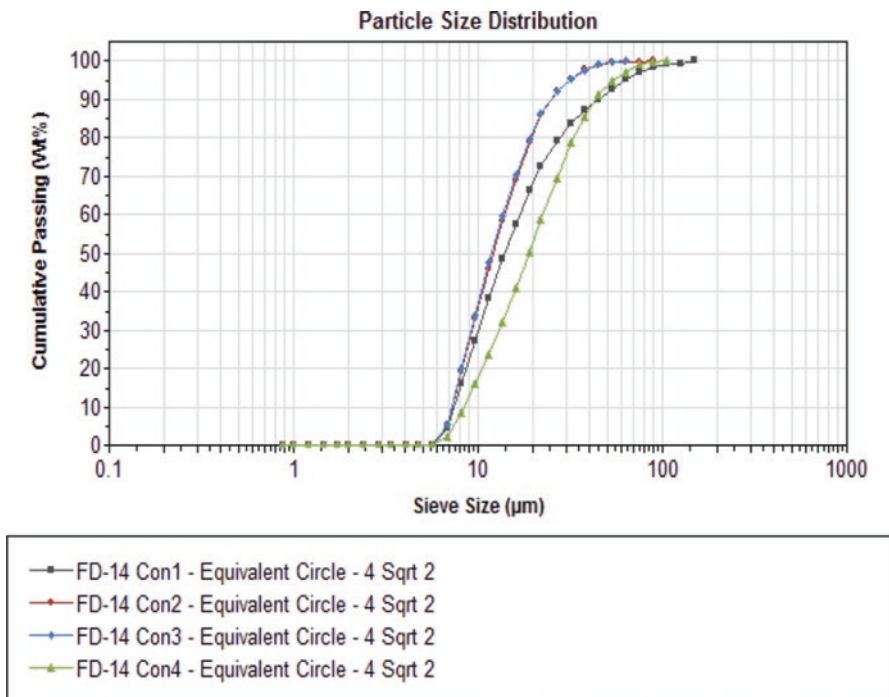
Mineral	Con 1 (0–45 s) (Wt%)	Con 2 (45 s–2 min) (Wt%)	Con 3 (2–8 min) (Wt%)	Con 4 (8–30 min) (Wt%)	Con composite (Wt%)
Monazite	1.98	1.89	1.64	1.16	1.71
Parisite	3.48	2.84	1.89	1.64	2.54
RE Minerals	7.28	6.62	4.68	3.13	5.62
Calcite	10.92	11.46	12.78	13.37	12.01
K-Feldspar	39.44	43.45	53.15	62.23	48.44

**Table 4.5** Select flotation experiment concentrate sample of minerals of interest for K55

Mineral	Con 1 (0–45 s) (Wt%)	Con 2 (45 s–2 min) (Wt%)	Con 3 (2–8 min) (Wt%)	Con 4 (8–30 min) (Wt%)	Con composite (Wt%)
Monazite	1.48	1.67	1.35	0.81	1.29
Parisite	2.32	2.41	1.70	1.18	1.83
RE Minerals	6.10	7.01	4.77	2.54	4.85
Calcite	15.91	17.57	12.38	7.94	12.87
K-Feldspar	46.87	39.94	50.51	63.41	51.46

Particle size distribution was calculated using MLA software. The P80 particle size for the concentrate sample from the second and third sampling periods are approximately 20 microns and the P80 particle size for the concentrate sample from the first and fourth sampling periods is approximately 30 microns. Similar particle size distributions are observed for all depressant flotation experiments. The results of the depressant flotation experiments are shown in Table 4.6 for recovery and Table 4.7 for increase in grade. Because this was a depressant study, calcite, iron oxide, potassium feldspar, and biotite are included.

Calculated gangue recovery is a combination of gangue recovered through flotation and gangue which are associated with REMs that are not fully liberated. Experiment 9, which used the T10 or the lower concentration of DGME and a high dosage of SHA, had the highest rare earth recovery of 83% and the highest gangue recovery for every mineral. The combination also resulted in the lowest increase in grade, only 19%, for rare earths and highest increase in grade (still lower than the feed) for potassium feldspar.



**Fig. 4.5** Particle size distribution for select flotation experiment with depressant of REM concentrate

**Table 4.6** Metallurgical recovery of REMs and gangue using depressants

Recovery (%)									
Exp.	Dosage	Dep.	RE	Monazite	Parisite	Calcite	Feldspar	Biotite	FeO
1	417	None	70%	69%	59%	54%	40%	73%	45%
2	417	K55	77%	72%	69%	63%	45%	74%	50%
3	417	T10	71%	72%	64%	51%	35%	67%	43%
4	1083	None	68%	66%	60%	53%	39%	71%	44%
5	1083	K55	72%	70%	65%	54%	38%	67%	47%
6	1083	T10	76%	76%	71%	52%	36%	67%	54%
7	750	None	70%	69%	62%	53%	40%	71%	46%
8	750	K55	64%	71%	54%	51%	37%	67%	46%
9	750	T10	83%	82%	80%	66%	51%	79%	64%
10	417	T12	80%	78%	76%	57%	42%	74%	62%
11	750	T12	78%	74%	77%	57%	41%	71%	56%
12	1083	T12	76%	73%	70%	53%	38%	68%	55%

**Table 4.7** Extraction efficiency for REMs and gangue using depressants

Grade (%)									
Exp.	Dosage	Dep.	RE	Monazite	Parisite	Calcite	Feldspar	Biotite	FeO
1	417	None	35%	18%	28%	11%	-16%	44%	14%
2	417	K55	47%	38%	25%	17%	-15%	42%	3%
3	417	T10	57%	51%	30%	26%	-18%	63%	-1%
4	1083	None	50%	35%	31%	12%	-15%	38%	6%
5	1083	K55	59%	65%	53%	20%	-18%	32%	28%
6	1083	T10	54%	69%	40%	14%	-17%	45%	34%
7	750	None	58%	61%	32%	9%	-16%	52%	8%
8	750	K55	46%	64%	30%	15%	-15%	44%	14%
9	750	T10	19%	33%	20%	17%	-11%	27%	8%
10	417	T12	24%	24%	10%	12%	-15%	35%	3%
11	750	T12	52%	80%	38%	17%	-18%	45%	27%
12	1083	T12	27%	29%	23%	7%	-13%	20%	29%

**Table 4.8** Flotation first-order rate constant for REM flotation using depressants

Flotation first-order rate constant, $k$							
Exp.	Dosage	Dep.	Calcite	FeO	Biotite	Monazite	Parisite
1	417	None	0.00	0.00	0.14	0.18	0.03
2	417	K55	0.73	0.33	0.04	0.37	0.53
3	417	T10	1.11	1.09	0.08	0.35	0.85
4	1083	None	0.00	0.98	0.18	0.42	0.48
5	1083	K55	0.81	0.28	0.04	0.50	0.05
6	1083	T10	0.06	0.00	0.31	0.73	0.70
7	750	None	0.00	0.35	0.07	0.04	0.14
8	750	K55	1.08	0.69	0.10	0.40	0.87
9	750	T10	0.12	1.49	0.38	0.82	1.13
10	417	T12	0.06	0.40	0.20	0.40	0.42
11	750	T12	0.41	1.43	0.09	0.84	1.13
12	1083	T12	0.00	1.72	0.07	0.88	0.79

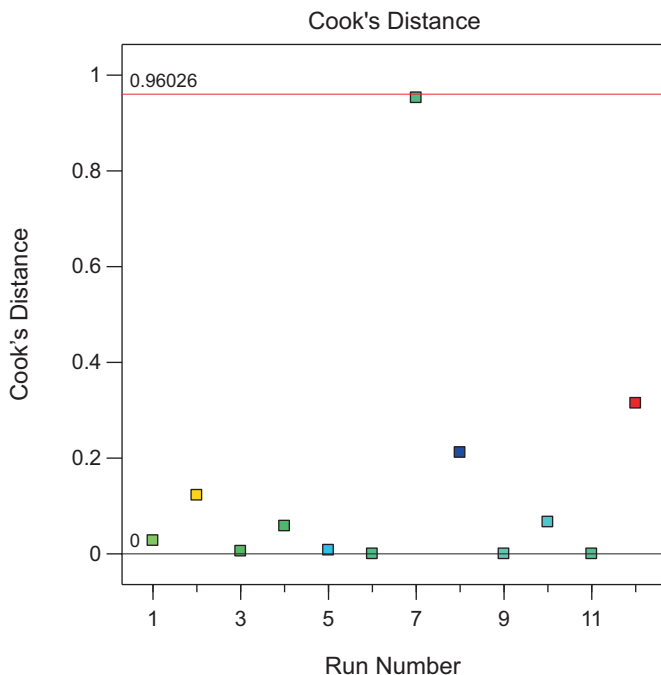
Kinetic parameters were also determined for parisite and monazite and the gangue. Potassium feldspar had a calculated rate constant of 0 for all experiments and is not shown. The flotation first-order rate constant for the design of experiments is shown in Table 4.8.

Biotite has a low rate constant across all experiments, from 0.04 to 0.38. Interestingly, at low collector dosage, 417 g/ton, the lowest rate constant is when no depressant is present for the REMs and gangue. However, this experiment resulted in a kinetic model with a high degree of error (28%), especially compared to the other models, (<10%). Given the wide range of results for the three depressants, an analysis of variance (ANOVA) for the design of experiments was performed.

Responses chosen for the design of experiments were monazite and parisite recovery; monazite and parisite increase in grade; and monazite and parisite

Design-Expert® Software  
(Monazite Recovery)<sup>-3</sup>

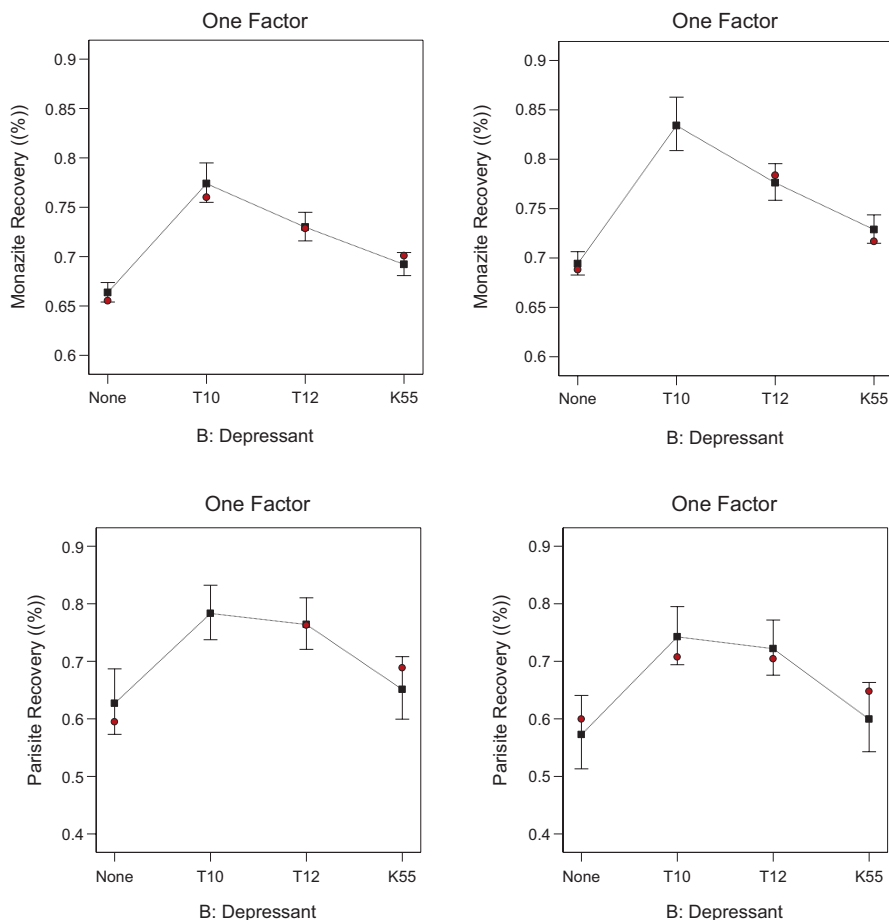
Color points by value of  
(Monazite Recovery)<sup>-3</sup>:



**Fig. 4.6** Cook's Distance for monazite recovery using depressants which identifies experiment 7 as an outlier

first-order rate constant. In addition, gangue recovery, grade, and first-order rate constant were also analyzed. Responses were analyzed using historical data in Design-Expert 10 as opposed to a two-factorial design. Given the nature of the experiments, a hierarchical design could not be developed. However, each response could be examined based off the ANOVA results which could result in either strictly a mean vs total, a linear model, or a two-factorial model. All increase in grade models resulted in a mean vs. total except for biotite. When diagnostics were performed on the monazite recovery model, the Cook's Distance on one of the experiments was found to indicate an outlier. The Cook's Distance for monazite recovery is shown in Fig. 4.6.

Cook's Distance identified experiment 7 as being an outlier to the rest of the data with a value equal to three times the mean Cook's Distance. Experiment 7 was performed without any depressant and at a collector dosage of 750 g/ton. A similar leverage value was obtained and so experiment 7 was not used for the ANOVA. Given the wide range of responses to be analyzed, the factors of interest will be analyzed, and the numerical optimization studies will be discussed. The effect of the depressants on monazite and parisite recovery is shown in Fig. 4.7, with the minimum collector dosage used for the model on the left and maximum collector dosage on the right and monazite recovery on top and parisite recovery on bottom.



**Fig. 4.7** Predicted monazite recovery using novel depressants as determined by ANOVA. Top: monazite recovery; Bottom: parisite recovery; Left: minimum collector dosage; Right: maximum collector dosage. The error bars identify 95% confidence interval

Maximum predicted monazite and parisite recovery is found using the T10 depressant at maximum collector dosage. The lowest predicted monazite recovery was when no depressant was used regardless of collector dosage. Similar parisite recoveries are noted between the no-depressant condition and the K55 depressant. An increase in recovery for monazite and parisite with the depressant use (all three for monazite, T10 and T12 for parisite) implies that the depressants are possibly preventing the adsorption of the collector onto the surface of the gangue and in the case of K55 on parisite as well. More of the collector is adsorbing onto the surface of monazite as it cannot adsorb onto the gangue. No significant change in parisite recovery is noted as a function of collector dosage. The increase in recovery whether it is by collection of more hydrophobic REMs or entrainment as the gangue with depressant are too large to transfer to the froth by water needed to be determined.

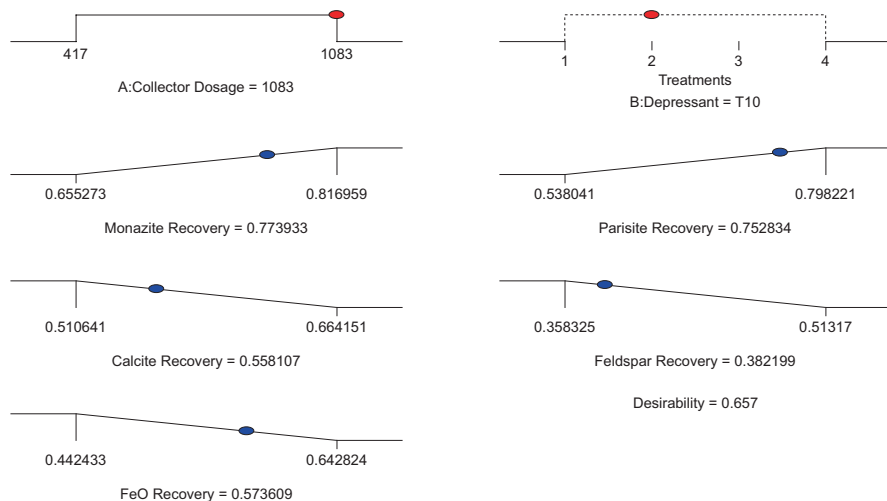
If monazite and parisite recovery are optimized and calcite, potassium feldspar and iron oxide are minimized, optimal conditions for flotation involves maximizing SHA dosage and using the depressant T10. The numerical optimization ramps for these conditions are shown in Fig. 4.8.

A desirability of 0.66 was obtained for these conditions. Feldspar and calcite recovery are minimized with the values close to the minimum obtained values. However, iron oxide recovery is not minimized as the optimized value is closer to the maximum experimental value. Parisite and monazite recovery are both close to maximum experimental values given these conditions.

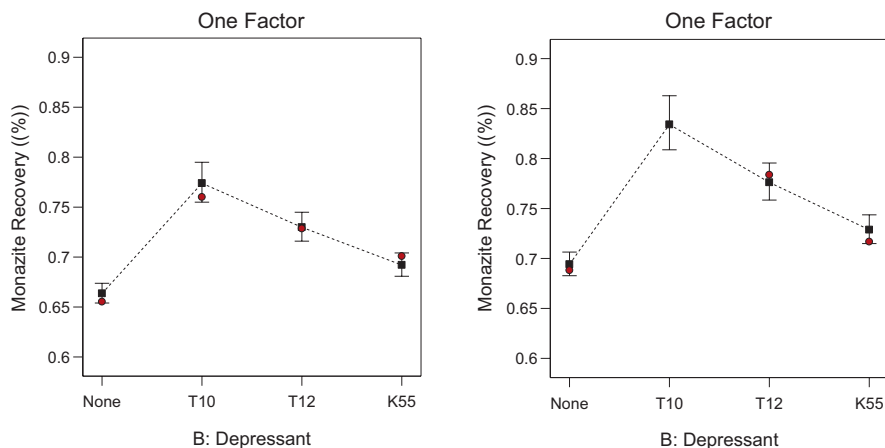
First-order rate constant ANOVA only resulted in significant models for monazite, calcite, and biotite. The effect of the depressant and collector dosage on the first-order rate constant is shown in Fig. 4.9 with monazite minimum collector dosage on the left and maximum collector dosage on the right.

The numerical optimization ramps for significant models for the flotation first-order rate constant are shown in Fig. 4.10. At maximum collector dosage and using the T12 depressant resulted in optimal conditions for the given constraints. Monazite  $K$  is optimized at the maximum experimental value and calcite and biotite are close to the minimum experimental  $K$  value. A desirability of 0.86 was achieved and almost all conditions were optimized.

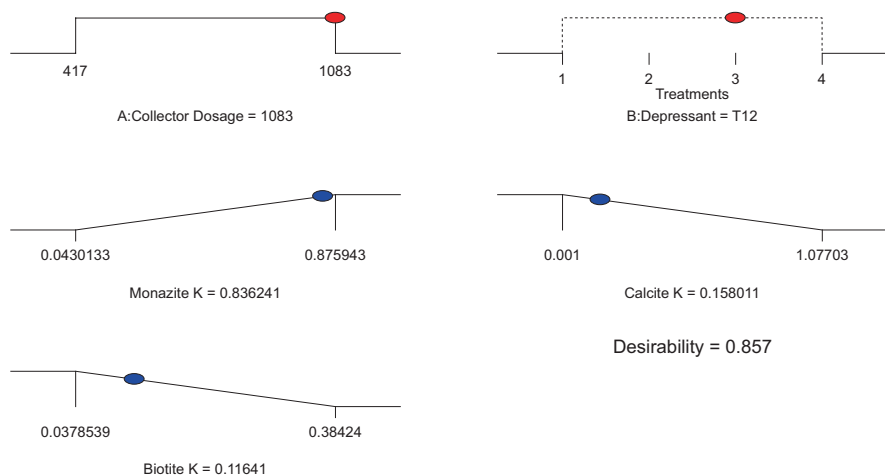
Diethylene glycol monobutyl ether results in higher recovery and faster flotation kinetics of REMs than the ionic copolymer with sodium sulfate. It is difficult to determine the actual mechanism for the observed behavior due to lack of information about the proprietary depressants. One possible explanation, however, is that the size and shape of the ionic copolymer hinder the kinetic behavior. Optimal conditions for minimizing the flotation performance of gangue are also achieved with DGME over the ionic copolymer. A lower concentration of DGME results in greater



**Fig. 4.8** Numerical optimization ramps for maximized REC and REP flotation and minimized gangue flotation



**Fig. 4.9** Predicted monazite recovery using novel depressants as determined by ANOVA. Left: minimum collector dosage; Right: maximum collector dosage. The error bars identify 95% confidence interval



**Fig. 4.10** Numerical optimization ramp for maximized flotation rate constant of monazite and minimized flotation rate constant of biotite and calcite

monazite recovery and minimal gangue recovery over a higher concentration of DGME. The implication of this trend is that DGME preferentially interacts with silicates, possibly aluminum, over REEs. At a sufficient concentration of DGME, this selectivity begins to disappear. When DGME concentration is increased, the number of floatable particles decreases as the available sites for the collector decrease. The first-order rate constant for particles that have been rendered hydrophobic should increase, which explains why T12 results in a more optimal condition when considering the first-order rate constant.

## 4.4 Conclusions

The flotation process was reviewed in general. Industrial examples with particular focus on REEs and REMs were given. It was stressed that REM flotation was very dependent on the mineral type because the REE coordination number and REE cation size were dependent on the associated anion (i.e., oxide, carbonate, phosphate, and silicate). Because the phenomenon could yield low REM flotation recoveries, it was emphasized that collector blends should be used. Following the review, a case study was presented to illustrate how the flotation performance in the presence of a single collector, salicyl hydroxamic acid (SHA), could also be improved by depressing the gangue present in the ore. For an ore with potassium feldspar as the prominent non-valuable mineral, the nonionic polymer diethylene glycol monobutyl ether (DGME) can be utilized as a depressant. REM recovery increases from a maximum of 69% with SHA alone to 83% with DGME. While these results were obtained at a maximum concentration of DGME, it was noted that REM recovery decreased with increasing DGME concentration. DGME will prevent the adsorption of an anionic collector onto a mineral surface preferentially toward aluminosilicates like potassium feldspar over REEs. The results show the potential for high REM recovery but a greater understanding is needed to determine why REM laboratory flotation results are not transferrable to the plant scale. Depressants can also reduce the flotation rate constant for gangue to essentially zero, limiting the ability to collect by solution chemistry and, to a smaller extent, by entrainment.

**Acknowledgments** Case study research was sponsored by the Army Research Laboratory and was accomplished under Cooperative Agreement Number W911NF-15-2-0020. The views and conclusions contained in this document are those of the authors and should not be interpreted as representing the official policies, either expressed or implied, of the Army Research Laboratory or the U.S. Government. The U.S. Government is authorized to reproduce and distribute reprints for Government purposes notwithstanding any copyright notation herein.

## References

1. B.S. Van Gosen, P.L. Verplanck, R.R. Seal II, K.R. Long, J. Gambogi, Chapter O: Rare-earth elements, in *Critical Mineral Resources of the United States – Economic and Environmental Geology and Prospects for Future Supply*, ed. by K.J. Schulz, J.H. DeYoung Jr., R.R. Seal II, D.C. Bradley, (U.S. Geological Survey, Professional Paper 1802, 2017), pp. O1–O31
2. Z. Hou, Y. Liu, S. Tian, Z. Yang, Y. Xie, Formation of carbonate-related giant rare-earth-element deposits by the recycling of marine sediments. *Sci. Rep.* **5**, 10231 (2015)
3. A. Jordens, Y.P. Cheng, K.E. Waters, A review of the beneficiation of rare earth element bearing minerals. *Miner. Eng.* **41**, 97–114 (2013)
4. V.R. Coterio, Optimization of Air-Injection Spargers for Column Flotation Applications, MS Thesis, Virginia Tech, Blacksburg, VA, USA, 2016, p. 96
5. S.M. Bulatovic, Chapter 4 – Modifying reagents, in *Handbook of Flotation Reagents: Chemistry, Theory and Practice*, (Elsevier, 2007), pp. 53–79



6. S.M. Bulatovic, Chapter 24 – Flotation of REO minerals, in *Handbook of Flotation Reagents: Chemistry, Theory and Practice*, (Elsevier, 2010), pp. 151–173
7. J.F. Boulanger, C. Bazin, K. Turgeon, Effect of depressants and temperature on bastnaesite and monazite flotation separation from a Canadian rare earth element (REE) ore. *Fortschr. Mineral.* **9**, 225–241 (2019)
8. C. Marion, R. Li, K.E. Waters, A review of reagents applied to rare-earth mineral flotation. *Adv. Colloid Interf. Sci.* **279**, 102142 (2020)
9. G. Galt, Adsorption of Salicylhydroxamic Acid on Selected Rare Earth Oxides and Carbonates, MS Thesis, Montana Tech, Butte, MT, USA, 2017, p. 137
10. F. Sime, Surface Chemistry and Modelling of Salicyl Hydroxamic Acid Adsorption at the Surface of Rare Earth Oxides, Carbonates and Phosphates, MS Thesis, Montana Tech, Butte, MT, USA, 2018, p. 104
11. S. Trant, Comparison of Salicyl Hydroxamate Adsorption on Rare Earth Phosphates to Oxides and Carbonates, MS Thesis, Montana Tech, Butte, MT, USA, 2018, p. 90
12. S. Trant, G. Galt, A. Das, C.A. Young, Fundamental understanding of the flotation chemistry of rare earth minerals, in *Peer-Reviewed Proceedings of Extraction 2018*, (2018), pp. 2581–2595
13. Greenland Minerals, September 2020 quarterly report, company website, 2020
14. R. McEwen, G.W. Hansen, G.F. Lee, Single-stage flotation of alkali feldspars, ilmenite, rutile, garnet, and monazite with mixed cationic/anionic collectors. *Trans. Soc. Min. Eng.* **260**, 97–100 (1976)
15. S.M. Bulatovic, Froth Flotation of Bastnasite, United States Patent US4772382A, 1988, p. 5
16. S.M. Bulatovic, G.C. Willett, A Monazite Beneficiation Process, Patent, WO 91/16986, World Intellectual Property Organization, 1991, pp. 1–40
17. C.J. Ferron, S.M. Bulatovic, R.S. Salter, Beneficiation of rare earth oxide minerals, in *International Conference on Rare Earth Minerals and Minerals for Electronic Uses*, ed. by B. Siribumrungsukha, S. Arrykul, P. Sanguansai, T. Punggrassami, L. Sikong, K. Kooptarmond, (Prince of Songkha University, Hat Yai, Thailand, 1991)
18. T.N. Chan, A new beneficiation process for treatment of supergene monazite ore, in *Peer-Reviewed Proceedings of Rare Earths: Resources, Science, Technology and Applications*, (Minerals, Metals & Materials Society, San Diego, CA, 1992), pp. 77–94
19. B. Yu, Y.O. Oyediran, M. Robart, Flotation development testwork on REE samples from the strange lake alkalic complex, in *Peer-Reviewed Proceeding of XXVIII International Mineral Processing Congress (IMPC)*, (Quebec, Canada, 2016)
20. L.Z. Li, X. Yang, China's rare earth ore deposits and beneficiation techniques, in *2014, ERES2014: Peer-Reviewed Proceedings of 1st European Rare Earth Resources Conference*, (Milos, Greece, 2014), pp. 26–36
21. P.L. Rozelle, T.J. Tarka, N. Mamula, *The Application of Current Mineral Processing and Extractive Metallurgy Technologies to Potential Rare Earth Ores in the U.S. Coal Measures: Near-Term Opportunities to Fill Out the U.S. Value Chain* (U.S. DOE Office of Fossil Energy, 2019). <https://doi.org/10.2172/1595955>
22. F.F. Aplan, Processing of rare earth minerals, in *Peer-Reviewed Proceedings of Rare Earths: Extraction and Preparation and Applications*, (The Minerals, Metals and Materials Society, 1989), pp. 15–34
23. P. Amelunxen, R. LaDouceur, Chapter 7.9: Applied flotation modeling, in *SME mineral processing and extractive metallurgy handbook*, ed. by R.C. Dunne, S.K. Kawatra, C.A. Young, (Society for Mining, Metallurgy & Exploration (SME), Englewood, 2019), pp. 1053–1065
24. P. Amelunxen, R. LaDouceur, R. Amelunxen, C. Young, A phenomenological model of entrainment and froth recovery for interpreting laboratory flotation kinetics tests. *Miner. Eng.* **125**, 60–65 (2018)
25. R. LaDouceur, High Fidelity Kinetic Model for Flotation: Applications to Rare Earth Elements and Copper/Molybdenum Separations, Dissertation, Montana Tech, 2018, p. 197

# Chapter 5

## Rare Earth Extraction from Ion-Adsorption Clays in U.S. Coal By-Products



Roe-Hoan Yoon

### 5.1 Introduction

In 2020, the global mine production of rare earth oxides (REOs) was 240,000 metric tons, of which China accounted for 58.3%, followed by the United States (15.8%), Burma (12.5%), Australia (7.1%), and other countries (6.3%) [1]. Since the U.S. mine production and much of that from Burma went to China for processing, one country controlled more than 80% of the global production.

Of the fifteen rare earth elements (REEs) of the lanthanide series, heavier elements are more in demand than lighter ones and hence command substantially higher prices. The major sources of the heavy rare earth elements (HREEs) are the IACs assaying typically 0.05–0.3% REEs, which are found in the regolith formed mainly from the weathering of granites. Despite the low grades, the low mining and processing costs make these ore deposits economically attractive. Approximately 40–90% of the REEs are physically adsorbed on the layer-structured minerals; therefore, they can be readily extracted by simple ion-exchange leaching processes without using the aggressive conditions required for processing the rare earth minerals such as bastnaesite, monazite, and xenotime. Virtually all the world's HREEs are produced from the ion-adsorption clays mined in South China [2].

Ion-adsorption clays are formed as a result of the in situ weathering of rare earth-rich host rocks such as granite. Clay minerals (e.g., kaolinite, halloysite) are made of layers of  $\text{SiO}_4$  tetrahedra and  $\text{AlO}_4(\text{OH})_2$  octahedra. During the process of forming these minerals, part of the  $\text{Si}^{4+}$  and  $\text{Al}^{3+}$  ions in the cross-linked polyhedra are isomorphically substituted by cations of lower formal charges (e.g.,  $\text{Si}^{4+}$  by  $\text{Al}^{3+}$  and  $\text{Al}^{3+}$  by  $\text{Mg}^{2+}$  ions), causing the basal surfaces of the clay minerals to be net negatively charged when they are submerged in aqueous media. Zhou et al. [3] measured

---

R.-H. Yoon (✉)

Department of Mining & Minerals Engineering, Virginia Tech, Blacksburg, VA, USA  
e-mail: [ryoon@vt.edu](mailto:ryoon@vt.edu)

the surface charge density ( $\sigma$ ) of kaolinite samples to be 0.19–0.24 C/m<sup>3</sup> depending on their origins. The surface charges of such origins are referred to as structural or permanent charges to be distinguished from the pH-dependent surface charges. The latter charges are created due to the adsorption of H<sup>+</sup> or OH<sup>-</sup> ions on the silanol (Si-OH) or aluminol (Al-OH) groups exposed on the edge surfaces of clay minerals [4, 5]. The lanthanide (Ln<sup>3+</sup>) ions in solution would adsorb on the negatively charged surfaces and enrich the clay minerals with rare earth ions by adsorption. The driving force for the adsorption mechanism is one of coulombic attraction; therefore, they can be readily displaced by other cations of higher affinity and chemical potentials. In the early 1970s, the ion-adsorption clay ores were treated by 1 M sodium chloride (NaCl) solutions, followed by precipitation of the displaced RE<sup>3+</sup> ions with oxalic acid (C<sub>2</sub>H<sub>2</sub>O<sub>4</sub>).

During the early 1980s, the 1 M NaCl solution was replaced by ~0.3 M ammonium sulfate ((NH<sub>4</sub>)<sub>2</sub>SO<sub>4</sub>) as lixiviant. Even today, (NH<sub>4</sub>)<sub>2</sub>SO<sub>4</sub> remains the preferred lixiviant for the recovery of HREEs despite the environmental concerns created by the extensive use of the reagents. The ion-exchange mechanism may be represented by the following reaction:



in which one mole of lanthanide ions (Ln<sup>3+</sup>) is displaced by three moles of ammonium ions. The kinetics of this reaction is fast as the REE ions are mostly attracted to the negatively charged basal surfaces of clay minerals by the weak coulombic attraction. It has been shown that Ln<sup>3+</sup> ions can indeed adsorb on the basal surfaces of kaolinite as outer-sphere complexes with 8–9 hydrated water molecules, while others adsorb as inner-sphere complexes via bridging oxygen especially at a high pH [6]. The latter species may be difficult to be displaced by the simple ion-exchange mechanism.

There are three major IAC deposits known to date: South China, Brazil, and Madagascar in Africa. At present, the IACs in South China alone account for ~80% of the world's HREE production, which is projected to reach a peak of 45,793 tons in 2024 [7], which appears to agree with the production data shown in Fig. 5.1 [8]. The decrease in production observed in recent years is due to the declining reserve base and the increased awareness of the environmental issues associated with the extraction of rare earth elements from ion-adsorption ores.

Recent studies conducted by the USGS and the National Energy Technology Laboratory (NETL) showed that significant amounts of REEs are present in coal and coal by-products such as fine coal waste, partings, underclays, waste rocks, fly ash, and bottom ash [9]. This conclusion was drawn on the basis of the correlation between the REE and aluminum (Al) contents in coal (Fig. 5.2). In selected coal basins, the REE concentrations in kaolinite are 5–10 times higher than coal as a whole. It has been estimated that 6 and 4.9 million tons of rare earths are associated with coal by-products in five western and four eastern coal-producing states at a 500 ppm cutoff grade. According to Renton et al. [10], the pH of coal swamps in the

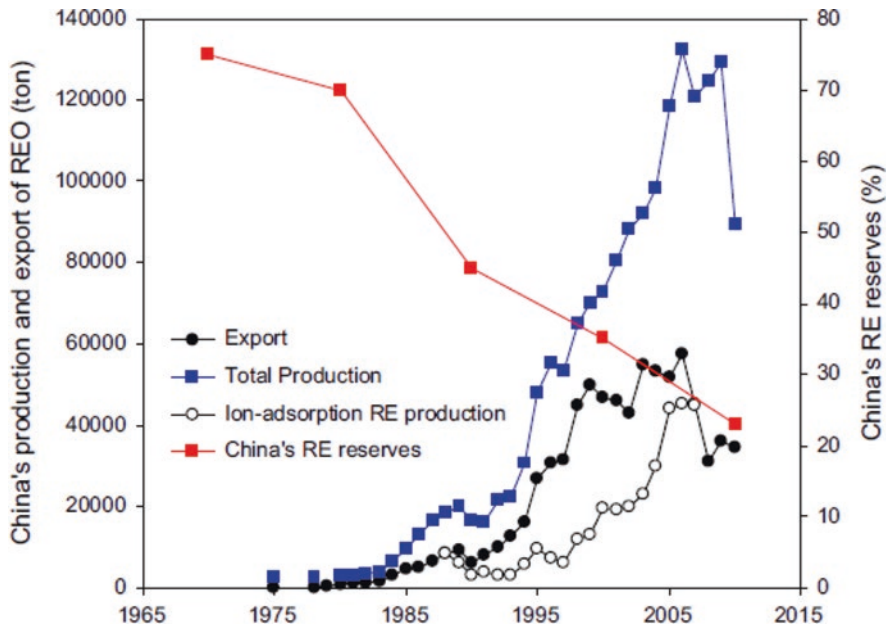


Fig. 5.1 Rare earth production in China [8]

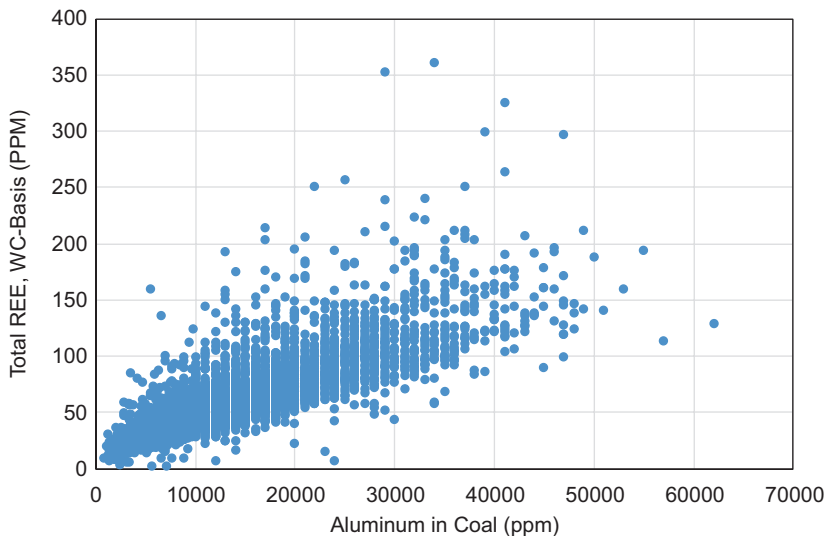


Fig. 5.2 Relationship between REE and Al contents eastern U.S. coals [9]

eastern United States was in the range of 4–6, which is similar to the condition under which IACs were formed in South China. Rozelle et al. [11] were the first to show that REEs can be extracted from clay samples isolated from a U.S. coal seam

using the ion-exchange leaching process. More recent work conducted by NETL extracted REEs from a series of different under clay samples associated with Central Appalachian coal seams using the ion-exchange leaching process [12].

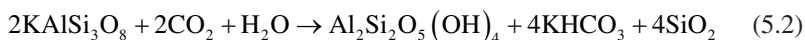
It is generally believed that IACs are formed under warm, humid, and slightly acidic conditions in subtropical areas, where the chemical weathering of granite can be sustained. Recent studies conducted by USGS showed, on the other hand, that IACs exist in the regolith formed on the granite horizon along the Central Appalachian mountains [2, 13]. This finding is consistent with the experimental results reported by Rozelle et al. [11] and Montrose [12]. Knowing that ~80% of the mineral matter in coal originates from clay minerals, it will be important to further develop the methods of extracting REEs from the clayey materials generated as wastes in the U.S. coal industry.

In this chapter, the mechanisms by which IACs are formed will be reviewed, and the possibility of extracting REEs from the clays and mineral matter present in U.S. coal by-products will be discussed. Despite what its name suggests, REEs are not rare. What makes them rare is the difficulty of extracting them efficiently and without creating environmental issues.

## 5.2 Formation of Ion-Adsorption Clay Deposits

### 5.2.1 *Enrichment of REEs in Clay Minerals*

The formation of IAC deposits is the consequence of the chemical weathering of granite, which is the most abundant continental rock consisting mainly of feldspar and quartz. Among the silicate rocks outcropped on the land surface, granite accounts for about 25% of the earth's surface [14]. Potassium feldspar, for example, is weathered by meteoric water, in which carbon dioxide (CO<sub>2</sub>) is dissolved, to produce kaolinite as follows:



Since the kaolinite is the end product, it is very stable and becomes the major component of the regolith. Part of the silica removed from feldspar is carried away by groundwater, precipitated as chert and nodules, or flows into the ocean to become the shells of microscopic animals. The other major component, quartz, is very resistant to weathering and hence remains unaltered except being fragmented. Other components of granite, muscovite, and biotite can undergo chemical changes to become different clay minerals.

Rare earth-bearing minerals that are referred to as accessory minerals are also weathered by the meteoric water under warm climate conditions, during the course of which various Ln<sup>3+</sup> ions are liberated into soil water. Some of the accessory minerals (e.g., bastnaesite, gadolinite-(Y), doverite, apatite) are more readily weathered than others (e.g., fergusonite, monazite, and alunite). Xenotime and zircon are most

resistant to weathering [15]. Although most of the rare earth and yttria (REY) in IACs originate from these accessory minerals, the rock-forming minerals themselves account for 24–28% of the REY in granite.

Figure 5.3 shows a typical weathering profile of a regolith-hosted ion-adsorption ore deposit. The profile is subdivided into four different horizons depending on the degrees of weathering: (A) humic layer which is thin with a thickness of 0–2 m for a 25-m-thick regolith. The color is dark and rich in organic matter and clay minerals; (B) completely weathered layer of 5–10 m thick, which is of mottled yellowish and orangish-red in color, rich in clay minerals (80%) and unaltered minerals (quartz, micas, etc.); (C) strongly weathered layer of 2–3 m thick, which is of spotted white, pinkish-brown in color, consists of ~30% clay minerals and rock-forming minerals; and (D) weathering front, interfacing unweathered bedrock.

Also shown in Fig. 5.3 are the changes in the REE concentration along the depth of the profile. As shown, the REE concentration is low in horizon A as the  $\text{Ln}^{3+}$  ions liberated into the soil water have already been transported to the lower section of the regolith layer by the flow of rainwater. The presence of the  $\text{HCO}_3^{2-}$  ions and  $\text{F}^-$  ions may act as complexing agents and help the  $\text{Ln}^{3+}$  ions stay liberated from the rare earth-bearing minerals.

As meteoric water flows through the regolith layer, the REE ions adsorb preferentially to the clay minerals formed via Reaction (5.2) as the mineral offers negatively charged substrates with large surface areas on which  $\text{Ln}^{3+}$  ions can adsorb. The particle sizes of the kaolinite and halloysite are in the range of 1–2  $\mu\text{m}$  and

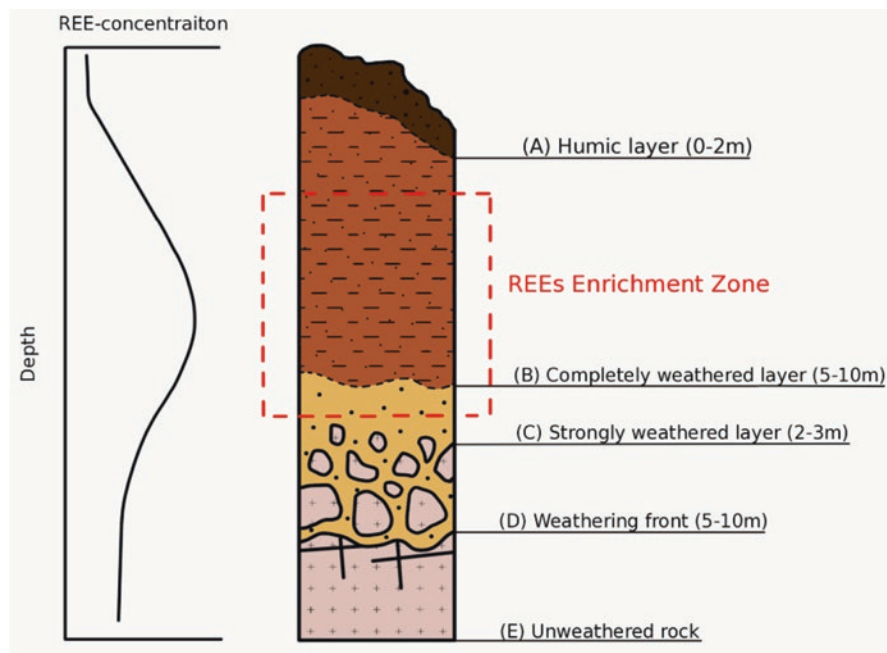
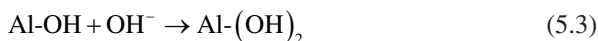


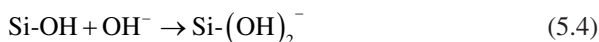
Fig. 5.3 Weathering profile of regolith-hosted ion-adsorption clay ore deposit [16]

0.5–2  $\mu\text{m}$ , respectively [15]. The latter is chemically similar to kaolinite, but the 1:1 layers are separated from each other by water molecules; therefore, its structural formula is written as  $\text{Al}(\text{OH})_4\text{Si}_2\text{O}_5 \cdot n\text{H}_2\text{O}$ . For the halloysite (10  $\text{\AA}$ ),  $n = 2$ , and for the halloysite (7  $\text{\AA}$ ),  $n = 0$ . Halloysite has a tubular structure with the aluminol groups (Al-OH) being exposed at the internal surface of the cylindrical structure, while the siloxane (Si-O-Si) groups are exposed at the external surface. The tubular structure gives large specific surface areas (SSA) of 20–80  $\text{m}^2/\text{g}$ . Thus, halloysite serves as the major absorbent for REEs in many IAC deposits despite the fact that it is less abundant than kaolinite.

The point of zero charge (PZC) of kaolinite is  $\text{pH} < 3$  [17]; therefore,  $\text{Ln}^{3+}$  ions should adsorb on the mineral surface via electrostatic interaction above this pH. The clay mineral has two adsorption sites, which include (1) the basal Si-O-Si surface that is negatively charged due to the isomorphic substitution of the  $\text{Si}^{4+}$  ions by the  $\text{Al}^{3+}$  ions and (2) the Al-OH and Si-OH sites exposed on the edge surfaces. The latter sites can adsorb  $\text{OH}^-$  as follows:



and



to become negatively charged sites at high pH, while the charges of the former sites are permanent or independent of pH as they are of structural origin [4, 5].

Borst et al. [6] studied the adsorption of Nd and Y as proxies for light and heavy REEs, respectively, on kaolinite using the X-ray absorption spectroscopy (XAS) and concluded that REEs adsorb on the basal surfaces as fully hydrated ions with eight and nine water molecules for heavy and light  $\text{Ln}^{3+}$  ions, respectively, as shown in Fig. 5.4. The fully hydrated ions that are referred to as outer-sphere complexes adsorb on the basal surfaces of the  $\text{AlO}_4(\text{OH})_2$  octahedra and the  $\text{SiO}_4$  tetra via electrostatic interactions. Therefore, they can be readily displaced by appropriate lixiviant (e.g.,  $\text{NH}_4^+$  ions), as shown by Reaction (5.1). On the edge surfaces of kaolinite,  $\text{Ln}^{3+}$  ions can adsorb as partially hydrated ions on the  $\text{Al}-(\text{OH})_2^-$  and  $\text{Si}-(\text{OH})_2^-$  groups and form inner-sphere complexes. According to Borst et al. [6], the inner-sphere complexes are difficult to be extracted by an ion-exchange mechanism.

It had been known previously that in acidic and near neutral solutions ( $\text{pH} < 6.5$ – $6.8$ ) most of the ion-exchangeable REEs adsorb on clay minerals as simple or hydrated cations as “clay-REE” or “clay-REE( $\text{H}_2\text{O}$ ) $_n$ ” species [18, 19]. At  $\text{pH} > 7$ , however, the adsorption occurs as “clay-O-REE $^{2+}$ ” species, which are irreversibly chemisorbed [20]. For this reason, ion-exchange leaching is carried out usually at  $\text{pH} 4.0$ – $5.5$ .

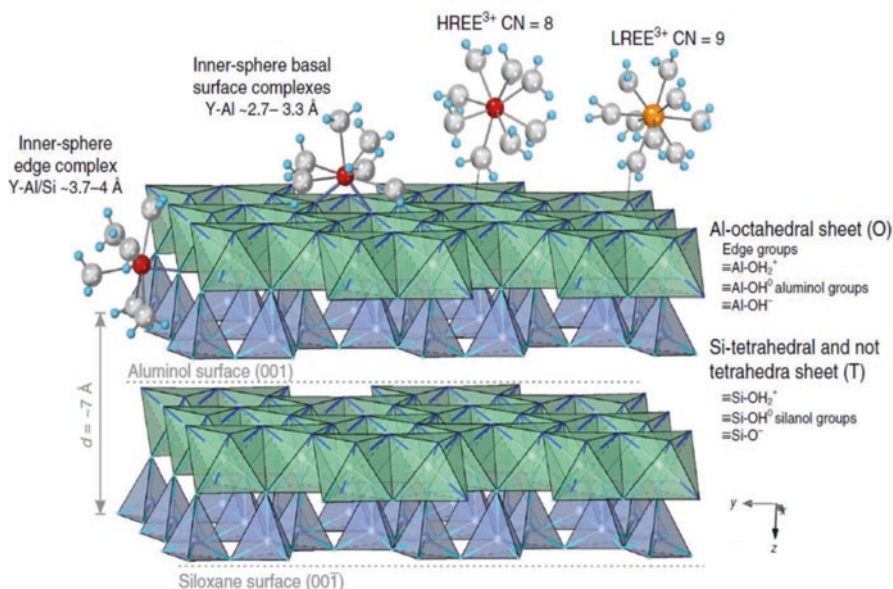


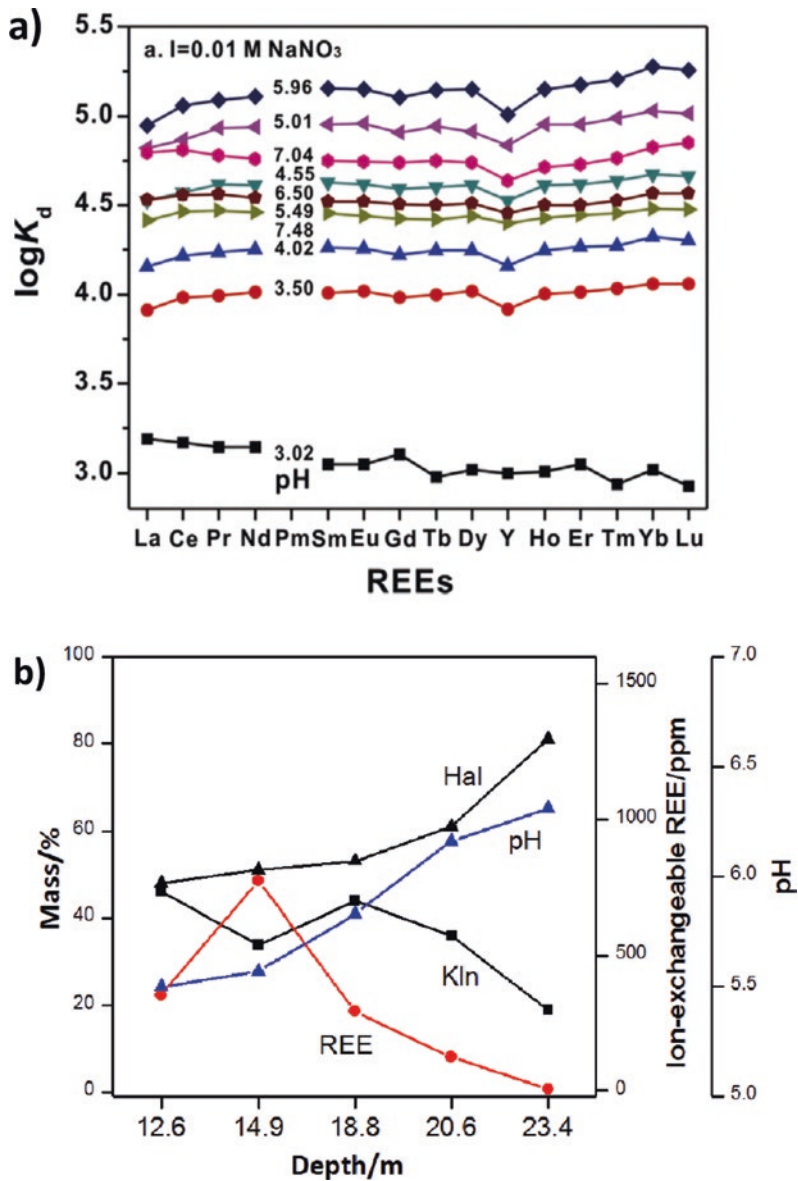
Fig. 5.4 A model for REE adsorption on the basal and edge surfaces of kaolinite [6]

### 5.2.2 Fractionation of REEs

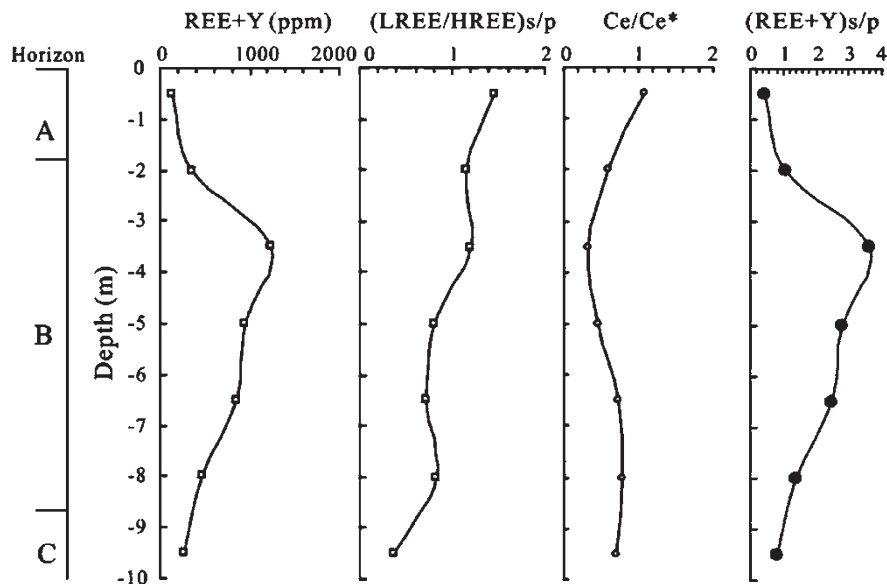
It is generally believed that HREEs can more readily form inner-sphere complexes than the light rare earth elements (LREEs) due to the smaller ionic radii associated with lanthanide contraction particularly at a higher pH, low lanthanide concentrations, and low ionic strengths [21]. Yang et al. [22] studied the adsorption of a full spectrum of REEs on halloysite and showed indeed that the REE adsorption increases with atomic number and pH (Fig. 5.5a). Also shown are the data obtained from an IAC deposit in Guangdong Province, China. Note that the concentration of the ion-exchangeable REEs increased from 355 to 775 ppm with increasing depth from 12.6 to 14.9 m, which may be attributed to the increase in pH, atomic number, and halloysite content (Fig. 5.5b). The decrease in the ion-exchangeable REE concentration at deeper depths may also be attributed to the propensity to forming inner-sphere REE complexes on the edges of clay minerals via mono- or bidentate oxygen ligands, making them resistant to ion-exchange leaching.

Mukai et al. [21] conducted microscopic analysis of the regolith-hosted IAC deposit using a laser ablation inductively coupled plasma mass spectrometry (LA-ICP-MS). The measurements were conducted on individual mineral (clay) particles before and after ion-exchange leaching using  $(\text{NH}_4)_2\text{SO}_4$  (0.5 M) as the lixiviant. The results showed that nearly half (45.5%) of the REEs remained in the kaolinitic particles after leaching, which was ascribed to the formation of inner-sphere complexes on the edge surfaces of clay minerals. It was found also that





**Fig. 5.5** (a) Coefficient of adsorption ( $K_d$ ) of REEs on halloysite; and (b) changes in pH, clay composition and ion-exchangeable REEs concentrations along the depth of a regolith-hosted IAC deposit [22]



**Fig. 5.6** Rare earth enrichment and fractionation along the depth of a regolith-hosted IAC ore deposit in Longnan, China [15]. Subscript *s/p* represents species concentration normalized by those of the parent rock. Ce/Ce represents the cerium anomaly

HREEs are more difficult to be removed than LREEs, which was consistent with the conclusions from Yang et al. [22]

It is well documented that the LREE/HREE ratio decrease with the depth of many IAC ore deposits as shown in Fig. 5.6. This observation has been explained by the theory that LREEs have a higher affinity toward clay minerals, which should allow smaller HREEs to migrate further down to the lower part of regolith and give rise to the fractionation [15]. Obviously, this mechanism does not agree with the more recent findings discussed in the foregoing paragraphs. A possible explanation for the apparent discrepancy may be attributed to the fact that HREEs could bond more strongly to both inorganic (e.g.,  $\text{CO}_3^{2-}$ ), and organic ligands, leading to a preferential depletion in regolith and corresponding enrichment in soil water, while LHEEs prefer to hydrolyze at a shallower depth to form REE oxides/hydroxides. The net result is that HREEs are mobilized toward depth and adsorb to clays [16, 23].

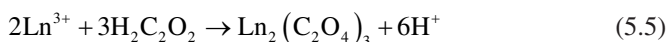
Figure 5.6 also shows that cerium concentrations are higher in the shallow part (0–0.7 m) than in the deeper part (3–4 m) due to the oxidation of  $\text{Ce}^{3+}$  to  $\text{Ce}^{4+}$  ions to form insoluble cerite, which is known as positive cerium anomaly. Note also that the REE+Y concentrations of the regolith-hosted IAC ore deposit in horizon B are 3–4 times higher than in the parent rock, which makes IACs valuable resources.

## 5.3 Extraction Processes

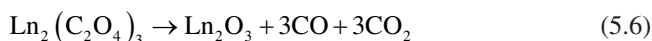
### 5.3.1 Ion-Exchange Leaching

Of more than 200 rare earth minerals identified to date, only four minerals are of commercial value in the sense that they account for ~95% of the world's REE+Y reserves. These include bastnaesite ((REE, Ce)(CO<sub>3</sub>)F) concentrates assaying 70–75% REO, monazite (REPO<sub>4</sub>) concentrates assaying 55–65% REO, xenotime (YPO<sub>4</sub>) concentrates assaying 55–60% REO, and IACs containing 0.05–0.3% REO [24]. Processing the first four rare earth minerals requires aggressive conditions involving NaOH baking and/or H<sub>2</sub>SO<sub>4</sub> cracking steps, which are costly. Processing IACs, on the other hand, involves simple ion-exchange processes as represented by Reaction (5.1). It would require in principle, only a fraction of the energy required to extract REEs from IACs to displace the physically adsorbed outer-sphere Ln<sup>3+</sup> complexes from the basal surfaces of clay minerals. It would be more difficult to displace the inner-sphere Ln<sup>3+</sup> complexes adsorbed to the edge surfaces and those chemisorbed at pH >7 as discussed in the foregoing section. Borst et al. [6] suggested that inner-sphere complexes can also form on the Al-OH groups on the basal surface of kaolinite, possibly at a higher pH.

The Ln<sup>3+</sup> ions extracted into solution are then precipitated with oxalic acid to form rare earth oxalate precipitate



which is subsequently roasted at 900 °C,



to obtain Ln<sub>2</sub>O<sub>3</sub> or rare earth oxides (REO). The sequence of Reactions (5.1), (5.5) and (5.6) are straightforward and do not involve aggressive reactions. Also, the IACs are rich in HREEs as compared to rare earth minerals (e.g., bastnaesite and monazite), for the enrichment mechanisms discussed above. Furthermore, the ion-exchange leaching yields very little thorium (Th) in solution. For these reasons, including low processing costs, high-value products plus the low Th concentrations in leach liquor, IACs account for more than 80% of the global HREE production despite the fact that their reserve base is only 1% of the world's REO resources, which has been reported to be 478.14 million metric tons [3].

Mining IAC ores started in Longnan Province, where NaCl rather than (NH<sub>4</sub>)<sub>2</sub>SO<sub>4</sub> was used as a lixiviant to extract the Ln<sup>3+</sup> ions into solution by the ion-exchange mechanism. The deposits with high yttrium (Y) contents (<65% of the REEs) have been mined out. The ore deposits that are currently mined in the Ganzhou and Xinfang provinces now contain Y contents in the range of 20–30% [25]. Table 5.1 shows a representative composition of the ores mined, which is close to an official Chinese estimate.

**Table 5.1** Composition of the Major IAC Mines in China [25]

REO	Average Weight %
La <sub>2</sub> O <sub>3</sub>	27.9
CeO <sub>2</sub>	3.3
Pr <sub>11</sub> O <sub>6</sub>	5.7
Nd <sub>2</sub> O <sub>3</sub>	17.8
Sm <sub>2</sub> O <sub>3</sub>	4.6
Eu <sub>2</sub> O <sub>3</sub>	0.9
Gd <sub>2</sub> O <sub>3</sub>	6.0
Tb <sub>4</sub> O <sub>7</sub>	0.7
Dy <sub>2</sub> O <sub>3</sub>	3.8
Er <sub>2</sub> O <sub>3</sub>	2.5
Ho <sub>2</sub> O <sub>3</sub> , Tm <sub>2</sub> O <sub>3</sub> , Yb <sub>2</sub> O <sub>3</sub> , Lu <sub>2</sub> O <sub>3</sub>	2.4
Y <sub>2</sub> O <sub>3</sub>	24.5
Sum	100

**Table 5.2** Extraction of REEs from the IAC samples from different continents [20]

REE (ppm)	Africa					Asia		South America
	A1	A2	A3	A4	A5	B1	B2	C1
Y	290	140	1801	120	100	1570	470	1200
La	1750	290	1790	460	250	70	980	450
Ce	260	170	220	450	280	60	200	120
Pr	280	70	270	450	280	60	200	980
Nd	1000	230		880	260	120	690	290
Sm	170	40	170	60	40	40	180	60
Eu	10	10	10	1.76	4.76	0.636	10	20
Gd	110	40	170	60	40	40	180	60
Tb	20	10	10	10	1.06	40	20	60
Dy	60	20	20	20	10	260	100	220
Ho	10	10	00	1.06	40	40	20	60
Er	20	10	150	120	10	380	250	210
Tm	2	0.869	0.685	0.0232	10	380	250	210
Yb	20	10	10	10	0	160	30	260
Lu	2.66	2.66	2.53	1.71	2.4	20	4.95	50
TREE	3990	1080	3800	1650	950	3000	3300	3260

Table 5.2 shows the results of the ion-exchange leaching tests conducted on the IAC samples from three different continents of the world—Africa, Asia, and South America. The extraction tests were conducted under benchmarked conditions: 0.5 M (NH<sub>4</sub>)<sub>2</sub>SO<sub>4</sub>, pH 5.2, 2:1 solid/liquid ratio, 30 min reaction time, and ambient temperature and pressure [20]. The extraction efficiencies (%E) varied in the range of 40–80%, which agrees well with the fraction of the ion-exchangeable REEs predicted by Chi and Tian [26]. The efficiencies decreased with increasing atomic number, which can be attributed to the decreasing ionic radii of the Ln<sup>3+</sup> ions due to

the lanthanide contraction and hence the increasing reactivity. Cerium (Ce) shows exceptionally low efficiencies due to the oxidation of Ce(III) to Ce(IV) during the weathering process.

That the overall extraction efficiencies were low is consistent with the adsorption model discussed in conjunction with Fig. 5.4. The  $\text{Ln}^{3+}$  ions forming outer-sphere complexes on the basal surfaces of clay minerals are ion-exchangeable as they are physically adsorbed, while those adsorbing on the edge surfaces by forming inner-sphere complexes are difficult to recover as they are chemically adsorbed.

During the early 1970s when the IAC industry began,  $\text{Ln}^{3+}$  and  $\text{Y}^{3+}$  ions were leached in  $\sim 1$  M NaCl solutions in ponds. A problem with this process was that the product qualities were low ( $<70\%$  REO) due to the coprecipitation of sodium oxalate. In the early 1980s, the industry began to use 0.3 M  $(\text{NH}_4)_2\text{SO}_4$  instead and increased the product quality to  $>92\%$  REO, which led to widespread deployment of the new lixiviant. After decades of intense and largely unregulated use of  $(\text{NH}_4)_2\text{SO}_4$  for pond and heap leaching, the industry is required to use in-situ leaching to minimize water pollution and landslides. According to Xiao et al. [27], the  $(\text{NH}_4)_2\text{SO}_4$  concentrations were 3500–4000 mg/L and 80–160 mg/L in groundwater and surface water, respectively, which may not be surprising in that 7–9 tons of the reagent are used per ton of REO produced. Many investigators are searching for greener lixiviants, which include magnesium sulfate ( $\text{MgSO}_4$ ) and aluminum sulfate ( $\text{Al}_2(\text{SO}_4)_3$ ).

Moldoveanu and Papangelakis [28] explained the ion-exchange mechanism on the basis of the enthalpy of hydration ( $\Delta H_{\text{hyd}}$ ) data given in Table 5.3. The fact that the three monovalent cations (i.e.,  $\text{Li}^+$ ,  $\text{Na}^+$ ,  $\text{NH}_4^+$ ), and  $\text{Cs}^+$  have nearly an order-of-magnitude less negative hydration enthalpies than the  $\text{Ln}^{3+}$  ions is an indication that these monovalent ions should be able to displace the latter from the surface of clay minerals, which is not surprising in that hydration enthalpy decreases with the increasing valence of cations. Note also that the  $\text{Na}^+$  ions have more negative  $\Delta H_{\text{hyd}}$  than the  $\text{NH}_4^+$  ions, which explains why the latter is a better lixiviant.

Table 5.3 shows also that the radii of the  $\text{RE}^{3+}$  ions decrease with increasing atomic number, causing the charge densities of the  $\text{Ln}^{3+}$  ions to increase. This explains why the heavier  $\text{RE}^{3+}$  ions have a higher propensity to adsorb on clay mineral surfaces than the lighter ones, providing an explanation for the IACs being the major source of HREEs. In effect, the clay minerals served as selective adsorbents (or collector) for HREE during the geological time scale.

### 5.3.2 Colloid Phase

The rare earths in the IAC ores in China exist in four different phases: (a) water-soluble, (b) ion-exchangeable, (c) colloidal sediment (oxides), and (d) minerals phase [29]. The first phase is negligibly small, the second (ion-exchangeable) phase accounts for  $\sim 80\%$ , and the colloid and mineral phases together account for  $\sim 20\%$  as shown in Table 5.4.

**Table 5.3** Ionic radii and enthalpies of hydration of cations [28]

Cations	Ionic radius (Å)	$\Delta H_{\text{hyd}}$ (kJ/mol)
La <sup>3+</sup>	1.06	-3285
Ce <sup>3+</sup>	1.03	-3340
Pr <sup>3+</sup>	1.01	-3384
Nd <sup>3+</sup>	0.99	-3420
Pm <sup>3+</sup>	0.98	-3445
Sm <sup>3+</sup>	0.96	-3465
Eu <sup>3+</sup>	0.95	-3508
Gd <sup>3+</sup>	0.94	-3522
Tb <sup>3+</sup>	0.92	-3553
Dy <sup>3+</sup>	0.91	-3577
Ho <sup>3+</sup>	0.89	-3621
Er <sup>3+</sup>	0.88	-3647
Tm <sup>3+</sup>	0.87	-3668
Yb <sup>3+</sup>	0.86	-3715
Lu <sup>3+</sup>	0.85	-3668
Li <sup>+</sup>	0.68	-520
Na <sup>+</sup>	0.95	-406
NH <sub>4</sub> <sup>+</sup>	1.48	-322
Cs <sup>+</sup>	1.69	-276

**Table 5.4** REE distribution in different phases (% wt) [29]

Ores	Water soluble	Ion-exchangeable	Colloidal oxide	Mineral
Longnan mine	$6.15 \times 10^{-3}$	80.62	5.30	13.36
Xingfeng mine	$8.14 \times 10^{-3}$	83.58	3.23	12.63
Ninghua mine	$1.47 \times 10^{-3}$	84.94	4.98	9.909

The Longnan (LN) IAC ore is rich in HREEs (87%), while the Xingfeng (XF) and Ninghua (NH) ores contain 44 and 41% HREEs, respectively. The colloidal phase should include the Ln<sup>3+</sup> ions adsorbed as chemisorbed species that are not removed by ion-exchange leaching using a 2% (NH<sub>4</sub>)<sub>2</sub>SO<sub>4</sub> solution. The residue of the first leaching step is subsequently leached in a 2 M hydrochloric acid (HCl) solution in the presence of a strong reducing agent (hydroxylamine hydrochloride (NH<sub>2</sub>OH·HCl)) to determine the amount of colloidal phase. The residue of the second step is then roasted at 900 °C to convert the rare earth minerals (e.g., monazite) to Ln<sub>2</sub>O<sub>3</sub>, followed by an HCl leaching. In the last step, the whole ore may be analyzed for comparison after roasting it at 900 °C in the presence of sodium peroxide (Na<sub>2</sub>O<sub>2</sub>) and NaOH.

Yanfei et al. [30] followed the sequential leaching procedure described above to determine the partitioning of REEs in three different phases (i.e., residual minerals phase, colloidal phase, and ion-exchangeable phase). The authors used an IAC ore

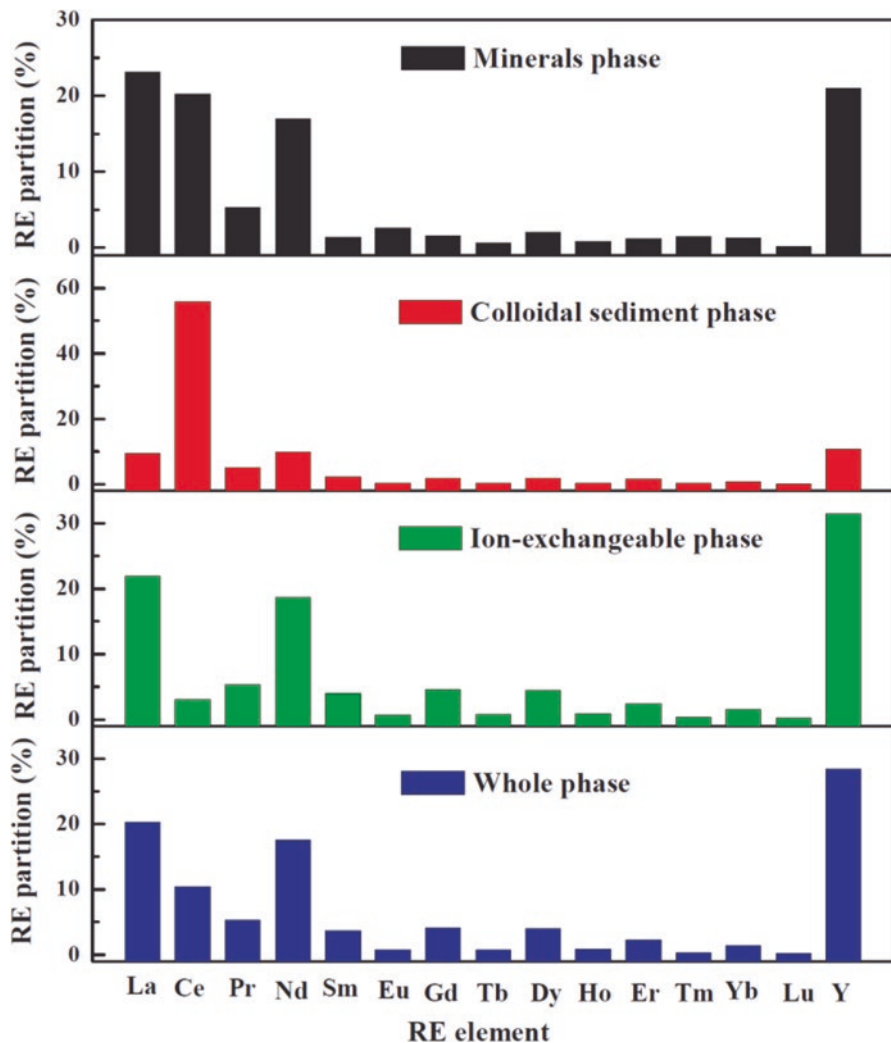


Fig. 5.7 Partitioning of REEs in different phases of the LT IAC ore [30]

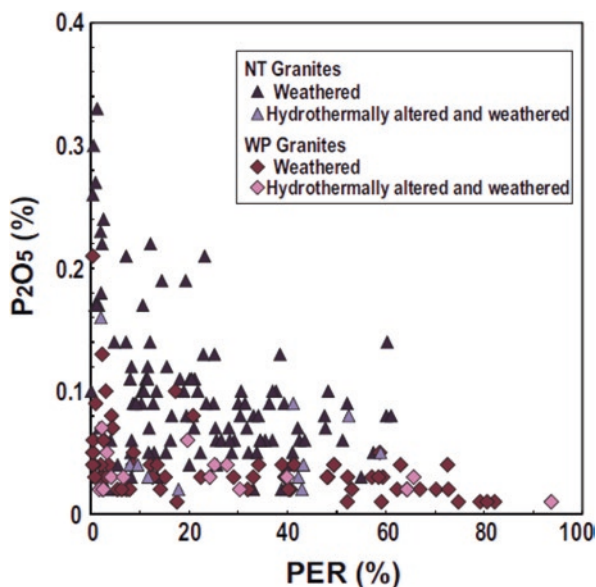
sample from the Liutang (LT) mine, China, and analyzed the leach solutions by inductively coupled plasma optical emission spectroscopy (ICP-OES). Results are presented in Fig. 5.7. The REE content was 1.8% in the whole ore, 1.5% in the ion-exchangeable phase, 0.14% the colloidal phase, and 0.18% in the minerals phase. The REE distribution in the minerals phase was similar to that of the whole ore as expected, with high concentrations of LREEs and Y. The major component of the colloidal phase was  $\text{CeO}_2/\text{Ce}(\text{OH})_4$ , with 55.84% by weight. The Ce(IV) compounds are insoluble in water; therefore, partitioning of Ce(III) to the ion-exchangeable phase is low, which is known as the negative Ce anomaly. The

ion-exchangeable phase, which accounts for 83.33% of the total, is rich in lanthanum (La), neodymium (Nd), and Y plus HREE (e.g., europium (Eu), gadolinium (Gd), and dysprosium (Dy)). In this LT ore, the colloidal and mineral phases accounted for 7.78 and 8.89%, respectively. It has been shown that one can extract REEs from the colloidal phase by using a reducing agent (e.g., ferric sulfate or ferric sulfate), to reverse the oxidation state from Ce(IV) to Ce(III) [31, 32].

### 5.3.3 Effect of Phosphate

It has been reported that the percentages of ion-exchangeable REY concentrations relative to whole rock REY contents (PER) vary with the  $P_2O_5$  contents of weathered granites, as shown in Fig. 5.8 [33]. Similar plots have been made for the IAC samples taken in the regolith of the Liberty Hill pluton, South Carolina [34]. A rationale for these observations was that the  $Ln^{3+}$  ions liberated into soil and groundwater are taken up by the phosphate minerals such as monazite and thereby limit their mobilities along the depth of a regolith. The phosphate minerals can be the residual monazite in the regolith or the secondary phosphate (e.g., rhabdophane), formed between the liberated  $Ln^{3+}$  and  $PO_4^{3-}$  ions in the soil water. Since the rare earth minerals are very stable with high pK values, they can act as powerful scavengers of the liberated  $Ln^{3+}$  ions from solution, reducing the mobility of the liberated  $Ln^{3+}$  ions and thereby decreasing the PER contents. Fu et al. [23] expressed a more optimistic view on the role of phosphorus by suggesting that the  $Ln^{3+}$  ions in soil water can maintain mobility by complexing with  $HCO_3^-$ ,  $CO_3^{2-}$ , and organic ligands.

**Fig. 5.8** A relationship between ion-exchangeable REEs (PER) and  $P_2O_5$  contents of weathered granites. North Thai (NT) granite has lower P content than Western Province (WP) granite [33]





### 5.3.4 Environmental Issues

Most of the global production of HREEs comes from the IAC ores mined in China. After several decades of intensive mining, the ore grades are declining in terms of remaining available resources, while the public awareness of environmental impacts has been growing. To address these issues, R&D efforts have been focusing on recovery improvement and finding nitrogen-free lixiviants. The REY recoveries were high (85–90%) when the industry was using the heap (or pond) leaching process. With the use of the in-situ leaching process, which is mandated in South China to minimize the environmental impacts, the recoveries are now in the range of 40–70% [25]. In this process, typically 1–5%  $(\text{NH}_4)_2\text{SO}_4$  solution is injected through the holes drilled into an ore body, kept in the ground for 150–400 days and then drained to recover the pregnant solution, followed by washing the ore with water. The process entails an 8–20% loss of the reagent.

The pregnant solution is cleaned of impurities, which include  $\text{Al}^{3+}$ ,  $\text{Fe}^{3+}$ ,  $\text{Mg}^{2+}$ , and  $\text{Ca}^{2+}$  ions. These impurities are removed by raising the pH from 3.5 to 5.0 using ammonium bicarbonate ( $\text{NH}_4\text{HCO}_3$ ). The leach solution substantially free of the impurities is then treated with oxalic acid to obtain  $\text{Ln}_2(\text{C}_2\text{O}_4)_3$ , which is calcined to obtain salable REO as shown in Reaction (5.5). The low recoveries obtained from the ion-exchange leaching may be in part due to the presence of the species that are not ion-exchangeable, which include the colloidal phase (oxides), residual and secondary minerals, and those adsorbed as inner-sphere complexes via chemisorption [21].

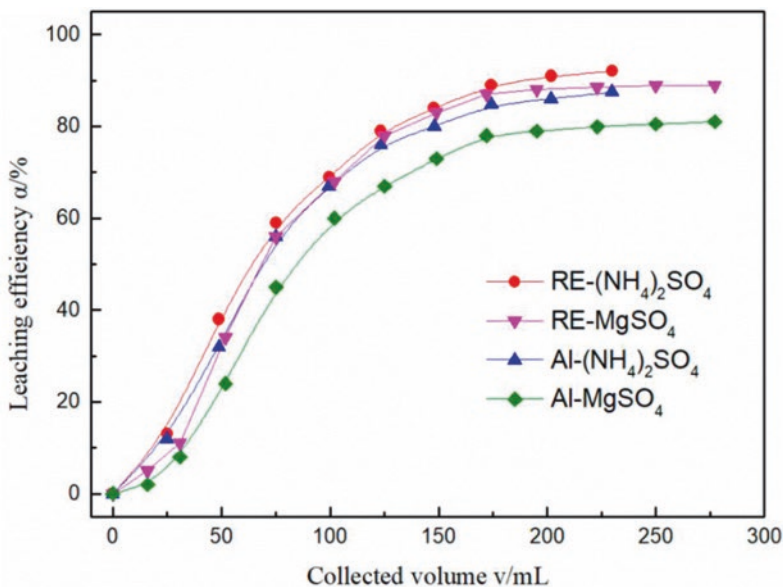


Fig. 5.9 Comparison of using  $(\text{NH}_4)_2\text{SO}_4$  and  $\text{MgSO}_4$  for the extraction of rare earth (RE) and aluminum ions from an IAC ore [35]

To address the environmental issues concerning the use of  $(\text{NH}_4)_2\text{SO}_4$  as a lixiviant, many investigators have explored the possibility of using  $\text{MgSO}_4$ . Figure 5.9 compares the results of using these two materials as lixiviants [35]. Rare earth recoveries were slightly higher with the former. On the other hand, the latter reagent released less of the aluminum ions into the solution. Thus, the use of  $\text{MgSO}_4$  may have two advantages: the elimination of nitrogen pollution and reduction of the generation of  $\text{Al}^{3+}$  ions into solution, which are major impurities in the leach liquor.

## 5.4 Ion-Adsorption Clays in the United States

### 5.4.1 Regolith-Hosted Deposit

It had been a general belief that IAC deposits are formed under humid and warm climates under subtropical weather conditions [36]. Recent studies conducted by the USGS showed, however, that both the climate and geological conditions in the United States were conducive to forming regolith-hosted IAC deposits in the granite plutons in Central Appalachia as shown in Fig. 5.10 [13].

Figure 5.11 compares the REE distributions obtained for the Stewartville regolith and the Heling IAC deposit, China [13]. The former exhibits a fourfold to 10-fold enrichment of REEs due to chemical weathering, which is comparable to what was observed with the latter. Note also that both the Stewartville and Heling regolith-hosted IAC ores exhibit Ce and Eu anomalies.

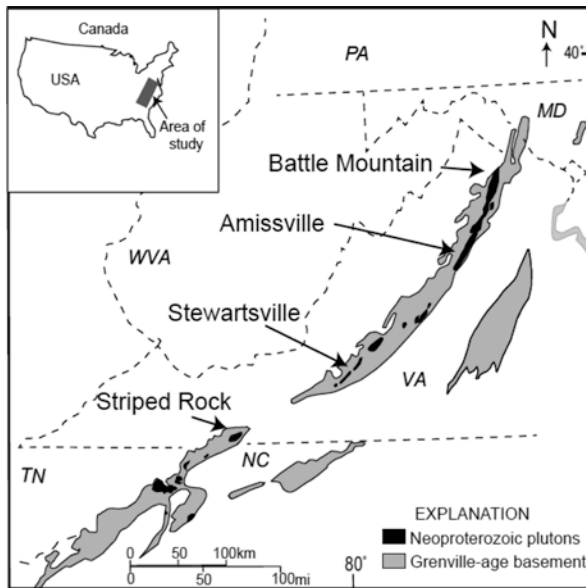
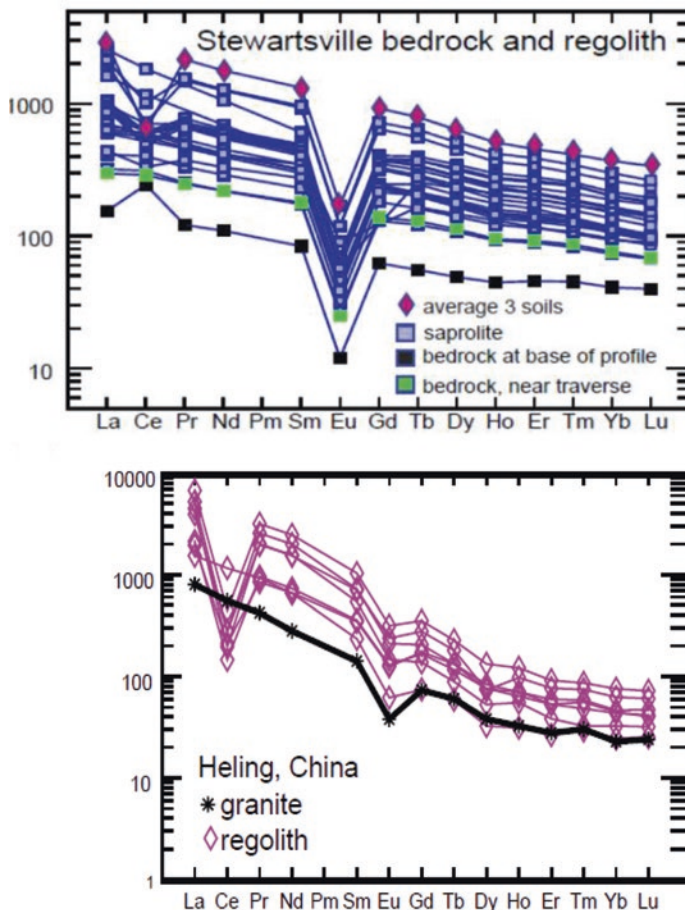
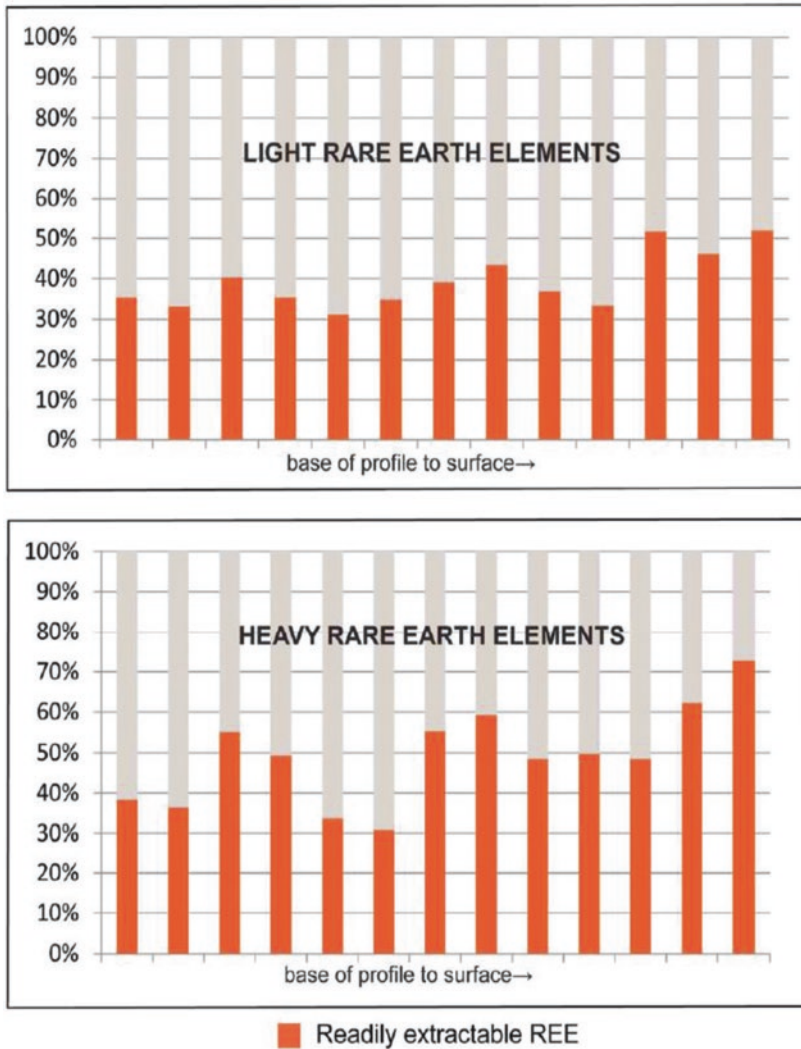


Fig. 5.10 IAC deposits in Central Appalachia [13]



**Fig. 5.11** Comparison of the REE patterns of a regolith-hosted ion-adsorption clay samples taken from Stewartville, Virginia, and Heling, China [13]

The Stewartville pluton is a medium-to-coarse-grained biotite granite, the accessory minerals of which include apatite, epidote, garnet, Nd-rutile, monazite, titanite, xenotime, gadolinite, and zircon. It is believed that the  $\text{Ln}^{3+}$  ions released from the Ln-bearing minerals have sufficient mobilities, which is essential for the regolith to be enriched with REEs during weathering. It has been shown, however, that the mobility of the liberated  $\text{Ln}^{3+}$  ions diminishes significantly if the regolith has a high phosphorus content [34]. In the presence of more stable phosphorus minerals (e.g., monazite, xenotime, and rhabdophane), the  $\text{Ln}^{3+}$  ions liberated from less stable accessory minerals (e.g., apatite), re-absorb onto the surfaces of the more stable minerals, and disappear from the soil water, thereby losing mobility, and failing to form ion-exchangeable IACs.

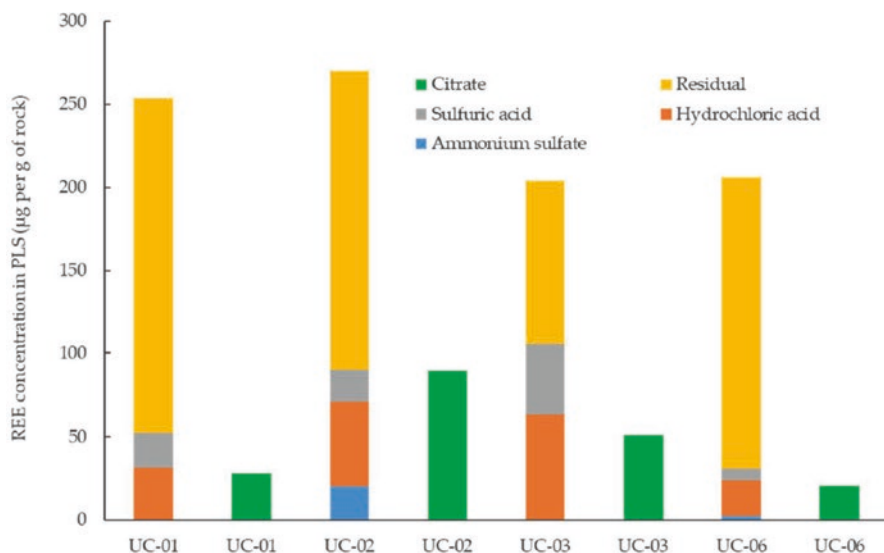


**Fig. 5.12** Sequential leaching tests conducted for selected regolith samples from Stewart profile [2]

Figure 5.12 shows the results of sequential extraction tests conducted on the Stewartville regolith samples taken at different depths [2]. The tests were conducted using sodium acetate ( $\text{NaO}_2\text{C}_2\text{H}_3$ ) as lixiviant at pH 5 and sodium pyrophosphate ( $\text{Na}_4\text{OP}_2\text{O}_7$ ) at pH 10. The maximum recoveries were 52% for LREEs and >70% for HREEs.

**Table 5.5** Reagents and conditions employed for sequential leaching [12]

Step	Reagent/target fraction	Solids (%)	Temp. (°C)	Time (h)	pH
1	0.5 M (NH <sub>4</sub> ) <sub>2</sub> SO <sub>4</sub>	22	22	4	5.0
	Exchangeable				
2	1 M HCl	22	22	24	1.0
	Colloid				
3	1.2 M H <sub>2</sub> SO <sub>4</sub>	70	70	1	0.86
	Colloid + mineral				
4	LiBO <sub>2</sub> -digestion	-	=	=	=
	Mineral + residual				

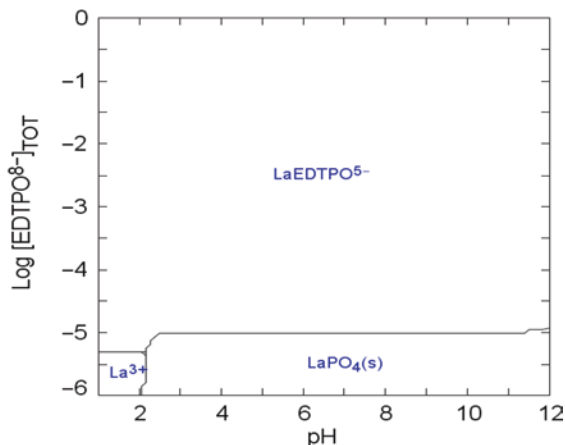
**Fig. 5.13** Results of the sequential leaching tests conducted on the underclay samples from Central Appalachian coal seams: Lower Freeport (UC-01), Middle Kittanning (UC-02), Pittsburg (UC-03), Lower Freeport (UC-06) [12]

### 5.4.2 Coal By-Products

Bryan et al. [9] suggested that the formation of coal generally occurs in a basin that may also contain REE-enriched sediments from the deposition and/or erosion of volcanic, intrusive, and detrital resources. Thus, the clayey materials formed in granite rocks may have been an integral part of coal formation. Recognizing that ~80% of the mineral matter in coal has been derived from kaolinite, illite, halloysite, and other clay minerals, it would be reasonable to explore the possibility of extracting REEs from the coal by-products such as underclay and thickener underflows.

Montrose et al. [12] did just that and conducted bench-scale extraction tests on a series of underclay samples associated with Central Appalachian coal seams. These

**Fig. 5.14** Stability diagram for  $\text{LaPO}_4(\text{s})$ , representing a passivated form of the  $\text{La}^{3+}$  ions adsorbed on kaolinite in the presence of EDTPO [37]



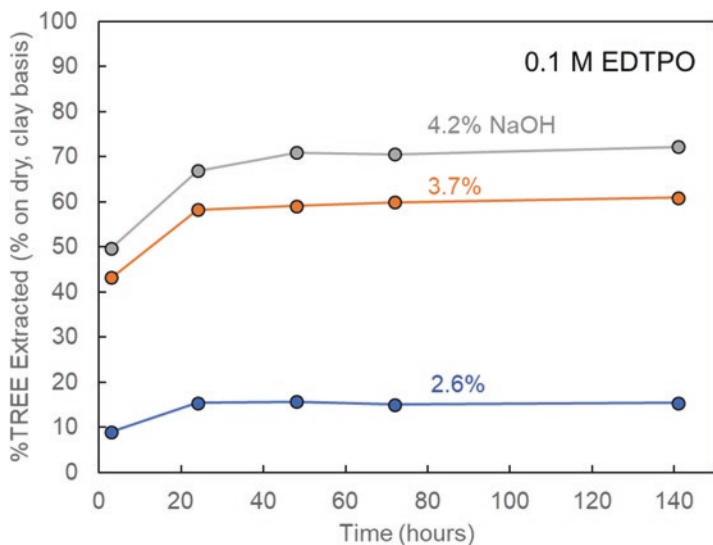
included Lower Freeport, Middle Kittanning, and Pittsburgh No. 5 coals. Each sample was subjected to sequential laboratory-scale extraction tests using the reagents and experimental conditions given in Table 5.5. The leaching experiments were designed to extract different phases of rare earths (i.e., ion-exchangeable, colloidal, minerals and total).

The results presented in Fig. 5.13 show that the  $(\text{NH}_4)_2\text{SO}_4$  leaching at pH 5 extracted only 0.3–7.5% of the total REEs, indicating that the ion-exchangeable fractions in the three U.S. coal samples were much smaller than those of the IAC ores mined in South China. Of the four samples tested, the Middle Kittanning coal sample (UC-02) responded well to the conventional ion-exchange leaching process using  $(\text{NH}_4)_2\text{SO}_4$  as the lixiviant. Including the recoveries obtained by HCl leaching, the recoveries were in the range of 11.4–36.0%. The HCl leaching most probably dissolved the colloidal phase which included iron (Fe) and manganese (Mn) oxides.

All four samples contained significant amounts of residual rare earth-bearing (carrier) minerals and secondary minerals mostly as phosphates, which may have contributed to reducing the mobility of the  $\text{Ln}^{3+}$  ions along the regolith profiles and hence the low ion-exchangeable contents.

The results obtained with a chelating agent (citric acid,  $\text{C}_6\text{H}_8\text{O}_7$ ) alone gave substantially higher recoveries than obtained with  $(\text{NH}_4)_2\text{SO}_4$ . For the UC-02 sample, the recovery was 33%. It is possible that the chelating agent dissolved  $\text{LnPO}_4(\text{s})$  that may have been formed on the IAC in the presence of the  $\text{PO}_4^{3-}$  ions that were derived from a less stable phosphate mineral (apatite).

Figure 5.14 represents a stability diagram for the  $\text{LaPO}_4(\text{s})$  in the presence of ethylenediamine-tetramethylene phosphonic acid (EDTPO), which is a strong chelating agent. The diagram suggests that it is thermodynamically possible to dissolve the  $\text{LaPO}_4(\text{s})$ , representing a passivated form of the lanthanide species adsorbed on the surface of an IAC, at a wide range of pH. The data presented in Fig. 5.15 show a set of leaching tests conducted on a clay sample that had been isolated from a thickener underflow sample from West Virginia. The tests were conducted at 0.1 M EDTPO, 2.6–4.2% NaOH at 80 °C. The use of NaOH was to desorb  $\text{PO}_4^{3-}$  ions from the  $\text{LaPO}_4(\text{s})$  surface. It is possible that REE ions were extracted into the leach



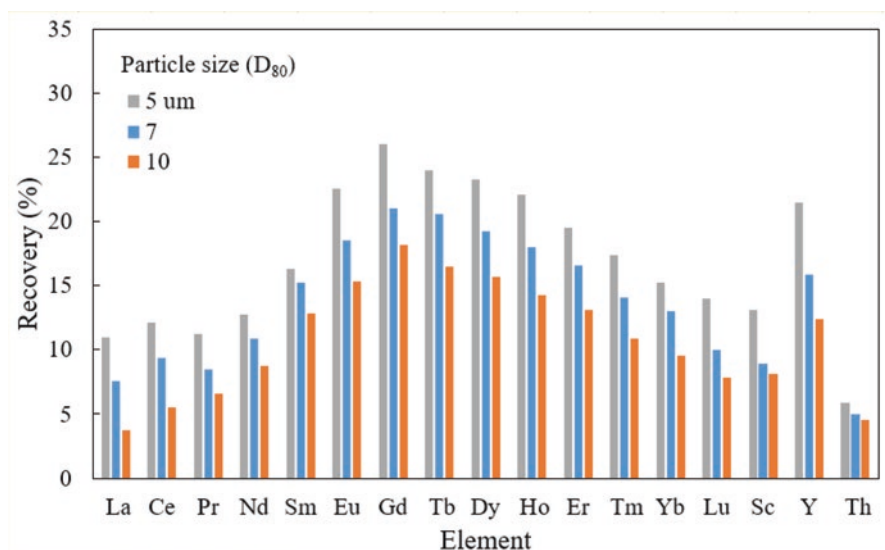
**Fig. 5.15** Percent extraction of REEs from the clay samples isolated from a thickener underflow of the Lower Kittanning coal in West Virginia [37]

liquor from both the  $\text{LnPO}_4(\text{s})$  and the residual minerals (monazite) that were co-present in the industrial sample. The experimental conditions employed for these tests were milder than typically employed to leach monazite. The role of the thickener was to collect the fine coal waste generated during the process of cleaning the Lower Kittanning coal before discarding it to an impoundment.

### 5.4.3 Challenges

The results presented in this chapter support the possibility that U.S. coal may be a significant source of HREEs. On the other hand, it is a challenge to extract them using the simple ion-exchange process represented by Reaction (5.1). Two possible reasons have been suggested for this difficulty. First, the REEs adsorbed on clay minerals are in a colloidal form possibly as oxides, hydroxides, and oxyhydroxides. A series of reductive leaching tests conducted on coal by-products did not yield promising results. Second, the ion-adsorption clays formed on granite rocks and transported to the coal basins may have been passivated by the  $\text{PO}_4^{3-}$  ions from solution, making it difficult to extract them by ion-exchange leaching. Promising results have, however, been obtained using chelating agents.

The presence of IACs in U.S. coals may be supported by the work reported by Foley et al. of the USGS [2, 13]. These investigations showed that the climate and geological conditions of the Central Appalachia region and South China were similar and that the REEs can be readily extracted using either by ion-exchange leaching



**Fig. 5.16** Element-by-element recovery of rare earth elements in a pregnant leach liquor obtained by leaching an underclay sample from Pennsylvania at 6 M HCl for 18 hrs. No significant leaching of the feed solids was observed. The smaller the particle size of a feed sample, the higher the recovery [37]

or by using appropriate complexing agents. A major difference between the two sources of clay (i.e., coal and granite) may lie in the fact that the former had been immersed in an aqueous phase during the geological time scale, while the latter had not.

There are three other challenges from the process engineering point of view. First, the REE concentrations are low (300–500 ppm), which makes it difficult to deploy a costly extraction process. Unless the prices of REOs are substantially elevated in the future, the contained values of coal by-products are too low to attract significant capital investments. Second, processing costs may be high to overcome the problems associated with colloidal and passivated forms of REEs. The fact that the particle sizes are small, mostly  $<10\ \mu\text{m}$ , may also contribute to the high costs. Third, coal by-products contain significant amounts of residual accessory minerals along with ion-adsorption clays. Processing of the former (e.g., monazite) will require aggressive extraction processes, while processing the latter will require milder reaction conditions. It may be necessary to process them in separate lines after appropriate separation.

The concentrations of different REE elements extracted into solution from leaching an underclay sample are presented in Fig. 5.16. Although the recoveries were low, the results show that the clay minerals in coal are excellent vehicles to enrich HREEs on the surface, which is a unique characteristic of IACs in general. Furthermore, the concentrations of Y and Th are low, which is another characteristic and advantage of extracting REEs from IACs.



## 5.5 Summary

Despite its low reserve base, IACs account for 80% of the global supply of HREEs that are essential for developing renewable energy resources, high-tech industries, and defense industries. Clay minerals provide negatively charged surfaces on which  $\text{Ln}^{3+}$  ions can adsorb physically as outer-sphere basal complexes, which can be readily extracted by other cations or by anions that can remove them by forming aqueous complexes.

Recent studies conducted by USGS showed that both the geological and climate characteristics of southeastern United States are conducive to forming regolith-hosted IACs, which has raised the prospect of turning coal mining wastes into a major resource for HREEs [13]. It has been found, on the other hand, that it is difficult to extract REEs from them using the ion-exchange leaching process as they may be passivated by  $\text{PO}_4^{3-}$  ions present in coal basins. Recent studies showed, however, that one can address this problem by using appropriate chelating agents. There are other challenges such as the presence of residual accessory minerals and low rare earth grades, both of which can be readily addressed with further future research.

**Acknowledgments** The author greatly appreciates the financial support from NETL (Grant No. DE-FE0029900), and technical guidance from Anthony Zinn and Charles Miller, who served as federal project managers, and from Mary Anne Alvin who served as NETL's Rare Earth Element and Critical Minerals Technology Manager. His appreciation is also extended to John Morris, Gordon Yee, Aaron Noble, Xu Feng, Rahaf Rousan, McAlister Council-Troche, Kaiwu Huang, Mohit Gupta, Ozgur Onel, Wei Liu, and Sara Price who have been working together as a coherent team.

## References

1. U.S. Geological Survey, Mineral commodity summaries, Jan, 2021
2. N. Foley, R. Ayuso, B. Hubbard, C. Bern, A. Shah, Geochemical and mineralogical characteristics of REE in Granite-Derived Regolith of the Southeastern United States, in *Mineral Resources in a Sustainable World. Proceedings of the 13th Biennial SGA Meeting*, vol. 2, (2015), pp. 725–729
3. B. Zhou, Z. Li, C. Chen, Global potential of rare earth resources and rare earth demand from Clean Technologies. *Fortschr. Mineral.* **7**(11), 203 (2017)
4. G.A. Parks, The isoelectric points of solid oxides, solid hydroxides, and aqueous hydroxo complex systems. *Chem. Rev.* **65**(2), 177–198 (1965)
5. R.H. Yoon, T. Salman, G. Donnay, Predicting points of zero charge of oxides and hydroxides. *J. Colloid Interface Sci.* **70**(3), 483–493 (1979)
6. A.M. Borst, M.P. Smith, A.A. Finch, G. Estrade, C. Villanova-de-Benavent, P. Nason, E. Marquis, K. Geraki, Adsorption of rare earth elements in Regolith-Hosted Clay Deposits. *Nat. Commun.* **11**(1), 1–15 (2020)
7. X. Wang, Y. Lei, J. Ge, S. Wu, Production forecast of China's rare earths based on the generalized Weng Model and policy recommendations. *Resour. Policy* **43**, 11–18 (2015)

8. X.J. Yang, A. Lin, X.L. Li, Y. Wu, W. Zhou, Z. Chen, China's ion adsorption rare earth resources, mining consequences and preservation. *Environ. Dev* **8**, 131–136 (2013)
9. R.C. Bryan, D. Richers, H.T. Andersen, T. Gray, *Assessment of Rare Earth Elemental Contents in Select United States Coal Basins* (United States National Energy Technology Laboratory, 2015)
10. J.J. Renton, C.B. Cecil, R. Stanton, F. Dulong, Compositional relationships of plants and peats from Modern Peat Swamps in support of a chemical coal model, in *Carboniferous Coal, Short Course and Guidebook*, vol. 3, (1979), pp. 57–102
11. P.L. Rozelle, A.B. Khadilkar, N. Pulati, N. Soundarrajan, M.S. Klima, M.M. Mosser, C.E. Miller, S.V. Pisupati, A study on removal of rare earth elements from US coal byproducts by ion exchange. *Metall. Mater. Trans. E* **3**(1), 6–17 (2016)
12. S.N. Montross, J. Yang, J. Britton, M. McKoy, C. Verba, Leaching of rare earth elements from central Appalachian coal seam underclays. *Fortschr. Mineral.* **10**(6), 577 (2020)
13. N. Foley, R. Ayuso, REE enrichment in Granite-Derived Regolith Deposits of the Southeastern United States: Prospective source rocks and accumulation processes. *Geol. Surv. Pap* **3**, 131–138 (2015)
14. P. Oliva, J. Viers, B. Dupré, Chemical weathering in granitic environments. *Chem. Geol.* **202**(3-4), 225–256 (2003)
15. Z. Bao, Z. Zhao, Geochemistry of mineralization with exchangeable REY in the weathering crusts of granitic rocks in South China. *Ore Geol. Rev.* **33**(3-4), 519–535 (2008)
16. Y.H.M. Li, W.W. Zhao, M.F. Zhou, Nature of parent rocks, mineralization styles and ore genesis of Regolith-Hosted REE Deposits in South China: An integrated genetic model. *J. Asian Earth Sci.* **148**, 65–95 (2017)
17. Y.H. Wang, C.B. Huang, Y.H. Hu, Y.M. Hu, Y. Lan, Beneficiation of diasporic-bauxite ore by selective flocculation with a polyacrylate flocculant. *Miner. Eng.* **21**(9), 664–672 (2008)
18. M.H. Bradbury, B. Baeyens, Sorption of Eu on Na- and Ca-montmorillonites: Experimental investigations and modelling with cation exchange and surface complexation. *Geochim. Cosmochim. Acta* **66**(13), 2325–2334 (2002)
19. W. Piasecki, D.A. Sverjensky, Speciation of adsorbed yttrium and rare earth elements on oxide surfaces. *Geochim. Cosmochim. Acta* **72**(16), 3964–3979 (2008)
20. G.A. Moldoveanu, V.G. Papangelakis, An overview of rare earth recovery by ion exchange leaching from ion adsorption clays of various origins. *Mineral. Mag.* **80**(1), 63–76 (2016)
21. H. Mukai, Y. Kon, K. Sanematsu, Y. Takahashi, M. Ito, Microscopic analyses of weathered granite in ion adsorption rare earth deposit of Jianxi Province, China. *Sci. Rep* **10**(1), 1–11 (2020)
22. M. Yang, X. Liang, L. Ma, J. Huang, H. He, J. Zhu, Adsorption of REEs on Kaolinite and Halloysite: A link to the REE distribution on clays in the weathering crust of granite. *Chem. Geol.* **525**, 210–217 (2019)
23. W. Fu, X. Li, Y. Feng, M. Feng, Z. Peng, H. Yu, H. Lin, Chemical weathering of S-type granite and formation of rare earth element (REE)-Rich Regolith in South China: Critical control of lithology. *Chem. Geol.* **520**, 33–51 (2019)
24. L.M. Suli, W.H.W. Ibrahim, B.A. Aziz, M.R. Deraman, N.A. Ismail, A review of rare earth mineral processing technology. *Chem. Eng. Res. Bull.* **19**, 20–35 (2017)
25. R. Schulze, F. Lartigue-Peyrou, J. Ding, L. Schebek, M. Buchert, Developing a life cycle inventory for rare earth oxides from ion adsorption deposits: Key impacts and further research needs. *J. Sustain. Metall* **3**(4), 753–771 (2017)
26. R. Chi, J. Tian, *Weathered Crust Elution-Deposited Rare Earth Ores* (Nova Science Publishers, 2008)
27. Y.F. Xiao, Z.Y. Feng, G.H. Hu, L. Huang, X.W. Huang, Y.Y. Chen, M.L. Li, Leaching and mass transfer characteristics of elements from ion adsorption type rare earth ore. *Rare Metals* **34**(5), 357–365 (2015)
28. G.A. Moldoveanu, V.G. Papangelakis, Recovery of rare earth elements adsorbed on clay minerals: I. Desorption mechanism. *Hydrometallurgy* **117**, 71–78 (2012)

29. R. Chi, J. Tian, L. Zhongjun, P. Cui, W. Yuanxin, L. Shirong, C. Wang, Z. Zhiang, Existing state and partitioning of rare earth on weathered ores. *J. Rare Earths* **23**(6), 756 (2005)
30. X. Yanfei, G. Guohua, H. Li, F. Zongyu, L. Fuguo, L. Zhiqi, A discussion on the leaching process of the ion adsorption type rare earth ore with the Electrical Double Layer Model. *Miner. Eng.* **120**, 35–43 (2018)
31. X.I.A.O. Yanfei, F.E.N.G. Zongyu, H.U. Guhua, L. Huang, X. Huang, C.H.E.N. Yingying, L.O.N.G. Zhiqi, Reduction leaching of rare earth from ion adsorption type rare earths ore with ferrous sulfate. *J. Rare Earths* **34**(9), 917–923 (2016)
32. F. Lai, G. Gao, L. Huang, Y. Xiao, R. Yang, K. Li, Compound leaching of rare earth from the ion adsorption type rare earth ore with magnesium sulfate and ascorbic acid. *Hydrometallurgy* **179**, 25–35 (2018)
33. K. Sanematsu, Y. Kon, A. Imai, Influence of phosphate on mobility and adsorption of REEs during weathering of granites in Thailand. *J. Asian Earth Sci.* **111**, 14–30 (2015)
34. C.R. Bern, T. Yesavage, N.K. Foley, Ion adsorption REEs in Regolith of the Liberty Hill Pluton, South Carolina, USA: An effect of hydrothermal alteration. *J. Geochem. Explor.* **172**, 29–40 (2017)
35. X. Ran, Z. Ren, H. Gao, R. Zheng, J. Jin, Kinetics of rare earth and aluminum leaching from Kaolin. *Fortschr. Mineral.* **7**(9), 152 (2017)
36. V.G. Papangelakis, G. Moldoveanu, Recovery of rare earth elements from clay minerals, in *Proceedings of the 1<sup>st</sup> Rare Earth Resources Conference, Milos*, (2014, September), pp. 191–202
37. R.-H. Yoon, C.A. Noble, M. Council-Troche, W. Liu, Methods for extracting rare earth elements from rare earth element sources. PCT, US2021/061917, December 4, 2021

# Chapter 6

## Solvent Extraction



Alain Rollat

### 6.1 Introduction

The chemical and physical properties of the final application using rare earth elements (REEs), as magnets, catalysis or phosphors for example, are specific to the different REEs and in most cases, these properties depend greatly on the purity of the REE used. Typically, it is quite usual in the rare earth (RE) industry to speak about purities as high as 99.9% (3 N) or 99.99% (4 N).

Since RE ores contain a mixture of all the lanthanides plus yttrium, and because the lanthanides and yttrium have similar chemical properties, producing such high purities is a challenge. Currently, this process step which is commonly called RE separation or RE refinery is done by solvent extraction (SX). Several companies and research teams are looking for alternative processes, but SX is still the only technology used in industry.

This step of the global RE process is key for several reasons.

- The performance of the final applications (magnets, catalysis, phosphors, etc.) depends mostly on the purity of the RE used.
- The cost of the refining step both in terms of capital expenditure (CAPEX) and operating expenditure (OPEX) is an important part of the overall cost of the REE industry.
- The life cycle assessment (LCA) of the RE oxides or metals shows the importance of the refining step in the global environmental footprint of the RE industry.

The focus of this chapter is to present the chemistry and the technology hidden behind the RE separation process and their consequences on the economics and the environmental footprint of the REE industry.

---

A. Rollat (✉)  
CARESTER, Lyon, France  
e-mail: [arollat75@gmail.com](mailto:arollat75@gmail.com)

## 6.2 A Short History of the Rare Earth Element Separation Processes

It is well known that all the REEs, the lanthanides, and yttrium have remarkably similar chemical behavior. This is the reason why these elements are always present together in the ores, and this characteristic also explains the complexity of the RE separation process.

Until the early 1950s, REEs were separated by fractional crystallization using various chemical reagents. On the other hand, if all the REEs exist as trivalent ions, with cerium being stabilized in the aqueous solution as a tetravalent ion and europium as a divalent ion, then these valence state differences were used to purify these REs. However, these processes were long, complex, and did not allow production of all the REs as pure individual elements.

In the 1950s, REE separation using ion exchange (IEx) was a first step in the development of the industrial production of pure individual elements. However, from the mid-1960s, the development of the color TV needed production of mass quantities of high purity europium and yttrium. Although IEx produces very pure REs, it has two drawbacks: it is a sequential process with an intrinsic low productivity, and it uses some expensive chemicals like aminopolyacetic acids which must be recycled. In this context, some companies in Europe, the United States, and Japan decided to develop a new process for RE separation based on the technology developed for the Manhattan project during the second world war, solvent extraction (SX). Among them were two companies, Molycorp in the United States and Pechiney-Saint Gobain (became Rhone-Poulenc, then Rhodia) in France, which were at that time the leaders of the RE industry.

From these early times, the situation of the RE industry has become both simpler and at the same time more complicated. In the early 1980s, a newcomer, China, started to develop its own RE industry based on the same principles as those already used in the western world [1]. Nowadays, all the industrial units in the world use SX for RE separation, but the competence for designing and running this technology has been progressively concentrated in China. Fortunately, a few teams around the western world have retained the expertise of RE separation.

## 6.3 Solvent Extraction Chemistry of Metallic Species—Application to the Rare Earths

Solvent extraction is widely used for metals recovery and purification, from very large volumes of base metals like copper to small quantities of high value elements like cobalt or uranium and even very costly elements like the platinum group metals [2]. SX of metallic species is based on the difference in behavior of metals during their transfer from an aqueous solution to an organic immiscible phase. Analyzing the behavior of metallic species according to the chemistry involved in the mass

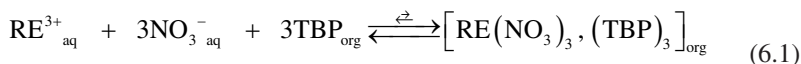
transfer is interesting from two standpoints. First-of-all, based on the chemical knowledge of the elements to be recovered, it allows for prediction and optimization of the conditions of their extraction, and then it also allows for understanding the mass transfer driving forces and economics of the process.

Insofar as the inorganic species are not soluble in most of the organic media, the transfer of a metallic species from an aqueous solution into an organic solution needs the help of some specific organic molecules to make the inorganic species compatible with the organic environment. The chemical form of these organic molecules, also called extractants, extracting molecules or ligands, is the basis for the classification of the various extraction systems for metallic species. These extraction systems can be classified into three categories according to the chemistry involved: neutral or solvating extraction (extraction of a neutral species (i.e., molecule or complex)); basic or ion pair extraction (extraction of anionic species); and acidic extraction (extraction of cations). Most often the active molecule is diluted in a diluent (typically an aliphatic—kerosene—or aromatic hydrocarbon, but other organic molecules can be considered) to lower the viscosity. This organic mixture to which some other species can be added is called the solvent of extraction.

The lanthanides and yttrium are all stable in trivalent oxidation state in aqueous solution. Because of the remarkably similar chemical properties of the trivalent cations, their purification is the most difficult separation among the metallic species. The specificities of each system (neutral, basic, and acidic) are shown below. However, two lanthanides, cerium and europium are also stable in a different oxidation state—tetravalent for cerium in a nitrate or sulfate solution and divalent for europium in a chloride solution. The specific behaviors of  $\text{Ce}^{4+}$  and  $\text{Eu}^{2+}$  compared to all  $\text{RE}^{3+}$  can also be used for purifying these elements (Sect. 6.3.4).

### 6.3.1 Neutral or Solvating Extraction of Trivalent RE

This system uses neutral molecules. The anion present in the aqueous phase is coextracted with the metallic cation meaning that this system can be used only if the metallic ion and the anion can form sufficiently stable complexes in the aqueous phase. In the case of REEs, this criterion limits the possibility of the use of neutral molecules to only nitrate solutions. Indeed, the chloride ions are not complexing enough versus REEs to be extracted by neutral molecules. Tributyl phosphate (TBP) is one of the neutral molecules widely used for REE separation [3]. The equilibrium of such an extraction system is shown below:



Where  $\text{RE}^{3+}$  = trivalent REE ion

The constant of this equilibrium can be expressed as:

$$K_{RE} = \left[ RE(NO_3)_3, (TBP)_{3org} \right] / \left( \left[ RE^{3+}_{aq} \right] * \left[ NO_3^-_{aq} \right]^3 * \left[ TBP_{org} \right]^3 \right) \quad (6.2)$$

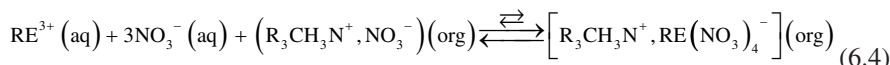
While the partition coefficient of REE ions between organic and aqueous phase is:

$$P_{RE} = \left[ RE(NO_3)_3, (TBP)_{3org} \right] / \left[ RE^{3+}_{aq} \right] = K_{RE} * \left[ NO_3^-_{aq} \right]^3 * \left[ TBP_{org} \right]^3 \quad (6.3)$$

The driving force of the RE extraction is the concentration of nitrate in aqueous solution. The equilibrium does not depend on the acidity of the aqueous solution as long as the acid concentration is low enough (at high acid concentration, nitric acid will be extracted by TBP and there will be a competition between the extraction of REE and the extraction of HNO<sub>3</sub>).

### 6.3.2 Basic or Ion Pair Extraction of Trivalent RE

This system uses organic cations. The metallic species is extracted as an anion formed between the metallic cation (M<sup>n+</sup>) and the anion present in the aqueous phase. This system can be used only if the metallic ion and the anion can form sufficiently stable complexes in the aqueous phase and in the case of REEs, this criterion limits the possibility of the use of ion pair extraction to nitrate solutions. Indeed, the chloride ions are not complexing enough with the REE to allow them to be extracted as ion pairs. Trioctyl methyl ammonium (commercial name Aliquat 336) is one of the organic cations used for REE separation [3]. The equilibrium of such an extraction system is shown below:



Where RE<sup>3+</sup> = trivalent REE ion and R = C<sub>8</sub>H<sub>17</sub>

The constant of this equilibrium can be expressed as:

$$K_{RE} = \left[ R_3CH_3N^+, RE(NO_3)_4^- \right]_{org} / \left( \left[ RE^{3+}_{aq} \right] * \left[ NO_3^-_{aq} \right]^{3*} \right) \quad (6.5)$$

While the partition coefficient of RE ions between organic phase and aqueous phase is:

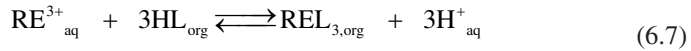
$$P_{RE} = K_{RE} * \left[ NO_3^-_{aq} \right]^{3*} \left[ R_3CH_3N^+, NO_3^- \right] \quad (6.6)$$

The driving force of the REE extraction is the concentration of nitrate in aqueous solution. Equilibrium does not depend on the acidity of the aqueous solution as long as the acid concentration is low enough (at high acid concentration, there will be a competition between the extraction of  $RE(NO_3)_4^-$  and the extraction of  $NO_3^-$ ).

It should be noted that anionic extraction as described below is a special case of extraction by ionic liquids to which various academic studies have been devoted in recent years [4]. It is therefore interesting to see that ionic liquids have been used industrially for several decades in the RE industry.

### 6.3.3 Acidic or Cationic Extraction of Trivalent RE

This system uses acidic organic molecules. The metallic species is extracted as a cation. It can be used whatever the aqueous solution's common acid ion, chloride, sulfate or nitrate may be. Ethylhexyl,ethylhexyl phosphonic acid (H(EH)EHP, commercial name P507 in China or PC88A in the western world) is one of the cationic molecules widely used for RE separation [3]. The equilibrium of such an extraction system is shown below:



Where  $RE^{3+}$  = trivalent REE ion and HL = Acidic organic molecule

The constant of this equilibrium can be expressed as:

$$K_{RE} = \left( [REL_3]_{org} * [H^+]_{aq}^3 \right) / \left( [RE^{3+}]_{aq} * [HL_{org}]^3 \right) \quad (6.8)$$

while its distribution coefficient is:

$$P_{RE} = K_{RE} * [HL_{org}]^3 / [H^+]^3 \quad (6.9)$$

The driving force of the RE extraction is the acidity of the aqueous solution. This driving force is linked to the acidity constant of the acidic molecule:

$$K_a = [L] * [H^+] / [HL] \quad (6.10)$$

For a given element, the higher the acidity constant, the more difficult the stripping of the RE from the organic solution and the more acid will be required.



### ***6.3.4 The Specific Case of Tetravalent Cerium and Divalent Europium***

All the lanthanides as well as yttrium are stable in the trivalent oxidation state in any type of common commercially used aqueous acidic solutions (chloride, nitrate, and sulfate). Chemical Eqs. 6.1, 6.2 and 6.3 reflect the chemical behavior of the trivalent RE cations.

However, cerium is also stable in the tetravalent oxidation state in sulfate and nitrate solutions and europium is stable in the divalent oxidation state in chloride solution.  $Ce^{4+}$  has a much more acidic chemical behavior than all the  $RE^{3+}$  while  $Eu^{2+}$  has a chemical behavior comparable to  $Sr^{2+}$ . These specific chemical behaviors can be used for purifying cerium and europium [3].

$Ce^{4+}$  can be obtained from  $Ce^{3+}$  by chemical oxidation or electrochemical oxidation in sulfate or nitrate solutions. The separation of  $Ce^{4+}$  from  $RE^{3+}$  can be done either by classical chemistry (selective precipitation) or by SX. Speaking about SX,  $Ce^{3+}$  is always between  $La^{3+}$  and  $Pr^{3+}$  whatever the extractant, but  $Ce^{4+}$  is much more extractable than all  $RE^{3+}$ . This difference is interesting from an industrial point of view because cerium represents almost half of the REE in many ores. Therefore, the SX of cerium first can be used to minimize the size of all the downstream processing.

$Eu^{2+}$  can be obtained from  $Eu^{3+}$  by chemical reduction with Zn or by electrochemical reduction in chloride solution.

Then, separation of  $Eu^{2+}$  from  $RE^{3+}$  is done either by classical chemistry using the difference of solubility between the  $Eu^{2+}$  species and the corresponding  $RE^{3+}$  species (selective precipitation of  $Eu^{2+}$  sulfate, the solubility of which is extremely low and close to the  $Sr^{2+}$  sulfate solubility) or by SX, the selectivity between  $RE^{3+}$  and  $Eu^{2+}$  is extremely high with any cationic type of molecule.

### ***6.3.5 Chemical Formula of Some Important Ligands***

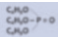

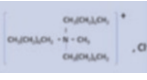
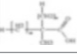
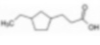
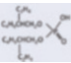
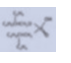
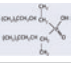
The most important ligands used for REE separation are shown in Table 6.1.

## **6.4 The RE Refining Process**

### ***6.4.1 A Global View of the RE Separation Process by SX***

Whatever the extracting molecule is, the selectivity of one single liquid-liquid extraction mass transfer is by far not sufficient to obtain pure products. This single effect needs to be repeated many times to allow reaching the required purity. Each mass transfer step (extraction) is followed by a coalescence step from which both

**Table 6.1** List of the main molecules used for REE separation

Extraction type	Chemical name and formula	Usual acronym	Commercial name
Solvation	Tri butyl phosphate 	TBP	TBP
	Di butylbutyl phosphonate 	DBBP	DBBP
Anionic	Triooctyl methyl quaternary ammonium 		Aliquat 336
Cationic	Methyl heptylic acid 		Versatic acid
	Cyclo pentyl alkyl carboxylic acid 	Naphtenic acid	Naphtenic acid
	Di ethyl2hexyl phosphoric acid* 	HDEHP D2EHPA	HDEHP (western world) P204 (China)
	Ethyl2hexyl, ethyl2hexyl phosphonic acid* 	HEH(EHP)	P507 (China), Ionquest 801 (Solvay) PC88A (Daihachi)
	Bis(2,4,4-trimethylpentyl) phosphonic acid* 	HBTMPP	Cyanex 272 (Solvay)
	Mixture of Ethyl2hexyl, ethyl2hexyl phosphonic acid and Bis(2,4,4-trimethylpentyl) phosphonic acid		Cyanex 572 (Solvay)

\*Among the phosphorus acids, the acidity constants are phosphinic < phosphonic < phosphoric

aqueous and organic phases are recovered separately. Then both aqueous and organic phases coming out of this first step are contacted again with a new organic and a new aqueous phase. This series of extractions-coalescences is done in specific equipment allowing the two phases, aqueous and organic, to circulate countercurrently. But how does such a series of extraction-coalescence steps allow us to produce pure REEs? In this type of process, the organic phase (the solvent) combines two actions:

- A conveyor, allowing the REs to move along the series of extraction-coalescence steps.
- A selector, allowing some REs to move more efficiently than the others.

The solvent as a conveyor, not being consumed during this process, is continuously recycled to repeat its conveying and selection actions.

The design of such equipment allowing the contact of the aqueous and organic phases countercurrently will be discussed later, but for the time being let us call it the SX battery.

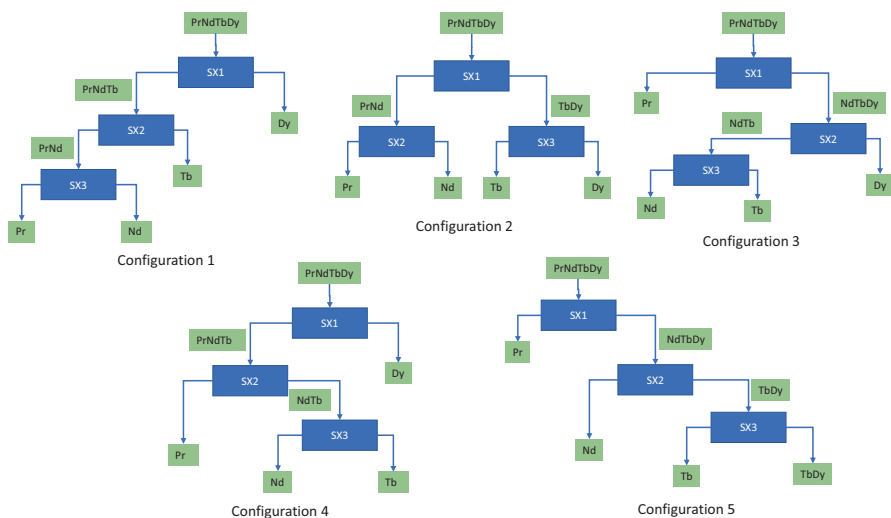
## The Classical Configuration of a SX Circuit (SX Battery)

Globally, a classical SX battery allows for the separation of a mixture of REs into two groups of REs, each of them being purified from the other or, if just a mixture of two REs, into two pure REs. The position of the cut between two adjacent REs can be anywhere along the lanthanide series if the separation factor between the two REEs to be separated (the ratio between the partition coefficient of both REE) is high enough. Industrially the lowest separation factor used is about 1.5. And so, the separation of a mixture of  $n$  REEs into  $n$  pure REEs needs  $n-1$  SX batteries. For example, the recycling of REEs from end-of-life permanent magnets leads to a mixture of four REEs—Pr, Nd, Tb, and Dy. The separation of this mixture into pure Pr, pure Nd, pure Tb, and pure Dy will need three SX batteries. Five different configurations of these three batteries can be designed (Fig. 6.1).

Even if all these configurations are potentially possible, they are not all equivalent from an economic point of view. The choice between these different configurations will be based on economic considerations and only a model can be used to make this comparison (i.e., the separation of a mixture of seven REEs into seven pure REEs can be done with 145 different configurations of six SX batteries!).

But how does each SX work? In other words, what is the principle of circulation of a solution containing a mixture of  $n$  REEs in a SX battery that allows this solution to be separated into two solutions of REEs each of them being completely separated from the other. This principle will be exemplified using SX1 of Configuration 2 (i.e., PrNd/TbDy separation).

Like all SX batteries for REEs separation, SX1 is made of four sections, loading, extraction, scrubbing, and stripping, each section having a certain number of stages:



**Fig. 6.1** Different configurations possible for Pr/Nd/Tb/Dy separation

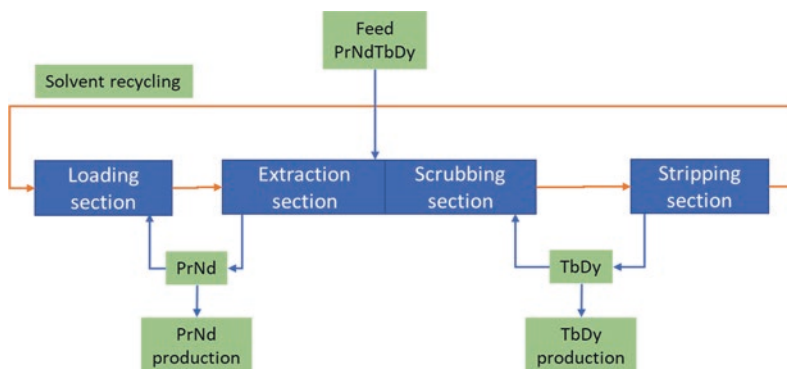
- In the loading section, the fresh solvent is loaded by mixing with an aqueous solution of Pr + Nd.
- In the extraction section, the loaded solvent containing Pr + Nd is fed countercurrently with the feed solution containing the four REEs. During this step, all the Tb and Dy ions contained in the feed are exchanged with the Pr and Nd coming with the loaded solvent.
- The solvent coming out of the extraction section contains all the Tb and Dy, but also part of the Pr and Nd coextracted with Tb and Dy. The aim of the scrubbing section is to exchange these Pr and Nd with Tb and Dy sent countercurrently to the solvent.
- In the stripping section, the solvent coming out of the scrubbing section is mixed countercurrently with an aqueous solution suitable to strip the Tb and Dy contained on the solvent.

The solvent coming out of the stripping section is pure of REEs and can be recycled as fresh solvent to the loading section. In other words, there is no consumption of the solvent which can be seen as the conveyor of the REE along the separation process.

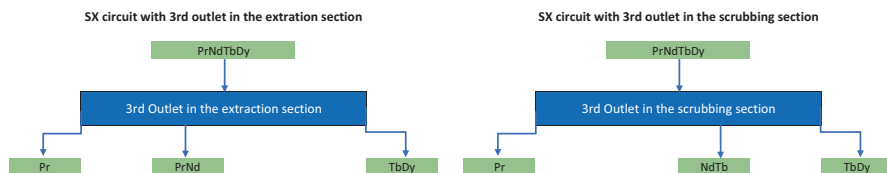
The circulation of the different streams is shown in Fig. 6.2.

### The Multioutlet SX Battery Configuration

In the classical configuration presented in Fig. 6.2, a mixture of four REEs (i.e., Pr, Nd, Tb, Dy) is separated into two mixtures of two REEs (Pr + Nd and Tb + Dy), this is a typical two outlets SX battery. It is also possible to design a SX battery with intermediate withdrawals of the aqueous phase. This type of configuration also called multioutlet configuration is widely used in China. It has an obvious advantage—it limits the number of SX batteries. It has also a significant drawback—it is not possible to get all the outlets pure.



**Fig. 6.2** Stream circulation in an RE SX battery. (\*Effluents and stripping streams are not represented in this figure)



**Fig. 6.3** A three outlet battery with a Nd concentrate withdrawal

An example of such a multioutlet SX battery is presented in Fig. 6.3 for the same feed as the one used in Fig. 6.2. The target is to obtain three products: pure Pr, Nd concentrate, and a TbDy mixture. Depending on its position, the third outlet can be either a concentrate of Nd with Pr if the aqueous withdrawal is in the extraction section, or a concentrate of Nd with Tb if the aqueous withdrawal is in the scrubbing section. It is impossible to obtain from the same circuit production of pure Pr, an outlet of pure Nd, and production of a Tb + Dy mixture without Nd.

### The Hyperlink Configuration

In the typical chloride route widely used in China, the loading section consumes alkali, usually caustic soda and the stripping section consumes acids, usually hydrochloric acid. Consumption of these chemical is by far the main cost of the RE separation process with the chloride route. To limit consumption, Chinese scientists have designed a new type of configuration called Hyperlink [5, 6]. The basic idea of this concept is to use the same loading section for several RE separations or in other words, the feed of one RE separation can be either an aqueous feed (i.e., the classical configuration) or an organic feed coming from the upstream SX separation. In this type of process, the different separations are overlapped and the flows coming from one to the other can be either aqueous or organic. A typical configuration for separation of three REEs is presented in Fig. 6.4.

In this configuration, the solvent is loaded once with an aqueous solution containing only A. The solvent containing B and C coming out of the A/(B)/C separation section is sent to the B/C section of the separation before being stripped. The aqueous phase containing A and B coming out of the A/(B)/C separation section is sent to the A/B separation. This principle can be theoretically reproduced as many times as desired when the target is to separate more than three REEs. In principle, one can design a multielement separation process with only one loading section and one stripping section. However, it is well known that the Chinese government prohibits the export of the RE technologies and the hyperlink process is considered as the most critical one. Under these conditions, it is not surprising that we did not find any Chinese publications presenting a global process flowsheet with a clear circulation of the different aqueous and organic streams for a separation with more than three REEs.

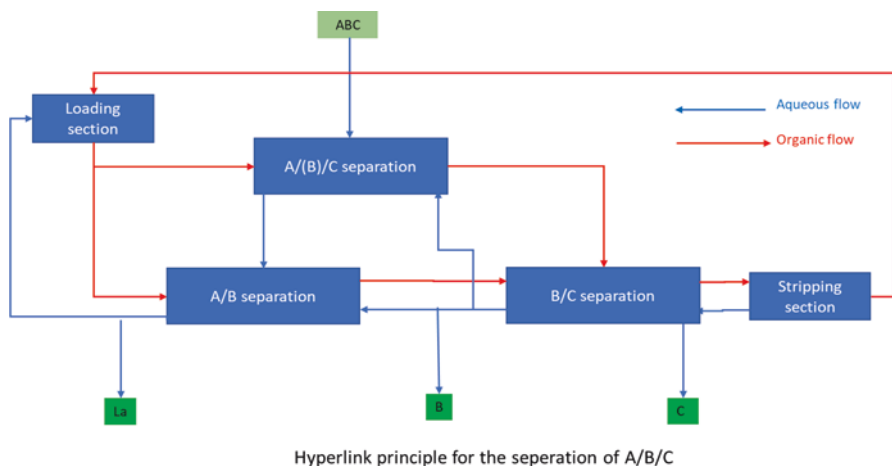


Fig. 6.4 Hyperlink configuration for separation of three elements

The main interest of this process is the savings of both alkaline solution during the loading step and of acid solution during the stripping step. Indeed, in the example shown in Fig. 6.4, instead of having two stripping sections (one for B + C and one for A) as with a classical separation flowchart, there is only one main stripping section for C in the hyperlink configuration. Of course, the acid consumption with the hyperlink is not equivalent to the acid consumption for C stripping only in the classical configuration, it will be much higher, but less than the global consumption in the classical configuration. Chinese scientists claim that the savings could be in the range of 30–50%; however, the model leading to this result is not provided.

On the other hand, the interweaving of the different separations makes their operation more delicate. Any deviation of one of them will automatically be transmitted to the others.

### 6.4.2 The Choice of the Solvent—An Economic and Environmental Decision

How to choose between the various potential extracting molecules and which aqueous/organic couple will be the best in terms of economy and environment? There is no absolute answer to these questions and the final decision depends on the composition of the feed solution, on the finished products targeted and on the local constraints. In the end, the decision will be based on three criteria—OPEX, CAPEX, and environmental footprint. But how does one relate these criteria to the characteristics of the system? Three characteristics must be considered:

- The selectivity of the organic ligand versus REEs.
- The chemistry associated to the organic ligand.
- The loading capacity of the solvent.

These three criteria will be discussed in the sections below considering only the chloride and nitrate media used industrially. In some RE industrial plants, the pregnant liquor solution (PLS) is obtained as a sulfate solution. In this case, the first SX separation can be operated in a sulfate medium, but with the target being to remove the non-RE impurities and at the same time to convert the purified mixed REs into a chloride or a nitrate solution.

## The Selectivity of the Organic Ligand

Selectivity is the first criterion to consider. Without selectivity, RE separation is not possible. Selectivity versus REE of the main molecules used for the RE separation is shown in Fig. 6.5.

Several important points can be highlighted:

- The three phosphorus-based acidic molecules, HDEHP, HEH(EHP), and HBTMPP, are selective all along the lanthanide series with quite similar separation factors and can be used for any REE separation.
- Naphthenic acid, which is a carboxylic acid, is selective only for the light rare earths (LREs), but one may notice that yttrium is located between La and Ce which is specific to this type of molecule and can be used for simplifying the yttrium purification.

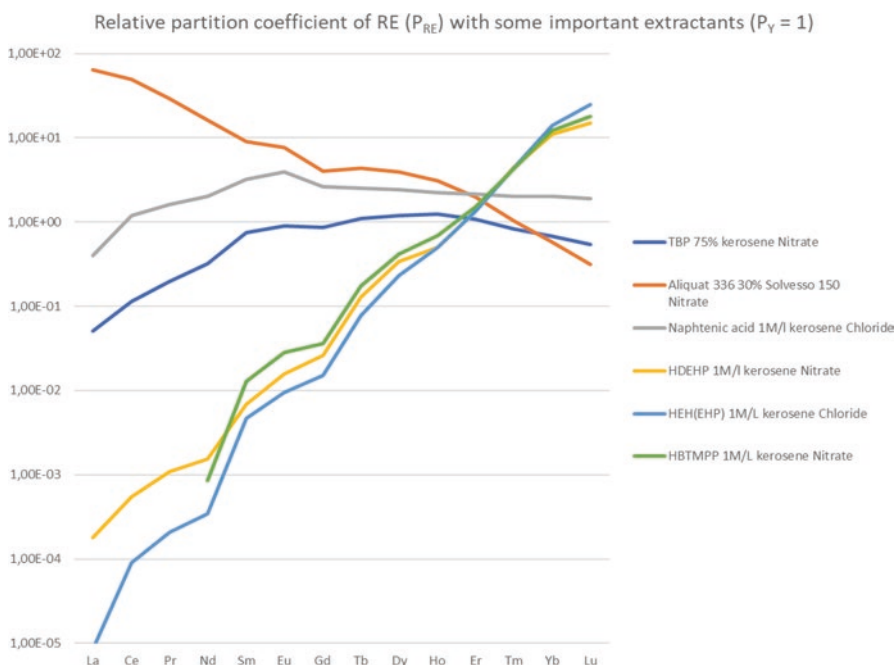


Fig. 6.5 Relative partition coefficients of REE for main industrial solvents ( $P_Y = 1$ )

- In a nitrate medium, the neutral molecule TBP is selective only for the LREs.
- In a nitrate medium, the basic extractant, Aliquat 336, is selective only for some groups of REE and has an inverse selectivity compared to the other extractants.

## The Chemistry of the Organic Ligand

The second important criterion to consider is the chemical nature of the ligand itself. Indeed, as it has been discussed above (Sect. 6.3), the mass transfer driving force between the aqueous and the organic phases will depend on the chemistry used and more specifically on the type of organic molecule used as an extractant.

Neutral molecules (i.e., TBP) or ion pairs (i.e., Aliquat 336) can be used only in a nitrate solution. In that case, the mass transfer driving force is the nitrate concentration in the aqueous phase. There is no need of any chemical addition during solvent extraction, but the aqueous solution must be concentrated during the extraction step (mass transfer from the aqueous phase to the organic phase) and diluted during the stripping phase (mass transfer from the organic phase to the aqueous phase). In other words, solvent extraction with neutral molecules or ion pairs will consume energy during the extraction step and water during the stripping step. No addition of chemicals also means that there is no chemical species to be removed from the system and so no wastewater released.

Cationic molecules (i.e., HDEHP (P204), HEH(EHP) (P507, Ionquest 801 or PC88A), HBTMP (Cyanex 272)) or their combination (Cyanex 572) can be used both in a chloride solution and in a nitrate solution. These molecules can also be used to extract REEs from a sulfate solution, but because of the low solubility of REEs in a sulfate medium and because of the risk of double salt precipitation ( $(\text{Na,RE})(\text{SO}_4)_2$ ), all the industrial processes use a chloride or a nitrate media (Sect. 4.3). The sulfate medium will not be considered here. The driving force of the extraction is the acidity of the aqueous phase. The extraction step (mass transfer from the aqueous phase to the organic phase) needs to have a low acidic aqueous phase and so will consume alkaline solution (caustic soda or ammonia) in the loading section. The stripping step (mass transfer from the organic phase to the aqueous phase) needs to have a high-acidic aqueous phase and so will consume acids (usually hydrochloric or nitric acids) in the stripping section. From Eq. 6.3, the higher the extraction constant, the more the acid consumption. For the three cationic molecules listed above, the acid consumption will increase in the order HBTMP < HEH(EHP) < HDEHP. The addition of these alkaline and acid solutions will generate salts (usually sodium chloride or ammonium nitrate) which need to be removed from the system and in the end will generate salty effluents.

The influence of the solvent extraction chemistry chosen based on the OPEX and environmental footprint is summarized in the Table 6.2.



**Table 6.2** Influence of the SX chemistry on the OPEX and environment

Type of extractant	Typical molecule	Aqueous phase	Chemical consumption	Energy consumption	Wastewater
Acidic	HDEHP, HEH(EHP), HBTMPP	Chloride or nitrate	Alkali and acids The higher the extraction constant the more the acid consumption	Low	Salty effluents
Neutral	TBP	Nitrate only	None	High	None
Ion pairs	Aliquat 336	Nitrate only	None	High	None

**Table 6.3** Maximum loading capacity of REEs in three solvents

Solvent	TBP 75% Kerosene 25%	H(EH)EHP 50% Kerosene 50%	Aliquat 336 30% Solvesso 150 70%
Loading capacity	RE = 0.75 M/l	RE = 0.20 M/l	RE = 0.20 M/l

### The Loading Capacity of the Solvent

The third important criterion is the loading capacity of the solvent. Indeed, as it has been discussed, the solvent is the conveyor of the REEs. In most of the RE separation processes, the solvents are saturated and so the higher the loading capacity, the higher the productivity.

In most cases, the active molecule (the extractant) cannot be used as such because of the high viscosity of these molecules. The extractant is diluted in an organic diluent, which is a mixture of aliphatic and aromatics molecules, from pure aliphatics to pure aromatics, depending on the process. This mixture (extractant + diluent) is the solvent for which the maximum loading capacity must be assessed.

The maximum loading capacity of three typical solvents used in RE separation is presented in Table 6.3.

### 6.4.3 Industrial Processes

In the block diagram presented in Fig. 6.2, the nature of the aqueous solutions is not specified. While REEs can exist in three different types of inorganic solutions (chloride, nitrate, and sulfate), only two of them (i.e., chloride and nitrate) are used industrially for the RE refining process. The sulfate medium has two main drawbacks with respect to its use industrially for refining: the solubility of RE sulfates is low (between 10 g REE per liter for La and 50 g REE per liter for Pr), and in the presence of alkaline ions (typically Na), REs form insoluble double salts (REE,Na)(SO<sub>4</sub>)<sub>2</sub>. Due to these drawbacks, all the RE industrial refining processes use either chloride or nitrate solutions, which is the reason why the processes are identified as

the “chloride route” or the “nitrate route.” The differences between these two routes which are discussed in Sects. 6.3.1 and 6.3.2 address only the chemistry of the process. In both cases, the equipment used industrially is always mixer-settlers. The possibility of using other types of equipment will be discussed in Sect. 6.

### Chloride Route

The chloride route was initially developed by Molycorp in the United States and Rhone-Poulenc in France in the 1960s. Then it was disseminated in China by Chinese scientists from the Baotou Research Industrial Center and the Beijing University, and now it is the most widely used process for RE separation around the world. All the Chinese RE plants as well as Lynas in its Malaysian plant use it.

The initial reason why the Chinese scientists have chosen this route is likely due to the high selectivity of HEH(EHP) which is also called PC88A in the western world or P507 in China. From Fig. 6.5, it is obvious that the organophosphorus acids are the most selective molecules for the REEs and that they can be used for any separation among the lanthanide series. The choice of HEH(EHP) rather than HDEHP is due to the lower acidic consumption of HEH(EHP) during the stripping step. Since this molecule can be used both with a chloride solution and a nitrate solution, the chloride medium has been chosen for cost reasons, as hydrochloric acid is cheaper than nitric acid. Nowadays, HEH(EHP) is the universal molecule chosen by all the RE separators using the chloride route for almost all the RE separations. The only exceptions are the final yttrium purification, which is usually done with a carboxylic acid, either Naphthenic acid or Versatic acid, and sometimes the separation of the heaviest RE, particularly Lu purification, which can be done with HTMPP or a mixture of HTMPP with a phosphonic ester commercialized by Solvay under the name of Cyanex 572. The use of HEH(EHP) for the heaviest RE separation leads to a very high consumption of HCl during the stripping step and Cyanex 572 is a good compromise for lowering the HCl consumption due to the phosphinic part of the formulation and improving the hydrodynamics of the liquid-liquid emulsion due to the phosphonic part of the formulation.

It is not possible to give a universal process design based on the chloride route and the choice of the solvent (couple extracting molecule plus diluent) does not give the final separation configuration. The chemical engineering designer must decide in which order the separation will be done (i.e., Fig. 6.1 showing five possible configurations for the recycling of RE from end-of-life magnets), and how to integrate some multioutlet SX batteries and possibly the hyperlink technology into the overall design. The final design will be an economic decision depending on the feed composition and on the REE to valorize. Each combination of the REE distributions in the mixed feed and the pure REEs to be produced is specific and only a calculation based on a simulation model (Sect. 5) will identify the best configuration for each case.

Because the main drawback of the chloride route is the consumption of chemicals (NaOH and HCl) and the associated salt release (NaCl), the Chinese

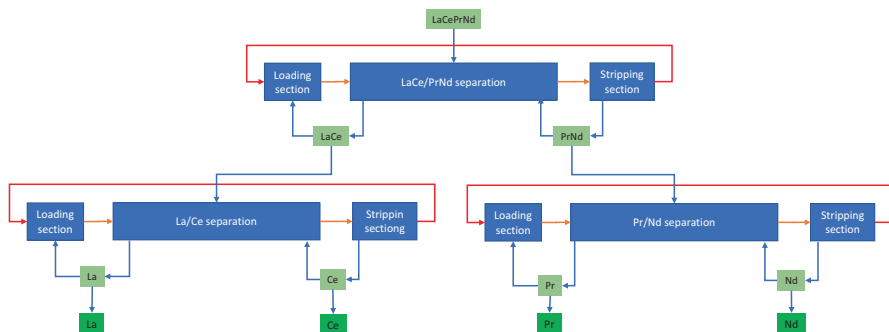
scientists extensively studied how to limit consumption as well as the global number of theoretical stages. These process improvements have been done in two steps: multioutlet configuration and hyperlink process. As it has been already stated, because of the Chinese governmental restriction to RE technology export, the detailed flowsheet of the hyperlink process is not publicly available. However, a tentative hyperlink flowsheet is shown in Fig. 6.6 in comparison with the traditional and multioutlet configurations for the light REE separation.

- In Configuration 1, each SX circuit is independent and the risk of cross-contamination from one to the others is limited.
- In Configuration 2, each circuit is also independent, but the third outlet of the first circuit needs a careful follow-up to avoid any difficulty in the Ce/Pr SX. The main interest of this configuration is the fact that the Ce/Pr separation corresponds to a small SX battery. But it should be noted that the first SX circuit is bigger than the first SX circuit of Configuration 1. The interest in this configuration compared to Configuration 1 must be assessed considering the feed composition and the targeted quality of each individual REE.
- In Configuration 3, all the circuits are interconnected and there is only one loading section with La and one stripping section with Nd. However, with the overlapping of the flows, both aqueous and organic, between the different separations leads to an extremely sensitive process which is difficult to control without a powerful simulation dynamic model. The big interest in this configuration is the potential savings of acid and alkali. Fu-Xiang Cheng [6] claimed that the theoretical savings of HCl and NaOH consumption compared to Configuration 1 are about 50%. These numbers are significant even if no model is available to permit confirmation of these data. Moreover, the fundamental chemistry remains a cationic exchange between the aqueous phase and the acidic molecule HEH(EHP). The consumption of acids and alkali cannot be avoided with this type of process unlike the use of neutral molecules in the nitrate route (Sect. 6.3.2).

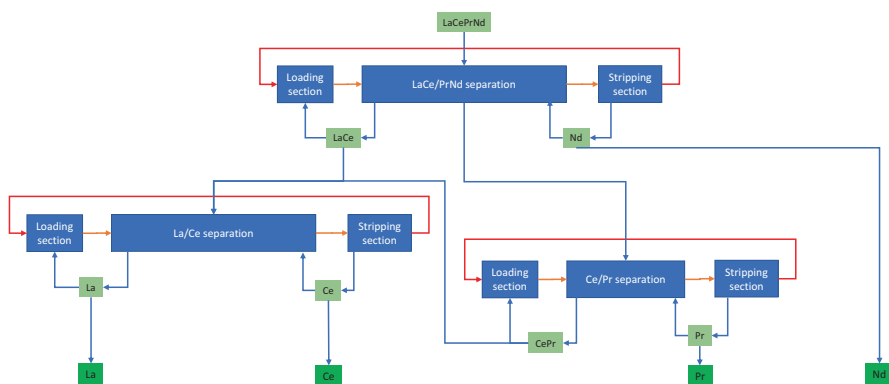
## Nitrate Route

It is paradoxical that at a time when industry everywhere in the world must commit to preserving the environment and developing processes with the lowest environmental footprint, some players in the RE industry are considering the nitrate route as an old process which cannot compete with the chloride route.

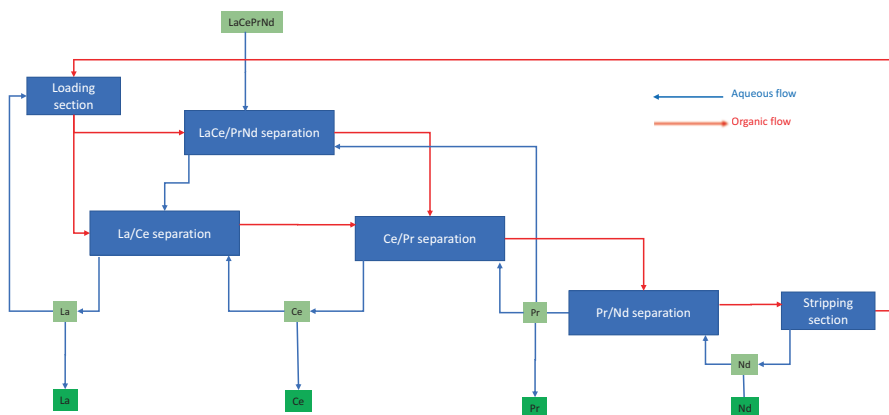
As it has been presented in Sect. 6.3.2, the main drawback of the chloride route is its high consumptions of chemicals (caustic soda and hydrochloric acid) and consequently its huge generation of salty effluents (NaCl). It is not surprising that Chinese scientists have tried to minimize this drawback with the hyperlink concept. But even if the hyperlink process can lower the chemical consumption, by using the same extractant as the classical chloride route it does not change fundamentally the chemical reaction and at the end leads to acids and alkali consumption and salt generation.



Configuration 1: traditional 2 outlets flowsheet



Configuration 2: 3 outlets flowsheet



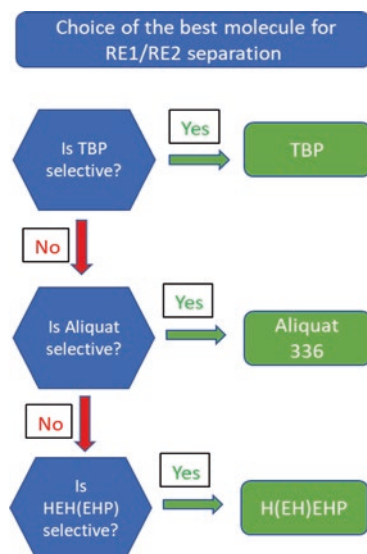
Configuration 3: Hyperlink flowsheet

Fig. 6.6 Block diagrams of La/Ce/Pr/Nd separations with three configurations

In the 1960s, scientists at Rhone-Poulenc in France were aware that the huge consumption of acids and alkali in the chloride route was intrinsic to the chemistry used, and they understood that only a change in terms of organic molecules could modify the chemistry and the consumption of chemicals. The first SX separation using the nitrate route instead of the chloride route was set up in 1968 at the La Rochelle plant in France for Nd/Pr separation. This way of thinking was fundamentally different from the Chinese process that used the hyperlink concept, since it acts not on the implementation of the chemistry (the process), but on the chemistry itself. The target of the nitrate route is the use of a wider range of chemicals and in particular neutral molecules or ion pairs that do not need acid and alkali as the driving force for mass transfer. The driving force for mass transfer of both neutral and ion pairs is the nitrate concentration. In other words, if the cationic molecules lead to the consumption of chemicals, the neutral molecules and ion pairs lead to the consumption of energy necessary to concentrate the aqueous nitrate solutions [7]. When both types of extractants have an appropriate selectivity, the final choice from purely an operational cost point of view is typically the use of neutral molecules or ion pairs.

And so, the target of a process engineer designing a process based on the nitrate route will be to minimize the usage of cationic molecules like HEH(EHP) and use as much as possible either neutral molecules or ion pairs. Between a neutral molecule and an ion pair, the choice will be based on the productivity (i.e., loading capacity). An example of such a choice is presented in Fig. 6.7. The engineer should choose among the three molecules—TBP, Aliquat 336, and HEH(EHP), and select the best material based on cost for the separation of two REEs (RE1 and RE2). Their decision will be based first on the possible use of these molecules for RE1/RE2 separation (Fig. 6.5) and then on the loading capacity (Table 6.3). This is summarized in the flowchart shown in Fig. 6.7.

**Fig. 6.7** Flowchart for the choice of molecule for separation between two REEs by the nitrate route



Using this flowchart and Fig. 6.5, a process engineer who should design an REE separation process with the nitrate route will choose:

- TBP for the LRE separations (La/Ce/Pr/Nd/other REE).
- Aliquat 336 for the some MRE and HRE separations.
- HEH(EHP) for all the others.

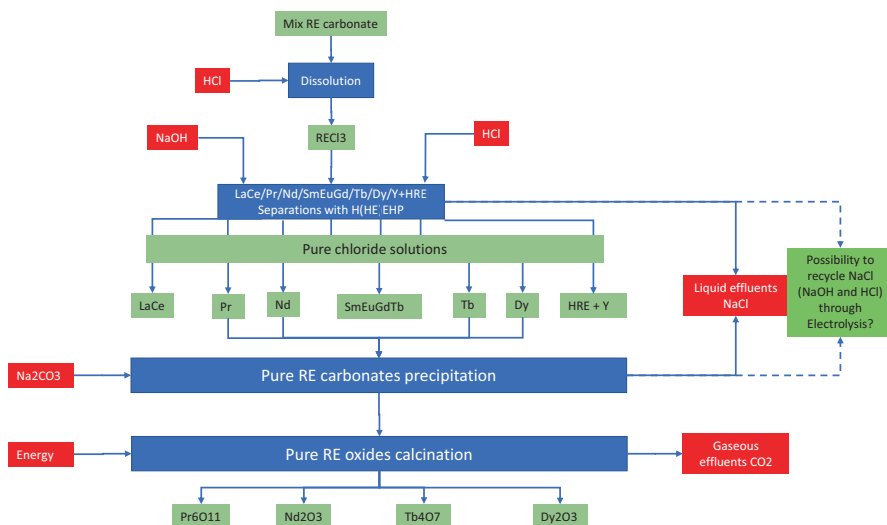
### Choosing Between Chloride and Nitrate Routes—An Economic and Environmental Decision

The choice between using the chloride and nitrate routes cannot be solely limited to an economic assessment of the separation unit but must also address the overall process from ore leaching/extraction to the separated individual and blended oxide production, and an environmental assessment.

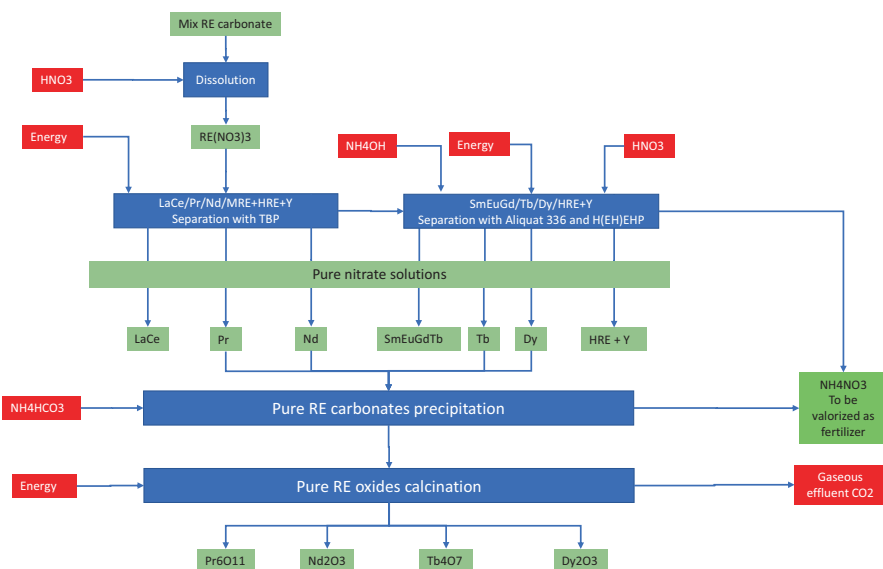
An example of such an overall process comparison is presented in Figs. 6.8 and 6.9. These figures show typical block diagrams for production of pure RE oxides for magnet applications (Pr oxide, Nd oxide, Tb oxide, and Dy oxide) from a mixed RE carbonate obtained after ore cracking.

Two important points must be highlighted:

- *Chemical consumption:* Both routes will consume chemicals for REE separation, but while the chloride route will need NaOH and HCl for all the separations, the nitrate route will use  $\text{NH}_4\text{OH}$  and  $\text{HNO}_3$  only for some MRE and HRE separations. Because very often the LRE portion in the mix RE concentrate to be separated is



**Fig. 6.8** Block diagram of pure Pr, Nd, Tb, and Dy oxide production from a mix RE carbonate with the chloride route



**Fig. 6.9** Block diagram of pure Pr, Nd, Tb, and Dy oxide production from a mix RE carbonate with the nitrate route

the main portion, this difference leads to a lower OPEX for the nitrate route. So, the higher the LRE portion, the more interesting the nitrate route becomes.

- *Liquid effluents:* The chloride route will generate a large quantity of  $\text{NaCl}$  solution which in most cases is released into the environment (case of all the Chinese plants as well as the Lynas plant in Malaysia). It is theoretically possible to recycle this effluent by producing  $\text{HCl}$  and  $\text{NaOH}$  from it. This was included in the initial design of the new Molycorp plant built in California in 2012, but the quality of this type of solution to be processed through electrolysis is very stringent and there is no evidence that this process really worked during the short time that the plant was operated at Mountain Pass.

The nitrate route will generate a  $\text{NH}_4\text{NO}_3$  solution and even if the quantity of the flow is much lower than the quantity of the  $\text{NaCl}$  effluent produced from the chloride route, this flow cannot be released into the environment and must be valorized as a by-product, as its quality is fitting for the fertilizer market. Several studies done in the past by several teams around the world have indicated a genuine interest in regenerating ammonia and nitric acid from ammonium nitrate by means of electro-membrane processing.

## 6.5 The Simulation of Rare Earth Separations

### 6.5.1 General Consideration

Only companies mastering the modeling of the REE separations can design and drive an REE separation unit. The mathematical models used for this type of simulation must be able to simulate the countercurrent mass transfer between an aqueous phase and an organic phase of all the 15 REEs (lanthanides plus yttrium) in more than 100 theoretical stages. There is no commercial software available, and the complexity of the mathematical model means that very few companies will have the capability to model an RE separation unit. There are two types of models: static models and dynamic models.

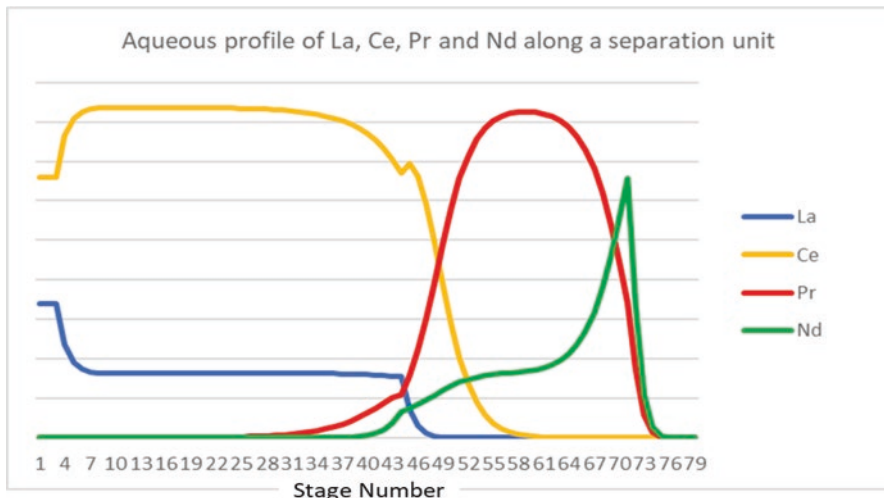
### 6.5.2 Static Simulation

A static simulation will give for any input conditions (number of theoretical stages for each section, position, flow rate, composition, and acidity of each inlet solution) the characteristics (concentrations and compositions) of each phase (organic and aqueous) at steady state. It will also give the qualities of the aqueous outlets which should be compliant with the initial target in terms of product quality. This is the base of the engineering design of a separation unit.

Another important output of the static simulation is the prediction of the RE inventory loading inside the separation equipment. Indeed, it is not often highlighted, but the quantity of REs stored inside the equipment (mixer-settlers) is huge and must be considered as a part of the CAPEX. An example of the output of a static simulation is presented in Fig. 6.10. The simulation shows that the Pr quantity stored inside the mixer-settlers is huge and its proportion versus other REs is much higher than in the feedstock.

Another purpose of a static simulation is to define the control parameters of separation. Indeed, if the target of separation represented in Fig. 6.10 is to get less than 10 ppm of Pr in LaCe and less than 10 ppm of Ce in PrNd, the operators need to have control parameters inside the separation to be able to react in advance before the outlets become off-specification but do have a concentration that is high enough to be easily analyzed. From Fig. 6.10, it can be seen that the Ce concentration and the Pr concentration have a sharp evolution in the stages between 35 and 60. The philosophy of control will be to follow Ce and Pr concentrations in one stage among these and to react accordingly to any deviation.





**Fig. 6.10** Aqueous profile of RE during the separation of LaCe/PrNd with TBP. (Figure from Carester in house software)

### 6.5.3 Dynamic Simulation

A static model as presented above does not consider the “life” of the separation. It gives the result of a separation unit if all the parameters (concentrations, compositions, flowrates, etc.) are perfectly stable. In real life, things are always moving, the composition of the feedstock is evolving, the flowmeters are not perfectly stable and the quality of different inlets also may vary. When one of these parameters is changing, the quality of the separation is modified and an engineer using a static model will try to recover the initial situation by adapting the process parameters to the new situation, but they will not be able to predict the time needed to get the final steady state or to choose the shortest way for reaching this new steady state.

It is the target of the dynamic model in combination with online analysis to keep the separations stable whatever the variations (composition, flow rates, etc.). While a static model gives only the final steady state calculated from fixed parameters, a dynamic model can predict the evolution over time for each characteristic and in each stage when any type of perturbation occurs. This is an immensely powerful tool for driving a separation unit, as well as for training operators, technicians, and engineers who can see their unit living like an airplane pilot sees his plane with a flight simulator.

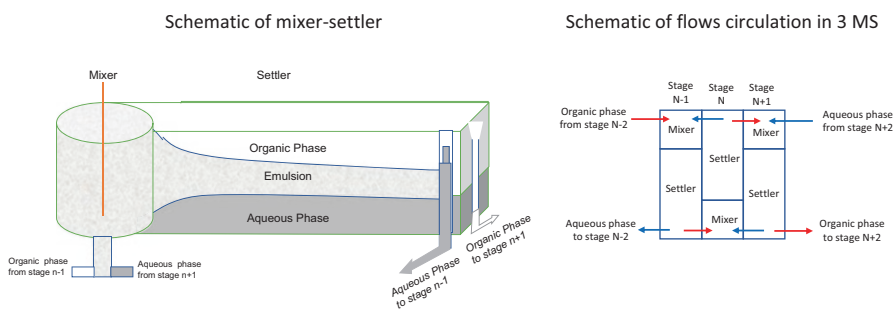
In November 2020, Carester announced a partnership with the French Commissariat for Nuclear Energy (CEA), to develop dynamic software for simulation of RE separations. It is essential in the nuclear industry, especially in the reprocessing of used fuels to address the various radioactive element concentrations over time. It was the ambition of the partnership between Carester and CEA to provide the RE industry with the most advanced tool for designing and operating an RE separation unit. It is now a reality.

## 6.6 Solvent Extraction Equipment

### 6.6.1 Mixer-Settlers

Currently all the industrial solvent extraction units dedicated to RE separation use batteries (or cascades) of mixer-settlers (MS) as countercurrent equipment [8].

The principle of the aqueous and organic flow circulation is shown in Fig. 6.11. Figure 6.12 shows a photo of such an impressive battery of mixer-settlers for industrial applications.



**Fig. 6.11** Simplified schematic of mixer-settler and of flows circulation in a series of three adjacent mixer-settlers



**Fig. 6.12** Rare earth solvent extraction battery in Solvay La Rochelle plant in France. (Photo from SoS RARE - Copyright Solvay)

This technology has several key industrial advantages:

- It can be applied whatever the chemical system (chloride medium, nitrate medium, neutral, basic or acidic extractants).
- With a proper design, each mixer-settler is close to one theoretical stage and the process design from the theoretical calculation is easy.
- It is a very mature technology, and the scale-up criteria are well known.
- During shutdown of the unit, the RE profiles of both aqueous and organic phases (Fig. 6.10) are maintained and there is no loss of time and materials after restart.

This technology has two important drawbacks:

- The large number of theoretical stages necessary for RE separation means a large number of mixer-settlers leading to high CAPEX.
- The solvents and RE inventories are huge, especially because of the size of the settlers and the corresponding cost is an important part of the CAPEX.

### ***6.6.2 Can Columns Be Used for RE Separation?***

In other fields of the industry, liquid-liquid extraction columns are widely used instead of mixer-settlers. The main advantage of columns is precisely to overcome the drawbacks of MS indicated above. Several types of extraction columns exist and have been developed over the years (i.e., pulsed packed columns, pulsed perforated-plate columns, rotating disk columns, Kühni column, etc.) [8], some of them having high efficiency in terms of throughput and mass transfer, but up to now none of these have been used industrially for REE separation. Understanding why the columns have not been used industrially for RE extraction is key to predicting the possibility of seeing this technology replace mixer-settlers in the future.

The extremely specific characteristic of REE separation compared to any other separation done by solvent extraction is the large number of theoretical stages needed for REE separation. A classical separation between two groups of REEs needs between 60 and 80 theoretical stages for one separation, and even if we consider the possibility of having one single column for each section (loading, extraction, scrubbing, and stripping), it is usual to have up to 40–50 theoretical stages for one section. Suppose for example that an engineer wants to design columns for doing the LaCe/PrNd separation as it is theoretically represented in Fig. 6.10 with one column for each section, they will need to design four columns with:

- Two theoretical stages for the loading section column.
- 42 theoretical stages for the extraction section column
- 28 theoretical stages for the scrubbing section column
- Eight theoretical stages for the stripping section column.

When speaking about mixer-settlers, each MS represents a theoretical stage, but when speaking about columns, the concept used by engineers to design a separation

system is the Height Equivalent to Theoretical Stage (HETS). A column of 10 m in height having an average HETS of 1 m for a specific mass transfer system, will be equivalent to ten theoretical stages. It is not the topic of this chapter to discuss the efficiency of solvent extraction columns and the theory behind it, but one should note that with the number of theoretical stages necessary for any REE separation, a column chosen for this target must have a HETS as low as possible and in any case the average HETS all along a column must be much lower than 1 m, preferably lower than 50 cm.

This is not the only constraint that a column dedicated to REE separation must respect. During the operation, each part of the column representing a theoretical stage has its own REE composition in both the aqueous and organic phases. Typically looking at Fig. 6.10, one can see that the aqueous Pr content in the part of the column representing stage 45 is about 10%, about 80% in the part representing stage 60, and about 40% in the part representing stage 70. But what will happen when the column is stopped? It is essential that this concentration profile is kept during any scheduled or unexpected shutdown. If the internal design of the column allows both phases to settle when the column is not running, the concentration profile along the column will be lost and it will take time to recover it after start-up and during this time, production will be off-spec and must be recycled.

Having these two constraints in mind (low HETS and capability to maintain the RE profile inside the column when it is not operating), one can look at the proposals for RE separation technologies based on columns.

One of the column-based technologies which is currently trying to overcome the drawbacks of the mixer-settlers for RE separation is the RapidSX™ technology proposed by UCORE (<https://ucore.com/rapidsx/>) [9]. *This technology has been sold to Ucore.* The company argues that the technology “reduces the number of SX separation stages by over 90%, leading to a significant reduction in capital expenditures [and also] leads to dramatic reductions in operating costs and time to process completion, when compared to conventional SX.”

There are little technical data publicly available to support this statement and to understand the principle of this technology. Making an objective assessment of the technology is therefore not realistic. However, from the presentations done by the company we can highlight some key points:

- The chemical process used is the classical chloride route with HEH(EHP).
- Solvent extraction columns representing several theoretical stages are used as countercurrent contactors. When the company states that “the number of SX separation stages are reduced by over 90%,” one should understand that although the number of equipment stages are reduced by 90% (number of columns compared to number of mixer-settlers), the number of theoretical stages are independent of the technology.
- It is likely that one essential point of the design is the ability to control the drop size of the emulsion aiming to get a low HETS.
- From photos presented at conferences, it is oblivious that there are no internal devices (i.e., packing, agitators or plates) visible inside the columns. It is likely

that the emulsion is obtained through an external effect which can be a field (magnetic or electrical).

From this one can infer that:

- The consumption of both acid and alkali is not modified compared to all plants using this chemical process and the statement about “the dramatic reductions in operating costs” is not understandable since consumption of both acid and alkali is by far the main portion of the OPEX.
- The technology clearly addresses the capital expenditure issue by replacing the mixer-settlers by columns.
- One of the constraints for using columns, low HETS, is probably addressed by using a special way to create the emulsion and controlling the drop size of the dispersed phase, but there are no data allowing us to assess the average HETS obtained by this technology.
- There is no evidence that the second constraint—capability to keep the RE profile inside the column when it is not operating, is achieved and from the pictures of the pilot plant presented by UCORE showing that the inside the column is empty, it is likely that both phases are decanted when the operation is stopped.

Once again, there are not enough public data available to give a definitive opinion on this technology, but the question of the capability to maintain the steady state profile during shutdown is essential and only an answer to this question can allow us to objectively assess RapidSX™ for RE separation.

Another column type technology developed by the Japan Atomic Energy Agency (JAEA) is the Emulsion Flow Extractor [10]. The main advantage claimed by JAEA with their Emulsion Flow Extractor is the ability to control the fine droplet sizes of the dispersed phase. But just as in the case of RapidSX™, the articles published by JAEA do not provide data allowing us to assess the HETS achieved, and the real efficiency of the Emulsion Flow extractor in terms of mass transfer cannot be adequately assessed. In addition, the picture of the column clearly shows that the column is empty. With this type of column, there is no possibility of keeping the RE profile along the column when it is not operating. Here again, one of the criteria aiming to validate the technology for RE separation—the capability to maintain the steady state profile during the shutdown, is not achieved.

## 6.7 Solid Phase Extraction—The New Holy Grail?

In the recent years, several teams in the world have worked on the possibility to use Solid Phase Extraction (SPE) for RE separation [11, 12]. SPE is not a new technology as such and is already used for some expensive products, but its application to RE separation, up to now, has been limited to analytical purposes.

The focus of this section is not to give a full picture of the state of the art, drawbacks, and interests of SPE applied to RE separation. Indeed, SPE is a complex process and a presentation of its status in the field of RE separation would merit a

full chapter. This section will therefore be limited to a few words on its principle and its potential interest for RE separation.

In this type of technology, a ligand is grafted or impregnated onto the surface of a high surface area solid, usually silica. This ligand must be able to create a selective bonding with the species targeted. The process works like a liquid chromatography with an eluent allowing the various species to move at different speeds along a column, and so allowing the separation between the species.

Two companies—one American, IBC Advanced Technology and one Norwegian, REEtec, have announced that they have succeeded in production of pure RE at pilot-scale and that they have the capability to design an industrial unit for RE separation based on their technology.

IBC calls its technology Molecular Recognition Technology (MRT) [13]. They have a wide range of Solid Phases, called Superlig, with different macrocycles grafted onto silica. Unfortunately, it is not possible to know which ligand is used for RE separation and no data allowing one to assess this technology in terms of CAPEX or OPEX for RE separation has been published.

REEtec claims that they have succeeded to separate RE with their technology at pilot-scale and that they have completed (in 2020) an industrial-scale demo plant [14]. REEtec, like IBC, does not provide any data allowing one to assess their technology. It is the assumption of the author of this chapter that they use a SPE with a phosphorous-based ligand impregnated onto the surface of silica, but there is no certitude about this. And even if this assumption is correct, it is by far not sufficient to assess their technology and compare it with SX.

The potential interest of SPE for RE separation is real. Indeed, this type of technology could potentially overcome some drawbacks of SX especially the ones linked to the mixer-settlers technology (i.e., high CAPEX and high RE inventory). But the companies promoting SPE do not give any data allowing one to compare their technology with SX and when they give qualitative information about the drawbacks of SX that they are able to overcome (high chemicals consumption, high liquid effluents, etc.), they clearly refer to the SX process based on cationic extractants and not to the most efficient SX process in terms of chemicals consumption and liquid effluents release, the nitrate route using neutral and anionic extractants. In other words, this information is more commercial in nature versus scientific data to help industrial companies choose the best technology.

## 6.8 Conclusions

All current industrial RE separations in the world are using solvent extraction, but this solvent extraction process is a specific one whose development is linked to the history of the RE industry.

After a first period until the late 1980s when the Europeans and Americans were dominating the technology, some Chinese research institutes started to disseminate everywhere in China a specific process (so called chloride route) that had been

initially developed in the western world. At the same time, the western industry as well as the academic community outside of China decided to drastically reduce work on RE separations. This decision led to a dramatic situation where all research and development on RE separation processes has been concentrated in China and more specifically has been focused on the chloride route. And when during the RE crisis in 2010, the western world discovered its dependency on the Chinese RE supply and decided to promote a non-Chinese RE supply chain, it appeared that the only available RE separation technology was the “Chinese” one and all newcomers struggled to obtain access to this technology.

The chloride route is based on a specific molecule, Ethyl2hexyl,ethyl2hexyl phosphonic acid (H(EH)EHP, also called P507 in China or PC88A outside of China, which has the specificity to be selective all along the RE series. But this interesting characteristic must be evaluated in the light of less positive characteristics. This molecule is an acid that requires large amounts of acid and base for its operation, thereby generating large amounts of saline effluent. There is a possibility to reduce dramatically the acid and base consumption by using other molecules, namely neutral molecules, and basic molecules, some of them being suitable for RE separation in nitrate solutions. The capability to design an RE separation process using much less chemicals and generating very few or even no waste waters is essential if the RE industry wants to change its image in terms of ecological footprint. This is possible by keeping a very mature process—solvent extraction, but thinking outside of the Chinese box, and considering that depending on the local specificities and constraints, one can use molecules other than the classical P507. It should be noted that most of the life cycle assessment (LCA) studies highlight the importance of the separation step in the global impact of the RE industry and consequently suggest replacing SX by another process. But there is an industrial process already available and able to lower the environmental footprint of the quasi-universal Chinese SX process, it is the SX nitrate route using other molecules than P507.

However, and whatever chemistry is used, solvent extraction technology with mixer-settlers leads to high CAPEX and RE inventory in the system. The capability to design a process using SX but with a technology other than mixer-settlers is likely an important potential improvement. This field of technological development is active, but as far as one can understand the current proposals, there are still some criteria that are essential when addressing industrial RE separation that are not achieved, particularly the capacity to keep the RE profile during shutdown of a unit.

It is likely that in the future, SX based on mixer-settlers will remain the main, if not the only technology used for industrial RE separation. However due to the growing attention to the environmental impact of the RE industry, the classical chloride route as developed by China will not remain the only option, and potentially the nitrate route will experience a new lease on life.

Does this mean that solvent extraction is unsurpassable and that any attempt to use an alternative technology is doomed to failure? No, and it is essential to pay particular attention to the development of Solid Phase Extraction dedicated to RE separation. But the assessment of these new technologies must be made by comparing them with the most efficient solvent extraction processes and not with a particular process even if it is still the most widely used.

## References

1. J. Zhang, B. Zhao, B. Schreiner, *Separation Hydrometallurgy of Rare Earth Elements* (Springer, 2016)
2. J. Rydberg, M. Cox, C. Musikas, G.R. Chopin, *Solvent Extraction Principles and Practice*, 2nd, Revised and Expanded edn. (CRC Press, Boca Raton, 2007)
3. A. Rollat, *Rare Earths, Science, Technology, Production and Use, Chapter 5* (Elsevier, Amsterdam, 2015)
4. A. Rout, K. Binnemans, Liquid–liquid extraction of europium (III) and other trivalent rare earth ions using a non-fluorinated functionalized ionic liquid. *Dalton Trans.* **43**, 1862–1872 (2013)
5. C. Liao, S. Wu, F. Cheng, S. Wang, Y. Liu, B. Zhang, C. Yan, Clean separation technologies of rare earth resources in China. *J. Rare Earths* **31**(4), 331 (2013)
6. C. Liao, F. Cheng, Green separation of RE resources in China, in *10th International Conference on f Elements*, (Lausanne, September 2018)
7. C. Berger, A. Rollat, A. Leveque, Rare earths: How to optimize the process design? in *Proceeding of the 59th Conference of Metallurgists*, (Toronto, August 2020)
8. T.C. Lo, M.H.I. Baird, C. Hanson, *Handbook of Solvent Extraction* (Wiley, New York, 1983)
9. Hexagon Resources, Disrupting the Rare Earths Supply Chain, January 2020 [PowerPoint Presentation \(hexagonresources.com\)](#)
10. N. Yanase, H. Nagawana, T. Nagano, J. Noro, New apparatus for liquid–liquid extraction, “emulsion flow” extractor. *Anal. Sci.* **27**, p171 (2011)
11. M. Ramzan, D. Kifle, G. Wibetoe, Comparative study of stationary phases impregnated with acidic organophosphorus extractants for HPLC separation of rare earth elements. *Sep. Sci. Technol.* **51**(3), 494–501 (2016)
12. M. Max-Hansen, H.-K. Knutson, C. Jönsson, M. Degerman, B. Nilsson, Modeling preparative chromatographic separation of heavy rare earth elements and optimization of thulium purification. *Ad. Mater. Phys. Chem.* **5**, 151–160 (2015)
13. S.R. Izatt, R.L. Bruening, K.E. Krakowiak, R.M. Izatt, Molecular recognition technology: Green chemistry separation and recovery of individual rare earth elements from primary and secondary sources, in *International Conference on Science, Technology and Applications of Rare Earths (ICSTAR-2018)*, (Tirupati, September 2018)
14. <https://www.reetech.no> (April 2022)



# Chapter 7

## Continuous Ion Chromatography



Richard Shaw and David Dreisinger

### 7.1 Introduction

In 1947, G. E. Boyd and his coworkers at the Oak Ridge National Laboratory and F. H. Spedding and his coworkers at the Ames Laboratory simultaneously published data demonstrating the separation of rare earth elements (REEs) using an ion exchange (IX) process [1, 2]. Spedding, Powell, and their coworkers further refined these IX separation process at the Ames Laboratory and began to prepare large quantities of individual rare earths that were 99.99% pure [3, 4].

The innovative processes developed at Ames resulted in the production of the purest rare earth metals in the world and at the same time led to significant reduction in the prices of these metals, expanding their economic applicability. Ion exchange was historically a batch process and its application to a process separating chemically similar REEs made it a very complex system which was capital intensive and difficult to control.

The development and wide-scale adoption of solvent extraction (SX) in hydro-metallurgy in the 1960s led to the displacement of IX technology as the main methodology for the separation of the REEs in large quantities. Solvent extraction systems were able to be operated on a continuous basis overcoming the batch limitations of IX. Ion exchange is still utilized for the production of small quantities of very high-purity rare earths (i.e., in excess of five-9's, 99.999%, purity) but SX has become the dominant separation technique for the production of the majority of the world's rare earths [6].

---

R. Shaw (✉)  
Fenix Hydromet, Benalla, VIC, Australia  
e-mail: [rshaw@fenixhydromet.com](mailto:rshaw@fenixhydromet.com)

D. Dreisinger  
University British Columbia, Vancouver, Canada

The polymer IX resins used in the 1950s were inferior to the modern generation of solid phase IX and chromatographic materials available today. To achieve the required rare earth separations, large numbers of columns in series were required and while the IX approach produced highly purified REEs, the technique could not compete with the mass transfer capabilities of SX.

Solvent extraction is not without its limitations. Commercial plants require a large number of mixer-settler stages to affect the separations which result in large inventories of organic extractants and flammable diluents as well as large, valuable product inventories. The Rhone Poulenc REE SX plant in France has some 1800 mixer settlers, while the Lynas Advanced Material Plant (LAMP) facility in Malaysia has over 700 mixer settlers [5, 7].

Advances in IX materials and techniques saw the introduction of pressurized IX columns using smaller particle size adsorbents [8, 9]. A number of different approaches were implemented to enable IX to be operated on a continuous or near continuous basis but many of these systems added additional complexities or involved resin transfer between stages. The potential advantages of continuous IX were recognized early on but the systems that were designed did not represent gains that could yet compete with SX techniques [10].

In the 1970s and early 1980s, a number of approaches were made to improve on IX separation of rare earths using techniques such as continuous separation by pressurized annular chromatography [11], rotating annular chromatography for continuous metals separation [12], continuous displacement chromatography [13], continuous IX using powdered resins and cross-flow filtration [14], and continuous annular sorption [15].

The introduction in the early 1980s of the first fully continuous ion exchange (CIX) system based upon a single multiport valve and subsequent design enhancements [16] led to a broader adoption of IX in a wide range of industries particularly in the food and pharmaceutical industries. This technological advancement provided the impetus for CIX in hydrometallurgical applications and the reevaluation of IX as a competitive technique to SX for the separation and production of REEs.

## **7.2 Continuous Ion Exchange (CIX)/Continuous Countercurrent Ion Exchange (CCIX)**

The early IX systems utilized multiple fixed-bed IX columns that were connected in series. For the early pilot plant work conducted in support of the Manhattan project, 24 columns each 103 mm in diameter and just over 3 m long (Fig. 7.1) were operated in series to create an effective column length of 72 m [4]. Industrial IX REE separation plants were constructed but required large numbers of tall columns operated in series to achieve the separations (Fig. 7.2) [17].

The development of modern CIX systems coupled with higher performing smaller particle size, monosphere, resin beads enabled an increase in separation performance with a greater simplicity of design and operation [18]. Early systems



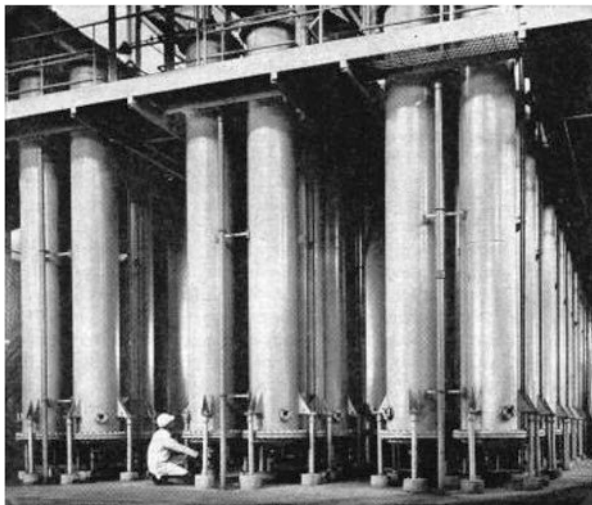
**Fig. 7.1** Ion exchange columns used to separate the rare earths from one another. Individual rare earths are collected in the large carboys as they are removed from the columns. The jars in front of the chemist contain the oxides of the individual rare earth elements [3]

utilized a multiport valve and around this was a rotating frame on which multiple IX columns were installed. This approach was referred to as a “carousel” system (Fig. 7.3).

A number of improvements and modifications have been made in the design of CIX/continuous ion chromatography (CIC) systems whereby the columns are fixed and the valve rotates. These multiport rotating valves simplify the cost while reducing the system footprint and complexity. At the same time, this approach adds a huge amount of flexibility with regard to rinse and recycle capabilities without requiring huge numbers of valves, piping, and control logic.

Valves and columns can be located and configured in a number of ways to suit a specific installation or processing need. Examples of companies offering multiport valve systems are provided in Table 7.1 and Figs. 7.4, 7.5 and 7.6. The successful economic application of CIX/CIC to a number of high-value metal separations such as nickel/cobalt (Ni/Co), scandium (Sc), germanium (Ge), molybdenum (Mo), and gallium (Ga) has demonstrated the effectiveness of the technique in modern hydro-metallurgical circuits [23].

**Fig. 7.2** Ion exchange columns for the separation of lanthanides at Michigan Chemical Corporation, St. Louis, Michigan [17]

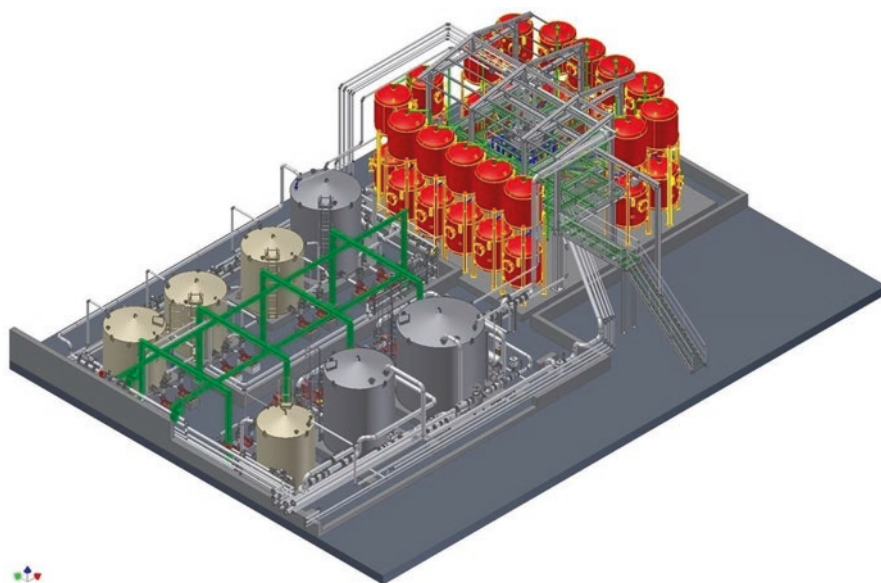


**Fig. 7.3** CIX “carousel” type system installed at a copper mine in 1996 [19]

An example of a modern CCIX system designed by PuriTech and marketed as the ION-IX system uses a single, multiport, distribution valve which enables continuous, countercurrent IX. The valve distributes the different flows to several resin cells in series or parallel and determines whether they are in an adsorption, regeneration, recycle or rinsing phase.

**Table 7.1** Multiport valve systems for CIX/CIC systems [20–22]

Company	Location	Brand name
PuriTech	Belgium	ION-IX™
Calgon carbon	USA	ISEP®/CSEP®
Ionex Separations Inc.	USA	IXSep



**Fig. 7.4** CIX industrial-scale plant design for metals separation. (Reproduced with permission PuriTech [23])

The columns are stationary around a central multiport valve and the process disk within the valve rotates around a central axis and distributes the different flow streams to the columns containing the IX resin. During a full rotation of the valve process disk, each column is subjected to an entire sorption cycle.

Adsorption and desorption imply mass transfer between a liquid and a solid phase. In IX, both adsorption and desorption occur together. Packed column adsorption is a dynamic process in which characteristic mass transfer profiles are established within the adsorbent bed.

Figure 7.7 shows the basic concept of a configuration for a CCIX system that separated uranium (U), thorium (Th), and zirconium (Zr) from REEs. Exhausted beds move out of the cascade at one end while new regenerated beds come into the cascade at the other end.



**Fig. 7.5** CIX industrial-scale plant installation for metals purification. (Reproduced with permission PuriTech [23])

### **7.2.1** *Valve Details*

The main process flow stream enters the valve from above the unit and leaves from an outlet on its underside (Fig. 7.8). Once inside, distribution channels divide the process stream and make the connection to the valve's external nozzles, which feed the columns that are filled with IX resin. The treated fluid collects in a lower channel and leaves the valve via the main outlet nozzle.

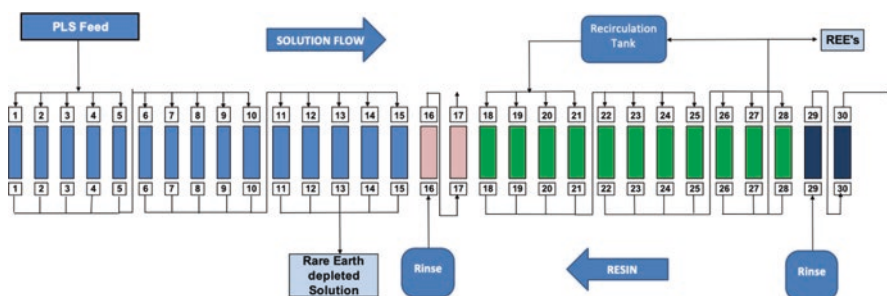
As shown in Fig. 7.8, other external nozzles convey rinse water and regeneration fluid into the valve, and effluent away from the system. Internal channels are separated from each other by two O-rings.

## **7.3** **Ion Exchange and Ion Chromatography**

Ion exchange is typically being employed as a preconcentration or impurity removal technique, and in the case of REE separation, ion chromatography is used in conjunction with complexing agents to separate groups or individual REEs.



**Fig. 7.6** CIX system alternative configuration over multiple levels. Two valves each controlling 30 columns. (Reproduced with permission PuriTech [23])



**Fig. 7.7** Schematic for separation of REEs from U, Th, Zr in a CIX system. (Reproduced with permission USA Rare Earth (unpublished information))

Helferich discusses the differences between chromatography for REEs as compared with conventional chromatography [24]. Typically, chromatographic separation relies on a sorption and a desorption step whereby the mixed product feed stream is reversibly sorbed onto the stationary phase or solid adsorbent, which then can be eluted with a solvent.

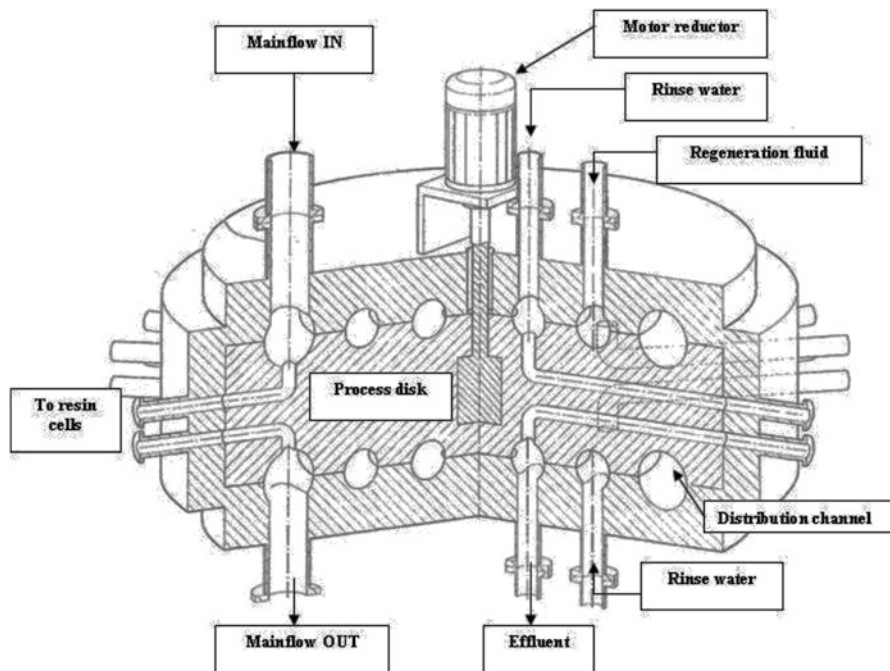


Fig. 7.8 Valve design of PuriTech's ION-IX systems. (Reproduced with permission PuriTech [23])

There is a very large body of work on the separation of REEs using IX and ion chromatography. Much of the chromatographic work has been developed to support the analysis of mixtures of REEs present in different samples as an analytical tool. These separation techniques are useful and informative but cannot be directly transferred to large-scale separation of REEs on a bulk industrial scale [25, 26]. The separation of milligram (mg) and microgram ( $\mu\text{g}$ ) quantities of REEs can be very effectively achieved using elution or extractive chromatography whereas bulk separation of REEs typically relies upon displacement chromatography as the most economical approach.

## 7.4 Chromatographic Techniques

Helferrich [25] and Chen et al [26] provide in depth description of the main chromatographic techniques that have been applied or studied with respect to REEs. These include:

1. Displacement Chromatography
2. Elution Chromatography
3. Gradient Elution Chromatography



4. Frontal Chromatography
5. Extraction Chromatography
6. Partition Chromatography
7. Ligand Exchange

Displacement and Ligand Exchange are the best suited techniques for bulk separation of REEs as they maximize the utilization and productivity of the resin. Elution and gradient elution techniques are commonly applied to analytical methods for quantitative analysis and typically only utilize a small proportion of the adsorbent capacity but can affect excellent, high-purity separations of the individual REEs.

Displacement chromatography utilizes a large percentage of the available binding sites within the adsorbent resin, where the loaded REEs are selectively displaced through the use of a complexing agent. The introduction of the complexing agent causes the REEs to separate into bands which elute from the column as they are displaced by the next band of REEs moving through the column. This is the fundamental approach developed and used by the Ames Laboratory and has been applied as a batch process [27].

The introduction of Continuous Ion Chromatography (CIC) enables the capability to switch from batch processing to continuous processing techniques including recycling of complexing agents to deliver high-efficiency, low-cost, separation. Information on these techniques can primarily be found in the patent literature [16, 28–34].

Variations on these approaches have also been studied, published, and patented such as the work by Purdue University on what they term Ligand-Assisted Displacement Chromatography which enhances approaches to Speddings' original separation strategies from the Ames Laboratory [35, 36].

## 7.5 Ion Exchangers and Adsorbents

A wide range of materials have been considered for the processing and separation of REEs [26, 37, 38]. At an early stage in the separation scheme, the rejection of impurities or recovery of other valuable leach components has been investigated using anion exchangers. This includes the removal of naturally occurring radioactive materials such as U and Th [39, 40]. These can be separated from the REEs due to their formation of anionic complexes in acidic sulfate solutions whereas the REEs do not readily form anionic complexes. Similarly, other impurities such as iron (Fe) can be separated from REEs using strong acidic chloride solutions, where Fe forms a strong chloride anionic complex [4, 38].

The majority of industrial REE separations have utilized polystyrene-based polymer beads functionalized with sulfonic acid (SO<sub>3</sub>H) groups referred to as Strong Acid Cation Exchangers (SAC). These resins are produced on a very significant scale by major specialty chemical producers around the globe [41]. Their availability as commodity materials makes them a very cost-effective production reagent.

These polystyrene-based functionalized polymers are stable across the entire pH range and are reusable through hundreds to thousands of cycles.

Work using anion exchangers for REE separations has been carried out with REEs present as anionic complexes such as carboxylic, hydroxy or amino acids [38]. The order of elution of REEs from anion exchangers is the reverse to that of cation exchangers. Elution of the heavy REEs usually occurs first with cation exchangers, while with anion exchangers it is the light REEs that elute first [38].

Strong Acid Cation polymer resins are typically significantly cheaper than their anion exchange analogs and usually exhibit a greater stability and longevity with less inclination to being fouled by contaminants such as silica ( $\text{SiO}_2$ ). Ehrlich and Lisichkin [37] identified a number of key parameters which influence the efficiency of cation exchangers for REE separations. These include:

- Nature and concentration of complexing agent
- Cation exchanger state (e.g., counter ion)
- Acidity of eluent
- Temperature (i.e., elevated temperatures usually increase separation factors)
- Presence of other complexing agents and metal ions
- Degree of cross-linking of the support/resin
- Operating parameters (e.g., flux rates, bed depth, and length)

There are additional factors such as the nature of the substrate or polymer type that can influence total loading capacity and kinetics due to changes in hydrophilicity. From an industrial perspective the mechanical properties of the resin are important with regard to stability, uniformity of particle size, operating pressures.

A wide range of other functionalized and impregnated supports have and continue to be studied for their applicability to the separation of REEs and associated impurities. A quite extensive summation of various adsorbents, their characteristics, and limitations has been documented [37].

A significant proportion of the numerous materials investigated for REE separation is for analytical applications [26] where modified, small particle size,  $\text{SiO}_2$  substrates are used as the stationary phase in High-Performance Liquid Chromatography (HPLC) separations.

For the direct recovery of REEs from strong acids and complex solutions, chelating cation exchangers have been investigated [37]. These include:

- Aminophosphonic acid ( $\text{NH}_2\text{PO}(\text{OH})_2$ )
- Aminomethylphosphonic acid ( $\text{CH}_2\text{NO}_3\text{P}$ )
- Iminodiacetic acid ( $\text{HN}(\text{CH}_2\text{CO}_2\text{H})$ )
- Di- and polyfunctional phosphonic/sulfonic acid ( $\text{PO}_3\text{H}_2$  and  $\text{HO}_3\text{S}$ )

These chelating resins do provide some direct separation of REEs and in many cases are useful for the separation of minor REE constituents from a semi-purified REE product [38]. Researchers have produced a range of complex functionalized materials that have been tested for REE separations including crown ethers, inorganic, solvent impregnated resins, and organic/inorganic hybrid composites [26, 42–44].

## 7.6 Complexing Agents

In conventional IX chromatographic separations, the ion exchanger is selected based upon its selectivity to separate the various ions present in solution. The REEs exhibit almost identical affinity for conventional SAC exchangers and so separation is achieved through the use of complexing agents.

Complexing anions can have greatly differing complex strengths with the REEs. Generally, a cation exchanger will exhibit a preference for the rare earth cations that form the weaker complexes [45]. Powell identified the following key characteristics of complexing agents for use in chromatographic REE separations: [25]

1. The reagent and its metal chelates must be reasonably soluble in an inexpensive but compatible solvent (i.e., preferably water).
2. The reagent must be selective in its chelating action.
3. The reagent must form rare earth chelates of sufficient stability to promote clean displacement of rare earths from the resin bed.
4. The reagent must form labile chelate species which must not be of such great stability that the accompanying cation-exchange process is hampered unnecessarily.

In early work, citrate ions were commonly used [27, 42]. Subsequently a wide range of complexing agents and ligands were documented. The major complexing agents that were studied were carboxylic acids, hydroxy acids, and aminopolycarboxylic acids.

- The carboxylic acids included acetic ( $\text{CH}_3\text{COOH}$ ), malonic ( $\text{CH}_2(\text{COOH})_2$ ), phthalic ( $\text{C}_6\text{H}_4(\text{CO}_2\text{H})_2$ ) [37].
- The hydroxy acids included glycolic ( $\text{HOCH}_2\text{CO}_2\text{H}$ ), lactic ( $\text{CH}_3\text{CHCOOH}$ ),  $\alpha$ -hydroxyisobutyric acid (HIBA,  $(\text{CH}_3)_2\text{C}(\text{OH})\text{COOH}$ ), 2-hydroxy-2-methylbutyrate, malic ( $\text{HO}_2\text{CCH}_2\text{CH}(\text{OH})\text{CO}_2\text{H}$ ), glycolate ( $\text{HOCH}_2\text{COOH}$ ), and tartaric ( $\text{HO}_2\text{CCH}(\text{OH})\text{CH}(\text{OH})\text{CO}_2\text{H}$ ). These have been successfully used to separate mixtures of rare earths [26, 37, 38, 46].
- The aminopolycarboxylic acids included aminoacetic acid ( $\text{NH}_2\text{-CH}_2\text{-COOH}$ ), aminopolyacetic acids, ethylenediaminetetraacetic acid (EDTA,  $[\text{CH}_2\text{N}(\text{CH}_2\text{CO}_2\text{H})_2]_2$ ), N-(2-hydroxyethyl) ethylenediaminetetraacetic acid (HEDTA,  $\text{HOCH}_2\text{CH}_2\text{N}(\text{CH}_2\text{CO}_2\text{H})\text{CH}_2\text{CH}_2\text{N}(\text{CH}_2\text{CO}_2\text{H})_2$ ), nitrilotriacetic acid (NTA,  $\text{N}(\text{CH}_2\text{CO}_2\text{H})_3$ ), cyclohexane-1,2-diaminetetraacetic ( $\text{C}_{14}\text{H}_{22}\text{N}_2\text{O}_8$ ), diethylenetriaminepentaacetic ( $[(\text{HOOCCH}_2)_2\text{NCH}_2\text{CH}_2]_2\text{NCH}_2\text{COOH}$ ), and iminodiacetic acid ( $\text{HN}(\text{CH}_2\text{CO}_2\text{H})_2$ ). These have been used to achieve highly effective separations [26, 37, 38, 42, 46].

The majority of these reagents are relatively low cost and environmentally friendly. The selection of the preferred complexing agent is driven by a number of factors which include cost, ability, and ease of recycling as well as selectivity and separation factors.

The carboxylic, hydroxy and amino acids are typically cheaper than the aminopolycarboxylic acids which tend to exhibit greater separation factors in chromatographic separation. HEDTA has been shown to achieve greater separation factors than EDTA but the relative costs and availability of these two reagents tend to result in EDTA being more commonly used [37, 38].

The use of ligands in conjunction with complexing agents adds an additional degree of complexity with respect to recycle and reuse of reagents in a large-scale production process especially when primary, impure feedstocks are used which contain other divalent cations.

## 7.7 CIX/CIC Industrial Applications

Continuous Ion Exchange and Continuous Ion Chromatography have a well-established track record in hydrometallurgy, pharmaceutical, food, chemical, and water treatment industries. A number of research groups have looked at the potential for the application of CIX/CIC to separating and recovering REEs from primary and secondary sources. Studies have been conducted to investigate the commercial applicability for the recovery of REEs from phosphoric acid ( $\text{H}_3\text{PO}_4$ ) and coal and coal waste materials [30, 31, 47].

From primary resources, Northern Minerals is in the process of commissioning the Browns Range heavy rare earth project in the East Kimberley region of WA, Australia [48]. A pilot program is in place utilizing CIX/CIC for the separation of individual REEs.

USA Rare Earth and Texas Minerals Resources are also applying CIX/CIC to their Round Top deposit in Texas [49]. The project is utilizing a sulfuric acid ( $\text{H}_2\text{SO}_4$ ) heap leach process with a CIX preconcentration followed by CIC for separation of individual REEs.

## 7.8 Conclusion

The application of CIC has grown rapidly in the past two decades in a wide variety of industries including hydrometallurgy. The proven capabilities of ion chromatography for REE separation were first demonstrated as part of the Manhattan project and subsequently practiced by the Ames Laboratory and industry. When combined with modern continuous IX equipment, the opportunity has expanded to recover and separate REEs from a range of both primary and secondary sources. Modern CCIX equipment enables low-cost, high-efficiency, separations to be performed with a small plant footprint, as well as the usage of low-toxicity reagents with the

ability to recycle the majority of reagents. The design of the current state of the art equipment requires low operator input as the majority of equipment is controlled by a single central valve which automates multiple steps from loading, rinse, elution, and recycle.

Continuous Ion Chromatography has the capability to compete with SX as an economical approach for REE separation and recovery at an industrial scale. Economic comparisons of IX and SX have been prepared by Rollat [44] but were focused predominantly on the methodologies using copper (Cu)—EDTA and its analogs. The selection of an optimal chelating agent is key to the economic competitiveness of IX techniques. The ideal chelator should be low cost, environmentally benign, and be capable of being recycled without needing to be precipitated which then requires the associated solid-liquid separation steps. Ion exchange methodologies are particularly advantageous for separation of the heavy rare earth elements (HREEs) for which SX methods commonly rely upon phosphonic extractants with high chemical consumption associated with the acid extraction and alkaline saponification steps as well as a large number of mixer settlers to affect high-purity separations. Advanced, modern IX-based REE separations also have the advantage, when compared with SX, of reduced hold of valuable REEs inventory in the circuit, smaller footprint, reduced chemical costs, and no requirement for heat input to control reagent viscosities nor the generation of vapors requiring fume extraction systems. The compatibility of IX techniques with H<sub>2</sub>SO<sub>4</sub> leach solutions, versus the more typical hydrochloric (HCl) and HNO<sub>3</sub> solutions used in SX, enables a further cost advantage simplifying materials of construction and enabling low-cost recovery operations such as heap leaching.

Where ore bodies can be directly leached without the need for fine grinding and beneficiation, IX lends itself even more so to the treatment of lower-grade feed solutions as it has done in other metal recovery scenarios such as that for the U industry [50]. The separation of partially purified concentrates and recycling of REE-containing materials such as magnets also offer the opportunity to recover small quantities of the more valuable less common HREEs found along with the lighter rare earth elements (LREEs).

These advantages of IX-based techniques and the separation capabilities of a continuous chromatographic column configuration provide the basis for a competitive technique to SX. The Ames Laboratory still produces very high-purity REEs using IX. Additionally, in the 1990s, an ion exchange production plant was brought online in China for the production of rare earth oxides (REOs) [42]. A number of companies are well progressed in their development, and additional commercial IX plants are likely to be implemented in the near future. The detailed specifics of circuit configurations, solid support chemistry, and chelation chemistry remain closely guarded proprietary aspects of the technology holders.

## References

1. G.E. Boyd, J. Schubert, A.W. Adamson, The exchange adsorption of ions from aqueous solutions by organic zeolites. I. Ion-exchange equilibria. *J. Am. Chem. Soc.* **69**(11), 2818–2829 (1947)
2. F.H. Spedding, E.I. Fulmer, T.A. Butler, E.M. Gladrow, M. Gobush, P.E. Porter, J.E. Powell, J.M. Wright, The separation of rare earths by ion exchange. III. Pilot plant scale separations. *J. Am. Chem. Soc.* **69**(11), 2812–2818 (1947)
3. K.A. Gscheneidner, *Rare Earth; The Fraternal Fifteen: Division of Technical Information* (U.S. Atomic Energy Commission, New York, 1967)
4. J.S. Fritz, Early milestones in the development of ion-exchange chromatography: A personal account. *J. Chromatogr. A* **1039**(1–2), 3–12 (2004)
5. J. Lifton, *Solvay's Toll Refining Services Redirect the Downstream Rare Earth Dream* (2014). <https://investorintel.com/markets/technology-metals/technology-metals-intel/first-come-first-served/>
6. F. Xie, T.A. Zhang, D. Dreisinger, F. Doyle, A critical review on solvent extraction of rare earths from aqueous solutions. *Miner. Eng.* **56**, 10–28 (2014)
7. T.S. Mackey, Recent developments in USA rare earth technology, in *New Frontiers in Rare Earth Science and Applications*, (Academic Press, 1985), p. 1131
8. S.D. Alexandratos, Ion-exchange resins: A retrospective from industrial and engineering chemistry research. *Ind. Eng. Chem. Res.* **48**(1), 388–398 (2009)
9. D.O. Campbell, Rapid Rare Earth Separation by Pressurized Ion Exchange Chromatography. *J. Inorg. Nucl. Chem.* **35**(11), 3911–3919 (1973)
10. R. McNeill, E.A. Swinton, D.E. Weiss, Continuous ion exchange. *JOM* **7**(8), 912–921 (1955)
11. C.D. Scott, R.D. Spence, W.G. Sisson, Pressurized, annular chromatograph for continuous separations. *J. Chromatogr. A* **126**, 381–400 (1976)
12. J.M. Begovich, W.G. Sisson, A rotating annular chromatograph for continuous metal separations and recovery. *Resour. Conserv.* **9**, 219–229 (1982)
13. V.T. Taniguchi, A.W. Doty, C.H. Byers, Large-scale chromatographic separations using continuous displacement chromatography (CDC), in *Rare Earths, Extraction, Preparation and Applications*, ed. by R.G. Bautiste, M.M. Wong, (The Minerals, Metals & Materials Society, 1988)
14. C.J. Cowan, C. Cox, B.T. Croll, P. Holden, J.B. Joseph, A.J. Rees, R.C. Squires, Development of exchange, a continuous ion exchange process using powdered resins and cross-flow filtration, in *Ion Exchange Advances*, ed. by M.J. Slater, (Springer, Dordrecht, 1992)
15. C.H. Byers, D.F. Williams, Efficient recovery of lanthanides by continuous ion exchange. *Ind. Eng. Chem. Res.* **35**(4), 993–998 (1996)
16. W.W. Berry, R.A. Schmeda, H.S. Kibler, *Advanced Separation Device and Method* US4522726 (1985)
17. F.A. Habashi, Textbook of hydrometallurgy, in *Quebec City, Metallurgie Extractive Quebec*, 2nd edn., (Distributed by Laval University Bookstore, 1993)
18. B.K. Ahlgren, R.U. Seneviratne, *Recent Advances in the Design and Operation of Continuous Ion Exchange Equipment in the Mining Industry* (Proceedings of the 7th International Symposium, Hydrometallurgy 2014 – Volume II, Canadian Institute of Mining, Metallurgy and Petroleum – ISBN: 978-1-926872-23-0, 2014)
19. D.B. Dreisinger, M.J. Gula, *The Ion Exchange Treatment of Copper Electrowinning Bleed Streams Using Diphonix™ Resin* (In the Minerals, Metals & Materials Society Annual Meeting, 1995)
20. <http://www.ixsep.com>
21. <https://www.calgoncarbon.com/products/isep/>
22. <https://www.puritech.be>

23. F. Rochette, Y. De Busscher, *Rare Earth and Precious Metals Recovered with CCIX-Continuous Countercurrent Ion Exchange* (ALTA 2018 Uranium-REE-Lithium Conference: 14th Annual Uranium Event Proceedings, 2018), p. 301
24. F.G. Helfferich, *Ion Exchange* (Courier Corporation, 1995)
25. J.E. Powell, *Non-Metallic Compounds – I*, vol 3 (Chapter 22 Separation Chemistry, 1979), pp. 81–109
26. B. Chen, M. He, H. Zhang, Z. Jiang, B. Hu, *Chromatographic Techniques for Rare Earth Elements Analysis*. *Phys. Sci. Rev.* **2**(4) (2017)
27. F.H. Spedding, E.I. Fulmer, J.E. Powell, T.A. Butler, The separation of rare earths by ion exchange. V. Investigations with one-tenth per cent. Citric acid-ammonium citrate solutions 1. *J. Am. Chem. Soc.* **72**(6), 2354–2361 (1950)
28. H. Li, Y. Zhao, Patent analysis of the rare earth extracting separation technology. *Appl. Mech. Mater.* **513–517**, 4597–4600 (2014)
29. W.W. Berry, G.J. Rossiter, *Process for Fractionating a Mixture of Rare Earth Metals by Ion Exchange*. EP0335538 (1989)
30. W.W. Berry, T.E. Baroody, *Processes for Rare Earths Recovery from Wet-Process Phosphoric Acid*. US2015167120 (2015)
31. N.L. Wang, H. Choi, D. Harvey, *Methods for Designing an Efficient Preparative Chromatographic Separation Process* (Publication number: US 20200348274, 2018)
32. N.L. Wang, L. Ling, *Ligand-Assisted Chromatography for Metal Ion Separation* (Publication Number: US 20200308668, 2019)
33. N.L. Wang, L. Ling, *Ligand-Assisted Chromatography for Metal Ion Separation* (Patent Number: US 10597751, 2015)
34. N.L. Wang, H. Choi, D. Harvey, *Preparation of Rare Earth Metals and Other Chemicals from Industrial Waste Coal Ash* (Patent Number: US 20190153562, 2018)
35. Y. Liang, H. Choi, N.L. Wang, *Rare Earth Elements Purification Using Ligand-Assisted Displacement Chromatography (August 4, 2016)* (The Summer Undergraduate Research Fellowship (SURF) Symposium. Paper 141, 2016)
36. Y. Ding, D. Harvey, N.H.L. Wang, Two-zone ligand-assisted displacement chromatography for producing high-purity praseodymium, neodymium, and dysprosium with high yield and high productivity from crude mixtures derived from waste magnets. *Green Chem.* **22**(12), 3769–3783 (2020)
37. G.V. Ehrlich, G.V. Lisichkin, Sorption in the chemistry of rare earth elements. *Russ. J. Gen. Chem.* **87**(6), 1220–1245 (2017)
38. D. Kołodyńska, Z. Hubicki, *Investigation of Sorption and Separation of Lanthanides on the Ion Exchangers of Various Types* (In *Ion Exchange Technologies*, 2012). <https://doi.org/10.5772/50857>
39. K.L. Ang, D. Li, A. Nikoloski, The effectiveness of ion exchange resins in separating uranium and thorium from rare earth elements in acidic aqueous sulfate media. Part 1. Anionic and cationic resins. *Hydrometallurgy* **174**, 147–155 (2017)
40. K.L. Ang, D. Li, A. Nikoloski, The effectiveness of ion exchange resins in separating uranium and thorium from rare earth elements in acidic aqueous sulfate media. Part 2. Anionic and cationic resins. *Miner. Eng.* **123**(2018), 8–15 (2018)
41. A.A. Zagorodni, *Ion Exchange Materials: Properties and Applications* (Elsevier, 2006)
42. Q. Dezhi, Chapter 6 – Ion-exchange and extraction chromatography separation of rare earth elements, in *Hydrometallurgy of Rare Earths*, ed. by D. Qi, (Elsevier, 2018)
43. B.H. Ketelle, G.E. Boyd, The exchange adsorption of ions from aqueous solutions by organic zeolites. IV. The separation of the yttrium group rare earths. *J. Am. Chem. Soc.* **69**(11), 2800–2812 (1947)
44. A. Rollat, *The Rare-Earths Refinery: Is There an Alternative Industrial Solution to Solvent Extraction?* (Rare Earths 2016 Sapporo, Japan, 2016)
45. J.P. Surls, G.R. Choppin, Equilibrium Sorption of Lanthanides, Americium and Curium on Dowex-50 Resin. *J. Amer. Chem. Soc.* **79**(4), 855–859 (1957)

46. S.P. Singh, in *Chapter 2 – Complexes of the Rare Earths*, ed. by S.P. Sinha, (Elsevier, Pergamon: Oxford, NY, 2013)
47. X. Heres, V. Blet, P. Di Natale, A. Ouaattou, H. Mazouz, D. Dhiba, F. Cuer, *Selective Extraction of Rare Earth Elements from Phosphoric Acid by Ion Exchange Resins*, vol 8 (Metals, 2018), p. 682
48. <http://wcsecure.weblink.com.au/pdf/NTU/02317302.pdf>
49. <https://www.usare.com>
50. D. Van Tonder, M. Kotze, *Uranium Recovery from Acid Leach Liquors: IX or SX?* (ALTA Uranium Conference, 2007)



# Chapter 8

## Ionic Liquids for the Processing of Rare Earth Elements



Tommee Larochelle

### 8.1 Introduction

This chapter provides an overview of the utilization of ionic liquids (ILs) for processing rare earth elements. Ionic liquids have been extensively researched and many historical perspectives have been published [1–4]. Ionic liquids are an established field of study with upwards of 3500 papers published annually [1]. The application of ILs to the rare earth industry is, however, relatively novel.

Ionic liquids are organic salts with melting points usually below ambient temperature. Their melting point is not definitive, and many authors specifically discretize room temperature ionic liquids (RTILs) as a subset of ILs. The definition generally accepted in the rare earths industry is that the melting point of ILs ought to be lower than the boiling point of water. The fundamental criteria distinguishing ILs from other liquid solvents are the absence of molecular species in the liquid phase.

The primary field of research for the utilization of ILs in the extraction and refining of rare earth elements (REE) is as a substitute for the organic phase(s) in the solvent extraction separation process. Ionic liquids are often described as a green alternative to organic solvent due to their negligible vapor pressure and high thermal stability [4]. Pham et al. [5] reviewed studies on the impact of ILs on the environment and concluded that the “green” designation may not be warranted since the high chemical and thermal stability of ILs combined with their low vapor pressure may be a Faustian bargain. The valuable characteristics of ILs will likely lead to persistence and accumulation in the environment. Most ILs, especially perfluorinated anions and long alkyl chain cations are particularly toxic to aquatic

---

T. Larochelle (✉)  
L3 Process Development, Bent Mountain, VA, USA  
e-mail: [tommee.larochelle@l3processdev.com](mailto:tommee.larochelle@l3processdev.com)

ecosystems. Due to their ionic nature, ILs solvents tend to be more soluble in aqueous phases than their molecular organic counterparts.

Other advantages of ILs as alternatives to the organic components in the solvent extraction systems include their significant variability with regard to viscosity, polarity, solubility, and coordination ability [4] allowing for their optimization with regard to specific extraction systems. While deep eutectic solvents such as choline chloride-carboxylic acid present characteristics and behaviors similar to ILs [6], they will be excluded from the present discussion since they do not meet the definition of ILs.

First, the primary ILs being investigated will be discussed followed by an overview of their usage in solvent extraction processes as replacement for conventional extractants and/or solvents. Specific comparisons will be presented for yttrium recovery processes where the value of ILs is most apparent. A new approach to solvent extraction using Aqueous Two-Phase Systems (ATPS) will also be discussed. Following the solvent extraction discussion, the recent investigations into applications of ILs to mineral processing will be reviewed. Finally, electrometallurgical applications of ILs will be discussed. All these applications for ILs in REE processing are integrated into the concept of solvometallurgy.

Solvometallurgy is a recent umbrella term that includes hydrometallurgy and systems with other nonmolecular organic solvents such as molten inorganic salts, deep eutectic solvents, polymer solvents, and ionic liquid solvents.

Similar to hydrometallurgy, the first step in solvometallurgical processing of REE is to solubilize the lanthanides. Ionic liquids such as betainium bis-(trifluoromethylsulfonyl)imide, [Hbet][NTf<sub>2</sub>] have been extensively studied for that purpose using various raw materials such as neodymium iron boron (NdFeB) waste magnets [7–9], bauxite (Al<sub>2</sub>O<sub>3</sub>·2H<sub>2</sub>O) residue [10–12], lamp phosphor [13, 14], and carbonatite ore [15]. In addition, and to a lesser extent, imidazolium-based ILs have been reported as leaching solutions for lanthanides [12, 16–18]. The direct utilization of [H][NTf<sub>2</sub>] for the leaching of rare earth carbonate prior to the electrodeposition has also been recently reported by Martinez [19]. Subsequent processing steps typically involve solvent extraction, aqueous two-phase systems selective precipitation using bases such as sodium hydroxide (NaOH) and/or acids such as oxalic acid (C<sub>2</sub>H<sub>2</sub>O<sub>4</sub>) and/or electrometallurgy.

A highly promising approach to solvometallurgy was recently developed by Pr. Binnemans' group at Katholieke Universiteit (KU) Leuven [20–22]. Rather than use acids to leach metals, they integrated chlorine to chloride ILs, generating [Cation][Cl<sub>3</sub>], ILs with oxidative capabilities toward metals [20]. Li et al. then applied this strategy to the separation of REE and transition metals from NdFeB permanent magnets using [P<sub>66614</sub>][Cl] as the IL underlying the system [21]. This approach only utilizes chlorine (Cl) and ammonia (NH<sub>3</sub>) as reagents, both of which are available as inexpensive commodity materials and which generate little wastewater. Other related processes such as the use of pyridinium chloride ((PyrH)(Cl)) are also investigated for the recovery of metals and alloys in solvometallurgical approaches. Orefice and Binnemans propose a closed loop process using such an approach where hydrochloric acid (HCl), C<sub>2</sub>H<sub>2</sub>O<sub>4</sub>, and NH<sub>3</sub> are the main reactants

[22]. In this process, conventional acidic extractants including 2-ethylhexyl phosphonic acid mono-2-ethylhexyl ester (EHEHPA) and Cyanex 923 are used in p-cymene (C<sub>10</sub>H<sub>14</sub>) along with C101 IL.

## 8.2 Nomenclature and Molecular Structure of Selected Ionic Liquids Cations and Anions

Ionic liquids are customarily named using both ions of the molecule in brackets, the cation on the left and the anion on the right. No formal naming convention currently exists, yielding various nomenclatures for the same molecules. Tables 8.1 and 8.2 present the usual nomenclature and alternate names for commonly used cation and anions in ILs. The structure of such ions is also presented in Figs. 8.1 and 8.2, respectively. It is customary to use elemental symbols for single elements such as [Cl] for a chloride ion or [Br] for a bromide ion. In addition to their trade names, complex molecules are customarily named using the first letter of the major functional groups in the molecule. 2-ethylhexyl phosphoric acid mono-2-ethylhexyl ester is thus commonly referred to as EHEHPA, P507, Ionquest801 or PC-88A. The cation portion of ILs can also be represented by its trade name, by convention using the anion base element and its molecular structure or by a generic molecular descriptor. The Aliquat 336 cation is thus alternatively referred to as [Aq336], [A336], [N<sub>1888</sub>], [R4N], and/or trioctylmethylammonium.

Acid-base ILs are formed when an acidic extractant is used as an anion for an IL and an ammonium or phosphonium salt is used as a cation. In this combination, it is customary to refer to the IL using the molecular structure of both ions. An acid-base IL formed using P507 and Aq336 would thus be named trioctylmethylammonium 2-ethylhexyl mono-2-ethylhexyl ester phosphate [N<sub>1888</sub>][EHEHP]. In most cases, the acidic extractant structure is used without the ending “A” since it is no longer an acid. This IL is also referred to as [A336][P507].

## 8.3 Solvent Extraction

Solvent extraction is a natural application for ionic liquids in REE processing as they can be substituted for every phase of the solvent extraction system. While the primary application of ILs in solvent extraction is replacement for the conventional extractants, the replacement of the organic phase with an IL also provides many significant advantages. The replacement of the aqueous phases with ILs has not been as extensively studied since solvometallurgical lixiviation is a nascent field of research.

The fundamental nature of ILs as molten salts composed as an anion and as a cation allows for the creation of highly effective ILs where both ions actively

**Table 8.1** Cations of ILs relevant to the processing of REE

Category/cation	Name	Figure	Note
<i>Ammonium-based cations</i>			
[N <sub>888</sub> ]/[Am336]/[A336]	Tri-n-octylammonium	8.1a	
[N <sub>1888</sub> ]/[Aq336]/[A336]/[TOMA]	Trioctylmethylammonium	8.1b	
[N <sub>4444</sub> ]/[TBA]	Tetrabutylammonium		
[N <sub>8888</sub> ]/[TOA]	Tetraoctylammonium	8.1c	
[TEHA]	Tri-(2-ethylhexyl)ammonium	8.1d	
[N <sub>6222</sub> ]	n-Hexyltriethylammonium	8.1e	
[OcGBOEt]	Trioctyl(2-ethoxy-2-oxoethyl)ammonium	8.1f	
[DEME]	N,N-Diethyl-N-methyl-N-(2-methoxyethyl)ammonium	8.1g	
[N <sub>444Bn</sub> ]	Benzyltributylammonium		
<i>Phosphonium-based cations</i>			
[P <sub>66614</sub> ]/[T <sub>66614</sub> ]/[THTP]	Trihexyl(tetradecyl)phosphonium	8.1h	
[P <sub>8884</sub> COOH]	(4-Carboxyl)butyl-trioctyl-phosphonium	8.1i	
<i>Imidazolium-based cations</i>			
[C <sub>(i)</sub> C <sub>(i)</sub> im]	Alkyl-alkyl-imidazolium	8.1j	R1 = 2,4,6,8,10 <sup>a</sup> , R2 = 1,2,4 <sup>a</sup>
[C <sub>(i)</sub> COOH C <sub>(i)</sub> im]	Alkyl-carboxyl-alkyl-imidazolium	8.1k	R1 = 3,4,5,6,7,8 <sup>a</sup> , R2 = 1,3 <sup>a</sup>
<i>Pyridinium-based cations</i>			
[C <sub>(i)</sub> C <sub>(i)</sub> Pyr]	Alkyl-alkyl-pyridinium	8.1l	R1 = 2,4,6,8,10 <sup>a</sup> , R2 = 1,2,4 <sup>a</sup>
[C <sub>(i)</sub> C <sub>(i)</sub> Pip]	n-Alkyl-n-alkyl-piperidinium	8.1m	R1 = 2,4,6, R2 = 1, 2
[N <sub>11</sub> N <sub>11</sub> PipGua]	Dis-1,2 methyl guanidinium piperidinium		R1 = 1,2 <sup>a</sup>
<i>Other cations</i>			
[EC]	Ethylene carbonate		
[N <sub>888DOPE</sub> ]	Trioctyl(2-(diethoxy-phosphoryl)ethyl)ammonium		

<sup>a</sup>Other alkyl chain lengths are possible but have not been tabulated in the surveyed literature

participate in the extraction process. This is referred to as acid-base coupling task-specific functional ionic liquids (ABC-TSFILs) and tends to produce the best results in terms of extraction efficiency when both ions have extraction capabilities by themselves. Most of the ABC-TSFIL research is targeted at combining such conventional extractants in an IL form. Since both ions are typically large, the resulting IL tends to be highly viscous, which reduces the phase mass transfer rate and prevents the usage of ABC-TSFILs as solvent. Thus, molecular organic solvents are still relevant.

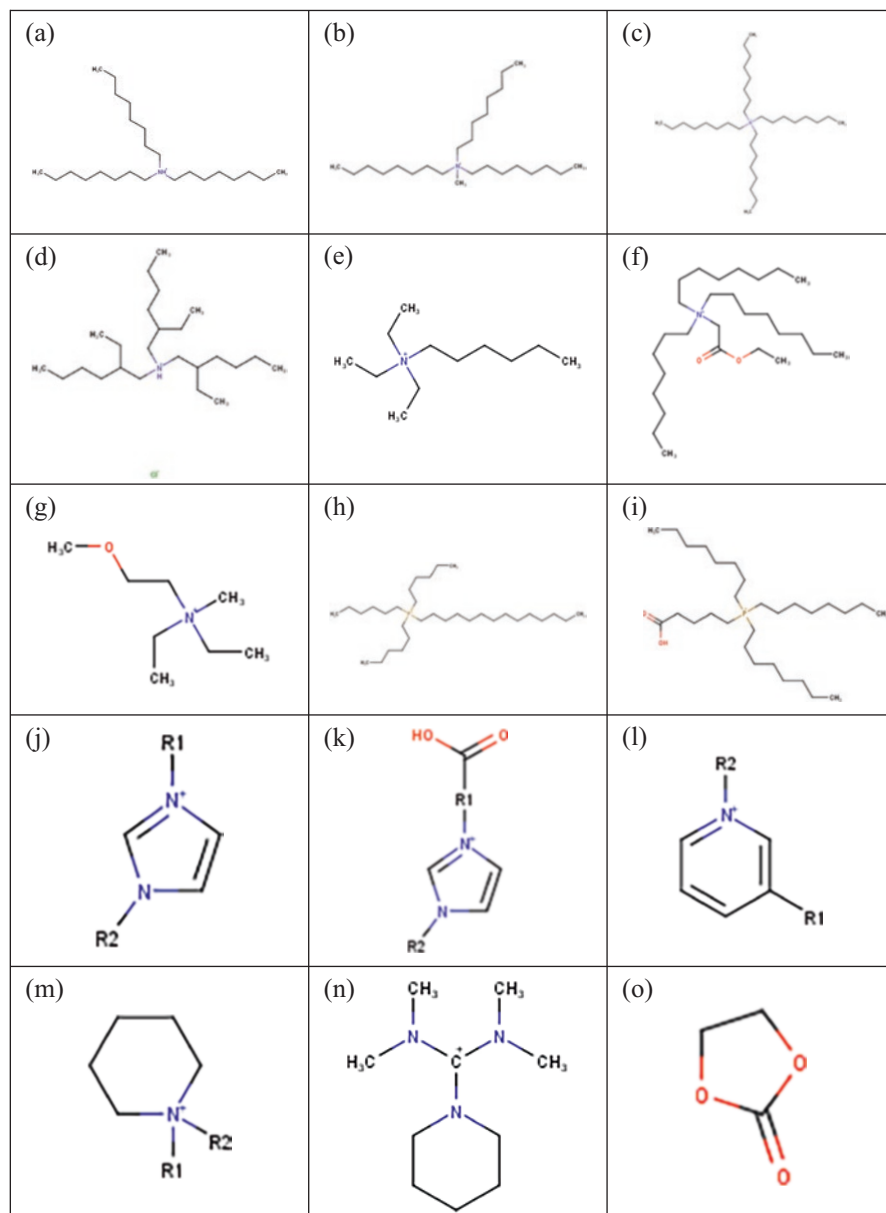
In parallel, research has been undertaken on the use of ILs as a replacement for molecular organic solvents. In contrast to ABC-TSFILs, ILs targeted for the

**Table 8.2** Anions of ILs relevant to the processing of REE

Category/anion	Name	Figure
<i>Fluorine-sulfur-nitrogen-based anions</i>		
[NTf <sub>2</sub> ]/[TFSI]/[TFSA]/[OTf]	Bis(trifluoromethylsulfonyl)azanide <sup>a</sup>	8.2a
[BETI]	Bis(perfluoroethanesulfonyl)azanide <sup>a</sup>	8.2b
[NfO]	Nonafluorobutanesulfonate	
[PF <sub>6</sub> ]	Hexafluorophosphate	8.2c
<i>Phosphorus-based anions</i>		
[C272]/[BTMPP]	Bis(2,4,4-trimethylpentyl)phosphinate	8.2d
[D2EHP]	Di(2-ethylhexyl)phosphate	8.2e
[EHEHP]	Mono-(2-ethylhexyl) 2-ethylhexyl phosphonate	8.2f
<i>Acetate-based anions</i>		
[SNPAA]/[CA100]	sec-Nonylphenoxyacetate (R1 = 7)	8.2g
[SOPAA]/[CA12]	sec-Octylphenoxyacetate (R1 = 6)	8.2g
[NOPAA]/[OCTPOA]	n-Octylphenoxyacetate (R1 = 8)	8.2g
[DMHPAA]/[POAA]	(2,6-Dimethylheptyl) phenoxy acetate	
[IOPAA]	4,4'-Isopropylidene bis (phenoxyacetate)	8.2h
[BDOAC]	Benzene-1,4-dioxydiacetate	8.2i
[MA]	Myristic acetate	
[DDA]	Dodecanedioic acetate	
<i>Organic acid-based anions</i>		
[BA]	Benzoate (R1 = Bz)	8.2j
[DA]	Decanoate (R1 = 9)	8.2j
[OI]/[OA]	Oleate (R1 = 17, monosaturated)	8.2j
[LA]	Laurate (R1 = 11)	8.2j
[PA]	Palmitate (R1 = 15)	8.2j
[LiA]	Linoleate (R1 = 17, monosaturated)	8.2j
<i>Diglycolamate-based anions</i>		
[BDGA]	Dibutyldiglycolamate (R1 = 4)	8.2k
[DHDGA]	Dihexyl diglycolamate (R1 = 6)	8.2k
[DODGA]	Diocetyl diglycolamate (R1 = 8)	8.2k
<i>Other anions</i>		
[D2EHOM]	Di(2-ethylhexyl)-oxamate	
[MA]	N,N,N',N'-tetra(2-ethyl-hexyl)malonate	8.2l
[MOx]	Methyl-oxalate	8.2n
[OPBOA]	2,2'-(1,2-Phenylenebis(oxy))dioctanoate	8.2o
[SCN]	Thiocyanate	
[AlCl <sub>3</sub> ]/[AlCl <sub>4</sub> ]	Aluminum chloride	

<sup>a</sup>Azanide is also referred to as "imide" or "amide"

replacement of molecular organic solvents tend to be composed of a large cation and a smaller halogen anion providing them with a lower viscosity. These include Cyphos 101 IL, [P<sub>66614</sub>][Cl] which contain functional ions and are referred to as task-specific functional (TSFILs), while others such as imidazolium salts [C<sub>(i)</sub>C<sub>(i)</sub>im]



**Fig. 8.1** Cations of ILs relevant to the processing of REE

[anion] are nonfunctional and are referred to simply as IL. It is important to note that many of the ILs investigated for the replacement of molecular organic solvents also exhibit a significant extraction potential for REE, allowing the design of very efficient systems through the combination of ABC-TSFIL extractants dissolved in TSFIL or in nonfunctional ILs.

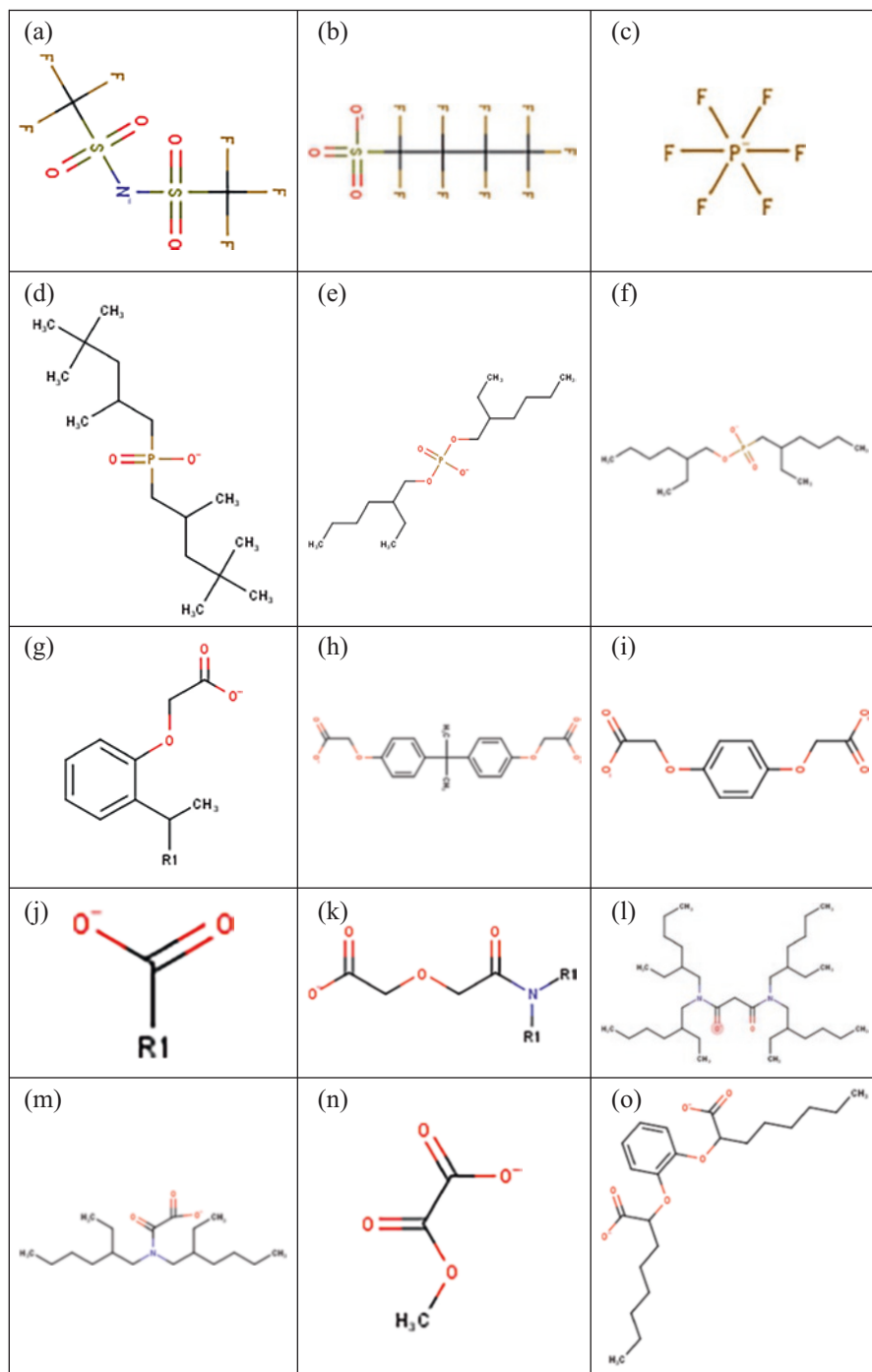


Fig. 8.2 Anions of ILs relevant to the processing of REE

In addition to the substitution of reagents in the conventional extraction systems, ILs also allow for the design of aqueous two-phase systems (ATPS) which are further discussed in a subsequent section. ATPS consist of an IL phase that is fully soluble in the aqueous phase under specific operating conditions but insoluble under different operating conditions.

Detailed literature reviews on the use of ILs for the solvent extraction of REE have been previously published [23–25] and technical aspects of the solvent extraction of rare earths have been discussed in Chap. 6. As such, this section will focus on providing the reader with an introduction to the utilization of ILs in the solvent extraction of REE as well as an update on the current state of the literature.

### 8.3.1 *Use of Ionic Liquids as Extractants*

The first entry of ILs in the REE industry will most likely be as the replacement of a conventional extractant by its IL equivalent. This process function has been addressed in numerous technical articles, which are summarized in Table 8.3. While the generally accepted benefits of using ILs (nonflammability, no vapor pressure, and high stability) may not be achieved by focusing on the extractant portion of the solvent extraction system, other benefits can be realized without engendering the downside of ILs (high losses in the aqueous phase). The most significant proposed benefits of a transition to ILs extractants are a potential reduction of the extraction system total volume and number of stages through either higher loading capacities and/or greater separation factors coupled by a potential reduction of wastewater generation through the elimination of saponification and in specific cases a reduction of the stripping acidity required. The losses of ILs extractant are also mitigated when using molecular organic solvent because of a more favorable aqueous partition ratio when compared to the equivalent acidic extractant. Su et al. [26] revealed that the solubility of [Aq336][EHEHP] was around an 0.5-order of magnitude lower than that of EHEHPA in the investigated system. A significant amount of research is still required to fully grasp the challenges and benefits of ILs with respect to their solubility in the aqueous phase.

The most studied acid-base coupling task-specific functional ILs are thus unsurprisingly a combination of the leading industrial extractants, D2EHPA and EHEHPA. To a much lesser extent, ABC-TSFILs based on HSOPAA and Cyanex 272 have also been investigated. Given the overlap, many investigations purport to compare ABC-TSFILs with their acidic anion; however, few offer a comparison properly using equivalent equilibrium conditions as a basis for comparison. A striking example involves most investigations into Cyanex 272-based ILs extractants which have been done using experimental conditions preventing a direct comparison with Cyanex 272 literature and thus are not worthy of discussing in detail. Some of the cases that do provide an appropriate comparison are summarized below. One such IL is Cyphos 104 IL which is a commercial IL of composition [P<sub>66614</sub>][C272] that is seeing increased activity in the literature.



**Table 8.3** Utilization of ionic liquids as extractant for rare earth elements separation

Anion	Cation	Ionic liquid	Rare earth element(s) Reference
[BA]	[P <sub>66614</sub> ]	[P <sub>66614</sub> ][BA]	Nd [27]
[BDOAC]	[P <sub>66614</sub> ] <sub>2</sub>	[P <sub>66614</sub> ] <sub>2</sub> [BDOAC]	Nd [28]
[BDGA]	[N <sub>1444</sub> ]	[N <sub>1444</sub> ][BDGA]	LREE [29]
[C272]	[N <sub>6222</sub> ]	[N <sub>6222</sub> ][C272]	La/Nd [30], Pr/Nd [31]
	[Am336]	[Am336][C272]	Pr/Nd [31, 32], La/Pr/Nd [32], Tb/Dy [33]
	[Aq336]	[Aq336][C272]	Lu [34], Pr/Nd/Fe/ [35], Tb/Dy [33], La/Y [36], HREE [37, 38]
	[N <sub>4444</sub> ]	[N <sub>4444</sub> ][C272]	HREE [37]
	[P <sub>66614</sub> ]	[P <sub>66614</sub> ][C272]/Cyphos 104	La/Ni [39], La/Y [36], Sm/Co [40, 41], REE [42, 43], HREE [44]
[Cl]	[N <sub>888DOPE</sub> ]	[N <sub>888DOPE</sub> ][C272]	Tm/Yb/Lu [45]
	[P <sub>66614</sub> ]	[P <sub>66614</sub> ][Cl]/Cyphos 101	Nd [46], REE [42, 47]
	[Aq336]	[Aq336][Cl]/Aliquat 336	REE [47], Nd [46], Sm/Co [48]
[NO <sub>3</sub> ]	[P <sub>8884COOH</sub> ]	[P <sub>8884COOH</sub> ][Cl]	REE/Co/Ni [49]
	[P <sub>66614</sub> ]	[P <sub>66614</sub> ][NO <sub>3</sub> ]	La/Sm/Co/Ni [50], Nd/Dy [51], REE [52, 53]
	[P <sub>8884COOH</sub> ]	[P <sub>8884COOH</sub> ][NO <sub>3</sub> ]	REE/Co/Ni [54]
	[Am336]	[Am336][NO <sub>3</sub> ]	REE [55]
	[Aq336]	[Aq336][NO <sub>3</sub> ]	REE [8, 52, 56, 57], Pr/Nd/Dy [58]
	[N <sub>1444</sub> ]	[N <sub>1444</sub> ][NO <sub>3</sub> ]	Nd/Fe [59], Pr/Nd [60]
[D2EHOM]	[C <sub>6</sub> mim]	[C <sub>6</sub> mim][D2EHOM]	REE [61]
[D2EHP]	[C <sub>6</sub> mim]	[C <sub>6</sub> mim][D2EHP]	REE [62]
	[C <sub>6</sub> mpy]	[C <sub>6</sub> mpy][D2EHP]	REE [62]
	[P <sub>66614</sub> ]	[P <sub>66614</sub> ][D2EHP]	REE [63]
	[Aq336]	[Aq336][D2EHP]	Pr/Nd/Fe/B [35], MREE [64, 65], REE [63, 66–68]
	[N <sub>2222</sub> ]	[N <sub>2222</sub> ][D2EHP]	REE [69]
	[N <sub>4444</sub> ]	[N <sub>4444</sub> ][D2EHP]	REE [62, 63, 69]
	[N <sub>8888</sub> ]	[N <sub>8888</sub> ][D2EHP]	REE [69]
	[Am336]	[Am336][D2EHP]	REE [70]
	[N <sub>88</sub> ]	[N <sub>88</sub> ][D2EHP]	REE [70]
[DGA]	[OcGBOEt]	[OcGBOEt][DHDGA]	REE [71, 72]
	[Aq336]	[Aq336][DHDGA]	REE [71, 72]
[EHEHP]	[Aq336]	[Aq336][EHEHP]	REE [26, 66, 68, 73–77]
	[N <sub>2222</sub> ]	[N <sub>2222</sub> ][EHEHP]	REE [69]
	[N <sub>4444</sub> ]	[N <sub>4444</sub> ][EHEHP]	REE [69], HREE [78]
	[N <sub>8888</sub> ]	[N <sub>8888</sub> ][EHEHP]	REE [69]
	[P <sub>66614</sub> ]	[P <sub>66614</sub> ][EHEHP]	Lu [34], REE [38]
	[N <sub>1888</sub> ]	[N <sub>1888</sub> ][EHEHP]	HREE [37]
[MA]	[P <sub>66614</sub> ]	[P <sub>66614</sub> ][MA]	REE [53]

(continued)

**Table 8.3** (continued)

Anion	Cation	Ionic liquid	Rare earth element(s) Reference
[MOx]	[C <sub>(i)</sub> mim]	[C <sub>(i)</sub> mim][MOx]	REE [61]
[PF <sub>6</sub> ]	[C <sub>(i)</sub> COOHpim]	[C <sub>(i)</sub> COOHpim][PF6]	Y [79]
[SCN]	[Aq336]	[Aq336][SCN]	Y/Eu [80], Sm/Co [48], Nd/Dy [51]
	[C <sub>(i)</sub> C <sub>(i)</sub> m <sub>3</sub> im]	[C <sub>(i)</sub> C <sub>(i)</sub> m <sub>3</sub> im][SCN]	Nd/Fe [81]
	[P <sub>66614</sub> ]	[P <sub>66614</sub> ][SCN]	Y/Eu [80], Nd/Dy [51]
[NTf <sub>2</sub> ]	[N <sub>1444</sub> ]	[N <sub>1444</sub> ][NTf <sub>2</sub> ]	REE [62]
	[P <sub>2225</sub> ]	[P <sub>2225</sub> ][NTf <sub>2</sub> ]	Nd/Pr/Tb/Dy [82]
	[P <sub>66614</sub> ]	[P <sub>66614</sub> ][NTf <sub>2</sub> ]	REE [83], Nd [27]
	[C <sub>(i)</sub> COOHpim]	[C <sub>(i)</sub> COOHmin][NTf <sub>2</sub> ]	Nd/Sm/Fe/Co [84], Sc [85]
	[N <sub>4</sub> BMalBBim]	[N <sub>4</sub> BMalBBim][NTf <sub>2</sub> ]	REE/Fe/Al [86]
	[PEGmim]	[PEGmim][NTf <sub>2</sub> ]	REE [87]
	[C <sub>(i)</sub> mpyr]	[C <sub>(i)</sub> mpyr][NTf <sub>2</sub> ]	REE [62]
	[C <sub>(i)</sub> bpyr]	[C <sub>(i)</sub> bpyr][NTf <sub>2</sub> ]	REE [83]
	[C <sub>(i)</sub> mim]	[C <sub>(i)</sub> mim][NTf <sub>2</sub> ]	REE [62, 63, 67, 88, 89]
[SOPA]	[P <sub>66614</sub> ]	[P <sub>66614</sub> ][SOPA]	HREE [90, 91], REE [47]
	[Aq336]	[Aq336][SOPA]	REE [47, 92], HREE [44, 91, 93]
[NOPA]	[Aq336]	[Aq336][NOPA]	Y [94]
[SNPA]	[Aq336]	[Aq336][SNPA]	REE [92]
[ND]	[Aq336]	[Aq336][ND]	REE [95]
[MA]	[N <sub>444Bn</sub> ]	[N <sub>444Bn</sub> ][MA]	REE [96]
[DDA]	[N <sub>444Bn</sub> ]	[N <sub>444Bn</sub> ][DDA]	REE [96]
[DMHPA]	[N <sub>1888</sub> ]	[N <sub>1888</sub> ][DMHPA]	REE [97]
[P227]	[Aq336]	[Aq336][P227]	HREE [98]
[C572]	[P81R]	[P81R][C572]	Nd/Tb/Dy [99]
[IOPA]	[P <sub>66614</sub> ]	[P <sub>66614</sub> ][IOPA]	REE [100]
[I]	[C <sub>(i)</sub> C <sub>(i)</sub> m <sub>3</sub> im]	[C <sub>(i)</sub> C <sub>(i)</sub> m <sub>3</sub> im][I]	Nd/Fe [81]
[DA]	[Aq336]	[Aq336][DA]	Sm/Co [101]
	[N <sub>888</sub> ]	[N <sub>888</sub> ][DA]	Nd/Dy/Ni [102]
[LA]	[Aq336]	[Aq336][LA]	Sm/Co [101]
[LiA]	[N <sub>7777</sub> ]	[N <sub>7777</sub> ][LiA]	REE [103]
[PA]	[Aq336]	[Aq336][PA]	Sm/Co [101]
[OA]	[Aq336]	[Aq336][OI]	Nd [104], Nd/Tb/Dy [105]
	[N <sub>7777</sub> ]	[N <sub>7777</sub> ][OA]	REE [103]
	[N <sub>8888</sub> ]	[N <sub>8888</sub> ][OI]	REE [61]
[OPBOA]	[P <sub>66614</sub> ]	[P <sub>66614</sub> ][OPBOA]	Nd/Co/Ni [106]

Neodymium (Nd); Lanthanum (La); Praseodymium (Pr); Terbium (Tb); Dysprosium (Dy); Nickel (Ni); Yttrium (Y); Samarium (Sm); Cobalt (Co); Thulium (Th); Ytterbium (Yb); Lutetium (Lu); Iron (Fe); Boron (B); Europium (Eu); mid rare earth elements (MREE); light rare earth elements (LREE); heavy rare earth elements (HREE)

A study on the extraction of yttrium by Devi and Sukla [36] revealed that [P<sub>66614</sub>][C272] presented a very similar extraction profile to [Aq336][C272], suggesting that the [C272] anion is the most significant ion in the extraction. Building on the promises of the [C272] anion, Zeng et al. [45] increased the functionality of the cation by adding a phosphoryl unit to the ammonium-based cation, pioneering

multifunctional ILs. The application of this novel  $[N_{888DOPE}][C272]$  IL to Tm, Yb, and Lu revealed increased extraction capabilities and separation factors compared to  $[N_{1888}][C272]$ . Hopefully the authors will further investigate this new extractant with regard to other REE.

Deng et al. utilized the steric hindrance property of a phenyl group toward Y [107] to theorize and synthesize a functional IL targeted at Y purification [96]. However, the separation factors for HREE and Y are lower than with either  $[P_{66614}][SOPA]$  or  $[N_{1888}][ND]$ . Using similar considerations, Hu et al. designed, synthesized, and tested the IL  $[(CH_2)_7COOHPyr][NTf_2]$ , which yielded separation factors between  $[P_{66614}][SOPA]$  and  $[N_{1888}][ND]$  [108]. While this later IL contains fluorine, its high separation factor suggests additional work with alternative anions would be warranted.

Of particular industrial interest is the replacement of Sec-octylphenoxy acetic acid (CA-12, SOPAA) by  $[P_{66614}][SOPA]$  evaluated by Dong Yamin et al. [109] for the separation and purification of Y. Dong Yamin et al. determined that the IL  $[P_{66614}][SOPA]$  had four times the extraction capacity of SOPAA and presented greater separation factors at equivalent operating conditions. In addition,  $[P_{66614}][SOPA]$  did not require saponification and could be stripped using distilled water as opposed to conventional SOPAA-TBP extraction systems requiring up to 3 molar acidity and 90% saponification [110]. A comparison of the separation factors for both systems is presented as Table 8.4.

In addition to SOPAA extraction systems, naphthenic acid and neodecanoic acid (NDA) are also used commercially and are the focus of IL research. The investigation of REE extraction by  $[N_{1888}][ND]$  by Su et al. revealed that the IL is significantly more efficient in the separation of yttrium from HREE than its NDA precursor [95]. A comparison of the separation factors for both systems is presented as Table 8.5.

The separation of Eu from gadolinium (Gd) using either D2EHFA or  $[Aq336][D2EHP]$  in both chloride and nitrate medium was investigated by Ismail et al. [64]. They found that at very low acidity in chloride medium,  $[Aq336][D2EHP]$  was

**Table 8.4** Separation factors for SOPAA and  $[P66614][SOPA]$

Extractant/separation factor	Ho/Y	Er/Y	Tm/Y	Yb/Y	Lu/Y	Reference
SOPAA	1.74	1.68	1.35	1.27	1.08	[110]
$[P_{66614}][SOPA]$	1.94	1.94	2.78	4.17	5	[109]

Holmium (Ho); Erbium (Er)

SOPAA: 0.7 M, 15% TBP in kerosene 90% saponified, 0.3 M REE, initial pH = 4

$[P_{66614}][SOPA]$ : 0.05 M in kerosene no saponification, 0.003 M REE, initial pH = 3.5

**Table 8.5** Separation factors for NDA and  $[N1888][ND]$

Extractant/separation factor	Ho/Y	Er/Y	Tm/Y	Yb/Y	Lu/Y	Reference
NDA	2.1	2.7	4.1	6.1	6.4	[95]
$[N_{1888}][ND]$	2.64	4.32	7.7	12.5	16.27	

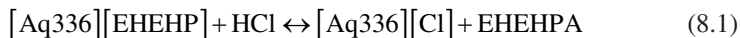
$[N_{1888}][ND]$  and NDA: 0.3 M, NDA is fully saponified. 0.15 M REE, pH = 5, O: A = 1

superior to D2EHPA but that around 3 M HCl, both extractants were equivalent. It was also determined that the nitrate media presented better extraction and separation efficiencies over the complete acidity range studies. Furthermore, [Aq336][D2EHP] was found to be superior to D2EHPA at all evaluated HNO<sub>3</sub> concentrations with optimum nitric acid concentrations of 3.5 and 3.0 M, respectively. Ismail et al. [64] used their data to simulate a countercurrent separation cascade and determined that the number of stages of the cascade could be halved by using [Aq336][D2EHP] instead of D2EHPA in the system. They reported that the extraction cascade could be reduced from eight stages to four stages and that the scrubbing cascade could be reduced from five stages to two stages. In a follow-up study, Ismail et al. [65] addressed the recovery of Sm from a MREE solution using [Aq336][D2EHP] using bench-scale data to model a cascade which was subsequently piloted. The separation factor Sm/(Eu-Gd) is on the same order of magnitude as the separation factor Sm/Eu = 1.6 and Sm/Gd = 2.53 as reported by Alstad et al. [111]

Investigation into an EHEHPA-based ABC-TSFIL extractant also produced similar results to D2EHPA-based extractants where extraction capabilities of the EHEHPA-based ABC-TSFILs are higher than EHEHPA under similar conditions while maintaining similar separation factors. In their comparative study of [Aq336][EHEHP] and EHEHPA on the extraction of HREE, Dong et al. [73] reported a 50% increased extraction capacity with similar separation factors for the extraction of HREE in chloride media. Although the [Aq336][EHEHP] system requires a slightly higher stripping solution acidity (0.2 M) than the EHEHPA system (0.13 M) to recover all REE from the organic phase, the stripping curve slope is less steep suggesting a better scrubbing efficiency at equivalent acidity.

Similar to acidic extractants, synergistic (antagonistic) interactions between ILs extractants have been proven to affect the extraction mechanism of the extraction system more than the sum of the effect of both extractants. Zhao et al. [34, 38] demonstrated that the system [P<sub>66614</sub>][EHEHP]/[Aq336][C272] produced an antagonistic effect on extraction with regard to using [Aq336][C272] by reducing the stability of the extracted species similar to the EHEHPA/C272 system [112]. This was further demonstrated by a lower required stripping acidity estimated at 1.5–2 M for the mixture of ILs compared to 3–4 M for the mixture of acidic extractants [113]. In addition, the IL mixture had substantial synergistic impact on the separation factor between the REE. This synergistic impact with regard to C272 was not significant in the acidic extractants study [112].

Notwithstanding the promises of ABC-TSFILs as extractants, similar to conventional solvent extraction research, it is essential to note that most studies are performed under dilute concentrations and may not be directly translatable to commercial applications. Of particular interest is the study of the stability of ILs. Quinn et al. [75, 76, 114] studied the effects of using a HCl medium with the extractant [Aq336][EHEHP]. They determined that under certain conditions, the IL reverted to a combination of its precursors through the extraction of HCl as shown by the following reaction:



Quinn et al. [76] studied this system over a range of pH and chloride ion concentration and concluded that:

Our results indicate that the combination of Aliquat 336 and EHEHPA behaves as a mixture of R4N EHEHP and R4N Cl<sup>-</sup> + EHEHPA, with the protonation dependent on the pH, and not as a different chemical form. Hence, regardless of how the IL has been prepared, once it is exposed to acid containing solutions, the acid-base behavior of the IL is indistinguishable from a mixture of the two reagents.

Undoubtedly, future studies will evaluate other acid-base coupling TSFILs and consider whether they too act as a combination of their precursors or as distinct extractants. Dong et al. [109] found that in the case of Cyphos 101 IL ([P<sub>66614</sub>][Cl]) and SOPAA, the ABC-TSFIL [P<sub>66614</sub>][SOPA] was significantly superior to the combination of its precursors indicating sufficient stability to be considered a distinct extractant.

### 8.3.2 Use of Ionic Liquids as Solvents

The utilization of ILs as a replacement for organic molecular solvents in rare earth solvent extraction processes has been the subject of a significant amount of research in the last decade. Table 8.6 presents a summary of the existing literature on the utilization of ILs as solvents for REE extraction systems.

Initial research focused on imidazolium [C<sub>(i)</sub>im] and pyridinium [C<sub>(i)</sub>pyr] cations using hexafluorophosphate [PF<sub>6</sub>] and bis(trifluoromethanesulfonyl)imide [NTf<sub>2</sub>] anions for their low viscosity and ease of utilization. Extraction of REE in these pure nonfunctional IL solvents did not prove significant and resulted in heavy losses of fluoride-based ILs in the aqueous phases. In order to increase the extraction capabilities of these systems, complexing agents such as carbamoylmethyl phosphine oxides (CMPO), diglycolamides (DODGA, TODGA), and conventional metal extractants such as Cyanex 923, D2EHPA, and EHEHPA have been investigated. However, environmental considerations reduced the incentive of using such ILs and the focus was reoriented toward nonfluoride ILs, especially TSFILs such as phosphonium and ammonium-based ILs using chloride or nitrate as an anion usually in combination with an extractant.

Perfluorinated imidazolium and pyridinium ILs were the first ionic liquids studied as potential replacement for organic solvents in the rare earth separation processes. While they show clear advantages such as their negligible vapor pressure and increased extraction capabilities, the cost of such ILs and the stability of the perfluorinated anion combined with its toxicity [138] in waste water effluents create significant barriers to their industrial application. To address those issues, biodegradable/incinerable ILs are increasingly the object of investigations. Such ILs are colloquially referred to as CHON ILs, referencing their elemental composition.

**Table 8.6** Utilization of ILs as solvents for REE extraction systems

Diluent	Extractant	Reference
[C <sub>2</sub> mim][Cl]	[P <sub>66614</sub> ][C272]	[39]
[P <sub>66614</sub> ][NO <sub>3</sub> ]	Self <sup>a</sup>	[50]
[P <sub>66614</sub> ][Cl]	D2EHPA	[115]
[P <sub>66614</sub> ][NTf <sub>2</sub> ]	[N <sub>4</sub> BMalBbim][NTf <sub>2</sub> ]	[86]
[Aq336][NO <sub>3</sub> ]	Self [Aq336][DGA] TBP Cyanex 923	[51, 52, 56] [55] [51] [51]
[N <sub>1444</sub> ][NTf <sub>2</sub> ]	Self [N <sub>444</sub> ][D2EHP] [C <sub>6</sub> mpyr][NTf <sub>2</sub> ] [C <sub>6</sub> mim][NTf <sub>2</sub> ]	[62]
[C <sub>6</sub> mpyr][NTf <sub>2</sub> ]	D2EHPA [C <sub>6</sub> mpyr][DEHP] [N <sub>444</sub> ][D2EHP]	[62]
[Aq336][SCN]	Self TBP Cyanex 923	[51, 80] [51] [51]
[P <sub>66614</sub> ][SCN]	Self TBP Cyanex 923	[51, 80] [51] [51]
[C <sub>2</sub> mim][PF <sub>6</sub> ]	D2EHPA	[116]
[C <sub>4</sub> mim][PF <sub>6</sub> ]	Self D2EHPA TPMDPO CMPO BzAc EHEHPA HQ	[117] [116] [118] [25, 119] [120] [121] [117]
[C <sub>6</sub> mim][PF <sub>6</sub> ]	TBP Cyanex 272 D2EHPA TOPO	[122] [122] [122] [123]
[C <sub>8</sub> mim][PF <sub>6</sub> ]	Self Cyanex 925 N1923 DEHEHP	[124] [125] [126] [127]
[C <sub>4</sub> mpyr][PF <sub>6</sub> ]	D2EHPA	[116]

(continued)

**Table 8.6** (continued)

Diluent	Extractant	Reference
[C <sub>4</sub> mim][NTf <sub>2</sub> ]	Self [Aq336][D2EHP] [C <sub>60</sub> COOHmin][NTf <sub>2</sub> ] CMPO DODGA DMDODGA TPMDPO Diaza-crown TBP TODGA	[128] [67] [85] [25] [129] [130] [118] [131] [128, 132] [132]
[C <sub>6</sub> mim][NTf <sub>2</sub> ]	[P <sub>66614</sub> ][D2EHP] [Aq336][D2EHP] D2EHPA [C <sub>6</sub> mim][D2EHP] [N <sub>4444</sub> ][D2EHP] [C <sub>60</sub> COOHmin][NTf <sub>2</sub> ] TOPO TBP	[63] [63, 67] [62, 133] [62] [62, 63] [85] [89, 123] [89, 133]
[C <sub>8</sub> mim][NTf <sub>2</sub> ]	[Aq336][D2EHP] EHEHPA DODGA [C <sub>60</sub> COOHpim][PF <sub>6</sub> ] [C <sub>60</sub> COOHmin][NTf <sub>2</sub> ]	[67] [134] [129] [79] [85]
[C <sub>10</sub> mim][NTf <sub>2</sub> ]	[Aq336][D2EHP] [C <sub>60</sub> COOHmin][NTf <sub>2</sub> ]	[67] [85]
[C <sub>12</sub> mim][NTf <sub>2</sub> ]	DODGA	[129]
[C <sub>60</sub> mim][BETI]	Self	[67]
[C <sub>(4,6,8,10)</sub> mim][BETI]	[Aq336][D2EHP]	[67]
[C <sub>(3,5,7)</sub> COOHmin][NTf <sub>2</sub> ]	Self	[84]
[PEGmim][NTf <sub>2</sub> ]	Self	[87]
[EC <sub>(4,8)</sub> pip][NTf <sub>2</sub> ]	DMDOHEMA	[135]
[C <sub>60</sub> C <sub>60</sub> m <sub>3</sub> im][I]	Self	[81]
[C <sub>60</sub> C <sub>60</sub> m <sub>3</sub> im][SCN]	Self	[81]
[N <sub>888</sub> ][DA]	Self	[102]
[P <sub>8884</sub> COOH][Cl]	Self	[54]
[P <sub>8884</sub> COOH][NO <sub>3</sub> ]	Self	[54]
[N <sub>1888</sub> ][NTf <sub>2</sub> ]	CMPO D2EHPA	[136]
[P <sub>66614</sub> ][OPBOA]	Self	[106]
[C <sub>(4,5,6)</sub> mim][NfO]	Self	[137]

<sup>a</sup>Diluent is also the extractant

Examples of such CHON ILs would include ammonium salts of fatty acids such as [N<sub>888</sub>][DA] [102, 139] or nitrates of ammonium salts such as [Aq336][NO<sub>3</sub>] [51, 52, 56]. Phosphonium-based ILs with CHON or nonfluorine halogen anions also show significantly higher degradation rates than perfluorinated anions ILs [140].

A noticeable additional advantage of the [Aq336][NO<sub>3</sub>] CHON IL investigated by Riano et al. [51] and Larsson et al. [52, 56] lies in the simultaneous usage of [Aq336][NO<sub>3</sub>] for both the extractant and the solvent. This allows for increased extraction capacity when an additional extractant is added to the IL solvent. Xiong et al. [115] compared using either [P<sub>66614</sub>][Cl] or [Aq336][NO<sub>3</sub>] as the solvent with DEHEHP as an extractant and found that the phosphonium IL has a higher extraction capability than the ammonium IL.

While these nonfluoride-based TSFILs have shown great potential for the replacement of organic solvent, their cost being one to one and a half order of magnitude higher is a major impediment to their widespread adoption in the rare earth industry. It is important to note that solvents are upwards of 35% of the solvent extraction circuit volume, which is a considerable amount for commercial separations plants. Solubility of ILs is also higher in aqueous acidic phases than their organic counterparts, leading to increased operating costs. It is currently unclear if the adoption of ILs solvents in other metals solvent extraction processes will lead to increases in production and reduction in sale prices, leading to a potential adoption by rare earth refiners.

### 8.3.3 Aqueous Two-Phase System

Aqueous Two-Phase Systems (ATPS), also referred to as Aqueous Biphasic Systems (ABS) consist of a polymer or IL phase that is fully soluble in an aqueous-rich phase under specific operating conditions but is insoluble under different operating conditions. Operating parameters involved in the phase chemistry of ATPS may include temperature, ionic strength, specific component concentration or exposure to a specific wavelength.

First proposed in the mid-1950s by Albertsson [141], ATPS were developed as an alternative to solvent extraction using a combination of a polymer, salt, and water. In 2012, Freire et al. [141] proposed a review of the ATPS literature relative to the effect of ILs on ATPS. They concluded that recent advances in IL chemistry are likely to lead to a greater adoption of the technology in the industrial sector based on the significant potential advantages of ATPS over conventional solvent extraction processes. These advantages include the absence of an organic phase, a very high mass transfer rate only limited by the reaction kinetics of the system since the extraction is undertaken in a homogeneous media and rapid phase separation. However, significant barriers remain to the mass adoption of IL-base ATPS industrial processes. The most important of which being the relatively high solubility of the IL phase in the aqueous phase after phase separation, leading to significant losses of ILs in the aqueous phase of the system.

Because of its potential value in the industry, the field of IL-based ATPS research for the separation of metal ions is seeing increased activity. The first reported extraction of a lanthanide using an IL-based ATPS was undertaken in the SolvoMet Group headed by Pr. Binnemans at KU Leuven by Hoogerstraete et al. [142] in 2013. Hoogerstraete used the IL betainium bis-(trifluoromethylsulfonyl)imide, [Hbet]



[NTf<sub>2</sub>], and the extractant betaine to extract REE and scandium (Sc) from an aqueous solution using temperature as a phase transition mechanism. They found that lanthanides had a distribution ratio slightly higher than 10 while Sc had a distribution ratio greater than 500. Building on the group's research, Depuydt et al. transitioned away from fluoride-base ILs and demonstrated that a carboxy-phosphonium IL could be used in a ATPS using sodium chloride (NaCl) concentration as a phase separation trigger [143]. The [Hbet][NTf<sub>2</sub>] and betaine extraction system were also used by Huang et al. to successfully extract REE from coal fly ash [144]. Unfortunately, none of these authors report losses of IL or fluoride in their experiments, a critical consideration for transition to industrial usage. This recognition lead Mikeli et al. to specifically investigate losses of [Hbet][NTf<sub>2</sub>] IL to its strip solution. The losses reported by Mikeli are unsatisfactory for commercial application of the concept even under optimized conditions [145].

Since 2015, additional ATP systems have been successfully investigated. These ATPS include [N<sub>1444</sub>][NO<sub>3</sub>]/NaNO<sub>3</sub> by Sun et al. [59] and [P<sub>4444</sub>][Br]/NaNO<sub>3</sub> by Chen et al. [146] both aiming at selectively extracting lanthanides from transition metals solutions. More recently, Vargas et al. [147] reported a very high separation efficiency for La/Ce using a [C<sub>2</sub>mim][Cl]/K<sub>2</sub>CO<sub>3</sub> ATPS and Alizarin Red S (ARS) as an extractant. In this study, a separation factor [DLa/DCe] of 2600 was obtained through the complexation of lanthanum ions with ARS, and its greater affinity for the IL phase following the phase separation trigger.

A novel configuration for ATPS involves its combination with traditional solvent extraction where the ATPS is contacted with an organic phase containing a traditional extractant, followed by tri-phase separation. Both three-phases organic-ATPS-based systems using a polymer and IL-based ATPS have been scarcely investigated, and they present an exciting research opportunity. Sun et al. [60] successfully used three-phase organic-IL ATPS to separate Nd from Pr and obtain a Nd-rich organic phase, a Pr-rich IL phase, and a depleted aqueous phase. In this study, Sun et al. used P507 diluted in dodecane for the organic phase, [N<sub>1444</sub>][NO<sub>3</sub>][NaNO<sub>3</sub>] for the IL phase, and a HNO<sub>3</sub>/NaNO<sub>3</sub> solution for the aqueous phase. Sun concluded that a separation factor as high as 3.5 could be attained by using a three-phase system which is much higher than the separation factor of 1.47 for the conventional solvent extraction process, or the separation factor of 1.22 obtained by ATPS separation. Interestingly, Sun also presented three-phase partitioning data pertaining to the extraction of lanthanides which strongly suggested that this system could be effectively used to separate lanthanides in light/medium and heavy groups with fewer stages than the current processes.

## 8.4 Mineral Processing

The usage of ILs in flotation was first applied in 2012 to the flotation of herbicides from yogurt [148]. In the minerals processing field, it is still a nascent research subject, with its first publication by Sahoo et al. on the flotation of quartz from naturally occurring banded hematite quartzite (BHQ) ore in 2014 [149]. Azizi et al. at

University Laval and Montreal Polytechnic had first applied the IL  $[N_{4444}][D2EHP]$  to the flotation of rare earth minerals, specifically monazite and bastnaesite [150] in 2016. They demonstrated that  $[N_{4444}][D2EHP]$  was superior to the hydroxamic-based collectors for the collection of monazite and bastnaesite from calcite, dolomite, and quartz.

Subsequently, Azizi et al. tested liquid-liquid mineral separation (i.e., a combination of heavy liquid separation and flotation) for the same material composed of bastnaesite, monazite, calcite, dolomite, and quartz using an aqueous phase containing 0.1 M  $KNO_3$  at various pHs and an organic phase containing either  $[N_{4444}][D2EHP]$ ,  $[N_{2222}][DiOctP]$  or  $[N_{2222}][DEHP]$  diluted in kerosene [151]. The experiment showed that the  $[N_{4444}][D2EHP]$  system was optimum and selective for REE minerals over gangue minerals and would outperform the equivalent flotation system discussed previously. Building on this novel research, Azizi and Larachi studied the liquid-liquid mineral separation of a mixture of bastnaesite, monazite, calcite, dolomite, and ankerite using a dual IL system [152]. In this study, the collecting IL was composed of  $[N_{4444}][D2EHP]$  while the continuous phase IL was composed of either  $[EtNH_3][NO_3]$ ,  $[Emim][SCN]$  or  $[Bmmim][BF_4]$ . The study demonstrated recoveries in the order bastnaesite > monazite > ankerite > calcite > dolomite, with both  $[EtNH_3][NO_3]$  and  $[Emim][SCN]$  outperforming the aqueous-IL liquid-liquid mineral separation system.  $[Bmim][BF_4]$  did not allow any separation, which led the author to conclude that viscosity is a significant factor in the system governing factors.

Research activity in the use of ILs for the flotation of rare earth mineral remains limited with publications on the flotation of bastnaesite using the IL  $[N_{2222}][EHEHP]$  by Li et al. in 2020 [153]. The study found that  $[N_{2222}][EHEHP]$  was effective for the flotation of hematite and bastnaesite from quartz minerals. However, the affinity was greater with hematite over bastnaesite, leading the author to test and recommend a two-stage approach in which hematite would be floated first by starving the system of the collector, followed by bastnaesite using increased collector dosages.

While the application of ILs for the mineral processing of rare earth ores appears to be promising for low iron-containing ores, the recovery of the IL from the separated minerals has not yet been addressed in the literature and may prove to be cost prohibitive. Further research in the area is expected given the high potential of this new field.

## 8.5 Electrometallurgy

The use of ILs in electrometallurgical processes promises to significantly reduce the environmental footprint associated with the production of rare earth metal by replacing the energy intensive molten salt electrolysis and metallothermic reduction processes. Key advantages of utilizing ILs in the electrochemical reduction of the lanthanides include a higher potential window than alternative mediums, virtually no vapor pressure at operating temperatures, a high-metal salt solubility, a higher conductivity than organic solvents, and more importantly a control over the water content of the electrolyte [154]. Additionally, the transition to a low-temperature

emission-free process would eliminate the large amount of carbon dioxide and per-fluorocarbon emissions currently resulting from conventional processes. It is important to note that the electrical conductivity of ILs at room temperature is approximately an order of magnitude lower than molten salts, resulting in lower electrical efficiency. This disadvantage can be mitigated by operating ILs units at high temperature ( $>100\text{ }^{\circ}\text{C}$ ) [155]. Similar to molten salt electrolysis, the existence of a stable +2 valence for samarium, europium, and ytterbium creates additional hurdles in ILs.

Table 8.7 presents a summary of relevant literature on the electrodeposition of REE in IL medium. Table 8.8 presents the nomenclature associated with the ILs listed in Table 8.7.

### 8.5.1 Imidazolium-Based ILs

The electrochemical behavior of europium in 1-hexyl-3-methylimidazolium bis(trifluoromethylsulfonyl)imide [ $\text{C}_6\text{mim}$ ][ $\text{NTf}_2$ ] medium was investigated by Rama et al. [181] Additionally, experiments were conducted where TBP and N, N-dihexyloctanamide (DHOA) were added to the system. A cyclic behavior was observed where Eu(III) would be reduced to Eu(II) at the cathode, but no metal was generated due to break down of the IL at lower voltage than reduction to metal.

Xu et al. [177] also reported that the reduction of rare earths in 1-ethyl-3-methylimidazolium dicyanamide [ $\text{Emim}$ ][DCA] at a voltage lower than the break down voltage of the IL was not possible. Xu et al. demonstrated that this issue could be circumvented by introducing Fe(II) as a co-deposition element. Similar to the electrodeposition of lanthanides in deep eutectic solvents, the addition of Fe(II) reduces the voltage needed and allows for co-deposition. It is believed that a catalytic reduction reaction occurs following the electrodeposition of a few atomic layers of iron on the cathode. It is important to note however, that the carbon residue from the degradation of the IL was found in the deposited metal. The authors concluded that additional investigation would be beneficial with a longer alkyl chain IL. This suggestion is in line with work previously undertaken in 2015 by Zhang et al. [178] where 1-butyl-3-methylimidazolium dicyanamide [ $\text{BMim}$ ][DCA] was used with lanthanum chloride to electrodeposit lanthanum while preserving the integrity of the electrolyte medium. The system presented by Zhang offers a promising avenue for the transition to an industrial process since it solves the anode reaction through the use of a chloride ion which is oxidized to chlorine.

### 8.5.2 Pyrrolidinium-Based ILs

The study of the electrodeposition of lanthanides in pyrrolidinium ILs revealed some discrepancies between the various pyrrolidinium ILs. Legeai et al. reported successful electrodeposition of lanthanum metal using 1-octyl-1-methyl-pyrrolidinium

**Table 8.7** Electrodeposition of REE in IL medium

Ionic liquid	Reduction to metal (V)	Cathodic limit (V)	Anodic limit (V)	Basis	Reference
[DEME][NTf <sub>2</sub> ]	-3.3 (Nd)	N/A	N/A	Ag/Ag <sup>+</sup>	[156]
[N <sub>1116</sub> ][NTf <sub>2</sub> ]	-3.0 (Nd)	N/A	N/A	Fc/Fc <sup>+</sup>	[157]
[P <sub>66614</sub> ][NTf <sub>2</sub> ]	-2.3 (Nd)	-3.3 (0.4% H <sub>2</sub> O) [158] -3.5 (0.1% H <sub>2</sub> O) [159]	N/A	Fc/Fc <sup>+</sup>	[158, 159]
[BMPyr][NTf <sub>2</sub> ]	-2.2 (La, Nd) -2.3 (Sm, Dy)	-3.4 to -3.5	N/A	Ag/AgCl	[155, 160]
	-2.45 (Eu)	-3.5	-1.7	Fc/Fc <sup>+</sup>	[161]
	[Me <sub>3</sub> NBu][NTf <sub>2</sub> ]	-2.2 (La) -1.95 (Ce) [162] -2.5 (Nd) -2.3 (Sm) -2.4 (Sm) [19] -2.0 (Eu) [19]	-3.6	N/A	Ag/AgCl
[Bu <sub>3</sub> MeN][NTf <sub>2</sub> ]	-2.4 (La) -2.85 (Sm) -3.0 (Eu)	-3.0	2.7	Fc/Fc <sup>+</sup>	[163]
	[Bu <sub>3</sub> MeN][NTf <sub>2</sub> ]	Simultaneous with IL break down	-1.9	2.85	Ref. Electrode
[Ln(TMP) <sub>3</sub> ][NTf <sub>2</sub> ]	-1.25 (Nd, Dy, Gd) -0.85 (Pr)	< -4	>1.5	Pt	[165]
	-2.1 (Nd)	< -4	>1.5	Ag/AgCl	[166]
	-2.5 (Sm)	-4	N/A	Pt	[167]
[Ln(DHOA) <sub>3</sub> ][NTf <sub>2</sub> ]	-3 (Nd, Eu, Dy)	N/A	N/A	Pd	[168]
[P <sub>2225</sub> ][NTf <sub>2</sub> ]	-2.5 (Nd) [169] -3.2 (Dy) [170]	-3.2	3	Fc/Fc <sup>+</sup>	[169, 170]
	[C <sub>6</sub> mim][NTf <sub>2</sub> ]	Not observed prior to IL break down	-1.75	N/A	Fc/Fc <sup>+</sup>
[C <sub>8</sub> MPyr][NTf <sub>2</sub> ]	-1.6 (La)	-2.5	N/A	AgCl/Ag	[171]
[N <sub>11</sub> N <sub>11</sub> PipGua][NTf <sub>2</sub> ]	-1 (Dy)	N/A	N/A	Pt	[172]
[Nd(DMI) <sub>x</sub> (NO <sub>3</sub> ) <sub>y</sub> ][CF <sub>3</sub> SO <sub>3</sub> ] <sub>3</sub>	-2.5 (Nd)	N/A	N/A	Ag/Ag <sup>+</sup>	[173, 174]
[BMPyr][DCA]	Simultaneous with IL break down	-2	N/A	Fc/Fc <sup>+</sup>	[175]
	-1.35 (NiLa)	-1.6	1.6	Ag/AgCl	[176]
[Emim][DCA]	-1.4 (Fe-Nd)	-1.5	N/A	Pt	[177]
[Bmim][DCA]	-1.05 (La)	-1.7	1.6	Ag/Ag <sup>+</sup>	[178]
[C <sub>4</sub> MPyr][DCA]	-2.0 (Nd)	-3.25	N/A	Fc/Fc <sup>+</sup>	[179]
[BMimCl][AlCl <sub>3</sub> ]	-1 (AlCe)	N/A	N/A	Al	[180]

Silver (Ag); Silver chloride (AgCl); Platinum (Pt); Palladium (Pd); Aluminum (Al)

**Table 8.8** Nomenclature for the ionic liquids used in electrodeposition of rare earth elements

Ionic liquid	Name
[DEME][NTf <sub>2</sub> ]	N,N-Diethyl-N-methyl-N-(2-methoxyethyl)ammonium bis(trifluoromethyl-sulfonyl)amide
[N <sub>1116</sub> ][NTf <sub>2</sub> ]	n-Hexyl-trimethyl-ammonium bis(trifluoromethyl-sulfonyl)amide
[P <sub>66614</sub> ][NTf <sub>2</sub> ]	Trihexyl(tetradecyl)phosphonium bis(trifluoromethylsulfonyl)azanide
[BMPyr][NTf <sub>2</sub> ]	1Butyl1methylpyrrolidinium bis(trifluoromethylsulfonyl)azanide
[Me <sub>3</sub> NBu][NTf <sub>2</sub> ]	N-trimethyl-N-butylammonium bis(trifluoromethylsulfonyl)azanide
[Bu <sub>3</sub> MeN][NTf <sub>2</sub> ]	Tri-Butylmethylammonium bis(trifluoromethylsulfonyl)azanide
[Ln(TMP) <sub>3</sub> ][NTf <sub>2</sub> ]	Lanthanide trimethylphosphate tribis(trifluoromethane) sulfonimide
[Ln(DHOA) <sub>3</sub> ][NTf <sub>2</sub> ]	Lanthanide dihexyloctanamide tribis(trifluoromethane) sulfonimide
[Ln(DMI) <sub>x</sub> (NO <sub>3</sub> ) <sub>y</sub> ][CF <sub>3</sub> SO <sub>3</sub> ] <sub>3</sub>	Lanthanide dimethylimidazolidinone nitrate trifluoromethanesulfonate,
[P <sub>2225</sub> ][NTf <sub>2</sub> ]	Triethyl-pentyl-phosphonium bis(trifluoromethane) sulfonimide
[C <sub>6</sub> mim][NTf <sub>2</sub> ]	1-Hexyl-3-methylimidazolium bis (trifluoromethylsulfonyl)imide
[C <sub>8</sub> MPyr][NTf <sub>2</sub> ]	1-Octyl-1-methyl-pyrrolidinium bis(trifluoromethylsulfonyl)imide
[N <sub>11</sub> N <sub>11</sub> PipGua][NTf <sub>2</sub> ]	Guanidinium bis(trifluoromethylsulfonyl)imide
[BMPyr][DCA]	Butylmethylpyrrolidinium dicyanamide
[Emim][DCA]	1-Ethyl-3-methylimidazolium dicyanamide
[Bmim][DCA]	1Butyl-3-methylimidazolium dicyanamide
[EC][AlCl <sub>3</sub> ]	Ethylene carbonate-aluminum chloride
[BMimCl][AlCl <sub>3</sub> ]	Aluminum chloride 1-butyl-3-methylimidazolium chloride

bis(trifluoromethylsulfonyl)imide [C<sub>8</sub>MPyr][NTf<sub>2</sub>]/lanthanum nitrate as an electrolyte [171]. However, the process as described was slow and inefficient. In an investigation of the electrodeposition of lanthanides in butyl methylpyrrolidinium dicyanamide medium, Razo et al. reported that a simultaneous reduction of the IL and lanthanides was occurring, preventing the utilization of [BMPyr][DCA] in such processes [182].

Pyrrolidinium ILs behave similarly to imidazolium ILs with regard to their behavior with water [183] and transition metal co-deposition. The simultaneous decomposition of the metal salt and IL can also be avoided in pyrrolidinium ILs by using a dual metal electrodeposition process where the transition metal acts as a catalyst [177]. The preparation of nickel lanthanum alloy with hydrogen evolution catalytic activity was achieved by Gao et al. using [BMPyr][DCA] in combination with lanthanum chloride and nickel chloride as an electrolyte [176]. The performance of the catalyst produced was superior to many comparable nickel rare earth catalyst, proving an interesting research avenue for solvometallurgists. [BMPyr][NTf<sub>2</sub>] was used by Manjum et al. for the co-electrodeposition of samarium cobalt SmCo7 alloy from samarium and cobalt triflimide salts [184]. However, it was noted that the morphology of the alloy as nanoparticles and nanowires caused issues with regard to its physical separation and washing from the IL medium.

In contrast, Bourbos et al. reported the successful reduction of lanthanum nitrate in 1Butyl1methylpyrrolidinium bis(trifluoromethane) sulfonimide [BMPyr][NTf<sub>2</sub>]

[160] and of lanthanum nitrate, neodymium nitrate, samarium trifluoromethanesulfonate, and dysprosium bistriflimide in both [BMPyr][NTf<sub>2</sub>] and in N-trimethyl-N-butylammonium bis(trifluoromethylsulfonyl)imide [Me<sub>3</sub>NBu][NTf<sub>2</sub>] [155]. Bourbos et al. noted that fluoride and sulfur were found in the metal product. It was not clear to the authors if the presence of these elements was the result of the sulfonimide ion adsorption or if it represented residual IL that was not washed properly. The authors rejected the possibility of IL breakdown following an analysis of the materials using Fourier transform infrared spectroscopy (FTIR) spectra where no breakdown residue could be observed [160].

Following their initial studies, Bourbos et al. successfully investigated a two-compartment process in which the anode reaction would not result in the breakdown of the IL anion [NTf<sub>2</sub>] by using neodymium chloride in dimethylsulfoxide (DMSO) in the anode compartment [155]. While the introduction of a two-compartment unit reduced the efficiency of the process, the use of a chloride salt as a feed material and the subsequent chloride oxidation to gaseous chlorine resulted in much more favorable economics and in a more environmentally friendly process.

A likely early industrial application of electrodeposition of rare earth in IL medium is the electroplating of NdFeB magnets with dysprosium and terbium followed by conventional heat treatment to increase the magnetic properties of the magnets. Suppan et al. used [BMPyr][NTf<sub>2</sub>] to electrodeposit dysprosium on NdFeB magnets and increased the magnets coercivity by 20% [185].

### 8.5.3 Phosphonium-Based ILs

The study of the electrodeposition of neodymium in phosphonium ILs revealed that phosphonium-based systems have significant inherent drawbacks to overcome before they can be implemented commercially. In order to reduce neodymium to metal in [P<sub>6614</sub>][NTf<sub>2</sub>] at low temperature with minimum degradation of the IL medium, it appears that a narrow neodymium concentration range (0.1–0.5 mol/kg) and water (0.1–2%) are required [159]. The presence of water allows for the electrodeposition process to occur in one step directly from the trivalent lanthanide as opposed to a two-step reduction from the trivalent phase to the divalent phase to the metal phase when the concentration of water is insufficient [186]. However, it is believed that the presence of water, while necessary to ensure proper speciation of neodymium in the IL, also leads to surface oxidation of the deposited metal [158] in addition to reducing the electrolyte electrochemical window [187]. The metal produced also contains significant amounts of phosphorus and sulfur which could either be caused by residual IL being present in the deposit or from break down of the IL itself.

While the effect of water is not explicitly addressed, Matsumiya suggests that increasing the temperature of the system also contributes to the successful reduction of lanthanides in phosphonium bis(trifluoromethane) sulfonimide medium [188]. It is yet to be determined whether operating at higher temperatures would be

preferable to the utilization of water with regard to a potential reduction of surface oxidation for the metal produced. In his investigations, Matsumiya successfully solubilized neodymium from a demagnetized NdFeB rod at the anode while simultaneously reducing it to metal at the cathode. His utilization of a Vycor glass filter around the anode prevented any iron from being deposited at the cathode [188].

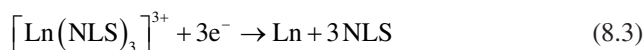
Early investigations of the electrolysis of neodymium in triethyl-pentyl-phosphonium bis(trifluoromethane) sulfonimide [P<sub>2225</sub>][NTf<sub>2</sub>] and [P<sub>1116</sub>][NTf<sub>2</sub>] by Kondo et al. had not assessed the impact of water in the system but have reached similar purity results as other investigators of this system [158, 159, 186–188] with regard to the metal produced. The poor metal reduction observed in [P<sub>1116</sub>][NTf<sub>2</sub>] was suggested to be related to the higher viscosity of [P<sub>1116</sub>][NTf<sub>2</sub>] compared to [P<sub>2225</sub>][NTf<sub>2</sub>], 153 mPa·s versus 88 mPa·s, respectively [169]. Kurachi et al. [170] failed to reduce dysprosium without breaking down the IL medium. The produced metal also contained significant amounts of sulfur, fluorine, and oxygen. Further studies by Kondo et al. evaluated the impact of lowering the water content of the ionic liquid [P<sub>2225</sub>][NTf<sub>2</sub>] and did not identify any significant impact on the electro-deposition of neodymium [189].

### 8.5.4 Neutral Ligand Complexation-Based ILs

Neutral ligand complexation-based ILs are formed by the dissolution of rare earth salts in neutral ligand solvents (NLS) such as tributyl-phosphate (TBP), trimethyl-phosphate (TMP), 1,3-dimethyl-2-imidazolidinone (DMI) or dihexyloctanamide (DHOA). The overall reaction for the formation of such ILs is represented by:



while [NTf<sub>2</sub>] is referenced in the equation, both [NTf<sub>2</sub>] and [CF<sub>3</sub>SO<sub>3</sub>] anions are currently being investigated for such systems. During the electrodeposition process, the cation portion of the IL is reduced to create a lanthanide metal and regenerate the NLS following the reaction:



Bagri et al. [165] and Sidhu [166] demonstrated that REE could be successfully deposited onto a cathode substrate using TMP as a NLS to generate a lanthanide IL cation through the dissolution of lanthanide tris(trifluoromethane) sulfonimide salt. Krishna et al. [168] achieved the same objective using DHOA as a NLS. This approach is likely to be successful commercially since the medium is very stable within the operating conditions (i.e., potential, acidity, and temperature) required for electrodeposition and the self-regeneration lends itself to a continuous process. However, similar to other IL mediums, additional research on the anodic reaction will be required to replace the decomposition of the [Ntf<sub>2</sub>] or [CF<sub>3</sub>SO<sub>3</sub>] anion with

a different anion and to allow for its reuse in the production of the lanthanide salt feed material.

Lanthanide neutral ligands complexes can also be dissolved in ILs such as the phosphonium-based IL  $[P_{2225}][NTf_2]$  and subsequently electrodeposited. Matsumiya et al. [190] demonstrated such a process following the extraction of the neodymium by TBP/ $[P_{2225}][NTf_2]$  from aqueous media. Unfortunately, as with other investigations of phosphonium-based electrodeposition, a significant amount of oxidation was present in the deposited metal [158, 159, 169, 187, 189].

### 8.5.5 Aluminum Chloride-Based ILs

The reduction of aluminum (Al) and Al alloys from aluminum chloride (AgCl)-based IL medium has been extensively investigated in the past [191–193]. However, these processes have yet been proven to be sufficiently economic to replace legacy industrial processes. The incentives with regard to REs such as the utilization of relatively inexpensive chlorides, the absence of fluorides, and a low operating temperature suggest that research into these systems is likely to increase drastically in the foreseeable future. The first foray in the subject in 1985 by Lipsztajn and Osteryoung [194] using aluminum chloride 1-methyl-3-ethylimidazolium chloride  $[AlCl_3][ImCl]$ /neodymium chloride as an electrolyte was considered a failure since it resulted in no neodymium deposition.

The first record of successful electrodeposition of a rare earth in aluminum chloride-based IL was achieved in 2001 by Tsuda et al. [195] using aluminum chloride 1-ethyl-3-methylimidazolium chloride  $[AlCl_3][EMiCl]$ /lanthanum chloride ( $LaCl_3$ ) in the presence of lithium chloride (LiCl) and thionyl chloride ( $SOCl_2$ ). It was noted however that the resulting metal layer was quickly passivated, ceasing lanthanum deposition. Building on work by Tsuda et al., Lisenkov et al. [180] investigated the electrodeposition of an aluminum cerium alloy as a corrosion inhibitor using an aluminum chloride 1-butyl-3-methylimidazolium chloride  $[AlCl_3][BMiCl]$ /cerium(III) chloride electrolyte. Unfortunately, the corrosion resistance of the deposited alloy was low due to the sequestration of chloride ions in the deposit.

## 8.6 Technology Outlook

The impact of ILs in the REE processing industry will undoubtedly increase tremendously in the coming years. The first point of entry in the commercial production sphere will likely be as a replacement for acidic extractants in the solvent extraction processes for the separation of the REE. The major impediments to this transition from research to industry lies in the inherently conservative nature of industrial separation process operators. The effort, cost, and risk associated with the retrofitting of existing processes will certainly delay and may potentially bar the



entry of ILs in the legacy industry. It is typical for such changes to be brought about by incumbents challenging the status quo. Such incumbents are currently plentiful in the United States as the government has resolved to reduce its dependence on the Chinese supply chain for REE.

A second point of entry lies in the application of ILs and solvometallurgy for the recycling of REE from spent magnets, electronics, and batteries. The industry is in its initial development and is expected to turn toward new technologies for competitiveness with legacy players. The integration of the full recycling process using ILs to dissolve, purify, and reduce the REE from such waste stream is expected to challenge the research community.

Finally, the increased attention toward environmentally friendlier ILs such as the CHON ILs may redeem the initial “green” designation that befelled perfluorinated ILs, further supporting their introduction to the industry as replacements from molecular organic solvents.

## References

1. T. Welton, Ionic liquids: a brief history. *Biophys. Rev.* **10**(3), 691–706 (2018). <https://doi.org/10.1007/s12551-018-0419-2>
2. J.S. Wilkes, A short history of ionic liquids – from molten salts to neoteric solvents. *Green Chem.* **4**(2), 73–80 (2002). <https://doi.org/10.1039/b110838g>
3. C. Austen Angell, Y. Ansari, Z. Zhao, Ionic liquids: past, present and future. *Faraday Discuss.* **154**(1), 9–27 (2012). <https://doi.org/10.1039/c1fd00112d>
4. A. Mohammad, Inamuddin, *Green Solvents II: Properties and Applications of Ionic Liquids* (Springer, Dordrecht, 2012)
5. T.P. Thuy Pham, C.W. Cho, Y.S. Yun, Environmental fate and toxicity of ionic liquids: a review. *Water Res.* **44**(2), 352–372 (2010). <https://doi.org/10.1016/j.watres.2009.09.030>
6. M. Francisco Casal, A. Bruinhorst, L.F. Zubeir, C.J. Peters, M.C. Kroon, Ionic liquids vs. deep eutectic solvents, in 248th ACS National Meeting & Exposition, August 10–14, 2014, San Francisco, California, 2014
7. D. Dupont, K. Binnemans, Recycling of rare earths from NdFeB magnets using a combined leaching/extraction system based on the acidity and thermomorphism of the ionic liquid [Hbet][Tf2N]. *Green Chem.* **17**(4), 2150–2163 (2015). <https://doi.org/10.1039/c5gc00155b>
8. M. Orefice, A. Van den Bulck, K. Binnemans, T. Vander Hoogerstraete, Metal coordination in the high-temperature leaching of roasted NdFeB magnets with the ionic liquid betainium bis(trifluoromethylsulfonyl)imide. *RSC Adv.* **8**(17), 9299–9310 (2018). <https://doi.org/10.1039/c8ra00198g>
9. M. Orefice, A. Van den Bulck, B. Blanpain, K. Binnemans, Selective roasting of Nd–Fe–B permanent magnets as a pretreatment step for intensified leaching with an ionic liquid. *J. Sustain. Metall.* **6**(1), 91–102 (2020). <https://doi.org/10.1007/s40831-019-00259-1>
10. P. Davris, E. Balomenos, D. Pnias, I. Paspaliaris, Leaching of bauxite residue using task specific ionic liquid HbetTf2N. *Proc. Eur. Metall. Conf. EMC 2015* **1**, 325–336 (2015)
11. P. Davris, E. Balomenos, D. Pnias, I. Paspaliaris, Selective leaching of rare earth elements from bauxite residue (red mud), using a functionalized hydrophobic ionic liquid. *Hydrometallurgy* **164**, 125–135 (2016). <https://doi.org/10.1016/j.hydromet.2016.06.012>
12. C. Bonomi, P. Davris, E. Balomenos, I. Giannopoulou, Ionometallurgical leaching process of bauxite residue: a comparison between hydrophilic and hydrophobic ionic liquids, in Proceedings of 35th International ICSOBA Conference, Hamburg, Germany, no. 636876, 2–5 October 2017, pp. 1–8

13. D. Dupont, K. Binnemans, Rare earth recycling using a functionalized ionic liquid for the selective dissolution and revalorization of  $Y_2O_3:Eu^{3+}$  from lamp phosphor waste. *Green Chem.* **17**(2), 856–868 (2015). <https://doi.org/10.1039/c4gc02107j>
14. B. Grymonprez, *Recovery of Rare Earths from Lamp Phosphor Waste: A Solvometallurgical Approach* (KU Leuven, Leuven, 2018)
15. P. Davris, D. Marinos, E. Balomenos, A. Alexandri, M. Gregou, D. Panias, I. Paspaliaris, Leaching of rare earth elements from “Rödberg” ore of fen carbonatite complex deposit, using the ionic liquid HbetTf2N. *Hydrometallurgy* **175**, 20–27 (2018). <https://doi.org/10.1016/j.hydromet.2017.10.031>
16. J.W. Freiderich, J.J. Stankovich, H. Luo, S. Dai, B.A. Moyer, Dissolution of the rare earth mineral bastnaesite by acidic amide ionic liquid for recovery of critical materials. *Eur. J. Inorg. Chem.* **2015**(26), 4354–4361 (2015). <https://doi.org/10.1002/ejic.201500509>
17. A.K. Sahin, D. Voßenkaul, N. Stoltz, S. Stopic, M.N. Saridede, B. Friedrich, Selectivity potential of ionic liquids for metal extraction from slags containing rare earth elements. *Hydrometallurgy* **169**, 59–67 (2017). <https://doi.org/10.1016/j.hydromet.2016.12.002>
18. N. Schaeffer, H. Passos, I. Billard, N. Papaiconomou, J.A.P. Coutinho, Recovery of metals from waste electrical and electronic equipment (WEEE) using unconventional solvents based on ionic liquids. *Crit. Rev. Environ. Sci. Technol.* **48**(13–15), 859–922 (2018). <https://doi.org/10.1080/10643389.2018.1477417>
19. B. Martinez, The electrochemical deposition of samarium and europium dissolved in ionic liquid solvent. UNLV Theses, Dissertations, Professional Papers, and Capstones, 3150, 2017
20. X. Li, A. Van Den Bossche, T. Vander Hoogerstraete, K. Binnemans, Ionic liquids with trichloride anions for oxidative dissolution of metals and alloys. *Chem. Commun.* **54**(5), 475–478 (2018). <https://doi.org/10.1039/c7cc08645h>
21. X. Li, Z. Li, K. Binnemans, Closed-loop process for recovery of metals from NdFeB magnets using a trichloride ionic liquid. *Sep. Purif. Technol.* **275**, 119158 (2021). <https://doi.org/10.1016/j.seppur.2021.119158>
22. K. Hu, H. Gao, Y. Nie, H. Dong, J. Yan, X. Zhang, F. Li, Efficient selective separation of yttrium from holmium and erbium using carboxyl functionalized ionic liquids. *Sep. Purif. Technol.* **269**, 117800 (2021). <https://doi.org/10.1016/j.seppur.2021.118774>
23. Y. Wang, C. Huang, F. Li, Y. Dong, X. Sun, Process for the separation of thorium and rare earth elements from radioactive waste residues using Cyanex®572 as a new extractant. *Hydrometallurgy* **169**, 158–164 (2017). <https://doi.org/10.1016/j.hydromet.2017.01.005>
24. L.Y. Wang, Q.J. Guo, M.S. Lee, Recent advances in metal extraction improvement: mixture systems consisting of ionic liquid and molecular extractant. *Sep. Purif. Technol.* **210**, 292–303 (2019). <https://doi.org/10.1016/j.seppur.2018.08.016>
25. Y. Baba, F. Kubota, N. Kamiya, M. Goto, Recent advances in extraction and separation of rare earth metals using ionic liquids. *J. Chem. Eng. Jpn.* **44**(10 Special Issue), 679–685 (2011). <https://doi.org/10.1252/jcej.10we279>
26. W. Su, J. Chen, Y. Jing, Aqueous partition mechanism of organophosphorus extractants in rare earths extraction. *Ind. Eng. Chem. Res.* **55**(30), 8424–8431 (2016). <https://doi.org/10.1021/acs.iecr.6b01709>
27. M. Panigrahi, M. Grabda, D. Kozak, A. Dorai, E. Shibata, J. Kawamura, T. Nakamura, Liquid–liquid extraction of neodymium ions from aqueous solutions of  $NdCl_3$  by phosphonium-based ionic liquids. *Sep. Purif. Technol.* **171**, 263–269 (2016). <https://doi.org/10.1016/j.seppur.2016.07.044>
28. X. Su, X. Guo, Z. Zhao, Y. Dong, Y. Wang, F. Li, X. Sun, An efficient and sustainable  $[P_6,6,6,14]_2[BDOAC]$  ionic liquid based extraction–precipitation strategy for rare earth recovery. *Chem. Eng. Res. Des.* **136**, 786–794 (2018). <https://doi.org/10.1016/j.cherd.2018.06.029>
29. L. Qiu, Y. Pan, W. Zhang, A. Gong, Application of a functionalized ionic liquid extractant tributylmethylammonium dibutylidiglycolamate ( $[A336][BDGA]$ ) in light rare earth extraction and separation. *PLoS One* **13**(8), 1–13 (2018). <https://doi.org/10.1371/journal.pone.0201405>

30. A. Kumari, M.K. Sinha, S.K. Sahu, B.D. Pandey, Extractive separation of La and Nd using ionic liquid as extractant, in 18th International Conference on Non-ferrous Minerals & Metals, vol. III, 2014, pp. 1–6
31. Y. Liu, H.S. Jeon, M.S. Lee, Solvent extraction of Pr and Nd from chloride solution by the mixtures of Cyanex 272 and amine extractants. *Hydrometallurgy* **150**, 61–67 (2014). <https://doi.org/10.1016/j.hydromet.2014.09.015>
32. Y. Liu, H.S. Jeon, M.S. Lee, Separation of Pr and Nd from La in chloride solution by extraction with a mixture of Cyanex 272 and Alamine 336. *Met. Mater. Int.* **21**(5), 944–949 (2015). <https://doi.org/10.1007/s12540-015-5113-3>
33. C.G. Oh, S.H. Son, M.S. Lee, Separation of Tb(III) and Dy(III) from chloride solution by extraction and scrubbing with ionic liquid prepared with Cyanex 272 and Aliquat 336. *J. Korean Inst. Met. Mater.* **57**(8), 499–505 (2019). <https://doi.org/10.3365/KJMM.2019.57.8.499>
34. Z. Zhao, H. Lyu, X. Guo, Y. Dong, Y. Wang, X. Sun, The synergistic extraction by combined ammonium and phosphonium type ionic liquids for rare earth elements separation. *Hydrometallurgy* **174**, 234–247 (2017). <https://doi.org/10.1016/j.hydromet.2017.05.020>
35. E. Padhan, K. Sarangi, Recovery of Nd and Pr from NdFeB magnet leachates with bifunctional ionic liquids based on Aliquat 336 and Cyanex 272. *Hydrometallurgy* **167**, 134–140 (2017). <https://doi.org/10.1016/j.hydromet.2016.11.008>
36. N. Devi, L.B. Sukla, Studies on liquid-liquid extraction of yttrium and separation from other rare earth elements using bifunctional ionic liquids. *Miner. Process. Extr. Metall. Rev.* **40**(1), 46–55 (2019). <https://doi.org/10.1080/08827508.2018.1481058>
37. X. Sun, Y. Dong, Y. Wang, Y. Chai, The synergistic extraction of heavy rare earth elements using EHEHP-type and BTMPP-type functional ionic liquids. *RSC Adv.* **5**(61), 49500–49507 (2015). <https://doi.org/10.1039/C5RA05884H>
38. Z. Zhao, X. Sun, Y. Dong, Y. Wang, Synergistic effect of acid-base coupling bifunctional ionic liquids in impregnated resin for rare earth adsorption. *ACS Sustain. Chem. Eng.* **4**(2), 616–624 (2016). <https://doi.org/10.1021/acsschemeng.5b01253>
39. A. Rout, S. Wellens, K. Binnemans, Separation of rare earths and nickel by solvent extraction with two mutually immiscible ionic liquids. *RSC Adv.* **4**(11), 5753–5758 (2014). <https://doi.org/10.1039/c3ra46261g>
40. B.B. Mishra, N. Devi, K. Sarangi, Recovery of samarium and cobalt from Sm–Co magnet waste using a phosphonium ionic liquid Cyphos IL 104. *J. Sustain. Metall.* **6**(3), 410–418 (2020). <https://doi.org/10.1007/s40831-020-00283-6>
41. B.B. Mishra, N. Devi, K. Sarangi, Solvent extraction and separation of samarium from transition and rare earth metals using phosphonium ionic liquid Cyphos IL 104. *Monatsh. Chem.* **152**(7), 767–775 (2021). <https://doi.org/10.1007/s00706-021-02792-w>
42. A. Kumari, M.K. Sinha, S.K. Sahu, B.D. Pandey, Solvent extraction and separation of trivalent lanthanides using Cyphos IL 104, a novel phosphonium ionic liquid as extractant. *Solvent Extr. Ion Exch.* **34**(5), 469–484 (2016). <https://doi.org/10.1080/07366299.2016.1207459>
43. B.B. Mishra, N. Devi, Solvent extraction and separation of europium (III) using a phosphonium ionic liquid and an organophosphorus extractant – a comparative study. *J. Mol. Liq.* **271**(III), 389–396 (2018). <https://doi.org/10.1016/j.molliq.2018.08.160>
44. L. Ma, Z. Zhao, Y. Dong, X. Sun, A synergistic extraction strategy by [N1888][SOPAA] and Cyphos IL 104 for heavy rare earth elements separation. *Sep. Purif. Technol.* **174**, 474–481 (2017). <https://doi.org/10.1016/j.seppur.2016.10.046>
45. Z. Zeng, X. Su, Y. Gao, G. Yu, S. Ni, J. Su, X. Sun, Separation of lutetium using a novel bifunctional ionic liquid based on phosphonate functionalization. *Sep. Purif. Technol.* **264**, 118439 (2021). <https://doi.org/10.1016/j.seppur.2021.118439>
46. T. Vander Hoogerstraete, E.R. Souza, B. Onghena, D. Banerjee, K. Binnemans, Mechanism for solvent extraction of lanthanides from chloride media by basic extractants. *J. Solut. Chem.* **47**(8), 1351–1372 (2018). <https://doi.org/10.1007/s10953-018-0782-4>

47. C. Huang, Y. Wang, B. Huang, Y. Dong, X. Sun, The recovery of rare earth elements from coal combustion products by ionic liquids. *Miner. Eng.* **130**, 142–147 (2019). <https://doi.org/10.1016/j.mineng.2018.10.002>
48. S. Sobekova Foltova, T. Vander Hoogerstraete, D. Banerjee, K. Binnemans, Samarium/cobalt separation by solvent extraction with undiluted quaternary ammonium ionic liquids. *Sep. Purif. Technol.* **210**, 209–218 (2019). <https://doi.org/10.1016/j.seppur.2018.07.069>
49. Y. Zhang, W. Guo, D. Liu, J. Xu, Rational design of novel carboxylic acid functionalized phosphonium based ionic liquids as high performance extractants for rare earths. *J. Rare Earths* **39**, 1435–1441 (2021). <https://doi.org/10.1016/j.jre.2020.10.005>
50. T. Vander Hoogerstraete, K. Binnemans, Highly efficient separation of rare earths from nickel and cobalt by solvent extraction with the ionic liquid trihexyl(tetradecyl)phosphonium nitrate: a process relevant to the recycling of rare earths from permanent magnets and nickel metal hydride batteries. *Green Chem.* **16**(3), 1594–1606 (2014). <https://doi.org/10.1039/c3gc41577e>
51. S. Riaño, S. Sobekova Foltova, K. Binnemans, Separation of neodymium and dysprosium by solvent extraction using ionic liquids combined with neutral extractants: batch and mixer-settler experiments. *RSC Adv.* **10**(1), 307–316 (2019). <https://doi.org/10.1039/c9ra08996a>
52. K. Larsson, K. Binnemans, Applying ionic liquids to rare earth separations, in 1st Conference on European Rare Earth Resources (ERES 2014), 2014, pp. 278–290
53. A. Rout, K. Binnemans, Liquid-liquid extraction of europium(III) and other trivalent rare earth ions using a non-fluorinated functionalized ionic liquid. *Dalton Trans.* **43**(4), 1862–1872 (2014). <https://doi.org/10.1039/c3dt52285g>
54. W. Zhang, R. Honaker, Process development for the recovery of rare earth elements and critical metals from an acid mine leachate. *Miner. Eng.* **153**, 106382 (2020). <https://doi.org/10.1016/j.mineng.2020.106382>
55. A. Rout, K. Binnemans, Solvent extraction of neodymium(III) by functionalized ionic liquid trioctylmethylammonium dioctyl diglycolamate in fluorine-free ionic liquid diluent. *Ind. Eng. Chem. Res.* **53**(15), 6500–6508 (2014). <https://doi.org/10.1021/ie404340p>
56. K. Larsson, K. Binnemans, Separation of rare earths by solvent extraction with an undiluted nitrate ionic liquid. *J. Sustain. Metall.* **3**(1), 73–78 (2017). <https://doi.org/10.1007/s40831-016-0074-4>
57. S. Acharya, S. Mishra, Studies on solvent extraction of La(III) using [A336][NO<sub>3</sub><sup>-</sup>] and modeling by statistical analysis and neural network. *Sep. Sci. Technol.* **52**(10), 1660–1669 (2017). <https://doi.org/10.1080/01496395.2017.1296870>
58. A. Kumari, K.K. Sahu, S.K. Sahu, Solvent extraction and separation of Nd, Pr and Dy from leach liquor of waste NdFeB magnet using the nitrate form of Mextral®336At in the presence of aquo-complexing agent EDTA. *Metals* **9**(2), 269 (2019). <https://doi.org/10.3390/met9020269>
59. P. Sun, K. Huang, W. Song, Z. Gao, H. Liu, Separation of rare earths from the transition metals using a novel ionic-liquid-based aqueous two-phase system: toward green and efficient recycling of rare earths from the NdFeB magnets. *Ind. Eng. Chem. Res.* **57**(49), 16934–16943 (2018). <https://doi.org/10.1021/acs.iecr.8b04549>
60. P. Sun, K. Huang, H. Liu, Separation of adjacent rare earth elements enhanced by “external push-pull” extraction system: an example for the separation of Pr and Nd. *Hydrometallurgy* **189**, 105136 (2019). <https://doi.org/10.1016/j.hydromet.2019.105136>
61. J.P. Leal, J. Marçalo, Deliverable D3.2: report on the perspectives of separation of REE from other metals by ionic liquids, 2017, pp. 1–21
62. A. Rout, J. Kotlarska, W. Dehaen, K. Binnemans, Liquid-liquid extraction of neodymium(III) by dialkylphosphate ionic liquids from acidic medium: the importance of the ionic liquid cation. *Phys. Chem. Chem. Phys.* **15**(39), 16533–16541 (2013). <https://doi.org/10.1039/c3cp52218k>
63. X. Sun, H. Luo, S. Dai, Solvent extraction of rare earth ions based on functionalized ionic liquids. *Talanta* **90**, 132–137 (2012). <https://doi.org/10.1016/j.talanta.2011.12.069>

64. N.A. Ismail, M.Y. Mohd Yunus, M.A. Abdul Aziz, M.A. Abidin, Comparison of optimal solvent extraction stages between P204 and [A336][P204] for the separation of europium and gadolinium. *IOP Conf. Ser. Mater. Sci. Eng.* **702**(1), 012044 (2019). <https://doi.org/10.1088/1757-899X/702/1/012044>
65. N.A. Ismail, M.A. Abd Aziz, A. Hisyam, M.A. Abidin, Separation of samarium from medium rare earth mixture using multi-stage counter-current extraction. *Chem. Eng. Commun.* **208**(5), 764–774 (2020). <https://doi.org/10.1080/00986445.2020.1746654>
66. H. Yang, W. Wang, H. Cui, D. Zhang, Y. Liu, J. Chen, Recovery of rare earth elements from simulated fluorescent powder using bifunctional ionic liquid extractants (Bif-ILEs). *J. Chem. Technol. Biotechnol.* **87**(2), 198–205 (2012). <https://doi.org/10.1002/jctb.2696>
67. X. Sun, H. Luo, S. Dai, Mechanistic investigation of solvent extraction based on anion-functionalized ionic liquids for selective separation of rare earth ions. *Dalton Trans.* **42**(23), 8270–8275 (2013). <https://doi.org/10.1039/c3dt50148e>
68. L. Guo, J. Chen, L. Shen, J. Zhang, D. Zhang, Y. Deng, Highly selective extraction and separation of rare earths(III) using bifunctional ionic liquid extractant. *ACS Sustain. Chem. Eng.* **2**(8), 1968–1975 (2014). <https://doi.org/10.1021/sc400541b>
69. X. Sun, K.E. Waters, The adjustable synergistic effects between acid-base coupling bifunctional ionic liquid extractants for rare earth separation. *AICHE J.* **60**(11), 3859–3868 (2014). <https://doi.org/10.1002/aic.14563>
70. S.N. Kalyakin, V.I. Kuz'Min, M.A. Mulagaleeva, Binary extraction of lanthanide(III) chlorides using carboxylates and dialkylphosphates of secondary and tertiary amines. *Hydrometallurgy* **151**, 116–121 (2015). <https://doi.org/10.1016/j.hydromet.2014.11.013>
71. M. Khodakarami, Development of functional ionic liquids for separation and recovery of rare earth elements. Doctoral Dissertations, Missouri University of Science and Technology, 2019
72. M. Khodakarami, L. Alagha, Separation and recovery of rare earth elements using novel ammonium-based task-specific ionic liquids with bidentate and tridentate O-donor functional groups. *Sep. Purif. Technol.* **232**, 115952 (2020). <https://doi.org/10.1016/j.seppur.2019.115952>
73. Y. Dong, X. Sun, Y. Wang, Y. Chai, The development of an extraction strategy based on EHEHP-type functional ionic liquid for heavy rare earth element separation. *Hydrometallurgy* **157**, 256–260 (2015). <https://doi.org/10.1016/j.hydromet.2015.09.004>
74. L. Shen, J. Chen, L. Chen, C. Liu, D. Zhang, Y. Zhang, W. Su, Y. Deng, Extraction of mid-heavy rare earth metal ions from sulphuric acid media by ionic liquid [A336][P507]. *Hydrometallurgy* **161**, 152–159 (2016). <https://doi.org/10.1016/j.hydromet.2016.01.015>
75. J.E. Quinn, K.H. Soldenhoff, G.W. Stevens, Solvent extraction of rare earth elements using a bifunctional ionic liquid. Part 2: Separation of rare earth elements. *Hydrometallurgy* **169**, 621–628 (2017). <https://doi.org/10.1016/j.hydromet.2017.04.003>
76. J.E. Quinn, K.H. Soldenhoff, G.W. Stevens, Solvent extraction of rare earths using a bifunctional ionic liquid. Part 1: Interaction with acidic solutions. *Hydrometallurgy* **169**, 306–313 (2017). <https://doi.org/10.1016/j.hydromet.2017.02.008>
77. H. Xu, L. Zhang, Z. Pang, Z. Wang, W. Li, J. Deng, The study on extraction behavior of [N1888][P507] and TRPO for heavy rare earths. *Miner. Eng.* **176**, 107339 (2022). <https://doi.org/10.1016/j.mineng.2021.107339>
78. X. Sun, K.E. Waters, Pyrolysis of heavy oil in the presence of supercritical water: the reaction kinetics in different phases. *AICHE J.* **61**(3), 857–866 (2015). <https://doi.org/10.1002/aic>
79. W. Wang, Y. Liu, A. Xu, H. Yang, H. Cui, J. Chen, Solvent extraction of yttrium by task-specific ionic liquids bearing carboxylic group. *Chin. J. Chem. Eng.* **20**(1), 40–46 (2012). [https://doi.org/10.1016/S1004-9541\(12\)60361-9](https://doi.org/10.1016/S1004-9541(12)60361-9)
80. R. Banda, F. Forte, B. Onghena, K. Binnemans, Yttrium and europium separation by solvent extraction with undiluted thiocyanate ionic liquids. *RSC Adv.* **9**(9), 4876–4883 (2019). <https://doi.org/10.1039/c8ra09797f>

81. S. Raiguel, D. Depuydt, T. Vander Hoogerstraete, J. Thomas, W. Dehaen, K. Binnemans, Selective alkaline stripping of metal ions after solvent extraction by base-stable 1,2,3-triazolium ionic liquids. *Dalton Trans.* **46**(16), 5269–5278 (2017). <https://doi.org/10.1039/c7dt00624a>
82. M. Matsumiya, D. Nomizu, Y. Tsuchida, Y. Sasaki, Separation of rare earth elements by synergistic solvent extraction with phosphonium-based ionic liquids using a  $\beta$ -diketone extractant and a neutral ligand. *Solvent Extr. Ion Exch.* **39**(7), 764–784 (2021). <https://doi.org/10.1080/07366299.2021.1889761>
83. M. Gras, N. Papaiconomou, E. Chainet, F. Tedjar, I. Billard, Separation of cerium(III) from lanthanum(III), neodymium(III) and praseodymium(III) by oxidation and liquid-liquid extraction using ionic liquids. *Sep. Purif. Technol.* **178**(III), 169–177 (2017). <https://doi.org/10.1016/j.seppur.2017.01.035>
84. Y. Chen, H. Wang, Y. Pei, J. Ren, J. Wang, pH-controlled selective separation of neodymium (III) and samarium (III) from transition metals with carboxyl-functionalized ionic liquids. *ACS Sustain. Chem. Eng.* **3**(12), 3167–3174 (2015). <https://doi.org/10.1021/acssuschemeng.5b00742>
85. Y. Chen, H. Wang, Y. Pei, J. Wang, Selective separation of scandium (III) from rare earth metals by carboxyl-functionalized ionic liquids. *Sep. Purif. Technol.* **178**(3), 261–268 (2017). <https://doi.org/10.1016/j.seppur.2017.01.058>
86. R. Boyd, C. Carroll, S. Dandil, C. Acikgoz, R. Ruhela, P. Nockemann, Malonamide-functionalized ionic liquid for recovery of rare earth metals from end-of-life products (lamp phosphors). *ACS Sustain. Chem. Eng.* **8**(50), 18706–18711 (2020). <https://doi.org/10.1021/acssuschemeng.0c07897>
87. X. Guo, W. Yao, Y. Chen, J. Fan, Y. Zhao, J. Wang, PEG-functionalized ionic liquids: a class of liquid materials for highly efficient extraction of rare earth metals from aqueous solutions. *J. Mol. Liq.* **236**, 308–313 (2017). <https://doi.org/10.1016/j.molliq.2017.04.044>
88. A.N. Turanov, V.K. Karandashev, V.A. Khvostikov, Synergistic extraction of lanthanides (III) with mixtures of TODGA and hydrophobic ionic liquid into molecular diluent. *Solvent Extr. Ion Exch.* **35**(7), 461–479 (2017). <https://doi.org/10.1080/07366299.2017.1355170>
89. M. Asadollahzadeh, R. Torkaman, M. Torab-Mostaedi, A. Hemmati, Enhancing cerium recovery from leaching solution of glass polishing powder waste using imidazolium ionic liquid. *Waste Biomass Valorization* **12**, 1529–1538 (2021). <https://doi.org/10.1007/s12649-020-01070-w>
90. Y. Dong, X. Guo, Y. Wang, Z. Zhao, C. Huang, X. Sun, A separation processing for industrial rare earth feed solution by phosphonium ionic liquid type saponification strategy. *J. Rare Earths* **35**(3), 290–299 (2017). [https://doi.org/10.1016/S1002-0721\(17\)60912-8](https://doi.org/10.1016/S1002-0721(17)60912-8)
91. C. Huang, B. Huang, Y. Dong, J. Chen, Y. Wang, X. Sun, Efficient and sustainable regeneration of bifunctional ionic liquid for rare earth separation. *ACS Sustain. Chem. Eng.* **5**(4), 3471–3477 (2017). <https://doi.org/10.1021/acssuschemeng.7b00159>
92. W. Wang, H. Yang, H. Cui, D. Zhang, Y. Liu, J. Chen, Application of bifunctional ionic liquid extractants [A336][CA-12] and [A336][CA-100] to the lanthanum extraction and separation from rare earths in the chloride medium. *Ind. Eng. Chem. Res.* **50**(12), 7534–7541 (2011). <https://doi.org/10.1021/ie2001633>
93. L. Chen, J. Chen, Y. Jing, D. Li, Comprehensive appraisal and application of novel extraction system for heavy rare earth separation on the basis of coordination equilibrium effect. *Hydrometallurgy* **165**, 351–357 (2016). <https://doi.org/10.1016/j.hydromet.2015.12.007>
94. X.G. Guo, R.O. Yang, Y. Gong, Z. Jiang, Y. Dong, X. Sun, Insights into the coordination and extraction of yttrium(III) ions with a phenoxyacetic acid ionic-liquid extractant. *Eur. J. Inorg. Chem.* **2017**(17), 2332–2339 (2017). <https://doi.org/10.1002/ejic.201601491>
95. H. Su, S. Ni, C. Bie, S. Wu, X. Sun, Efficient and sustainable separation of yttrium from heavy rare earth using functionalized ionic liquid [N1888][NDA]. *Sep. Purif. Technol.* **285**, 120302 (2022). <https://doi.org/10.1016/j.seppur.2021.120302>

96. Y. Deng, Y. Ding, Z. Huang, Y. Yu, J. He, Y. Zhang, Boosting the extraction of rare earth elements from chloride medium by novel carboxylic acid based ionic liquids. *J. Mol. Liq.* **329**, 115549 (2021). <https://doi.org/10.1016/j.molliq.2021.115549>
97. Y. Wang, Y. Wang, H. Zhou, F. Li, X. Sun, Extraction kinetics of mixed rare earth elements with bifunctional ionic liquid using a constant interfacial area cell. *RSC Adv.* **7**(63), 39556–39563 (2017). <https://doi.org/10.1039/c7ra07851j>
98. L. Chen, J. Chen, H. Li, M. Yang, D. Zou, Y. Deng, Y. Liu, Applying basic research on a dialkylphosphoric acid based task-specific ionic liquid for the solvent extraction and membrane separation of yttrium. *Sep. Purif. Technol.* **207**, 179–186 (2018). <https://doi.org/10.1016/j.seppur.2018.06.042>
99. S. Pavón, A. Fortuny, M.T. Coll, A.M. Sastre, Neodymium recovery from NdFeB magnet wastes using Primene 81R-Cyanex 572 IL by solvent extraction. *J. Environ. Manag.* **222**, 359–367 (2018). <https://doi.org/10.1016/j.jenvman.2018.05.054>
100. H. Zhou, Y. Wang, X. Guo, Y. Dong, X. Su, X. Sun, The recovery of rare earth by a novel extraction and precipitation strategy using functional ionic liquids. *J. Mol. Liq.* **254**, 414–420 (2018). <https://doi.org/10.1016/j.molliq.2018.01.078>
101. Q. Chen, S. Ni, G. Ai, T. Zhang, X. Sun, A recovery strategy of Sm, Co for waste SmCo magnets by fatty acid based ionic liquids. *Miner. Eng.* **158**, 106581 (2020). <https://doi.org/10.1016/j.mineng.2020.106581>
102. M. Matsumoto, T. Yamaguchi, Y. Tahara, Extraction of rare earth metal ions with an undiluted hydrophobic pseudoprotic ionic liquid. *Metals* **10**(4), 2–7 (2020). <https://doi.org/10.3390/met10040502>
103. F. Li, Z. Xiao, J. Zeng, J. Chen, X. Sun, Recovery of REEs from leaching liquor of ion-adsorbed-type rare earths ores using ionic liquid based on cooking oil. *Hydrometallurgy* **196**, 105449 (2020). <https://doi.org/10.1016/j.hydromet.2020.105449>
104. E. Obón, A. Fortuny, M.T. Coll, A.M. Sastre, Experimental and modelling studies of neodymium solvent extraction from chloride media with methyl-tri(octyl/decyl)ammonium oleate ionic liquid diluted in kerosene. *Hydrometallurgy* **174**, 216–226 (2017). <https://doi.org/10.1016/j.hydromet.2017.10.021>
105. E. Obón, A. Fortuny, M.T. Coll, A.M. Sastre, Mathematical modelling of neodymium, terbium and dysprosium solvent extraction from chloride media using methyl-tri(octyl/decyl)ammonium oleate ionic liquid as extractant. *Hydrometallurgy* **173**, 84–90 (2017). <https://doi.org/10.1016/j.hydromet.2017.08.011>
106. X. Su, W. Xie, X. Sun, A sustainable [P6,6,6,14]2[OPBOA]-based separation process of rare earth and transition metal in waste NiMH battery. *Miner. Eng.* **160**, 106641 (2021). <https://doi.org/10.1016/j.mineng.2020.106641>
107. C.G.N. War, Steric effects in solvent extraction of yttrium and lanthanum by hydrogen 2-ethylhexyl phenacylphosphonate. *J. Inorg. Nucl. Chem.* **23**(1947), 103–108 (1961)
108. K. Hu, H. Gao, Y. Nie, H. Dong, J. Yan, Efficient selective separation of yttrium from holmium and erbium using carboxyl functionalized ionic liquids. *Sep. Purif. Technol.* **269**, 118774 (2021). <https://doi.org/10.1016/j.seppur.2021.118774>
109. Y. Dong, X. Sun, Y. Wang, C. Huang, Z. Zhao, The sustainable and efficient ionic liquid-type saponification strategy for rare earth separation processing. *ACS Sustain. Chem. Eng.* **4**(3), 1573–1580 (2016). <https://doi.org/10.1021/acsschemeng.5b01499>
110. Y. Wang, W. Liao, D. Li, A solvent extraction process with mixture of CA12 and Cyanex272 for the preparation of high purity yttrium oxide from rare earth ores. *Sep. Purif. Technol.* **82**(1), 197–201 (2011). <https://doi.org/10.1016/j.seppur.2011.09.018>
111. J. Alstad, J.H. Augustson, T. Danielsen, L. Farbu, A comparative study of the rare earth elements in extraction by HDEHP/Shell Sol T from nitric and sulfuric acid solution. *Proc. Int. Solvent Extr. Conf.* **2**, 1083–1102 (1974)
112. J.E. Quinn, K.H. Soldenhoff, G.W. Stevens, N.A. Lengkeek, Solvent extraction of rare earth elements using phosphonic/phosphinic acid mixtures. *Hydrometallurgy* **157**, 298–305 (2015). <https://doi.org/10.1016/j.hydromet.2015.09.005>

113. T. Liu, J. Chen, H. Li, K. Li, D. Li, Further improvement for separation of heavy rare earths by mixtures of acidic organophosphorus extractants. *Hydrometallurgy* **188**, 73–80 (2019). <https://doi.org/10.1016/j.hydromet.2019.06.008>
114. J.E. Quinn, Synergistic solvent extraction of rare earth elements. PhD Thesis, The University of Melbourne, 2017
115. Y. Xiong, W. Kuang, J. Zhao, H. Liu, Ionic liquid-based synergistic extraction of rare earths nitrates without diluent: typical ion-association mechanism. *Sep. Purif. Technol.* **179**, 349–356 (2017). <https://doi.org/10.1016/j.seppur.2017.02.026>
116. S.J. Yoon, J.G. Lee, H. Tajima, A. Yamasaki, F. Kiyono, T. Nakazato, H. Tao, Extraction of lanthanide ions from aqueous solution by bis(2-ethylhexyl)phosphoric acid with room temperature ionic liquids. *J. Ind. Eng. Chem.* **16**(3), 350–354 (2010). <https://doi.org/10.1016/j.jiec.2009.09.063>
117. Z. Pan, S. Zhao, T. Wu, J. Pan, Extraction behavior of rare earths in ion liquid extraction system using 1-butyl-3-methyl-imidazolium hexafluorophosphate and 5,7-dichloro-8-hydroxy quinoline. *Appl. Mech. Mater.* **189**, 75–79 (2012). <https://doi.org/10.4028/www.scientific.net/AMM.189.75>
118. A.N. Turanov, V.K. Karandashev, V.E. Baulin, Effect of ionic liquids on the extraction of rare earth elements by bidentate neutral organophosphorus compounds from chloride solutions. *Russ. J. Inorg. Chem.* **53**(6), 970–975 (2008). <https://doi.org/10.1134/S0036023608060272>
119. K. Nakashima, F. Kubota, T. Maruyama, M. Goto, Ionic liquids as a novel solvent for lanthanide extraction. *Anal. Sci.* **19**(8), 1097–1098 (2003). <https://doi.org/10.2116/analsci.19.1097>
120. Z. Pan, C. Ma, Y. Zhang, Y. Huang, X. Chen, X. Zhang, Extraction behavior of rare earths in ion liquid extraction system using 1-butyl-3-methyl-imidazolium hexafluorophosphate and benzoyl acetone. *Adv. Mater. Res.* **335–336**, 1428–1432 (2011). <https://doi.org/10.4028/www.scientific.net/AMR.335-336.1428>
121. Z. Pan, G. Li, L. Lin, Extraction behavior of scandium cation in ion liquid extraction system using 1-butyl-3-methyl-imidazolium hexafluorophosphate and 2-ethylhexyl phosphonic acid-2-ethylhexyl ester. *Adv. Mater. Res.* **306–307**, 1524–1527 (2011). <https://doi.org/10.4028/www.scientific.net/AMR.306-307.1524>
122. M. Asadollahzadeh, R. Torkaman, M. Torab-Mostaedi, A. Hemmati, A. Ghaemi, High performance separation of gadolinium from samarium with the imidazolium ionic liquid through selective complexation of organophosphorus extractants. *Environ. Technol. Innov.* **19**, 100979 (2020). <https://doi.org/10.1016/j.eti.2020.100979>
123. M. Asadollahzadeh, R. Torkaman, Extraction of dysprosium from waste neodymium magnet solution with ionic liquids and ultrasound irradiation procedure. *Korean J. Chem. Eng.* **39**(1), 134–145 (2022). <https://doi.org/10.1007/s11814-021-0970-6>
124. Y. Zuo, Y. Liu, J. Chen, Q. De Li, The separation of cerium(IV) from nitric acid solutions containing thorium(IV) and lanthanides(III) using pure [C<sub>8</sub>mim]PF<sub>6</sub> as extracting phase. *Ind. Eng. Chem. Res.* **47**(7), 2349–2355 (2008). <https://doi.org/10.1021/ie071486w>
125. X. Sun, D. Wu, J. Chen, D. Li, Separation of scandium (III) from lanthanides (III) with room temperature ionic liquid based extraction containing Cyanex 925. *J. Chem. Technol. Biotechnol.* **82**(3), 267–272 (2007)
126. Y. Zuo, J. Chen, D. Li, Reversed micellar solubilization extraction and separation of thorium(IV) from rare earth(III) by primary amine N1923 in ionic liquid. *Sep. Purif. Technol.* **63**(3), 684–690 (2008). <https://doi.org/10.1016/j.seppur.2008.07.014>
127. Y. Zuo, Y. Liu, J. Chen, D.Q. Li, Extraction and recovery of cerium (IV) along with fluorine (I) from bastnasite leaching liquor by DEHEHP in [C<sub>8</sub>mim]PF<sub>6</sub>. *J. Chem. Technol. Biotechnol.* **84**(7), 949–956 (2009). <https://doi.org/10.1002/jctb.2116>
128. S. Mekki, C.M. Wai, I. Billard, G. Moutiers, J. Burt, B. Yoon, J.S. Wang, C. Gaillard, A. Ouardi, P. Hesemann, Extraction of lanthanides from aqueous solution by using room temperature ionic liquid and supercritical carbon dioxide in conjunction. *Chemistry* **12**(6), 1760–1766 (2006). <https://doi.org/10.1002/chem.200500559>



129. F. Yang, Y. Baba, F. Kubota, N. Kamiya, M. Goto, Extraction and separation of rare earth metal ions with DODGAA in ionic liquids. *Solvent Extr. Res. Dev.* **19**, 69–76 (2012). <https://doi.org/10.15261/serdj.19.69>
130. Q. Chen, C. Lu, Y. Hu, Y. Liu, Y. Zhou, C. Jiao, M. Zhang, H. Hou, Y. Gao, G. Tian, Extraction behavior of several lanthanides from nitric acid with DMDODGA in [C4mim][NTf2] ionic liquid. *J. Radioanal. Nucl. Chem.* **327**(1), 565–573 (2021). <https://doi.org/10.1007/s10967-020-07525-7>
131. A.N. Turanov, V.K. Karandashev, V.E. Baulin, Extraction of lanthanides(III) with N,N'-bis(diphenylphosphinyl-methylcarbonyl)diaza-18-crown-6 in the presence of ionic liquids. *Solvent Extr. Ion Exch.* **30**(3), 244–261 (2012). <https://doi.org/10.1080/0736629.9.2011.639248>
132. A.N. Turanov, V.K. Karandashev, M. Boltoeva, Solvent extraction of intra-lanthanides using a mixture of TBP and TODGA in ionic liquid. *Hydrometallurgy* **195**, 105367 (2020). <https://doi.org/10.1016/j.hydromet.2020.105367>
133. M. Asadollahzadeh, R. Torkaman, M. Torab-Mostaedi, Recovery of gadolinium ions based on supported ionic liquid membrane: parametric optimization via central composite design approach. *Int. J. Environ. Sci. Technol.* **17**(9), 3983–3996 (2020). <https://doi.org/10.1007/s13762-020-02743-8>
134. F. Kubota, Y. Koyanagi, K. Nakashima, K. Shimojo, N. Kamiya, M. Goto, Extraction of lanthanide ions with an organophosphorous extractant into ionic liquids. *Solvent Extr. Res. Dev.* **15**, 81–87 (2008)
135. G. Arrachart, J. Couturier, S. Dourdain, C. Levard, S. Pellet-Rostaing, Recovery of rare earth elements (REEs) using ionic solvents. *Processes* **9**(7), 1–29 (2021). <https://doi.org/10.3390/pr9071202>
136. A. Rout, K.A. Venkatesan, Synergic extraction of europium(III) in hydrophobic ammonium ionic liquid containing neutral and acidic extractants. *J. Mol. Liq.* **312**, 113377 (2020). <https://doi.org/10.1016/j.molliq.2020.113377>
137. N. Kozonoi, Y. Ikeda, Extraction mechanism of metal ion from aqueous solution to the hydrophobic ionic liquid, 1-butyl-3-methylimidazolium nonafluorobutanesulfonate. *Monatsh. Chem.* **138**(11), 1145–1151 (2007). <https://doi.org/10.1007/s00706-007-0727-x>
138. N.S.M. Vieira, S. Stolte, J.M.M. Araújo, L.P.N. Rebelo, A.B. Pereira, M. Markiewicz, Acute aquatic toxicity and biodegradability of fluorinated ionic liquids. *ACS Sustain. Chem. Eng.* **7**(4), 3733–3741 (2019). <https://doi.org/10.1021/acssuschemeng.8b03653>
139. P. Oulego, J. Faes, R. González, J.L. Viesca, D. Blanco, A.H. Battez, Relationships between the physical properties and biodegradability and bacteria toxicity of fatty acid-based ionic liquids. *J. Mol. Liq.* **292**, 111451 (2019). <https://doi.org/10.1016/j.molliq.2019.111451>
140. M. Sydow, M. Owsianiak, G. Framski, M. Woźniak-Karczewska, A. Piotrowska-Cyplik, Ł. Ławniczak, A. Szulc, A. Zgoła-Grzeškowiak, H.J. Heipieper, Ł. Chrzanowski, Biodiversity of soil bacteria exposed to sublethal concentrations of phosphonium-based ionic liquids: effects of toxicity and biodegradation. *Ecotoxicol. Environ. Saf.* **147**, 157–164 (2018). <https://doi.org/10.1016/j.ecoenv.2017.08.026>
141. M.G. Freire, A.F.M. Cláudio, J.M.M. Araújo, J.A.P. Coutinho, I.M. Marrucho, J.N. Canongia Lopes, L.P.N. Rebelo, Aqueous biphasic systems: a boost brought about by using ionic liquids. *Chem. Soc. Rev.* **41**(14), 4966–4995 (2012). <https://doi.org/10.1039/c2cs35151j>
142. T. Vander Hoogerstraete, B. Onghena, K. Binnemans, Homogeneous liquid-liquid extraction of metal ions with a functionalized ionic liquid. *J. Phys. Chem. Lett.* **4**(10), 1659–1663 (2013). <https://doi.org/10.1021/jz4005366>
143. D. Depuydt, W. Dehaen, K. Binnemans, Solvent extraction of scandium(III) by an aqueous biphasic system with a nonfluorinated functionalized ionic liquid. *Ind. Eng. Chem. Res.* **54**(36), 8988–8996 (2015). <https://doi.org/10.1021/acs.iecr.5b01910>
144. L. Stoy, V. Diaz, C. Huang, Preferential recovery of rare earth elements from coal fly ash using a recyclable ionic liquid. *Environ. Sci. Technol.* **55**(13), 9209–9220 (2021). <https://doi.org/10.1021/acs.est.1c00630>

145. E. Mikeli, E. Balomenos, D. Pnias, Utilizing recyclable task-specific ionic liquid for selective leaching and refining of scandium from bauxite residue. *Molecules* **26**(4), 1–11 (2021). <https://doi.org/10.3390/molecules26040818>
146. Y. Chen, H. Wang, Y. Pei, J. Wang, A green separation strategy for neodymium (III) from cobalt (II) and nickel (II) using an ionic liquid-based aqueous two-phase system. *Talanta* **182**(III), 450–455 (2018). <https://doi.org/10.1016/j.talanta.2018.02.018>
147. S.J.R. Vargas, J.C. Quintão, G.M.D. Ferreira, L.H.M. Da Silva, M.C. Hespanhol, Lanthanum and cerium separation using an aqueous two-phase system with ionic liquid. *J. Chem. Eng. Data* **64**(10), 4239–4246 (2019). <https://doi.org/10.1021/acs.jced.9b00293>
148. N. Li, R. Zhang, L. Nian, R. Ren, Y. Wang, H. Zhang, A. Yu, Extraction of eight triazine and phenylurea herbicides in yogurt by ionic liquid foaming-based solvent floatation. *J. Chromatogr. A* **1222**, 22–28 (2012). <https://doi.org/10.1016/j.chroma.2011.12.019>
149. H. Sahoo, S.S. Rath, B. Das, Use of the ionic liquid-tricaprylmethyl ammonium salicylate (TOMAS) as a flotation collector of quartz. *Sep. Purif. Technol.* **136**, 66–73 (2014). <https://doi.org/10.1016/j.seppur.2014.08.034>
150. D. Azizi, F. Larachi, M. Latifi, Ionic-liquid collectors for rare earth minerals flotation—case of tetrabutylammonium bis(2-ethylhexyl)-phosphate for monazite and bastnäsite recovery. *Colloids Surf. A Physicochem. Eng. Asp.* **506**, 74–86 (2016). <https://doi.org/10.1016/j.colsurfa.2016.06.011>
151. D. Azizi, A. Sarvaramini, F. Larachi, Liquid-liquid mineral separation via ionic-liquid complexation of monazite and bastnäsite—an alternate route for rare earth mineral beneficiation. *Colloids Surf. A Physicochem. Eng. Asp.* **520**, 301–323 (2017). <https://doi.org/10.1016/j.colsurfa.2017.01.079>
152. D. Azizi, F. Larachi, Immiscible dual ionic liquid-ionic liquid mineral separation of rare earth minerals. *Sep. Purif. Technol.* **191**, 340–353 (2018). <https://doi.org/10.1016/j.seppur.2017.09.061>
153. R. Li, C. Marion, E.R.L. Espiritu, R. Multani, X. Sun, K.E. Waters, Investigating the use of an ionic liquid for rare earth mineral flotation. *J. Rare Earths* **39**, 866–874 (2021). <https://doi.org/10.1016/j.jre.2020.09.003>
154. A.P. Abbott, K.J. McKenzie, Application of ionic liquids to the electrodeposition of metals. *Phys. Chem. Chem. Phys.* **8**(37), 4265–4279 (2006). <https://doi.org/10.1039/b607329h>
155. E. Bourbos, I. Giannopoulou, A. Karantonis, I. Paspaliaris, D. Pnias, Reduction of light rare earths and a proposed process for Nd electrorecovery based on ionic liquids. *J. Sustain. Metall.* **4**, 395 (2018)
156. M. Matsumiya, M. Ishii, R. Kazama, S. Kawakami, Electrochemical analyses of diffusion behaviors and nucleation mechanisms for neodymium complexes in [DEME][TfSA] ionic liquid. *Electrochim. Acta* **146**, 371–377 (2014). <https://doi.org/10.1016/j.electacta.2014.09.066>
157. N. Sasaya, M. Matsumiya, K. Tsunashima, Solvation and electrochemical analyses of neodymium complexes in TfSA-based ionic liquids dissolving the nitrates synthesized from spent Nd-Fe-B magnets. *Polyhedron* **85**, 888 (2015)
158. L. Sanchez-Cupido, J.M. Pringle, A.I. Siriwardana, M. Hilder, M. Forsyth, C. Pozo-gonzalo, Correlating electrochemical behavior and speciation in neodymium ionic liquid electrolyte mixtures in the presence of water. *ACS Sustain. Chem. Eng.* **8**(37), 14047–14057 (2020). <https://doi.org/10.1021/acssuschemeng.0c04288>
159. L. Sanchez-Cupido, J.M. Pringle, A.L. Siriwardana, A. Unzurrunzaga, M. Hilder, M. Forsyth, C. Pozo-Gonzalo, Water-facilitated electrodeposition of neodymium in a phosphonium-based ionic liquid. *J. Phys. Chem. Lett.* **10**, 289 (2019)
160. E. Bourbos, I. Giannopoulou, A. Karantonis, I. Paspaliaris, D. Pnias, Electrodeposition of rare earth metals from ionic liquids, in *Rare Earths Industry Technological, Economic, and Environmental Implications*, (Elsevier, Amsterdam, 2016), pp. 199–207. <https://doi.org/10.1016/B978-0-12-802328-0.00013-9>

161. C. Jagadeeswara Rao, K.A. Venkatesan, K. Nagarajan, T.G. Srinivasan, P.R. Vasudeva Rao, Electrochemical behavior of europium (III) in N-butyl-N-methylpyrrolidinium bis(trifluoromethylsulfonyl)imide. *Electrochim. Acta* **54**(20), 4718–4725 (2009). <https://doi.org/10.1016/j.electacta.2009.03.074>
162. D.W. Hatchett, J. Drossler, J.M. Kinyanjui, B. Martinez, K.R. Czerwinski, The direct dissolution of  $Ce_2(CO_3)_3$  and electrochemical deposition of Ce species using ionic liquid trimethyl-n-butylammonium bis(trifluoromethanesulfonyl)imide containing bis(trifluoromethanesulfonyl)imide. *Electrochim. Acta* **89**, 144–151 (2013). <https://doi.org/10.1016/j.electacta.2012.10.083>
163. A.I. Bhatt, I. May, V.A. Volkovich, D. Collison, M. Helliwell, I.B. Polovov, R.G. Lewin, Structural characterization of a lanthanum Bistriflimide complex,  $La(N(SO_2CF_3)_2)_3(H_2O)_3$ , and an investigation of La, Sm, and Eu electrochemistry in a room temperature ionic liquid,  $[Me_3NnBu][N(SO_2CF_3)_2]$ . *Inorg. Chem.* **44**(14), 4934–4940 (2005). <https://doi.org/10.1021/ic048199u>
164. L.M. Glukhov, A.A. Greish, L.M. Kustov, Electrodeposition of rare earth metals Y, Gd, Yb in ionic liquids. *Russ. J. Phys. Chem.* **84**(1), 104–108 (2010). <https://doi.org/10.1134/S0036024410010206>
165. P. Bagri, H. Luo, I. Popovs, B.P. Thapaliya, Trimethyl phosphate based neutral ligand room temperature ionic liquids for electrochemical separation of rare earth elements. *Electrochem. Commun.* **96**, 88–92 (2018). <https://doi.org/10.1016/j.elecom.2018.10.001>
166. P. Sidhu, Investigation of the electro-winning of neodymium oxide in room temperature ionic liquid. Thesis, 2019
167. C. Andrew, M. Dhivya, M. Jayakumar, Electrochemical and spectroscopic investigation of samarium in a neutral ligand based ionic liquid. *J. Electroanal. Chem.* **895**, 115398 (2021). <https://doi.org/10.1016/j.jelechem.2021.115398>
168. G.M. Krishna, A. Rout, K.A. Venkatesan, Voltammetric investigation of some lanthanides in neutral ligand ionic liquid. *J. Electroanal. Chem.* **856**, 113671 (2020). <https://doi.org/10.1016/j.jelechem.2019.113671>
169. H. Kondo, M. Matsumiya, K. Tsunashima, S. Kodama, Attempts to the electrodeposition of Nd from ionic liquids at elevated temperatures. *Electrochim. Acta* **66**, 313–319 (2012). <https://doi.org/10.1016/j.electacta.2012.01.101>
170. A. Kurachi, M. Matsumiya, K. Tsunashima, S. Kodama, Electrochemical behavior and electrodeposition of dysprosium in ionic liquids based on phosphonium cations. *J. Appl. Electrochem.* **42**(11), 961–968 (2012). <https://doi.org/10.1007/s10800-012-0463-8>
171. S. Legeai, S. Diliberto, N. Stein, C. Boulanger, J. Estager, N. Papaiconomou, M. Draye, Room temperature ionic liquid for lanthanum electrodeposition. *Electrochem. Commun.* **10**(11), 1661–1664 (2008). <https://doi.org/10.1016/j.elecom.2008.08.005>
172. C.A. Berger, M. Arkhipova, G. Maas, T. Jacob, Dysprosium electrodeposition from a hexaalkylguanidinium-based ionic liquid. *Nanoscale* **8**(29), 13997–14003 (2016). <https://doi.org/10.1039/c6nr01351a>
173. B. Zhang, L. Wang, K. Pan, W. Zhang, Y. Liu, Y. Zhang, L. Zhang, Z. Shi,  $LiNO_3$ -supported electrodeposition of metallic Nd from Nd-containing solvate ionic liquid. *J. Phys. Chem. C* **125**(38), 20798–20805 (2021). <https://doi.org/10.1021/acs.jpcc.1c06335>
174. A.M. Liu, Y. Yao, M.X. Guo, Y.B. Liu, Z.N. Shi, F.G. Liu, X.W. Hu, W.C. He, Z.W. Wang, Physicochemical properties of DMI– $LiNO_3$  solvated ionic liquid and its application in electrodeposition of neodymium at room temperature. *Trans. Nonferrous Met. Soc. China (Engl. Ed.)* **31**(8), 2522–2531 (2021). [https://doi.org/10.1016/S1003-6326\(21\)65672-8](https://doi.org/10.1016/S1003-6326(21)65672-8)
175. V. Zinovyeva, C. Cannes, C. Le Naour, Comparison of the electrochemical behavior of some rare earth elements in butyl methylpyrrolidinium dicyanamide ionic liquid. *Int. J. Electrochem. Sci.* **14**, 10431–10447 (2019). <https://doi.org/10.20964/2019.11.16>
176. M.Y. Gao, C. Yang, Q.B. Zhang, J.R. Zeng, X.T. Li, Y.X. Hua, C.Y. Xu, Y. Li, Electrochemical preparation of Ni-La alloy films from N-butyl-N-methyl pyrrolidinium dicyanamide ionic liquid as electrocatalysts for hydrogen evolution reaction. *J. Electrochem. Soc.* **164**(12), D778–D784 (2017). <https://doi.org/10.1149/2.1751712jes>

177. X. Xu, S. Sturm, J. Zavasnik, K.Z. Rozman, Electrodeposition of a rare earth iron alloy from an ionic-liquid electrolyte. *ChemElectroChem* **6**(11), 2860–2869 (2019). <https://doi.org/10.1002/celec.201900286>
178. Q.B. Zhang, C. Yang, Y.X. Hua, Y. Li, P. Dong, Electrochemical preparation of nanostructured lanthanum using lanthanum chloride as a precursor in 1-butyl-3-methylimidazolium dicyanamide ionic liquid. *Phys. Chem. Chem. Phys.* **17**(6), 4701–4707 (2015). <https://doi.org/10.1039/c4cp05266h>
179. K. Periyapperuma, J.M. Pringle, L. Sanchez-Cupido, M. Forsyth, C. Pozo-Gonzalo, Fluorine-free ionic liquid electrolytes for sustainable neodymium recovery using an electrochemical approach. *Green Chem.* **23**(9), 3410–3419 (2021). <https://doi.org/10.1039/d1gc00361e>
180. A. Lisenkov, M.L. Zheludkevich, M.G.S. Ferreira, Active protective Al-Ce alloy coating electrodeposited from ionic liquid. *Electrochem. Commun.* **12**(6), 729–732 (2010). <https://doi.org/10.1016/j.elecom.2010.03.018>
181. R. Rama, A. Rout, K.A. Venkatesan, M.P. Antony, P.R. Vasudeva Rao, Electrochemical behavior of Eu(III) in imidazolium ionic liquid containing tri-n-butyl phosphate and N,N-dihexyloctanamide ligands. *J. Electroanal. Chem.* **757**(III), 36–43 (2015). <https://doi.org/10.1016/j.jelechem.2015.09.005>
182. M. Razo-Negrete, R. Ortega-Borges, V. Zinovyeva, C. Cannes, C. Le Naour, G. Trejo-Cordova, Y. Meas, Comparison of the electrochemical behavior of some rare earth elements in butyl methylpyrrolidinium dicyanamide ionic liquid. *Int. J. Electrochem. Sci.* **14**, 10431–10447 (2019). <https://doi.org/10.20964/2019.11.16>
183. K. Orme, D.L. Baek, R.V. Fox, A. Atifi, Water interplays during dysprosium electrodeposition in pyrrolidinium ionic liquid: deconvoluting the pros and cons for rare earth metalization. *ACS Sustain. Chem. Eng.* **9**(43), 14631–14643 (2021). <https://doi.org/10.1021/acssuschemeng.1c06189>
184. M. Manjum, N. Serizawa, A. Ispas, A. Bund, Y. Katayama, Electrochemical preparation of cobalt-samarium nanoparticles in an aprotic ionic liquid. *J. Electrochem. Soc.* **167**(4), 042505 (2020). <https://doi.org/10.1149/1945-7111/ab79a8>
185. G. Suppan, M. Ruehrig, A. Kanitz, H.J. Gores, Electroplating dysprosium from IL-based solutions: a promising electrochemical step to produce stronger high performance Nd(Dy)-Fe-B sintered magnets. *J. Electrochem. Soc.* **162**(8), D382–D388 (2015). <https://doi.org/10.1149/2.0911508jes>
186. R. Kazama, M. Matsumiya, N. Tsuda, K. Tsunashima, Electrochemical analysis of diffusion behavior and nucleation mechanism for Dy(II) and Dy(III) in phosphonium-based ionic liquids. *Electrochim. Acta* **113**, 269–279 (2013). <https://doi.org/10.1016/j.electacta.2013.09.082>
187. A.M. O'Mahony, D.S. Silvester, L. Aldous, C. Hardacre, R.G. Compton, Effect of water on the electrochemical window and potential limits of room temperature ionic liquids. *J. Chem. Eng. Data* **53**(12), 2884–2891 (2008). <https://doi.org/10.1021/je800678e>
188. M. Matsumiya, Electrodeposition of rare earth metal in ionic liquids, in *Rare Earths Industry Technological, Economic, and Environmental Implications*, (Elsevier, Amsterdam, 2016), pp. 199–207
189. H. Kondo, M. Matsumiya, K. Tsunashima, S. Kodama, Investigation of oxidation state of the electrodeposited neodymium metal related with the water content of phosphonium ionic liquids. *ECS Trans.* **50**(11), 529–538 (2013). <https://doi.org/10.1149/05011.0529ecst>
190. M. Matsumiya, Y. Kikuchi, T. Yamada, S. Kawakami, Extraction of rare earth ions by tri-n-butylphosphate/phosphonium ionic liquids and the feasibility of recovery by direct electrodeposition. *Sep. Purif. Technol.* **130**, 91 (2014)
191. Y. Zhao, T.J. VanderNoot, Electrodeposition of aluminium from room temperature AlCl<sub>3</sub>-TMPAC molten salts. *Electrochim. Acta* **42**(11), 1639–1643 (1997). [https://doi.org/10.1016/S0013-4686\(96\)00271-X](https://doi.org/10.1016/S0013-4686(96)00271-X)
192. T. Jiang, M.J. Chollier Brym, G. Dubé, A. Lasia, G.M. Brisard, Electrodeposition of aluminium from ionic liquids: Part 1 – Electrodeposition and surface morphology of aluminium from aluminium chloride (AlCl<sub>3</sub>)-1-ethyl-3-methylimidazolium chloride ([EMIm]Cl) ionic liquids. *Surf. Coat. Technol.* **201**(1–2), 1–9 (2006). <https://doi.org/10.1016/j.surfcoat.2005.10.046>

193. J.K. Chang, S.Y. Chen, W.T. Tsai, M.J. Deng, I.W. Sun, Electrodeposition of aluminum on magnesium alloy in aluminum chloride (AlCl<sub>3</sub>)-1-ethyl-3-methylimidazolium chloride (EMIC) ionic liquid and its corrosion behavior. *Electrochem. Commun.* **9**(7), 1602–1606 (2007). <https://doi.org/10.1016/j.elecom.2007.03.009>
194. M. Lipsztajn, R.A. Osteryoung, Electrochemistry in neutral ambient-temperature ionic liquids. I. Studies of iron(III), neodymium(III), and lithium(I). *Inorg. Chem.* **24**(5), 716–719 (1985). <https://doi.org/10.1021/ic00199a016>
195. T. Tsuda, T. Nohira, Y. Ito, Electrodeposition of lanthanum in lanthanum chloride saturated AlCl<sub>3</sub>-1-ethyl-3-methylimidazolium chloride molten salts. *Electrochim. Acta* **46**(12), 1891–1897 (2001). [https://doi.org/10.1016/S0013-4686\(01\)00434-0](https://doi.org/10.1016/S0013-4686(01)00434-0)

# **Part II**

## **Metal Refining**

# Chapter 9

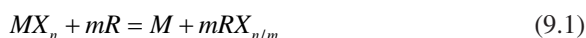
## Reduction of Rare Earth Elements Through Electrochemical and Metallothermic Methods



Patrick R. Taylor, Matthew Earlam, and Sridhar Seetharaman

### 9.1 Introduction and Thermodynamics Considerations

The pertinent thermodynamics of rare earth metal production pertains to reactions as



where M is the rare earth metal to be produced, and X is the anion that M is bound to which could either be the starting ore compound (e.g., oxide) or an intermediate compound such as fluorine (F) or chlorine (Cl) [1]. R is the reducing agent which may be carbon monoxide (CO (g)), hydrogen (H<sub>2</sub> (g)) or a metal (e.g., magnesium (Mg) or lithium (Li)). For typical rare earth compounds, n is 3/2 for oxides and is 3 for chlorides and fluorides. The coefficient m is the stoichiometric amount of X required in the compound with M.

Equation 9.1 can be written as



Since these reactions are associated with standard free energies of mixing,  $-\Delta G_0^{MX_n}$  and  $m \Delta G_0^{RX_{n/m}}$ , the overall Gibbs Free Energy for Eq. 9.1 is

---

P. R. Taylor (✉) · M. Earlam · S. Seetharaman  
Colorado School of Mines, Golden, CO, USA  
e-mail: [prtaylor@mines.edu](mailto:prtaylor@mines.edu)

$$\Delta G_1 = m\Delta G_0^{RX_{n/m}} - \Delta G_0^{MX_n} + RT \ln \left( \frac{a_M a_{RX_{n/m}}^m}{a_R^m a_{MX_n}} \right) \quad (9.4)$$

For a thermodynamically favorable reduction condition  $\Delta G_1 < 0$ . Since compounds ( $RX_{n/m}$  and  $MX_n$ ) are generally at unit activity, Eq. 9.4 will depend on:

- The standard free energies  $G_0^{MX_n}$  and  $\Delta G_0^{RX_{n/m}}$ , which will have the largest contribution to  $\Delta G_1$ . The standard free energies can be written as,  $\Delta G_0^i = \Delta H_0^i - T\Delta S_0^i$ .
- The activity of the product metal,  $a_M$ , which can be reduced by producing an alloy as opposed to a pure metal.
- The activity (or fugacity) of the reductant,  $a_R$ .
- The temperature ( $T$  (K)) which also appears in the standard free energies.

Table 9.1 lists standard Gibbs energies for the formation for several rare earth oxides (REOs) and the only effective metallothermic reduction material (i.e., calcium (Ca)) as a function of temperature. Figure 9.1 shows the standard Gibbs energies for formation of several REOs, and Fig. 9.2 gives standard Gibbs energies for the formation of REOs and potential reductants.

Figure 9.3 shows the temperature dependence of the standard Gibbs energy (i.e., the Ellingham diagram) for the reactions listed in Tables 9.1 and 9.2. From Eq. 9.4, if the activities are all unity, this means that a particular REO can be reduced by reducing agents whose standard Gibbs energy lies beneath them. Thus, with unit rare earth metal activity, only Ca can accomplish this. The situation is similar for fluorides (Table 9.3).

Table 9.2 and Fig. 9.2 show the corresponding information for chlorides, and it can be seen that Ca, potassium (K), sodium (Na), Li, and carbon ((C) at high enough temperatures to form CO(g)) can reduce rare earth chlorides.

In the case of an electrochemical reaction, electric power is used to drive a reaction where the chemical free energy is positive. The reaction is separated as anode and cathode half-cell reactions and rewritten as separate reactions, following dissolution of  $MX_n$  into an electrolyte:



**Table 9.1** Standard Gibbs energies of select REOs and CaO as a function of temperature

Oxide	$\Delta G^\circ$ (kJ/mole O <sub>2</sub> ) 500 K	$\Delta G^\circ$ (kJ/mole O <sub>2</sub> ) 1000 K	$\Delta G^\circ$ (kJ/mole O <sub>2</sub> ) 1500 K	$\Delta G^\circ$ (kJ/mole O <sub>2</sub> ) 2000 K
Nd <sub>2</sub> O <sub>3</sub>	-1109	-1016	-924	-829
Pr <sub>2</sub> O <sub>3</sub>	-1108	-1016	-922	-829
Dy <sub>2</sub> O <sub>3</sub>	-1140	-1045	-952	-857
CaO	-1164	-1061	-950	-837



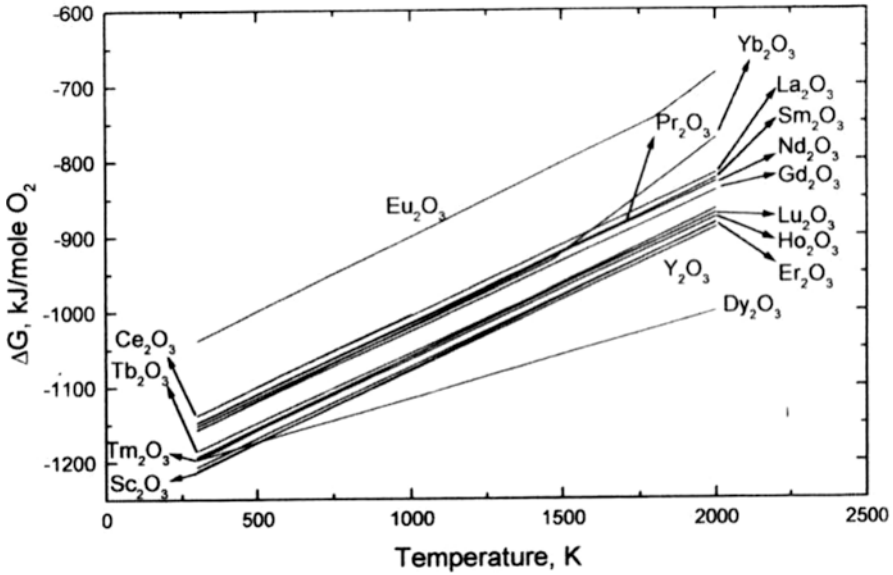


Fig. 9.1 Standard Gibbs energies for formation of the REOs versus temperature [1]

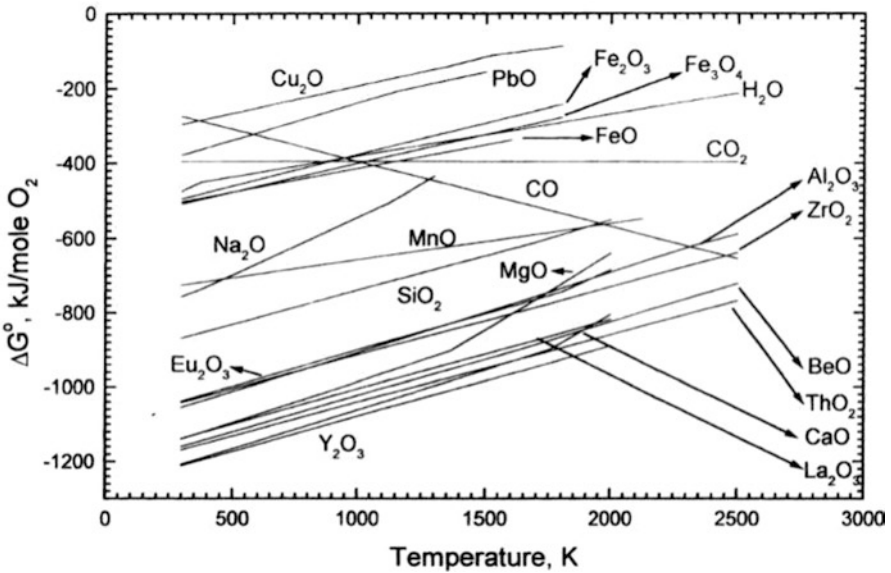


Fig. 9.2 Standard Gibbs energies for the formation of REOs and potential reductants [1]

In the case of electrochemical reactions, the free energies in Eq. (9.4) are replaced by electric potentials through the Nernst Equation,  $\Delta G_i^j = -nFE_i^j$ , free energies for Eqs. 9.5 and 9.6 are converted to electric potentials, and the thermodynamically minimum electric potential [2] to accomplish reduction will be:

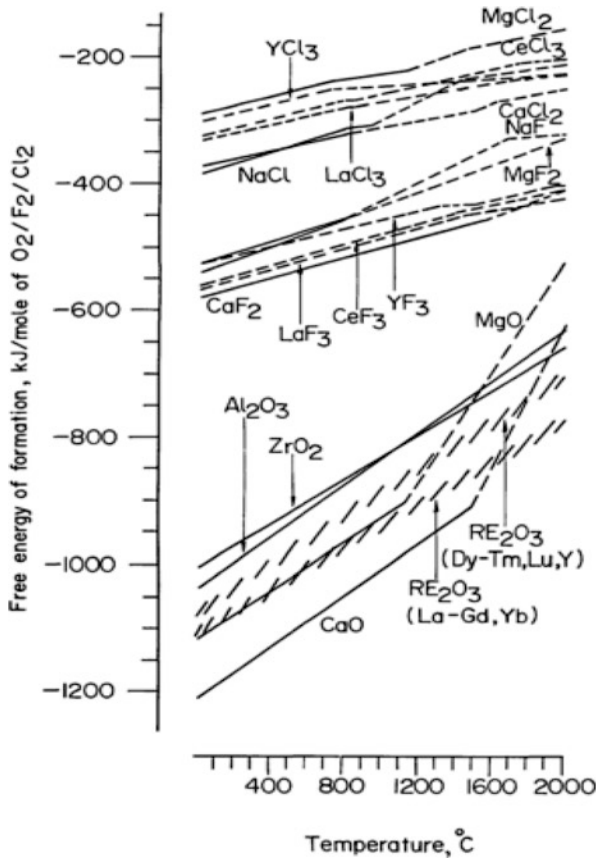


Fig. 9.3 Ellingham diagram for various rare earth oxides and halides

Table 9.2 Gibbs energy of formation for potential chlorides and Ca, K, Na, and Li as reductants for two temperatures

Chloride	$\Delta G^\circ$ (kJ/mole $\text{Cl}_2$ ) 500 K	$\Delta G^\circ$ (kJ/mole $\text{Cl}_2$ ) 1000 K	$\Delta G^\circ$ (kJ/mole $\text{Cl}_2$ ) 1500 K	$\Delta G^\circ$ (kJ/mole $\text{Cl}_2$ ) 2000 K
$\text{NdCl}_3$	-611	-534	-477	-425
$\text{PrCl}_3$	-620	-543	-484	-430
$\text{DyCl}_3$	-571	-484	-413	-345
$\text{CaCl}_2$	-718	-645	-585	-531
$\text{KCl}$	-778	-683	-620	-564
$\text{NaCl}$	-730	-638	-575	-523
$\text{LiCl}$	-735	-659	-607	-559

$$E = \left( E_{M/M^{z+}}^0 - E_{R/R^{z+m}}^0 \right) - \frac{RT}{nF} \ln \frac{a_M a_R^{z+m}}{a_M^{z+} a_R} \quad (9.7)$$

**Table 9.3** Gibbs energy of formation for rare earth fluorides and Ca as a reductant for two temperatures

Fluoride	$\Delta G^\circ$ (kJ/mole F <sub>2</sub> ) 500 K	$\Delta G^\circ$ (kJ/mole F <sub>2</sub> ) 1000 K	$\Delta G^\circ$ (kJ/mole F <sub>2</sub> ) 1500 K	$\Delta G^\circ$ (kJ/mole F <sub>2</sub> ) 2000 K
NdF <sub>3</sub>	-1036	-957	-880	-812
PrF <sub>3</sub>	-1041	-962	-885	-817
DyF <sub>3</sub>	-1042	-962	-888	-830
CaF <sub>2</sub>	-1141	-1058	-978	-911

**Table 9.4** Relevant half-cell potentials

Element	Half-cell reaction	E <sup>0</sup> (V)	Element	Half-cell reaction	E <sup>0</sup> (V)
Sr	Sr <sup>-</sup> + e <sup>-</sup> = Sr(s)	-4.101	Li	Li <sup>+</sup> +C <sub>6</sub> (s) + e <sup>-</sup> = LiC <sub>6</sub> (s)	-2.84
Ca	Ca <sup>+</sup> +e <sup>-</sup> = Ca(s)	-3.8	Eu	Eu <sup>2+</sup> +2e <sup>-</sup> = Eu(s)	-2.812
Pr	Pr <sup>3+</sup> +e <sup>-</sup> = Pr <sup>2+</sup>	-3.1	Ra	Ra <sup>2</sup> + 2e <sup>-</sup> = Ra(s)	-2.8
Li	Li <sup>+</sup> +e <sup>-</sup> = Li(s)	-3.0401	Ho	Ho <sup>3+</sup> +e <sup>-</sup> = Ho <sup>2+</sup>	-2.8
Cs	Cs <sup>+</sup> +e <sup>-</sup> = Cs(s)	-3.026	Bk	Bk <sup>3+</sup> +e <sup>-</sup> = Bk <sup>2+</sup>	-2.8
Er	Er <sup>3+</sup> +e <sup>-</sup> = Er <sup>2+</sup>	-3.0	Yb	Yb <sup>2+</sup> +2e <sup>-</sup> = Yb(s)	-2.76
Rb	Rb <sup>+</sup> +e <sup>-</sup> = Rb(s)	-2.98	Na	Na <sup>+</sup> +e <sup>-</sup> = Na(s)	-2.71
K	K <sup>+</sup> +e <sup>-</sup> = K(s)	-2.931	Mg	Mg <sup>+</sup> +e <sup>-</sup> = Mg(s)	-2.70
Ba	Ba <sup>2+</sup> +2e <sup>-</sup> = Ba(s)	-2.912	Nd	Nd <sup>3+</sup> +e <sup>-</sup> = Nd <sup>2+</sup>	-2.7
Fr	Fr <sup>+</sup> +e <sup>-</sup> = Fr(s)	-2.9	Sm	Sm <sup>2+</sup> +2e <sup>-</sup> = Sm(s)	-2.68
Sr	Sr <sup>2+</sup> +2e <sup>-</sup> = Sr(s)	-2.899	Pm	Pm <sup>3+</sup> +e <sup>-</sup> = Pm <sup>2+</sup>	-2.6
Ca	Ca <sup>2+</sup> +2e <sup>-</sup> = Ca(s)	-2.868	Dy	Dy <sup>3+</sup> +e <sup>-</sup> = Dy <sup>2+</sup>	-2.6

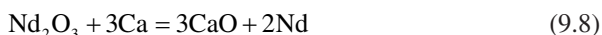
The standard half-cell reactions (Table 9.4) are written as reduction reactions, and n represents the number of electrons transferred. F is Faraday's constant = 96,487 °C/mole equivalent.

## 9.2 Metallothermic Reduction

Metallothermic reduction is based upon the relative thermodynamic stability of metal oxides, chlorides or fluorides as compared to a different metal. There have been many papers written on this topic; examples are given in the references [1, 3–10].

The rare earth precursors (e.g., oxide, fluoride or chloride) must be purified before reduction as minor impurities that are more noble will also be reduced and cannot be easily removed. This purification step is accomplished through mineral processing and hydrometallurgy using leaching, solvent extraction, and ion exchange. The purified product is typically an oxide. To form pure chlorides or fluorides, additional chemical processing is required to convert the oxide.

A typical oxide reaction can be written as



To perform this reaction, one would need a reactor in which the REO and metal reductant are placed. This is then heated up to a temperature that allows the kinetics of the reaction to take place. Most of the reactions are exothermic, so some of the thermal energy required is provided. Ideally, the rare earth metal is formed above its melting point so that metal separation can be achieved, and an ingot can be poured. If not, then mineral processing or leaching of the slag can be used to separate the various materials into metal powders from the slag. This concept is used in many other metal production scenarios (e.g., The Kroll process for Ti and Zr).

The standard state Gibbs Energy (pure and one atmosphere) order of stability for

- Reduction of oxides is:  $\text{CaO} > \text{RE}_2\text{O}_3 > \text{MgO} > \text{Al}_2\text{O}_3 > > \text{SiO}_2$ .
- Fluorides:  $\text{CaF}_2 > \text{REF}_3 > \text{LiF} > \text{NaF} > \text{MgF}_2 > \text{AlF}_3$ .
- Chlorides:  $\text{KCl} > \text{NaCl} > \text{LiCl} > \text{CaCl}_2 > \text{RECl}_3 > \text{MgCl}_2 > > \text{AlCl}_3$ .

Thus, under standard conditions, Ca can reduce the rare earth oxides and fluorides. Rare earth chlorides can be reduced by K, Na, Li, and Ca.

These relative Gibbs Energies may be manipulated by reducing the activity of the rare earth metal product, either through forming an alloy containing the metal, forming a slag containing the metal or by generating a metal vapor phase that is removed as it is formed.

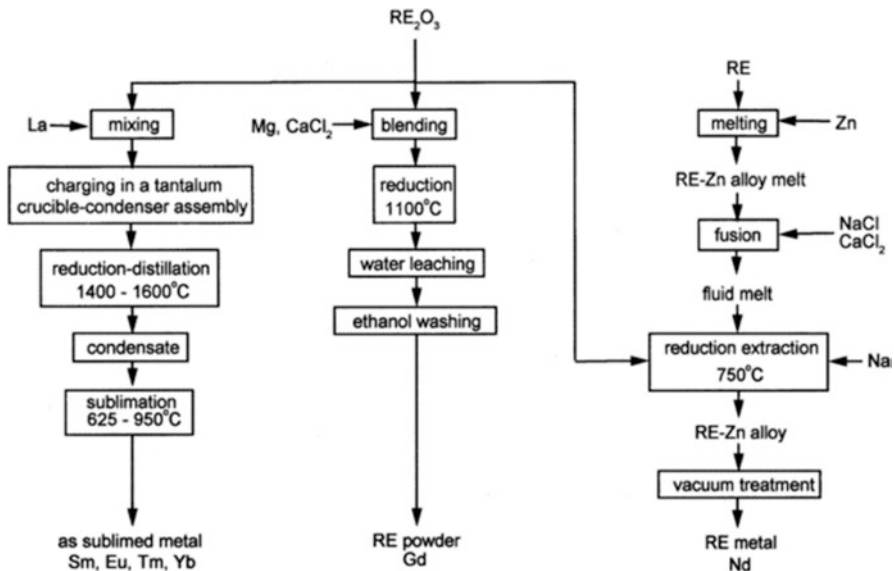
Important factors to consider in metallothermic reduction are melting point, boiling point, vapor pressure, densities, viscosities, chemical activities, and alloying behavior of the reactants and products. In addition, the cost of the metal reductant is very important. Table 9.5 provided additional characteristics that may be important in metallothermic reduction.

Metallothermic reduction of rare earths can produce rare earth metals in the form of ingots, sponges or powders. Fluoride systems typically produce products in the form of ingots, while chloride systems typically produce products in the form of sponges. Oxide systems typically produce products in the form of powders. In the case of a powder or sponge product, the metal can be separated through vacuum distillation or by leaching away the slag. A flow sheet for metallothermic reduction of oxides is shown in Fig. 9.4. These do not require the pretransformation of the REOs into halides. It is typically labor and energy intensive because rare earth oxides are very stable. Reducing agents include Ca and lanthanum (La is sometimes used to reduce the heavier rare earth metals). Magnesium and zinc (Zn) are used to form an alloy to decrease the activity of the metal product. Both Mg and Zn are recovered by vacuum distillation.

Metallothermic reduction of rare earth halides requires the transformation of the REOs into halides. Both chloride and fluoride reduction are meant to be oxygen-free processes. Rare earth halides are less stable than oxides, thus there are more options available for reducing agents and less energy required for reduction.

**Table 9.5** Properties and characteristics of metallothermic reactions

Characteristics	Property
Kinetics and yield	Solid state heterogeneous kinetics depends upon particle sizes of feed, temperature, and time
Molten metal product and slag	Melting point of the metal and slag with sufficient time to allow the phases to separate
Separation of slag and metal	Densities of the metal (more dense) and slag (less dense)
Thermally self-sustaining reaction	Exothermicity of the reaction and well-insulated reactor
High purity	Impurities initially present or introduced by the reductant, reductant product or reactor
Safety	Engineered to assure safe performance and handling
Reactor design	Commercially available reactors and refractories
Reactor atmosphere	Ideally open but may be inert



**Fig. 9.4** Flow sheet of the most common processes used for the direct reduction of REOs [1]

### 9.2.1 Rare Earth Chlorides

#### Preparation of Rare Earth Chlorides

Three primary processes have been used to produce rare earth chlorides. These include:

- Wet Method—Hydrated RECl<sub>3</sub> is crystallized out of a HCl solution of REOs and dehydrated by heating under a dry flow of hydrochloric acid (HCl) [1].

- Dry Method—Direct chlorination: Heating REOs with ammonium chloride ( $\text{NH}_4\text{Cl}$ ) or heating REOs under the flow of chlorine gas [1, 11].
- Carbochlorination—Chlorination process utilizes carbon in the reaction to provide more favorable thermodynamics. One example is the Goldschmidt process (Fig. 9.5) that was developed in industry to produce rare earth chlorides directly from rare earth ores. Process temperature ranges from 800 to 1000 °C. The ore is crushed, mixed with carbon and a binder, pressed into briquettes, placed in a reactor, and heated under the flow of dry chloride gas. Product yields are between 97 and 99%.

## Metallothermic Reduction of Rare Earth Chlorides

Metallothermic reduction of rare earth chlorides have been demonstrated for cerium (Ce), neodymium (Nd), gadolinium (Gd), La, yttrium (Y), and praseodymium (Pr). Typically, metallothermic reduction of rare earth chlorides is only used for the light rare earths due to the volatility of chlorides at high temperatures. Reducing agents include Mg, Ca, Li, and Na. Purity levels range from 61 to 99%. A flow sheet is shown in Fig. 9.6.

### 9.2.2 Rare Earth Fluorides

#### Preparation of Rare Earth Fluorides

A wet and a dry method have been developed to produce rare earth fluorides [1]. The wet method usually involves dissolving a REO in HCl and then adding hydrofluoric acid (HF) to precipitate a hydrated fluoride. The dry method is usually hydrofluorination with HF gas at elevated temperatures (e.g., 700 °C) for 8 h using 200% excess HF gas.

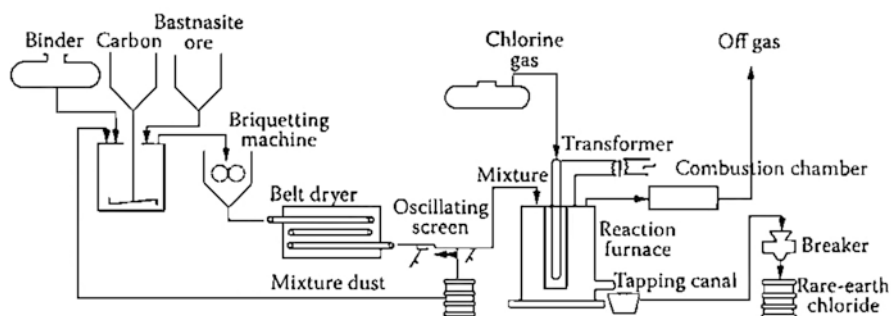


Fig. 9.5 Flow sheet illustrating the Goldschmidt process [1]

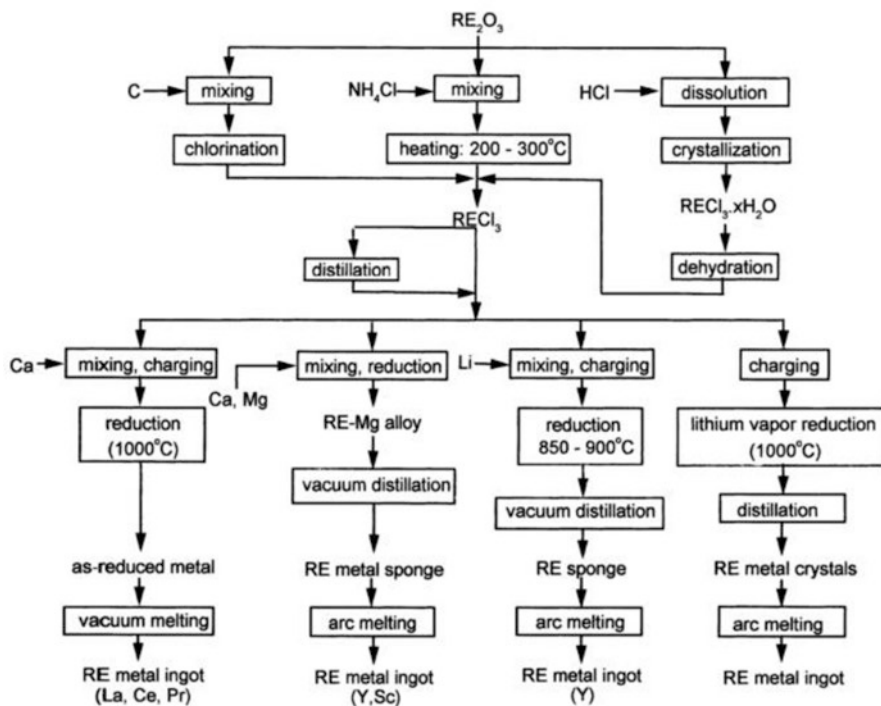


Fig. 9.6 Flowchart of the most common processes used for the reduction of rare earth chlorides [1]

### Metallothermic Reduction of Rare Earth Fluorides

Metallothermic reduction of rare earth fluorides has been demonstrated for all rare earth elements. Processes can be less problematic than chloride reduction because fluorides are less volatile than chlorides. Reducing agents include Ca, Li, and Mg (alloy process). Purity levels range from 97 to 99.85%. Typically, fluoride reduction is more expensive than chloride reduction due to the higher operating temperatures and cost of chemicals. A flow sheet is shown in Fig. 9.7.

## 9.3 Lanthanotherapy

Lanthanotherapy [8–10] is similar to the Pidgeon Process [12] for Mg (Fig. 9.8). It is based upon the formation of a volatile metal product that can be removed and quenched in a separate chamber. This then promotes the reaction Gibbs energy to be more negative. It can be used for the production of samarium (Sm), europium (Eu), and ytterbium (Yb), which is not obtained through halide routes, being based upon vapor pressure measurements of the rare earth metals. These measurements indicate

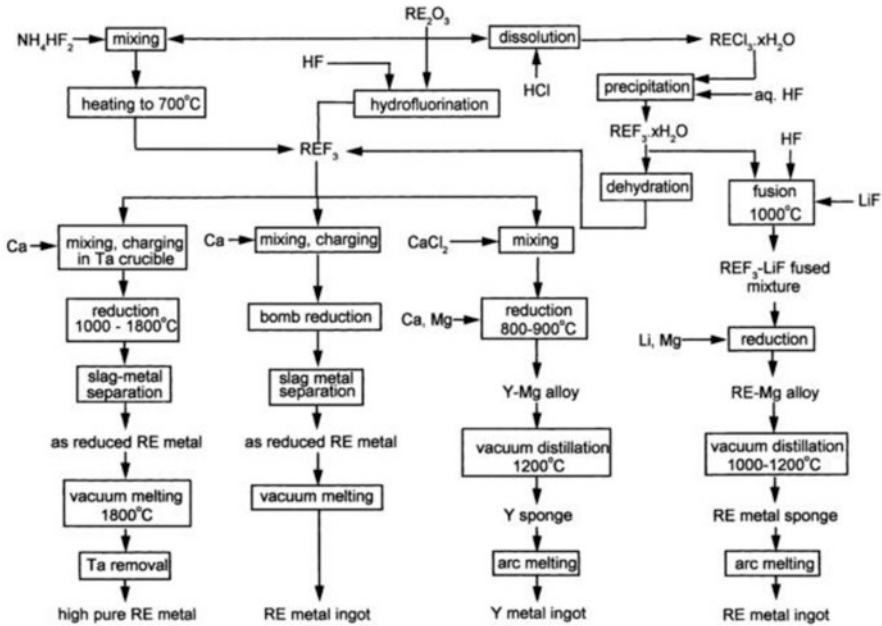
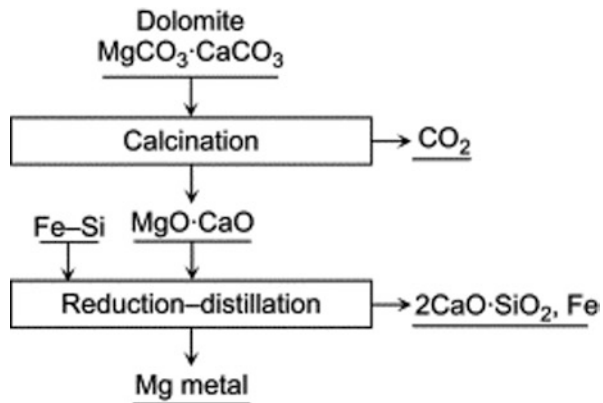


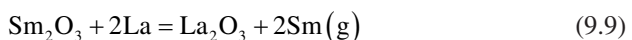
Fig. 9.7 Flowchart of the most common processes used for the direct reduction of rare earth fluorides [1]

Fig. 9.8 Schematic for the Pidgeon process [11]



that La is the least volatile of the rare earths and that Dy had a vapor pressure nearly 300 times higher. Samarium and Eu are also very volatile.

As lanthanum oxide has one of the highest (–negative) heats of formation among the REOs, this led to a process for reducing select rare earth oxides with La and volatilizing the products. Samarium is the rare earth metal that is primarily produced by La reduction. Samarium is used in producing all of the samarium-cobalt (Sm-Co) magnets (Fig. 9.9). The reaction of interest follows:



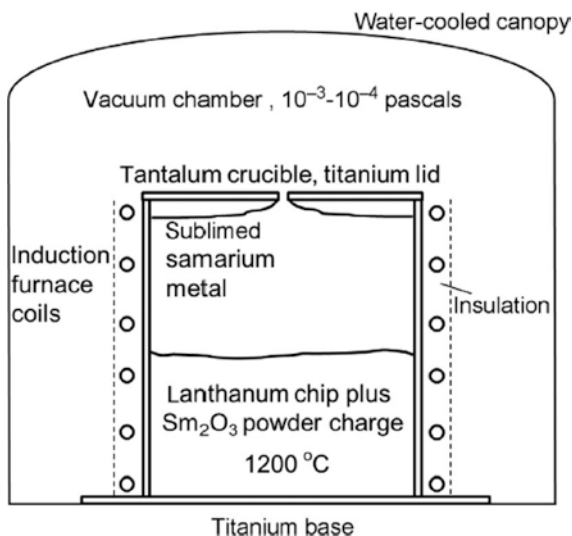


## 9.4 Molten Salt Electrolysis

### 9.4.1 Industrial Production of Rare Earth Metals by Electrolysis

The industrial production of rare earth metals by molten salt electrolysis is a commercial method to produce Ce, La, Nd, Pr, DyFe, and NdPr (known as didymium). Mischmetal is also produced. Mischmetal is the name of the alloy produced by electrolysis of oxides or chlorides of nonseparated rare earths. These alloys are dominated by Ce as it is the most abundant rare earth, typically at 40–50% of the total alloy content. Rare earths alloys do not exhibit melting point suppression, as they are chemically similar and do not interact in the molten state. The electrolytes used in these processes are selected based on the melting point of the electrowon metal. Cerium metal has a relatively low melting point of 798 °C. Of the metals electrowon, this is lowest as shown in Table 9.6. The Dy-Fe eutectic which is used in the magnet industry has a low melting point. When chloride electrolytes are used, residual chlorides can cause corrosion issues in the product, and as a result, either the fluoride route or metallothermic reduction with La and Ca is used. Didymium is the name given to Nd-Pr alloys. These alloys do not have a specific composition, and the natural ratio of approximately 3:1 that is found in bastnaesite ore is often used. Mischmetal can be composed of all the light rare earths, or alternately a Ce-La mischmetal is produced with a 65% Ce/35% La ratio. The metal melting point for these materials and electrolysis route is shown in Table 9.6. Praseodymium is rarely electrowon as pure metal.

**Fig. 9.9** Schematic of a Sm lanthanothermy system [10]



**Table 9.6** Melting points of rare earth metals produced by electrolysis

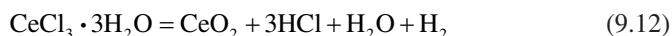
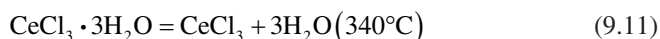
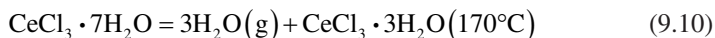
Metal	Electrometallurgy route	Melting point
Cerium	Chloride-based	795–798 °C
Lanthanum	Oxide/fluoride	920 °C
Neodymium	Oxide/fluoride	1021 °C
Praseodymium	Oxide/fluoride	931 °C
Nd:Pr (3:1) didymium	Oxide/fluoride	~990 °C
DyFe eutectic	Oxide/fluoride	~860 °C
Mischmetal	Chloride-based	>800 °C

### 9.4.2 Industrial Production of Cerium and Mischmetal

Industrial production of mischmetal began as a by-product metal produced from the extraction of thorium (Th). Thorium was extracted from monazite producing a light rare earth stream. It was found that the light rare earths when alloyed with iron (Fe) were very useful in the production of lighter flints. There had been a demand for flints for cigarette lighters and in industrial applications (e.g., starters for welding torches). Treibacher in Austria produced these materials which are still used today. The market for personal lighters has decreased as the piezoelectric lighters have taken a significant portion of the market share of flints for personal use. A primary use in the current market is the production of inoculants for steel making and nickel hydride batteries. There is a new application where cerium is alloyed with aluminum (12% Ce) to produce a nonheat treatable alloy.

The electrolysis of mischmetal and Ce is conducted in a molten salt electrolyte using the rare earth chloride with potassium and sodium chloride and small additions of fluorite (CaF<sub>2</sub>). The electrolysis is conducted at temperatures greater than 800 °C to produce a molten metal product. Graphite anodes are used with steel, graphite or tungsten (W) cathodes. The metal is collected by hand dipping the metal from the bottom collection well of the electrolytic cell.

The production of metal by this process requires the conversion of the rare earth chloride hydrates to an anhydrous rare earth chloride. The process of hydration of cerium chloride heptahydrate (CeCl<sub>3</sub>·7H<sub>2</sub>O) takes place by first removing the four waters of hydration at approximately 170 °C (Eq. 9.10), followed by the removal of the final three waters of hydration at approximately 235 °C [13]. While it appears that (CeCl<sub>3</sub>·7H<sub>2</sub>O) could undergo a hydrolysis reaction forming an oxychloride, the formation of CeO<sub>2</sub> is favored. This oxide is not electrolyzed but is a loss in the conversion of the chloride.



For other rare earths such as La, the oxychloride is favored. For these chlorides, waters of hydration usually are six, as they do not exhibit the +4 valence which favors the hydrolysis reaction.



The molten light rare earth chlorides have a large metal solubility in their respective rare earth metal. For example, cerium chloride ( $\text{CeCl}_3$ ) can significantly dissolve in cerium metal [14]. This limits the material that can be used for cell construction as the dissolved metal will reduce most oxide refractories. This can damage the refractory and dissolve alkali earth metals (Ca, Mg) and silicon (Si) into the bath where they are reduced at the cathode and thus contaminate the metal product. As a result, steel and graphite are often used for the lining of the cell. Carbon steel can also be used as some products require the addition of Fe into the final product. Preventing air regression in the cell is very important as steel will oxidize at high temperature. Notably, the oxide scale is soluble in the bath causing extensive wear. Reported performance for various electrolytic cell architectures is shown in Table 9.7 [1].

Larger cells as those that have been operated at 12KA by Remacor in Washington, Pennsylvania [16] are shown in Figs. 9.10 and 9.11. The production of La takes place in a similar electrolyte, and it has been shown that the performance of the cell is similar to that of the  $\text{CeCl}_3$  process. At bench-scale, the current yield was reported as high as 90% [17]. Lithium chloride (LiCl), KCl, NaCl, and  $\text{LaCl}_3$  electrolytes were used, with current density on the anode of about 0.8 A/cm<sup>2</sup>.

There is very little documentation on the process for the direct production of La metal. Lanthanum metal has been produced via the oxide/fluoride process in the laboratory. The chloride route can be used when producing a mischmetal. Chloride electrolysis is much easier to control as the rare earth chloride content is very high whereas in the fluoride process the solubility of the oxide is much lower [18]. The melting point of the La metal is at the extreme end of the temperature range where chloride electrometallurgy can be employed. The vapor pressure of lithium and potassium chloride is very high at this temperature leading to bath losses.

**Table 9.7** Reported performance for cell architectures

Cell type	Ceramic	Ceramic	Graphite [15]
Cell body material	Fire brick	Fire clay and cement	Graphite
Anode	Carbon	Graphite	Graphite
Cathode	Iron	Iron	Steel
Electrolyte	NaCl-CeCl <sub>3</sub>	CaCl <sub>2</sub> -CaCl <sub>3</sub>	KCl-NaCl-CeCl <sub>3</sub> -CaF <sub>2</sub>
Operating temperature	850 °C	850 °C	1000 °C
DC Amps	2300	1500	2000
Volts	14	12	12
kWh/IB	45	50	
Current yield	45%	50%	70%

## 9.5 Electrowinning of Nd, Nd-Pr, and Dy-Fe

The process for electrowinning Nd, Nd-Pr, and ferrodysprosium (Dy-Fe) takes place at temperatures ( $>1000\text{ }^{\circ}\text{C}$ ) which are difficult to operate with a chloride-based electrolyte. The bath species are very volatile at these temperatures and the rare earth chloride retains the hygroscopic nature it has at room temperature. Exposure of the electrolyte to air will result in a hydrolysis reaction forming insoluble oxychloride compounds that settle out in a slag layer at the bottom of the cell.

Before the discovery of the  $\text{Nd}_2\text{Fe}_{14}\text{B}$  magnet compositions, the demand for neodymium, praseodymium, and dysprosium alloys could be met with metallothermic reduction of these fluorides or chloride. The retorts in the reduction process typically were constructed from tantalum (Ta), resulting in significant production cost. Electrolysis processes lend themselves to scaling once the basic chemistry and materials of construction have been determined on a small scale. Some NdPr was produced by chloride electrolysis in the early stages of magnet industry development. The residual chloride in the metal produced sometimes presented corrosion problems with the magnet. This led to the decline of this process in favor of an oxide feed/fluoride bath process similar in some ways to Hall-Heroult process. The metal solubility in this type of bath is much lower than the chloride electrolyte and very little hydrolysis occurs. The hydrolysis reaction for neodymium chloride is exactly as reported for lanthanum chloride as shown above (Eq. 9.13).

Fig. 9.10 Remacor cell



**Fig. 9.11** Metal harvest from Remacor Ce cell



The oxide feed/fluoride bath process was developed by the U.S. Bureau of Mines (USBM) for light rare earth oxides in the 1960–1970s [19]. When the process was applied to cerium [20], it was found to require a partial reduction of  $\text{CeO}_2$  to  $\text{Ce}_2\text{O}_3$  since the +4 valance is not stable in molten fluorides and  $\text{Ce}_2\text{O}_3$  slowly converts back to ceric oxide over time. The reduction method requires carbon (C) or hydrogen ( $\text{H}_2$ ) to produce cerous oxide. Direct addition of the  $\text{CeO}_2$  to the electrolyte flashes off some of the oxygen [21]. At the cell operating temperature, this is very reactive when graphite shells and anodes are used, causing wear.

Similarly, direct addition of praseodymium oxide ( $\text{Pr}_6\text{O}_{11}$ ) to fluoride flashes off oxygen resulting in cell wear. Praseodymium oxide is readily converted to  $\text{Pr}_2\text{O}_3$  by heating in slightly reducing conditions. The solid solution of Pr-Nd oxides results in stability of  $\text{Pr}_2\text{O}_3$  [22]. The process was applied to lanthanum oxide ( $\text{La}_2\text{O}_3$ ) [23]. For La, Nd, and NdPr, the stability of the trivalent metal ion provides for solubility of the oxide in the electrolyte so that metal electrowinning can be conducted [24].

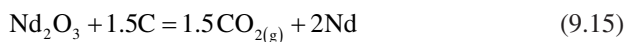
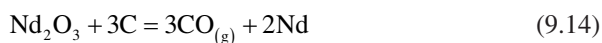
### 9.5.1 Commercial Production of Nd, Nd-Pr, and Dy-Fe

The demand from Nd, Nd-Pr, and Dy-Fe increased dramatically with development of the  $\text{Nd}_2\text{Fe}_{14}\text{B}$  magnets. Estimates of over 110,000 tons of these metals are produced annually for magnet production. Recycle rates for these magnets are very low. Cuttings or the swarf from magnets are recycled. Hydrometallurgical

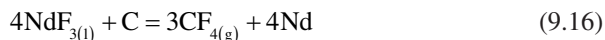
processing similar to the extraction of the rare earths from ore is practiced. The process generates oxides that then are electrowon to produce metals, alloys or ferrodysprosium (eutectic DyFe).

As discussed above, the processes for production of Nd, Nd-Pr, and Dy-Fe were developed by the USBM in the 1960s [19–23, 25, 26] where oxide solubility was on the order 3% [26]. This resulted in development of a control process that avoids the “*anode effect*” which is similar to that of the Hall-Heroult process. The major difference is the configuration of the anode and cathode—the Hall-Heroult process uses horizontal electrodes, and the anode and cathodes of the rare earth cells are vertical. Vertical electrodes have the advantage of the buoyancy of the anode off-gas using the gas lift to help keep the anodes fed with oxide. In both the Hall-Heroult process and rare earth electrowinning, the anode effect produces tetrafluoromethane [27]. The bath composition in electrowinning Nd and NdPr uses the highest (86–90%) concentration of rare earth fluoride with additions of lithium fluoride to reduce the melting point of the electrolyte. Ideally the electrolyte should melt approximately 100 °C below that of the metal produced (Table 9.6). The cell should operate with enough superheat as to impart to the melt enough heat that it does not freeze in the handling equipment. Typical cells now operate in a 2000–4000 ampere load, without lids, and as a result they are not very thermally efficient. Typical operating parameters are shown in the Table 9.8 [28].

Anode wear occurs because of the production of CO at the anode. Mechanical wear is a strong function of the geometry of the cell. In the operation of the cell, most of the anode gas is CO unlike in the aluminum process where CO<sub>2</sub> is produced. Reactions occurring at the anode include



The anode effect reaction occurs when the concentration of dissolved oxide falls to low concentration.



An estimate of the combination of mechanical wear and electrochemical wear was determined by Lynas [29]. Production of CO results in wear rate of about 0.12 kg C/kg Nd, whereas total wear is estimated about 0.45 kg C/kg Nd [29]. Measurement of this value is very important with respect to the economics for production of Nd and NdPr, as graphite is consumed as a raw material and can cost \$4–11/kg. Figure 9.12 shows a typical Nd cell.

Ferrodysprosium is produced in a similar cell configuration. The demand for ferrodysprosium in the production of Nd<sub>2</sub>Fe<sub>14</sub>B magnets is only about 2% [28]. While only percent additions of Nd or NdPr are used in sintered magnets, very little is used in the production of bonded magnets. Ferrodysprosium can be produced by

**Table 9.8** Nd cell operating parameters [28]

Operation parameter	Value
Cell voltage	9–11 V
Cell current	1.8–2.5 kA
Current yield	65–78%
Anode current density	1–1.25 A/cm <sup>2</sup>
Cathode current density	5–6.5 A/cm <sup>2</sup>
Power consumption	11–13 kWh/kg
Material yield	95%

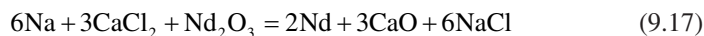
electrolysis in a DyF<sub>3</sub>-LiF bath [30], where the melting point of the iron-dysprosium (Fe-Dy) eutectic is approximately 860 °C. In the production of ferrodysprosium, both the anode and cathode current densities are controlled. The composition of the consumable Fe cathode is controlled through the use of low-carbon steels with low concentrations of other transition metals such as manganese (Mn) and chromium (Cr).

### 9.5.2 Alternative Rare Earth Electrodeposition

There are two methods for conversion of rare earth oxide to metals exclusive of molten salt electrolysis or metallothermic reduction. The Fray Farthing Chen (FFC) method [31] has been applied to ceria (CeO<sub>2</sub>) and neodymium oxide (Nd<sub>2</sub>O<sub>3</sub>). Room temperature ionic liquids (ILs) have been studied in Nd electrolysis [12].

#### Neochem Process

During the initial development of the Nd<sub>2</sub>Fe<sub>14</sub>B magnets, it was necessary to develop a method to produce large amounts of Nd. The electrowinning method developed for mischmetal is difficult to operate at 1100 °C, where the Nd has enough superheat to be tapped from a cell. The fluoride process developed by the USBM has not been commercialized [18]. To meet this need, Sharma and others at GM [32–34] developed a two step metallothermic process where Na can be used as reductant.



This process was developed and installed at Delphi (at the time a subsidiary of GM) [30]. Lime (CaO) and NaCl are not recycled. The process has the advantage of using Na metal instead of the more expensive and higher melting calcium. Once mixed, the Na metal reduces the calcium chloride (CaCl<sub>2</sub>) to Ca metal, which then reduces the Nd<sub>2</sub>O<sub>3</sub>. Calcium oxide has a high solubility in CaCl<sub>2</sub> which allows the process to proceed without interfering with the reduction process. In this process,



**Fig. 9.12** Neodymium cell. (Cell was operated by Great Western Resources which has a W cathode center electrode [29])

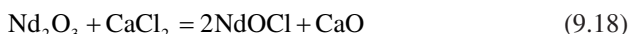
pure Nd metal was not produced, but a eutectic of neodymium and iron (Nd-Fe) or neodymium-zinc (Nd-Zn) resulted. This allowed the process to operate at approximately 750 °C [32]. The process was commercialized as part of the Magnaquench process to produce magnets; however, it fell into disfavor once the electrowinning production methods were developed.



### The FFC Process

The FFC (Fray, Farthing, and Chen) process has been used to reduce  $\text{CeO}_2$  to Ce metal in a  $\text{CaCl}_2$  bath [34]. The process used a graphite anode and  $\text{CeO}_2$  pellets held either in a basket or with wires being attached to the cathode. The process produces Ce metal with some contamination of Ca metal. A significant amount of cerium oxychloride is formed during the reaction. Current yields are approximately 60–70% [34]. As the oxide solubility in Ce metal is low, a good quality deposit was produced. This work was conducted on a very small scale, and scale-up to a larger process has not been attempted.

The reduction of  $\text{Nd}_2\text{O}_3$  by the FFC process has been attempted; however, this process is not very viable as  $\text{Nd}_2\text{O}_3$  reacts chemically with the bath to form a neodymium oxychloride ( $\text{NdOCl}$ ).



The reduction of  $\text{NdOCl}$  can proceed after the  $\text{NdOCl}$  has been sintered [31]. This process was studied using a yttria ( $\text{Y}_2\text{O}_3$ )-stabilized membrane anode. No current yield data were reported.

### Inorganic Liquids

The use of ILs, also referred to as Ionic Liquids, has the appeal of operating at room temperature. These solutions have been used to study electrolysis. Inorganic liquids are similar to molten salts, however organic molecules are used. The organic molecules have higher viscosities of solution compared to conventional molten salts. Work has been conducted by first creating a salt. Neodymium oxide is first refluxed with bis-(trifluoromethyl sulfonyl)imide acid ( $\text{Nd}(\text{TFSI})_3$ ), which is then washed with dichloromethane, and subsequently the electrolyte is formulated with trimethyl phosphate. Electrolysis is conducted in this liquid. Very small deposits of Nd metal were formed [12]. It was found that electrowinning with this process was not useful, and that only electrorefining could be conducted. In electrowinning, some of the bis was destroyed and decomposed on the anode [12].

## 9.6 Environmental Concerns

Reduction processes can have considerable environmental effects. The carbon footprint can be significant depending on the embedded carbon in the raw materials used in metallothermic reduction and the source of the electric power in electrolysis.

Also important is the formation of fluorocarbons. Using Nd as an example, processing results in depleting the electrolyte of neodymium fluoride ( $\text{NdF}_3$ ) and can

result in the emission of carbon tetrafluoride (CF<sub>4</sub>), a greenhouse gas that is 6200 times more potent than CO<sub>2</sub>. Preventing fluorocarbon emissions requires expensive off-gas scrubbing. The use of an anode that is inert to bath conditions represents a significant advancement over the state-of-the-art carbon anode technology.

## 9.7 Conclusions

Once the rare earth metals are separated from one another, they must be reduced from the oxides to the respective metals in relatively pure form to be useful for applications such as permanent magnets. Due to the thermodynamic instability of the metals, this final reduction adds substantially to the cost and energy to the rare earth metals manufacturing process. Both electrolytic and metallothermic processes have been used to reduce rare earths. The electrolytic processes have the advantages that (1) they can be operated continuously and (2) can replace the use of costly reactive metal reductants with electric power which would be expected to become more cost-effective and have a lower embedded carbon footprint as a result of renewable power penetration. Additionally, refining requirements, to remove residual metal reductants, are not required for the electrolytic reduction route.

## References

1. C.K. Gupta, N. Krishnamurthy, *Extractive Metallurgy of Rare Earths, Chapter 4* (CRC Press, 2005)
2. A.J. Bard, R.L. Faulkner, *Electrochemical Methods, Fundamentals and Applications, Chapter 2*, 2nd edn. (2001)
3. M. Albander, *Chemical Extraction, Beneficiation, Production, and Application of the Rare Earths Metals* (Tech. Print, 2012)
4. F.E. Block, T.T. Campbell, R.E. Mussler, G.B. Robidart, Preparation of High-Purity Yttrium by Metallic Reduction of Yttrium trichloride. Bureau of Mines RI 5588 (1960)
5. A.H. Daane, F.H. Spedding, Preparation of yttrium and some heavy rare earth metals. *J. Electrochem. Soc.* **100**(10), 442–444 (1953)
6. M.R. Esquivel, A.E. Boh, D.M. Pasquevich, Carbochlorination of cerium dioxide. *Mineral Processing and Extractive Metallurgy* **111.3**, 149–155 (2002)
7. P.M.J. Gray, The production of pure cerium metal by electrolytic and thermal reduction processes. *Trans. Inst. Mining. Met* **61.1** (1952)
8. N. Krishnamurthy, C.K. Gupta, Extractive metallurgy of rare earths. *Int. Mater. Rev.* **37.1**, 197–248 (1992)
9. R.A. Sharma, Metallothermic Reduction of Rare Earth Oxides. U.S. Patent No. 4,578,242. (25 Mar. 1986)
10. F. Habashi, Metallothermic reactions – Past, present and future. *Res Rep Metals* **2**, 1 (2018)
11. L.M. Pidgeon, W.A. Alexander, Thermal production of magnesium – Pilot plant studies on the retort ferrosilicon process. *Trans. AIME* **159**, 315 (1944)
12. P. Sindhu, Investigation of the Electrowinning of Neodymium Oxide in Room Temperature Ionic Liquid. Colorado school of Mines, MS Thesis (2019)

13. S. Xue, W. Wu, X. Bian, Y. Wu, Dehydration, hydrolysis and oxidation of cerium chloride heptahydrate in air atmosphere. *J. Rare Earths* **V35**, 1156–1163 (2017)
14. D. Cuvicciotti, Metal-salt interactions at high temperature: The Cerium-chloride system. *J. Am. Chem. Soc.* **71 I 12**, 4119–4121 (1949)
15. A.N. Zelikeman, O.E. Krein, G.V. Samsonov, *Metallurgy of Rare Metals. Izsatel'stovo Metallurgiya* (1964), p. 293
16. Remacor Sale Brochure 1994
17. D.K. Sahoo, H. Singh, Current efficiency in electro-winning of lanthanum and cerium metals from molten chloride electrolytes. *Rare Metals* **32(3)**, 305–311 (2013)
18. E.S. Shedd, J.D. Marchant, T.A. Henrie, Electrowinning and Tapping of Lanthanum Metal. USBM RI 6882 (1966)
19. E. Morrice, M.M. Wong, Fused salt electrowinning and electrorefining of rare earths and yttrium metals. *Min. Sci. Eng. J.* (1979)
20. E. Morrice, B. Porter, E.A. Brown, C. Wyche, R.G. Knickenbocker, Electrowinning Cerium-Group and Yttrium Group Metals. USBM RI 5868. 1961
21. B. Porter, E.S. Shedd, C. Wyche, J.D. Marchant, R.G. Knickenbocker, Higher purity ingot cerium from molten salts. *J. Met.*, 798–803 (Oct 1960)
22. E. Morrice, E.S. Shedd, T.A. Henrie, Direct Electrolysis of Rare Earth Oxides to Metals and Alloys in Fluoride Melts. USMB RI 7146, 1968
23. E. Morrice, C. Wyche, T.A. Henrie, Electrowinning Molten Lanthanum from Lanthanum Oxide. USBM RI 6075 1962.
24. I.S. Hirschhorn, Commercial production of rare earth metals by fused salt electrolysis. *JOM*, 19–23 (March 1968)
25. E. Morrice, E.S. Shedd, T.A. Henrie, Direct Electrolysis of Rare Earth Oxides to Metals and Alloys in Fluoride Melts. USBM Ri 7146 (1968)
26. D.K. Dysinger, J.E. Murphy, Electrowinning of Neodymium from a Molten Oxide-Fluoride Electrolyte. USBM RI 9504 (1994)
27. S. Liu, L. Chen, B. Li, L. Wang, B. Yan, M. Liu, Anode process for Nd electrowinning from LiF-NdF<sub>3</sub>-Nd<sub>2</sub>O<sub>3</sub> melt. *Electrochim. Acta* **V147**, 82–86 (2014)
28. H. Vogel, B. Friedrich, Developments and research trends of the neodymium-electrolysis – A literature review. *Proc. EMC* (2015)
29. Environ Australia Pty. Environmental Effects Report for Didymium Pilot Plant. June 13, 2013. p.12
30. W. Shi, Method for Preparing Dy-Fe Alloy through Oxide Molten Salt Electrolysis, Patent, CN 102140656 A 8/3/2011
31. J. Song, M. Gua, A. Mukherjee, B. Blanpain, J. Fransaer, Extraction of neodymium by direct reduction of NdOCl in molten calcium chloride. *Electrochim. Acta* **V257**, 463–472 (2017)
32. R.A. Sharma, Neodymium production processes. *J. Met.* **39**, 33–37 (1987)
33. R.A. Sharma, R.N. Seefurth, A Molten Salt Process for Producing Neodymium and Neodymium- Iron Alloys. *Metall. Trans. B* **20B**, 805–812 (Dec 1989)
34. B. Claux, J. Serp, J. Fouletier, Electrochemical reduction of cerium oxide into metal. *Electrochimica Acta* **V56**, 2771–2780 (2011)

# Chapter 10

## Rare Earth Element Reduction to Metals



**Tommee Larochelle**

### 10.1 Introduction

This chapter presents an overview of the current processes for the reduction of rare earth elements (REE) to metals which is a critical step in the supply chain of many REE used in technological applications. The magnet elements (praseodymium (Pr), neodymium (Nd), samarium (Sm), terbium (Tb), and dysprosium (Dy)) possess unique properties rendering them difficult to replace in permanent magnet applications because of their very high strength to weight ratio. Permanent magnets are used in a multitude of applications, with the main applications including:

- Office equipment: Hard drives, printer drives, and copiers.
- Appliances: Air conditioners, refrigerators, washing machines, and shavers.
- Motors: Elevators, Robots, injection molding, linear and voice coil motors.
- Automobiles: Hybrid/electric drives, generators, air conditioners, power steering, audio system, and sensors.
- Other: MRIs, train motors, wind turbines, and electric bicycles.

The most common REE permanent magnet is neodymium-iron-boron (NdFeB), with samarium cobalt (SmCo) making up a smaller percentage of the market. NdFeB magnets have the highest magnetic strength per weight of all the permanent magnets and no tooling is required in their fabrication. However, they corrode easily, can lose their magnetic strength at relatively low temperatures, and are difficult to initially magnetize [1]. Samarium cobalt magnets are resistant to corrosion, stable in a wide range of temperatures, but they can be expensive as their price is strongly linked to the cobalt (Co) spot price as they require large amounts of Co and are more difficult to make, only coming in simple shapes [1]. Other rare earth

---

T. Larochelle (✉)  
L3 Process Development, Bent Mountain, VA, USA  
e-mail: [tommee.larochelle@l3processdev.com](mailto:tommee.larochelle@l3processdev.com)

metals, such as Dy or Tb, can replace small amounts of the Nd in the NdFeB alloy to alter and upgrade specific properties of the magnets. Dysprosium is added to increase the coercivity and corrosion resistance of the magnet while Tb is added to increase the allowable operating temperature.

A mixed REE alloy is used in the anode of the batteries to improve durability and manipulation characteristics. Typically, La is the alloying REE of choice, but the anodes also contain a variety of other metals. Rare earths make up 3 to 14% of the mass of a battery cell inclusive of its casing [2], which come in various sizes and are used in a multitude of applications. Large batteries are typically used in automobile and energy applications while smaller batteries are used in portable electronic devices such as computers, cell phones, power tools, medical equipment, and other applications.

Metallurgical applications of the REE are mainly comprised of hydrogen ( $H_2$ ) storage, mischmetal, and specialty alloys. While  $H_2$  fuel is a potential source of alternative fuels being heavily discussed, it presents challenges for storage. High pressures are required because of the gas cryogenic nature (very low-temperature boiling point) and low energy density, requiring a substantial amount of the material. Hydrogen has many beneficial properties as a combustion fuel source since it is not a hydrocarbon (contains no carbon), its combustion only generates heat and water. The favored alternative to high-pressure hydrogen storage is molecular storage [3]. In this process,  $H_2$  is absorbed in or on a compound, forming bonds in a similar fashion as water in hydration bonds. The result is a storage method that does not require high operation pressures, but still maintains a low storage volume per unit of  $H_2$ . Lanthanum-nickel ( $LaNi_5$ ) alloys can store up to 2.2% of their weight through  $H_2$  absorption [4]. This alloy favorably compares to its alternatives and its use is growing.

Light REEs, primarily cerium (Ce) and La, with small amounts of Pr and Nd form an alloy referred to as mischmetal. Mischmetal is added to steel during the steelmaking process in order to bind with contaminant elements such as oxygen ( $O_2$ ) and sulfur (S) to improve properties of the steel, such as corrosion resistance. When REEs react with  $O_2$  and S, they form rare earth oxysulfides which replace manganese sulfide (MnS) and various oxide inclusions from the steel slag, increasing the overall steel strength and resistance to cracking [5]. High-carbon (C) steels and stainless steels can also be doped with Y and Ce to increase their temperature performance, oxidation resistance, ductility, and other thermal and mechanical properties [5]. Finally, REEs can also be used as alloying elements in a variety of alloys such as magnesium (Mg), aluminum (Al), and zinc (Zn) alloys. The most promising alloy is the aluminum-scandium (AlSc) alloy, which is expected to allow for the welding of aircraft bodies instead of the current riveting processes, reducing weight considerably.

Rare earth metals are produced industrially by metallothermic reduction and by molten salt electrolysis processes. Molten salt electrolysis is a process using electricity as the reducing vector to convert rare earth salts or oxides to metals in a molten salt medium. The molten salt medium is selected to allow for the

solubilization of the rare earth and for operation above the rare earth melting temperature. It is currently the most important commercial process for the reduction of rare earth compounds on a throughput basis. Rare earths heavier than Nd cannot be reduced in the molten salt electrolysis process because their melting temperature is either higher than available molten salt mixture or because they possess multiple stable valences. These rare earth metals are produced using a metallothermic reduction process, in batch or semi-batch mode at relatively low production volumes. The metallothermic reduction processes use a metal with higher stability to reduce the rare earth. The produced rare earth metal is then either distilled or gravity separated from the oxidized slag.

The starting reduction materials are composed of chloride, fluoride, oxide or a mixture thereof. It is important to note that REEs have varying thermodynamic properties and that different reduction processes may be optimal for different elements. The high electropositivity of the REE coupled with their reactivity with water ( $\text{H}_2\text{O}$ ) and  $\text{O}_2$  prevents the use of aqueous media for their electroreduction. Any attempt to electrodeposit the lanthanides in aqueous media would result in the production of hydrogen at the cathode rather than the reduction of the rare earth.

The current industrial reduction processes for lanthanides have been extensively described by Krishnamurthy and Gupta in their opus on the Extractive Metallurgy of Rare Earths [6] and by Habashi in his Handbook of Extractive Metallurgy [7], both are foundation references in the past and current practices in the industry. Habashi also published a short paper summarizing the current industrial reduction processes in 2013 [8], which in addition of the two previously cited handbooks will serve as a basis for the summary of current industrial rare earth reduction processes contained herein. This summary will be augmented with recent advances in the field when applicable.

Promising innovative reduction processes such as the Electrolysis in Ionic Liquids [9–22], the FFC-Cambridge [23–25], the Infinium Fueled Anode Electrolysis [26–28], and the Carboxylate Reduction Process [29] will also be discussed.

## 10.2 Industrial REE Reduction Processes

### 10.2.1 *Metallothermic and Carbothermic Reduction*

Metallothermic reduction processes use a molten metal which reacts with the rare earth compound to form a liquid or solid compound and the rare earth metal. Highly reactive metals usually in the alkali (lithium (Li), sodium (Na), potassium (K)) or alkali-earth (Ca) groups are used for this purpose. The reduction potential of metals toward the lanthanides is a reverse function of their stability. As such, Ca is the only metal more stable than rare earth fluoride and oxides whereas the full suite of common alkali metals (Li, Na, K) and Ca are more stable than rare earth chlorides and can be used to reduce the lanthanide chlorides [30].

The general equation (unbalanced) representing lanthanide metallothermic reduction is:



where Ln is a lanthanide, X is comprised of [F, Cl, O], and M is the reducing metal.

Lanthanide chlorides have the largest suite of suitable reductants possible among the industrial raw materials for the reduction of rare earths. However, the difficulty and cost of producing and handling anhydrous rare earth chloride salts result in a much lower metal product purity rendering chlorides an unattractive medium. Instead, historical metallothermic processes relied on fluoride medium and on the reduction-distillation process of oxides [6]. In the fluoride medium processes, lanthanide oxides were either reacted with hydrofluoric acid (HF) in an aqueous solution and dehydrated using an HF atmosphere (wet process) or directly converted to fluorides using anhydrous HF or ammonium hydrogen fluoride ( $\text{NH}_4\text{HF}_2$ ) (dry process). The rare earth fluoride was then reduced using Ca under vacuum in a batch furnace lined with tantalum (Ta) and the system was cooled down. The metal ingot was separated from the calcium fluoride ( $\text{CaF}_2$ ) slag and recovered. Unfortunately, these calciothermic reduction process would leave a significant amount of Ca and Ta in the metal, up to 2% and 0.5% by weight respectively [30]. In order to reduce contamination, the calciothermic process operating temperatures were lowered through the simultaneous introduction of a lower-melting temperature alloying element such as Zn or Mg and/or calcium chloride ( $\text{CaCl}_2$ ). These added compounds would react to form a lower-melting eutectic  $\text{CaF}_2$  slag [31]. The alloying metal was then distilled under vacuum and recovered, similarly to the Kroll process [32]. In a study by Carlson et al., the Y produced using this intermediate alloy technique had less than 0.01% by weight total Ca and Mg and only contained minor amounts of Ta [31]. The subsequent introduction of Li metal as a replacement for  $\text{CaCl}_2$  in the process leads to further lowering of the reaction temperature through the formation of a lithium fluoride (LiF) slag which has a lower melting point than the  $\text{CaF}_2$ - $\text{CaCl}_2$  slag [30].

While the fluoride reduction process proved commercially viable for most rare earths, it was not applicable to the elements possessing a divalent stable state (Sm, europium (Eu), ytterbium (Yb)). During the reduction process, these elements are reduced to their respective divalent salt and never reach the metal state [30]. In order to produce these metals, the reduction process must start from the oxide material. Unfortunately, the use of Ca as a reduction agent for the lanthanide oxides is not a viable commercial production route because of the very high melting temperature of calcium oxide (CaO) resulting in inefficient processing conditions. A specific reduction process referred to as Reduction-Distillation, Lanthanothermic Reduction or as Lanthanothermy [6] was developed using molten La as a reducing agent. In this process, the rare earths oxides are reduced using La metal and subsequently distilled from the molten lanthanum. This process is based on a higher stability of lanthanum oxide ( $\text{La}_2\text{O}_3$ ) and on the lower vapor pressure of La metal with regard to other lanthanides.

Aluminothermic reduction is primarily used industrially to reduce scandium oxide ( $\text{Sc}_2\text{O}_3$ ) in situ [33] and produce an AlSc alloy for use in the industry. Scandium availability and pricing do not currently support a mass adoption of AlSc alloys, but many prospective producers are advancing their projects as the aerospace industry is evaluating such alloys for the next generation of commercial airliners. Once sufficient low-cost supply capacity exists in the market, it is expected that the AlSc alloys will become ubiquitous in all applications where weight to strength ratio is important.

Calciothermic reduction is still used industrially for the production of high-purity heavy rare earth metals such as gadolinium (Gd), Tb, Dy, holmium (Ho), erbium (Er), Lu, and Y, while lanthanothermic reduction is used industrially for the production of Sm, Eu, Tb, and Yb [34].

Carbon is with Ca, the only other element having the thermodynamic potential to reduce lanthanides. However, no successful industrial processes have been developed for the reduction of lanthanides using carbothermic reduction as a basis because it has many drawbacks such as the formation of carbides and the vaporization of rare earth metal at operating temperatures leading to the reverse reaction occurring in the gas phase with carbon monoxide (CO) [30].

General Motor Corporation has developed and patented a molten salt calciothermic reduction process applicable to oxides [35], oxychlorides [36], and fluorides [37] in which the lanthanides are reduced by Ca metal in a molten  $\text{CaCl}_2$  medium. The process is most efficient due to lower operating temperatures when utilized in combination with Fe as an alloying element for the preparation of neodymium-iron (Nd-Fe) alloys, a precursor to the NdFeB magnet alloy. Sharma has also demonstrated that Na metal could be used in lieu of Ca in this process to allow for the in situ reduction of Ca from  $\text{CaCl}_2$  [35].

### 10.2.2 Molten Salt Electrolysis

Molten salt electrolysis (MSE) is an electrochemical reduction process using molten salt as a medium instead of an aqueous solution. The high reactivity of the lanthanide metals with water precludes aqueous electrowinning. MSE is currently the most important industrial process for the reduction of REE by production volume due to its lower comparative energy requirements and its continuous operation mode unlike metallothermic reduction which occurs in batch or semi-batch mode. In the MSE process, a rare earth compound (usually a chloride, fluoride or an oxide) is dissolved in a molten salt medium under an inert atmosphere while an electrical current is circulated through the unit. Historically, the chloride system was favored by the industry; however, intensification imperatives lead to the conversion toward the oxide-fluoride system around the year 2000. Chloride systems offer current efficiencies below 50% while oxide-fluoride systems offer current efficiencies up to 87% [38].



The applicability of molten salt electrolysis as a reduction process for lanthanides is limited to lower-melting lanthanide metals such as La, Ce, Pr, and Nd [34] or to low-temperature melting alloys made with Fe, Mg, Zn, and cadmium (Cd) [30, 39]. Higher-melting lanthanides have melting temperatures resulting in high losses of molten salt medium through vaporization, or above the boiling point of the salt medium.

The molten salt electrolysis of light rare earths (La, Ce, Pr, and Nd) has traditionally been undertaken in small circular 3kA cells using vertical graphite (C) anodes and either tungsten (W) or molybdenum (Mo) cathodes [40]. Recent advances have maintained the design but increased the capacity of the cells to 4–6 kA, and more recently to 10kAV using rectangular cells instead of cylindrical [41, 42]. Typical electrolytes are composed of a mixture of lanthanide fluoride and LiF in proportion 4 to 9:1. Specific operating parameters are usually maintained as trade secrets by Chinese firms, but Milicevic reports a ratio of 7:1 as the proper proportion of lanthanide fluoride to LiF to maximize solubility without detrimentally affecting the physical properties of the electrolyte [43]. The electrolytical reaction system for the electrolysis of Nd, the most important product in value and volume, is described using the following equations: [38, 44]

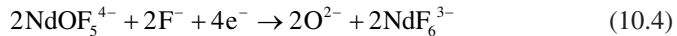
Neodymium dissolution reaction:



Cathode reaction:



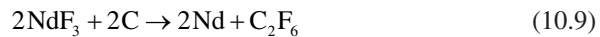
Anode reactions:



Overall reaction (carbon unbalanced):



In addition, perfluorocarbons ( $\text{C}_x\text{F}_y$ ) are emitted at the anode due to an anode effect in the system. The anode effect can be described by the following reactions [45]:



Although  $C_xF_y$  production from the LiF electrolyte is theoretically possible, its significantly higher voltage requirement makes it unlikely to be a significant contributor to  $C_xF_y$  production [44]. Nevertheless modern molten salt electrolysis processes for the reduction rare earths present significant sustainability challenges especially with regard to  $C_xF_y$  emissions from anode effect and greenhouse gases emissions as highlighted in numerous life cycle assessments [39, 42]. They are also much more expensive to operate than many other metal reduction processes, prompting researchers to work on optimizing the current processes and on developing a new generation of more sustainable technologies.

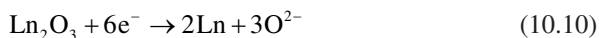
## 10.3 Novel REE Reduction Processes

### 10.3.1 FFC Cambridge Process

The FFC-Cambridge Process [22] is a zero liquid discharge process initially discovered by Fray, Farthing, and Chen of Cambridge that is currently being developed by Metalysis for the production of titanium (Ti), Ta, Al, and high-entropy alloys. Metalysis has reported successful production of Ce, Nd, and Y metals using the FFC-Cambridge process and it claims its process is suitable for all rare earth with the exception of La [22]. Lanthanum oxide reacts with molten  $CaCl_2$  salt to form an oxychloride which does not electro-reduce to metal. However, it was determined by Zhu et al. [23] that sintering  $La_2O_3$  with nickel oxide (NiO) at sufficiently high temperature prior to the FFC-Cambridge process allowed for the production of  $LaNi_5$   $H_2$  storage alloy powder.

The FFC-Cambridge Process for lanthanides can be described by the following reactions:

Cathode deoxygenation reaction:



Anode reactions:



Overall reaction (carbon unbalanced):



The FFC-Cambridge process is a batch electro-deoxidation process in molten salt medium where the metal oxide is pelletized and reduced in situ at the cathode yielding a metal or metal alloy pellet. The metal pellet is then ground and washed to yield a metal powder product [25]. While it is unlikely that the FFC-Cambridge

process will challenge the oxide-fluoride molten salt electrolysis for light REE, it presents a valuable alternative to metallothermic reduction processes used for the heavier lanthanides and could present an interesting alternative for the production of complex magnetic alloys. The nanometric metal powder nature of the product also increases the attractiveness of the FFC-Cambridge process, enabling the direct production of bonded and sintered magnets.

### ***10.3.2 Fueled Anode Molten Salt Electrolysis***

The Fueled Anode Molten Salt Electrolysis process [26] that was being developed by Infinium prior to its closure is a significant evolution of the oxide-fluoride molten salt electrolysis process. It was commercially operated at a small scale to produce ferro-dysprosium alloy (80:20 DyFe) and the company was expected to offer other rare earth elements to the market [26].

In Infinium's molten salt electrolysis process, an oxygen ion ( $O_2^-$ ) permeable membrane is used to separate the anode from main electrolyte reservoir. Following dissolution, the rare earth ions are reduced at the cathode while the  $O_2^-$  is oxidized in the presence of fuel at the anode. Contrary to conventional molten salt electrolysis, the Infinium process used an inert liquid metal anode such as liquid silver (Ag), copper (Cu) or tin (Sn). The injection of fuel in the anodes serves many beneficial purposes such as an increase in energy efficiency and for oxidation protection [27, 28].

Infinium's process was revolutionary in that its configuration and its  $O_2$  permeable membrane precluded the electrolysis of the fluoride ion ( $F^-$ ) and when operated with a truly inert anode emitted no carbon dioxide ( $CO_2$ ).

### ***10.3.3 Carboxylate Reduction***

The Carboxylate Reduction Process (CRP) is a zero liquid discharge process developed by Hela Novel Metals that is currently being scaled up to demonstration-scale following the successful piloting of the technology. It represents a significant challenge to the legacy molten salt electrolysis and metallothermic reduction processes both from a capital and an operating standpoint. The patent application US20200047256A1 is currently pending on this novel technology [29].

CRP can be operated either as a continuous process in a series of rotary kilns or as a batch process in a static furnace. The configuration versatility of the process is expected to allow its profitable implementation at various scales. CRP uses a proprietary mixture of nitrogen ( $N_2$ ), ammonia ( $NH_3$ ), CO, and  $H_2$  to sequentially dehydrate, reduce, and refine rare earth elements into their respective pure metal powders. The process also allows mixtures of metal oxalates to be reduced to an alloy powder mixture of the elements such as NdFeB, SmCo, and AlNiCo alloys. In the first step, a metal oxalate salt is dehydrated into an anhydrous metal oxalate salt at a

temperature between 200 and 440 °C while avoiding any oxalate decomposition. In the second step, the anhydrous metal oxalate powder is decomposed to its metal state and a mixture of oxalic acid ( $C_2H_2O_4$ ) and ammonium oxalate ( $(NH_4)_2C_2O_4$ ) is recovered as a by-product. The reduction step is operated between 320 and 720 °C under pressure. In the final process step, the metal powder is refined to remove any loosely bonded nonmetal impurities such as  $O_2$ , S, and C under a different variation of the proprietary gas mixture at a temperature between 700 and 1300 °C.

As an added benefit, CRP produces a micropowder, allowing the direct utilization of the REE for bonded and sintered magnets. Hela Novel Metal recently submitted a patent application for a process to manufacture rare earth magnetic blocks from carboxylate salts in a single proprietary furnace.

While CRP shows great promise for the reduction of REE to their respective metals or alloys, it is important to note that Hela Novel metals have also demonstrated the applicability of the CRP process to many other critical metals and alloys thereof such as Ti-6Al-4 V, ferroniobium, nuclear grade zirconium (Zr) alloys, and Co alloys. In addition, Hela Novel Metal has identified alternative carboxylates such as ammonium metal carboxylates which provide for reduced energy requirement from the process.

### ***10.3.4 Ionic Liquid Electrodeposition***

Details on the ionic liquid (IL) electrodeposition process are provided in detail in Chap. 8. Salient points from that chapter follow.

The use of ILs in electrometallurgical processes promises to significantly reduce the environmental footprint associated with the production of rare earth metal by replacing the energy-intensive molten salt electrolysis and metallothermic reduction processes. A few ventures have already been established to develop a commercial ionic liquid electrodeposition process, but none has yet to succeed.

Key advantages of the utilization of ILs in the electrochemical reduction of the lanthanides include a higher potential window than alternative medium, virtually no vapor pressure at operating temperatures, a high metal salt solubility, a higher conductivity than organic solvents, and more importantly a control over the water content of the electrolyte [9]. In addition, the transition to a low-temperature emission-free process would eliminate the large amount of  $CO_2$  and  $C_xF_y$  emissions currently resulting from conventional processes.

It is important to note that the electrical conductivity of ILs at room temperature is approximately an order of magnitude lower than molten salts, resulting in lower electrical efficiency. This disadvantage can be mitigated by operating IL units at high temperature ( $>100$  °C) [10]. Similar to molten salt electrolysis, the existence of a stable +2 valence for Sm, Eu, and Yb creates additional hurdles in ILs.

Various ionic liquids are being investigated for the electrodeposition of rare earth elements.

- *Imidazolium ILs*: Significant issues have been reported using imidazolium ( $C_3H_5N_2^+$ )-based ILs, notably related to the decomposition of the IL under operating conditions [11, 12]. One potential avenue is the production of transition metal alloys of REE [13].
- *Pyrrolidinium ILs*: Successful deposition of REE metals was observed using pyrrolidinium ( $C_4H_{10}N^+$ ) ILs. Notably, Bourbos et al. successfully prevented the breakdown of the IL anion  $[NTf_2]$  by using neodymium chloride in dimethylsulfoxide (DMSO) in a separate anode compartment [10]. This two-compartment design allowed for the utilization of neodymium chloride ( $NdCl_3$ ) as a feed material and the production of gaseous chlorine rather than the decomposition products of the  $[NTf_2]$  anions, resulting in much more favorable economic prospects in a more environmentally friendly process.
- *Phosphonium ILs*: All investigations of phosphonium ( $PH_4^+$ ) ILs as a medium for the electrodeposition of REE have highlighted the critical role played by water in the system. Water is both required for the process to operate and deleterious to the product [14–16]. As such, the potential of phosphonium ILs for the electrodeposition of rare earth elements is rather dubious.
- *Neutral Ligand Complexation ILs*: These represent one of the most promising approaches to the electrodeposition of rare earth metals in ILs. Recent investigations demonstrated that REE could indeed be successfully deposited onto a cathode substrate using a neutral ligand solvent (NLS) to generate a lanthanide IL cation through the dissolution of a lanthanide triflimide salt [17–19]. The potential commercial success of this approach lies in the electrostability of the medium and with its implicit self-regeneration. However, similar to other IL mediums, additional research on the anodic reaction will be required to replace the decomposition of the  $[Ntf_2]$  anion with a different anion and allow for its reuse in the production of the lanthanide salt feed material.
- *Aluminum Chloride ILs*: The reduction of Al and Al alloys from aluminum chloride ( $AlCl_3$ )-based IL medium has been extensively investigated in the past [20–22]. However, these processes have yet been proven to be sufficiently economical to replace legacy industrial processes. The incentives with regard to rare earths such as the utilization of relatively inexpensive chlorides, the absence of fluorides, and a low operating temperature suggest that research into these systems is likely to increase drastically in the foreseeable future. A subsequent distillation step would be required for the purification of the rare earth metal, not unlike current lanthanothermic processes.

## 10.4 Technology Outlook

Global economics and geopolitical considerations in the last two decades allowed China to consolidate the RE industry vertically. This situation currently raised some alarming flags with respect to RE supply chain and pricing.

No significant REE metal reduction plants exist outside of China with the exception of a small Japanese integrated supply chain. More importantly, the two main obstacles to the establishment of an REE reduction plant outside of China are a stable availability of high-purity separated REE raw materials and the absence of a significant market for the rare earth metals produced. All novel processes discussed in this chapter were also being designed for the production of other technological metals for which conventional processes are onerous and complicated such as for Ti, Zr, and advanced alloys.

The development of a novel more efficient process for rare earth reduction such as the FFC-Cambridge, the Infinium, and the Carboxylate reduction process is not enough in themselves to challenge the domination of the Chinese industry. They can however be part of a larger effort by the Occident to reestablish an industry supply chain starting from deposits to separation to reduction and finally to the production of REE-containing products. The commercialization of new processing technologies across the supply chain would then be the key to a rebalancing of market forces.

In the next decade, additional research on ILs electrodeposition is likely to lead to its implementation in China as a replacement for both the molten salt electrolysis and the metallothermic reduction processes. Its adoption outside of China will likely be precluded by the market forces described above.

## References

1. D. Brown, B.M. Ma, Z. Chen, Developments in the processing and properties of NdFeB-type permanent magnets. *J. Magn. Magn. Mater.* **248**(3), 432–440 (2002). [https://doi.org/10.1016/S0304-8853\(02\)00334-7](https://doi.org/10.1016/S0304-8853(02)00334-7)
2. L.E.O.C. Rodrigues, M.B. Mansur, Hydrometallurgical separation of rare earth elements, cobalt and nickel from spent nickel-metal-hydride batteries. *J. Power Sources* **195**(11), 3735–3741 (2010). <https://doi.org/10.1016/j.jpowsour.2009.12.071>
3. J. Graetz, New approaches to hydrogen storage. *Chem. Soc. Rev.* **38**(1), 73–82 (2009). <https://doi.org/10.1039/b718842k>
4. S.K. Pandey, A. Srivastava, O.N. Srivastava, Improvement in hydrogen storage capacity in LaNi<sub>5</sub> through substitution of Ni by Fe. *Int. J. Hydrog. Energy* **32**(13), 2461–2465 (2007). <https://doi.org/10.1016/j.ijhydene.2006.12.003>
5. J.F. Collins, V.P. Calkins, J.A. McGurty, *Applications of Rare Earths to Ferrous and Non-Ferrous Alloys*. <https://doi.org/10.2172/4215576>
6. Gupta C. K. and Krishnamurthy, N., *Extractive Metallurgy of Rare Earths*. 2004
7. F. Habashi, *Handbook of Extractive Metallurgy: Precious Metals, Refractory Metals, Scattered Metals, Radioactive Metals, Rare Earth Metals* (Wiley-VCH, 1997)
8. F. Habashi, *Extractive Metallurgy of Rare Earths* **52**(3), 224–233 (2013). <https://doi.org/10.1179/1879139513Y.0000000081>
9. A.P. Abbott, K.J. McKenzie, Application of ionic liquids to the electrodeposition of metals. *Phys. Chem. Chem. Phys.* **8**(37), 4265–4279 (2006). <https://doi.org/10.1039/b607329h>
10. E. Bourbos, I. Giannopoulou, A. Karantonis, I. Paspaliaris, D. Pantias, Reduction of light rare earths and a proposed process for Nd electrorecovery based on ionic liquids. *J. Sustain. Met.* **4**, 395 (2018)

11. R. Rama, A. Rout, K.A. Venkatesan, M.P. Antony, P.R. Vasudeva Rao, Electrochemical behavior of Eu(III) in imidazolium ionic Liquid containing Tri-n-Butyl phosphate and N,N-dihexyloctanamide ligands. *J. Electroanal. Chem.* **757**, No. **iii**, 36–43 (2015). <https://doi.org/10.1016/j.jelechem.2015.09.005>
12. X. Xu, S. Sturm, J. Zavasnik, K.Z. Rozman, Electrodeposition of a rare-earth iron alloy from an ionic-liquid electrolyte. *ChemElectroChem* **6**(11), 2860–2869 (2019). <https://doi.org/10.1002/celec.201900286>
13. Q.B. Zhang, C. Yang, Y.X. Hua, Y. Li, P. Dong, Electrochemical preparation of nanostructured lanthanum using lanthanum chloride as a precursor in 1-Butyl-3-methylimidazolium dicyanamide ionic liquid. *Phys. Chem. Chem. Phys.* **17**(6), 4701–4707 (2015). <https://doi.org/10.1039/c4cp05266h>
14. A.M. O'Mahony, D.S. Silvester, L. Aldous, C. Hardacre, R.G. Compton, Effect of water on the electrochemical window and potential limits of room temperature ionic liquids. *J. Chem. Eng. Data* **53**(12), 2884–2891 (2008). <https://doi.org/10.1021/je800678e>
15. L. Sanchez-Cupido, J.M. Pringle, A.L. Siriwardana, A. Unzurrunzaga, M. Hilder, M. Forsyth, C. Pozo-Gonzalo, Water-facilitated electrodeposition of neodymium in a phosphonium-based ionic liquid. *J. Phys. Chem. Lett.* **10**, 289 (2019)
16. L. Sanchez-cupido, J.M. Pringle, A.I. Siriwardana, M. Hilder, M. Forsyth, C. Pozo-Gonzalo, Correlating electrochemical behavior and speciation in neodymium ionic liquid electrolyte mixtures in the presence of. *Water* **8**(37), 14047–14057 (2020). <https://doi.org/10.1021/acssuschemeng.0c04288>
17. P. Bagri, H. Luo, I. Popovs, B.P. Thapaliya, Trimethyl phosphate-based neutral ligand room temperature ionic liquids for electrochemical separation of rare earth elements. *Electrochem. Commun.* (2018). <https://doi.org/10.1016/j.elecom.2018.10.001>
18. P. Sidhu, *Investigation of the Electrowinning of Neodymium Oxide in Room Temperature Ionic Liquid, Colorado School of Mines* (Arthur Lakes Library, 2019)
19. G.M. Krishna, A. Rout, K.A. Venkatesan, Voltammetric investigation of some lanthanides in neutral ligand-ionic liquid. *J. Electroanal. Chem.* **856**, 113671 (2020). <https://doi.org/10.1016/j.jelechem.2019.113671>
20. Y. Zhao, T.J. VanderNoot, Electrodeposition of aluminium from room temperature AlCl<sub>3</sub>-TMPAC molten salts. *Electrochim. Acta* **42**(11), 1639–1643 (1997). [https://doi.org/10.1016/S0013-4686\(96\)00271-X](https://doi.org/10.1016/S0013-4686(96)00271-X)
21. T. Jiang, M.J. Chollier Brym, G. Dubé, A. Lasia, G.M. Brisard, Electrodeposition of aluminium from ionic liquids: Part I-electrodeposition and surface morphology of aluminium from aluminium chloride (AlCl<sub>3</sub>)-1-Ethyl-3-methylimidazolium chloride ([EMIm]Cl) ionic liquids. *Surf. Coatings Technol.* **201**(1–2), 1–9 (2006). <https://doi.org/10.1016/j.surfcoat.2005.10.046>
22. J.K. Chang, S.Y. Chen, W.T. Tsai, M.J. Deng, I.W. Sun, Electrodeposition of aluminum on magnesium alloy in aluminum chloride (AlCl<sub>3</sub>)-1-Ethyl-3-methylimidazolium chloride (EMIC) ionic liquid and its corrosion behavior. *Electrochem. Commun.* **9**(7), 1602–1606 (2007). <https://doi.org/10.1016/j.elecom.2007.03.009>
23. A.J. Fenn, G. Cooley, D. Fray, L. Smith, Exploiting the FFC Cambridge process. *Adv. Mater. Process.* **162**(2), 51–53 (2004)
24. Y. Zhu, D. Wang, M. Ma, X. Hu, X. Jin, G.Z. Chen, More affordable electrolytic LaNi<sub>5</sub>-type hydrogen storage powders. *Chem. Commun.* No. **24**, 2515–2517 (2007). <https://doi.org/10.1039/b701770g>
25. G.Z. Chen, The FFC Cambridge process and its relevance to valorisation of ilmenite and titanium-rich slag, *trans. Institutions min. Metall. Sect. C Miner. Process. Extr. Metall.* **124**(2), 96–105 (2015). <https://doi.org/10.1179/1743285514Y.0000000073>
26. Infinium. <http://www.infiniummetals.com/>. Accessed 16 Dec 2020
27. A.C. Powell, S. Pati, U.B. Pal, S.J. Derezinsky III, S.R. Tucker, Liquid Anodes and Fuels for the Production of Metals from Their Oxides by Molten Salt Electrolysis with a Solid Electrolyte, 9,206,516 (2012)
28. A.C. Powell, S.J. Derezinsky III, Primary Production of Elements, 8,795,506 (2013)

29. H.W. Kasaini, Methods for the production of fine metal powders from metal compounds (US20200047256A1). U.S. Patent and Trademark Office (2020)
30. N. Krishnamurthy, C.K. Gupta, *Extractive Metallurgy of Rare Earths, Second Edition* (2015)
31. O.N. Carlson, J.A. Haefling, F.A. Schmidt, F.H. Spedding, Preparation and refining of yttrium metal by Y-mg alloy process. *J. Electrochem. Soc.* **107**(6), 540 (1960). <https://doi.org/10.1149/1.2427739>
32. O. Takeda, T. Uda, T.H. Okabe, Ch. 2.9 Rare earth, titanium group metals, and reactive metals production, in *Treatise on Process Metallurgy 3: Industrial Processes*, (Elsevier Ltd, 2014), pp. 995–1069
33. J. Røyset, N. Ryum, Scandium in aluminium alloys. *Int. Mater. Rev.* **50**(1), 19–44 (2005). <https://doi.org/10.1179/174328005X14311>
34. J.C.K. Lee, Z. Wen, Rare earths from mines to metals: Comparing environmental impacts from China's main production pathways. *J. Ind. Ecol.* **21**(5), 1277–1290 (2017). <https://doi.org/10.1111/jiec.12491>
35. R.A. Sharma, Metallothermic Reduction of Rare Earth Oxides, 4,578,242 (1984)
36. R.A. Sharma, Metallothermic Reduction of Rare Earth Chlorides, 4,680,055 (1987)
37. R.A. Sharma, Metallothermic Reduction of Rare Earth Fluorides, 5,314,526 (1990)
38. H. Zhu, *Encyclopedia of Applied Electrochemistry* (2014)
39. E. Vahidi, F. Zhao, Assessing the environmental footprint of the Production of rare earth metals and alloys via molten salt electrolysis. *Resour. Conserv. Recycl.* **139**(April), 178–187 (2018). <https://doi.org/10.1016/j.resconrec.2018.08.010>
40. A. Schreiber, J. Marx, P. Zapp, W. Kuckshinrichs, Comparative life cycle assessment of neodymium oxide electrolysis in molten salt. *Adv. Eng. Mater.* **22**(6), 1901206 (2020). <https://doi.org/10.1002/adem.201901206>
41. B. Yao, B. Cai, F. Kou, Y. Yang, X. Chen, D.S. Wong, L. Liu, S. Fang, H. Liu, H. Wang, L. Zhang, J. Li, G. Kuang, Estimating direct CO<sub>2</sub> and CO emission factors for industrial rare earth metal electrolysis. *Resour. Conserv. Recycl.* **145**(January), 261–267 (2019). <https://doi.org/10.1016/j.resconrec.2019.02.019>
42. H. Vogel, B. Flerus, F. Stoffner, B. Friedrich, Reducing greenhouse gas emission from the neodymium oxide electrolysis. Part I: Analysis of the anodic gas formation. *J. Sustain. Metall.* **3**(1), 99–107 (2017). <https://doi.org/10.1007/s40831-016-0086-0>
43. K. Milicevic, D. Feldhaus, B. Friedrich, Conditions and mechanisms of gas emissions from didymium electrolysis and its process control, *miner. Met. Mater. Ser. Part F4*, 1435–1441 (2018)
44. H. Vogel, B. Friedrich, Development and research trends of the neodymium electrolysis – A literature review. *Proc. – Eur. Metall. Conf. EMC 2015* **2**, 689–701 (2015)
45. L. Zhang, X. Wang, B. Gong, Perfluorocarbon emissions from electrolytic reduction of rare earth metals in fluoride/oxide system. *Atmos. Pollut. Res.* **9**(1), 61–65 (2018). <https://doi.org/10.1016/j.apr.2017.06.006>



**Part III**  
**Applications – Product Manufacturing**

# Chapter 11

## Rare Earth Markets and Their Industrial Applications



Gaétan Lefebvre and Nicolas Charles

### 11.1 Introduction

The first occurrence of rare earth elements (REEs) in industrial applications can be traced back as early as 1885 when cerium (Ce) was used in urban lighting in the city of Vienna, Austria. The uses of REEs were very limited until 1960s with no more than a few thousand tons produced worldwide. A great diversification has emerged from 1970s and 1980s with the development of technological applications in nuclear, magnetic, electronic, optical and catalytic fields using exceptional properties of REEs. As a result of continuous technological progress and broadening of knowledge base, REEs enabled significant advances in technologies in the defense industry, electronics, and renewable energies [1–6]. In the future, REEs will be essential in the development of critical sectors such as robotics, electric mobility and artificial intelligence [5, 7].

Throughout the history of the REE market development and discovery, a recurring theme was observed. The rise and fall of many of the different discoveries and technological breakthroughs where REEs are involved seem to follow two trends. The first one is the evolution of consumer's demand for applications using specific REEs, playing a central role together with finding substitution technologies. The second one, which is interconnected to the first one, is the need to find new applications for some of the excess REEs extracted along with the specific REEs used in the applications. For example, production of neodymium (Nd), which is used in magnets also produces an excess of lanthanum (La) and Ce that would otherwise accumulate in large quantities with a loss of asset value.

This chapter presents a historical approach of the different REE market needs that have arisen and sometimes have disappeared following the continuous

---

G. Lefebvre (✉) · N. Charles  
BRGM-French Geological Survey, Orleans, France  
e-mail: [g.lefebvre@brgm.fr](mailto:g.lefebvre@brgm.fr)

discoveries of unique REE chemical and physical properties. It will focus on three key examples which best illustrate the trends described above. The first one is the discovery of pyrophoric alloys, then of phosphors in color television and finally of REE-based permanent magnets. Bearing in mind the diversity of REE properties, a trend toward continuous innovation involving REEs is anticipated in the future, which will continue to increase their role in modern societies.

## 11.2 1790s–1900s: Discovery of Rare Earth Elements (REEs) and First Industrial Applications: Gas Mantle and Mischmetal

The history of the REEs began in 1788 in Sweden [8]. Lieutenant and chemist C.A. Arrhenius found a black mineral in Ytterby, located twenty kilometers to the northeast of Stockholm. In 1794, Professor J. Gadolin at the University of Abo in Finland (later named Turku) studied this mineral and named it “ytterbia” (shortened 3 years later to “yttria” and then named “gadolinite” in memory of the scientist). J. Gadolin found for the first time a new kind of “earth” which he called “rare earth” (Fig. 11.1). At that time, “earth” was how the metallic oxides were described (i.e., bitter earths (magnesia), zirconium earths (zirconia) and beryllium earths (beryllia)).

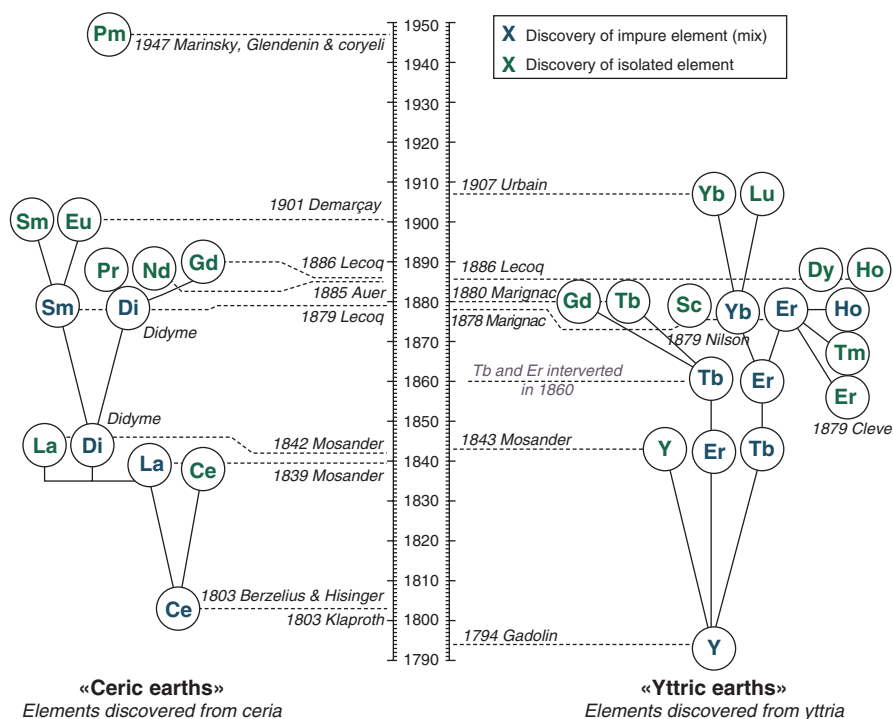


Fig. 11.1 Filiation of successive discoveries of rare earth elements [9]

In 1803, M.H. Klaproth and independently J.J. Berzelius and W. Hisinger isolated a new “earth” from another reddish and heavy mineral found by the Swedish mineralogist A.F. Cronstedt in the Bastnäs copper (Cu) mine, near the village of Ridderhyttan, 150 km to the west of Stockholm. They named it “ceria,” in reference to the asteroid Ceres discovered 2 years earlier. It would later be called “bastnäsite.” In this mineral, the researchers found new earths which they named “ochroite earths” because upon heating of the mineral a yellow substance resulted with ochre color.

In 1839, C.G. Mosander began for the first time to systematically analyze the mixed rare earths [10]. The work on rare earths individual elements was carried forward by several scientists and achieved particularly useful results through the work of R.W. Bunsen and G. Kirchhoff, who introduced spectroscopy as a control instrument for the detection of the REEs.

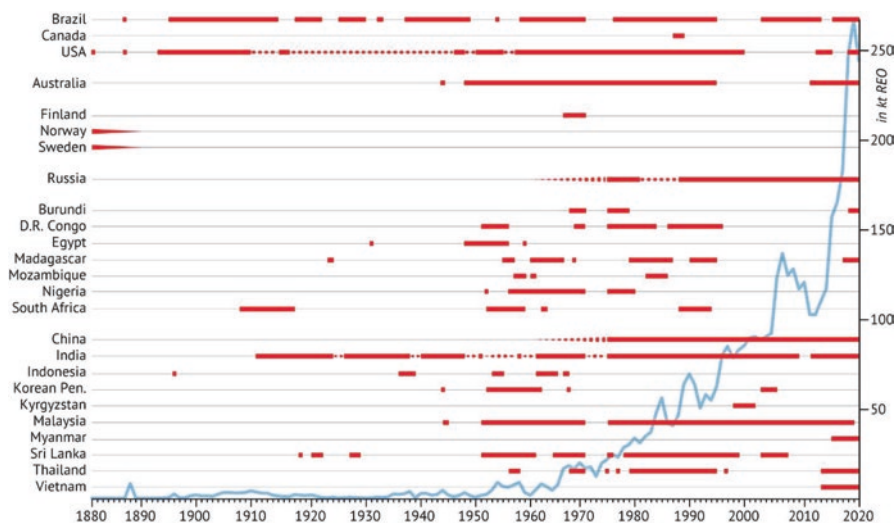
Still, REE in pure elemental form, and as derived compounds meeting strict user specifications, became only available in larger quantities during the second part of the twentieth century, thanks to the independent work of Austrian, French and American chemists, namely F. Lecoq, J.C.G. de Marignac, P.T. Cleve and E.A. Demarçay [11]. In Austria, Carl Auer von Welsbach separated Nd and praseodymium (Pr) in 1885, by fractional crystallization, noticing the strong luminescence of some REEs. Subsequently, he developed the cerium/thorium (Ce/Th) oxides soaked “Auer” gas mantles that revolutionized Europe’s urban lighting in the first part of the twentieth century. In 1903, he invented the modern lighting flint which is still widely used in cigarette lighters and consists of a ductile cerium-iron (Ce-Fe) alloy [12].

In France, Georges Urbain also worked on the separation of individual REEs using fractional crystallization, which led him in 1907 to the discovery of the last known REE, lutetium (Lu). In 1919, Georges Urbain was one of the founders of the “Société des Terres Rares,” an enterprise devoted to REEs and radioactive materials, producing gas mantles and lighting flints in the REE processing plant at Serquigny, in Normandy. Eventually, promethium (Pm) was discovered in 1947 in uranium (U) fission products from the Oak Ridge reactor (the United States).

The three major REE uses (up to the year 1930) were related either directly or indirectly to light. Two of these important inventions stem from the Austrian scientist, inventor and entrepreneur, Carl Auer von Welsbach [12, 13].

In 1889, C. Auer von Welsbach reported one of his first patents for the Auer incandescent mantle [14], which was composed of 99% thorium oxide ( $\text{ThO}_2$ ) and 1% cerium oxide ( $\text{CeO}_2$ ). This light was cheaper and more efficient than electric light for a few decades. Consequently, until the year 1935, approximately five billion incandescent mantles had been produced and consumed in the world. “Auer” gas mantles revolutionized Europe’s urban lighting in the first part of the twentieth century.

Gadolinite and bastnäsite from Sweden served at first as raw materials for the REEs and Th. Later, it was necessary to seek new raw materials as the so-called Carolina sand. This monazite-enriched sand was discovered in the United States in some gold (Au)-panning areas. Finally, a nearly inexhaustible reserve of monazite was discovered in Brazil, which guaranteed raw material supplies far into the next decades (Fig. 11.2).

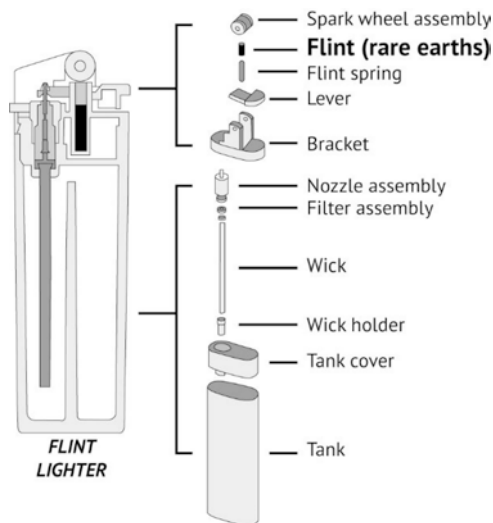


**Fig. 11.2** REE production per country and world production for the period 1880–2020. Red lines represent proven periods of production per country. Dashed red lines illustrate assumed periods of production per country. Blue Line shows rare earth oxides annual world production (in metric kt REO) [15–19]

Two situations led to new discoveries according to Auer von Welsbach. They already illustrate the specific dynamic where substitution and the need to find new applications for some of the REEs are involved. The first one was the large quantities of REEs that were left over from the production of Auer incandescent mantles and which had accumulated in large waste piles. The second one implies technology and reacting to consumer's need: the necessity for finding a simple ignition system for Auer lamps.

Thus in 1903, Carl Auer von Welsbach discovered pyrophoric alloys [13]. He was granted a patent in 1906 [20] for a pyrophoric metal alloy (“flintstone”) composed of 70% mischmetal and 30% Fe. Mischmetal (from German, *mischmetal*, metallic mixture) originally referred to an unseparated light rare earth alloy in which the natural proportions of each element are found (i.e., approximately 50% Ce, 20–25% La, 15–17% Nd and 5–10% Pr, 1% samarium (Sm) etc.).

To produce mischmetal from the large dumps resulting from the production of Auer incandescent mantles, Auer von Welsbach founded in 1907 the *Treibacher Chemische Werke* in the rooms of an iron works. In 1908, for the first time, he succeeded in producing pore-free mischmetal by fused salt electrolysis. In 1908, 800 kg of mischmetal iron flints were brought to the market. Still today, lighter flints are made of pyrophoric alloys containing 74% mischmetal and 23% Fe with small quantities of iron oxide ( $\text{Fe}_2\text{O}_3$ ) and magnesium oxide ( $\text{MgO}$ ) added for strength. The pyrophoric nature of this material means that it emits sparks when struck or scratched with steel (Fig. 11.3). The market for lighter flints was relatively important until the 2000s but has since been decreasing with progressive replacement by



**Fig. 11.3** Structure of a cigarette lighter equipped with a REE-bearing lighting flint

piezoelectric lighters. Today, major manufacturers of the pyrophoric alloy include Treibacher Industrie of Austria (which produces flints comprising 47–55% Ce, 25–36% La, 8–15% Nd and 3–7% Pr) and the Baotou Flint factory in Inner Mongolia province, China. In 2014, the global annual consumption of mischmetal for this application was <1000 tons per year [21].

The third major invention for the use of REE was the addition of rare earth fluoride as a wick in arc light carbons, which at that time, were used for a wide range of lighting purposes and later for cinema production and for searchlights as well. This use of rare earth compounds is based on the intensive arc light developed by Beck in Germany in 1910. It would be later substituted by high pressure – argon (Ar) arc lights, particularly in cinema projectors and in searchlights.

In the 22 years between 1908 and 1930, about 1100 to 1400 tons of flints were produced as the most important rare earth product. This required the consumption of about 1300 to 1800 tons of rare earth oxides (REO) in the form of rare earth chloride. If one adds to this the other applications, the consumption was probably between 2000 and 3000 tons of REO. On the other hand, at the same time, about 7500 tons of thorium nitrate ( $\text{Th}(\text{NO}_3)_4$ ) were needed for Auer incandescent mantles. If one assumes that monazite contains 6%  $\text{ThO}_2$  and 60% REE, then 30,000 tons of REO were produced during this period of which only about 10% was consumed [12].

One fact unique to REEs is that they are often extracted together as aggregate lanthanide elements, with a few exceptions, which is due to their similar characteristics with respect to their ionic radii and oxidation states. This enables them to substitute for one another in crystalline structures and explains the occurrence of multiple REEs within a single mineral [22, 23]. It is therefore also a key geological

feature of REE-bearing minerals and deposits, which leads to challenges for their extraction and separation [24]. Any extracting and processing technology to extract REEs cannot focus on one specific REE but generally leads to the concentration of all 15 lanthanides, some of them potentially having lower market value. It is also why industry has always tried to find new applications for REEs in order to maximize economic benefits from their extraction. This appears to be a trend that can be traced back to the 1930s.

### **11.3 1930s–1960s: Diversification of Uses and the Development of REE-Based Phosphors in Color Televisions**

Between 1930 and 1940, significant progress was made to develop various REE applications. Particularly successful was the production of sunglasses (“Neophan”), polishing media from REOs to replace  $\text{Fe}_2\text{O}_3$ , decolorization of glass using  $\text{CeO}_2$ , pure  $\text{CeO}_2$  as an opacifier in ceramic glazes, use of cerium oxalate ( $\text{Ce}_2(\text{C}_2\text{O}_4)_3$ ) in “peremesin” to tackle seasickness and nausea during pregnancy, and neodymium in “Thrombodym” to combat thromboses [12]. However, all these applications had only relatively small impact on REE consumption as the supply of REEs outpaced the demand. For example, the use of  $\text{ThO}_2$  as a catalyst in plants for the production of gasoline by the Fischer–Tropsch process required processing of large quantities of monazite ore (although  $\text{MgO}$  replaced  $\text{ThO}_2$  in this application after a few years). As a result, other REEs co-extracted contributed to the accumulated stockpiles with no home for their consumption. Hence the constant search for new applications.

In the 1950s, major research programs focused on the development of atomic energy first in the United States and England, then later in other countries, which was an important step in the history of REE applications. The large stockpile purchases of Th as feed material for atomic breeder reactors left behind huge quantities of REE by-products at the end of the 1950s and beginning of the 1960s.

Separation of individual REEs was one of the areas of research among others pursued in the 1950s that led to the generation of a large volume of scientific results on the properties of the rare earth metals. In this regard, the large atomic energy programs provided a great advantage for the rare earth industry. F. Spedding and his team, working for the Manhattan project at the Ames Laboratory, Iowa, made a breakthrough in 1956, by developing an effective ion-exchange process to separate individual REEs, which was better than fractionated crystallization [25]. During the same period, the Mountain Pass Carbonatite in California was discovered and mining of bastnäsite mineral was started. It was the beginning of the “Mountain Pass era” of REE production (Fig. 11.4) dominated by the United States.

The period following World War II coincided with economic prosperity and high level of consumption of material goods. This further reinforced with the Cold War context favored promoting the American way of life on the international scene. It

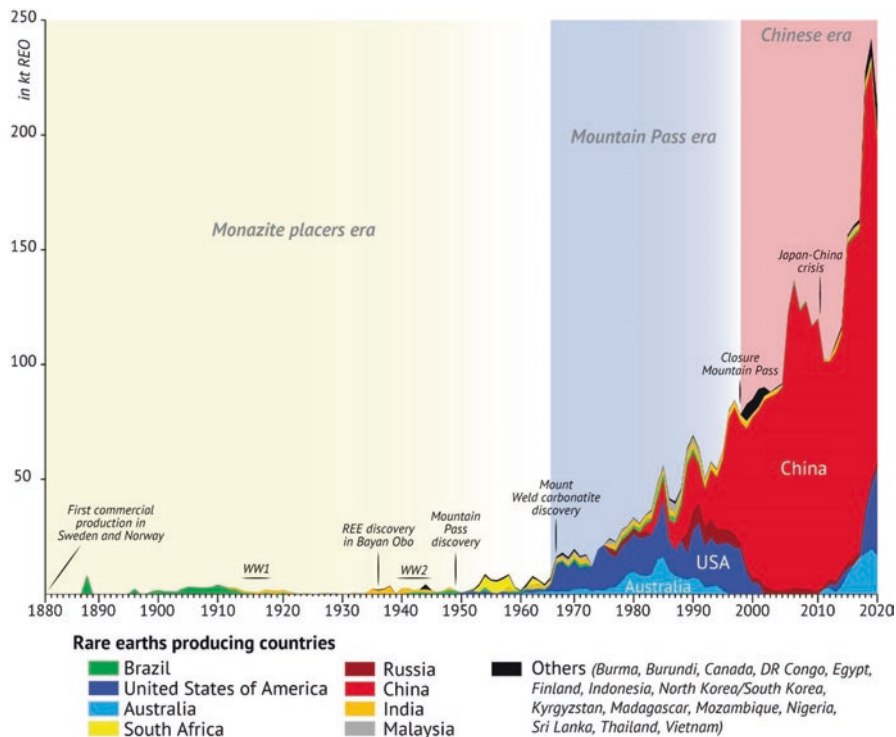


Fig. 11.4 Rare earths oxides annual world production (metric kt REO) by country from 1880 to 2020 [15–19, 26, 27]

was the beginning of widespread use of television. Although limited color broadcasts took place during the 1950s, it was not until the early 1960s that color TV started to take off, thanks in large part to the National Broadcasting Company (NBC), culminating in the color revolution of 1965.

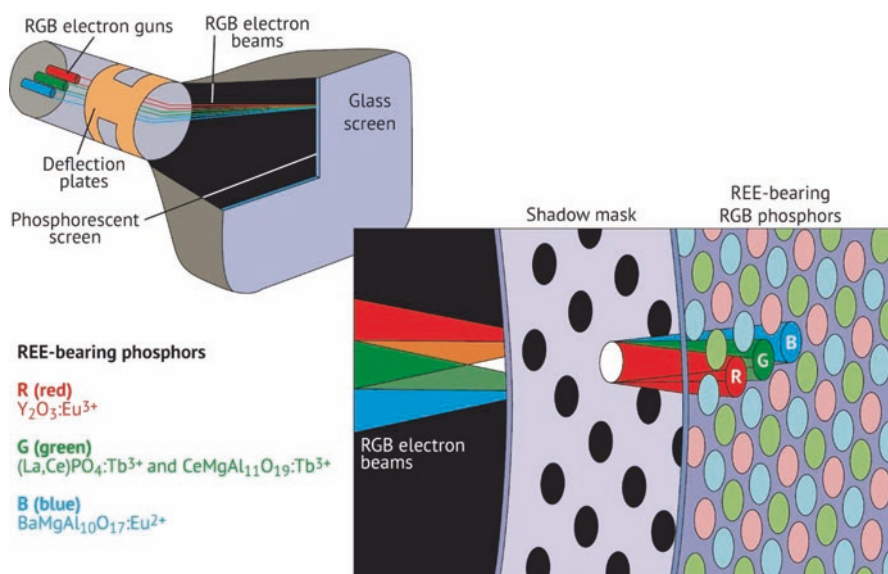
On January 12, 1950, the general public was introduced to color television for the very first time when the Columbia Broadcasting System (CBS) demonstrated its field sequential color system (FSC) on eight television sets in the Walker Building, in Washington [28]. It is noteworthy that the FSC developed by Peter Carl Goldmark was shown to the press in 1940. Then, the first commercial color broadcast took place on Monday, June 25, 1951, when CBS offered an hour-long program entitled “Premiere” to an ad hoc network of five stations in New York City, Boston, Philadelphia, Baltimore and Washington [29]. Thousands were able to watch the first color broadcast in auditoriums, department stores and hotels in these five cities, but the general public was literally left in the dark. Because the CBS color system was incompatible with existing black and white television sets, for the hour the color special was on the air, viewers tuned to CBS in these five cities saw only a blank screen [30].



For a variety of reasons, including a lack of adequate production facilities for color television sets, the expense involved in converting existing television stations to color broadcast transmissions, and the cost of color sets for the general public, the adoption of color television was slow. During the first 6 months of 1954, fewer than 8500 color television sets were manufactured in the United States [31]. Moreover, for those households that owned a color set, only a small percentage of network broadcasts were in color. During the entire 1954–1955 television season, for example, CBS only made 19 color broadcasts [32].

By the beginning of the 1960s, the markets for some of the REEs had been established. For example, there was already a market for La in the optical glass industry, for cerium as a polishing media and for praseodymium/neodymium (Pr/Nd, so-called didymium) in the glass industry for coloring and decolorization. However, no one found the need to use Sm and europium (Eu), which were other by-products. This situation suddenly changed thanks to the work of Levine and Palilla [33]. The use of expensive Eu together with yttrium (Y) made a major leap forward for the rare earth industry as red phosphors in the color TV screens (Fig. 11.5).

Due to the strong and sharp emission line of Eu at 610 Å, without a yellow component, which is perceived by the eye as a wonderfully saturated red color tone, it was possible to achieve in color TVs an evenly colored picture. This resulted in a rapidly growing color TV market, driven by consumer's demand. Thanks to such a development, in 1966, the REE world production exceeded the 10,000 tons REO threshold for the first time (Fig. 11.4). Television broadcasting stations and networks in most parts of the world upgraded from black-and-white TVs to color



**Fig. 11.5** Structure of a cathode ray tube television using REE-bearing phosphors. (Modified from [34])

transmission in the 1960s and 1970s. Throughout this period, the United States was the first producer of REEs worldwide thanks to the extraction at Mountain Pass, a situation that lasted until the 1980s.

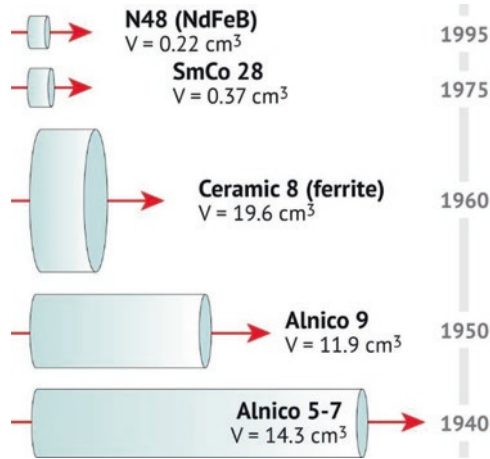
The development of REE-based phosphors in color television illustrates a great example of interplay between technological innovations driven by market needs and vice versa. The time span necessity to find new applications for some of the REEs accumulated in the mining stockpiles has been the greatest challenge for REE market expansion through history. In the case of the discovery of REEs in permanent magnets, which occurred in the following decade (1970s–1980s), a third important factor appears, for REEs played the role of a substitute in making permanent magnets.

## 11.4 1970s–1980s: The Rise of REE-Based Permanent Magnets

The first modern permanent magnet material was Alnico. It was invented in 1931 as an alloy of aluminium (Al), nickel (Ni) and Fe and progressively used in the 1940s (Fig. 11.6). A permanent magnet is a material that when inserted into a strong magnetic field will not only begin to exhibit a magnetic field of its own, but also continue to exhibit a magnetic field once removed from the original field. This field would allow the magnet to exert force (ability to attract or repel) on other magnetic materials. The ability to continue exhibiting a field while withstanding different conditions (temperature, demagnetizing field etc.) helps to define the capabilities and types of applications in which a magnet can be successfully used. Figure 11.6 exhibits the miniaturization trend of permanent magnets throughout the twentieth century. Note the dramatic decrease in size of the magnet for the same magnetic field performance.

In the 1950s, the second major permanent magnet invention was hard ferrite magnets. Although it did not present any improvement in size, its main advantages were that material costs were really low and the resistance to demagnetization was adequately high for many uses. Thus, it developed rapidly and no significant improvement in performance was considered imperative until after 45 years of production, with the introduction of lanthanum-cobalt-ferrite ( $\text{CoFe}_2\text{O}_4$ ) grades shortly after 2000 [36]. In 2014, ferrite magnets still accounted for 88% of global production of permanent magnets [21].

In the 1960s, research progress continued globally, aimed at combining REEs with transition metals, especially cobalt (Co) [37]. At that time, samarium oxide ( $\text{Sm}_2\text{O}_3$ ) continued to remain unused from monazite and bastnäs site extraction. In 1966, a first patent for samarium cobalt ( $\text{SmCo}_5$ ) magnet was granted to the U.S. Materials Laboratory [38] followed by other patents in 1970s [36, 39, 40]. At that time, SmCo magnets offered three times the strength of commercially available Alnico magnets.



**Fig. 11.6** Miniaturization evolution of permanent magnets thanks to the use of new REE-based material.  $V$  represents the volume of permanent magnet in  $\text{cm}^3$ . (Adapted from Constantinides et al. [35])

Researcher K. Strnat, credited for the invention of  $\text{SmCo}_5$  material, continued working with A. Ray and H. Mildrum at the University of Dayton, Ohio, seeking to reduce the need for cobalt because of its price and supply issues. This resulted in  $\text{Sm}_2\text{Co}_{17}$  material, which benefited from a modest reduction of Cobalt from 65% to approximately 50% in weight with substitution by Fe, which increased residual induction providing a higher energy product. The addition of Cu and zirconium (Zr) provided adequate coercivity. Still, thermal processing was more difficult than for  $\text{SmCo}_5$  and it took several years for the material to become widely produced and used. By 1975,  $\text{Sm}_2\text{Co}_{17}$  had been developed with a higher energy product and a high anisotropy field. In terms of volume, SmCo magnets were 32 times smaller compared to a “Alnico 9” and 53 times smaller compared to a “Ceramic 8” ferrite magnet for the same performance (Fig. 11.6).

However, in 1978 the price of Co increased by a factor 6.5 in a matter of months, resulting in dramatic price increases for SmCo magnet products and initiating a search for rare earth magnets based on Fe, a widely available and inexpensive element. Researchers, however, in the late 1970s to early 1980s continued to look for stronger and lower cost magnets with increasing attempts to substitute Co.

Numerous laboratories were combining REEs with Fe, but the resulting materials exhibited low coercivity until, by accident, N. Koon and B. Das, working at the U.S. Naval Research Laboratory (NRL) added a modest amount of boron (B) in an attempt to make a rapidly quenched REE-Fe amorphous material. The resulting material, produced in early 1980, exhibited both moderate residual induction and coercivity and resulted in two U.S. patents being issued to the U.S. Navy. The first one for the composition and the hard magnetic powder [41] and the second one for the production process for making the alloy [42]. However, as the U.S. Navy does not commercialize inventions, it remained for both M. Sagawa at Sumitomo and

J. Croat at General Motors to optimize the composition and provide practical manufacturing processes for sintered magnets [43] and powder for bonded magnets [44]. Credit for first commercial sintered magnet product went to Crucible Magnetics in November 1984 [36].

The first major application for neodymium-iron-boron (NdFeB) was in hard disk drives (HDDs), a market that was rapidly growing concurrent with the introduction of NdFeB. By 1990, it was reported that 75% of NdFeB was going into the voice coil motors (compression bonded magnets) and the spindle drive motors of HDDs (sintered magnets). The invention and rapid commercialization of NdFeB had a chilling effect on research for improved SmCo. Indeed, from 1984 through the late 1990s, almost no reference to SmCo publications was available, while research into NdFeB was extensive and continues to the present.

Despite the increasing competition with NdFeB magnets produced at a lower cost, SmCo magnets remain a high-value, speciality product as they have the best-known resistance to demagnetization, smaller size and greater stability at high temperatures (up to 550 °C). They are preferred in certain applications requiring high performances in harsh environments. As of 2014, global production of permanent magnets was estimated to be 738,800 tons, of which ferrite magnets accounted for 88%, NdFeB magnets 11% (approximately 80,000 tons), AlNiCo magnets less than 1% and SmCo magnets less than 0.5% (1300 tons) [21].

## 11.5 1990s–2020s: Entering the “Chinese Era” and Associated Challenges

The development of REE magnetic applications was a trigger point for China to become one of the most important world producers of REEs in the 1990s (Figs. 11.2 and 11.4).

The start of REE production in China began in the middle 1950s [45]. In those days, monazite was only processed to produce rare earth metals for lighter flints and  $(\text{Th}(\text{NO}_3)_4)$  for gas mantles. In 1956, the research team led by Professor Zou Yuanxi at the Shanghai Institute of Metallurgy succeeded in developing a process for making REE-Si-Fe alloy, in which rare earths were recovered from blast furnace slag containing 4–6% REO by using ferrosilicon as a reductant. It was the initiation of recovering REEs from the Bayan Obo deposit in Inner Mongolia and making REE-Si-Fe alloy in China. Following in the 1960s, great importance was attached to a more comprehensive use of the Bayan Obo deposit. Technical personnel associated with REEs throughout the country were deployed to undertake research into the comprehensive recovery of REE, as well as their popularization and application, thus promoting all-round development of the REE industry.

In 1965, a number of researchers from the Baotou Research Institute of Rare Earths successfully worked out a new process for increasing the REE content of the slag mentioned above. After a series of pilot plant tests performed in the Shanghai

Ferroalloy plant in 1966, regular commercial production of the slag was carried out in Baotou Rare Earth Ferroalloy plant (formerly Baotou Dongfeng Iron and Steel plant) in 1969. The slag that was obtained contained over 100% more REO than the common blast furnace slag. This increase in REO greatly reduced the consumption of energy and raw materials and increased the recovery of REE. This in turn, lowered the price of REE and created favorable conditions for promoting their application in iron and steel manufacturing. This process has been used so far to produce REE master alloy in China. It was the first step that revolutionized the Chinese REE industry.

In the 1970s, scientific research institutions engaged in research on permanent magnet materials, which mainly included the Central Research Institute of Iron and Steel in Beijing, the Baotou Research Institute of Rare Earths, General Research Institute of Non-ferrous Metals in Beijing and the Shanghai Research Institute of Iron and Steel. However, during this period, consumption volumes of REE both in China and abroad were more important in sectors such as metallurgy, catalysis, glass and ceramics, which together accounted for more than 85% of the total REE production [45].

China's production levels progressed rapidly, especially from 1980 to 1990, with yearly increase rates close to 20%. By the 1990s, China had become the largest REE producer in the world (Fig. 11.4) with permanent magnetic materials being the largest REE consuming sector in the field of high technology. Tens of REE-bearing permanent magnet producers appeared to answer domestic demand and develop export activities. Such development was strongly supported by the Chinese central government over these decades with massive financial support (subsidies) and strong control (production levels, environmental permitting etc.).

Furthermore, from 1990 to 2010, there was a process for concentrating REE activities in China, which consisted of merging a large number of mid-sized players into large industrial conglomerates, thus creating companies with international weight and over which control was easier. Such consolidation started with mining producers and metallurgical processors of REE, but it was then extended to NdFeB permanent magnets producers [46]. All of these joint efforts resulted in strengthening the control of a few Chinese groups over the entire supply chain of REE production and permanent magnets, keeping production costs low and mastering the crucial step of creating benefit. It resulted in Chinese dominance over the global REE industry and allowed the country to even run an aggressive strategy in the development of mining projects outside China.

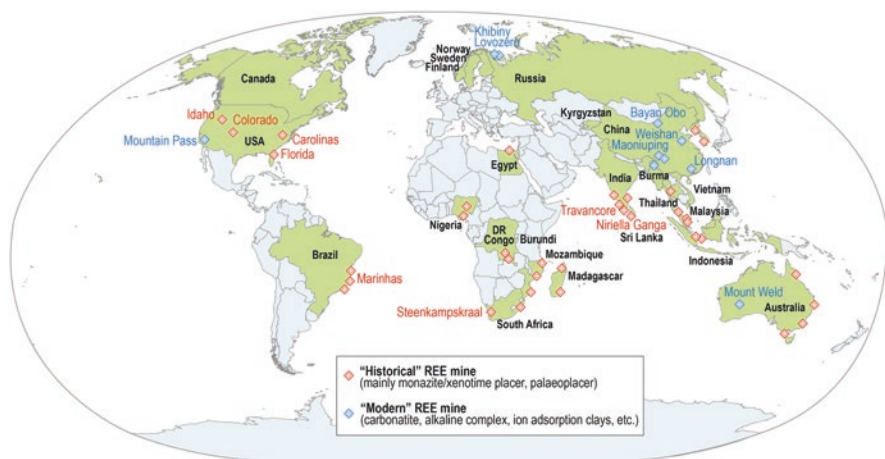
In the North of China, vertical integration has been particularly successful. In the main production area in Inner Mongolia province (Bayan Obo mining complex), the consortia China Northern Rare Earth Group and Inner Mongolia Baotou Rare Earth Magnetic Material merged. These alone represented by 2015, a production capacity of 60,000 tons of REO and 30,000 tons of NdFeB magnets per year.

In the South of China, the concentrating process had proven to be more complex because the ionic adsorption clay deposits [47, 48] responsible for the extraction of heavy REEs were numerous, small in size and scattered in six provinces (i.e.,

Hunan, Yunnan, Jiangxi, Fujian, Guangdong and Guangxi). The merger of the five already powerful industrial groups in this area has been more problematic.

Between 1990 and 2000, China’s production increased over 350% from 16,000 tons REO to about 73,000 tons REO. During the same period, production from other countries declined almost 60% from 44,000 tons to about 16,000 tons. As a result, world production increased from about 60,000 tons to almost 91,000 tons between 1990 and 2000 (Fig. 11.4). By 2009, world production reached about 132,000 tons with Chinese production at 129,000 tons and production from other countries was only 3000 tons [49]. The situation of monopoly led to the 2010 crisis, which began as a diplomatic incident between China and Japan, but rapidly spread to other consuming countries realizing their dependency on the REE primary supply [50–54].

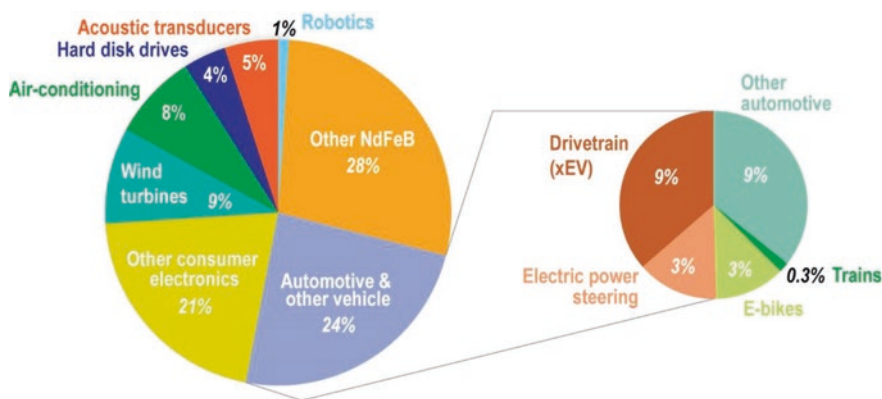
In the years that followed this crisis, a renewal of exploration activities from various countries took place, in order to find new deposits and try to develop “modern REE mines” (Fig. 11.7). As of 2020, the result has been a decrease of China’s share of total REE mine production at around 65%, followed by the United States (12%) and Australia (10%). Still, one of the greatest challenges for any new producer is to be able to master the steps of separating REEs and manufacture magnetic alloys in order to secure production of NdFeB magnets.



**Fig. 11.7** Map of historical and modern REE mines in the world. Historical REE mines are represented by heavy REE-bearing minerals placers and paleoplacers, while modern REE mines exhibit a more various geology with alkaline complexes, carbonatites and ion adsorption clays. Light REE and heavy REE distribution is controlled by the type of deposit and REE-bearing minerals. (Compiled from [15–19, 26, 27, 55–57])

## 11.6 Future Trends for the REE Market

In the last two decades (2000–2020), NdFeB permanent magnets were a particularly important driver of the global REE demand. If electronics (Hard Disk Drives) were the first application sector for NdFeB magnets in the 1990s, their use rapidly spread to a large number of applications. Figure 11.8 illustrates the diversity of application sectors, nearly 70% of these uses being in the form of electric motors [58]. Thanks to the reduction of volume and weight required for equivalent magnetic performance, NdFeB permanent magnets have thus enabled a significant reduction in the dimensions and mass of the devices using them. They have been an essential factor in the miniaturization of electric motors in several fields (information and communication technologies, automotive, defense etc.). The corresponding demand for REE in permanent magnets has been growing since the end of the 1990s at a rate of around 7% per year. Since the 2010s, it has always represented the main driver for demand for all REEs and the sector with the strongest growth since 2012 [46]. According to Roskill, the consumption of rare earth oxides (REO) for the manufacture of permanent magnets alone would have increased from 24,000 tons in 2012 to 41,000 tons in 2019, representing 30% of the total demand in 2019, compared to 20% in 2012 [59]. It is due both to their use in a large number of technologies using various electric motors and to the development of renewable energies. This trend



Sectors	Applications
Aerospace & defence	Stepper motors, electronic compasses, sensors, clutch and brake systems, radar devices, missile guidance systems, accelerometers.
Automotive	Starters, anti-lock braking system, injection pumps, electric motors for accessories (window lifters, windscreen wipers, seats, etc.), audio systems (loudspeakers), generators and drive motors for hybrid vehicles.
Electronics	Computers (hard disk drives), printers and photocopiers, digital camera, smartphone, DVD player, MP3 player, loudspeakers, camcorder, etc.
Consumer electrical equipment	Washing machine, fridge, air-conditioner, electric shaver, food processor, tools, e-bikes, etc.
Renewable energies	Wind turbine generator, etc.
Other	Industrial robots, magnetic separator, lifts, etc.

Fig. 11.8 Main application sectors of NdFeB magnet. (Modified from [11, 59])

that is likely to continue in the coming years is particularly due to the deployment of electric vehicles and wind power, which require increasing quantities of NdFeB permanent magnets.

In the field of wind power, since 2005, permanent magnet generators have gained popularity, especially in offshore turbines, as they allow for high power density and small size with the highest efficiency at all speeds, offering a high annual production of energy with a low lifetime cost. Most direct-drive turbines are equipped with permanent magnet generators that typically contain Nd and smaller quantities of dysprosium (Dy). The same, although on a different scale, is true for several gear-box designs [7]. In 2018, generators containing permanent magnets were used in nearly all offshore wind turbines in Europe and in approximately 76% of offshore wind turbines worldwide [60]. However, the same does not apply for onshore wind turbines, for which the need for powerful generators with reduced size and weight is not as strict. In onshore applications, it is possible to replace permanent magnet generators by other technologies such as the ones using asynchronous generators (e.g., Squirrel Cage Induction Generator (SCIG) or Double Fed Induction Generator (DFIG)) or synchronous generators using copper windings (Direct Drive Synchronous Generator (DDSG)). Wind power today consumes 9% of the global NdFeB permanent magnets volume. Volumes are expected to double by 2030 [59].

The increase is even higher for electric vehicles, with 30% of the total market for NdFeB magnets by 2025 and 50% to 70% by 2030, representing total volumes between 50,000 tons to 70,000 tons REO [61]. Some analysis suggests that with the existing permanent magnet technology, gradual replacement of conventional passenger car production by hybrid (HV), plug-in hybrid (PHV) or electric (EV) along with electric bikes and wind turbines will require a total increase of 191% in Nd and 168% in Dy supplies, respectively [62]. Other market development such as the development of robotics could increase such numbers by consuming the growing volumes of NdFeB permanent magnets. Today, the share for robotics, only at its early development, accounts for around 1% of NdFeB uses.

Therefore, it is expected that NdFeB permanent magnets will remain the main driver for REE uses and innovation for the next decade. Still, there may be some changes, substitutions or technological breakthroughs, which could radically modify market needs for REEs after 2030. The next section discusses such perspectives.

First, possibilities are that NdFeB permanent magnets will be substituted in the future. Rare earth free, high-performance magnetic materials such as amorphous Fe or iron nitride ( $\text{Fe}_2\text{N}$ ) are known. Since 2010, some research centers have been engaged in finding artificial substitutes for REEs. For example, the U.S. Department of Energy (DOE) has been funding several innovative projects through the Advanced Research Projects Agency-Energy (ARPA-E) program. One of these can be cited, related to the University of Delaware, Hitachi and General Electric, regarding nano-composites that would make alternative, strong magnets that do not need REE [63]. Another ARPA-E funding research project, led by the University of Nebraska, was trying to enhance permanent magnets with FeCo alloy [64]. In 2012, Hitachi, for instance, presented a 11 kW prototype electric motor using an amorphous iron



magnetic material instead of REE permanent magnets. Someday, superconducting materials may revolutionize the way wind turbines are built, phasing out the need for REE permanent magnets. As for conventional hard disk drive technologies as we know them, they are likely to be challenged in the future by new technologies that may not rely on the use of REEs.

On the other hand, other market developments could reinforce the use for REE materials in the future, relying on the same dynamics that were previously illustrated. For example, one possibility is new geological feedstock becoming available; another is new applications with high commercial potential.

The first one could be linked for instance in the use of Th in future nuclear programs. Two countries in particular are very active in this field: China and India. Should there be a development of the Th nuclear industry, Th would no longer be a waste but a valuable coproduct and its association with REEs in geological deposits would open new perspectives. Although the technology will take many decades to be realized, China could be the first to have a shot at commercializing it. Tests have begun in 2021 to build an experimental nuclear reactor using Th as fuel in Wuwei which is on the outskirts of the Gobi Desert. The reactor is unusual in that it has molten salts circulating inside it instead of water (H<sub>2</sub>O) [65].

In terms of new applications, one that is known for some time but has not yet found its commercial application is magnetic refrigeration. Magnetic refrigeration uses gadolinium (Gd) where it is used in an alloy in association with NdFeB magnetic magnets as a solid-state alternative to traditional refrigeration techniques. Refrigeration technology using REEs has been researched for several decades, but changes to chlorofluorocarbons (CFCs) and hydrofluorocarbons (HFCs) policy used in traditional compress/expand refrigeration (hydrochlorofluorocarbon (HCFC)-type refrigerants are due to be phased out by 2030 as part of the Kyoto protocol) have increased interest in its development as an alternative to traditional refrigeration. Modern prototypes rely on alloys of Gd as a refrigerant, which is stored in a tube, around which a cylinder of NdFeB magnets is moved to trigger magnetocaloric effect (MCE) in the alloy. The alloy is heated when the magnetic field increases and cooled when the magnetic field decreases.

Magnetic refrigeration offers a less toxic, solid state and nonpolluting liquid alternative. Magnetic refrigeration also has a higher cooling efficiency than traditional refrigeration, and this leads to smaller quantities of carbon dioxide (CO<sub>2</sub>) release. The lack of a compressor also reduces noise and vibration for the user. Around 15% of the world's energy consumption is related to the use of air conditioning, refrigeration, freezing and chilling based on traditional vapor compression/expansion technology across industrial, commercial, agricultural, household, military and aerospace applications, both stationary and mobile, so there is a large potential market. Estimates on a timescale for commercialization range from 5 to 10 years, although there is some concern over the limited availability and high cost of Gd, which may hinder development, particularly for low-cost applications. Semiconductor thermoelectric effect refrigeration is another alternative technology, but it is only suitable for small-scale applications. Some of the key companies likely to start commercial production include Cooltech Applications, which was working

with Whirlpool and other refrigerator manufacturers. The Baotou Research Institute of Rare Earths (BRIRE) has also developed magnetic refrigerators using around 750 g of Gd to 200 g of La-based alloys and, in 2014, it was reported that it has collaborated with the Haier Group on this research. The company Santoku produces magnetic refrigeration alloys in Japan.

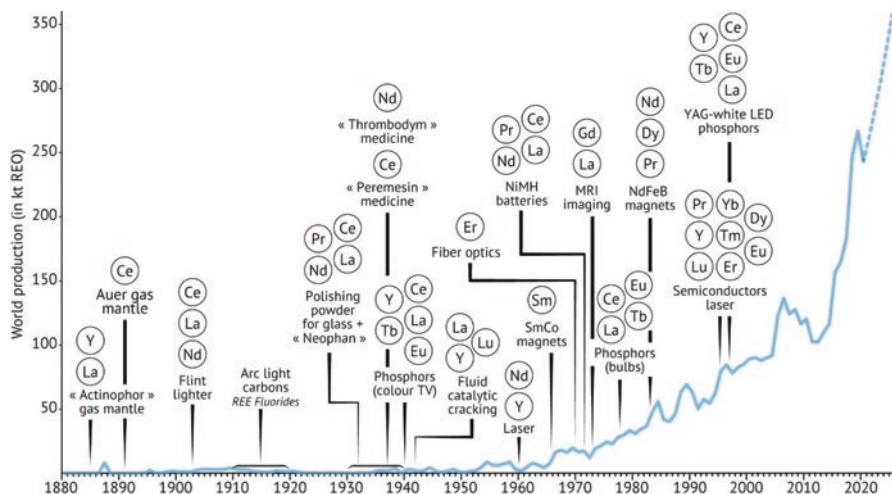
Still in the field of magnetic refrigeration, La-based alloys offer a lower cost alternative to Gd-based alloys but require more treatment. Testing is also being carried using superconducting magnets to create greater change in magnetic field strength of around 5T. The rare earth alloy gadolinium-silicon-germanium  $Gd_5(Si_2Ge_2)$  is commonly used in this new application, which has the potential to become a disruptive technology.

Another disruptive application could be phosphor thermometry, particularly with the development of the Internet of Things (IoT), increasing the numbers of sensors in daily appliances. So far, this method of temperature measurement based on REE phosphors is used in difficult environments, for instance, for biological and surgical applications because the fiber optic probes are small and low in thermal mass. Another one is in corrosive, explosive and high-voltage settings because the probes are inert and nonconductive. Future applications could include coatings inside operating microelectronic equipment, on textiles during microwave drying, or on steel surfaces during production. Functioning is based on a phosphor's decay time, which is used to detect and measure a variety of properties such as temperature. Some phosphors are also sensitive to pressure, and sensors have been developed based on this characteristic. A small pellet of the phosphor  $Eu:La_2O_3S$ ,  $Eu:Gd_2O_3S$  or  $Sm:BaFCl$  is used as an emitting sensor, and an optical fiber is used to carry exciting radiation to the phosphor and to return its emission, which is temperature sensitive, to the spectro-electronic instrumentation. Temperatures can be measured to an accuracy of 0.1 °C over the range  $-100$  °C to  $+300$  °C.

## 11.7 Conclusion

Since the discovery of REEs, the evolution of consumer's demand has been a strong driver enhancing discoveries of REE applications throughout history (Fig. 11.9). In the face of new challenges related to climate change, REEs will play an important role in new technologies to ensure an energy transition (e.g., renewable energies and electric mobility). In other words, REE applications will continue to develop in the next decades and REE world production will continue to grow. This growing demand for REE poses a challenge in terms of securing supplies of these metals, the real "vitamins" of new technologies. Thus, some companies will turn to more technological innovations to substitute REEs in the development of critical sectors such as robotics, electric mobility and artificial intelligence.

However, REEs still have a bright future ahead of them, as evidenced by the many deposits being explored around the world and the increasing diversification of supply sources outside of China. Despite the production of REEs outside China, the



**Fig. 11.9** Major historical technological innovations that have driven REE consumption over 150 years. Blue Line shows the REE world production in metric kt REO. (See references used for compilation in Figs. 11.2 and 11.4 captions). Blue dashed line is a prevision of REE world production based on an annual rate of 7% [11]. Abbreviations: Laser (Light Amplification by Stimulated Emission of Radiation), MRI (Magnetic Resonance Imaging), NiMH (Nickel-Metal Hydride), YAG-LED (Yttrium Aluminium Garnet-Light-Emitting Diode)

country remains in a monopoly position, especially in the processing and development of new technologies using REEs. While REEs have been the source of major technological advances for the past 150 years, they also seem to have become a major geopolitical tool in recent years. Thus, this family of remarkable chemical elements will remain a major player in new technologies, markets and the balance of power between major industrial countries for several decades to come.

## References

1. W.D. Judge, Z.W. Xiao, G.J. Kipouros, Application of rare earths for higher efficiencies in energy conversion, in *Rare Metal Technology 2017*, (Springer, Cham, 2017), pp. 37–45
2. V. Balaram, Geoscience frontiers rare earth elements: A review of applications, occurrence, exploration, analysis, recycling and environmental impact. *Geosci. Front.* **10**, 1285–1303 (2019)
3. European Commission (EC), The European Green Deal. COM(2019) 640 final (2019), 24 p
4. European Commission (EC), *Masterplan for a Competitive Transformation of EU Energy-Intensive Industries Enabling a Climate-Neutral, Circular Economy by 2050* (Publications Office of the European Union, 2019), 56 p. <https://doi.org/10.2873/854920>
5. S. Bobba, S. Carrara, J. Huisman, F. Mathieux, C. Pavel, *Critical Raw Materials for Strategic Technologies and Sectors in the EU* (European Commission, 2020), 98 p. ISBN 978-92-76-15337-5
6. N. Dushyantha, N. Batapola, I. Ilankoon, S. Rohitha, R. Premasiri, B. Abeysinghe, N. Ratnayake, K. Dissanayake, The story of rare earth elements (REEs): Occurrences,

- global distribution, genesis, geology, mineralogy and global production. *Ore Geol. Rev.* **122**, 103521 (2020)
7. P. Alves Dias, S. Bobba, S. Carrara, B. Plazzotta, *The Role of Rare Earth Elements in Wind Energy and Electric Mobility*, EUR 30488 EN (Publication Office of the European Union, Luxembourg, 2020). <https://doi.org/10.2760/303258>, JRC122671. ISBN 978-92-79-27016-4
  8. C.H. Evans, *Episodes from the History of the Rare Earth Elements* (Springer Science, Dordrecht, 1996), 268 p. ISBN 978-0-7923-4101-7
  9. N. Charles, J. Tuduri, G. Lefebvre, O. Pourret, F. Gaillard, K. Goodenough, Ressources en Terres Rares de l'Europe et du Groenland: un Potentiel Minier Remarquable mais Tabou ? in *Ressources Métalliques: Cadre Géodynamique et Exemples Remarquables*, ed. by P. Boulvais, S. Decrée, (ISTE Science Publishing Ltd-Wiley, 2021)
  10. C.G. Mosander, On the new metals, lanthanum and didymium, which are associated with cerium; and on erbium and terbium, new metals associated with yttria. *Philos. Mag.* **23**(152), 241–254 (1843)
  11. K. Bru, P. Christmann, J.-F. Labbé, G. Lefebvre, Panorama Mondial 2014 du marché des Terres Rares. Public report BRGM/RP-65330-FR (2015), 194 p
  12. E. Greinacher, *History of Rare Earth Applications, Rare Earth Market Today*. ACS Symposium Series (American Chemical Society, Washington, DC, 1981)
  13. E. Baumgartner, Carl Auer Von Welsbach: A pioneer in the industrial application of rare earths, in *Episodes from the History of the Rare Earth Elements. Chemists and Chemistry*, ed. by C.H. Evans, vol. 15, (Springer, Dordrecht, 1996)
  14. United States Patent Office, Carl Auer Von Welsbach, of Vienna, Austria-Hungary. Assignor to the Welsbach Incandescent Gas Light Company, of New Jersey. Letters Patent No. 409528, US409528A (1889)
  15. British Colonial Geological Surveys Statistical Summary of the Minerals Industry (Period 1942–1971). <https://www2.bgs.ac.uk/mineralsuk/statistics/worldArchive.html>
  16. British Geological Survey (BGS) World Mineral Statistics Archive. <https://www2.bgs.ac.uk/mineralsuk/statistics/worldArchive.html>
  17. Mineral Statistics of the British Empire and Foreign Countries (Period 1913–1947). <https://www2.bgs.ac.uk/mineralsuk/statistics/worldArchive.html>
  18. United States Geological Survey (USGS) Minerals Yearbook. <https://www.usgs.gov/centers/national-minerals-information-center/rare-earths-statistics-and-information>
  19. United States Bureau of Mines Minerals Yearbook. <https://www.usgs.gov/centers/national-minerals-information-center/bureau-mines-minerals-yearbook-1932-1993>
  20. United States Patent Office, Carl Auer Von Welsbach, of Vienna, Austria-Hungary. Assignor to the Pyrophoric Alloy. Letters Patent No. 837017, US837017A (1906)
  21. Roskill Information Services, *Rare Earths: Market Outlook to 2020*, 15th edn. (2015), 337 p
  22. S.B. Castor, J.B. Hendrik, Rare earth elements, in *Industrial Minerals and Rocks: Commodities, Markets, and Uses*, ed. by S.B. Castor, J.B. Hendrik, J.E. Kogel, N.C. Trivedi, J.M. Barker, S.T. Krukowski, 7th edn., (Society for Mining Mineralogy, Littleton, 2006), pp. 769–792
  23. J. Tuduri, N. Charles, G. Guyonnet, J. Melleton, P. Pourret, A. Rollat, Projet ANR ASTER. Rapport de Tâche 4. Potentialité de Stocks Géologiques de Terres Rares en Europe et au Groenland. Rapport final. BRGM/RP-64910-FR (2015)
  24. C.K. Gupta, N. Krishnamurthy, *Extractive Metallurgy of Rare Earths* (CRC Press, Boca Raton, 2005)
  25. H.J. Hettel, V.A. Fassel, Quantitative Separation of Small Amounts of Rare Earths from Thorium, Uranium and Zirconium by Ion Exchange. M.S. Thesis. Iowa State College, Ames, Iowa. Work performed under contract no. W-7405-eng-82. (US Atomic Energy Commission, 1956), 71 p
  26. H.B.C. Nitze, Monazite and monazite deposits in North Carolina. North Carolina Geological Survey Bulletin **9**, 57 p (1895)
  27. W.C. Overstreet, The Geologic Occurrence of Monazite. U.S. Geological Survey Professional Paper 530 (1967), 338 p
  28. New York Times, Public Sees Color Television for the First Time; Demonstration Is Ordered by the FCC, 30 (1950, January 13). <https://www.tvobscurities.com/articles/color60s/>

29. New York Times, Adams, Val. Color TV is Here, 85 (1951, June 24)
30. Wall Street Journal, Commercial Color TV To Have Its 'Premiere' Over CBS Monday, 14 (1951, June 22)
31. New York Times, Television in Review, 33 (1954, August 11)
32. New York Times, CBS to Increase Color Shows to 73, 63 (1955 September 7)
33. A.K. Levine, F.C. Palilla, A new, highly efficient red emitting cathodoluminescent phosphor (YVO<sub>4</sub>:Eu) for color television. *Appl. Phys. Lett.* **5**, 118 (1964)
34. B.A. Wandell, L.D. Silverstein, Chapter 8 – Digital color reproduction, in *The Science of Color*, ed. by S.K. Shevell, 2nd edn., (Elsevier, Amsterdam, 2003), 339 p. ISBN 978-0-444-51251-2
35. S. Constantinides, J. De Leon, *Permanent Magnet Materials and Current Challenges* (Arnold Magnetic Technologies, 2011), 18 p. <https://www.arnoldmagnetics.com/wp-content/uploads/2017/10/Permanent-Magnet-Materials-and-Current-Challenges-Constantinides-and-DeLeon-PowderMet-2011-ppr.pdf>
36. S. Constantinides, D. Maybury, U. Wyss, G. Martinek, *Extending the Limits of the Sm<sub>2</sub>Co<sub>17</sub> System* (Arnold Magnetic Technologies Publications, Rochester, USA, 2010)
37. K.J. Strnat, G. Hoffer, J.C. Olson, W. Ostertag, J.J. Becker, A family of new cobalt-base permanent magnet materials. *J. Appl. Phys.* **38**(3), 1001–1002 (1967)
38. United States Patent Office, Magnetic Rare Earth-Cobalt Alloys. US3421889A (1966)
39. United States Patent Office, Permanent Magnet. US3677947A (1972)
40. United States Patent Office, Samarium-Cobalt Magnet with Grain Growth Inhibited SmCo<sub>5</sub> Crystals. US4075042A (1978)
41. N.C. Koon, U.S. Patent Documents. Patent Number: 4402770. International Classification: C04B 3500 (1983)
42. N.C. Koon, U.S. Patent Documents. Patent Number: RE34322. International Classification: H01F 104 (1993)
43. M. Sagawa, U.S. Patent Documents. Patent Number: US4601875A (1983)
44. United States Patent Office, Bonded Rare Earth-Iron Magnets. US49262983A (1983)
45. M. Wang, X. Dou, The history of China's rare earth industry, in *Episodes from the History of the Rare Earth Elements. Chemists and Chemistry*, ed. by C.H. Evans, vol. 15, (Springer, Dordrecht, 1996)
46. G. Lefebvre, Sursaut sur le Marché des Terres Rares en 2017. *Écomine* 20 Oct. 2017 (2017). <http://www.mineralinfo.fr/ecomine/sursaut-marche-terres-rares-en-2017>
47. Z. Bao, Z. Zhao, Geochemistry of mineralization with exchangeable REY in the weathering crusts of granitic rocks in South China. *Ore Geol. Rev.* **33**, 519–535 (2008)
48. R. Chi, T. Tian, *Weathered Crust Elution Deposited Rare Earth Ores* (Nova Science Publishers, Inc, New York, 2008), 286 p
49. P.K. Tse, China's Rare Earth Industry. U.S. Geological Survey Open File Report 2011-1042 (2011), 11 p
50. European Commission (EC), Tackling the Challenges in Commodity and Markets and on Raw Materials. COM(2011)0025 Final (2011)
51. European Commission (EC), The 2017 List of Critical Raw Materials for the EU. COM(2017) 490 Final (2017)
52. D. Sebastiaan, N. Mancheri, A. Tukker, T. Brown, E. Petavratzi, L. Espinoza, Report on the Current Use of Critical Raw Materials. Solutions for Critical Raw Materials – A European Expert Network (2017), 91 p.
53. L.S. Lauri, P. Eilu, T. Brown, G. Gunn, P. Kalvig, H. Sievers, Identification and Quantification of Primary CRM Resources in Europe. SCRREEN Deliverable 3.1 (2018), 65 p
54. G.A. Blengini, C.E.L. Latunussa, U. Eynard, C. Torres de Matos, D. Wittmer, K. Georgitzikis, C. Pavel, S. Carrara, L. Mancini, M. Unguru, D. Blagoeva, F. Mathieux, D. Pennington, Study on the EU's List of Critical Raw Materials (2020). Final Report. European Commission (2020), 158 p. <https://doi.org/10.2873/11619>, ISBN 978-92-76-21049-8
55. K.L. Kithil, Monazite, Thorium and Mesothorium. U.S. Bureau of Mines, Technical Paper 110, Mineral Technology 8 (1915), 40 p

56. J.B. Hedrick, Rare earth minerals and metals, in *Minerals Yearbook*, vol. 1, (U.S. Department of the Interior, Washington, DC, 1985), pp. 791–803
57. J.B. Hedrick, D.A. Templeton, Rare earth minerals and metals, in *U.S. Bureau of Mines Minerals Yearbook* (1991), pp. 825–844
58. S. Constantinides, The Technology and Market Issues of Magnetic Materials. Arnold Magnetic Technologies Corp. Presentation, 158 slides (2014)
59. Roskill Information Services, *Rare Earths: Outlook to 2029*, 19th edn (2019). ISBN 978-1-910922-80-4
60. Joint Research Center, *Raw Materials Demand for Wind and Solar PV Technologies in the Transition towards a Decarbonised Energy System*, EUR 30095 EN, (Publications Office of the European Union, Luxembourg, 2020)
61. Adamas Intelligence, *Rare Earth Magnets Market Outlook to 2030* (2020), 173 p
62. A. Filippas, G. Sempros, C. Sarafidis, Critical rare earths: The future of Nd & Dy and prospects of end-of-life product recycling. *Mater. Today, Proc.* **37**(4), 4058–4063 (2021)
63. K. Bourzac, New Magnets Could Solve Our Rare Earth Problems. *Technology Revue* January 20. (Institute of Technology (MIT), Massachusetts, 2011). <http://www.technologyreview.com>
64. A. Aston, China's Rare Earth Monopoly. *Technology Revue* October 15 (Institute of Technology (MIT), Massachusetts, 2010). <https://www.technologyreview.com>
65. S. Mallapaty, China prepares to test thorium fuelled nuclear reactor. *Nature* **597**, 311–312 (2021)

# Chapter 12

## Rare Earth Magnets: Manufacturing and Applications



James Bell

### 12.1 Introduction

One of the most important and wide range of applications for rare earth (REs) containing materials is the production of permanent magnets. Since the 1960s, this class of magnets has given designers and engineers the ability to increase performance, reduce the size of devices and even create applications that would not be possible with other magnet materials. Although magnets are seldom seen, they are everywhere and nearly everything around us that has moving parts is a candidate for designing with permanent magnets. Motors, generators, sensors and holding devices in every type of product are likely to be using permanent magnets, from exotic applications such as the Mars rover to totally mundane items like the magnetic catch on a purse, you will find them everywhere if you look hard enough. From children's toys to high energy physics, RE permanent magnets are the choice of designers and engineers.

The following sections describe how magnets are made, where they are used and some of the major companies who depend on them as well as the key magnet manufacturers worldwide.

---

J. Bell (✉)  
MagnetoDynamics LLC, Pittsburgh, PA, USA  
e-mail: [James@MagnetoDynamics.com](mailto:James@MagnetoDynamics.com)

## 12.2 Basic Magnet Compositions

The two main types of RE magnets in commercial production are samarium cobalt (SmCo) and neodymium iron boron (NdFeB). Both of these contain other elements which are added to control properties but for simplicity this chapter will use the basic compositional abbreviations.

### 12.2.1 *Samarium Cobalt Magnets*

Discovered in the 1960s by Strnat and Ray [1], SmCO magnets were the first RE-based permanent magnets to be commercialized and which eventually exhibited properties far higher than the standard magnet materials of the time. One of the great gifts that the developers gave to the world was the ability to experiment and improve this class of magnets without the hinderance of patent restrictions, which may have been due to Strnat receiving U.S. Air Force funding at the Wright Patterson facility where he was working. Although the very first example of these compositions had somewhat mediocre magnetic properties, by about 1970 improvements to composition and processing enabled a doubling of the energy product that was available from commercial permanent magnets.

SmCo magnets offered the combination of high remanence (field strength), very high coercivity (resistance to demagnetization) and stability at high temperatures, not just with respect to magnetic properties but also chemical stability in terms of resistance to oxidation damage. SmCo magnets were very expensive compared to the other commercial permanent magnets of the time (ferrite and alnico) and also had poor mechanical properties which resulted in cracking and chipping, properties which were shared with the dominant ceramic ferrites (Fig. 12.1).

The first compositions developed were of the 1:5 type (SmCo<sub>5</sub>) and by the early 1970s a second crystalline phase of the 2:17 type (Sm<sub>2</sub>Co<sub>17</sub>) was discovered [3]. With the additions of elements such as cobalt (Co), copper (Cu), zirconium (Zr) and iron (Fe), the magnetic properties were enhanced significantly although at the expense of more complicated processing.

The manufacturing process for SmCo<sub>5</sub> magnets is much the same as described below for neodymium magnets (also known as NdFeB or Neo magnets), but because the worldwide production quantity is so much lower, most manufacturing processes have not developed to the same extent as they have with NdFeB, and production is therefore more typical of the low volume NdFeB manufacturers. Melting and slab casting, rather than strip casting, are still standard practices as are batch sintering furnaces.

SmCo magnets were used in a wide range of applications, some due to the thermal and chemical stability of these compositions particularly in military, aerospace and physics equipment, and in other industrial applications that allow for



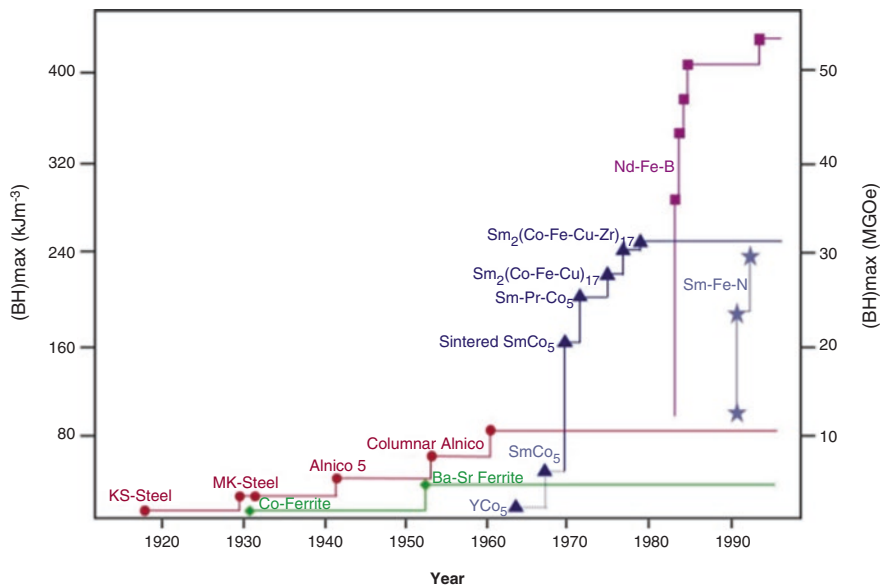


Fig. 12.1 The development of permanent magnets in the twentieth century [2]

miniaturization of devices such as earbuds and other electronic devices. Even though many applications were addressed later with lower cost NdFeB magnets, they are still widely used in the most demanding application areas.

### 12.2.2 Neodymium Iron Boron Magnets

With research and development having been focused on RE intermetallic alloys for over a decade, the early 1980s delivered the next major discovery – NdFeB alloys. The discovery was made independently by two different groups – Sagawa et al. [4] at Sumitomo in Japan and Croat et al. [5] at General Motors in the United States. Allegedly, the GM team was tasked with finding an alternative to SmCo for use in various automotive applications. This alternative material was not to contain Sm due to its high price, nor Co due to the volatility of its supply and pricing. The addition of boron (B) to the NdFe alloy resulted in the stabilization of a particular tetragonal crystalline phase with extremely good magnetic properties. The actual composition of this hard magnetic phase was identified as Nd<sub>2</sub>Fe<sub>14</sub>B. Sagawa and Croat developed completely different ways of creating magnets with a high proportion of Nd<sub>2</sub>Fe<sub>14</sub>B. The sintered magnet method developed by Sumitomo has always dominated production volumes due to higher magnetic performance and being a more cost-effective production route.

## Sintered NdFeB Magnets

The Sumitomo production method followed conventional powder metallurgical techniques similar to those used to manufacture ceramic ferrite materials. Small powder particles consisting of a single grain of the alloy were shown to have significantly higher magnetic properties along one crystalline axis. When large numbers of particles were aligned in a magnetic field prior and then sintered, the resulting material had greatly enhanced magnetic strength in the aligned direction in comparison to materials formed from a random, un-aligned, assemblage that was then sintered. The ferrite process used a water-based slurry of very fine ferrite powders that are pumped into a die cavity. Water is extracted through pressure, leaving a “green” compact that has sufficient strength to be put through a high temperature sintering process. During the sintering stage, the compact densifies through solid-state diffusion as well as liquid-assisted densification processes.

The Sumitomo process similarly converts a block of the alloy to fine powder, aligns the particles in a die using a magnetic field and pressed into a handleable, semi-densified shape that is then sintered. One difference between the Sumitomo process and the ceramic ferrite material production process is that a water-based slurry cannot be used due to the reactivity of the NdFeB powder. Therefore, a mold is filled with dry powder, aligned and pressed.

Alloy compositions are specific to the grade of material being produced and commonly included element additions as aluminum (Al), cobalt (Co), silicon (Si), refractory metals as well as the heavy rare earth (HRE) metals dysprosium (Dy) and terbium (Tb) which enhance coercivity and high temperature performance. Manufacturers consider their alloy compositions to be proprietary and purchasing the same grade from two different producers does not mean that the compositions will be the same.

The basics of this process have changed very little over the decades of manufacturing; however, numerous process improvements and more efficient production methods have been implemented which have progressively improved performance and reduced manufacturing costs. A diagram showing the different manufacturing stages is provided in Fig. 12.2.

A typical manufacturing operation now uses alloy that has been melted and rapidly cooled through strip casting before being exposed to hydrogen which breaks the flakes down to a friable powder. The control and high cooling rates experienced in strip casting enable a more uniform product to be formed that avoids the formation of undesirable phases which are typically generated through much slower cooling as seen in slab cast alloys.

Alloy flakes are then jet milled to create a powder – typically 5–10 microns in size, that is then pressed into blocks under an applied magnetic field on highly automated hydraulic presses. For increased densification prior to sintering, these blocks may be isostatically pressed. Sintering furnaces are now commonly multichamber continuous units with more accurate and repeatable temperature and inert atmosphere control. The sintering schedule may have several temperature stages where the sintering and heat treatment processes are performed. Many smaller

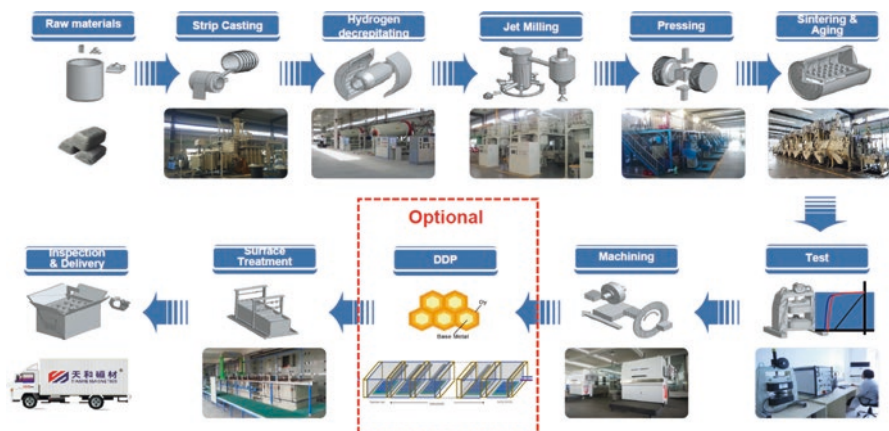


Fig. 12.2 Diagram of sintered magnet production steps [6]

manufacturers that cannot justify the high cost of these elaborate sintering furnaces still use simple batch sintering furnaces and therefore cannot take advantage of the improved consistency and efficiency that the latest equipment offers.

With sintering, shrinkage and surface contamination results which means the surface of the block needs to be removed by cutting or grinding, to leave a clean, flat, rectangular block that can be further processed by cutting or grinding to give the final magnet size. If the final shape required is a rectangular block or plate, then a relatively new technique – multi-wire cutting [7] – is frequently used which had been developed for the silicon wafer industry. Although equipment costs are high, the increased efficiency, precision, automation and capacity means that these latest advancements are particularly effective for the production of small or thin rectangular magnets. The multi-wire cutting machines also require much less floor space than single wire, electrical discharge machines (EDM) and abrasive slitting wheel. With one multi-wire machine, up to 50 of the older, simpler machines that had been used for decades are replaced. For curved surfaces, profile grinders can be used. However, these are only suitable for large production volumes due to the high cost of diamond impregnated (profiled) grinding wheels, and equipment setup time. For lower quantities, EDM or abrasive single wire cutting machines are commonly used.

The next stage in the process is a relatively new addition to magnet production – the diffusion of heavy rare earth (HRE) metals into the magnet structure which is shown in the production process diagram as DDP. DDP was initially dysprosium diffusion processing but now also includes Tb. Improved coercivity and high temperature performance have been achieved for decades by the addition of these elements to the basic magnet alloy compositions. This results in a fairly even distribution of those elements throughout the body of the finished magnet. Since these elements are very expensive, diffusion from the magnet surface which results in concentrating the additions at grain boundaries where they are particularly effective, minimizes the quantity of added HRE. This process was described as far back as 2000

[8], but it is only over the last 7–10 years that the process has been widely adopted in the industry. The metal (or oxide, fluoride or other compound) is deposited on the surface and during the subsequent heat treatment diffusion into the body takes place. Because diffusion results in decreasing concentration with increase in distance from the surface, this process is most effective in thin sections of magnet, typically 5–8 mm.

For protection of the magnet against oxidation or corrosion, a coating may then be applied. There are a wide range of coating options from simple passivation to multilayer, multi-material coatings for aggressive environments. The most common of these is a Ni-Co-Ni trilayer electrodeposited coating.

Finally, the magnet may be magnetized prior to shipment. It is usually recommended that magnetization is performed as late in the assembly process as possible in order to minimize the attraction of magnetic debris that could be present.

### **Bonded NdFeB Magnets**

As was discussed earlier, NdFeB magnets were simultaneously discovered at Sumitomo and at General Motors (Magnequench). The GM process involved extremely high cooling rates for the alloy using modified strip casting equipment that was developed for amorphous metal production which they called jet casting or more commonly melt spinning. A thin jet of molten metal was deposited onto a rapidly rotating cooled wheel, resulting in a cooling rate in the region of  $10^6$  °C per second. The near amorphous structure that was produced enabled a subsequent heat treatment to create a very fine microstructure of NdFeB, with a grain size of typically 20–30 nm, which is over 100× smaller than what is produced in sintered NdFeB magnets. This extremely fine grain size gives the material a high coercivity. However, because the grains are randomly oriented, the resulting metal flake is isotropic and therefore will not align magnetically as in the case of sintered NdFeB. The main benefit of this flake is that it is easy to bond together with epoxy resins or plastics to form complex magnet shapes with little or no waste from cutting or grinding.

One of the biggest early applications for this type of magnet was in thin-walled rings for disk drive spindle motors (Fig. 12.3). Shapes like this are impossible to make effectively using sintered magnets. The relatively high cost per kilogram for the flake material was easily absorbed with the need for miniaturization. The magnetic performance is related to the volume percent of flake in the finished magnet, with early product reaching 10 MGOe for compression molded magnets (epoxy binder) and about 6.5 MGOe for injection molded (thermoplastic bonded) product. The reason for the lower performance in injection molding is the need for the molten material to flow and fill the molding cavity which limits the solid loading. A third technique, extrusion, was developed by Seiko Epson [9] for making thin-walled rings, where approximately 9 MGOe could be achieved as the process does



**Fig. 12.3** Bonded magnet rings that can be made by extrusion [10]

not require the same degree of flow that is necessary for complex shaping in injection molding and therefore a higher powder loading is possible.

With compression molding, shapes are limited by the need to eject the molded part from the die, so they tend to require a consistent cross-sectional shape, whereas injection molding allows for true three-dimensional shaping. Extrusion is also limited to “2D” shaping and with lower performance compared to compression molding, it was never adopted by other manufacturers.

Unlike sintered NdFeB magnets, which have increased in energy product (Fig. 12.1 (BH)<sub>max</sub>) by about 50% since their first volume production, the Magnequench powders have seen a relatively small increase in magnetic performance for a “standard grade” compression molded product at 10 MGOe in the late 1980s, and top end levels currently of around 12 MGOe [11]. Many new powder grades have been developed by Magnequench that are tailored to magnetic performance, specific applications and lower cost formulations for price sensitive applications. Two “deviations” from the standard jet casting process are powders with a more amorphous structure used for hot pressing and gas atomized spherical powders which were targeted at injection molding because of their improved flow performance. The problem with the spherical powder strategy is that the magnetic performance is lower than a jet cast powder so the volume of powder needed to achieve the same energy product is greater, negating the benefit of improved flow. Also, the cost reduction was not sufficient to warrant the use of a higher percentage of filler for the same performance. Both of these variants seem to be obsolete as they are not listed in current Magnequench materials product data.

## Anisotropic Bonded NdFeB Magnets

Magnequench powders are isotropic and therefore cannot be aligned during forming which limits the energy product of their materials. However, if a stable form of anisotropic powder could be produced, that could be magnetically aligned, there is a potential to double the performance. About 30 years ago, Takeshita et al. at Mitsubishi [12] discovered that treating the alloy with hydrogen resulted in an anisotropic powder. This process was called hydrogen decrepitation disproportionation and recombination (HDDR). It had been known for many years that the RE alloys would absorb large amounts of hydrogen and that the swelling of the structure caused the alloy to fracture into a friable material that was then much easier to grind down to the very fine powder sizes needed for sintered magnet production. The hydrogen decrepitation (HD process) had become fairly standard in magnet manufacturing operations.

What was discovered at Mitsubishi was that if the hydrogenated material was heated, under moderate hydrogen pressures, then the alloy disproportionated into a very finely distributed mixture of phases. These included unaltered boride particles that retained the original orientation of the parent grain, and when hydrogen was removed these particles acted as nuclei for regrowth of the NdFeB main phase. Rather than forming a large single grain, as in the starting alloy, the grain size was much finer with the individual sub-grains having the same orientation as the parent grain. The fine sub-grain size imparts an inherent coercivity, while the material can be aligned in a magnetic field during compression or injection molding. Energy products are around 18–20 MGOe can be achieved in either compression or injection molding. The main producer of these powders is now Aichi Steel in Japan. Mitsubishi had exited the magnet materials market only a few years after the discovery, and Aichi Steel created a variant of HDDR [13], developing it into a scalable manufacturing process.

## Hot Formed NdFeB Magnets

Apart from sintered and bonded forming techniques, there is a third category which is hot pressing or hot forging to form NdFeB magnets. This technique was pioneered by Magnequench using their melt spun powders in the 1980s for their two magnet products MQ2 and MQ3 (MQ1 being the bonded designation) [14]. If the melt spun powder is quenched but not heat treated to develop a high degree of crystallization, this powder can be pressed in a heated die to near full density of the NdFeB alloy (7.5 g/cc) without the use of any binder, and the result is a higher energy product (i.e., 14 MGOe) when compared to the energy product of a bonded magnet. This type of magnet is still isotropic and due to the additional time and cost of hot pressing, the increase in performance was not sufficient to carve out a niche in applications, particularly with limited shaping capability. However, if a hot pressed magnet is then hot forged by a process called die upset forging, using a die that is larger than the magnet, the material flow imparts anisotropy and magnets with

energy products of about 27 MGOe were initially produced [14]. Eventually, process improvements increased this to over 35 MGOe. Magnequench spent a lot of time and effort designing dies and process conditions to be able to make the “butterfly”-shaped voice coil magnets (VCM) for disk drives. Processing was once again met without a large degree of commercial success.

One of the most elegant processes derived for Magnequench’s MQ3 was back extrusion where the hot alloy was pressed into a fairly deep cylindrical die and the “punch” that was used was a smaller diameter than the inner diameter of the die. The hot alloy material would therefore flow up the sides of the punch resulting in a hollow cylinder [15]. In this case, the anisotropy developed is radial. Trimming the ends and surface grinding could produce a fairly thin-walled ring with radial anisotropy which would be perfect for many motor applications. Cost, however, was high and the process was not widely licensed which probably stifled cost reduction and development of more efficient variants. Notably, Magnequench’s MQ2 and MQ3 are no longer mentioned on the Magnequench website [11].

More recently, radially anisotropic, fully dense, rings have been produced by the hot pressing of anisotropic (e.g., sinterable) powders under an applied radial field [16] as well as variants where the pressure is applied in a localized circular motion similar to rotary forging.

### ***12.2.3 Other Magnet Types and Processes***

Over the years, there have been a number of promising techniques and material discoveries which looked like they would eventually become mainstream. In terms of magnet materials, the only major discovery since NdFeB is samarium iron nitride (SmFeN) [17]. Magnetic properties are good, with the powder being anisotropic, but because of temperature stability that prevents sintering, it was limited to bonded magnets. Today, there is very little of this material being produced although a reasonable amount is incorporated into the Aichi Steel anisotropic NdFeB powder blends to enhance performance.

In the late 1980s, the group at Philips developed a composite hard/soft magnetic magnet structure that had very promising properties [18]. The soft phase was so finely distributed that the “exchange spring” effect resulted in the magnets with low RE content, but these did demonstrate appreciable coercivity. Unfortunately, these were never developed to production scale.

Currently, there is interest in reducing Nd content by substitution with cerium (Ce) [19]. Reduced magnetic performance results, which although the magnet may still be adequate for many devices, substitution may not adequately reduce cost when compared with current sintered and bonded magnets.

A RE-containing magnet that is usually forgotten is the high-performance, sintered ferrite that was developed in Japan [20]. Doping these ceramic compositions with lanthanum (La) increases magnetic performance. These, however, are not really considered RE magnets.

In terms of processes, the gas atomization for production of bondable powders mentioned earlier never delivered sufficient cost savings. Similarly, magnet powders produced by high energy ball milling and magnets made by explosive compaction [21], magnetic compaction [22] and other forming methods never delivered commercially useful benefits.

### ***12.2.4 Current Development Focus***

Rare earth magnet manufacturing is now a fairly mature process with incremental improvements being made to properties and production efficiency. The most recent major advancement was in HRE diffusion, where Tb or Dy is diffused in through the surface of a finished magnet rather than incorporated into the starting alloy as discussed earlier. This may become the next battleground in patent infringement since Hitachi does not allow its “licensees” access to the many patents that Hitachi has filed on this development.

Another promising direction is to reduce the grain size of the finished magnet by starting with powders that have been jet milled to smaller sizes. This increases coercivity without the need for HRE additions, but complicates the milling and powder handling processes because of higher reactivity.

Currently, there is nothing on the horizon (i.e., RE-containing or not) that is threatening the dominance of existing RE magnet materials, and with more sources of raw material being developed outside of China, this should help in stabilizing price volatility or even reducing overall pricing, which will in turn remove pressure to replace RE-based magnets altogether.

## **12.3 Major Applications**

### ***12.3.1 The Automotive Industry***

Permanent magnets have been used in automotive applications for over a century. The first car radio and speaker came in the 1920s, but long before that, drivers relied on magnet-driven speedometers. Originally patented in the 1880s, the basic concept of a rotating magnet inducing eddy currents, and therefore drag, on a metal cup or disk was still in use for this application over 100 years later. As more convenience features were added to vehicles such as wiper motors, power windows and seat motors, the number of magnets being used exploded. Initially, most of these components used sintered ferrite magnets but as the auto industry started to focus on weight reduction as a way of improving fuel economy many of these started to incorporate RE magnets. In the 1990s, it was almost obligatory to use a diagram like the one shown in Fig. 12.4 in any presentation pertaining to permanent magnet applications.



### Automotive applications

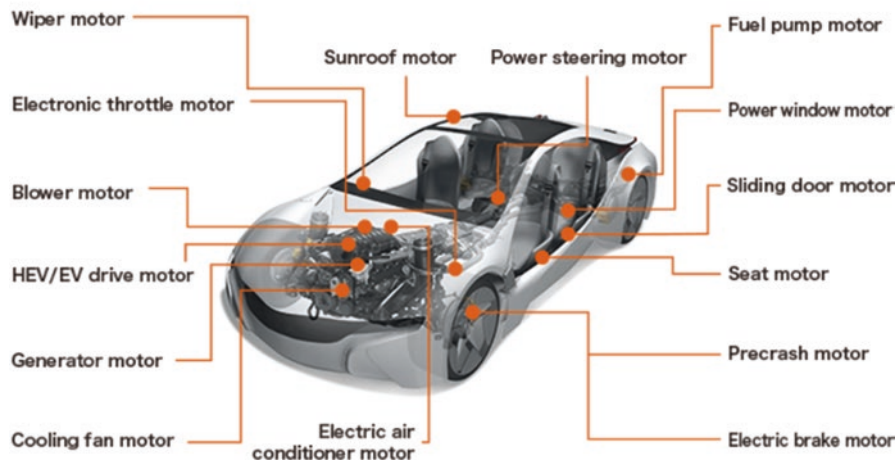


Fig. 12.4 Some of the uses of permanent magnets in automotive applications [23]

Today, this sort of diagram would be unreadable because of the huge number of devices that use permanent magnets. Add to this the proliferation in the number of devices in any one application and the total number of magnets in a single vehicle is now counted in the hundreds. For example, with a power seat often having four or more motors per seat – each with two magnets, the number of magnets quickly adds up. Audio systems, originally with one speaker, have become a huge market for RE magnets. For example, the Tesla model 3 using 16 RE magnet powered speakers for a total magnet weight of over 500 g places this automotive application in second place only exceeded by the potential for electric vehicle (EV) traction motors [24]. The improved energy efficiency of electric rather than mechanical or hydraulic-driven devices along with the transition to EVs is sure to create a total “drive-by-wire” vehicle and ensure that RE magnet usage continues to grow.

### 12.3.2 The Electronics Industry: Computers

One of the first important application areas for both sintered and bonded NdFeB magnets was in computer hard drives. The strength of the magnetic field that sintered magnets can produce enabled the read head actuator, called a voice coil motor, to operate faster and with reduced size and mass, while the spindle motor used thin-walled rings that could be very efficiently made by compression molding of bonded magnets. A fairly short-lived computer storage device, the Zip drive [25], which offered a removable disk with a “massive” 100 Mb of storage as compared to standard floppy disks with 1.44 Mb, used bonded NdFeB magnets in both the head

actuator and the spindle motor. Then came compact disks (CDs), digital versatile disks or dual-layer disks (DVDs) and other optical storage drives that used combinations of bonded and sintered neo magnets for the two movement functions. Thirty years ago, with the invention of the solid-state drive (SSD), predictions about a short life for conventional hard drives were common but through increased storage density, lower manufacturing costs and increased reliability they are still competitive. That fate did, however, come to the optical drive formats with the convenience and low cost of flash drives, and for audio and video players because of downloading and streaming.

### ***12.3.3 The Medical Industry***

Probably, the most commonly cited application for RE magnets in the medical field is magnetic resonance imaging (MRI). For many of these systems, the magnetic field is produced by superconducting magnets, but the advantages of portability and simplicity that RE magnet-generated fields give means that they are often the preferred field source. Extremely accurate, whole body superconducting magnet systems have their place but for smaller single limb examination or for less claustrophobic open magnet geometries, RE magnets can be more cost effective. Systems can weigh a few hundred kilograms or as much as several tonnes, so the number of systems produced does not need to be high to make this a significant use of RE magnets.

But MRI is just one of many, extremely varied applications in the medical field. Movement is again an indicator that magnets may be present. From peristaltic pumps to high speed bone drills to air movement, the power or miniaturization that RE magnets can provide are the key to their use. With respect to air movement this could be inflation of an air mattress (i.e., on a bed with RE magnet motors for positioning) which can give a patient variable support, or in ventilators for people with breathing difficulties. In the United States, two manufacturers of the sleep apnea continuous positive air pressure (CPAP) machines produce over two million units a year generating revenue of approximately \$2.5 billion in 2021 [26], each one with a RE magnet powered blower motor. Pencil-thin high speed “power tools” will be found in every operating theater. Even the separation of red blood cells from plasma results from the interaction of iron in hemoglobin with a magnetic field.

Another application involves very large magnets in combination with some of the smallest RE magnets used anywhere. Stereotaxis manufactures systems which can guide a catheter along arteries by magnetic forces acting on a minute RE magnet (Fig. 12.5). The large external magnets can steer the tip through right angle turns or even acute angles that cannot be done by mechanically guided methods.

The movement of remote or robotic controlled surgery equipment again relies of the precision of RE magnet containing motors and actuators.



Fig. 12.5 Stereotaxis Remote Magnetic Navigation (RMN) system [27]

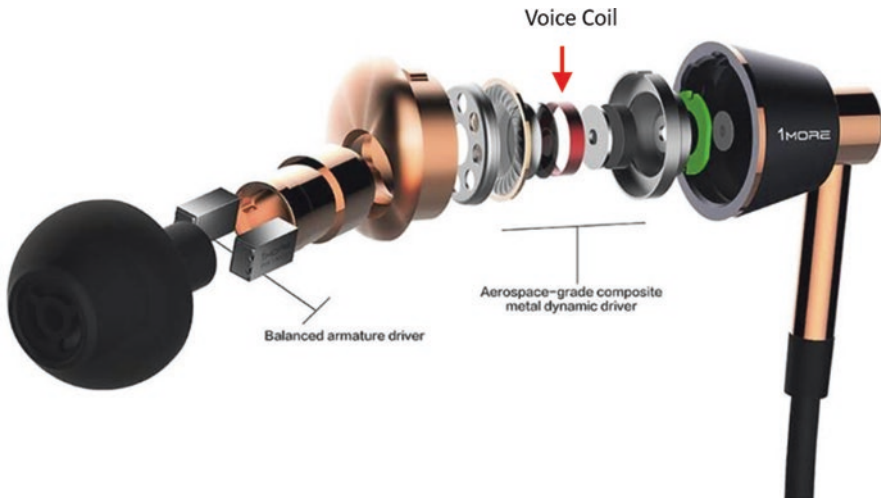
### 12.3.4 Industrial Products

Industrial products span a wide range of applications and industries, many of which are using high-performance brushless direct current (DC) or stepper motors, such as in robotics, material handling systems and fluid pumps. RE magnets are used in levitation, eddy current brakes, magnetic separation, clamps or work holding devices, reduction in hard water scale deposits, flow and level measurement and a host of other applications that would easily fill a chapter on its own.

### 12.3.5 Consumer Products

Although the majority of large home appliances still use induction motors, the smaller ones are increasingly using RE magnets. Traditional vacuum cleaners boast about the amount of power they consume, never mentioning that the efficiency of conversion of that power to actual suction is very poor. Dyson reinvented the vacuum cleaner using very high-speed RE magnet motors that are small, light and energy efficient [28]. Now other manufacturers are following suit and when it comes to handheld rechargeable units, the increased efficiency results in longer runtime or a smaller battery which again saves weight.

The same logic applies to handheld power tools which are increasingly moving toward cordless formats. With the improvements in energy density of batteries and the use of brushless DC RE magnet-containing motors, lower cost tools still have respectable runtimes, and for more professional use all-day battery packs can be a reality. Manufacturers such as Milwaukee Electric focus on the high-performance, high durability segment of the market which would not be possible without RE magnets [29].

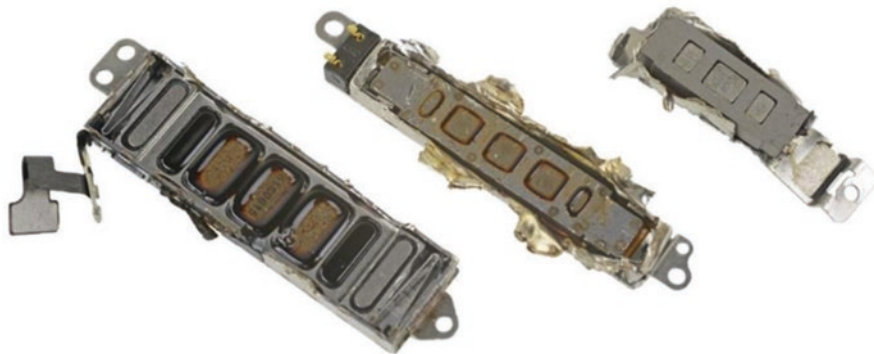


**Fig. 12.6** Earbud schematic illustrating the inclusion of three separate drivers each using NdFeB magnets [30]

Audio applications for RE magnets have proliferated in recent years with Bluetooth personal speakers, sound bars for TV, headphones and earbuds. Often used in marketing, the term “*Neodymium Magnets*” frequently appears despite the general public knowing little about why this is a good thing. Again, the combination of size, weight and efficiency is driving growth and many of these are battery powered so time between charges is important. The exploded diagram of a top end earbud shown in Fig. 12.6 has one traditional voice coil driver and two balanced armature drivers all containing NdFeB magnets.

Which section to place mobile phone applications in is difficult – consumer device, computer or electronics. Whichever section they should be in, phones are a good example of miniaturization through the use of powerful NdFeB magnets. A slightly different geometry of the speaker driver is used because of the thickness of the devices. And for the vibration generator there are a number of designs, either with a rotating unbalanced rotor or a linear oscillator as used in iPhones, which is called the “taptic engine” (Fig. 12.7). The linear device can give near-real-time response and variable strength and frequency.

A new application for NdFeB magnets is the Magsafe assembly [32] that will be used in iPhones that enables a variety of add-on devices (i.e., cameras, chargers and pop sockets) to be precisely aligned and attached to the phone. Consisting of a ring of 36 magnets with an extra two for rotational positioning, the number of magnets used in a phone just increased dramatically.



**Fig. 12.7** Three versions of Apple Taptic™ engines using multiple RE magnets [31]

### ***12.3.6 Green Energy***

The reason why green energy-related applications have been split out as a separate section is because of two applications: wind generators and electric vehicles (EV). These are relatively new, high consumption, areas for RE permanent magnets. Going back a decade, these two markets were already seen as a big potential impact in terms of stressing the supply chain, due to high growth rates. Those previous predictions were somewhat optimistic in terms of demand and so far, we have not seen a significant effect on the supply chain and therefore have avoided shortages and price fluctuations caused by additional demand. Despite the growth not being as rapid as predicted, they are still significant applications – wind power consuming huge amounts of sintered magnets for each generator, and EVs in terms of the number of traction motors being produced.

### ***12.3.7 Electric Vehicle Traction Motors***

Although any type of motor could be used for traction applications, the EV market appears to be standardizing on one form of permanent magnet motor – an internal permanent magnet (IPM) structure, where the magnets are embedded inside a steel rotor and the rotational forces produced are a combination of those produced by the magnets directly as well as through reluctance from the steel core [33]. This combination appears to give a cost-effective design with attractive torque/speed characteristics.

In the United States, the first EV production volume has been Tesla, using induction motors for their vehicles (i.e., no magnets). Tesla has, however, moved to using a combination of IPM and induction motors or in some models, only IPM. A tear-down study of different EVs was performed by Munro and Associates [34],

## Motor Side-by-Side Analysis

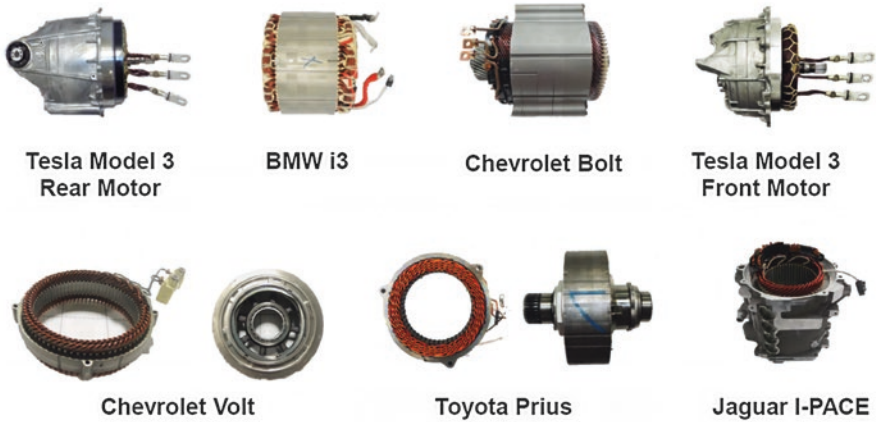


Fig. 12.8 EV (+ Hybrid) traction motors

covering every aspect of vehicle construction, including a section on the traction motors used by the various manufacturers (Fig. 12.8). This study has dimensional details of all components and includes the amount of magnet material used in each design.

There are several variants of IPM motor designs, with the magnets in a flat or “V” configuration and with one or more layers of magnets. The magnet configuration (i.e., single layer, “V”) for the Tesla design is shown below Fig. 12.9. In total, the motor uses about 1.8 kg of sintered NdFeB.

The reason why each magnet slab is made from four pieces is to reduce eddy currents in the magnet caused by fluctuation of the applied field and increases motor efficiency. The rotor is made from four separate lamination stacks, fixed together, but with the center pair “twisted” by a few degrees, to simulate a skew to the magnet pattern, which affects performance as well as vibrational noise.

To translate magnet usage in a single motor to industry demand, let us assume that if the United States produces eight to ten million cars and trucks a year, and by 2030, 50% of these are EVs, then the total RE magnet usage would be about 5000 tons. This assumes that not all EVs will use permanent magnet rotors and that the average weight per motor will decrease to around 1.5 kg. To put that into perspective, 5000 tonnes per year would be the total output of a medium-sized sintered NdFeB factory in China today.

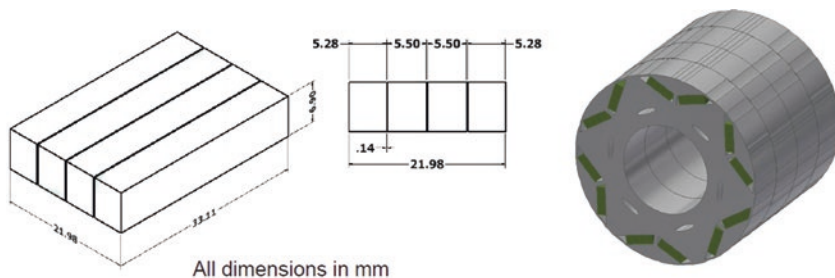


Fig. 12.9 Tesla magnet and configuration [34]

### 12.3.8 Wind Generators

At the other end of the spectrum, in terms of units built, wind generators are often given as an application that could stress the supply chain. Not all turbines use permanent magnets and those that do can be split into two categories, depending on whether they are direct drive or have incorporated gearboxes. Since the gearbox can require maintenance or may cause failure, wind turbines that are hard to access (e.g., offshore) favor direct drive, and these require a larger quantity (500 kg and more) of magnet material per MW of generator power. With generator rated capacity rising, now pushing 10 MW, the amount of magnet material per unit is measured in tonnes. With the DOE Wind Energy report [35] predicting an average of 9 GW of new U.S. generator capacity per year, from 2031 to 2050 and assuming about 50% of these are direct drive, this translates to 2000–3000 tonnes of magnets per year. Significant quantities but well within the elasticity of magnet production and RE supply.

### 12.3.9 The Defense and Aerospace Industry

One of the reasons why the loss of U.S. manufacturing capability for high-performance RE magnets is a concern is because of applications in military and aerospace systems that rely on REs being supplied from another country. Aircraft have moved to fly by wire which means that moving parts are now controlled with precision motors and actuators, which need to be small, light and powerful [36]. In high temperature applications such as in engines and rocket motors, only the highest performance SmCo magnets can be used because magnetic strength decreases with increasing temperature. Above a critical temperature (Curie temperature), magnetic strength actually drops to zero.

One of the plant closures that produced a lot of bad press was when Magnequench closed the Ugimac plant that had been producing RE magnets for the JDAM weapons system [37]. This was just one example, but all aircraft and many weapons

systems today rely on high-performance RE magnet for their successful operation. In September 2022, deliveries of the F35 fighter were put on hold because starter/generator magnet components were found to have come from China which is forbidden under DFARS (Defense Federal Acquisition Regulations Supplement) regulations [38]. There are manufacturers in “friendly” countries (i.e., Europe and Japan) that can supply what is needed, but only having one well-established sintered RE magnet producer in the United States, that is limited to SmCo is a strategically dangerous position.

## 12.4 Intellectual Property

The subject of NdFeB patents has been a thorny issue ever since the “dual” discovery by GM and Sumitomo. Although the basic crystal structure and magnetic phases present in both variants were the same, the manufacturing processes were sufficiently different for the two companies to retain their patent filings and to coexist in the market, through a cross-licensing agreement which divided the market up into bonded (i.e., Magnequench) and sintered (i.e., Sumitomo) magnet technologies. The basic compositional patents expired many years ago but the patent situation is now much more complex than it was two decades ago. Many of the patents that were filed by Sumitomo were transferred to a company called Neomax (i.e., a merger in 2004 of the Sumitomo and Hitachi permanent magnet operations) and then eventually to Hitachi. This means that Hitachi controls a large proportion of the patents that have been filed on NdFeB development, and they claim to have over 600 patents related to RE magnet production and applications. This was recognized as a strategic advantage by both Sumitomo and Hitachi and effectively leveraged as a method of generating royalty income, licensing companies around the world to use their patent portfolio without fear of legal action as long as royalties were paid on all their NdFeB magnet production. This would then inhibit the growth of competitors provided that the IP owners were seen to take legal action against “infringing” companies. There were several legal actions initiated by Sumitomo/Hitachi and Magnequench essentially to support their licensees and maintain the flow of royalty income.

The value of the patent portfolio to Hitachi is more to do with the quantity rather than the quality of those patents. This was illustrated well in the International Trade Commission (ITC) case (337-TA-855) filed by Hitachi in 2012 [39], claiming infringement by a large number of end-product manufacturers for using NdFeB magnets that were not produced by Hitachi licensees, as well as a number of magnet distributors/fabricators and three Chinese magnet manufacturers who did not have licensing from Hitachi. From that vast collection of intellectual property (IP), Hitachi selected four patents and attempted to show infringement. Obviously, these patents would be the ones that Hitachi considered to be the strongest weapons in their IP arsenal.



Many of the end-product manufacturers and distributors signed agreements to only purchase from licensed companies in the future to avoid the high cost of a protracted legal defense. However, some manufacturers and distributors did not, and the Chinese manufacturers had no option but to defend themselves. This defensive action displayed the weakness of some of those patents, either due to substantial prior art or to the inability to prove infringement, and days before the case was due to go to court, Hitachi backed down and offered the three Chinese companies licensing agreements instead. This was not the intention, and the five Chinese companies with existing Hitachi licenses were more than a little upset with the outcome of the action.

With Hitachi recently announcing that they are looking to get out of the magnet business by attempting to divest of Hitachi Metals (now Proterial Ltd.) [40], it will be interesting to see whether whoever ends up with the patent portfolio will see the same strategic advantage in terms of royalty generation.

## 12.5 U.S. Magnet Manufacture

Since the early 1990s, the United States has lost the vast majority of its capability in producing RE magnets. The decay in magnet-manufacturing capability started earlier than this with the gradual loss of plants that made sintered ferrites because of low-cost sources in China. With the higher value of RE magnets, the United States was able to absorb the higher cost structure for a while, but eventually all the sintered RE magnet producers, with the exception of one, became uncompetitive and either closed or moved production to China. The 1990s also saw considerable consolidation in the U.S. magnet industry with Arnold/SPS Technologies acquiring several businesses (i.e., 3M, Flexmag and RJF) in the bonded and flexible magnet area as well as RE magnet producer Swift-Levick in the United Kingdom [41]. Plants such as IG Technologies/Ugimag which had been acquired by Magnequench and then closed. Similarly, the Hitachi facility in Edmore, MI, was no longer competitive and also closed production. Even Arnold/SPS eventually moved a lot of production offshore, with the exception of the Flexmag ferrite/rubber business in Ohio.

The only remaining sintered RE plant from that period is operated by Electron Energy Corporation (EEC) in Pennsylvania. The reason they have survived is because they focus almost exclusively on SmCo, and particularly in military, aerospace and high energy physics applications which are the highest value and, to some degree, are strategically protected. Hitachi did attempt to set up a new sintered NdFeB plant at their China Grove site during the ITC case, but this was because they had to show that a U.S.-manufacturing operation was being damaged by the “infringers” rather than being based on cost-effective production. That plant never reached volume production and the equipment was sold off at a huge discount.

One new facility that has recently been built by Urban Mining (now Noveon) in Texas is based on sourcing the raw materials (i.e., magnets) from end-of-life devices or manufacturing scrap, and then crushing, milling and adding small amounts of RE

metal compounds to counteract any further volatilization that occurs in the sintering operation [42]. There is little evidence that operation will be cost competitive with Chinese production, or that their products will have the consistency over time that is required by major magnet users. The technology is based on research that was done at the University of Birmingham in the United Kingdom [43].

Bonded RE magnet production in the United States was more resilient, partly because they are less of a “commodity” and again are higher value, with minimal labor content. Thanks to the high price and sole source for the bondable NdFeB powders produced by Magnequench, there was little advantage to purchasing finished magnets from outside the United States and businesses such as Magnet Applications (i.e., currently Bunting-DuBois), Tengam, Electrodyne and Phoenix are still operating although the latter two companies have little RE production. Kane Magnetics (formerly Stackpole Magnet Division) was one of the RE bonded magnet companies that did not survive even though they were once Magnequench’s No. 1 customer by a significant margin in the United States. The company made strategic mistakes and suffered badly through the closure of the sintered ferrite magnet production facilities.

The state of US and European RE manufacturing facilities is currently being addressed by a number of companies such as MP Materials, USA Rare Earth, Vacuumsmeltze, GKN, Quadrant and others. With support from national governments it is likely that three to four substantial RE magnet manufacturing plants will be brought online starting as early as 2024. Added to this, there are projects in other parts of the supply chain including RE separation, metal making and recycling of end of life RE magnets that will help in re-building a robust supply chain.

There are also a host of fabricator/distributor companies in the United States, several of which describe themselves as magnet manufacturers but are more accurately described as magnet assembly manufacturers. The magnets used in these assemblies are normally imported from China, and therefore end users need to be aware that these are not U.S. products. Particular care needs to be taken if the end-product is for a military or other sensitive application that has to meet International Traffic in Arms Regulations (ITAR)/Defense Federal Acquisition Regulation Supplement (DFARS) requirements.

## 12.6 Major Players in the RE Magnet Supply Chain

With hundreds of RE magnet-manufacturing plants in China and very few in the rest of the world, there is almost complete dominance of the supply chain by China. Not only is the largest source of RE minerals in China (i.e., a by-product of mining iron ore), but separation, purification, alloy making and magnet making are skills that the Western world has either lost or is close to losing. With the decades of pressure from China and the closure of nearly all major magnet manufacturers, there has been little research and development (R&D) done in the United States or people trained in those industries. Not only is the Western world losing manufacturing

capability, but it has also lost the human capital that is necessary to support an industry.

There are some bright spots, with the once dominant U.S. RE mine at Mountain Pass (MP), CA, being back in operation and with Lynas now producing considerable quantities of materials in Australia. But until all the downstream processes have been regenerated there is still a reliance for these from China.

Of the sintered magnet plants in China, a few of them have the scale, the quality systems and state-of-the-art equipment that distinguishes them from the pack. Ningbo Yunsheng, Beijing Zhong Ke San Huan, Yantai Zhenghai, JL Mag, Baotou Tianhe Magnetics Technology and AT&M are in the group that major customers rely on.

In Japan, Hitachi (for now), TDK, Shin-Etsu and Daido Steel are all major, quality manufacturers. In Europe, where the loss of manufacturing has been almost as dramatic as in the United States, the Arnold SmCo plant in Switzerland, MS Schramberg (also bonded) and Vacuumshmelze in Germany are still operational. For bonded magnets Germany has Kolektor (i.e., Widia) and Magnet Fabrik Bonn, France has Arelec and the United Kingdom has Bunting (i.e., Magnet Applications).

## 12.7 Conclusions and Final Outlook

The growth in RE magnet markets over the last four or five decades has not only been substantial in value terms but their presence has resulted in a host of lower cost, higher-performance applications that may not even have existed without them. They are used in almost every manufacturing sector but largely go unnoticed by the public because the devices in which they are used are usually hidden inside the finished product. Certainly, many current applications could adopt material substitutions if the metal price volatility is controlled, if there were promise of new mining operations in many parts of the world, and the current focus on establishing multiple supply chains free from geopolitical constraints are moderated. With no new magnet materials on the horizon RE magnets are likely to hold onto their position of being the most valuable segment of permanent magnet material markets for decades.

Looking forward at what factors will impact growth and risk, the green energy applications of wind power and electric vehicles will probably be the dominant drivers of growth but at the same time, these applications are likely to be the biggest risk as well. Growth forecasts in these areas are indicating stress on existing supply chains and if major new resources are not developed quickly there will be supply shortages which will not only limit growth but will create price volatility and the need to find solutions that do not require rare earth metals.

With substantial resources for mining in Australia, Africa, North America and many other countries, along with multiple plans for separation, metal making, magnet manufacture and recycling underway, the future looks positive, provided that all of these stages of production deliver on their plans.

## References

1. K. Strnat, G. Hoffer, J. Olson, W. Ostertag, J. Becker, A family of new cobalt-base permanent magnet materials. *J. Appl. Phys.* **38**, 1001–1002 (1967). <https://doi.org/10.1063/1.1709459>
2. Magnetic Materials History. <https://www.birmingham.ac.uk/Documents/college-eps/metallurgy/research/Magnetic-Materials-Background/Magnetic-Materials-Background-1-History.pdf>
3. A. Ray, K. Strnat, Easy directions of magnetization in Ternary R<sub>2</sub>(Co, Fe)<sub>17</sub>phases. *IEEE Trans. Magn.* **8**, 516–518 (1972). <https://doi.org/10.1109/TMAG.1972.1067471>
4. M. Sagawa, S. Fujimura, N. Togawa, *J. Appl. Phys.* **55**, 2083 (1984)
5. J. Croat, J. Herbst, R. Lee, F. Pinkerton, *J. Appl. Phys.* **55**, 2078 (1984)
6. J. Bell, Magnets in EV/HEV Traction Motors. Designs and State of the Art Manufacturing. Magnetics 2021 Conference, Orlando, FL (2021, February 8)
7. Likia Tech Product Brochures. [www.likaicnc.com](http://www.likaicnc.com)
8. K. Park, K. Hiraga, M. Sagawa, Effect of metal-coating and consecutive heat treatment on coercivity of thin Nd-Fe-B sintered magnets, in *Proc 16th International Workshop on Rare Earth Magnets and Their Applications*, Sendai (2000), p. 257
9. US6387293, Composition for Rare Earth Bonded Magnet Use, Rare Earth Bonded Magnet and Method for Manufacturing Rare Earth Bonded Magnet, Seiko Epson (2002)
10. Newland Magnetics Product Literature. <https://www.newlandmagnetics.eu>
11. Neo Performance Materials – Product type MQ1–12. <https://mqitechnology.com/products/magnets/magnetic-properties/>
12. T. Takeshita, R. Nakayama, Development of HDDR process and anisotropic Nd-Fe-B bonded magnets. *IEEE Transl. J. Magn. Jpn.* **8**(10), 692–700 (1993)
13. C. Mishima, N. Hamada, H. Mitarai, Y. Honkura, Dependence of the hydrogen pressure on the magnetic properties of NdFeB anisotropic magnet powders produced by the HDDR method. *J. Magn. Soc. Jpn.* **24**, 407–410 (2000). <https://doi.org/10.3379/jmsjmag.24.407>
14. US4844754A – Iron-Rare Earth-Boron Permanent Magnets by Hot Working
15. N. Yashikawa, T. Iriyama, H. Yamada, Y. Kasai, V. Panchanathan, Radially orientated high energy product Nd-Fe-B ring magnets. *IEEE Trans. Magn.* **35**, 3268–3270 (1999)
16. US20090246063A1 – Method and Apparatus for Producing Radially Oriented Ring Magnet
17. J. Coey, H. Sun, D. Hurley, Intrinsic magnetic properties of new rare-earth iron intermetallic series. *J. Magn. Mater.* **101**, 310–316 (1991)
18. R. Coehoorn, D.B. de Mooij, C. De Waard, Meltspun permanent magnet materials containing Fe<sub>3</sub>B as the main phase. *J. Magn. Mater.* **80**(1), 101–104 (1989)
19. Lower-Cost Commercial Grade Ce Enhances Performance and Reduces Cost in Gap Magnets. <https://www.ameslab.gov/cmi/research-highlights/>
20. US20150170811A1 – Ferrite Magnetic Material, Ferrite Sintered Magnet, and Motor
21. S. Guruswamy, M. McCarter, J. Shield, V. Panchanathan, Explosive compaction of magnenquench Nd-Fe-B magnetic powders. *J. Appl. Phys.* **79**, 4851–4853 (1996). <https://doi.org/10.1063/1.361631>
22. B. Chelluri, *Powder Consolidation Using Dynamic Magnetic Compaction (DMC) Process* (2008). <https://doi.org/10.1002/9780470294574.ch22>
23. [https://www.aichi-steel.co.jp/ENGLISH/products/electromagnetic/bonded\\_magnet/example.html](https://www.aichi-steel.co.jp/ENGLISH/products/electromagnetic/bonded_magnet/example.html)
24. <https://www.iea.org/reports/global-ev-outlook-2022/executive-summary>
25. <https://www.howtogeek.com/658287/even-25-years-later-the-iomega-zip-is-unforgettable/>
26. <https://marketresearchcommunity.com/cpap-device-market/>
27. <https://www.stereotaxis.com/products/>
28. <https://www.dyson.co.uk/vacuum-cleaners/cordless/hyperdymium-motor>
29. <https://www.milwaukeetool.com/Products/Power-Tools>
30. <https://www.ecoustics.com/reviews/1more-triple-driver-earphones/>

31. <https://www.maclife.de/news/taptic-engine-analysiert-deshalb-dominiert-apple-touch-feedback-100113835.html>
32. <https://www.macrumors.com/2020/11/02/apple-magsafe-design-guidelines-accessory-makers/>
33. US8294320B2 – Interior Permanent Magnet Machine
34. <https://www.leandesign.com>
35. Projected Growth of the Wind Industry From Now Until 2050 – <https://www.energy.gov/maps/map-projected-growth-wind-industry-now-until-2050>
36. What Are Fly-By-Wire Systems? BAE Systems. <https://www.baesystems.com/en-us/definition/what-are-fly-by-wire-systems>
37. <https://abcnews.go.com/Politics/Vote2008/story?id=4757257&page=1>
38. <https://www.defensenews.com/air/2022/09/07/pentagon-suspends-f-35-deliveries-over-chinese-alloy-in-magnet/>
39. <https://www.federalregister.gov/documents/2012/09/21/2012-23325/certain-sintered-rare-earth-magnets-methods-of-making-same-and-products-containing-same-institution>
40. <https://www.hitachi-metals.co.jp/e/>
41. History of Arnold Magnetic Technologies. <https://web.archive.org/web/20110707170418/http://www.arnoldmagnetics.com/History.aspx>
42. W. Liu, C. Li, M. Zakotnik, M. Yue, D. Zhang, X. Huang, Recycling of waste Nd-Fe-B sintered magnets by doping with dysprosium hydride nanoparticles. *J. Rare Earths* **33**(8), 846–849 (2015)
43. M. Zakotnik, E. Devlin, I.R. Harris, A.J. Williams, Hydrogen decrepitation and recycling of NdFeB-type sintered magnets, in *Proceedings of the 19th International Workshop on Rare Earth Magnets & Their Applications*, (Beijing, 2006)

# Chapter 13

## Role of Rare Earths as Catalysts in the Chemical, Petroleum and Transportation Industries



Aaron Akah

### 13.1 Introduction

Rare earth elements, also known as the lanthanide series in the periodic table of elements, are a series of chemical elements found in the Earth's crust that are applied in many modern technologies such as consumer electronics, computers and networks, communications, clean energy, advanced transportation, health care, environmental mitigation, national defense and many others [1–5]. The introduction of the Welsbach incandescent lamp, which made use of the oxides of zirconium (Zr), lanthanum (La) and yttrium (Y) during the 1880s, marked the first commercial application of rare earths [1]. Since then, rare earths have found applications in various fields and their consumption has grown to over 100,000 metric tons annually as shown in Table 13.1.

Rare earths form a critical and essential part of many modern technologies as they sometimes act like technology building blocks. This is because their application in alloys and compounds can have a profound effect on the performance of complex engineered systems, some of which include automotive catalytic converters, petroleum refining catalysts, glass manufacture and polishing, ceramics, permanent magnets, metallurgical additives and alloys and rare earth phosphors for lighting, television, computer monitors, radar and X-ray intensifying film [1, 2, 6–8].

The demand for rare earth elements is a direct result of their integration as catalysts into end-use products. Catalysts represent a large market for rare earths where they provide properties desired for effective catalysis in petroleum refining, fuel additives and the transportation and chemical industry [1, 9–11].

---

A. Akah (✉)  
Saudi Aramco R&D Center, Dhahran, Saudi Arabia  
e-mail: [aaron.akah@aramco.com](mailto:aaron.akah@aramco.com)

**Table 13.1** Rare Earth Consumption by Market Sector [1]

Rare earth oxide	Amount by Market Sector (metric tons)								
	Catalyst	Ceramics	Glass	Metallurgy	Magnets	Battery alloys	Phosphors	Other	Total
CEO <sub>2</sub>	8820	840	18,620	5980		4040	990	2930	42,220
Dy <sub>2</sub> O <sub>3</sub>	–	–	–	–	1310	–	–	–	1310
Eu <sub>2</sub> O <sub>3</sub>	–	–	–	–	–	–	441	–	441
Gd <sub>2</sub> O <sub>3</sub>	–	–	–	–	525	–	162	75	762
La <sub>2</sub> O <sub>3</sub>	18,180	1190	8050	2990	–	6050	765	1430	38,655
Nd <sub>2</sub> O <sub>3</sub>	228	840	360	1900	18,200	1210	–	1130	23,868
Pr <sub>6</sub> O <sub>7</sub>	152	420	694	633	6140	399	–	300	8738
SmO	–	–	–	–	–	399	–	150	549
Tb <sub>6</sub> O <sub>7</sub>	–	–	–	–	53	–	414	–	467
Y <sub>2</sub> O <sub>3</sub>	–	3710	240	–	–	–	6230	1430	11,610
Other			480						480
Total	27,380	7000	28,444	11,503	26,228	12,098	9002	7445	129,100

## 13.2 Application of Rare Earths in Fluid Catalytic Cracking Catalysts

Fluid catalytic cracking (FCC) is a process for conversion of heavy oil fractions into high octane gasoline, light fuel oils and olefin-rich light gases. The process employs a catalyst in the form of microspheres, which behave as a fluid when aerated. Fluid catalytic cracking is an endothermic process during which carbon is deposited onto the catalyst. This carbon, known as coke, reduces the activity of the catalyst and the catalyst must be regenerated.

The fluidized catalyst is continuously circulated from a reaction zone, where the cracking reactions occur, to a regeneration zone where the catalyst is reactivated as illustrated in Fig. 13.1 [12].

During the FCC process, hydrocarbon (HC) feed is injected into the riser section of the FCC reactor where it is cracked into lighter more valuable products upon contacting hot catalyst from the catalyst regenerator. The catalyst and HC vapors are carried up the riser to the disengagement section of the FCC reactor where they are separated. Subsequently, the catalyst flows into a stripping section where the HC vapors entrained with the catalyst are stripped by steam injection. Following the stripping of HCs from the spent cracking catalyst, the stripped catalyst is recirculated to the catalyst regenerator.

Typically, catalyst is regenerated by introducing air into the regenerator and burning off the coke to restore catalyst activity. Coke combustion is an exothermic reaction and it is used to supply heat to the regenerated catalyst. The hot, reactivated catalyst flows through the regenerated catalyst standpipe back to the riser to complete the catalyst cycle. The coke combustion exhaust gas stream rises to the top of the regenerator and leaves the regenerator as flue gas. Flue gas generally contains

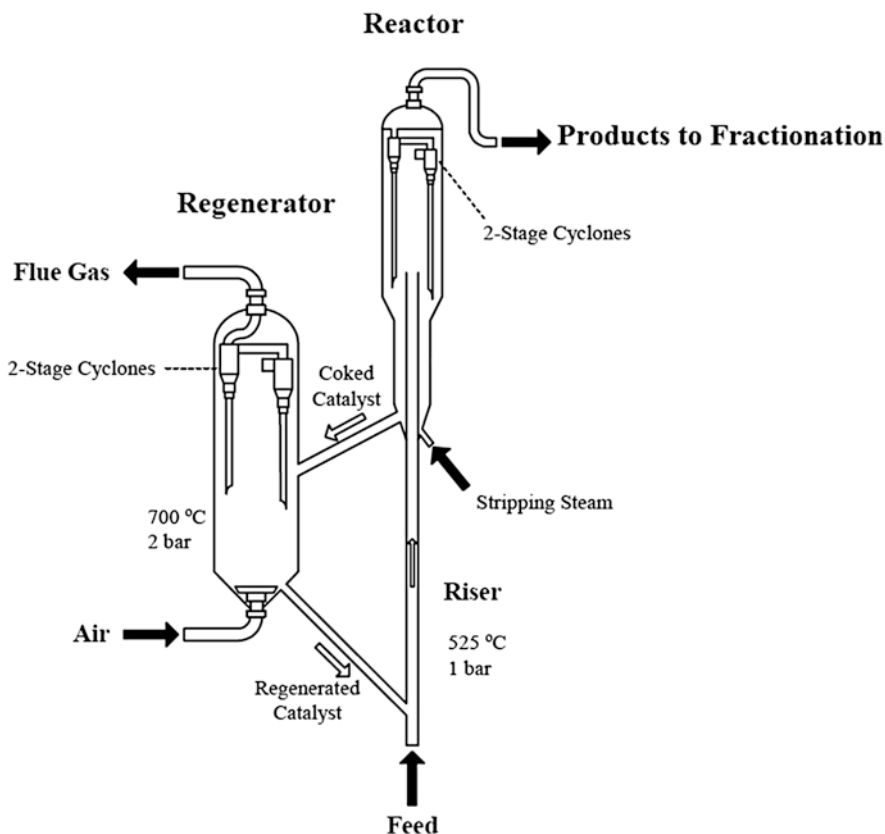


Fig. 13.1 Schematic of a conventional FCC unit [12]

nitrogen oxides ( $\text{NO}_x$ ), sulfur oxides ( $\text{SO}_x$ ), carbon monoxide ( $\text{CO}$ ), oxygen ( $\text{O}_2$ ), hydrogen cyanide ( $\text{HCN}$ ) or ammonia ( $\text{NH}_3$ ), nitrogen ( $\text{N}_2$ ) and carbon dioxide ( $\text{CO}_2$ ).

In addition to providing the catalytic action, the catalyst is also the vehicle for the transfer of heat from the regeneration to the reaction zone. Catalyst performance is an integral part of the techno-economic evaluation of the catalytic cracking process as it affects the capital cost in terms of the amount of material required, and the quantity and quality of the reaction products generated.

Rare earth oxides have been widely investigated in catalysis as structural and electronic promoters to improve the activity, selectivity and thermal stability of catalysts [1, 2, 10, 13–31]. Since the introduction of rare earths in fluid catalytic cracking (FCC) catalysts in the early 1960s, the FCC continues to play a major role in the catalytic application of rare earths [9]. The use of rare earths can help preserve catalyst effectiveness and increase the yield of the gasoline fractions by cracking the heavier oil fractions. Rare earths, such as lanthanum (La), are used in FCC catalysts to refine crude oil into gasoline, distillates, lighter oil products and other fuels.

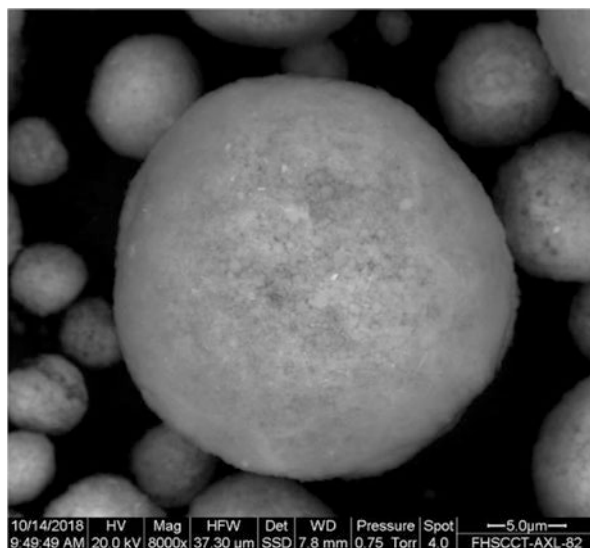


FCC catalysts operate between moderate to high temperatures (500–800 °C) in the presence of steam, especially during the regeneration step. These severe conditions strongly influence the performance of the catalysts. Thus, thermal and hydrothermal stability of zeolites (i.e., hydrated aluminosilicate minerals,  $M_xAl_xSi_{1-x}O_2 \cdot yH_2O$  where M is either a metal ion or  $H^+$ ) are among the most important parameters for FCC heterogeneous catalysts.

One of the factors that affects the design and operation of an FCC unit is the type of catalyst to be employed in the process. Most FCC catalysts consist of an active component (e.g., zeolite), a matrix such as amorphous silica-alumina ( $SiO_2-Al_2O_3$ ) which also provides catalytic sites and larger pores, a binder (e.g., bentonite clay ( $Ca, Na, H)(Al, Mg, Fe, Zn)_2(Si, Al)4O_{10}(OH)_2 \cdot nH_2O$ )), and a filler. Fig. 13.2 is a micrograph of an FCC catalyst showing the spherical particles that are suitable for application in a fluidized circulating reactor. Large voids and pores in the spherical catalyst particle are necessary to allow for mass transport of the heavy HCs.

Ultra-stabilized zeolite Y ( $M_{3.5}[Al_7Si_{17}O_{48}] \cdot 32H_2O$ , M = Ca, Na, K, Mg) is used as the main active zeolite in today's conventional FCC process. This material contains an internal porous structure in which acid sites are present, which can convert larger molecules to the desired gasoline range molecules. Although the FCC unit was developed purposely to assist in the conversion of low value feed into more gasoline, the unit and the process have undergone several modifications, some of which are aimed at tackling the increasing demand for some of its by-products, such as propylene. For the purpose of producing more propylene and olefins, ZSM-5 (i.e., Zeolite Socony Mobil-5:  $Na_nAl_nSi_{96-n}O_{192} \cdot 16H_2O$ ) is being used as the main active component of the catalyst in the FCC unit [35–42]. Metal contaminants usually have their biggest influence on the zeolite active components, and it is through the zeolite that rare earths are usually introduced into the FCC catalysts.

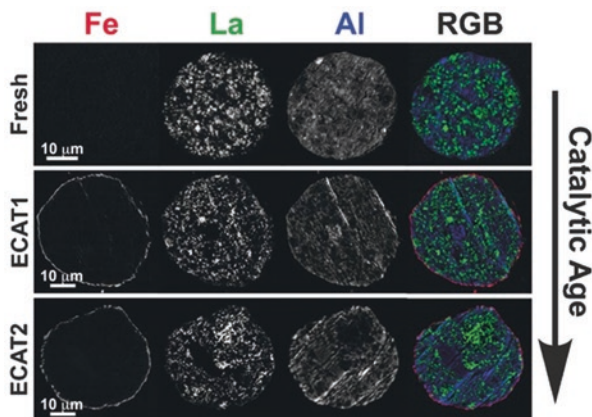
**Fig. 13.2** Microscopic image of an FCC catalyst



The matrix of an FCC catalyst serves both physical and catalytic functions [32, 43–49]. Physical functions include providing particle integrity and attrition resistance, acting as a heat transfer medium, and providing a porous structure to allow diffusion of HCs into and out of the catalyst microspheres [20, 41–43, 45, 47, 48]. The matrix can also affect catalyst selectivity, product quality and resistance to poisons. Various alumina ( $\text{Al}_2\text{O}_3$ ) and silica ( $\text{SiO}_2$ ) sources are used to produce a meso- and macroporous matrix that allows access to, and pre-cracks the larger molecules in the heavy oil or crude oil. In addition, these components are used to bind the system together. Additional components may comprise rare earth metals or specific metal traps for trapping nickel (Ni) and vanadium (V) that are present in the feed source. The components are typically mixed in an aqueous slurry, and then spray-dried to form more or less uniform spherical particles that can be fluidized in a regenerator.

For the modern conventional FCC process, the desired catalyst properties are as follows: [33]

- Good stability to high temperature and to steam. The catalysts must have the thermal stability to maintain particle and catalytic integrity under severe regeneration conditions. The continuous cycle of cracking and regeneration in the FCC leads to dealumination as a result of the harsh hydrothermal conditions in the regenerator, and metal deposition from the feed. Dealumination leads to the loss of Bronsted acidity, while metal deposition can lead to occluded pores and unwanted secondary reactions. Kalirai [34] studied dealumination in FCC catalysts using scanning transmission X-ray microscopy (STXM) with La as a localization marker for the zeolite particles. Results revealed that the loss of activity in FCC catalysts is a combination of deposited metal-mediated pore accessibility loss and zeolite dealumination. Fig. 13.3 elucidates physical changes that occur within zeolite in the catalyst as a result of metal deposition and dealumination [34]. The thin ring of iron (Fe) deposition on ECAT 1 and ECAT2 (i.e., equilibrium



**Fig. 13.3** Elucidation of zeolite dealumination using fresh and equilibrium FCC catalyst (ECAT) [34]

catalysts) is a result of the catalyst being exposed to feeds that contain contaminant metals (e.g., Fe). The deposited contaminant metals are primarily present on the surface of the catalyst.

- High activity to carry out conversion of the feed before any significant amount of thermal cracking sets in. Thermal cracking leads to undesirable products such as methane ( $\text{CH}_4$ ), ethane ( $\text{C}_2\text{H}_6$ ) and some propane ( $\text{C}_3\text{H}_8$ ). Catalytic cracking produces relatively fewer  $\text{C}_1$  and  $\text{C}_2$  fragments and a larger number of olefins ( $\text{C}_n\text{H}_{2n}$ ) are produced.
- Large pore sizes to crack larger molecules so that can get into smaller pores.
- Good resistance to attrition to maintain particle morphology under the severe impact and erosion forces that exist in the FCC unit.
- Low coke production so the catalyst can remain active for a longer period.

The main goal of the FCC unit is to upgrade low value HCs such as residue feeds, which often contains higher levels of contaminants that can degrade catalyst activity such as nickel (Ni), vanadium (V), sodium (Na), iron (Fe), and calcium (Ca) [32, 50, 51]. Of all these metals, V presents the most deleterious effect as it is mobile and can move from one catalyst particle to another, thereby contaminating newer active sites and aged catalysts. Figure 13.4 illustrates the distribution of Ni and V in the FCC catalyst before and after regeneration. It shows that Ni remains on the surface of the zeolite, while V is more mobile and penetrates into the pores of the zeolite. The mobility of V is facilitated during the regeneration process by the hydrothermal environment that is produced during the combustion of coke and HCs to steam and  $\text{CO}_2$ .

The concentration of V in the spent catalyst is sometimes used as a determinant for the amount of fresh catalyst that is needed to be added to the FCC to maintain catalytic activity [24]. Vanadium also promotes dehydrogenation reactions leading to more dry gas and coke [52–56]. It also attacks the zeolite crystalline structure leading to structure collapse and a loss in surface area as the pore structure is no longer maintained.

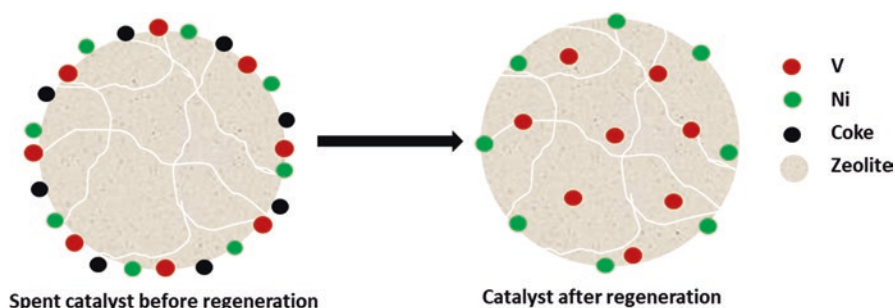


Fig. 13.4 Distribution of Ni and V in equilibrium FCC catalyst

### 13.2.1 Use of Rare Earths to Passivate Metal Contaminants

As described in the previous section, a common practice for maintaining the FCC unit activity is by adjusting fresh catalyst addition, based on the level of metal contaminants in the feed [57]. Fresh catalyst additions are increased when feed metals begin to increase, and the opposite applies when the metal content in the feed is low. Consequently, when dealing with feeds that have a higher metals content, adding more fresh catalyst alone may not be an effective catalyst management strategy as this will not reduce the impact of contaminant metals and the activity and stability of the catalyst will be adversely affected.

It is therefore important to have an appropriate catalyst formulation, which can effectively trap metal contaminants. The metal trap technology works by capturing the volatile and mobile metal contaminants, primarily V, to form a stable and catalytically inactive compound in a process known as *metal passivation*. Rare earths are used to passivate (trap) V through the formation of stable vanadates, thus preventing V from attacking the zeolite structure. The severe conditions under which the catalytic cracking process is carried out make it particularly difficult for V blocking. A suitable V trap for FCC catalysts should fulfill most of the following conditions: [58]

- The substance should be stable at a temperature up to 800 °C in an oxidizing environment (i.e., regenerator) and in the presence of about 20% water vapor and from 60 to 2000 ppm sulfuric acid (H<sub>2</sub>SO<sub>4</sub>).
- That the substance be stable at a temperature of 550 °C in a strongly reducing environment (i.e., reactor) and in the presence of water vapor (i.e., stripper).
- That the substance possesses a greater affinity for V than for the zeolite or the catalyst components.
- The amount of substance required for the effective protection of the catalyst must be low enough to avoid excessive dilution of the catalyst and in that way avoids loss of catalytic activity and selectivity.
- The rate of V capture must be high enough to avoid damaging the catalyst.
- The substance ought to maintain its capability to capture V while it remains within the cracking unit.
- If the substance contains metallic elements, these must not be interchanged by the zeolite cations.
- The substance must not be damaging to either the catalyst or its metallic structure.
- The substance ought to be able to be incorporated within the catalyst particle during its production (i.e., integral particle), and/or to be able to be prepared in the form of particles that are able to be fluidized having good abrasion strength, in order that they can flow together with the catalyst in the unit (i.e., dual particle).
- The substance must be cheaper than the catalyst since it is charged to the catalyst cost in order to decrease the fresh catalyst addition and in this manner to diminish the operation cost.

- It must be acceptable from the viewpoint of environmental preservation. The substance must not require particular handling conditions, it must not generate toxic materials during its preparation, nor can it be apt to be converted into a dangerous contaminant after being used.
- It must not possess dehydrogenating activity nor facilitate Ni and V dehydrogenating action.

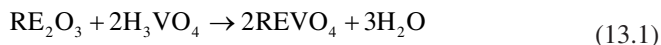
Despite a great deal of investigation, no substance has been found which meets all the requirements with respect to an ideal trap for retaining vanadium.

The use of rare earths for the preparation of V-tolerant FCC catalysts provides a way forward because of the following attributes: [24]

- They can process high metal-containing feeds.
- They can capture and immobilize V in a nondestructive form.
- They irreversibly bind V so that V cannot migrate back to the catalyst.
- They have a high capacity to remove a considerable amount of V from the catalyst.
- They show negligible interaction with other acidic species (e.g., sulfur (S) as H<sub>2</sub>SO<sub>4</sub>).
- Vanadium migration to the trap is significantly faster than the migration of V to the zeolite.

Metal *passivation* reduces the harmful effects of metals without substantial reduction in catalyst activity and without removing the metal from the unit. Nickel and V which constitute the most relevant poisons for catalytic cracking catalysts are usually associated metal porphyrins. Porphyrins are organometallic compounds found in the higher boiling range oil fractions, and distillation concentrates Ni and V in the fractions typically sent to the FCC unit. It is during the FCC process that the metals form a deposit on the catalyst surface, damaging the zeolite structure [19, 24]. Therefore, the use of rare earths will help reduce the deleterious effect of V and Ni.

Rare earth oxides such as La<sub>2</sub>O<sub>3</sub> are basic in nature and can neutralize vanadic acid (H<sub>3</sub>VO<sub>4</sub>) to form rare earth vanadates [24, 55, 59, 60], thereby preventing the rapid hydrolysis of the zeolite framework. The reaction of rare earths with acidic vanadium compounds forming vanadates is represented by Reaction 13.1



where RE<sub>2</sub>O<sub>3</sub> is a rare earth oxide, which leads to the formation of stable vanadium compounds [61].

Therefore, the introduction of rare earths into the zeolite helps to reduce metal poisoning and results in the retention of the aluminum framework and improved stability of the zeolite structure [10, 24, 62–72].

### ***13.2.2 Use of Rare Earths to Improve Catalyst Stability***

Most catalysts used in processes involving high severity operation, such as high temperatures and steam, face the inherent problem of hydrothermal deactivation that has to be mitigated. FCC catalysts operate between moderate to high temperatures (i.e., 500–800 °C), in the presence of steam, especially during the regeneration step. These severe conditions strongly influence the performance of the catalysts especially during catalyst regeneration which usually takes place at temperatures as high as 800 °C and in the presence of steam. With such severe conditions, zeolite dealumination becomes a real problem. For instance, USY (i.e., ultra-stable Y) zeolites used in standard FCC catalyst usually have a framework Si/Al ratio of approximately 5 before reaction and after regeneration, the equilibrium catalyst has a Si/Al ratio close to 20, showing the extent of dealumination in the FCC regenerator [20, 73]. Therefore, thermal stability and hydrothermal stability of zeolites are among the most important parameters for catalyst manufacturers.

To mitigate the problem of catalyst deactivation, rare earths can be used to improve the hydrothermal stability of FCC catalysts [5, 18, 67, 72–81]. Lanthanum and cerium (Ce) are the two main rare earths used in FCC catalysts [1, 2, 6–8, 82, 83]. These metals limit the extent to which zeolite dealumination occurs, thereby stabilizing the structure under the conditions of the FCC unit [75]. A study carried out at BASF [84] shows the differences in catalyst hydrothermal stability with and without rare earth (Fig. 13.5). Rare earth zeolite Y (REY) shows a greater thermal stability than  $\text{NH}_4\text{Y}$  (i.e., ammonium form of zeolite Y where the proton is replaced by  $\text{NH}_4^+$  ion through ion exchange). This is because rare earths provide hydrothermal stability to the zeolite by improving retention of the catalysts' surface area, as well as inhibiting dealumination, resulting in greater preservation of the acid sites [84].

### ***13.2.3 Effect of Rare Earths on the Activity of Catalysts***

Zeolites used in cracking catalysts undergo reactions in the high-temperature steam environment of the regenerator that destroy the active sites. As catalysts age in the FCC regenerator, the unit cell size drops due to dealumination of the zeolite, through the reaction of the active sites with steam. The rare earth ions in the zeolite retard this deleterious reaction from occurring, thus preventing the collapse of the crystal structure. This active site preservation helps to maintain the activity of the catalysts. Manipulation of the active site density of the catalysts with rare earths translates into improved catalyst activity and/or selectivity profiles that are available to refiners [22].

The fact that rare earths inhibit the dealumination of a zeolite, means that a higher concentration of acid sites will be found in a rare earth ion-exchange catalyst, leading to improved activity and hydrothermal stability. On average, the acid sites

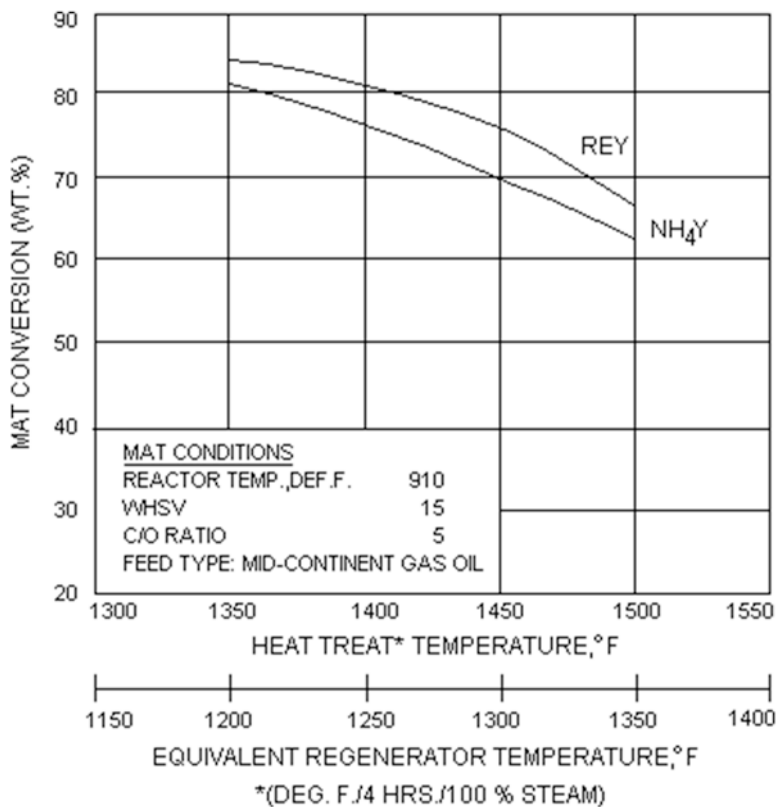


Fig. 13.5 Effect of rare earths on the hydrothermal stability of Y zeolite [84]

are weaker and in closer proximity to each other than those found in a more highly dealuminated catalyst that is characterized by lower unit cell size measurements.

As a result of the greater number of active sites, the cracking activity of the catalyst increases. Therefore, the incorporation of rare earths in catalytic cracking catalysts enhances gasoline yield. Figure 13.6 shows a plot of gasoline yield at varying conversion levels for two standard cracking catalysts with different levels of rare earths. These data suggest a strong correlation between rare earth content and gasoline yield.

Therefore, by restricting the loss of aluminum atoms from zeolite, rare earths increase the activity and gasoline yield of FCC catalysts [85].

Whether a rare earth or non-rare earth catalyst is used in the refinery operation depends on the type of feed and desired products. If a refinery is interested in processing residue feed into gasoline, a rare earth cracking catalyst will be desired.

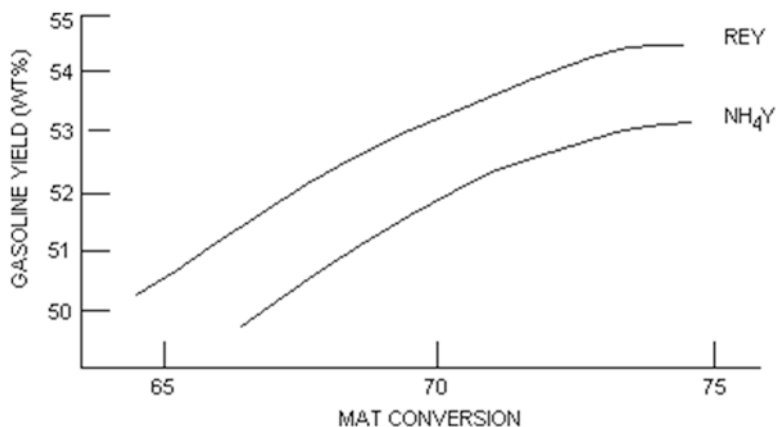


Fig. 13.6 Effect of rare earths on gasoline yield [84]

### 13.3 Application of Rare Earths in the Transportation Industry

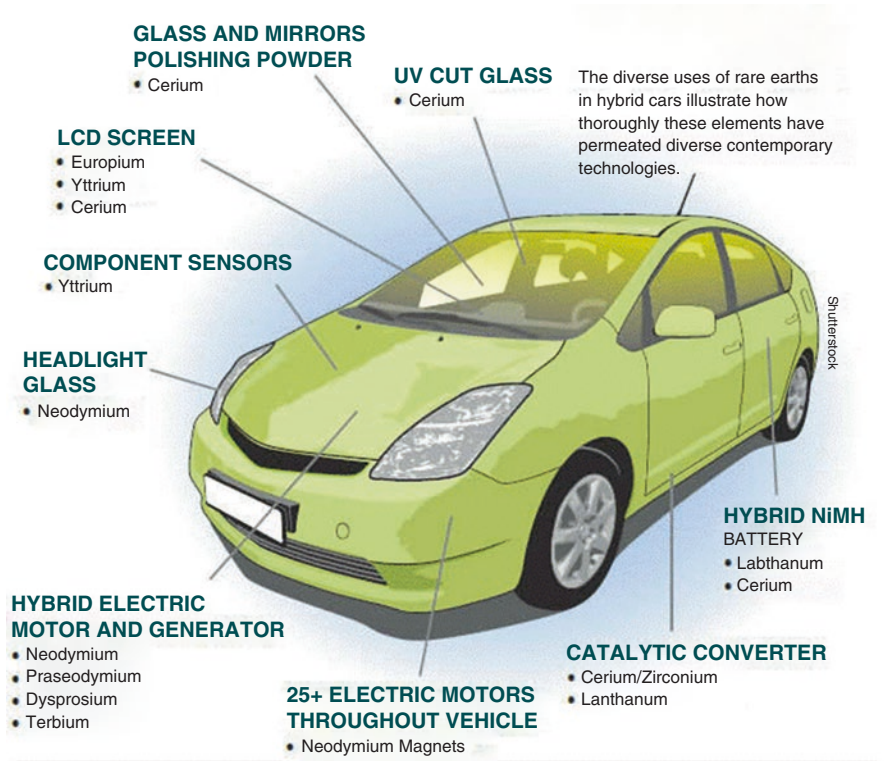
From a glance, it might look as if the use of rare earths in the transportation sector is limited, but taking an in-depth look suddenly reveals the widespread use of rare earths in the automotive industry. For instance, rare earths find applications in several car parts such as windshield wipers, antilock brakes, airbags, electric windows, power steering and in the control of vehicle emissions.

#### 13.3.1 Use of Rare Earths in Car Components

Figure 13.7 illustrates the widespread use of rare earths in the automotive industry [86], with neodymium (Nd) being the rare earth metal that is most widely used. The use of Nd was also confirmed in a study carried out by Alonso et al. [87] where approximately 0.44 kg of rare earths was estimated for use in a typical conventional sedan with approximately 80% of the rare earth content in magnets. This study also indicated that Ce, the second most widely used rare earth, was incorporated into catalytic converters.

It is expected that electrification of the automotive industry will reshape the role played by some rare earths and limit their applications as components such as catalytic converters that will no longer be required. The advent of electric vehicles (EVs) is seen as a key technology to reduce air pollution in densely populated areas. Electrification of the automotive industry will provide alternative pathways to diversification of energy, as well as contributing to reduction in greenhouse gas emissions. Coupled with the low-carbon electricity sector, electrification of the





**Fig. 13.7** Application of rare earths in the automotive industry [86]

automotive sector has a huge potential to reduce greenhouse gas emissions through zero tailpipe emissions and better efficiency in comparison to internal combustion engine vehicles [88].

Other rare earth applications include batteries to power the electric vehicles. These batteries will require high-efficiency magnets to convert energy to torque where the force of the spinning axle is used to power the wheels of an electric car.

The strength of a magnet is determined by its coercive force and flux density. Magnets made using rare earths such as Nd are known to have high coercivity and flux density, and it is this combination that makes them perfect for high-powered EVs. Neodymium magnets can only be used at low temperatures as they lose their magnetism at temperatures around 60–80 °C. To permit higher-temperature use, other rare earth elements such as dysprosium (Dy) and terbium (Tb) can be added, increasing operating temperatures to above 160 °C. The coercivity of the magnet can also be increased by adding Dy and praseodymium (Pr). The composition of EV magnets is approximately 24% Nd, 7.5% Dy and 6% Pr [86].

In most hybrid or EVs, around 2–5 kg of rare earth magnets are used depending on the design [87–89], primarily in the heating, ventilation and air-conditioning (HVAC) systems.

It is projected by 2030, that the growth in EVs will lead to a rise in demand for magnetic systems [88], and it is anticipated that rare earth magnets will continue to play a fundamental role in the design of the EV. Thus, the increase in demand for rare earth magnets will drive the demand for rare earths in the future automotive industry.

### 13.3.2 Role of Rare Earths in Catalytic Converters

A catalytic converter (Fig. 13.8) is a unit that fits into the front part of the exhaust system of a vehicle, close to the engine, to reduce the emission of gaseous pollutants, such as carbon monoxide (CO), nitrogen oxides (NO<sub>x</sub>) and HCs. When exhaust gas from the engine enters the catalytic converter, it passes through the inner catalyst honeycomb. Here the engine exhaust gas comes into contact with catalysts that will ignite the chemical reactions needed to convert the harmful pollutants into more benign gas-phase chemical species. There are two main types of catalysts that will control these reactions: oxidation catalysts and reduction catalysts.

The catalyst formulation is comprised of three key constituents: (1) precious or noble metals (platinum (Pt), palladium (Pd) and rhodium (Rh)); (2) alumina (Al<sub>2</sub>O<sub>3</sub>) and (3) rare earth-based materials which enhance catalytic activity of the precious metals. Rare earths promote noble metal dispersion, increase thermal stability of the alumina support, promote the water-gas shift and the steam reforming reactions and store and release oxygen under conditions fluctuating between oxidizing and reducing. Cerium is typically used in this capacity.

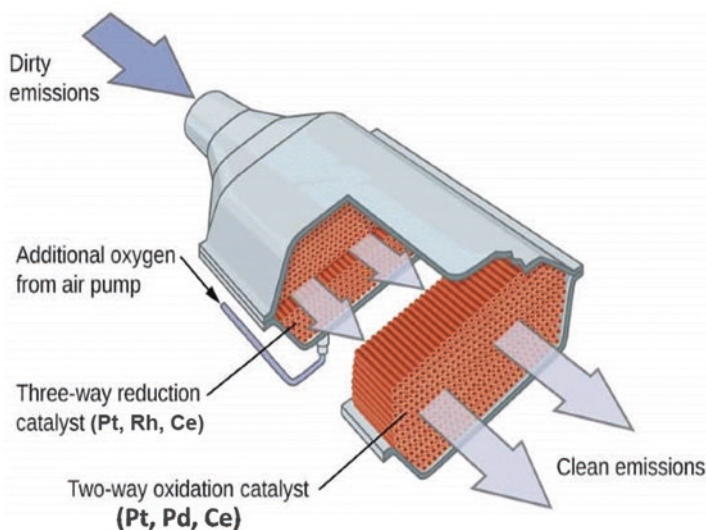


Fig. 13.8 Illustration of the catalytic converter. (Modified from Sokol [90])

Three-way reduction catalysts are designed to perform multiple oxidation and reduction reactions simultaneously, as well as convert  $\text{NO}_x$  into oxygen ( $\text{O}_2$ ) and nitrogen ( $\text{N}_2$ ). The two-way oxidation catalysts are designed to perform two simultaneous reactions, primarily converting CO and HCs to  $\text{CO}_2$  and  $\text{H}_2\text{O}$ . The reason that two different types of catalysts are necessary is because CO and HCs require a lean fuel/air mixture for conversion to occur, while  $\text{NO}_x$  conversion requires a rich fuel/air mixture. Rare earths are now incorporated in catalytic converters because of the benefits that they bring.

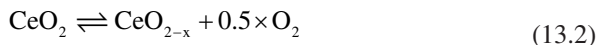
## 13.4 Role of Rare Earths in Environmental Protection

Rare earth such as La and Ce have been used as structural and electronic promoters in several applications in the field of environmental catalysis. For example, lanthanum oxide ( $\text{La}_2\text{O}_3$ ) is used as surface area stabilizer of  $\text{Al}_2\text{O}_3$  and zirconia ( $\text{ZrO}_2$ ) support substrates [3], while cerium oxide ( $\text{CeO}_2$ ) is used to increase the oxygen storage/release properties of three-way catalyst formulations. Although rare earths can be introduced into the catalyst substrate in several forms, in general, they are used in the form of oxides in catalyst formulations. Rare earths do not act alone but always in combination with other elements. Their role is, therefore, being either catalyst promoters (i.e., structural or electronic) or stabilizers to improve the activity and selectivity or increase the thermal stability of the catalyst [91]. Two application areas are combustion and air pollution control.

### 13.4.1 Rare Earths in Catalytic Combustion

Ceria ( $\text{CeO}_2$ ) or ceria-based materials are used as a promoter due to ceria's oxygen storage capacity (OSC). Without any OSC function, the ratio of oxygen to fuel needs to be tightly controlled with a specific stoichiometric ratio to achieve the best conversion rates [92]. This is because while CO and HCs are converted to  $\text{CO}_2$  under oxidizing conditions, the reduction of  $\text{NO}_x$  to  $\text{N}_2$  only shows good conversion efficiency under reducing conditions. Cerium ions can easily switch between  $3^+$  and  $4^+$  oxidation states via the creation and regeneration of oxygen vacancies, which allows the ceria-containing catalyst material to store oxygen from the exhaust stream when it is in stoichiometric excess, promoting conversion of  $\text{NO}_x$ , as well as release oxygen to the exhaust stream when it is deficient, promoting conversion of CO and HCs to  $\text{CO}_2$ . This expands the air-to-fuel ratio "window" under which acceptable catalyst performance is achieved for all three reactants. Typically, a  $\text{CeO}_2$ - $\text{ZrO}_2$  blend is used to improve thermal stability. Platinum or palladium are used as the active oxidative catalyst, with Rh is included for the reduction of  $\text{NO}_x$  to  $\text{N}_2$  [92].

The success of  $\text{CeO}_2$  in redox and combustion catalysts is related to its ability to shift easily between a reduced and an oxidized state as a result of a change in gas-phase oxygen concentration according to the following reaction:



This allows  $\text{CeO}_2$  to act as an oxygen buffer providing oxygen under rich conditions and removing it under lean conditions for optimal conversion in a three-way catalyst (TWC) system.

Most FCC catalysts contain zeolites or molecular sieves as active components [33]. Zeolites improve the activity and selectivity of the catalysts for the desired cracking reactions. The porous nature of the zeolites means they are susceptible to coke formation during catalysis, which leads to deactivation of catalytic activity. The catalyst will then have to be regenerated by burning off the coke. To reduce the coke content of zeolites during regeneration, the degree of coke burnoff must be increased to promote the formation of  $\text{CO}_2$  as a combustion product, as opposed to forming  $\text{CO}$ . The formation of  $\text{CO}_2$  rather than  $\text{CO}$  increases the amount of heat released in the regenerator and reduces the amount of pollution control treatment needed before the regenerator flue gas can be passed into the atmosphere. In addition to the degree of coke burnoff, the rate of coke burnoff in the catalyst regenerator is also important. A faster burnoff rate allows a smaller amount of catalyst to be used in the regenerator and allows the regenerator to be sized smaller than would otherwise be possible.

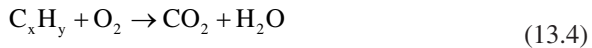
It is known that the degree of coke burnoff and the rate of coke burnoff in an FCC catalyst regenerator can be increased by adding a promoter, such as a catalytic metal, to the FCC catalyst. Rare earths have been found to be suitable promoters in FCC catalysts because they are stable and can withstand the continuous cycling between the high-temperature cracking reaction zone in the FCC system and the even higher-temperature regeneration zone [12]. In addition to their role in coke burnoff, rare earths can also help to improve product yields and reduce the amount of coke formed in the reaction zone. They are usually introduced in the FCC catalysts via ion exchange or impregnation. The amount of rare earth metals utilized is calculated on the basis of  $\text{RE}_2\text{O}_3$ . The application alleges that catalysts promoted with the rare earth metals acquire excellent selectivity, providing a relatively high yield of gasoline and reducing coke production [23].

### ***13.4.2 Use of Rare Earths in Air Pollution Control***

Anthropogenic activities (e.g., release of greenhouse gases) have led to an increase in air pollution, leading to a major public health concern, particularly in urban areas. More stringent legislation to control and limit pollutant emissions has been proposed to combat this problem. For the automotive sector, stringent environmental legislation has led to the development of the catalytic converter technology to

control and treat these pollutants. Initially, Pt/Pd or Pt/Rh oxidation catalysts were developed to limit HC and CO emissions which were later developed into TWC systems that also converted NO<sub>x</sub> emissions.

Although the main reactions for exhaust purification using the TWC are the oxidation of CO and HCs to CO<sub>2</sub> and H<sub>2</sub>O, and the reduction of NO<sub>x</sub> to N<sub>2</sub>, other reactions, such as the water-gas shift reaction or reaction of pollutants with H<sub>2</sub>O or H<sub>2</sub> can occur as well: [92]



Three-way catalysts consist of a monolith substrate, high surface area washcoat with oxygen storage promoter materials, the active catalyst (platinum group metals (PGMs)) and promoter materials [92, 94].

Alumina and thermally stabilized variations of Al<sub>2</sub>O<sub>3</sub> are important automobile catalysts as they provide high surface area for dispersion of active PGMs as very small crystallites (e.g., initially less than 10 nm). Within a high surface area support, the PGM crystallites are dispersed which assists in mitigating their high-temperature sintering and deactivation. Alumina also absorbs poisons (e.g., S, phosphorus (P) and metals) which helps retain catalytic performance, and it also helps binding the catalyst layer to the substrate. Ceria in various forms also has several roles [92]. It has a stabilizing effect on the Al<sub>2</sub>O<sub>3</sub> surface area at high temperatures, and it is also capable of stabilizing the PGM dispersion, especially Pt. In addition, CeO<sub>2</sub> allows for two other performance enhancing phenomena to take place: (1) oxygen storage and (2) the water-gas shift reaction (Reaction 13.6).



Ceria stores O<sub>2</sub> as CeO<sub>2</sub> (Ce(IV)) when the exhaust gas is lean (i.e., a reducing or fuel gas environment) and releases O<sub>2</sub> when the gas becomes rich (i.e., an oxidizing or flue gas environment), forming Ce<sub>2</sub>O<sub>3</sub> (Ce(III)), and enables CO and HC adsorbed on the catalyst to be oxidized during rich excursions when there is insufficient O<sub>2</sub> in the gas [93]. This improves the oxidation performance of the catalyst under rich operating conditions, and leads to the production of H<sub>2</sub> from the water-gas shift reaction, as well as the decomposition of NO<sub>x</sub>. Originally, CeO<sub>2</sub> was incorporated into the catalyst matrix. Today, various mixed ceria oxides which demonstrate enhanced stability are used. Although exact catalyst formulations are proprietary, it is clear from publications in the literature the performance of the catalyst is influenced by the forms and methods in which components are incorporated into the catalyst.

The beneficial effects of rare earth metals in exhaust catalysts have been recognized [10]. The rare earth metals promote noble precious metal dispersion, increase thermal stability of the alumina support, promote the water-gas shift and the steam reforming reactions as well as store and release O<sub>2</sub> under conditions fluctuating between oxidizing and reducing.

Development of TWC technology has been critical in maintaining air-quality regulations for gasoline engines via the conversion of pollutants from the internal combustion engine exhaust. The development of improved TWC formulations is an important challenge for the automotive industry. To meet increasingly stringent environmental regulations around the world, the development of more efficient catalysts will require a complete understanding of the many parameters related to TWC design.

## 13.5 Application of Rare Earths in the Chemical Industry

One area that is beginning to see the emergence of catalysts containing rare earths is chemical processing where the introduction of rare earths leads to increased catalyst performance.

### 13.5.1 Use of Rare Earths in Methanol Synthesis

Methanol (CH<sub>3</sub>OH) is one of the most important basic industrial chemicals, with considerable potential as feed for the production of organic raw materials. Methanol derivatives end up in products such as paints, solvents, engineered wood, plastics, polyethylene terephthalate (PET) bottles, safety glass, carpets, mattress foam, fertilizer and furniture using resins. The value chain for CH<sub>3</sub>OH is shown in Fig. 13.9.

Methanol was discovered in the seventeenth century by Robert Boyle via wood distillation [94, 95]. Boyle's process continued to be used until the beginning of the twentieth century when Sabatier introduced the first synthetic pathway for the production of methanol by reacting CO with H<sub>2</sub> [95]. Based on the Sabatier's synthetic process, BASF patented a syngas-based methanol production process [96], where syngas (CO, CO<sub>2</sub> and H<sub>2</sub>) was supplied via coal gasification. The BASF process was carried out over a zinc oxide/chromium oxide (ZnO/Cr<sub>2</sub>O<sub>3</sub>) catalyst at high temperature and pressure (e.g., 300–400 °C and 25–35 MPa). As this process was highly inefficient, research efforts continued to develop and improve not only the process operating conditions, but also the catalyst and the use of cleaner produced syngas. Operating temperatures were reduced to 300 °C, and pressures to 10 MPa by Imperial Chemical Industries (ICI) in 1966 [94, 95], and then further reduced by Lurgi [94, 95] to 230–250 °C and 4–5 MPa, respectively.

Although a typical methanol synthesis catalyst mostly consists of copper (Cu), zinc (Zn) and aluminum (Al), the use of catalysts incorporating rare earth elements

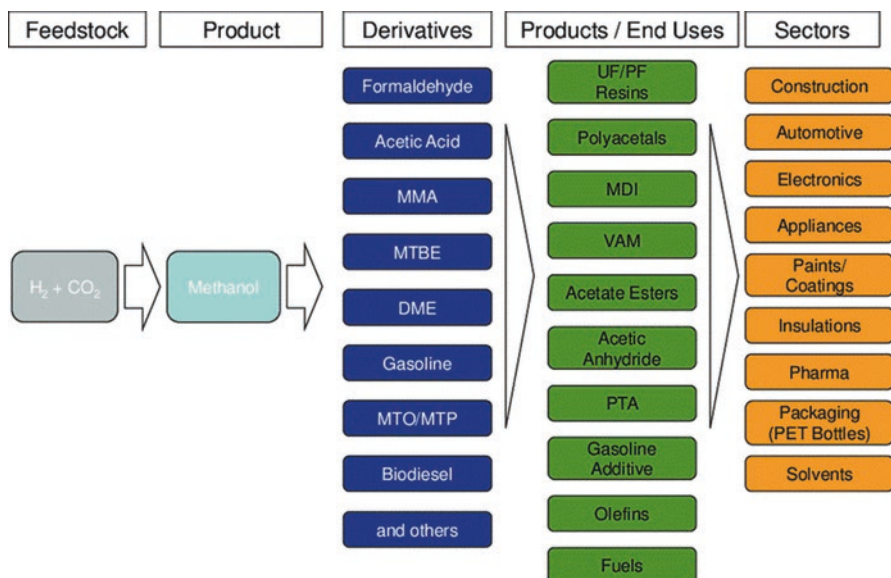


Fig. 13.9 Methanol value chain [94]

has been shown to improve the catalytic performance [94, 95]. Recent catalyst development efforts [97] show that Pd supported on  $La_2O_3$  is an active and selective catalyst for methanol synthesis. The application of rare earths in methanol synthesis is attributed to their ability to influence the surface basicity of the catalyst. Properties such as strength of basic sites, ionic radius and electronegativity have been found to be correlated with the activity or selectivity of the catalyst. More research is needed to better understand the role of rare earths either as supports or promoters.

### 13.5.2 Applications of Rare Earths in Coordination Chemistry

Rare earths react with many organic molecules to form organolanthanide complexes. These complexes are increasingly being incorporated in the design and application of coordinated complexes as catalysts for polymerization and organic synthesis [98]. This has led to the development of more efficient or selective catalysts to produce high added-value stereoregular polymers or copolymers.

Rare earths are also being incorporated into metal organic frameworks (MOFs) because of their coordination chemistry [98]. Rare earth MOFs have been studied for a wide variety of potential applications, including sensing, gas adsorption, chemical separations, catalysis, drug delivery, near-infrared emission, proton conductivity, single molecule magnets and lighting applications [99].

## 13.6 Summary and Outlook

Rare earths are a key component of FCC catalysts, providing stability to the zeolite catalyst structure, as well as affecting the selectivity of the catalyst for specific reactions. The quantity of rare earths influences the behavior of the zeolite active component with regard to its response to the hydrothermal deactivation and contaminant metals. The presence of rare earths influences the rates of hydrogen transfer reactions, which in turn, have an impact on catalyst deactivation by coke formation.

Rare earths also find wide application in the transport industry and they are also used as catalysts for cleaner combustion and air pollution control in car exhausts.

There is also a continuous and growing interest in the application of rare earths in other fields such as methanol synthesis and coordination chemistry where the rare earths are used as supports or promoters. The challenge to fully understand the interaction mechanism between rare earths and other oxides and metals still remains. It is expected that recent developments in the field of nanotechnology, material science, analytical and characterization techniques will provide new opportunities to address this challenge and also lead to more research into new ways of designing and preparing high-performance catalysts.

The wide range of rare earth applications will subsequently lead to an increase in their demand. As the demand for rare earth catalysts continues to grow, the tendency to generate more spent catalysts also increases. The current practice is to send spent catalysts to landfills, which is not sustainable. Therefore, it is important to develop a recycling strategy for spent catalysts as well as recovery techniques for rare earths.

## References

1. T.K. Swift, M.G. Moore, H.R. Rose-Glowacki, E. Sanchez, *The Economic Benefits of the North American Rare Earths Industry* (Rare Earth Technology Alliance, 2014), pp. 1–32
2. T.G. Goonan, *Rare Earth Elements – End Use and Recyclability*, in *Scientific Investigations Report 2011–5094* (U.S. Department of the Interior, U.S. Geological Survey, 2011), pp. 1–22
3. N. Curtis, Rare Earths, We Can Touch Them Every day. Lynas Presentation in JP Morgan Australia Corporate Access Days, 27–28 September 2010 (New York, 2010)
4. B. Jurd, J. Nolde, Lanthanum Oxide Product Stewardship Summary. <https://grace.com/en-us/environment-health-and-safety/ProductStewardship/>
5. Y. Yung, K. Bruno, Low Rare Earth Catalysts for FCC Operations (2012), pp. 1–10. [www.digitalrefining.com/article/1000347](http://www.digitalrefining.com/article/1000347)
6. M. Humphries, Rare earth elements: The global supply chain, in *CRS Report for Congress* (2013, Congressional Research Service), R41347, pp. 1–31
7. E. Alonso, A.M. Sherman, T.J. Wallington, M.P. Everson, F.R. Field, R. Roth, R.E. Kirchain, Evaluating rare earth element availability: A case with revolutionary demand from clean technologies. *Environ. Sci. Technol.* **46**(6), 3406–3414 (2012)
8. G.P. Hatch, Dynamics in the global market for rare earths. *Elements* **8**(5), 341–346 (2012)
9. A. Akah, Application of rare earths in fluid catalytic cracking: A review. *J. Rare Earths* **35**(10), 941–956 (2017)



10. W. Zhan, Y. Guo, X. Gong, Y. Guo, Y. Wang, G. Lu, Current status and perspectives of rare earth catalytic materials and catalysis. *Chin. J. Catal.* **35**(8), 1238–1250 (2014)
11. E. Greinacher, History of rare earth applications, rare earth market today, in *Industrial Applications of Rare Earth Elements*, (American Chemical Society, Washington, DC, 1981), pp. 3–17
12. J.A. Moulijn, M. Makkee, A.E. van Diepen, *Chemical Process Technology* (Wiley, New York, 2013)
13. A. Trovarelli, C. de Leitenburg, M. Boaro, G. Dolcetti, The utilization of ceria in industrial catalysis. *Catal. Today* **50**(2), 353–367 (1999)
14. M.L. Occelli, P. Ritz, The effects of Na ions on the properties of calcined rare earths Y (CREY) zeolites. *Appl. Catal. A Gen.* **183**(1), 53–59 (1999)
15. L.A. Pine, Vanadium-catalyzed destruction of USY zeolites. *J. Catal.* **125**(2), 514–524 (1990)
16. G. de la Puente, E.F. Souza-Aguiar, F.M.A. Zanon Zotin, V.L. Doria Camorim, U. Sedran, Influence of different rare earth ions on hydrogen transfer over Y zeolite. *Appl. Catal. A Gen.* **197**(1), 41–46 (2000)
17. J. Du, Z. Li, Y. Wang, Z. Da, J. Long, M. He, Development of structure stabilized SSY zeolite. *Stud. Surf. Sci. Catal.* **154**, Part C, 2309–2315 (2004)
18. F. Lemos, F. Ramo'a Ribeiro, M. Kern, G. Giannetto, M. Guisnet, Influence of lanthanum content of LaHY catalysts on their physico-chemical and catalytic properties. *Appl. Catal.* **39**, 227–237 (1988)
19. C. Liu, X. Gao, Z. Zhang, H. Zhang, S. Sun, Y. Deng, Surface modification of zeolite Y and mechanism for reducing naphtha olefin formation in catalytic cracking reaction. *Appl. Catal. A Gen.* **264**(2), 225–228 (2004)
20. E.F. Sousa-Aguiar, F.E. Trigueiro, F.M.Z. Zotin, The role of rare earth elements in zeolites and cracking catalysts. *Catal. Today* **218–219**, 115–122 (2013)
21. E.T.C. Vogt, B.M. Weckhuysen, Fluid catalytic cracking: Recent developments on the grand old lady of zeolite catalysis. *Chem. Soc. Rev.* **44**(20), 7342–7370 (2015)
22. D. Wallenstein, K. Schäfer, R.H. Harding, Impact of rare earth concentration and matrix modification in FCC catalysts on their catalytic performance in a wide array of operational parameters. *Appl. Catal. A Gen.* **502**, 27–41 (2015)
23. R. Wormsbecher, W.-C. Cheng, D. Wallenstein, *Role of the Rare Earth Elements in Fluid Catalytic Cracking*, vol 108 (Grace Davison Catalogram, 2010), pp. 19–26
24. S.Q. Yu, H.P. Tian, Y.X. Zhu, Z.Y. Dai, J. Long, Mechanism of rare earth cations on the stability and acidity of Y zeolites. *Wuli Huaxue Xuebao/Acta Phys. – Chim. Sin.* **27**(11), 2528–2534 (2011)
25. T.J. Dougan, U. Alkemade, B. Lakhanpal, L.T. Boock, New vanadium trap proven in commercial trials. *Oil Gas J.* **92**(39), 81–91 (1994)
26. R. Fei, L. Qianqian, Z. Yuxia, Performance of FCC catalyst improved with vanadium trapping components. *China Pet. Process. Petrochem. Technol.* **16**(2), 8–11 (2014)
27. P. Diddams, M. Evans, R. Fletcher, Unconventional Means of Increasing Propylene Yield in Residue Operations. Paper ID: 20100362, in *Petrotech-2010* (New Delhi, 2010)
28. C. Deng, J. Zhang, L. Dong, M. Huang, L. Bin, G. Jin, J. Gao, F. Zhang, M. Fan, L. Zhang, Y. Gong, The effect of positioning cations on acidity and stability of the framework structure of Y zeolite. *Sci. Rep.* **6**, 23382 (2016)
29. S.-J. Yang, Y.-W. Chen, L. Chiuping, The interaction of vanadium and nickel in USY zeolite. *Zeolites* **15**(1), 77–82 (1995)
30. S.-J. Yang, Y.-W. Chen, C. Li, Vanadium-nickel interaction in REY zeolite. *Appl. Catal. A Gen.* **117**(2), 109–123 (1994)
31. S.-J. Yang, Y.-W. Chen, C. Li, Metal-resistant FCC catalysts: Effect of matrix. *Appl. Catal. A Gen.* **115**(1), 59–68 (1994)
32. C. Perego, R. Millini, Porous materials in catalysis: Challenges for mesoporous materials. *Chem. Soc. Rev.* **42**(9), 3956–3976 (2013)

33. A. Akah, M. Al-Ghrami, Maximizing propylene production via FCC technology. *Appl. Petrochem. Res.* **5**(4), 377–392 (2015)
34. S. Kalirai, P.P. Paalanen, J. Wang, F. Meirer, B.M. Weckhuysen, Visualizing dealumination of a single zeolite domain in a real-life catalytic cracking particle. *Angew. Chem. Int. Ed.* **55**(37), 11134–11138 (2016)
35. X. Zhao, T.G. Roberie, ZSM-5 additive in fluid catalytic cracking. 1. Effect of additive level and temperature on light olefins and gasoline olefins. *Ind. Eng. Chem. Res.* **38**(10), 3847–3853 (1999)
36. J.M. Arandes, I. Torre, M.J. Azkoiti, J. Ereña, M. Olazar, J. Bilbao, HZSM-5 zeolite as catalyst additive for residue cracking under FCC conditions. *Energy Fuel* **23**(9), 4215–4223 (2009)
37. J.S. Buchanan, The chemistry of olefins production by ZSM-5 addition to catalytic cracking units. *Catal. Today* **55**(3), 207–212 (2000)
38. T.F. Degan, G.K. Chitnis, P.H. Schipper, History of ZSM-5 fluid catalytic cracking additive development at Mobil. *Microporous Mesoporous Mater.* **35–36**(19), 245–252 (2000)
39. M.A. Abul-Hamayel, A.M. Aitani, M.R. Saeed, Enhancement of propylene production in a downer FCC operation using a ZSM-5 additive. *Chem. Eng. Technol.* **28**(8), 923–929 (2005)
40. A. Akah, M. Al-Ghrami, M. Saeed, M.A.B. Siddiqui, Reactivity of naphtha fractions for light olefins production. *Int. J. Ind. Chem.* **8**(2), 221–233 (2017)
41. J.M. Arandes, I. Abajo, I. Fernández, M.J. Azkoiti, J. Bilbao, Effect of HZSM-5 zeolite addition to a fluid catalytic cracking catalyst. Study in a laboratory reactor operating under industrial conditions. *Ind. Eng. Chem. Res.* **39**(6), 1917–1924 (2000)
42. M.A.B. Siddiqui, A.M. Aitani, M.R. Saeed, N. Al-Yassir, S. Al-Khattaf, Enhancing propylene production from catalytic cracking of Arabian Light VGO over novel zeolites as FCC catalyst additives. *Fuel* **90**(2), 459–466 (2011)
43. L.D. Silverman, W.S. Winkler, J.A. Tiethof, A. Witoshkin, Matrix effects in catalytic cracking, in *NPRA Meeting*, (Engelhard Corporation, Los Angeles, 1986)
44. R. Von Ballmoos, C.-M.T. Hayward, Matrix vs zeolite contributions to the acidity of fluid cracking catalysts. *Stud. Surf. Sci. Catal.* **65**, 171–183 (1991)
45. M.P. Gamero, M.C. Maldonado, M.J.C. Moreno, M.O. Guzman, M.E. Mojica, S.R. Gonzalez, Stability of an FCC catalyst matrix for processing gas oil with resid. *Stud. Surf. Sci. Catal.* **111**, 375–382 (1997)
46. A. Humphries, J.R. Wilcox, Zeolite components and matrix composition determine FCC catalyst performance. *Oil Gas J. (United States)* **87**(6), 45–50 (1989)
47. S. Al-Khattaf, The influence of alumina on the performance of FCC catalysts during hydrotreated VGO catalytic cracking. *Energy Fuel* **17**(1), 62–68 (2002)
48. R.L.V. Mao, N. Al-Yassir, D.T.T. Nguyen, Experimental evidence for the pore continuum in hybrid catalysts used in the selective deep catalytic cracking of n-hexane and petroleum naphthas. *Microporous Mesoporous Mater.* **85**(1–2), 176–182 (2005)
49. H.T. Yan, R.L.V. Mao, Hybrid catalysts used in the catalytic steam cracking process (CSC): Influence of the pore characteristics and the surface acidity properties of the ZSM-5 zeolite-based component on the overall catalytic performance. *Appl. Catal. A Gen.* **375**, 63–69 (2010)
50. A. Claude, Holding the key, in *Hydrocarbon Processing* (Hydrocarbon Engineering, 2008), pp. 1–7. [www.hydrocarbonengineering.com](http://www.hydrocarbonengineering.com)
51. M. Larocca, H. De Lasa, H. Farag, S. Ng, Cracking catalysts deactivation by nickel and vanadium contaminants. *Ind. Eng. Chem. Res.* **29**(11), 2181–2191 (1990)
52. P.F. Schubert, C.A. Altomare, Effects of Ni and V in catalysts on contaminant coke and hydrogen yields. *ACS Symp. Ser.: Fluid Catal. Crack.* **375**(375), 182–194 (1988)
53. O. Bayraktar, E.L. Kugler, Effect of pretreatment on the performance of metal-contaminated fluid catalytic cracking (FCC) catalysts. *Appl. Catal. A Gen.* **260**(1), 119–124 (2004)
54. U.J. Etim, B. Xu, Z. Zhang, Z. Zhong, P. Bai, K. Qiao, Z. Yan, Improved catalytic cracking performance of USY in the presence of metal contaminants by post synthesis modification. *Fuel* **178**, 243–252 (2016)

55. H.J. Jeon, S.K. Park, S.I. Woo, Evaluation of vanadium traps occluded in resid fluidized catalytic cracking (RFCC) catalyst for high gasoline yield. *Appl. Catal. A Gen.* **306**, 1–7 (2006)
56. L.-E. Sandoval-Díaz, J.-M. Martínez-Gil, C.A. Trujillo, The combined effect of sodium and vanadium contamination upon the catalytic performance of USY zeolite in the cracking of n-butane: Evidence of path-dependent behavior in Constable–Cremer plots. *J. Catal.* **294**, 89–98 (2012)
57. M.K. Maholland, Improving FCC Catalyst Performance. *Catalysis* (2006). [www.digitalrefining.com/article/1000302](http://www.digitalrefining.com/article/1000302)
58. C.A. Trujillo, U.N. Uribe, L.A.O. Aguiar, Vanadium Traps for Catalyst for Catalytic Cracking. US Patent 6159887 (2000)
59. W. Huai-Ping, W. Fang-Zhu, W. Wen-Ru, Effect of vanadium poisoning and vanadium passivation on the structure and properties of REHY zeolite and FCC catalyst. *ACS Fuels* **45**, 623–628 (2000)
60. B.A. Feron, P. Gallezot, M. Bourgogne, Hydrothermal aging of cracking catalysts: V. Vanadium passivation by rare earth compounds soluble in the feedstock. *J. Catal.* **134**(2), 469–478 (1992)
61. T. Myrstad, Effect of vanadium on octane numbers in FCC-naphtha. *Appl. Catal. A Gen.* **155**(1), 87–98 (1997)
62. B. Li, S. Li, N. Li, C. Liu, X. Gao, X. Pang, Structure and acidity of REHY zeolite in FCC catalyst. *Chin. J. Catal.* **26**(4), 301–306 (2005)
63. A. Corma, V. Fornes, J.B. Monton, A.V. Orchilles, Structural and cracking properties of REHY zeolites. Activity, selectivity and catalyst-decay optimization for n-heptane cracking. *Ind. Eng. Chem. Prod. Res. Dev.* **25**(2), 231–238 (1986)
64. X. Du, H. Zhang, G. Cao, L. Wang, C. Zhang, X. Gao, Effects of La<sub>2</sub>O<sub>3</sub>, CeO<sub>2</sub> and LaPO<sub>4</sub> introduction on vanadium tolerance of USY zeolites. *Microporous Mesoporous Mater.* **206**, 17–22 (2015)
65. E.L. Kugler, D.P. Leta, Nickel and vanadium on equilibrium cracking catalysts by imaging secondary ion mass spectrometry. *J. Catal.* **109**(2), 387–395 (1988)
66. A. Corma, J.M. López Nieto, Chapter 185, The use of rare-earth-containing zeolite catalysts, in *Handbook on the Physics and Chemistry of Rare Earths*, (Elsevier, San Diego, 2000), pp. 269–313
67. C. Baillie, R. Schiller, Zero and Low Rare Earth FCC Catalysts. PTQ Q4 (2011). [www.digitalrefining.com/article/1000137](http://www.digitalrefining.com/article/1000137)
68. B.D. Graaf, Y. Tang, J. Oberlin, P. Diddams, Shale Crudes and FCC: A Mismatch from Heaven? Processing Shale Feedstocks (2014). [www.digitalrefining.com/article/1000921](http://www.digitalrefining.com/article/1000921)
69. R.E. Roncolato, Y.L. Lam, Effect of vanadium on the deactivation of FCC catalysts. *Braz. J. Chem. Eng.* **15**(2) (1998). <https://doi.org/10.1590/S0104-66321998000200002>
70. X. Du, H. Zhang, X. Gao, Z. He, Z. Li, Effect of nickel and vanadium on structure and catalytic performance of FCC catalyst. *Shiyou Xuebao, Shiyou Jiagong Acta Pet. Sin. (Petroleum Processing Section)* **31**(5), 1063–1068 (2015)
71. X. Du, X. Li, H. Zhang, X. Gao, Kinetics study and analysis of zeolite Y destruction. *Chin. J. Catal.* **37**(2), 316–323 (2016)
72. H.S. Cerqueira, G. Caeiro, L. Costa, F. Ramôa Ribeiro, Deactivation of FCC catalysts. *J. Mol. Catal. A Chem.* **292**(1–2), 1–13 (2008)
73. F. Maugé, P. Gallezot, J.-C. Courcelle, P. Engelhard, J. Grosmangin, Hydrothermal aging of cracking catalysts. II. Effect of steam and sodium on the structure of LaHY zeolites. *Zeolites* **6**(4), 261–266 (1986)
74. F. Lemos, F.R. Ribeiro, M. Kern, G. Giannetto, M. Guisnet, Influence of the cerium content of CeHY catalysts on their physicochemical and catalytic properties. *Appl. Catal.* **29**(1), 43–54 (1987)
75. O. Topete, C. Baillie, R. Schiller, Optimizing FCC operations in a high rare-earth cost world: Commercial: Update on Grace Davison's low and zero rare-earth fcc catalysts, in *Grace Davison Catalogram*, pp. 2–12
76. S. Ismail, Fluid catalytic cracking (FCC) catalyst optimization to cope with high rare earth oxide price environment, in *BASF Technical Note* (BASF, 2011). [www.catalysts.basf.com/refining](http://www.catalysts.basf.com/refining)

77. J. Scherzer, Octane-enhancing, zeolitic FCC catalysts: Scientific and technical aspects. *Catal. Rev.* **31**(3), 215–354 (1989)
78. N. Rahimi, R. Karimzadeh, Catalytic cracking of hydrocarbons over modified ZSM-5 zeolites to produce light olefins: A review. *Appl. Catal. A Gen.* **398**, 1–17 (2011)
79. F. Ding, S.H. Ng, C. Xu, S. Yui, Reduction of light cycle oil in catalytic cracking of bitumen-derived crude HGOs through catalyst selection. *Fuel Process. Technol.* **88**(9), 833–845 (2007)
80. I. Shimada, K. Takizawa, H. Fukunaga, N. Takahashi, T. Takatsuka, Catalytic cracking of polycyclic aromatic hydrocarbons with hydrogen transfer reaction. *Fuel* **161**, 207–214 (2015)
81. X. Gao, Z. Qin, B. Wang, X. Zhao, J. Li, H. Zhao, H. Liu, B. Shen, High silica REHY zeolite with low rare earth loading as high-performance catalyst for heavy oil conversion. *Appl. Catal. A Gen.* **413–414**, 254–260 (2012)
82. M. Hunger, G. Engelhardt, J. Weitkamp, Solid-state  $^{23}\text{Na}$ ,  $^{139}\text{La}$ ,  $^{27}\text{Al}$  and  $^{29}\text{Si}$  nuclear magnetic resonance spectroscopic investigations of cation location and migration in zeolites  $\text{LaNaY}$ . *Microporous Mater.* **3**(4), 497–510 (1995)
83. F.E. Trigueiro, D.F.J. Monteiro, F.M.Z. Zotin, E. Falabella Sousa-Aguiar, Thermal stability of Y zeolites containing different rare earth cations. *J. Alloys Compd.* **344**(1–2), 337–341 (2002)
84. BASF, Effects of Rare Earth Oxides in FCC Catalysts, in *Catalyst Reports: Section 4 – The Effects of FCC Catalyst Characteristics on FCC Yields and Product Properties*. <http://www.refiningonline.com/engelhardkb/>. BASF Catalysts
85. L. Zhang, Q. Li, Y. Qin, X. Zhang, X. Gao, L. Song, Investigation on the mechanism of adsorption and desorption behavior in cerium ions modified Y-type zeolite and improved hydrocarbons conversion. *J. Rare Earths* **34**(12), 1221–1227 (2016)
86. L. Borowsky, Sourcing rare earths and critical minerals, in *Mines Magazine* (2011). <https://minesmagazine.com/1737/>
87. E. Alonso, T. Wallington, A. Sherman, M. Everson, F. Field, R. Roth, R. Kirchain, An assessment of the rare earth element content of conventional and electric vehicles. *SAE Int. J. Mater. Manuf.* **5**, 473 (2012)
88. IEA, *Global EV Outlook 2020* (IEA, Paris, 2020). <https://www.iea.org/reports/global-ev-outlook-2020>
89. P. Fears, Rare Earth Magnets in Electric Vehicle Motors (2021). <https://www.buntingeurope.com/rare-earth-magnets-in-electric-vehicle-motors/>
90. E. Sokolc, 6 Ways How to Quiet a Rattling Catalytic Converter (2022). <https://betersoundproofing.com/how-to-quiet-a-rattling-catalytic-converter/>
91. S. Colussi, C. de Leitenburg, G. Dolcetti, A. Trovarelli, The role of rare earth oxides as promoters and stabilizers in combustion catalysts. *J. Alloys Compd.* **374**(1), 387–392 (2004)
92. S. Rood, S. Eslava, A. Manigrasso, C. Bannister, Recent advances in gasoline three-way catalyst formulation: A review. *Proc. Inst. Mech. Eng. D: J. Automob. Eng.* **234**(4), 936–949 (2020)
93. M.V. Twigg, Catalytic control of emissions from cars. *Catal. Today* **163**(1), 33–41 (2011)
94. F. Ausfelder, C. Beilmann, M. Bertau, S. Bräuninger, A. Heinzl, R. Hoer, W. Koch, F. Mahlendorf, A. Metzethin, M. Peuckert, L. Plass, K. Räuchle, M. Reuter, G. Schaub, S. Schiebahn, E. Schwab, F. Schüth, D. Stolten, G. Teßmer, K. Wagemann, K.-F. Ziegahn, Energy storage as part of a secure energy supply. *ChemBioEng Rev.* **4**(3), 144–210 (2017)
95. D. Sheldon, Methanol production; a technical history. *Johnson Matthey Technol. Rev.* **61**(3), 172–182 (2017)
96. G. Bozzano, F. Manenti, Efficient methanol synthesis: Perspectives, technologies and optimization strategies. *Prog. Energy Combust. Sci.* **56**, 71–105 (2016)
97. A. Mittasch, M. Pier, K. Winkler, BASF AG, ‘Ausführung Organischer Katalysen’, German Patent 415,686 (1925)
98. I. Cota, Developments in the use of rare earth metal complexes as efficient catalysts for ring-opening polymerization of cyclic esters used in biomedical applications. *Phys. Sci. Rev.* **2**(4), 1–24 (2017)
99. F. Saraci, V. Quezada-Novoa, P.R. Donnarumma, A.J. Howarth, Rare-earth metal–organic frameworks: From structure to applications. *Chem. Soc. Rev.* **49**(22), 7949–7977 (2020)

# Chapter 14

## High-Performance Aluminum Castings Containing Rare Earth Elements



David Weiss

### 14.1 Introduction

Auto manufacturers are under commercial and regulatory pressure to improve engine efficiency. Potential solutions include direct fuel injection, higher compression ratios and turbochargers. All these solutions can lead to higher component and/or system-operating temperatures and pressures. Al-Si-Mg or Al-Si-Cu-Mg alloys that are typically solution-treated and aged are used for automotive products because of their good mechanical properties at room temperature and ease of processing [1]. However, these alloys rapidly lose strength above their aging temperature which is around 155 °C. For engines to be able to operate between 180 °C and 300 °C, a different paradigm for alloy design is needed. The need for temperature tolerant alloys does not go away with the clean energy transition. Hydrogen (H<sub>2</sub>) internal combustion engines, for example, are low-emission alternatives in the trucking industry that operate at exhaust gas temperatures of between 300 and 600 °C [2].

Several strategies have been employed to improve the performance characteristics of Al alloys. The addition of copper (Cu) generally improves both room temperature and high-temperature strength. There can be an impact on corrosion because of a greater change in electrode potential with variations in amount of Cu in solid solution and the presence of non-uniformities in solid solution concentration [3]. The addition of transition metals such as zirconium (Zr), manganese (Mn) and vanadium (V) is being used to stabilize the precipitates in alloys of the Al-Cu-Mg and Al-Si-Mg system [4, 5]. Although many types of metal matrix composites have been developed that will generally improve modulus, yield strength and elevated temperature properties, the composites are generally less ductile and are more difficult to process [6].

---

D. Weiss (✉)  
Eck Industries, Inc., Manitowoc, WI, USA  
e-mail: [David.Weiss@eckindustries.com](mailto:David.Weiss@eckindustries.com)

Turning to rare earths, the addition of Ce has been shown to improve the performance characteristics of both solid solution-strengthened and precipitation-strengthened Al alloys, particularly at elevated temperatures. The use of large volumes of Ce in Al castings can be viewed possibly as a means to improve the rare earth supply balance and potentially the overall production process economics by effectively utilizing one of the most abundant oxides present in most rare earth deposits.

## 14.2 Background and History

The oxides of rare earth elements with limited use such as Ce and lanthanum (La) are the predominant oxides found globally during mining operations. Often, these by-products are regarded as waste and are discarded. Repurposing these waste products into useful products adds value and reduces the cost and ecological impact of rare earth mining. Using Ce and La in high volume applications could stabilize demand and increase the profitability of extraction of the heavy rare earths [7, 8].

Mondolfo [9] reviewed the Al-Ce and the Al-Ce-Fe systems and reported that small additions of Ce do not produce appreciable improvements in mechanical properties and that the alloys did not have a wide application. He reported that a eutectic is formed with 13 wt% Ce at 638 °C. In a later work, Mondolfo [10] reported that an increase of strength without loss of conductivity and improved machinability occurred for Ce additions to Al alloys. He referenced sources that claimed an Al-CeAl<sub>4</sub> eutectic formed at approximately 12 wt% Ce.

An analysis of the Al-Ce-Fe system produced via powder metallurgy showed extraordinary strengths in an Al-8Fe-4Ce alloy at temperatures up to 343 °C [11]. There was, however, no documented attempt to cast these materials.

There has been some experimental work conducted to use Ce as an alloying element in cast Al alloys. Shikun [12, 13] reviewed the effect of Ce additions on the cast microstructure and solidification range of an Al-4.5Cu alloy. He concluded that the addition of Ce improved castability but the mechanical properties were not studied. Belov [14] explored Ce for the development of creep-resistant Al alloys in combination with transition metals such as Zr, Mn, chromium (Cr), iron (Fe) and nickel (Ni). Later Belov [15] focused on the Al-Ce-Ni system. He concluded that alloys of the Al-Ce-Ni ternary eutectic system had high mechanical properties at room and elevated temperatures along with good casting characteristics.

Al-Si alloys are the most important Al-based foundry alloys. They have good mechanical properties, narrow solidification ranges and good fluidity. Gröbner [16] considered Al alloys containing up to 25 at.% Ce and 45 at.% Si and studied several Al-Ce-Si systems where Al was held at a constant 90 at.% with the concentrations of Ce and Si being varied between 0% and 10%. He showed that small Ce additions could provide high-temperature stable AlCeSi phases in equilibrium with Al-Si-rich melt. He concluded that Ce between 1% and 5 at.% could be used as a grain refiner.

In a recent comprehensive review of the Al-Ce system, Czerwinski [17] suggested that high amounts of Ce along with transition metals can contribute to the formation of amorphous structures.

The development of Al-Ce casting alloys is driven by the increasing demands for high-temperature-tolerant Al alloys and the use for the excess Ce that was available as a by-product of the production of the higher atomic number rare earths.

### 14.3 Metallurgical Aspects of the Al-Ce System

The equilibrium diagram, Ce-Al crystal structure data and Ce-Al lattice parameter data were reviewed in 1988 [18] and a eutectic composition of Al and  $\text{Al}_{11}\text{Ce}_3$  was shown at 4 at.% Ce at 640 °C. This reference confirms the Al-rich compound had previously been incorrectly identified as Al-CeAl<sub>4</sub>. Recently calculated ThermoCalc data predicted a eutectic of  $\text{Al}_{11}\text{Ce}_3$  at 580 °C at 10 wt % (2.09 at.%) [19].

Typical microstructures of the Al-Ce binary composition are shown in Fig. 14.1 [20]. The as-cast microstructures show a very fine interconnected  $\text{Al}_{11}\text{Ce}_3$  eutectic microstructure in a pure Al phase. The intermetallic can be as small as 50 nm wide at permanent mold cooling rates of 4–5 °C/s. These structures are stable up to the melting point of the Al phase. The intermetallics cannot dissolve since Ce has extremely low solubility in the Al matrix. A solubility diagram for the binary Al-Ce system is shown in Fig. 14.2. Yield strength retention is about three times conventional alloys when tested at 300 °C. When Ce is used with solid solution-strengthening elements such as Mg or zinc (Zn), room temperature properties remain stable regardless of exposure times with exposure temperatures up to 400 °C. The data in Fig. 14.3 show an actual increase in room temperature properties after exposure at 400 °C. This is due to the homogenization of the Mg that is not uniformly distributed because of low and variable cooling rates in the cast structure. In solid solution-strengthened alloys, there are no phases that dissolve or coarsen such as the  $\text{Mg}_2\text{Si}$  in 300 series alloys or the  $\text{Al}_2\text{Cu}$  in 200 series alloys.

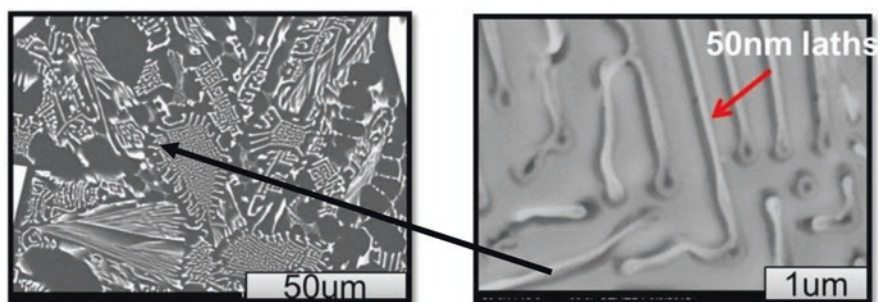
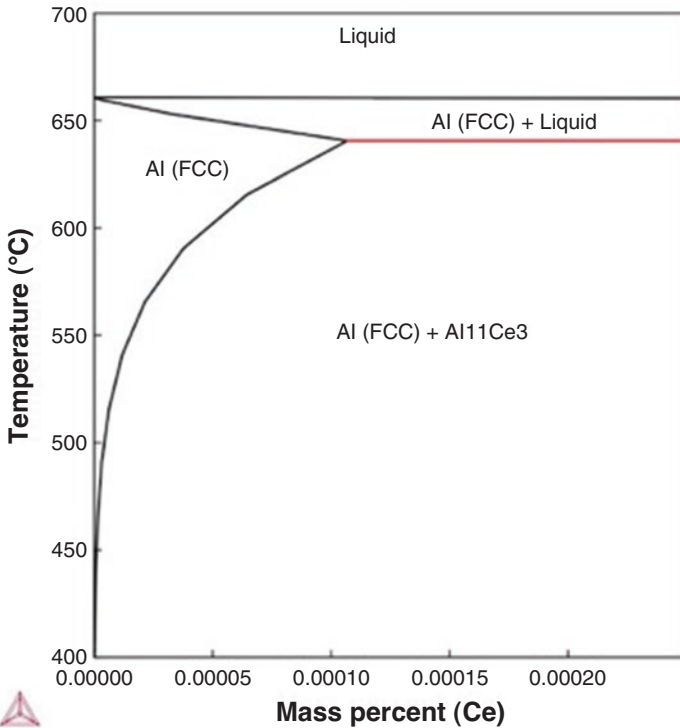


Fig. 14.1 As cast microstructure of Al-Ce binary alloy. (The phase shown is  $\text{Al}_{11}\text{Ce}_3$  phase)



**Fig. 14.2** Cerium solubility in aluminum

Load-partitioning studies in compression conducted by Oak Ridge National Laboratory at their Vulcan Beam Line show unusual load-sharing behavior between the matrix and the Al<sub>11</sub>Ce<sub>3</sub> intermetallic. As illustrated in Fig. 14.4, as the compressive stress increases, a higher proportion of that stress is transferred to the intermetallic. Weiss [20] provides an extensive analysis of the strengthening mechanisms and microstructural analysis of the Al-Ce system.

## 14.4 Alloying Element Interactions

At room temperature, the Al<sub>11</sub>Ce<sub>3</sub> intermetallic is not an effective strengthening mechanism. Mechanical properties for pure binary compositions are shown in Table 14.1 [20]. To develop reasonable room temperature strengths, alloying elements such as Mg, Zn, Cu, Si or others can be added along with Ce to strengthen the aluminum matrix. Sun [21] reported on a comprehensive study of 19 binary systems



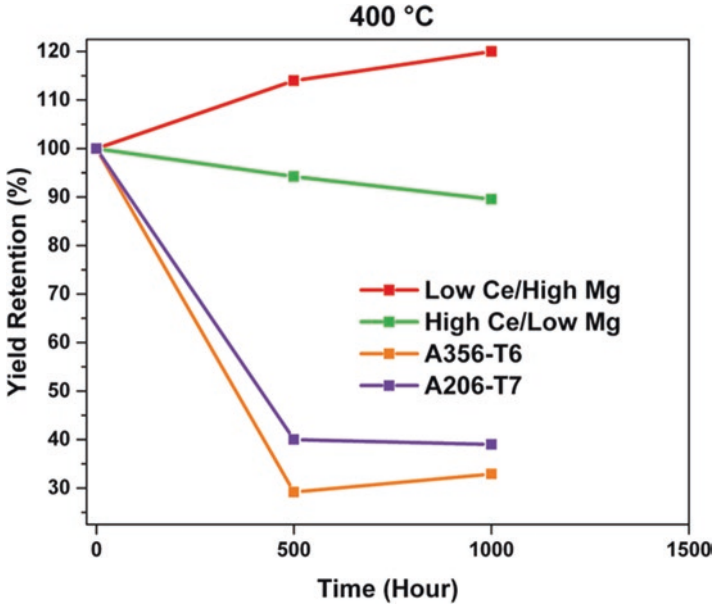


Fig. 14.3 Yield strength retention after long-term exposure of Al-Ce alloys measured at room temperature compared to some standard casting alloys

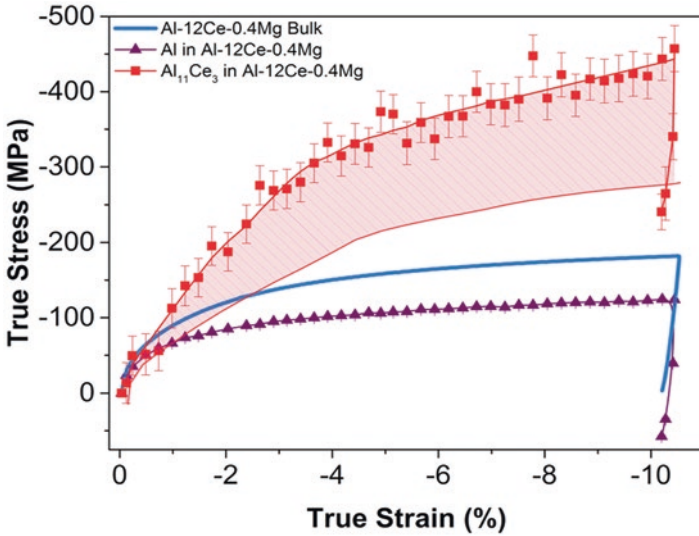


Fig. 14.4 Phase load sharing for Al-12Ce-0.4 Mg under compressive load. Shaded region denotes differences between binary and ternary alloy composition’s mechanical response [19]

**Table 14.1** Mechanical properties of Al-Ce binary alloys [20]

	Tensile strength, MPa	Yield, MPa	Elongation, %
Al-16Ce	144	68	2.5
Al-12Ce	163	58	13.5
Al-10Ce	152	50	8
Al-8Ce	148	40	19
Al-6Ce	103	30	25

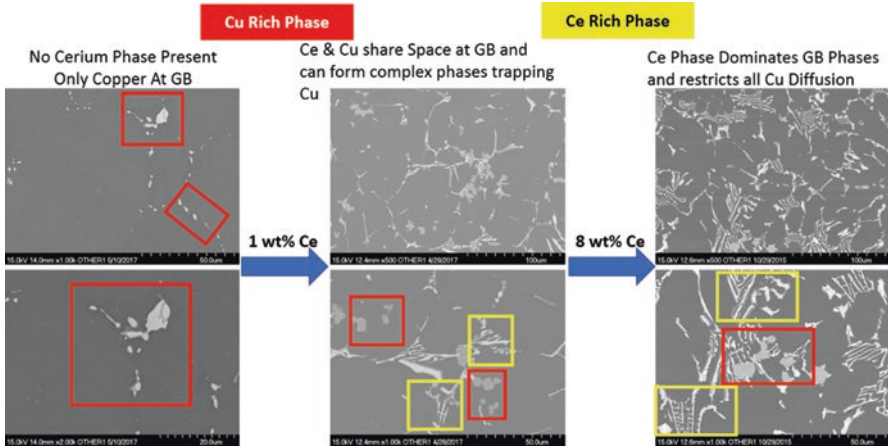
of Ce and 4d or 5d transition metals using high-throughput first principles calculations. He showed that many common alloying elements used in Al systems, such as Fe, Ni, Cu and Zn will form compounds with Ce, while others, such as Zr would not. Subsequent experimentation demonstrated that his theoretical conclusions were correct with one exception. While Sun showed no compounds would form with titanium (Ti,) experimentally a detrimental Ce-Ti intermetallic forms that significantly reduces ductility when Ti levels are above 0.05%.

Understanding the reaction mechanics between Ce and other alloying elements can be used to identify elements that could independently strengthen the Al matrix without interference from the Ce, as well as those that form compounds with Ce that can synergistically increase the strength or potentially immobilize elements required for strengthening during heat treatment.

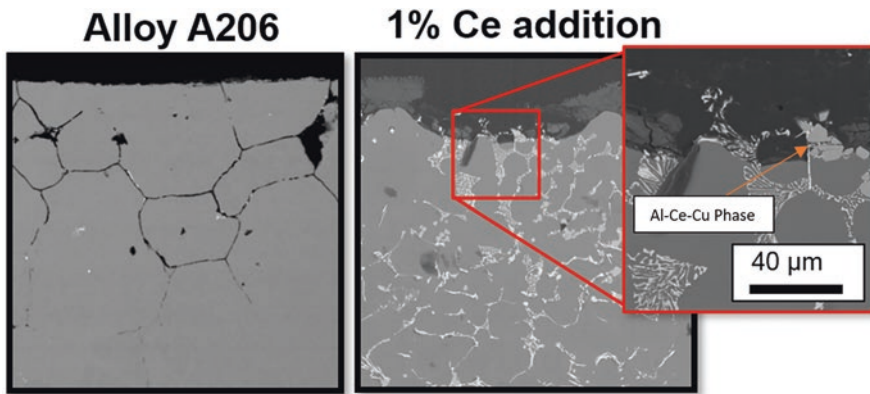
In commercially pure Al, Mg in solid solution gives a near-linear concentration dependence of strength at a given strain. Solid solution hardening is a result of an interaction between the mobile dislocations and the solute atoms [22]. In an Al-8Ce alloy, the addition of 10% Mg increases the yield strength by over 300% from about 50 MPa to about 162 MPa. There is no evidence that the formation of some CeMg intermetallic is a significant factor in the strength increase, as the primary mechanism for matrix strengthening is the inclusion of Mg.

The addition of Cu to the alloy forms immobile Cu-Ce phases. This is illustrated in Fig. 14.5 using a 4.5 wt% Cu alloy with the addition of 1 and 8 wt% Ce. Most of the Cu is not free to strengthen the alloy since it is tied up with the Ce phase. On the other hand, modification of the traditional grain boundary phases improves the hot tear resistance of the alloy and reduces intergranular corrosion. Additional Cu needs to be added to create “free Cu” that can participate in the heat treat response. As shown in Fig. 14.6, for Cu-containing alloys such as A206, Ce acts as a diffusion barrier preventing the formation of Cu-depleted zones. In all alloys tested, the addition of small amounts of Ce increases their resistance to intergranular corrosion (Fig. 14.7).

The addition of scandium (Sc) to Al-Ce alloys has been investigated [23]. At levels of 0.4% Sc, room temperature hardness levels increased by 20%, and room temperature hardness values after 300 °C exposure for 100 h increased by 60%. While the ternary Al-Ce-Sc system had good thermal stability, the room temperature hardness values are not sufficient for structural castings. The addition of Mg at levels of up to 12.15% resulted in significant improvement in hardness at room and elevated temperatures. Ekaputra [24] investigated Al-Ce alloys modified with Sc, Zr



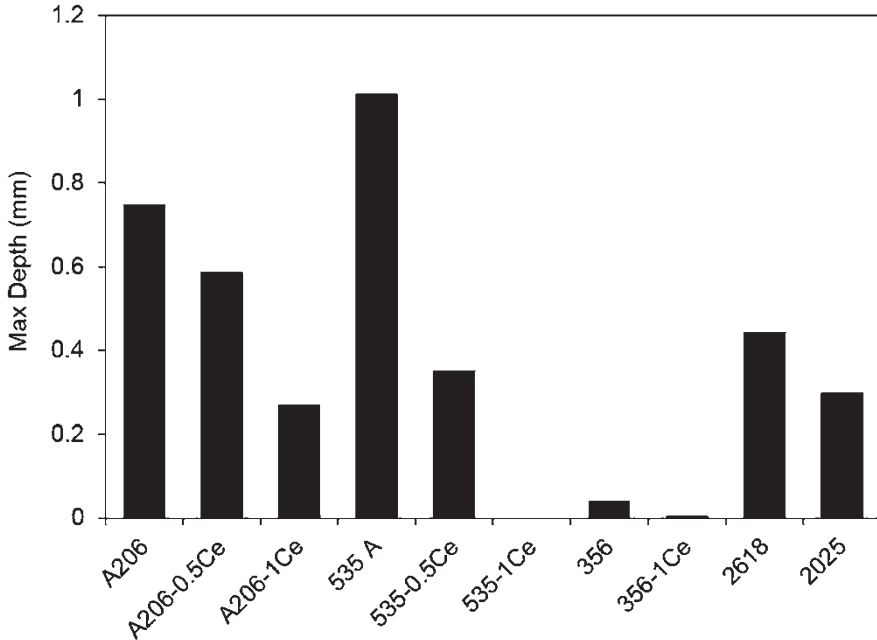
**Fig. 14.5** Increasing cerium addition precipitates immobile Al-Ce and Ce-Cu phases at the grain boundary (GB)



**Fig. 14.6** The addition of Ce to Al-Cu alloys creates an Al-Ce-Cu phase that acts as a diffusion barrier

and erbium (Er) micro-additions. He showed that peak hardness is higher for alloys containing Ce and  $L1_2$   $Al_3(Sc,Ze,Er)$  precipitates than their Ce-free counterparts.

Silicon as an alloying element in Al reduces its coefficient of thermal expansion [25]. While increasing the Si in a binary composition with Al will reduce the solidification range up to the eutectic composition, the addition of Ce will increase that range which may make the alloy more difficult to feed in traditional casting applications. The solidification range of a standard Al7Si alloy is approximately 70 °C. Using thermal analysis, it was experimentally determined that as the ratio of Ce to Si in an alloy increases, the solidification range increases as well. At a Ce/Si ratio of 3.16, the solidification range increases to 120 °C. At a Ce/Si ratio of 0.46,

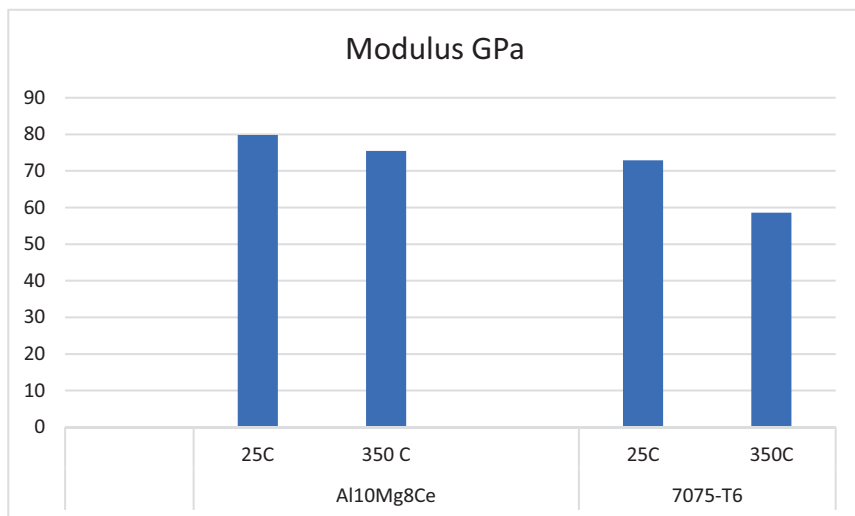


**Fig. 14.7** ASTM G110-92 intergranular attack [20] (Test coupons were submerged in hydrogen peroxide ( $H_2O_2$ ) with sodium chloride (NaCl))

the solidification range is reduced to 82 °C. Generally, maintaining a Ce/Si ratio of about 0.5 results in an alloy with excellent castability. Cerium will also form CeSi phases making some of the Si unavailable for combining with Mg when added to form  $Mg_2Si$ -strengthening precipitates. However, Si-rich alloys contain enough excess Si so that the response to heat treatment is not affected.

## 14.5 Composite Potential in Al-Ce Alloys

In conventional hard particle-reinforced Al alloys, failure at elevated temperature can occur when the matrix softens and causes interfacial decohesion and void growth at the particle/matrix interface and particle corners [26]. Secondly, Al loses stiffness at high temperature, minimizing the modulus improvement attempted by the introduction of high modulus particles. Alloys containing Ce retain a higher percentage of their modulus at elevated temperatures. Figure 14.8 shows the modulus retention of an as-fabricated Al10Mg8Ce-F alloy compared with 7075-T6 (Al/5.6–6.1% Zn, 2.1–2.5% Mg, 1.2–1.6% Cu with less than 0.5% Si, Fe, Mn, Ti, Cr and other metals).



**Fig. 14.8** Comparison of room temperature and 350 °C moduli for Al10Mg8Ce-F and 7075-T6

Preliminary work has been completed using silicon carbide (SiC) and carbon (C) nanotubes as reinforcement in AlCe and AlCeSi alloys as well as alumina ( $\text{Al}_2\text{O}_3$ ) in AlCeMg alloys. The addition of 50 nm  $\text{Al}_2\text{O}_3$  at reinforcement levels of about 0.1% results in a tensile strength improvement of 12%. The results are promising but require more data and functional testing to fully understand the use of Al-Ce alloys as a composite matrix material.

## 14.6 Product Forms

### 14.6.1 Castings

Much of the early work in the Al-Ce system concentrated on casting alloys. The casting characteristics of the binary Al-Ce systems is as good as the Al-Si system but can change as additional alloying elements are added [27]. When other alloying elements are used such as Si, Mg or Cu, the solidification range is determined primarily by the secondary alloying elements. Standard systems for melting, degassing and alloy cleaning of cast alloys can be used without modification for the conventional casting of Al-Ce alloys.

At solidification rates typical of castings in Ce alloys that contain more than 7% Mg, a homogenization heat treat can be used to improve mechanical properties [28]. This treatment reduces the size and volume fraction of Mg pools that can segregate in high Mg alloys. The amount of Ce does not affect the segregation behavior. The alloys have been cast successfully in most traditional casting processes, such as



**Fig. 14.9** Air-cooled cylinder head poured from Al-Ce binary alloy

sand, permanent mold, low-pressure permanent mold and die casting. Figure 14.9 shows a cylinder head poured as a gravity casting showing the good fluidity of the alloy system.

Mechanical properties for the ternary Al-Ce-Mg system have been studied at both room and elevated temperatures (Table 14.2). The room temperature properties can be improved by both homogenization and hot isostatic pressing. One of the key attributes in the Al-Ce-Mg system is the recovery of mechanical properties at room temperature when exposed to elevated temperatures for prolonged periods of time. This alloy system does not contain any precipitates that become unstable after prolonged high-temperature exposure.

### 14.6.2 Extrusions

Extrusions have been produced for applications where improved high-temperature performance or resistance to corrosion is desired. In these alloys, extrusion improves the properties through a combination of work hardening and alignment of the inter-metallic. Extrusions have been produced at 300 °C billet temperatures and at extrusion ratios of 5.75 to 1 and 52 to 1 from an Al10Mg8Ce alloy. A comparison of average permanent mold properties to extruded properties is shown in Table 14.3. As the extrusion ratio increases, tensile strength remains constant, with the elongation increasing and yield strength decreasing. The mechanical properties can be affected by the starting microstructure of the billet. Structural extrusions have also been produced as shown in Fig. 14.10.

**Table 14.2** Room and elevated temperature properties of Al-10 Mg-8Ce compared to common piston alloys

Alloy	Temperature	Time hours	At temperature			At room temperature After heating		
			Tensile, MPa	Yield, MPa	% E	Tensile, MPa	Yield, MPa	% E
<b>Al-10Mg-8Ce</b>	260 °C	0.5	137	131	4			
	260 °C	336	137	97	5	159	137	1
	315 °C	0.5	97	55	20			
	315 °C	216	94	56	13.8	172	159	1
	400 °C	120				218	191	1.5
	500 °C	500				252	185	3
<b>2618-T61</b>	260 °C	0.5	90	62	50			
	315 °C	0.5	52	31	80			
<b>4032-T6</b>	200 °C	0.5	90	62	30			
	300 °C	0.5	38	24	70			
<b>Baseline room temperature properties of Al-10 Mg-8Ce</b>					As cast	228	186	1
					T4	248	200	2
					HIP	262	207	2
		Typical	2618-T61		Forged	440	370	10
		Typical	4032-T6		Forged	380	315	9

All Al-Ce properties as cast unless otherwise noted

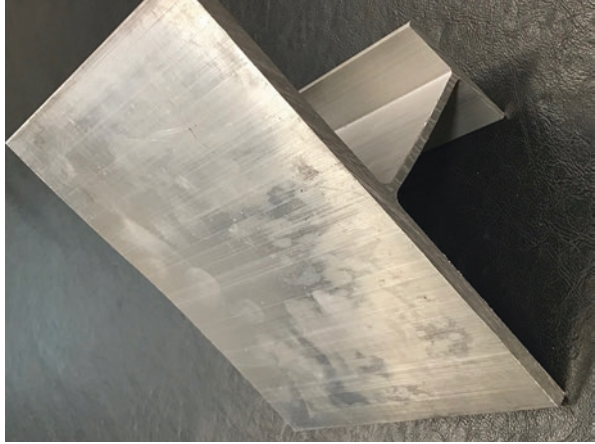
**Table 14.3** Comparison of extruded data at different extrusion ratios for cast Al10Mg8Ce

	Tensile, MPa	Yield, MPa	% E
Extrusion 5:1	375	342	6
Extrusion 52:1	364	274	12
Permanent mold	228	186	1

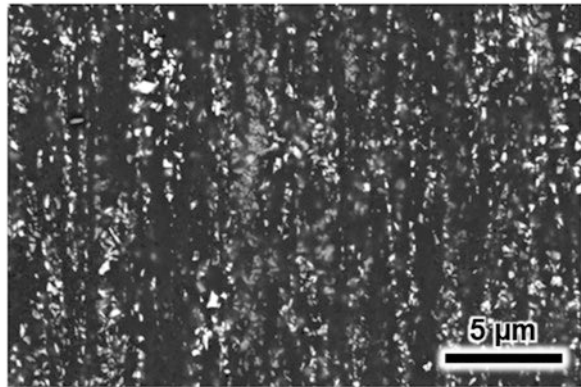
### 14.6.3 Additive Manufacturing

The Al-Ce alloy system has been used for both the direct write and powder bed fusion. Manca [29] has reported high mechanical properties of Al-3Ce-7Cu in both high-temperature tension and compression testing via selective laser melting. Fine eutectic phases of  $\text{Al}_{11}\text{Ce}_3$  and  $\text{Al}_{6.5}\text{CeCu}_{6.5}$  were found in the microstructure. High hardness values were noted after annealing at 400 °C due to the precipitation of nanosized particles. Hyer [30] demonstrated yield strength and tensile strength of 377 and 468 MPa, respectively, in a ternary Al-8wt%Ce-10 wt% Mg composition produced in laser powder bed fusion with a power of 200 W traversing at 800 mm/s. Kessler [31] in a wire-based additive technique, used induction heated Al-Ce binary alloy wire to take advantage of the inherent rheology of molten Al-Ce and the high enthalpy of fusion for the reactive Ce-containing intermetallic. This intermetallic phase enhances the surface energy and stabilizes the extruded filament, imparting shape stability and facilitating layer to layer joining.

**Fig. 14.10** Structural extrusion produced for the marine industry



**Fig. 14.11** Extruded powder microstructures



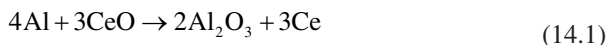
#### **14.6.4 Consolidated Powders**

The size range of powders for additive manufacturing in Al alloys is typically between 20 and 60 microns. The yield of good powders can be anywhere between 40% and 80%, leaving a substantial amount of powder as waste that is discarded or recycled. The coarse and fine powders can be consolidated via forging or extrusion. In extrusion, the intermetallic is broken up into fine particles on the length scale of the lath thickness, as shown in Fig. 14.11. In work done with the Al10Mg8Ce alloys, ultimate tensile strengths exceeding 600 MPa were achieved using mixed coarse and fine particles.



## 14.7 Economics of Al-Ce Alloys

As an alloying element used typically in the 1–10% weight range, Ce is relatively inexpensive. Its cost is in the range of \$4–5/lb and is widely available. Similarly, the as-alloyed cost of Al-Ce material is competitive with other high-performance Al alloy systems. Further cost reduction in Ce is enabled by direct metallothermic reduction of CeO<sub>2</sub>. Luna et al. [32] directly reduced the oxide on a laboratory scale in Al alloys containing between 0.5 and 4.0 wt% Mg. Current development work by the author has shown the successful reduction of both CeO<sub>2</sub> and cerium carbonate (Ce<sub>2</sub>CO<sub>3</sub>) in batch sizes of 200 kg. The reduction reaction for the oxide is given as



The produced aluminum oxide (Al<sub>2</sub>O<sub>3</sub>) is removed during standard degassing or through filtering down to a size range of approximately 1–5 micron. This remaining oxide serves to dispersion strengthen the alloy. Improvements of 8% in tensile strength and 20% in yield strength versus the alloy produced conventionally with Ce metal have been demonstrated.

## 14.8 Conclusions

Aluminum-cerium alloys are being rapidly developed as alternatives to Al-Si and Al-Cu alloys. These alloys have good fabrication characteristics and excellent corrosion performance. The alloys have superior performance at elevated temperatures and long exposure times. The use of the least expensive of the rare earth elements and standard processing methods make the transition to use of Al-Ce alloys available for lightweight, high-performance applications in the automotive, trucking, aerospace and other industrial sectors.

## References

1. A. Tanwir, A.H. Ansari, Review on aluminium and its alloys for automotive applications. *Int. J. Adv. Technol. Eng. Sci* **5**, 278–294 (2017)
2. S. Sterlepper, M. Fischer, J. Claßen, V. Huth, S. Pischinger, Concepts for hydrogen internal combustion engines and their implications on the exhaust gas after-treatment system. *Energies* **14**(23), 8166 (2021). <https://doi.org/10.3390/en14238166>
3. Prepared under the direction of the ASM Handbook Committee; William H. Clobberly, Director of Reference Publications. *Metals Handbook* 9th, vol 13 (ASM International, 1987) p. 585
4. V. Zakharov, About alloying of Aluminum alloys with transition metals. *Metal Sci. Heat Treat.* **59**(8), 1–5 (2017)

5. V. Zakharov, T.D. Rostova, Effect of scandium, transition metals, and admixtures on strengthening of Aluminum alloys due to decomposition of the solid solution. *Metal Sci. Heat Treat.* **49**(9), 435–442 (2007)
6. S. Priyaranjan, P.R. Vundavilli, A. Meher, M.M. Mahapatra, Recent Progress in Aluminum metal matrix composites: A review on processing, mechanical and Wear properties. *J. Manuf. Process.* **59**, 131–152 (2020)
7. Z.C. Sims, M.S. Kesler, H.B. Henderson, A. Castillo, T. Fishman, P. Singleton, S. McCall, O. Rios, How cerium and lanthanum as coproducts promote stable rare earth production and new alloys. *J. Sustain. Metall.* **8**, 1225–1234 (2022). <https://doi.org/10.1007/s40831-022-00562-4>
8. R.T. Nguyen, D.D. Imholte, *JOM* **68**, 1948 (2016)
9. L.F. Mondolfo, *Metallography of Aluminum Alloys* (Wiley, 1943)
10. L.F. Mondolfo, *Aluminum Alloys: Structure and Properties* (Butterworths & Co Ltd, 1976)
11. W.M. Griffith, R.E. Sanders, G.J. Hildeman, *Elevated Temperature Aluminum Alloys for Aerospace Applications. High-Strength Powder Metallurgy Aluminum Alloys*, Proceedings of a symposium sponsored by the Powder Metallurgy Committee of the Metallurgical Society of AIME, February 17–18, 1982
12. X. Shikun, Y. Rongxi, G. Zhi, X. Xiang, H. Chagen, G. Xiuyan, Effects of rare earth Ce on casting properties of Al-4.5Cu alloy. *Adv. Mater. Res.* **136**, 1–4 (2010)
13. X. Shikun, A. Yongping, G. Zhi, X. Xiang, Y. Rongxi, G. Zhi, G. Xiuyan, Effects of Ce addition on the mobility and hot tearing tendency of Al-4.5Cu alloy. *Adv. Mater. Res.* **146–147**, 481–484 (2010)
14. N.A. Belov, Principles of optimizing the structure of creep-resisting casting Aluminum alloys using transition metals. *J. Adv. Mater.* **1**(4), 321–329 (1994)
15. N.A. Belov, E.A. Naumova, D.G. Eskin, Casting alloys of the Al–Ce–Ni system: A microstructural approach to alloy design. *Mater. Sci. Eng. A* **271**(1), 134–142 (1999)
16. J. Gröbner, D. Mirkovic, R. Schmid-Fetzer, Thermodynamic aspects of the constitution, grain refining, and solidification enthalpies of Al-Ce-Si alloys. *Metall. Mater. Trans. A* **35A**, 3349 (2004)
17. F. Czerwinski, Cerium in Aluminum Alloys. *J. Mater. Sci.* **56**(12). <https://doi.org/10.1007/s10853-019-03892-z>
18. K. Gschneidner, F.W. Calderwood, The Al-Ce (Aluminum-Cerium) system. *Bull. Alloy Phase Diagr.* **9**(6), 699–672 (1988)
19. Z. Sims, O. Rios, D. Weiss, P. Turchi, A. Perron, J. Lee, T. Li, J. Hammons, M. Bagger-Hansen, T. Willey, K. An, Y. Chen, A. King, S. McCall, High performance Aluminum-cerium alloys for high-temperature applications. *Mater. Horiz.* **4**, 1070 (2017)
20. D. Weiss, Improved high-temperature Aluminum alloys containing cerium. *J. Mater. Eng. Perform.* **28**, 1903–1908 (2019)
21. X. Sun, Y. Lei, R. Zhou, B. Zhang, Novel compounds of cerium binary alloys from high-throughput first-principles calculations. *J. Appl. Phys.* **123**, 235102 (2018)
22. Ø. Ryen, B. Holmedal, O. Nijs, E. Nes, E. Sjölander, H. Ekström, Strengthening mechanisms in solid solution Aluminum alloys. *Metall. Mater. Trans. A* **37A**, 1999–2006 (2006)
23. D. Weiss, Developments in Aluminum-scandium ceramic and Aluminum-scandium cerium alloys, in *Light Metals*, ed. by C. Chesonis, (The Minerals, Metals & Materials Society, 2019)
24. C. Eputra, J. Rakhmonov, D. Weiss, J. Mogonye, Microstructure and mechanical properties of cast Al-Ce-Sc-Zr-(Er) alloys strengthened by Al<sub>11</sub>Ce<sub>3</sub> micro-platelets and L<sub>12</sub> Al<sub>3</sub>(Sc,Zr,Er) nano-precipitates. *Acta Mater.* **240**, 118354 (2022)
25. F. Stadler, H. Antrekowitsch, W. Fragner, H. Kaufmann, E.R. Pinatel, P.J. Uggowitzer, The effect of Main alloying elements on the physical properties of Al–Si foundry alloys. *Mater. Sci. Eng. A* **560**, 481–491., ISSN 0921-5093 (2013). <https://doi.org/10.1016/j.msea.2012.09.093>
26. N. Chawla, K.K. Chawla, *Metal Matrix Composites* (Springer Science+Business Media, Inc., Berlin, 2006), p. 272
27. D. Weiss, *Development and Casting of High Cerium Content Aluminum Alloys*, Transactions of the American Foundry Society 17-013 (American Foundry Society, 2017)

28. D. Weiss, *Thermal Treatment of Al-Mg-Ce Alloys*, Transaction of the American Foundry Society 18-101 (American Foundry Society, 2018)
29. D.R. Manca, A. Churyumov, A.V. Pozdniakov, A. Prosviryakov, D. Ryabov, A. Krokhin, V.A. Korolev, D. Daubarayte, Microstructure and properties of novel heat resistant Al–Ce–Cu alloy for additive manufacturing. *Met. Mater. Int.* **25**, 633–640 (2019). <https://doi.org/10.1007/s12540-018-00211-0>
30. H. Hyer, A. Mehta, K. Graydon, N. Kljestan, M. Knezevic, D. Weiss, B. McWilliams, K. Cho, Y.H. Sohn, *Addit. Manuf.* **52**, 102657 (2022). Available online February 2, 2022. <https://doi.org/10.1016/j.addma.2022.102657>
31. M. Kesler, M. Neveau, W. Carter, H. Henderson, Z. Sims, D. Weiss, T. Li, S. McCall, M. Glicksman, O. Rios, Liquid direct reactive printing of structural Aluminum alloys, *applied. Mater. Today* **13**, 339–343 (2018)
32. J.S. Luna, A.A. Flores, V.R. Muñiz, A.F. Fuentes, J. Torres, N. Rodríguez, J.C. Ortiz, P. Orozco, Cerium extraction by Metallothermic reduction using cerium oxide powder injection. *J. Rare Earths* **29**(1), 74 (2011)

# Chapter 15

## Scandium in Commercial Wrought Aluminum Alloys



Timothy J. Langan and Thomas Dorin

### 15.1 Introduction

Scandium is a transition element that has been classed as a rare earth element (REE) by the International Union of Pure and Applied Chemistry (IUPAC) along with yttrium (Y) and the lanthanides. It is the most potent strengthening element when added to Al. This means that only a very low amount of Sc is needed to provide a significant strengthening effect (i.e., increase of yield strength), with reports of up to 100 MPa per 0.05 wt% addition [1]. Scandium has also been reported to enhance formability and corrosion resistance of some Al alloys [1–4]. The remarkable effects that Sc has on the properties of Al comes from its effects on the microstructure which can be referred to as the four pillars of Sc – grain refinement, increased recrystallization temperature, dispersoid strengthening and nucleation of strengthening precipitates.

Despite the known benefits of Sc additions to Al, the industrial uptake has been hampered by historical high price and limited supply of Sc. Scandium has been considered for use in a range of Al alloys which resulted in numerous patented compositions. This chapter will summarize the Sc-containing Al alloys registered by Al associations. The applications where Al-Sc alloys have been or are currently used will also be reviewed. We will not focus on the extensive fundamental research and alloy development efforts undertaken over the past 60 years in the United States, Europe and Former Soviet Union countries. Extensive research and development efforts are currently underway in China but at this point it is not clear to what extent Sc-containing Al alloys have been commercialized by Chinese manufacturers.

---

T. J. Langan (✉)  
Sunrise Energy Metals, Melbourne, VIC, Australia  
e-mail: [tlangan@sunriseem.com](mailto:tlangan@sunriseem.com)

T. Dorin  
Deakin University, Institute for Frontier Materials, Geelong, VIC, Australia

Scandium additions are very beneficial in Al alloys developed for additive manufacturing (AM) including the Scalmalloy<sup>®</sup> alloy powder developed by AP Works in Germany [5]. Wire-based and powder Sc-containing alloys will also not be discussed in this chapter.

## 15.2 The “Four Pillars” of Scandium in Aluminum

One of the main uses of Sc is as an alloying element in Al alloys as it results in significant improvement of a number of key properties including strength, corrosion resistance, weldability and formability. The impact that Sc additions have on alloy properties varies with parameters of the thermomechanical process and alloy composition. The benefits from Sc come from the various influences it has on alloy microstructure which can be summarized as four main effects, referred to as the “four pillars” of Sc as summarized in Fig. 15.1. These four pillars will be discussed in more detail in this section.

### 15.2.1 Grain Refinement

Control of an alloy’s microstructure during solidification is of high importance in the manufacturing of high-quality Al products. The formation of a fine-scale, equiaxed microstructure is beneficial for several reasons, which range from increasing the mechanical properties to reducing the tendency to hot tearing. The control of the grain microstructure is traditionally done through the addition of melt inoculants as master alloys of aluminum-titanium-boron (Al-Ti-B) and aluminum-titanium-carbon (Al-Ti-C).

The binary Al-Sc phase diagram is dominated by a eutectic reaction in the Al-rich end, where liquid Al transforms into  $\alpha(\text{Al})$  and  $\text{Al}_3\text{Sc}$  [2]. As can be seen in Fig. 15.2, the eutectic composition is 0.55 wt% Sc. For Sc to act as an effective grain refiner, it needs to be added in excess of the eutectic composition. In that case, the  $\text{Al}_3\text{Sc}$

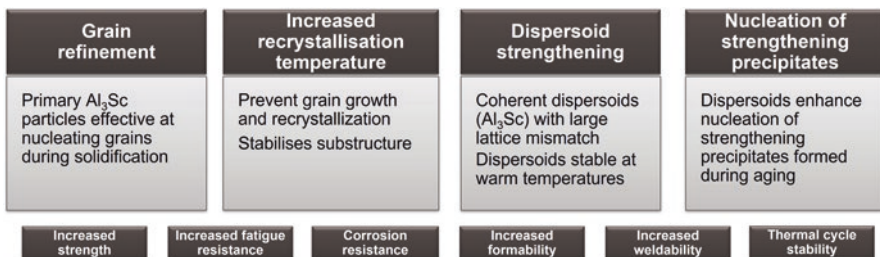
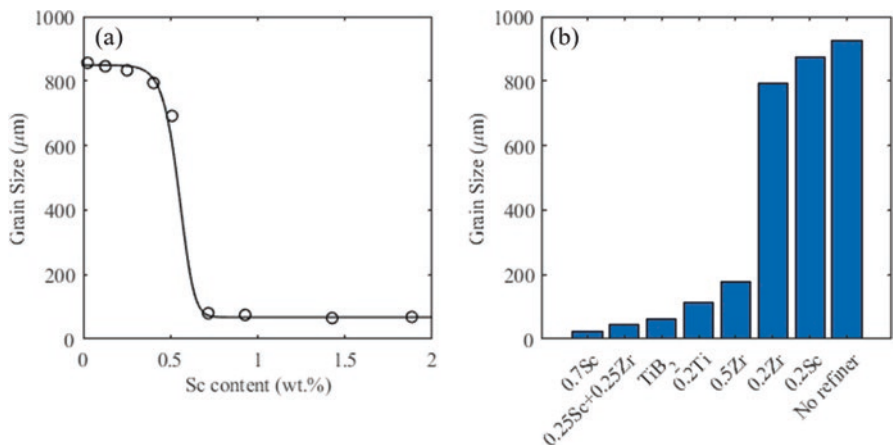
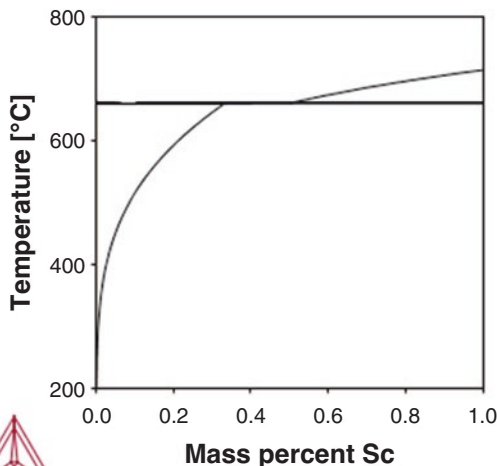


Fig. 15.1 The “four pillars” of Sc addition in Al

**Fig. 15.2** Al-rich end of the Al-Sc phase diagram calculated via ThermoCalc



**Fig. 15.3** (a) Grain size in the as-solidified alloy as a function of Sc content [6]. (b) Grain size as a function of element addition after solidifying with a cooling rate of ~1000 K/s. TiB<sub>2</sub> corresponds to grain size for similar castings made with typical commercially used TiB<sub>2</sub>/Ti master alloy additions [7]

particles will form in the melt and act as a nucleus for the  $\alpha(\text{Al})$  leading to significant grain refinement.

Early work by Drits et al. [6] recorded the dramatic grain refinement in Al-Sc cast ingots when Sc was increased above 0.55 wt% (Fig. 15.3a). These results were later confirmed by Norman et al. [7] who reported grain refinement by over an order of magnitude when comparing Al-0.2wt%Sc to an Al-0.7wt%Sc alloy. Norman et al. further compared the grain refinement potentials of Sc, zirconium (Zr), titanium (Ti), titanium diboride (TiB<sub>2</sub>) and co-additions of Sc and Zr. Hypereutectic

additions of Sc were reported to provide the most efficient grain refinement for a range of cooling rates between 100 and 1000 K/s using a wedge mold. The second-best refinement was obtained by adding 0.25 wt% Sc with 0.25 wt% Zr, followed by  $\text{TiB}_2$ , Ti and Zr. The as-cast grain sizes at the tip of the wedge mold (i.e., cooling rate  $\sim 1000$  K/s) for the different alloying additions are shown in Fig. 15.3b.

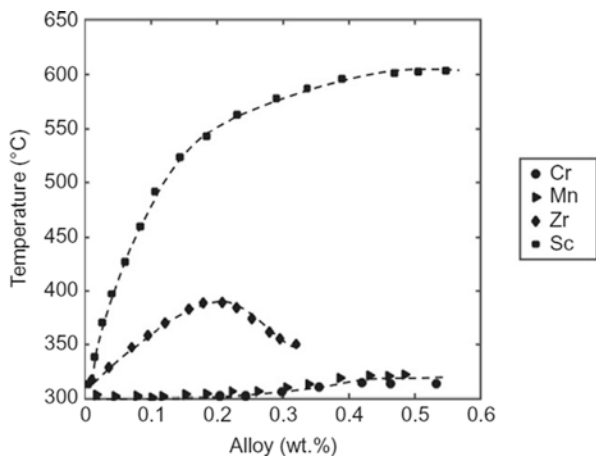
The  $\text{Al}_3\text{Sc}$  phase has a  $\text{L1}_2$  crystal structure with a lattice parameter close in size to the Al FCC crystal structure. The close match in lattice parameters can explain the exceptional ability of the  $\text{Al}_3\text{Sc}$  phase to heterogeneously nucleate the  $\alpha(\text{Al})$  grains. The extreme grain refinement obtained in the 0.25Sc + 0.25Zr alloy (Fig. 15.3b) can be explained by the fact that Zr substitutes in the  $\text{L1}_2$  structure to create  $\text{Al}_3\text{Sc}_x\text{Zr}_{1-x}$  inoculants. As a result, the addition of Zr together with Sc promotes grain refinement even for hypoeutectic Sc additions.

### 15.2.2 Increased Recrystallization Temperature

Metal processing commonly involves the use of large strains which result in an increase in the strength and a decrease in the ductility of the processed metal. Recovery and recrystallization are the thermal processes behind restoring the strained material to a softer state.

Recrystallization in Al alloys is generally undesired as it results in a drop in strength and local strength heterogeneities. Small additions of transition metals that form thermally stable dispersoids are commonly used to control the evolution of the grain structure during thermomechanical processing and restrain grain growth.

Zirconium is commonly used in aluminum-copper-lithium (Al-Cu-Li) alloys as it produces  $\text{Al}_3\text{Zr}$  dispersoids which are extremely efficient recrystallization inhibitors. One common parameter which is used to evaluate the recrystallization of Al alloys is the recrystallization temperature which corresponds to the temperature at which 50% recrystallization is achieved. The evolution of the recrystallization temperature as a function of alloying content for Sc, Zr, manganese (Mn) and chromium (Cr) is given in Fig. 15.4. Figure 15.4 clearly highlights the exceptional ability of Sc to inhibit Al recrystallization. A rapid increase in recrystallization temperature results as Sc is increased from 0 to 0.2 wt%. The changes in the recrystallization temperature become more marginal for larger Sc contents. The recrystallization temperature of Al-Sc alloys is further improved by adding Zr as it forms the thermally stable  $\text{Al}_3\text{Sc}_x\text{Zr}_{1-x}$  phase. The starting temperature for recrystallization of an Al-Sc alloy was found to be improved by up to 100 °C through Zr additions [2]. Similarly, the recrystallization temperature of the ternary Al-Zr-Sc system is higher when compared to the binary Al-Zr system [8] further demonstrating the synergistic effect of co-additions of Sc and Zr to Al.



**Fig. 15.4** Effect of alloying with Cr, Mn, Zr and Sc on the recrystallization temperature of cold-rolled Al sheets. (Data extracted from Zakharov [9])

### 15.2.3 Dispersoid Strengthening

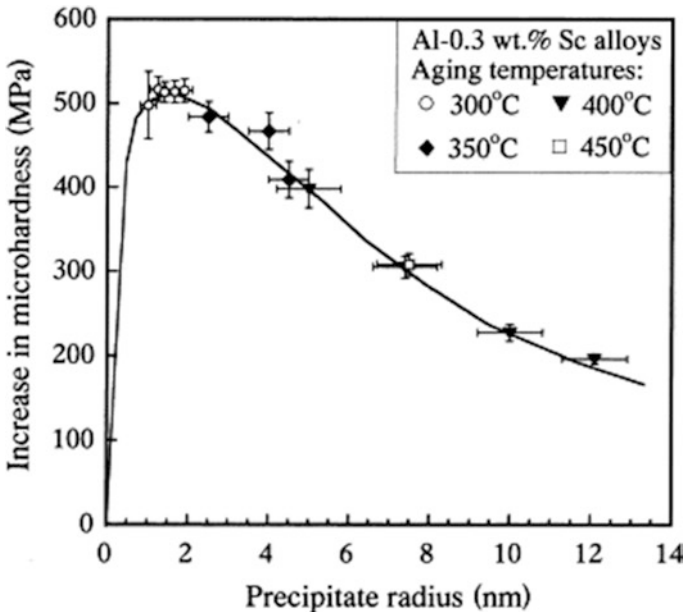
In Al-Sc alloys, maximum strengthening is obtained by precipitation of a fine  $L1_2$ -type  $Al_3Sc$  dispersoids. The average yield strengthening resulting from the fine dispersoids is on the order of 50 MPa per 0.1 wt% Sc addition [1]. This remarkable strengthening potential makes Sc the element providing the most strengthening in Al. One of the most studied precipitation system in physical metallurgy is Al-Cu and the precipitation of the  $\theta'$  precipitates [10]. Copper (Cu) additions typically result in around 5–10 MPa strength improvement per 0.1 wt% Cu addition, an order of magnitude lower than for Sc additions. The main difference is that the maximum solubility of Cu is much larger than that of Sc, allowing for larger amounts of Cu (up to 5–6 wt%) to be added. This in turn results in alloys with superior strength. Comparatively the maximum solubility of Sc is 0.33 wt% which provides for less freedom to add larger amounts of Sc and limits the maximum strength achievable. However, one of the key benefits of Sc is the potential of developing Al alloys with low alloy content with an exceptional combination of properties, such as strength, conductivity, corrosion resistance and formability. Strengthening from the fine Sc-containing dispersoids can be also used in combination with other strengthening precipitates to develop ultrahigh-strength alloys.

The exceptional strengthening potential of Sc additions to Al was first discovered in the 1960s. A majority of the early work was conducted in Russia and is summarized in a comprehensive book by Toropova et al. [2] The strength improvement from Sc additions is mainly provided by the formation of fine  $L1_2$ -type  $Al_3Sc$  dispersoids. The level of strengthening depends on the size and number density of these dispersoids. Temperatures in the range 250–350 °C are usually preferred to



nucleate a high number of small  $\text{Al}_3\text{Sc}$  precipitates. The use of higher temperatures will most commonly generate coarser particles with less strengthening potential.

The increment of yield strength and corresponding dislocation mechanisms related to  $\text{Al}_3\text{Sc}$  precipitates was systematically investigated by Seidman et al. [11] When deforming at room temperature, the dislocation/precipitate interaction mechanisms determine the level of strengthening through two mechanisms – precipitate shearing and precipitate bypassing. The shearing mechanism involves chemical, coherency, modulus mismatch and antiphase boundary (APB) strengthening. For larger precipitates, a moving dislocation will bow all the way around the precipitates and leave a dislocation loop [12]. Seidman et al. systematically generated microstructures with different precipitate sizes at approximately constant volume fraction in an Al-0.3wt%Sc alloy. The hardness increment as a function of average precipitate radius is presented in Fig. 15.5. The maximum strength increment is found to occur for a precipitate radius of approximately 1.5–2 nm. The shape of the curve in Fig. 15.5 is characteristic of a transition between precipitate shearing and precipitate bypassing. The transition between shearing and bypassing was confirmed through analytical models and a transition radius of 2.1 nm was predicted, confirming the experimental results. The maximum strengthening achieved in Seidman's study was about 500 MPa (HV) which translates to a yield strength increment of approximately 167 MPa.



**Fig. 15.5** Hardness increment from  $\text{Al}_3\text{Sc}$  precipitates as a function of precipitate radius at approximately constant precipitate volume fraction. (Taken from Seidman et al. [11])

### 15.2.4 Nucleation of Other Strengthening Phases

The presence of second phase particles in an Al matrix is known to influence the breakdown of solid solutions. Various mechanisms have been proposed to explain the role of the interface in modifying nucleation, including vacancies sinks, solute segregation at precipitate interfaces and reduced surface energy for nucleation. Scandium and  $\text{Al}_3\text{Sc}$  dispersoids have been reported to influence precipitation mechanisms in age-hardenable alloy systems with most of the reports addressing additions of Sc in the 2xxx and 6xxx-series of Al alloys.

#### Al-Cu-Based 2xxx-Series Alloys

The addition of Sc has been reported to modify precipitation and stability of strengthening phases in 2xxx-series alloys resulting in an increase [13–16] or a decrease [17] of the alloy performance. These conflicting results can be explained by the different precipitation routes used in these different studies. The report of negative impact of Sc on mechanical properties generally comes from the formation of the non-strengthening W-AlCuSc phase that traps part or all the Sc and some of the Cu and hence leads to a decrease in strength upon Sc additions. For instance, Toropova et al. [2] reported that early work by Fridlyander et al. found that Sc additions (i.e., 0.2 and 0.45 wt%) reduced strengthening from Al-Cu precipitates during aging at 190 °C in an extruded commercial Al-Cu with 6 wt% Cu.

Recent work has shown that the heat treatment of Al-Cu-Sc alloys can be tailored to avoid the formation of the detrimental W-phase [18]. The addition of Zr is also key so that thermally stable core-shell  $\text{Al}_3(\text{Sc},\text{Zr})$  dispersoids can form during an initial multistep homogenization and remain stable for the rest of the thermomechanical process. The high number density of dispersoids was then found to act as nucleation sites for the  $\theta'$ -phases during artificial aging. This nucleation effect resulted in a significant refinement of the  $\theta'$  precipitates which provided significant additional strengthening. Rouxel et al. [14] characterized the effect of Sc/Zr dispersoids on nucleation of strengthening precipitates in an Al-4 Cu alloy with and without pre-stretch and at two different aging temperatures. Results show that even without plastic deformation prior to aging, the  $\theta'$  precipitates are strongly refined by dispersoids.

#### Al-Mg-Si 6xxx-Series Alloys

The 6xxx-series are the most commonly used Al alloys in the automotive industry as they can achieve medium to high strength while remaining relatively lean, providing for excellent corrosion resistance and formability compared to other high strength alloys. 6xxx-series alloys as aluminum-magnesium-silicon (Al-Mg-Si) obtain most of their strengthening from the formation of coherent GP-zones and

$\beta''$ -precipitates. Copper is commonly added to Al-Mg-Si alloys to promote the formation of  $Q'$ -AlMgSiCu precipitates.

The work on Sc in Al-Mg-Si alloys is limited and while some work reports a positive impact, a number of papers report a detrimental impact on mechanical properties. These conflicting results are due to the strong interactions between Si and Sc and the formation of the detrimental AlSiSc, which is referred as  $\tau$  or V-phase. Recent work has revealed that the V-phase forms at temperatures greater than 450 °C [19]. As a result, this phase can occur at traditional solution treatment temperatures for these alloys.

Under the right heat treatment conditions, the addition of Sc and Zr has been shown to lead to a significant strength increment increase in Al-Mg-Si alloys. Atom probe tomography revealed that the rodlike  $\beta''$ -precipitates were systematically associated with Al<sub>3</sub>Sc dispersoids [20]. These associations between dispersoids and  $\beta''$ -precipitates were confirmed via systematic transmission electron microscopy (TEM) characterization by Babaniaris et al. [21] This nucleation effect was found to result in a refinement of the  $\beta''$  precipitates. Babaniaris et al. also reported increased stability of  $\beta''$  precipitates with a retardation of their transition to  $\beta'$ . Similarly, Kwon et al. [22] suggested that the presence of Sc-rich dispersoids retarded the precipitation kinetics and over-aging rate of the  $\beta$  series precipitates.

### 15.3 Development and Applications of Sc-Containing Wrought Alloys

As discussed in the previous section, Sc additions strengthen Al alloys by modifying key features in the microstructure including refining grain size, reducing recrystallization, forming stable coherent dispersoids and enhancing precipitation of strengthening phases. The first patent for Sc-containing Al alloys [23] was awarded to Alcoa in 1970. According to this invention, additions of Sc improve performance for alloys designated by the American Aluminum Association in the 7xxx, 6xxx, 5xxx, 3xxx and 2xxx-series including 7075, 7039, 6061, 5083, 3003, 2219 and 2024. Examples in this patent demonstrated that Sc provides for dramatic increases in yield strength for cold worked alloys after aging at temperatures ranging from 100 to 425 °C. In addition, Sc reduces recrystallization and improves strength after warm temperature (less than 350 °C) exposure. Strengthening effects for these different alloy series are reviewed in detail by Royset [3] and Toropova et al. [2] Royset provides direct comparisons of strength with and without Sc additions and concluded that the largest strength increase is observed in non-heat treatable alloys. These data, along with unpublished results from Clean TeQ, were plotted by Carr and presented by Clean TeQ [24] (Fig. 15.6).

Compositions for “commercial” Sc-containing alloys are shown in Tables 15.1 and 15.2. This includes alloys currently registered with the American Aluminum Association [25] and alloys that are listed in the Russian standard GOST

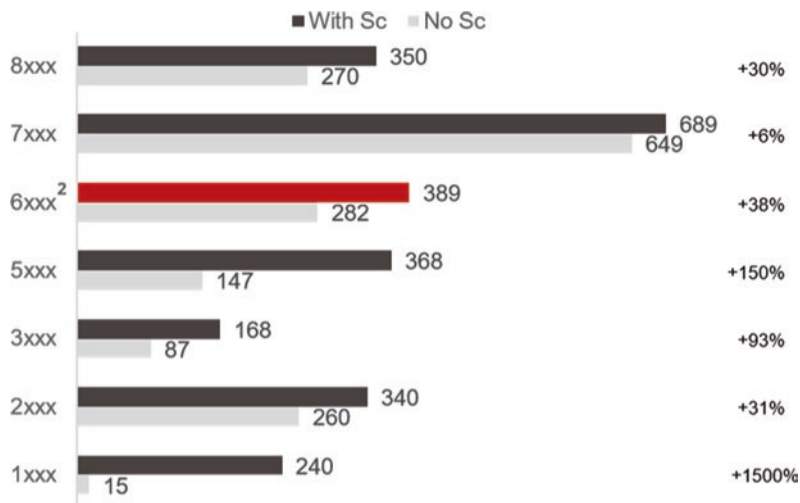


Fig. 15.6 Effect of Sc addition on yield strength in wrought Al alloys [24]

4784-2019 [26]. Nominal compositions are listed for alloys that have seen commercial applications but do not have a registered composition. The sections below provide specific examples of development and applications for these commercial Sc-containing wrought Al alloys.

### 15.3.1 Al-Mg-Li (14XX-Series) Alloys

The aluminum-magnesium-lithium (Al-Mg-Li) alloy 01420 was developed in the 1960s. This alloy was used in riveted fuselage structures of the YAK36 and YAK38 aircraft [33] and in the welded fuselage structure of the “supersonic MiG29 fighter.” [34] A modified version of alloy 01420 containing 0.17 wt% Sc (i.e., alloy 1421) was developed to increase yield strength [29, 35] and improve weldability for use in fuselage structures. This modified alloy went into commercial production in 1985 [36]. No specific references were found in the open literature for its application in construction of military or commercial aircraft. The compositions of alloys 01420 and 1421 were further modified to create alloy 1424, where the Li content was reduced, and Zn was added. Alloy 1424 was evaluated [33] for use in fuselage structure on commercial aircraft as part of a program between DaimlerChrysler, All-Russian Institute of Aircraft Materials, Kamensk-Uralsky Metallurgical Plant and Hugovens. This class of Al-Mg-Li alloys was also evaluated for potential applications in U.S. space launch systems but were not selected for service [29, 37].

**Table 15.1** Commercial Sc-containing Al-Mg (Mn) alloys

Alloy designation	Mg	Mn	Sc	Zr	Others
Al-Mg (Mn)					
01515 [27]	1.15		0.3	0.1	
01523 [27]	2.1		0.3	0.15	
01535 [27]	4.2		0.3	0.1	
01545K [26]	4.5–4.9	0.19–0.35	0.17–0.27	0.05–0.12	<b>Be</b> 0.0002–0.005; <b>Cr</b> 0.01–0.04; <b>Ce</b> 0.0001–0.0009; <b>Ti</b> 0.01–0.04; <b>Cu</b> 0.1; <b>Zn</b> 0.1, <b>Fe</b> 0.12; <b>Si</b> 0.1
01570 [26]	5.3–6.3	0.2–0.6	0.15–0.35	0.05–0.15	<b>Be</b> 0.0002–0.005; <b>Ti</b> 0.01–0.05; <b>Zn</b> 0.1; <b>Cu</b> 0.1; <b>Si</b> 0.2; <b>Fe</b> 0.3
01570C [26]	5.0–5.6	0.2–0.5	0.18–0.26	0.05–0.12	<b>Si</b> and <b>Fe</b> 0.005–0.12; <b>Be</b> 0.0002–0.005 <b>Ti</b> 0.01–0.03; <b>Ce</b> 0.0002–0.0009
01570C [26]	5.7–6.3	0.3–0.6	0.20–0.28	0.05–0.12	<b>Si</b> and <b>Fe</b> 0.005–0.12; <b>Be</b> 0.0002–0.005 <b>Ti</b> 0.01–0.03; <b>Ce</b> 0.0002–0.0009
1571 [26]	5.8–6.8	max 0.3	0.2–0.5	0.05–0.15	<b>Cr</b> 0.05–0.15; <b>Be</b> 0.0005–0.005 <b>Ti</b> 0.02–0.05; <b>Zn</b> 0.2; <b>Ce</b> 0.0002–0.0009; <b>B</b> 0.01–0.005; <b>Cu</b> 0.15; <b>Si</b> 0.2; <b>Fe</b> 0.3
1575 [26]	5.4–6.4	0.35–0.6	0.2–0.3	0.05–0.15	<b>Be</b> 0.0002–0.005 <b>Ti</b> 0.07; <b>Cu</b> 0.1; <b>Cr</b> 0.05–0.15; <b>Si</b> 0.2; <b>Fe</b> 0.3
1575–1 [26]	5.5–6.5	0.5–0.85	0.12–0.2	0.05–0.2	<b>Be</b> 0.0002–0.005 <b>Ti</b> 0.02–0.006; <b>Cu</b> 0.1; <b>Cr</b> 0.1–0.25; <b>Zn</b> 0.1–0.6; <b>Si</b> 0.2; <b>Fe</b> 0.3
1580 [26]	4.9–5.3	0.4–0.8	0.05–0.14	0.06–0.18	<b>Be</b> 0.003 <b>Ti</b> 0.15; <b>Cu</b> 0.1; <b>Cr</b> 0.08–0.18; <b>Zn</b> 0.25; <b>Si</b> 0.06–0.16; <b>Fe</b> 0.12–0.18; <b>Ca</b> 0.0005; <b>Na</b> 0.0003
1597 [26]	5.5–6.5	0.5–0.8	0.36–0.5	0.05–0.25	<b>Be</b> 0.001–0.005 <b>Ti</b> 0.01–0.05; <b>Cu</b> 0.1–0.2; <b>Cr</b> 0.08–0.18; <b>Zn</b> 0.05–0.25; <b>Si</b> 0.1; <b>Fe</b> 0.15
5025 [25]	4.5–6.0	0.2 max	0.05–0.55	0.1–0.25	<b>Si</b> 0.25 max; <b>Fe</b> 0.25 max; <b>Cu</b> 0.1 max; <b>Cr</b> 0.1 max; <b>Zn</b> 0.25 max; <b>Ti</b> 0.05–0.2; <b>Be</b> 0.0008
5024 [25]	3.9–5.1	0.2 max	0.1–0.4	0.05–0.2	<b>Si</b> 0.25 max; <b>Fe</b> 0.4 max; <b>Cu</b> 0.2 max; <b>Cr</b> 0.2 max; <b>Zn</b> 0.25 max; <b>Ti</b> 0.2 max;
5028 [25]	3.2–4.8	0.3–1.0	0.02–0.4	0.05–0.15	<b>Si</b> 0.3 max; <b>Fe</b> 0.4 max; <b>Cu</b> 0.2 max; <b>Cr</b> 0.05–0.15; <b>Zn</b> 0.05–0.5; <b>Ti</b> 0.05–0.15;
5081 [25]	4.9–5.3	0.4–0.8	0.05–0.14	0.06–0.18	<b>Si</b> 0.06–0.16; <b>Fe</b> 0.12–0.18; <b>Cu</b> 0.1; <b>Cr</b> 0.08–0.18; <b>Zn</b> 0.25; <b>Ti</b> 0.15; <b>Be</b> 0.03 <b>V</b> 0.1; <b>Ca</b> 0.1
5181 [25]	4.3–5.3	0.4–0.8	0.01–0.09	0.08–0.18	<b>Si</b> 0.06–0.16; <b>Fe</b> 0.12–0.22; <b>Cu</b> 0.1; <b>Cr</b> 0.08–0.18; <b>Zn</b> 0.25; <b>Ti</b> 0.15; <b>V</b> 0.1; <b>Ca</b> 0.1
C557 [28]	4.0	0.6	0.2	0.1	<b>Si</b> 0.06; <b>Fe</b> 0.1; <b>Ti</b> 0.02

Beryllium (Be), Boron (B), Calcium (Ca), Cerium (Ce), Chromium (Cr), Copper (Cu), Iron (Fe), Manganese (Mn), Silicon (Si), Sodium (Na), Titanium (Ti), Zinc (Zn)

**Table 15.2** Other commercial Sc-containing alloys

Alloy designation	Mg	Zn	Cu	Li	Sc	Zr	Others
<i>Al-Mg-Li</i>							
01421 [29]	5.2			2.1	0.17	?	
1424 [26]	4.1–6	0.1–1.5		1.5–1.9	?	?	
<i>Al-Cu (Li)</i>							
2023 [25]	1.0–1.6		3.6–4.5		0.01–0.06	0.05–0.15	<b>Mn</b> 0.3; <b>Fe</b> 0.1; <b>Si</b> 0.15; <b>Ti</b> 0.05; <b>Cr</b> 0.1
1460 [29]			3.0	2.0	0.1	?	
1469 [30]	0.3		4.18	0.92	0.06	0.1	<b>Ag</b> 0.38
<i>Al-Zn-Mg (Cu)</i>							
V1963	?	?	?		?	?	<b>Ag</b>
01970 [26]	2.0	5.2	0.4		0.2	0.1	<b>Mn</b> 0.3
01975 [26]	2.0	5.2	?		0.07	0.1	<b>Mn</b> 0.3
1977 [26]	4.2–5	3.2–3.9	0.4–1		0.17–0.3	0.07–0.14	<b>Si</b> 0.1; <b>Fe</b> 0.15; <b>Mn</b> 0.25; <b>Cr</b> 0.1; <b>Ti</b> 0.01–0.05; <b>Be</b> 0.00001–0.005
7042 [25]	2.0–2.8	6.5–7.9	1.3–1.9		0.18–0.5	0.11–0.2	<b>Mn</b> 0.2–0.4; <b>Fe</b> 0.2; <b>Si</b> 0.2; <b>Cr</b> 0.05
7xa [31]	1.9–2.4	5.1–5.4			0.10–0.14	0.12–0.18	<b>Ag</b> 0.04–0.08
7X0X [32]	5.0	2.0			0.1	0.14	
7X1X [32]	5.2	2.0	0.3		0.1	0.14	
7X5X [32]	8.1	2.2	1.9		0.1	0.15	
<i>Al-Mg-Si</i>							
1370 [26]	0.7–1.4	0.2–0.8	0.6–1.4		0.01–0.1	0.05–0.12	<b>Si</b> 0.6–1.2; <b>Mn</b> 0.2–0.5; <b>Cr</b> 0.01–0.1; <b>Ti</b> 0.01–0.1; <b>Ni</b> 0.05–0.2; <b>Ce</b> 0.005–0.05; <b>Fe</b> 0.15

Lithium (Li), Nickel (Ni), Silver (Ag)

### 15.3.2 Al-Mg (Mn) (5xxx/15xx-Series) Alloys

Aluminum-magnesium-(manganese) (Al-Mg (Mn)) alloys see widespread commercial applications based on the combination of high strength and resistance to environmental attack. These alloys are primarily strengthened by Mg in solid solution, thus artificial aging is not required. Scandium additions are known to increase strength in these alloys. No ternary phases (e.g., AlMgSc) are present in the Al-rich corner of the Al-Mg-Sc phase diagram. Efforts have focused on developing Sc-containing Al-Mg alloys for various applications including aircraft structures, space launch systems and marine structures. A list of “commercial” Sc-containing Al-Mg (Mn) alloys is presented in Table 15.1. Aluminum and aerospace companies have actively worked to capture intellectual property associated with adding Sc to Al-Mg (Mn) alloys (Table 15.3). The commercial alloys shown in Table 15.1

Table 15.3 Summary of key patents for Sc-containing Al-Mg alloys

No.	Date	Assignee	Mg	Sc	Zr	Mn	
US 5,554,428	9/1/94	Alcoa	2.0–11.0	0.05–1	≤0.3		<b>Zn</b> ≤ 5.0; <b>Si</b> and <b>Fe</b> ≤ 0.2; <b>Cu</b> ≤ 1.0; opt. <b>Er</b> , <b>Th</b> , <b>Lu</b> , <b>Yt</b> , <b>Hf</b> , <b>Y</b>
US 5,624,632	1/31/95	Alcoa	3.0–7.0	0.05–0.5	0.05–0.2	0.2–1.2	<b>Si</b> < 0.15; <b>Cu</b> < 0.25; <b>Zn</b> free
RU2085607	6/30/95	Joint-stock company open type All-Russian Institute light alloys, Central Scientific Research institute construction materials Prometheus	3.9–4.9	0.2–0.5	0.05–0.15		<b>Ti</b> 0.01–0.1; <b>Be</b> 0.0001–0.0005; <b>Ce</b> 0.001–0.004
RU2081934	7/13/95		5.3–6.5	0.17–0.35	0.02–0.15	0.2–0.7	<b>Cr</b> 0.01–0.25; <b>Li</b> 0.01–0.25; <b>Be</b> 0.0001–0.0005
RU2082809	7/25/95	Joint-stock company open type All-Russian Institute light alloys	5.8–6.8	0.2–0.5	0.02–0.15		<b>Be</b> 0.0001–0.01; <b>Cr</b> , <b>V</b> , <b>Ti</b> 0.02–0.2; <b>Ce</b> 0.001–0.01; <b>B</b> 0.001–0.01
US 6,531,004	8/21/98	Airbus	5.0–6.0	0.05–0.5	0.05–0.15	0.05–0.12	<b>Zn</b> 0.1–0.4; <b>Ti</b> 0.01–0.2; <b>Cu</b> 0.1–0.2; <b>Tb</b> 0.05–0.5
US 6,139,653	8/12/99	Kaiser	4.0–8.0	0.05–0.6	0.05–0.2	0.1–0.8	<b>Zn</b> 0–2; <b>Cu</b> 0.5–2; <b>Hf</b> and/or <b>Zr</b> ; <b>Cu</b> and/or <b>Zn</b>
US 6,258,318	8/14/99	EADS	3.0–5.0	0.05–0.50	0.05–0.15	0.05–0.12	<b>Ti</b> 0.01–0.2; opt. lanthanide series
US 6,551,424	12/17/99	Aleris	3.0–6.0	0.01–0.4		≤1.0	<b>Zn</b> ≤ 2.0; <b>Si</b> ≤ 0.3; <b>Fe</b> ≤ 0.3; <b>Cu</b> ≤ 0.3; <b>Li</b> 0.4–3.0; <b>Ag</b> ≤ 0.5; at least one of <b>Sc</b> or <b>Hf</b> , <b>Ti</b> , <b>V</b> , <b>Nd</b> , <b>Zr</b> , <b>Cr</b> , <b>Y</b> and <b>Be</b>
US 6,383,314	6/14/00	Pechiney	4.55–6	<0.5	<0.5	≥0.98	<b>Cr</b> < 0.25; <b>Si</b> < 0.3; <b>Fe</b> < 0.4 UTS <sup>3</sup> 68ksi
US 6,676,899	12/14/01	EADS	5.0–5.6	0.18–0.30	0.05–0.15	0.05–0.18	<b>Zn</b> 0.05–0.15; <b>Ti</b> 0.01–0.05; <b>Si</b> 0.04–0.24; <b>Fe</b> 0.04–0.24; <b>Cu</b> 0.05–0.15; <b>Be</b> 0.0001–0.0005; <b>Ce</b> 0.001–0.004; <b>Fe:Si</b> 1:5

DE10248594	10/17/02	Airbus D&S	1.0–5.0	0.1–1.0	0.05–1.0 opt	0–2.0	<b>Zn</b> 0–2.0; <b>Cu</b> 0–1.0; 0–1.0 <b>Ag</b>
RU2268319	5/20/04	Federal State Unitary Enterprise Central Scientific Research Institute of Structural Prometheus materials	5.5–6.6	0.1–0.2	0.05–0.2	0.5–1.0	<b>Cr</b> 0.1–0.25; <b>Zn</b> 0.1–1.0; <b>Ti</b> 0.02–0.15; <b>B</b> 0.003–0.015; <b>Be</b> 0.0002–0.005; <b>Sc</b> + <b>Mn</b> + <b>Cr</b> > 0.85
RU2280705	9/15/04	Open Joint Stock Company Kamensk-Ural's Metallurgical Plant (RU)	4.2–6.5	0.05–0.3	0.05–0.3	0.5–1.2	<b>Cr</b> ≤ 0.2; <b>Zn</b> ≤ 0.2; <b>Ti</b> ≤ 0.15; <b>Si</b> ≤ 0.25; <b>Fe</b> ≤ 0.3; <b>Cu</b> ≤ 0.1; opt <b>Sc</b> or <b>Be</b> , <b>Y</b> , <b>Nd</b> , <b>Ce</b>
FR2889852	8/16/05	Aleris	3.5–6.0	<0.5	<0.5	0.4–1.2	<b>Cr</b> < 0.3; <b>Zn</b> < 1.7; <b>Ti</b> 0.03–0.2; <b>Si</b> < 0.5; <b>Fe</b> < 0.5; <b>Cu</b> < 0.15; <b>Li</b> < 0.5; <b>Ag</b> < 0.4; opt <0.5 <b>Er</b> , <b>Y</b> , <b>Hf</b> , <b>V</b>
US 7,998,402	8/14/06	Aleris	3.5–6	0.1–0.3	0.05–0.25	0.4–1.2	<b>Cr</b> 0.03–0.3; <b>Ti</b> 0.05–0.2; <b>Fe</b> 0.06– < 0.5; <b>Cu</b> < 0.05; <b>Ag</b> < 0.4; <b>Zn</b> none
EPI917373	8/14/06	Aleris	3.8–4.3	0.1–0.3	0.05–0.25	0.4–1.2	<b>Cr</b> 0.05–0.1; <b>Zn</b> 0.35–0.6; <b>Ti</b> 0.05–0.1; <b>Si</b> < 0.12; <b>Fe</b> < 0.14; <b>Cu</b> < 0.05; <b>Ag</b> < 0.4; <b>Li</b> < 0.5
US 9,039,848	11/5/08	Aleris	3.0–7.0	0–0.5	0.04–0.4Opt	0.6–2.8	<b>Zn</b> 0.6–2.8; <b>Si</b> < 0.3; <b>Fe</b> < 0.3; <b>Cu</b> 0–1.0; at least 1 from <b>Zr</b> , <b>Cr</b> , <b>Ti</b> or <b>Hf</b> 0.04–0.4; opt <b>Cr</b> 0.04–0.4; opt <b>Ti</b> 0.01–0.3
US 9,169,544	2/9/13	Aleris	3.5–6	0.1–0.3	0.05–0.25	0.4–1.2	<b>Cr</b> 0.03–0.1; <b>Ti</b> 0.05–0.11; <b>Fe</b> < 0.14; <b>Si</b> < 0.12; <b>Cu</b> < 0.05; <b>Ag</b> < 0.4; <b>Zn</b> 0.2–0.65

(continued)



Table 15.3 (continued)

No.	Date	Assignee	Mg	Sc	Zr	Mn	
US 9,255,315	5/5/14	Aleris	4.0-6.0	≤0.5	<0.3	0.2-1.4	<b>Cr</b> < 0.3; <b>Zn</b> < 0.9; <b>Ti</b> ≤ 0.3; <b>Si</b> < 0.45; <b>Fe</b> < 0.5; <b>Cu</b> < 0.25
US 10,335,841	1/21/15	Aleris	2.5-6	0-1.0	0.03-0.4 optional	0-1.2	<b>Zn</b> 0-2; <b>Si</b> 0-0.25; <b>Fe</b> 0-0.4; <b>Cu</b> 0-2; <b>Ag</b> 0-0.5; <b>Li</b> 0-3; opt <b>Er</b> ; <b>Dy</b> , <b>Gd</b> , <b>Hf</b> 0.03-0.3; opt <b>Cr</b> 0.03-0.4; opt <b>Ti</b> 0.005-0.3
US20190249285	10/17/17	Constellium	3.8-4.2	0.1-0.3	0.07-0.15	0.3-0.8	<b>Cr</b> < 0.01; <b>Zn</b> 0.1-0.4; <b>Ti</b> 0.01-0.05; <b>Si</b> < 0.1; <b>Fe</b> < 0.15
US 6,695,935	5/4/20	Aleris	4-5.6	no Sc (0.01-0.5 abstract)	<0.25	0.4-1.2	<b>Cr</b> < 0.3; <b>Zn</b> 0.4-1.5; <b>Ti</b> < 0.2; <b>Si</b> < 0.5; <b>Fe</b> < 0.5; <b>Cu</b> < 0.4; <b>Bi</b> 0.01-0.1
DE60002061T3		Aleris	4.6-5.6	0.01-0.5 (included in 1 or more)	0.05-0.25	0.4-0.9	<b>Cr</b> < 0.3; <b>Zn</b> 0.4-1.5; <b>Ti</b> < 0.2; <b>Si</b> < 0.5; <b>Fe</b> < 0.5; <b>Cu</b> < 0.4; one or more from <b>Bi</b> 0.01-0.1; <b>Sn</b> 0.03-0.1; <b>Sc</b> 0.01-0.5; <b>Li</b> 0.01-0.5; <b>Ce</b> 0.01-0.3; <b>Y</b> 0.01-0.3
WO2019201994		SBD	2.4-5.6	0.03-0.55	0.1-0.3	0.11-0.31	<b>Zn</b> 0.11-0.31

Erbium (Er), Terbium (Tb), Lutetium (Lu), Ytterbium (Yb), Hafnium (Hf), Vanadium (V), Neodymium (Nd), Dysprosium (Dy), Gadolinium (Gd), Bismuth (Bi)

resulted from these patents, but widespread adoption of these alloys has been somewhat muted due to the lack of a stable Sc supply.

Scandium-containing alloys were developed to improve performance of the Al-Mg-Li alloys used in welded structures [33, 34] on Soviet military and commercial aircraft. Based in part on this success, the German Government initiated a program with All-Russia Institute of Light Alloys (VILS) to develop welded fuselage structures for commercial aircraft. The AlMgSc alloy KO8242/AA5024 was developed under this program [38]. Further development by Aleris led to the improved alloy AA5028. An ongoing program at Airbus [38] demonstrated a low-cost approach for fabrication of welded Al-Mg-Sc alloy aircraft fuselage structures. In the past, these structures were fabricated from the Al-Cu-Mg alloy 2024 using a stretching and riveting process that required up to twenty-two steps. This can be replaced with a nine-step process involving laser beam welding and creep forming with an Al-Mg-Sc alloy to fabricate fuselage structures [38]. The Al-Mg-Sc alloy can be substituted as a one-to-one replacement for AA2024, the currently used alloy, without a design change, reducing weight by 4% and increasing manufacturability. The good corrosion resistance led workers at Airbus to investigate substituting unclad 5028 for clad 2024 [39]. Benefits from this approach include reducing weight due to an increase in load bearing strength across the entire thickness of the sheet and reduced rework issues associated with damage to soft clad layers. Widespread adoption has not yet occurred partially due to supply concerns associated with Sc. The primary focus of the effort has moved away from welded structures and Aleris is working to fully qualify AA5028 for airframe applications [40].

Trade studies [28, 41] were performed to characterize cost and performance advantages associated with substituting Al-Mg-Sc alloys for high-strength Al-Cu-Li alloys. Scandium increases the cost for raw materials required to cast ingots and billets, but it does not require modified casting schedules. Lithium adds to both the raw material costs and manufacturing cost due to required modifications to casting equipment and schedules. One study led by Vorel [41] at Airbus Defense and Space evaluated properties and performance for the Al-Mg-Mn-Sc alloy 5028 relative to alloys currently used to build propellant tankage for space launch vehicles. Yield strength for 5028 is slightly lower than the conventional Al-Cu alloy 2219 (325 MPa vs. 360 MPa) and much lower than the Al-Cu-Li alloy 2195 (yield strength of 550 MPa). However, the lower density 2.67 g/cm<sup>3</sup> for 5028 vs. 2.84 g/cm<sup>3</sup> for 2219 and 2.71 g/cm<sup>3</sup> for 2195 make the alloy attractive based on high-specific properties. The specific Young's modulus (27.7) is higher than 2219 (25.6) and close to 2195 (28.0). This work determined that the Al-Mg-Sc alloy 5028 offers advantages for design of lightweight inter-tank structures and interstage structures. In addition to good specific properties, Al-Mg alloys have good corrosion resistance and compatibility with different propellants (e.g., H<sub>2</sub>O<sub>2</sub>). Work at NASA [42] showed that Alcoa's Al-Mg-Sc alloy C557 has stability in the H<sub>2</sub>O<sub>2</sub> propellant and that it can be classified as Class 1 (i.e., Unlimited use materials — Can be used for long-term contact with H<sub>2</sub>O<sub>2</sub> as storage containers.) Domak and Dicus [28] characterized the mechanical performance of C557 for aerospace applications including aircraft and launch vehicles structures. Their work focused on strength toughness behavior at temperatures from -184 °C to 107 °C to establish service temperature applicability,

and after exposures of up to 10,000 h at 107 °C to evaluate thermal stability. They concluded that “*yield strength and apparent fracture toughness values of C557 were within 10% of established values for 2024-T3 sheets.*”

In 2000, Filatov et al. [27] reviewed the development and potential applications for “New” Russian Sc-containing Al-Mg alloys. They reviewed work that was initiated at VILS in the 1970s and discuss alloys with Mg levels ranging from approximately 6 wt% (i.e., 01570 and 01571) down to approximately 1 wt% (i.e., 01515). Nominal compositions for these alloys are provided in Table 15.1. The early work at VILS demonstrated casting of thick ingots with non-dendritic structures when a critical Sc level is maintained. Thus, Sc levels of between 0.2 and 0.3 wt% are present in these alloys. The high Mg alloy 01571 was developed as a filler metal alloy where 85% joint efficiencies are obtained when it is used to tungsten inert gas (TIG) weld the high-strength alloy 01570. The medium-strength alloy (i.e., 01535) has high strength and shows good properties in cryogenic applications which make it a good candidate for the production of welded structures for liquid hydrogen (H<sub>2</sub>)/liquid oxygen (O<sub>2</sub>) tanks. Alloy 01523 which contains 2.1 wt% Mg maintains the good corrosion resistance inherent in low Mg alloys but has much higher strength. Potential applications for this include welded tankers and tank cars. These authors note that “*scandium-bearing alloys are still expensive and applied rarely.*” Eskin [43] provides an update on the review by Filatov et al. [27] and cites unique examples of applications for Al-Mg-Sc alloys in welded aerospace applications.

As discussed in Sect. 15.2, Sc levels greater than approximately 0.2 wt% are typically required to refine the cast structure during casting of ingots and billets used to fabricate wrought products (e.g., extrusions, plate, sheet and forgings). In a recent patent application, Krokhin et al. [44] pointed out “*that commercial Al-Mg-Sc alloys typically contain approximately 0.2 wt% Sc.*” Recent work at Rusal [45] has focused on benefits from low Sc additions (<0.1 wt%) in Al-Mg alloys in an attempt to reduce the cost of these alloys. This work shows (Fig. 15.7) that most of the

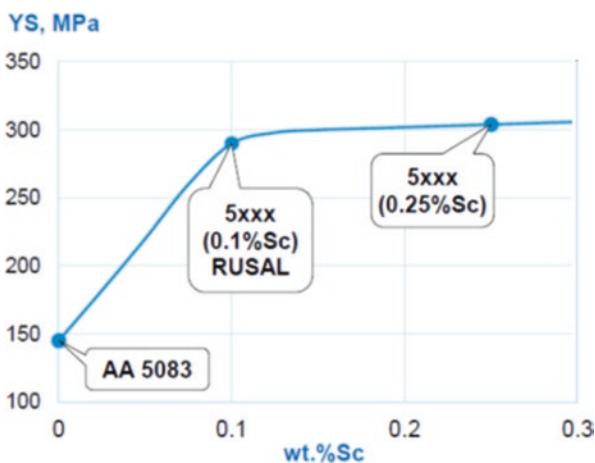
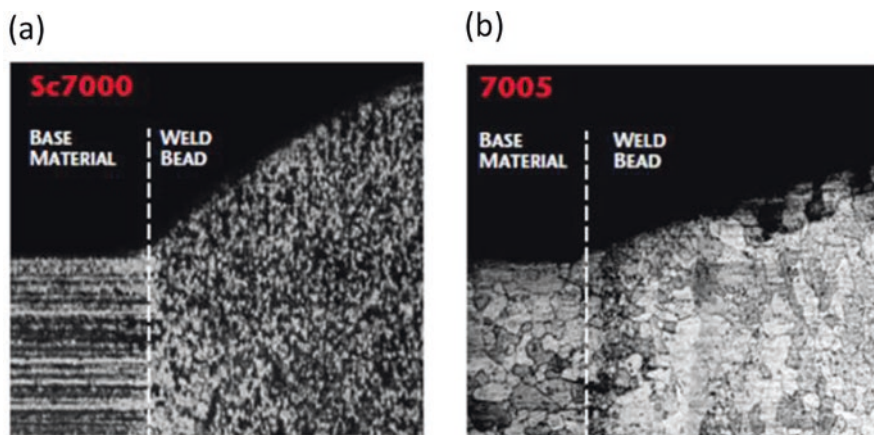


Fig. 15.7 Increase in strength for Al-Mg-Sc wrought alloys associated with Sc level [45]

increase in strength for AlMgSc is imparted by 0.1 wt% Sc [45]. Two new Al-Mg-Sc alloys (Table 15.1) were registered with the American Aluminum Association: low Sc (5081–0.1 wt%) and very low Sc (5181–0.03 wt%). Rusal is currently working to commercialize these “low-Sc” corrosion-resistant Al-Mg-Sc alloys for marine and aerospace structures. This effort relies on the supply of scandium oxide ( $\text{Sc}_2\text{O}_3$ ) using their novel approach to remove Sc from red mud (i.e., bauxite residue produced during processing of bauxite ( $\text{Al}_2\text{H}_2\text{O}_4$ ) into alumina ( $\text{Al}_2\text{O}_3$ ) using the Bayer process).

### 15.3.3 Al-Zn-Mg (Cu) (7XXX/19XX-Series) Alloys

Ashurst Technology was awarded a patent [46] that teaches the benefits of combining Sc with Zr to improve performance in 2xxx, 7xxx and 6xxx-series Al alloys. Materials engineers and scientists at Ashurst Technology worked with Kaiser Aluminum and various Institutes in Ukraine to commercialize a family of ultrahigh-strength and high-strength weldable Sc-containing alloys. Highly worked tubular products were fabricated from these Sc-containing alloys and used to manufacture sporting good products (e.g., baseball bats and bicycle frames). The trace addition of Sc reduces recrystallization and the materials remained unrecrystallized during the draw/anneal steps required to make thin-walled products. Ashurst worked with Kaiser Aluminum and Easton Sports to develop tubes for bicycle frames from a weldable high-strength Sc-containing alloy (i.e., Sc7000) with a composition close to 7X0X (Table 15.2). A novel Sc-containing Al-Mg-Sc alloy (i.e., AA5025) was developed as a filler metal for fusion welding of the bike frames. As shown in Fig. 15.8, the combination of Sc in the base alloy and in the filler resulted in a



**Fig. 15.8** Weldment in (a) Weldable Sc-containing Al-Zn-Mg alloy Sc7000 welded with Sc-containing Al-Mg alloy and (b) Conventional weldable 7005 alloy with conventional filler

refined microstructure in weldments. Easton designed lightweight durable bike frames based on the weldability of these high-strength tubes.

The ability to maintain refined grains during extensive drawing and swagging allowed Easton to fabricate thin-walled high-performance ball bats. Alcoa developed a similar Cr-containing alloy that was used by Easton's competition in the ball bat market. Both products were commercially successful. Unfortunately, the performance was "too good" and these bats were banned from competition.

An ultrahigh-strength Sc-containing 7xxx-series alloy was used by companies, including Yuan Aluminum Company in South Korea, to manufacture high-performance tent poles. The Yunan Scandium PF poles are designed with a yield strength of 109 ksi compared with 83 ksi for conventional AA7001 poles [47].

Smith and Wesson were awarded a U.S. patent [48] for the use of Sc in firearms. They developed and commercialized a high-strength Sc alloy for handgun frames.

In the mid-2000s, Surface Treatment Technologies (ST2) developed and patented [49] a high-strength corrosion-resistant Sc-containing Al alloy (i.e., 7xa) for use in marine structures. ST2 worked with ship builders to qualify the patented alloy for a demanding shipboard application. Extensive testing was performed to develop specifications for the alloy and components were fabricated using the conventional U.S.-based supply chain (i.e., master alloy production, billet casting, extrusion, heat treating and machining). Scandium oxide was sourced on the "open market" which primarily came from China or former Soviet Union (FSU) countries. Finished components were delivered and installed on ships. The alloy did not ultimately see widespread use due to restrictions in the supply of  $\text{Sc}_2\text{O}_3$ .

These "supply disruptions" caused the price for Sc to rise drastically, with the price for the Al-Sc master alloy increasing from approximately \$40/kg to close to \$200/kg. While this price increase could have been temporarily absorbed in high-value applications, it became increasingly difficult to source the  $\text{Sc}_2\text{O}_3$  that was necessary to support U.S. industry. As a result, a less-suitable Sc-free alloy was qualified.

### ***15.3.4 Al-Mg-Si (Cu) (6XXX/13XX-Series) Alloys***

Very few Sc-containing Al-Si-Mg 6xxx-series-type alloys have been commercialized due to the deleterious interaction between Sc and Si [50, 51]. This interaction is known to reduce beneficial effects of Sc additions in these alloys by (1) substituting for Al in the  $\text{Al}_3\text{Sc}$  dispersoids which modifies nucleation, resulting in coarsening (i.e., loss in strengthening), and (2) formation of a coarse incoherent non-strengthening Al-Sc-Si ternary phase [19, 50] which removes Si and Sc from solution reducing strength. Work by Zakharov [52] and Booth-Morrison et al. [53] demonstrated that Si enhances breakdown of the Sc solid solution.

The patent by Willey [23] demonstrated that Sc additions can be used to increase strength in 6xxx-series alloys. He provided examples of Sc additions to commercial Al-Mg-Si alloys including 6061, 6351, 6161 and 6063. One example shows a 10 ksi

**Table 15.4** Strength of Al-Mg-Si alloy sheet with and without 0.3 wt% Sc addition

Alloy	Tensile strength, ksi	Yield strength, ksi	Elongation, %
Al-0.7 Mg-0.4Si (No Sc)	22.4	14.2	13
Al-0.7 Mg-0.4Si (0.3 Sc)	31.2	24.4	13

Cast ingots with 75% cold roll reduction. Aged for 8 h at 285–290 °C after cold work

**Table 15.5** Mechanical properties of Sc-modified Al-Mg-Si 6061 alloy with 0.4 wt% Sc [54]

Alloy	Yield strength (YS)	Ultimate tensile strength (UTS)	Elongation, %
6061	30.7	35.1	19
M6061	40.2	45.7	13

increase in yield strength (Table 15.4) for an Al-0.7 Mg-0.4Si model alloy (i.e., composition falls within registered range for AA6063) after aging for 4 h at 177 °C and 8 h at 288 °C. Strengths in a peak-aged T6-type temper was not disclosed in this patent so it is not clear how the Sc addition affected the precipitation Mg-Si  $\beta'$ -type strengthening precipitates in these alloys.

Tack [54] disclosed that adding 0.4 wt% Sc to the Al-Mg-Si alloy 6061 increased strength by approximately 10 ksi in a T6-type temper and reduced hot cracking during welding (Table 15.5).

The Russian alloy 1370 was developed as an advanced material to be used in place of the Al-Cu-Mg alloy AA2024 [55]. Kurenkov et al. [56] reported that the alloy “*is used as skin on fuselages of hydroplanes and in naval aviation.*” This alloy is strengthened by Mg<sub>2</sub>Si ( $\beta$ ) and Al<sub>5</sub>Cu<sub>2</sub>Mg<sub>8</sub>Si (Q) precipitates and is reported to have similar Mg, Si and Cu levels with AA6065 but also contains Zr, Sc and Ni. No effects of the Sc addition on precipitation of these strengthening phases were reported in the work by Kolobnev and coworkers [55, 57]. Work by Litynska-Dobrzynska [58] showed that needlelike Q-type strengthening phases coexist with fine spherical Al<sub>3</sub>Sc dispersoids after heat treatment and artificial aging in an Al-1.0 Mg-0.6Si-1.0Cu-0.4Sc-0.2Zr wrought alloy.

Recent work [59] has focused on developing heat treatment schedules that promote precipitation of fine Al-Sc-strengthening dispersoids that can be used to augment and enhance strengthening from the Mg-Si and Mg-Si-Cu precipitates that are typically found in 6xxx-series-type alloys. Novel heat treatment schedules have been disclosed in the U.S. patent application by Langan and Dorin [59] that optimize nucleation of dispersoids and extract all of the strengthening from the Sc addition.

Work [20, 60, 61] performed at Deakin University and Michigan Tech demonstrated that trace Sc additions increased strength in conventional low-strength 6xxx-series alloys (i.e., 6005) by as much as 100 MPa. One key outcome of this work found that the addition of Sc did not adversely impact extrudability of these alloys [60]. This is commercially important because these 6xxx-series alloys are typically selected based on low product cost. Thus, a high-strength Sc-containing variant can potentially be produced cheaper than conventional highly alloyed 6xxx-series alloys (e.g., 6111).

### 15.3.5 Other Alloy Systems

“High-strength” Sc-containing Al alloys with good electrical conductivity have been developed for use in electric wire. Aluminum alloys are used extensively in overhead transmission cable based on their low density relative to Cu giving them much high specific conductivity [62]. Alloying to increase strength typically reduces conductivity in Al alloys. Conductor grade alloys [63] such as AA1350 have high conductivity (e.g., 60.9% IACS (International Annealed Copper Standard)) but low strength (e.g., UTS of only 180 MPa). Higher-strength alloys such as AA6201 (e.g., UTS 330 MPa) are used in overhead cable but the conductivity is much lower (e.g., 52.5% IACS).

The Fe-containing, 8xxx-series alloys have been developed for cable applications. Iron additions increase strength and creep resistance (i.e., cables can heat up during service) due to precipitation of Al-Fe phase. Zhang et al. [64] looked at increasing strength and creep resistance in an 8xxx-series alloy by adding Sc. They pointed out that precipitation strengthening using the REE europium (Er) and transition elements Sc and hafnium (Hf) increases mechanical properties without degrading conductivity.

Work led by Professor Dunand and Seidman at NWU has focused on understanding nucleation of L12 precipitates in Al alloys. A key part of this work focused on finding alloying elements that can substitute for Sc [65]. NanoAl LLC was formed to commercialize Al alloys containing heavy rare earth elements (HREE), particularly Er and Yb that supplement or substitute for Sc. NanoAl LLC and General Cable [66] disclosed an approach that utilized inoculant elements to modify nanoscale precipitation of Zr in Al alloys including Al-Fe 8xxx-type alloys that can contain Sc. Zhang et al. [67] demonstrated that adding Sc to Al-Zr alloys significantly improves creep resistance. Testing is ongoing to qualify these materials for commercial applications.

NanoAl LLC is also working [68] to develop an Al-Sc-Zr alloy that can be used to encapsulate ceramic reinforcement tiles in hybrid composite armor systems. The Sc-containing alloy can be used in the as-cast condition, where no high-temperature heat treatment is required. Moderate strength can be obtained in this alloy using a two-step aging schedule designed to minimize thermal stress on the encapsulated ceramic tiles; 4 h at 300 °C plus 8 h at 425 °C. Research on this system was supported by NanoAL LLC and the U.S. Army.

Deutschland GmbH and Co KG [69] disclosed a Sc-containing Al alloy for bonding wire. The patent specifies composition and processing that ensure that 30% of the Sc is present in fine Al<sub>3</sub>Sc dispersoids having a diameter of less than 25 nm. This wire [70] demonstrated considerable improvement in lifetime after wire bonding in microelectronic applications.

## 15.4 Scandium Supply

In 2020, the world market for  $\text{Sc}_2\text{O}_3$  was estimated to be approximately between 15 and 30 tonnes, the bulk of which came from Chinese suppliers. As far as metal markets go, the Sc market is small, opaque and highly concentrated. There is no primary mine supply, with material mostly recovered from waste-processing operations. The Sc market is classically chicken and egg. Widespread commercial adoption has been hampered by lack of supply, with customers unprepared to commit to single-source or ‘high-risk’ supply chains. In turn, the lack of supply growth has kept prices too high to motivate commercial adoption. Scandium oxide prices are extremely volatile and are highly influenced by volumes and delivery times. Over recent years, oxide prices have been quoted from \$1000/kg to over \$4000/kg. In addition, price supply has been controlled for political reasons. As reported by the Congressional Research Service [71], “...in July 2010, China announced that it would reduce its export quota of rare earth elements by 70% during the second half of 2010 over the previous year’s level (or a 40% drop for the full year over 2009 levels).” The same report goes on to state that “In September 2010, China reportedly delayed shipments of rare earth to Japan (the world’s largest rare earth importer) for about two months because of a territorial dispute.”

Of the approximately 15–30 tonnes of  $\text{Sc}_2\text{O}_3$  consumed each year, it is estimated that more than half is consumed in solid oxide fuel cells (SOFC). Bloom Energy Corporation [72] accounts for most of this demand. The balance of demand is consumed mostly in the production of high-strength Al-Sc alloys used in aerospace programs (e.g., China and Russia) and a variety of other military applications.

Future commercialization of Sc-containing alloys will be contingent upon development of a market for supply of Sc. A key factor in the development of the market is establishing a stable price. At present, the price per weight percent Sc addition in a wrought alloy is directly related to the price of  $\text{Sc}_2\text{O}_3$  (Fig. 15.9). Royset and Ryum [4] suggest that the cost for Sc in the master alloy needs to fall to an equivalent price of \$400/kg Sc before widespread adoption of Sc-containing alloys can take place.

A review [73] of sources for recovery of Sc concluded that red mud and Ni-laterite mining provide the most promising resources for increased future production of Sc. Other sources currently under evaluation include mining of Sc and other REE from deep-sea sediments.

### 15.4.1 Mining Sc-Containing Minerals

“High concentrations” of Sc are found in two minerals – thortveitite ( $(\text{Sc},\text{Y})_2\text{Si}_2\text{O}_7$ ) and kolbeckite ( $\text{ScPO}_4 \cdot 2\text{H}_2\text{O}$ ). Thortveitite can contain up to 45% Sc in the form of  $\text{Sc}_2\text{O}_3$  [74]. Deposits containing these minerals are rare and it was estimated that



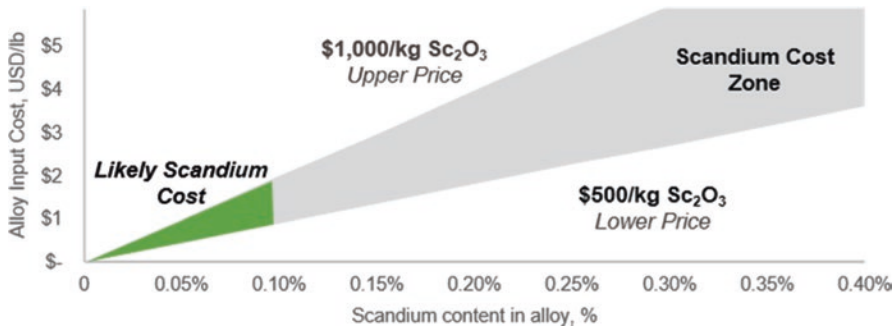


Fig. 15.9 Alloy input cost in USD/lb. as a function of Sc content in alloy

only about 20% of the Sc supply came these sources in 2003 [73]. These minerals are mined from deposits in Madagascar and Norway [75]. Scandium has also been recovered from  $(\text{Sc},\text{Y})_2\text{Si}_2\text{O}_7$  tailings at the crystal mountain fluorite mine near Darby, Montana, in the United States [73].

### 15.4.2 Extraction of Scandium as a Coproduct

#### Rare Earth Mining

Scandium is present in solid solution in REE-containing minerals (e.g., aegirine ( $\text{NaFeSi}_2\text{O}_6$ ), bastnaesite ( $(\text{M})(\text{CO}_3)\text{F}$ ;  $\text{M} = \text{Light rare earth element (LREE), Ca}$ ) and monazite ( $(\text{M})\text{PO}_4$ ;  $\text{M} = \text{Ce, La, Nd, Th}$ )). A paper published in 2018 by Williams-Jones and Vasyukova [76] reports that “Approximately 90% of global scandium production (15 tonnes) comes from the Bayan Obo deposit in China.” Unfortunately, this claim is not supported by the reference they cite [77]. They [76] also report that “... the scandium resource has been estimated at 140,000 tonne.” The operation of this mine may reportedly [78] be controlled by the newly formed Inner Mongolia Baotou Steel Rare-Earth (Group) Hi-Tech Co, but Grandfield [72] reports that Sc extraction is no longer active at the Bayan Obo mine in China.

#### Iron/Uranium Mining

High concentrations of Sc (approximately 100 ppm) are present in a polymetallic ore body near Zhovti Vody in Ukraine [77]. Scandium recovered at the Nova Fe/uranium (U) mine in this ore body was used in high-strength Al alloys during Soviet times. In the mid-1990s, a Canadian company, Ashurst Technologies Corp., worked under a joint venture with their Ukrainian partners (VostGOK and The Institute for Problems in Materials Science (IPMS)) to mine Sc at the Nova Mine and produce

Al-Sc master alloy. This venture successfully created demand for Sc but was unsuccessful at generating supply. It is reported that the Nova mine was permanently closed in 2004 [77].

Dalur, JCS, a subsidiary of Atomredmetzoloto (ARMZ) Uranium Holding Company/Mining Division of Rosatom State Atomic Energy Corporation, announced commissioning of mobile sorption units to increase Sc output during in-situ U leaching [79]. The United States Geological Survey (USGS) reported production capacities in Dalur, Kurgan region of 570 kg  $\text{Sc}_2\text{O}_3$  per year and 24.5 tonnes of Al-Sc alloy per year [80].

### Nickel Laterite Mining

A Sc-refining plant designed to recover 7.5 tonnes of  $\text{Sc}_2\text{O}_3$  per year is currently operated by Sumitomo in association with the Taganito HPAL Ni/cobalt (Co) project in the Philippines [81].

Research and development efforts focused on Sc extraction are currently underway at the Nikel Kobalt Ni laterite mine in Gordes, Turkey [82, 83]. The USGS reports that a pilot plant at this facility produced small quantities (less than 1 kg) of ammonium scandium hexafluoride ( $\text{NH}_4)_3\text{ScF}_6$ ) in 2021 [80].

Several projects under development in Australia bring promise of directly mining for Sc. Clean TeQ's Sunrise Project [24] hosts one of the world's largest and highest-grade accumulations of Sc ever discovered. Here Sc will be produced as a by-product, making production costs very low, with initial production estimated at 85 tpa  $\text{Sc}_2\text{O}_3$ , with the potential to be easily expanded (i.e., 2x). A large-scale pilot plant campaign was carried out in 2015 on ore from Sunrise to produce  $\text{Sc}_2\text{O}_3$  samples for potential customers.

### 15.4.3 Extraction of Scandium from Mining and Industrial Waste Streams

#### TiO<sub>2</sub> Production Waste Stream

Historically, most of the  $\text{Sc}_2\text{O}_3$  from China has been extracted from acid waste generated during production of titania ( $\text{TiO}_2$ ) pigment. A 2018 review by CM Group authored by John Grandfield [72] reported that the total  $\text{Sc}_2\text{O}_3$  production capacity in China was 60 tonnes/year with an additional 20 tonnes of capacity "*in the pipeline*." They also reported a utilization rate of only 20% in 2017 resulting in a total production of only 12 tonnes of  $\text{Sc}_2\text{O}_3$ .

Several projects outside of China have also focused on recovery of Sc from  $\text{TiO}_2$  waste streams. In one such effort, the Clean TeQ's Clean-iX® continuous ion-exchange process was optimized. This work culminated in operation of a large-scale

Sc recovery pilot plant with a major Japanese TiO<sub>2</sub> producer in 2015. Unfortunately, recovery of Sc does not reduce the volume of the waste that must be disposed. This resulted in limited adoption of this process by western pigment producers. The SCALE and ScaVanger projects [84, 85] funded by the European Union (EU) are revisiting the approach for developing production of Sc from European metallurgical wastes. TRONOX, a global leader in mining, processing and manufacture of TiO<sub>2</sub> pigment, is participating in these projects and is providing samples from its waste stream as part of the SCALE project.

Recent work by Rio Tinto [86] resulted in development of “*an innovative process to extract high purity scandium oxide from the waste streams of titanium dioxide production, at its ilmenite mine in Havre-Saint-Pierre, Quebec.*” This facility, scheduled to initiate commercial production in 2021, will be the first Sc recovery facility in North America that is capable of producing three tonnes of Sc<sub>2</sub>O<sub>3</sub>/year.

### **Red Mud – Waste Stream from Processing Bauxite into Alumina**

Scandium is naturally associated in Al ore (bauxite) with aluminum-phosphate minerals containing up to 0.8% Sc<sub>2</sub>O<sub>3</sub> [73]. The Bayer Process that is used to extract Al from bauxite enriches the Sc level in the waste residue (i.e., red mud). Notably, Sc in red mud can be twice the level contained in the ore. Wang [73] estimated that 4100 tonnes of Sc<sub>2</sub>O<sub>3</sub> could theoretically be extracted annually. They assumed an 80% recovery rate from the 102.5 Mt. of red mud with an average Sc<sub>2</sub>O<sub>3</sub> content of 50 ppm that was generated worldwide in 2008.

The EU initiated a major initiative, SCALE, to develop technologies required to extract Sc from dilute mediums [84]. Recovery methods were being developed to produce Sc compounds and Al-Sc alloys from by-products of Al and Ti mining and processing.

Rusal [87] is continuing pilot studies for production of Sc from red mud at the Urals Al smelter (UAZ) in Russia. This facility will produce approximately 3 tonnes of Sc<sub>2</sub>O<sub>3</sub>/year [87].

### **Extraction of Scandium from Coal Fly Ash**

A number of reviews and laboratory studies have identified fly ash from coal-fired power generation as a potential source for Sc [75, 88, 89]. Scandium levels in fly ash vary based on origin of coal, with levels from 0.5 to 297 ppm reported in the literature [75]. Chernoburova and Chagnes [90] report that processes for extracting Sc have “*reached the commercialization level.*” It is interesting to note that the USGS does not include a discussion about Sc in their Fact Sheet entitled “*Rare Earth Elements in Coal and Coal Fly Ash.*” [91]

### Phosphogypsum Waste – Residual from Phosphorus Fertilizer

Phosphate rock (fluorapatite ( $\text{Ca}_5(\text{PO}_4)_3\text{F}$ )) is digested to generate the phosphoric acid ( $\text{H}_3\text{PO}_4$ ) used in the production of the phosphorus fertilizer DAP (Diammonium Phosphate ( $(\text{NH}_4)_2\text{HPO}_4$ )) and MAP (Monoammonium Phosphate ( $\text{NH}_4\text{H}_2\text{PO}_4$ )). Up to 6 tonnes of waste are produced for every tonne of phosphorus pentoxide ( $\text{P}_2\text{O}_5$ ) produced [92], with approximately 200 million tonnes/year of waste produced worldwide [92–94]. The bulk (i.e., 65–95 wt%) of the waste phosphogypsum (synthetic  $\text{CaSO}_4 \cdot 2\text{H}_2\text{O}$ ) product is made up of gypsum (naturally occurring  $\text{CaSO}_4 \cdot 2\text{H}_2\text{O}$ ) [94] which cannot be used in construction because the waste contains trace metals and radioactive elements. Only about 15 tonnes of the synthetic  $\text{CaSO}_4 \cdot 2\text{H}_2\text{O}$  has been recycled [94], with more than 7 billion tonnes [93] held in large untreated stockpiles. The synthetic  $\text{CaSO}_4 \cdot 2\text{H}_2\text{O}$  waste stream, which contains up to 1 wt% REE [92–94], has been identified as a potential source for Sc recovery [75]. A waste synthetic  $\text{CaSO}_4 \cdot 2\text{H}_2\text{O}$  sample from Florida contained 218 ppm of total REEs with only 1 ppm of Sc [94].

## 15.5 Production of Scandium Master Alloys

Suzdaltsev [95] reviewed advantages and disadvantages associated with producing Al-Sc master alloys using conventional approaches including (1) direct fusion of Sc with Al, (2) aluminothermic synthesis using Sc salts or oxide and (3) electrowinning in molten salts using Sc salts or oxide.

Direct alloying of pure Sc with Al provides the most control of composition and allows higher levels of Sc to be added. Unfortunately, production of pure Sc is difficult and expensive. Royset [3] points out that the cost of producing master alloys from pure Sc is approximately ten times more expensive than from  $\text{Sc}_2\text{O}_3$ .

The master alloy used to produce Sc-containing wrought alloys is currently produced primarily using proprietary aluminothermic-type approaches. Direct reduction of Sc-fluoride ( $\text{ScF}_3$ ) or  $\text{Sc}_2\text{O}_3$  with Al is difficult because Sc is more electronegative than Al. These reactions may progress with formation of an intermediate aluminum scandium ( $\text{Al}_3\text{Sc}$ ) phase [95]. An early Soviet patent awarded to Skorovarov [96] extracts Sc from scandium fluoride ( $\text{ScF}_3$ ) in molten Al under vacuum. A patent [97] awarded to Alcoa demonstrated that Al-Sc master alloy can be produced by placing pellets of pressed Al and  $\text{Sc}_2\text{O}_3$  powder into molten Al. Examples from this patent identified low Sc levels (approximately 0.5 wt%) in the master alloy. In another approach [95], a two-step process was used to manufacture Al-Sc master alloy by extracting Sc from  $\text{ScF}_3$  or  $\text{Sc}_2\text{O}_3$ . In the first step, potassium (K) and Na fluorine-scandates are formed by reacting  $\text{ScF}_3$  or  $\text{Sc}_2\text{O}_3$  in a molten flux: NaF-KCl with  $\text{ScF}_3$  and NaF-KCl-AlF<sub>3</sub> with  $\text{Sc}_2\text{O}_3$ . The scandates ( $\text{K}_3\text{ScF}_6$  or  $\text{Na}_3\text{ScF}_6$ ) are reacted with molten Al to form the Al-Sc master alloy. A Russian patent using a similar approach was awarded to Borisovich and Yurievich [98]. Modified approaches involving reaction with scandium sulfide ( $\text{Sc}_2\text{S}_3$ ) are currently under investigation [99].

Extensive research and development (R&D) [95, 100, 101] has been devoted to developing electrowinning approaches for extracting  $\text{Sc}_2\text{O}_3$  into Al-Sc master alloys. A number of patents have been awarded or filed based on this approach including [102, 103], however, the authors of this chapter are currently unaware of any commercial application of this method.

## 15.6 Conclusions

The benefits of Sc when used as an alloying element in Al are well established. These benefits largely come from the formation of nm-size  $\text{L1}_2 \text{Al}_3\text{Sc}$  dispersoids that provide significant strengthening to the Al alloys. This strengthening comes from various mechanisms, summarized as the “*Four pillars*” of Sc in Al which include

- Grain refinement
- Increase of recrystallization temperature
- Dispersoids strengthening
- Nucleation of additional strengthening phases.

Scandium has also been reported to positively influence a range of other properties such as formability, weldability and corrosion resistance. Despite all of these benefits, the number of commercial applications to date has been very limited and restricted to a few niche low-volume markets. For the industry to widely adopt Sc, a larger and reliable supply of Sc is required. When this can be achieved, a long-term supply of low-cost Sc will ensure the use of Sc in a wide range of industrial sectors.

## References

1. T. Dorin, M. Ramajayam, A. Vahid, T. Langan, Aluminium scandium alloys, in *Fundamentals of Aluminium Metallurgy*, (Elsevier, 2018), pp. 439–494. <https://doi.org/10.1016/B978-0-08-102063-0.00012-6>
2. L.S. Toropova, D.G. Eskin, M.L. Kharakterova, *Advanced Aluminum Alloys Containing Scandium: Structure and Properties* (Eds., Gordon & Breach, Amsterdam, 1998)
3. J. Royset, Scandium in aluminium alloys, physical metallurgy, properties and applications. *Metall. Sci. Technol.* **25**(2) (2007)
4. J. Røyset, N. Ryum, Scandium in aluminium alloys. *Int. Mater. Rev.* **50**(1), 19–44 (2005). <https://doi.org/10.1179/174328005X14311>
5. F. Palm, *Hypereutectic High Strength AlMgSc Profile Materials Melt-Spun Scalmalloy – A New Family of Weldable and Corrosion Free Al Alloys with 500–850 MPa Strength* (AeroMat, 2006)
6. M.E. Drits, L.S. Toropova, Y.G. Bykov, F.L. Guschina, V.I. Yelagin, Y.A. Filatov, Metastable state diagram of the Al-Sc system in the range rich in aluminium. *Russ. Metall (USSR)* **1**, 150 (1983)

7. A.F. Norman, P.B. Prangnell, R.S. McEwen, The solidification behaviour of dilute aluminium–scandium alloys. *Acta Mater.* **46**(16), 5715–5732 (1998). [https://doi.org/10.1016/S1359-6454\(98\)00257-2](https://doi.org/10.1016/S1359-6454(98)00257-2)
8. Z. Jia, J. Røyset, J.K. Solberg, Q. Liu, Formation of precipitates and recrystallization resistance in Al–Sc–Zr alloys. *Trans. Nonferrous Metals Soc. China* **22**(8), 1866–1871 (2012). [https://doi.org/10.1016/S1003-6326\(11\)61399-X](https://doi.org/10.1016/S1003-6326(11)61399-X)
9. V.V. Zakharov, Effect of scandium on the structure and properties of aluminum alloys. *Met. Sci. Heat Treat.* **45**(7–8), 8 (2003)
10. I. Polmear, D. St. John, J.-F. Nie, M. Qian, *Light Alloys: Metallurgy of the Light Metals* (Butterworth-Heinemann, 2017)
11. D.N. Seidman, E.A. Marquis, D.C. Dunand, Precipitation Strengthening at Ambient and Elevated Temperatures of Heat-Treatable Al(Sc) Alloys. *Acta Mater.* **50**(16), 4021–4035 (2002). [https://doi.org/10.1016/S1359-6454\(02\)00201-X](https://doi.org/10.1016/S1359-6454(02)00201-X)
12. E. Nembach, *Particle Strengthening of Metals and Alloys* (Wiley, New York, 1997)
13. T. Dorin, M. Ramajayam, T.J. Langan, Impact of scandium and zirconium on extrudability, microstructure and hardness of a binary Al–Cu alloy. *Mater. Today Proc.* **10**, 242–247 (2019). <https://doi.org/10.1016/j.matpr.2018.10.402>
14. B. Rouxel, M. Ramajayam, T.J. Langan, J. Lamb, P.G. Sanders, T. Dorin, Effect of dislocations, Al<sub>3</sub>(Sc,Zr) distribution and ageing temperature on  $\Theta'$  precipitation in Al–Cu–(Sc)–(Zr) alloys. *Materialia* **9**, 100610 (2020). <https://doi.org/10.1016/j.mtla.2020.100610>
15. L. Jiang, B. Rouxel, T. Langan, T. Dorin, Coupled segregation mechanisms of Sc, Zr and Mn at  $\theta'$  interfaces enhances the strength and thermal stability of Al–Cu alloys. *Acta Mater.* **206**, 116634 (2021). <https://doi.org/10.1016/j.actamat.2021.116634>
16. B.A. Chen, L. Pan, R.H. Wang, G. Liu, P.M. Cheng, L. Xiao, J. Sun, Effect of solution treatment on precipitation behaviors and age hardening response of Al–Cu alloys with Sc addition. *Mater. Sci. Eng. A* **530**, 607–617 (2011)
17. V.V. Zakharov, T.D. Rostova, On the possibility of scandium alloying of copper-containing aluminum alloys. *Met Sci Heat Treat* **37**(2), 65–69 (1995). <https://doi.org/10.1007/BF01157047>
18. T. Dorin, M. Ramajayam, J. Lamb, T. Langan, Effect of Sc and Zr additions on the microstructure/strength of Al–Cu binary alloys. *Mater. Sci. Eng. A* **707**, 58–64 (2017). <https://doi.org/10.1016/j.msea.2017.09.032>
19. J. Dumbre, S.K. Kairy, E. Anber, T. Langan, M.L. Taheri, T. Dorin, N. Birbilis, Understanding the formation of (Al,Si)<sub>3</sub>Sc and V-Phase (AlSc<sub>2</sub>Si<sub>2</sub>) in Al–Si–Sc alloys via ex situ heat treatments and *in Situ* transmission electron microscopy studies. *J. Alloys Compd.* **861**, 158511 (2021). <https://doi.org/10.1016/j.jallcom.2020.158511>
20. T. Dorin, M. Ramajayam, S. Babaniaris, T.J. Langan, Micro-segregation and precipitates in as-solidified Al–Sc–Zr–(Mg)–(Si)–(Cu) alloys. *Mater. Charact.* **154**, 353–362 (2019). <https://doi.org/10.1016/j.matchar.2019.06.021>
21. S. Babaniaris, M. Ramajayam, L. Jiang, T. Langan, T. Dorin, Tailored precipitation route for the effective utilisation of Sc and Zr in an Al–Mg–Si alloy. *Materialia* **10**, 100656 (2020). <https://doi.org/10.1016/j.mtla.2020.100656>
22. E.P. Kwon, K.D. Woo, S.H. Kim, D.S. Kang, K.J. Lee, J.Y. Jeon, The effect of an addition of Sc and Zr on the precipitation behavior of AA6061 alloy. *Met. Mater. Int.* **16**(5), 701–707 (2010). <https://doi.org/10.1007/s12540-010-1002-y>
23. L. A. Willey, *Aluminum Scandium Alloy*. 3619181, November 9, 1971.
24. R. Friedland, *Syerston Nickel Cobalt Scandium Project*, Investor Presentation, February 2017. <https://wcsecure.weblink.com.au/clients/sunriseenergy/v2/headline.aspx?headlineid=3464171>
25. Aluminum Association. *International Alloy Designations and Chemical Composition Limits for Wrought Aluminum and Wrought Aluminum Alloys*, (2015)
26. Aluminium and Wrought Aluminium Alloys Grades. GOST 4784-2019 (2019)

27. Y.A. Filatov, V.I. Yelagin, V.V. Zakharov, New Al–Mg–Sc alloys. *Mater. Sci. Eng. A* **280**(1), 97–101 (2000). [https://doi.org/10.1016/S0921-5093\(99\)00673-5](https://doi.org/10.1016/S0921-5093(99)00673-5)
28. M.S. Domack, D.L. Dicus, *Evaluation of Sc Bearing Aluminum Alloy C557 for Aerospace Applications April 2002*; NASA/TM-2002-211633 (2002)
29. J.N. Fridlyander, W. Bozich, The properties of semi-products of 1460 alloy (Al–Cu–Li–Sc) and 1421 alloy (Al–Mg–Li–Sc) at 293K and 77K. *Proc. 6th Int. Conf. Alum. Alloys (ICAA-6)* **2**, 937–941 (1998)
30. M. Jia, Z. Zheng, Z. Gong, Microstructure evolution of the 1469 Al–Cu–Li–Sc alloy during homogenization. *J. Alloys Compd.* **614**, 131–139 (2014). <https://doi.org/10.1016/j.jallcom.2014.06.033>
31. Surface Treatment Technologies. *Alloy Data Sheet for Alloy 7xa* (2009)
32. T. Langan, *Sporting Good Alloys Developed by Ashurst Technologies, Inc* (2000)
33. I.N. Fridlyander, Aluminum Alloys in Aircraft in the Periods of 1970–2000 and 2001–2015. *Metal Sci. Heat Treat.* **43**(1), 6–10 (2001)
34. I.N. Fridlyander, From the history of aluminum alloys: A developer’s memoir. *Her. Russ. Acad. Sci.* **78**(4), 416–420 (2008). <https://doi.org/10.1134/S101933160804014X>
35. I.N. Fridlyander, S.F. Danilov, E.N. Malysheva, T.A. Gorokhova, N.N. Kirkina, Structure and properties of Al–Li alloys alloyed with scandium, in *Aluminum Lithium*, vol. 1, (Sixth International Aluminum–Lithium Conference, Garmisch-Partenkirchen, 1992), pp. 381–386
36. I.N. Fridlyander, A.G. Bratukhin, V.G. Davydov, *Soviet Al–Li Alloys of Aerospace Application*, vol 1 (Sixth International Aluminum–Lithium Conference, Garmisch-Partenkirchen, 1992), pp. 35–42
37. J.R. Pickens, T.J. Langan, E. Barta, Weldability of Al-5 Mg-2 Li-0. 1 Zr alloy 01420, in *Aluminium-lithium alloys III*, (Institute of Metals, 1986), pp. 137–147
38. Lenczowski, B., Innovative Aluminum Lightweight Technologies for Aerospace Applications, 2016. [https://www.amap.de/fileadmin/files/Kolloquium/27.\\_Kolloquium/2016\\_AMAP\\_Innovative\\_Aluminium\\_Blanka\\_Lenczowski\\_AGI-AMAP-S.PDF](https://www.amap.de/fileadmin/files/Kolloquium/27._Kolloquium/2016_AMAP_Innovative_Aluminium_Blanka_Lenczowski_AGI-AMAP-S.PDF)
39. T. Mertens, *Investigation on the Corrosion Behavior of Clad Free Aluminium Alloys* (2019). <https://asm.confex.com/asm/aero19/webprogram/Paper47937.html>. Accessed 11 May 2021
40. S. Spangel, A. Bürger, P. Rumpf, P. Meyer, Y. Marchal, *AlMgSc Alloys – A Novel Approach for Various Aircraft Applications*. <https://asm.confex.com/asm/aero19/webprogram/Paper47979.html>. Accessed 11 May 2021
41. M. Vorel, S. Hinsch, M. Konopka, M. Scheeree, AlMgSc Alloy 5028 Status of Maturation, in *Proceedings of the 7th European Conference for Aeronautics and Space Sciences*, (Proceedings of the 7th European Conference for Aeronautics and Space Sciences. Milano, Italy, 3–6 July 2017, Milano, 2017), p. 9 <https://doi.org/10.13009/EUCASS2017-633>
42. J.A. Lee, P.S. Chen, Aluminum–Scandium Alloys: Material Characterization, Friction Stir Welding, and Compatibility with Hydrogen Peroxide (*MSFC Center Director’s Discretionary Fund Final Report, Project No. 04–13*); NASA/TM—2004–213604; NASA (2004)
43. D.G. Eskin, Scandium Applications in Aluminum Alloys: Overview of Russian Research in the 20th Century, in *Light Metals 2018*, The Minerals, Metals & Materials Series, ed. by O. Martin, vol. 2018, (Springer, Cham), pp. 1565–1572. [https://doi.org/10.1007/978-3-319-72284-9\\_204](https://doi.org/10.1007/978-3-319-72284-9_204)
44. A.Y. Krokhin, V.K. Mann, D.K. Ryabov, N.A. Babitskiy, Effect of Treatment Parameters on Structure, Mechanical and Corrosion Properties of Al–Mg–Sc Alloy Forgings with Reduced Concentration of Scandium, in *Light Metals 2018*, The Minerals, Metals & Materials Series, ed. by O. Martin, (Springer, Cham, 2018), pp. 1573–1580. [https://doi.org/10.1007/978-3-319-72284-9\\_205](https://doi.org/10.1007/978-3-319-72284-9_205)
45. D. Fokin, *High-Strength Al–Mg–Sc Alloy with 0.1wt.%Sc Content* (2017). [https://www.scaletechnology.eu/wp-content/uploads/2018/12/16-D.-Fokin\\_High-Strength-Al-Mg-Sc\\_alloys.pdf](https://www.scaletechnology.eu/wp-content/uploads/2018/12/16-D.-Fokin_High-Strength-Al-Mg-Sc_alloys.pdf). Accessed 12 May 2021
46. W.T. Tack, I.L.H. Hansson, *Aluminum Alloys Containing Scandium with Zirconium Additions*. US 5620652, April 15, 1997

47. *Atlas Poles – antsol2*. <https://sites.google.com/site/antsol2/home/atlas-poles>. Accessed 24 May 2021
48. T.C. Stall, N. Grosvenordale, J. Luty, K.R. Fleury, N.W. Spencer, *Scandium Containing Aluminum Alloy Firearm*. US 6,711,819, March 30, 2004.
49. T. Langan, *Aluminum-Zinc-Magnesium-Scandium Alloys and Methods of Fabricating Same*. 8,133,331, March 13, 2012.
50. M.L. Kharakterova, D.G. Eskin, L.S. Toropova, *Precipitation Hardening in Ternary Alloys of the Al-Sc-Cu and Al-Sc-Si Systems*. 6 (n.d.)
51. J. Royset, H. Hovland, N. Ryum, An investigation of dilute Al-Sc-Si alloys. *Mater. Sci. Forum* **396–402**, 619–624 (2002)
52. V.V. Zakharov, Stability of the solid solution of scandium in aluminum. *Met Sci Heat Treat* **39(2)**, 61–66 (1997). <https://doi.org/10.1007/BF02467664>
53. C. Booth-Morrison, Z. Mao, M. Diaz, D.C. Dunand, C. Wolverton, D.N. Seidman, Role of Silicon in Accelerating the Nucleation of Al<sub>3</sub>(Sc,Zr) Precipitates in Dilute Al–Sc–Zr Alloys. *Acta Mater.* **60(12)**, 4740–4752 (2012). <https://doi.org/10.1016/j.actamat.2012.05.036>
54. W.T. Tack, *Aluminum-Scandium Alloys*. US 5597529, January 28, 1997
55. N.I. Kolobnev, L.B. Khokhlatova, S.V. Samokholav, A.A. Alekseev, S.V. Sbitneva, T.I. Tararaeva, V.I. Popov, Heat treatment effect on properties of AlMgSiCu 1370 alloy. *Mater. Sci. Forum* **519–521**, 519–524 (2006)
56. Y.A. Kuzenkov, S.V. Oleinik, S.A. Karimova, T.G. Pavlovskaya, Chromate-free conversion coatings on 1370 aluminum alloy. *Prot. Met. Phys. Chem. Surf.* **48(7)**, 784–789 (2012). <https://doi.org/10.1134/S2070205112070106>
57. N.I. Kolobnev, L.B. Ber, L.B. Khokhlatova, D.K. Ryabov, Structure, properties and application of alloys of the Al – Mg – Si – (Cu) system. *Met. Sci. Heat Treat.* **53(9–10)**, 440–444 (2012). <https://doi.org/10.1007/s11041-012-9412-8>
58. L. Lityńska-Dobrzyńska, Precipitation of phases in Al-Mg-Si-Cu alloy with Sc and Zr additions during heat treatment. *SSP* **130**, 163–166 (2007). <https://doi.org/10.4028/www.scientific.net/SSP.130.163>
59. T.J. Langan, T. Dorin, *Heat Treatment of Aluminum Alloy Containing Silicon and Scandium*. US20190249283A1 (n.d.)
60. S. Babaniaris, M. Ramajayam, L. Jiang, R. Varma, T. Langan, T. Dorin, Effect of Al<sub>3</sub>(Sc,Zr) dispersoids on the hot deformation behaviour of 6xxx-series alloys: A physically based constitutive model. *Mater. Sci. Eng. A* **793**, 139873 (2020). <https://doi.org/10.1016/j.msea.2020.139873>
61. T. Dorin, M. Ramajayam, S. Babaniaris, L. Jiang, T.J. Langan, Precipitation sequence in Al–Mg–Si–Sc–Zr alloys during isochronal aging. *Materialia* **8**, 100437 (2019). <https://doi.org/10.1016/j.mtla.2019.100437>
62. J.R. Davis, *Aluminum and Aluminum Alloys* (ASM International, 1993)
63. F.U. Flores, D.N. Seidman, D.C. Dunand, N.Q. Vo, Development of high-strength and high-electrical-conductivity aluminum alloys for power transmission conductors, in *Light Metals 2018*, The Minerals, Metals & Materials Series, ed. by O. Martin, (Springer, Cham, 2018), pp. 247–251. [https://doi.org/10.1007/978-3-319-72284-9\\_34](https://doi.org/10.1007/978-3-319-72284-9_34)
64. J. Zhang, X. Jiang, M. Ma, B. Jiang, B. Wang, D. Yi, Effect of scandium micro-alloying on the creep resistance properties of Al-0.7Fe alloy cables. *Mater. Sci. Eng. A* **699**, 194–200 (2017). <https://doi.org/10.1016/j.msea.2017.05.088>
65. N.Q. Vo, D.C. Dunand, D.N. Seidman, Improving aging and creep resistance in a dilute Al–Sc alloy by microalloying with Si, Zr and Er. *Acta Materialia* **63**, 73–85 (2014). <https://doi.org/10.1016/j.actamat.2013.10.008>
66. S. Srinivas, C.A. Muojekwu, J.S. Sekunda, R.S. Baker, N.J. Duer N.Q. Vo, Cables and Wires Having Conductive Elements Formed from Improved Aluminum-Zirconium Alloys. 10,450,637, October 22, 2019



67. J. Zhang, B. Wang, H. Wang, C. Zhang, Improvement in compressive creep resistance of Al-0.2Zr alloy with L12 structured Sc-enriched precipitates. *Mater. Charact.* **159**, 110024 (2020). <https://doi.org/10.1016/j.matchar.2019.110024>
68. N.Q. Vo, J. Sorensen, E.M. Klier, A. Sanaty-Zadeh, D. Bayansan, D.N. Seidman, D.C. Dunand, Development of a precipitation-strengthened matrix for non-quenchable aluminum metal matrix composites. *JOM* **68**(7), 1915–1924 (2016). <https://doi.org/10.1007/s11837-016-1896-z>
69. E. Milke, S. Thomas, U. Geissler, M. Schneider-Ramelow, *Aluminum Alloy Wire for Bonding Applications*. US 9,397,064, July 19, 2016
70. U. Geissler, S. Thomas, M. Schneider-Ramelow, B. Mukhopadhyay, K.-D. Lang, Aluminum-scandium: A material for semiconductor packaging. *J. Elec. Mater.* **45**(10), 5456–5467 (2016). <https://doi.org/10.1007/s11664-016-4756-2>
71. The Congressional Research Service. *Rare Earth Elements in National Defense: Background, Oversight Issues, and Options for Congress*. R41744, 44 (2013)
72. J. Grandfield, *10-Year Outlook for the Global Scandium Market to 2028*. <http://scale-project.eu/scandium-workshop/>. Accessed 4 Jan 2022
73. W. Wang, Y. Pranolo, C.Y. Cheng, Metallurgical processes for scandium recovery from various resources: A review. *Hydrometallurgy* **108**(1–2), 100–108 (2011). <https://doi.org/10.1016/j.hydromet.2011.03.001>
74. K. Pyrzyńska, K. Kilian, M. Pęgiel, Separation and purification of scandium: From industry to medicine. *Sep. Purif. Rev.* **48**(1), 65–77 (2019). <https://doi.org/10.1080/15422119.2018.1430589>
75. A.B. Botelho Junior, D.C.R. Espinosa, J. Vaughan, J.A.S. Tenório, Recovery of scandium from various sources: A critical review of the state of the art and future prospects. *Miner. Eng.* **172**, 107148 (2021). <https://doi.org/10.1016/j.mineng.2021.107148>
76. A.E. Williams-Jones, O.V. Vasyukova, The economic geology of scandium, the runt of the rare earth element litter. *Econ. Geol.* **113**(4), 973–988 (2018). <https://doi.org/10.5382/econgeo.2018.4579>
77. W.P.C. Duyvesteyn, G.F. Putnam, *White Paper – Scandium; A Review of the Element, Its Characteristics, and Current and Emerging Commercial Applications EMC Metals Corporation (TSX: EMC.TO)*. <https://scandiummining.com/site/assets/files/5740/scandium-white-paperemc-website-june-2014-.pdf>. Accessed 5 Jan 2022
78. *Chinese Rare Earth Giant Born*. *Mining.com*. <https://www.mining.com/chinese-rare-earth-giant-born-62354/>. Accessed 5 Jan 2022
79. ARMZ Uranium Holding Co. – *Dalur Commissioned Mobile Sorption Units to Increase Scandium Output*. <https://www.armz.ru/en/press-center/news/2407-dalur-commissioned-mobile-sorption-units-to-increase-scandium-output>. Accessed 18 Jan 2022
80. J. Gambogi, Scandium, *U.S. Geological Survey, Mineral Commodity Summaries*, January 2021
81. *Sumitomo to Launch Scandium Recovery Business* | S&P Global Market Intelligence. [https://www.spglobal.com/marketintelligence/en/news-insights/trending/qlunwrl\\_e4fvbhfsa7a-xcg2](https://www.spglobal.com/marketintelligence/en/news-insights/trending/qlunwrl_e4fvbhfsa7a-xcg2). Accessed 9 Nov 2022
82. S. Kaya, *Critical Raw Materials Data Management & European Scandium Inventory Workshops – Scale Project*. <http://scale-project.eu/scandium-workshop/>. Accessed 18 Jan 2022
83. *Meta Nikel Kobalt A.Ş. | Gördes Meta Nickel Cobalt Facility*. <http://www.metanikel.com.tr/en/gordes-meta-nickel-cobalt-facility/srch-scandium>. Accessed 18 Jan 2022
84. *SCALE Project – Scandium – Aluminium Europe*. <http://scale-project.eu/>. Accessed 18 Jan 2022
85. *Scavanger – Home*. <https://www.scavanger.eu/>. Accessed 1 Feb 2022
86. J. Gambogi, Scandium, *U.S. Geological Survey (Mineral Commodity Summaries, 2020)*
87. *RUSAL Produces First Output of Scandium Oxide*. [https://rusal.ru/en/press-center/press-releases/rusal\\_produces\\_first\\_output\\_of\\_scandium\\_oxide/](https://rusal.ru/en/press-center/press-releases/rusal_produces_first_output_of_scandium_oxide/). Accessed 23 Mar 2021
88. D.T. Bradshaw, L. Tolhurst, *Commercial Recovery of Metals from Coal Ash*. 9.

89. R.S. Blissett, N. Smalley, N.A. Rowson, An investigation into six coal fly ashes from the United Kingdom and Poland to evaluate rare earth element content. *Fuel* **119**, 236–239 (2014). <https://doi.org/10.1016/j.fuel.2013.11.053>
90. O. Chernoburova, A. Chagnes, The Future of Scandium Recovery from Wastes. *Mater. Proc.* **5**(1), 55 (2021). <https://doi.org/10.3390/materproc2021005055>
91. Fact Sheet, (2019). <https://doi.org/10.3133/fs20193048>
92. E. Saadaoui, N. Ghazel, C. Ben Romdhane, N. Massoudi, Phosphogypsum: Potential uses and problems – A review. *Int. J. Environ. Stud.* **74**(4), 558–567 (2017). <https://doi.org/10.1080/00207233.2017.1330582>
93. O. Yahorava, Hydrothermal Modification of Phosphogypsum to Improve Subsequent Recovery of Rare Earths (2018)
94. H. Liang, P. Zhang, Z. Jin, D. DePaoli, Rare Earths Recovery and Gypsum Upgrade from Florida Phosphogypsum. *Miner. Metall. Proc.* **34**(4), 201–206 (2017). <https://doi.org/10.19150/mmp.7860>
95. A.V. Suzdaltsev, A.Y. Nikolaev, Y.P. Zaikov, *A Modern Ways for Al-Sc Master Alloy Production* (Ariel University Press, 2019), pp. 161–167
96. D. Skorovarov, *Method of Producing Aluminium-Scandium Alloying Composition*. SU873692A1 (n.d.)
97. G.P. Tarcy, P. Boro, *Method for Making a Light Metal Rare Earth Metal Alloy*. 5,037,608, August 6, 1991
98. S. Borisovich, S. Yurievich, *Method for Obtaining Aluminium-Scandium Alloy Combination*. RU2507291 (n.d.)
99. C. Stinn, A. Allanore, Selective sulfidation for rare earth element separation, in *Rare Metal Technology 2022*, The Minerals, Metals & Materials Series, ed. by T. Ouchi, G. Azimi, K. Forsberg, H. Kim, S. Alam, N.R. Neelameggham, A.A. Baba, H. Peng, (Springer, Cham, 2022), pp. 259–278. [https://doi.org/10.1007/978-3-030-92662-5\\_25](https://doi.org/10.1007/978-3-030-92662-5_25)
100. A.V. Suzdaltsev, A.A. Filatov, A.Y. Nikolaev, A.A. Pankratov, N.G. Molchanova, Y.P. Zaikov, Extraction of scandium and zirconium from their oxides during the electrolysis of oxide–fluoride melts. *Russ. Metall.* **2018**(2), 133–138 (2018). <https://doi.org/10.1134/S0036029518020180>
101. X. Wang, Preparation of aluminum master alloys by electrolytic co-deposition in Hall-Héroult cells, in *Light Metals 2022*, The Minerals, Metals & Materials Series, ed. by D. Eskin, (Springer, Cham, 2022), pp. 392–401. [https://doi.org/10.1007/978-3-030-92529-1\\_53](https://doi.org/10.1007/978-3-030-92529-1_53)
102. D. Shangchao, W. Wang, L. Yeda, L. Mingchuan, S. Ninglei, L. Dong, L. Guo, *The Method of Electrolytic Preparation Aluminium-Scandium Alloy*. CN 10,755,7817A, January 9, 2018.
103. A.C. Powell, M.R. Earlam, S.A. Barriga, R. Salvucci, *Method of Aluminum-Scandium Alloy Production*. US 2020/0407863 A1 (n.d.)

# Chapter 16

## Rare Earth Oxide Applications in Ceramic Coatings for Turbine Engines



David L. Poerschke and Jessica A. Krogstad

### 16.1 Protective Ceramic Coating Applications and Requirements

Gas turbines underpin the global energy and transportation infrastructure. Presently, turbine engines provide propulsion for most commercial cargo and passenger aircraft. Natural gas turbines have grown in importance for both base and peak-load electrical generation, and currently provide approximately 40% of U.S. electricity demand [1]. Ceramic coatings play a critical role in protecting structural components in the hot section of these turbines, enabling higher operating temperatures for improved efficiency and performance. These coatings serve two primary functional roles. Thermal barrier coatings (TBC) insulate internally cooled components, implying the selection of materials and microstructures that lead to low thermal conductivity ( $\kappa$ ) of the coating [2–4]. Environmental barrier coatings (EBC) are used to protect the components from degradation caused by reactions with corrosive species in the combustion gases [5–7]. For EBCs, the primary requirements are low permeability of oxidizing species including oxygen and water vapor, and resistance to volatilization either by direct evaporation of the coating material or by reactions with water vapor that form gaseous hydroxides.

In addition to these primary functions, the coatings must satisfy additional performance and durability requirements. First, the coatings must be mechanically robust. A core challenge is managing the thermo-cyclic stresses that arise due to a coefficient of thermal expansion (CTE,  $\alpha$ ) mismatch ( $\Delta\alpha$ ) between the coating and

---

D. L. Poerschke (✉)  
University of Minnesota Twin Cities, Minneapolis, MN, USA  
e-mail: [dpoersch@umn.edu](mailto:dpoersch@umn.edu)

J. A. Krogstad  
University of Illinois Urbana Champaign, Urbana, IL, USA

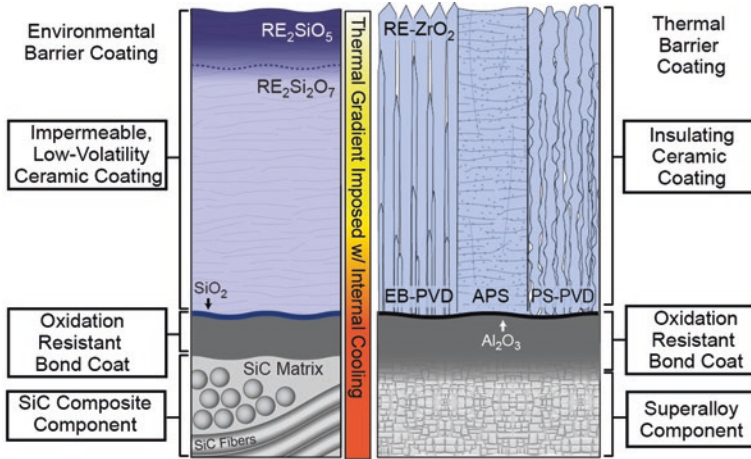
component or between coating layers. The magnitude of the thermal stress (or stored elastic strain energy) in the coating is determined by the product of the degree of mismatch and temperature change ( $\Delta\alpha\Delta T$ ), the coating stiffness and the coating thickness. To limit these stresses, it is necessary to either select a coating material that minimizes  $\Delta\alpha$  or to employ compliant porous or segmented microstructures to decrease the coating stiffness. High coating toughness, achieved through a combination of material selection and architecture control, is also important to limit coating cracking caused by thermal stresses or foreign object impact. Second, the coatings must be thermochemically stable in the combustion environment. This requires (1) a high melting temperature, (2) thermodynamic compatibility with the substrate and other coating layers, (3) the absence of deleterious phase transformations when heating and cooling over the service temperature range, (4) low volatility, and for porous coatings, (5) resistance to sintering [3, 7]. Additionally, the coatings must resist degradation caused by corrosive sulfate and oxide deposits that arise when ingested debris (i.e., salts, dusts, ashes) accumulates on the coating surfaces [8, 9].

This broad list of performance requirements significantly limits the menu of suitable coating materials and often necessitates the use of multilayer coating architectures to achieve the desired characteristics. With few exceptions, RE oxides play a critical role in most commercially relevant and prospective coating materials. Historically, the industrially preferred materials contained RE oxides that are present in minor fractions to stabilize specific crystal structures. However, materials comprising RE oxides as a primary component are growing in prominence. The utilization of RE oxides will continue to increase in future generations of coating architectures, due to growing demand for turbine engines, increasing utilization of coatings and increased concentration of RE oxides in these coatings. This chapter reviews the current coating applications, introduces relevant RE-containing material families and discusses the coating development trends and anticipated impacts on REO utilization.

### ***16.1.1 Thermal Barrier Coatings (TBC) for Ni-Based Alloys***

Today, TBCs are used primarily to protect nickel-based superalloys which are used throughout the turbine hot section, including combustor liners, shrouds, vanes (nozzles) and blades (buckets). The TBC system comprises multiple layers that each serve specific functions. An oxidation-resistant metallic or aluminide bond coat protects the underlying alloy by forming an adherent, slow-growing alpha-alumina ( $\alpha\text{-Al}_2\text{O}_3$ ) thermally grown oxide (TGO). RE metals are often used as a component of these bond coats to improve the oxidation characteristics and TGO adherence, as elaborated elsewhere in this book. An insulating ceramic top coat is then deposited to provide thermal protection. The typical architecture is shown in Fig. 16.1.

The CTEs of the superalloys which fall in the range of  $14 \times 10^{-6}/\text{K}$  to  $18 \times 10^{-6}/\text{K}$  [10, 11] exceed those of most ceramic materials capable of high temperature



**Fig. 16.1** Schematic showing typical TBC architecture on a Ni-based superalloy deposited using various techniques, and EBC architecture on a SiC-based ceramic matrix composite. (Adapted from Poerschke et al. [8] Typical coating thicknesses range from  $\sim 100 \mu\text{m}$  to  $\sim 1 \text{ mm}$  depending on the component geometry and application requirements)

service. The most used TBC materials are RE-stabilized zirconia ( $\text{ZrO}_2$ ) and RE zirconates that have CTEs in the range of  $10 \times 10^{-6}/\text{K}$  to  $12 \times 10^{-6}/\text{K}$  [12–14]. It is generally assumed that at high temperature the thermal stresses are relaxed due to creep in the alloy. Upon cooling at the end of the service cycle, compressive stresses generated because of this negative  $\Delta\alpha$  between the TBC and alloy can drive coating delamination. To reduce the magnitude of these thermal stresses the coatings are typically deposited with a porous or segmented microstructure which reduce the in-plane stiffness and the total thermal conductivity of the coating.

Several effective techniques have been developed to achieve these engineered microstructures [15, 16]. The selection of the coating material, including the identity of the RE oxide, is influenced by the capabilities (and limitations) of the processing methods. Electron-beam physical vapor deposition (EB-PVD) utilizes electron-beam heating to evaporate a source material within a vacuum chamber, and the component to be coated is rotated through the vapor plume. A combination of preferential growth of specific crystallographic directions and shadowing effects associated with the component rotation result in the growth of columnar grains. The size, shape and distribution of porosity in these coatings can be tuned through process parameter control [17–20]. EB-PVD coatings provide good functional performance and durability, but the vacuum processing requirements increase cost. There are also technical limitations for depositing materials containing components with disparate vapor pressures, which can lead to significant composition variations through the thickness of the deposited coating [21, 22]. In contrast, for atmospheric plasma spray (APS) deposition particles of the ceramic feedstock are injected into a plasma torch directed toward the substrate. The particles melt in flight, forming a splat-like morphology as they impact and accumulate on the component surface.

Processing parameters can be tuned to control the coating density, toughness and to induce controlled vertical cracks to reduce the in-plane stiffness [23, 24]. This deposition approach is more efficient and thus lower cost than EB-PVD and is also amenable to a larger range of materials. However, reduced compliance and the incidence of microstructure defects can reduce durability compared to EB-PVD coatings. Hybrid processing approaches utilizing plasma torches with liquid solution or suspension precursors (i.e., suspension or precursor plasma spray, SPS or PPS), or plasma spray at reduced pressures (i.e., plasma spray PVD, or PS-PVD) can capture desirable attributes of both techniques [25, 26].

Degradation caused by the accumulation of ingested debris on coating surfaces is a core challenge to overcome in future coating designs. These deposits which are commonly termed “CMAS” owing to the common presence of calcium oxide, magnesium oxide, alumina and silica ( $\text{CaO}$ ,  $\text{MgO}$ ,  $\text{Al}_2\text{O}_3$  and  $\text{SiO}_2$  – CMAS), form when ingested silicious debris adheres to coating surfaces and melts. This melt readily penetrates the open porosity used to achieve thermal strain tolerance. Upon cooling, elevated stresses in the stiffened coating drive premature coating cracking and spallation [27, 28]. There is a strong tendency for reactions to occur between the adhered debris and the RE oxides present in many coating materials. In some cases, the reactions destabilize the coating materials further contributing to the accelerated degradation [29]. In other cases, the reactions have proven to be beneficial by rapidly crystallizing the infiltrating melt [30]. Understanding the relationships between the REO chemistry in the coating and the reactions with various CMAS deposits has been an area of intense interest. The effectiveness of RE oxides to partially mitigate the degrading effects of CMAS on TBCs influences decisions related to the selection of specific RE compositions in coating materials, and is partially responsible for the increased REO utilization in coatings [8, 31].

Today, ongoing TBC development efforts focus on identifying new materials, architectures and processing pathways to further increase the temperature capabilities and durability of the coating systems. As elaborated in Sect. 16.3, the broad trend is toward multilayer coating architectures that combine multiple RE-containing coating materials to meet specific performance requirements.

### ***16.1.2 Environmental Barrier Coatings (EBC) for Ceramics and Ceramic Composites***

There is significant interest in leveraging the lower mass density and increased temperature capability of monolithic ceramics or ceramic fiber-reinforced ceramic matrix composites (CMC) based on silicon carbide (SiC), silicon nitride ( $\text{Si}_3\text{N}_4$ ) and  $\text{Al}_2\text{O}_3$  to replace metallic turbine components [32]. Si-based ceramics form a slow-growing  $\text{SiO}_2$  TGO which protects the ceramic from high temperature oxidation in dry environments. However, the presence of water vapor significantly accelerates

oxidation due to increased oxidant transport through the silica-TGO and volatilization of the protective TGO via the formation of volatile silicon hydroxides [33–35]. Without protection, the SiC loss rate can approach 1 mm per 1000 h under typical turbine operating conditions which significantly limits the lifetime of components that are typically only several millimeters thick [36]. For Al<sub>2</sub>O<sub>3</sub>-fiber-reinforced composites, water vapor increases the fiber creep rate and reduces the creep lifetime [37, 38]. Volatilization via reactions forming gaseous aluminum hydroxides also leads to surface recession [35, 39].

EBCs have been developed to protect ceramics from these deleterious reactions by limiting access of the combustion gases to the structural ceramic. This application requires a dense, low-permeability structure (Fig. 16.1). SiC and Si<sub>3</sub>N<sub>4</sub> have CTEs around  $5 \times 10^{-6}/\text{K}$ . Early EBCs for SiC used ZrO<sub>2</sub>-based materials. Testing showed that the tensile stresses generated in the coating upon cooling due to the positive  $\Delta\alpha$  caused cracks to penetrate from the surface through the coating and into the underlying composite. Localized degradation occurred when combustion gas penetrated these cracks [40, 41]. Subsequent development efforts focused on identifying materials that minimize the  $\Delta\alpha$ , and have identified several families of RE silicates offering desirable property combinations [6]. The higher CTE of alumina-based composites (approximately  $8 \times 10^{-6}/\text{K}$ ) requires EBC materials with CTEs falling between those of the RE-zirconia and RE-silicate coating materials. Their development has focused on RE aluminates and RE oxides [42, 43]. EBCs are typically deposited by plasma spray processing owing to the ability to deposit diverse materials chemistries and to produce dense microstructures [6, 44, 45]. There are also ongoing efforts to develop slurry-based processing approaches for improved control over coating microstructure and chemistry [46].

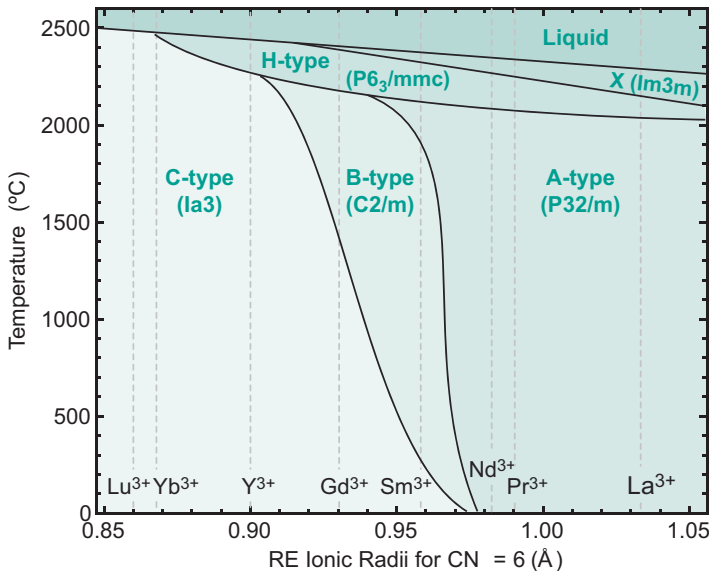
## 16.2 Coating Material Families and Properties

Today, most commercially relevant TBC and EBC materials are based on RE-stabilized ZrO<sub>2</sub>, zirconate compounds comprising roughly equimolar combinations of RE oxides and ZrO<sub>2</sub>, and RE silicate compounds. Other material families, including RE aluminates, phosphates and tantalates have been studied at the laboratory scale for prospective future use in coating architectures. In some cases, the choice of the specific REO is driven by specific materials chemistry or property considerations. In other cases, the selection is more heavily influenced by techno-economic factors such as processibility, cost and availability. This section reviews the relevant REO chemistry and then introduces each of these materials families along with key properties and performance characteristics that drive materials selection for coatings applications.

### 16.2.1 Rare Earth Oxide Chemistry

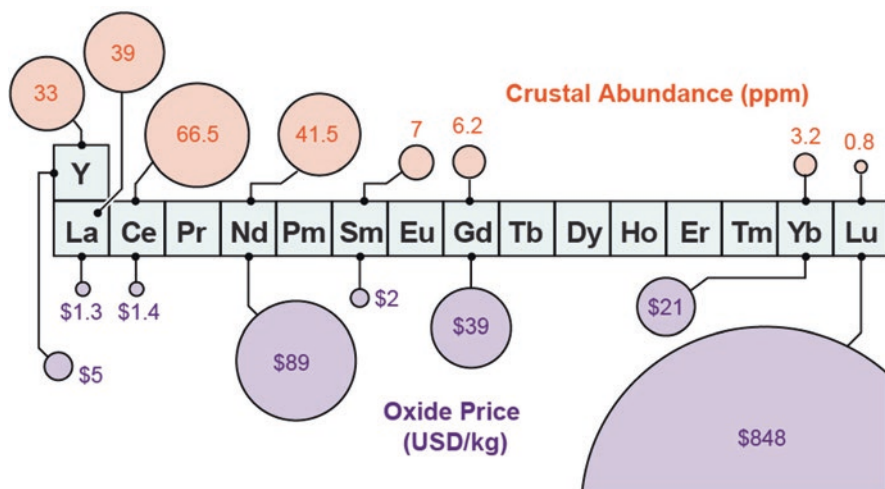
The RE elements, defined here to include yttrium (Y) and the lanthanides, predominantly form trivalent sesquioxides ( $\text{RE}_2\text{O}_3$ , or on a single-cation basis,  $\text{REO}_{1.5}$ ) [47, 48]. Exceptions include cerium (Ce) which readily forms a dioxide ( $\text{CeO}_2$ ) and praseodymium (Pr) and terbium (Tb) which can form complex ordered phases between  $\text{RE}_2\text{O}_3$  and  $\text{REO}_2$ . Owing to the similarity in the valence electron configuration, the chemistry of the sesquioxides is determined primarily by  $\text{RE}^{3+}$  cationic size which decreases by approximately 20% when moving across the period from lanthanum (La) to lutetium (Lu). As pure oxides, the smaller  $\text{RE}^{3+}$  tend to form a cubic structure (C-type, space group  $\text{Ia}\bar{3}$ ) in which each cation is coordinated by six oxygen anions (Fig. 16.2). The stable coordination number increases with the  $\text{RE}^{3+}$  size. At intermediate  $\text{RE}^{3+}$  size, the stable B-type structure ( $\text{C}2/\text{m}$ ) contains a combination of 6- and 7-coordinate cation sites. The A-type structure favored by the larger  $\text{RE}^{3+}$  has a coordination number of seven. Upon heating above 2000 °C, all  $\text{RE}_2\text{O}_3$  except lutetium(III) oxide ( $\text{Lu}_2\text{O}_3$ ) undergo polymorphic transformations prior to melting.

Figure 16.3 shows known abundance of various RE elements in the earth's crust [50] and the current market prices for refined oxides of the RE elements that have received the most interest with respect to coating development. There is



**Fig. 16.2** Stability of RE sesquioxides as a function of cationic radius and temperature based on thermodynamic assessment of each oxide. (Stability data adapted from Zinkevich [48] using ionic radii from Shannon [49])





**Fig. 16.3** Crustal abundance [50] and approximate wholesale oxide price [51] for RE oxides used commercially or widely studied for use in TBCs and EBCs

considerable variation in cost and availability. In general, the lighter RE elements (e.g., Y, La and Ce) have higher abundance and lower cost. Neodymium (Nd) is also abundant, but the significant demand on this element for permanent magnet manufacturing leads to higher market competition and price. The smaller, heavier REs tend to be less abundant and more expensive. Based solely on cost and abundance, lanthanum oxide ( $\text{La}_2\text{O}_3$ ) and cerium(IV) oxide ( $\text{CeO}_2$ ) would be the obvious choice for coating applications. However, as elaborated in later sections, processing challenges and inferior properties for some of the relevant phases favor the use of other, more expensive, RE oxides in the coating materials.

The C-type  $\text{RE}_2\text{O}_3$  show reasonable stability in combustion environments [52] and their CTE is comparable with  $\text{Al}_2\text{O}_3$ , making them viable choices for protecting  $\text{Al}_2\text{O}_3$ -based ceramic composites. For this application, development has focused on  $\text{Y}_2\text{O}_3$  owing to its lower cost and higher abundance compared to similarly sized cations [42, 43]. The tendency for temperature-dependent transformations from C- to B-type or B- to A-type for the intermediate-size RE oxides [48] complicates their use for TBC and EBC applications as pure oxides. Of the larger RE cations, direct use of  $\text{La}_2\text{O}_3$  is not favored due to its propensity for hydration which would cause coating failure as the oxide is converted to a friable hydroxide upon exposure to water. Likewise, the reducibility of  $\text{CeO}_2$  to cerium(III) oxide ( $\text{Ce}_2\text{O}_3$ ) presents challenges for coating stability during processing and in service.

### 16.2.2 Zirconia and Hafnia-Based Coating Materials

Zirconia offers many desirable attributes for use in TBCs including high melting temperature and resistance to hydroxide-mediated volatilization in the combustion environment. However, polymorphic transformations in pure  $\text{ZrO}_2$  preclude its use directly as a coating material. At room temperature,  $\text{ZrO}_2$  exists with a monoclinic crystal structure ( $m$ ,  $P2_1/c$ ). It transforms to tetragonal ( $t$ ,  $P4_2/nmc$ ) around  $1170^\circ\text{C}$  and then to the cubic fluorite structure ( $F$ ,  $Fm\bar{3}m$ ) around  $2370^\circ\text{C}$ . The martensitic  $t$ - to  $m$ - $\text{ZrO}_2$  transformation upon cooling is accompanied by a shear strain of 0.16 and a  $\sim 5\%$  volume expansion [53, 54]. These strains generate significant local stresses within the material, leading to microcracking and eventual comminution upon thermal cycling. The addition of RE oxides to  $\text{ZrO}_2$  can suppress this transformation by stabilizing the tetragonal phase against spontaneous transformation to monoclinic upon cooling. Further REO additions stabilize the cubic fluorite phase allowing the material to be shifted away from a composition space where  $m$ - and  $t$ - $\text{ZrO}_2$  are stable (Fig. 16.4). As an additional benefit, the aliovalent substitution of  $\text{RE}^{3+}$  for  $\text{Zr}^{4+}$  introduces oxygen vacancies that reduce the thermal conductivity by acting as phonon-scattering centers [55].

Most  $\text{ZrO}_2$ -based materials contain several percent hafnia ( $\text{HfO}_2$ ) based on their natural mineral abundance, and the difficulty in separating the elements due to their chemical similarity. However, when separated and used intentionally,  $\text{HfO}_2$  provides benefits in TBC and EBC applications. First, solid solutions involving an increased fraction of  $\text{Hf}^{4+}$  on  $\text{Zr}^{4+}$  sites can further reduce the thermal conductivity

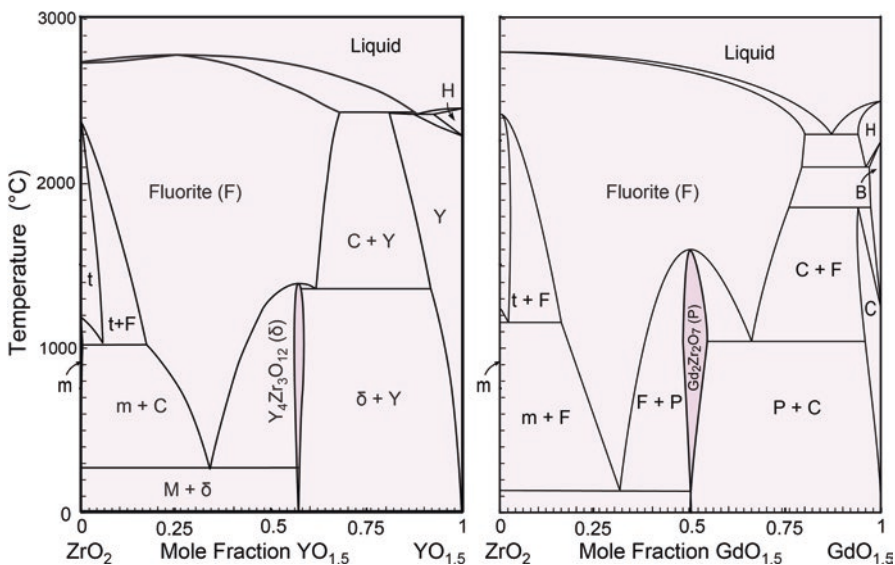


Fig. 16.4 Equilibrium phase diagrams for the  $\text{YO}_{1.5}$ - $\text{ZrO}_2$  and  $\text{GdO}_{1.5}$ - $\text{ZrO}_2$  systems. (Adapted from Leckie et al. [56] and Fabrichnaya et al. [57])

of the ceramics because the mass contrast between the  $\text{Hf}^{4+}$  on  $\text{Zr}^{4+}$  can inhibit phonon transport [55, 58]. This behavior presents a distinct advantage for the stabilized tetragonal phases, wherein the  $\text{RE}^{3+}$  content is insufficient to achieve a similar effect. Nonetheless, for zirconate (or hafnate) compounds, it is more cost-effective to select a  $\text{RE}^{3+}$  that shows mass contrast with  $\text{Zr}^{4+}$  than to introduce a significant amount of  $\text{HfO}_2$  into the material. Second, some reports suggest that  $\text{HfO}_2$  and some RE hafnate compound exhibit lower CTE than the equivalent  $\text{ZrO}_2$ -based phases [59–61]. This would be advantageous in their use as coatings on ceramic composites. However, significant price differential and limitations on availability presently limit the commercial adoption of  $\text{HfO}_2$ -containing materials.

The remainder of this section introduces RE-stabilized zirconia phases and RE zirconate and hafnate compounds that are relevant to TBC and EBC technology.

### Rare Earth-Stabilized Tetragonal Phases

The earliest studies of potential TBC systems, which were all based on air plasma-sprayed zirconias, explored the relationship between yttria content and coating longevity. By the late 1970s, the relationship between the tetragonal phase and durability was solidified – coatings comprised of  $\text{ZrO}_2 + 7$  to 8 wt% (7.6–8.7 mol%)  $\text{YO}_{1.5}$ , commonly referred to as 7YSZ, delivered maximum resistance to cyclic failure [62]. More than 40 years later, 7YSZ remains the dominant industrial standard for TBCs even as other compositions expand their market share to address the challenges introduced by increasing operating temperatures [63]. The success of “non-transformable” tetragonal ( $t'$ ) 7YSZ lies in the fact that this composition remains tetragonal across all temperatures in the thermal cycle [64, 65]. This metastable tetragonal phase ( $t'$ ) benefits from activation of a ferroelastic toughening mechanism, not available in the fully stabilized cubic phases [3, 66], yet avoids the stress-induced phase transformations that earned transformable zirconia the name of “ceramic steel” [67–70]. Thus, microcracks arising from the significant volume change can be suppressed in a thermally cycled environment. In reality, this “non-transformable” phase is a metastable, supersaturated composition that falls in the tetragonal + fluorite two-phase field in the equilibrium diagram shown in Fig. 16.4 at typical operating temperatures above 1000 °C, and which ultimately decomposes into a Y-lean tetragonal phase ( $t$ ) and a Y-rich cubic fluorite phase ( $F$ ) after sufficient time at the turbine operating temperature. Following this phase separation reaction, the  $\text{YO}_{1.5}$ -depleted  $t$ - $\text{ZrO}_2$  is prone to phase transformation to the monoclinic structure upon cooling with the associated undesirable volume changes, while the fluorite phase that is formed lacks the intrinsic toughness of the  $t'$ - $\text{ZrO}_2$ . Historically, this slow destabilization process has not been life-limiting, but increasing operating temperatures increases the rate of destabilization and must be more carefully considered in the future [71–73].

Tetragonal zirconia TBCs stabilized by other  $\text{RE}^{3+}$  cations have been studied in some depth, but the systematic differences in the zirconia-rich side of the binary phase space are subtle and, likewise, contribute only subtle changes in the overall

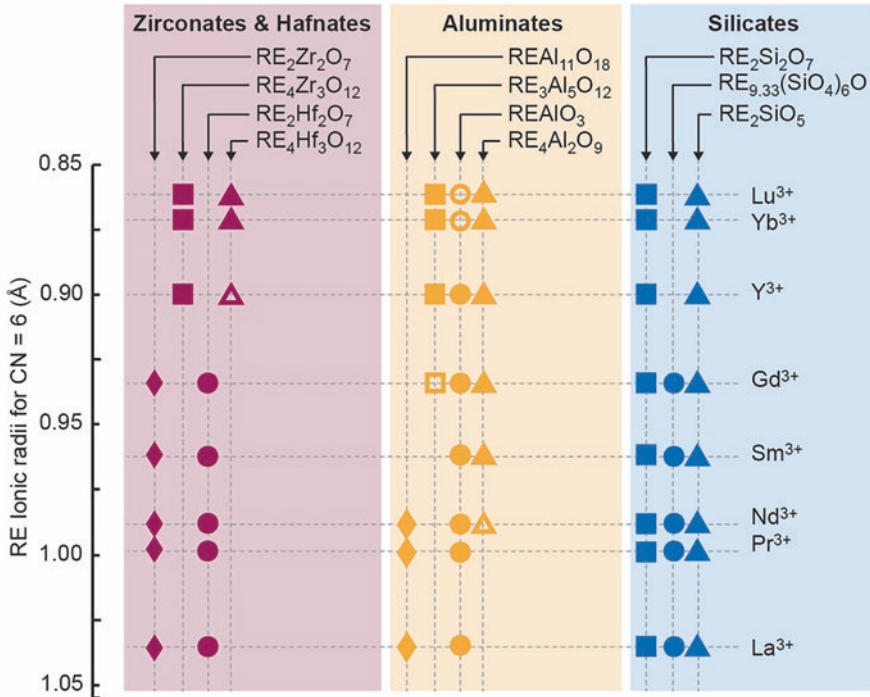
performance of tetragonal zirconia coatings [2, 74, 75]. For example, the compositional width of the  $t + F$  phase field systematically decreases with decreasing ionic radius of the  $RE^{3+}$  cation – as a result the compositional window for the nontransformable  $t'$ -phase is reduced, but so too is the driving force for its destabilization. This effect was most clearly demonstrated by Cairney et al. when comparing Y and ytterbium (Yb) doped tetragonal zirconia [76]. Co-doping zirconia with both Y and an additional RE cation has met some success in reducing the sinterability of the coatings, especially with the RE cation is larger than Y (e.g., La) [77]. This strategy has also been reported to reduce the thermal conductivity as was already noted for mixtures of  $Hf^{4+}$  and  $Zr^{4+}$  cations [57], but the effect is somewhat minimized by the compositional restrictions necessary to maintain the tetragonal phase (e.g., sum of  $Y^{3+} + RE^{3+} < 7$  to 8 mol%).

Co-doping strategies have expanded beyond the bounds of trivalent lanthanide rare earth oxides, to include  $CeO_2$ , titania ( $TiO_2$ ), tantalum(V) oxide ( $Ta_2O_5$ ), niobium(V) oxide ( $Nb_2O_5$ ) and numerous iterations that include at least one trivalent cation. These ternary spaces have largely been explored in hopes of identifying a fully stabilized tetragonal phase to avoid the longer-term destabilization issues associated with 7YSZ while maintaining enhanced toughness through maximization of ferroelastic toughening mechanisms. Both goals have been realized to some extent in the  $ZrO_2$ - $CeO_2$ - $TiO_2$  [77–79] and  $ZrO_2$ -Yb(Y) $O_{1.5}$ - $TaO_{2.5}$  ternary systems [21, 80–82]. However, as the compositional complexity of these novel coating systems increases, the processing challenges associated with achieving the necessary compositionally homogenous coatings also expand. Thus, there are presently no public reports of the practical application of such ternary zirconia-based coatings in commercial service.

## Rare Earth Zirconates and Hafnates

Increasing the  $RE_2O_3$  content in zirconia beyond the RE-stabilized tetragonal phase further reduces the thermal conductivity by increasing the concentration of phonon-scattering oxygen vacancies. Despite their lower thermal conductivity, coatings based on the cubic fluorite structure with moderately higher RE concentrations than the  $t$ - $ZrO_2$  counterparts (e.g., in the range of 25–30 mol%  $REO_{1.5}$ ) have not found utility as TBCs because their combination of low toughness and poor sintering resistance reduces their durability.

Instead, the development of lower- $\kappa$ ,  $ZrO_2$ -based materials has focused on RE zirconate compounds based on the pyrochlore ( $RE_2Zr_2O_7$ ,  $Fm\bar{3}m$ ) and  $\delta$ -phase ( $RE_4Zr_3O_{12}$ ,  $R\bar{3}$ ) structure. As illustrated in Fig. 16.5, the pyrochlores are stable for the larger  $RE^{3+}$ , and the  $\delta$ -phase is stable for the smaller  $RE^{3+}$ . These compositions exhibit improved thermal stability, sintering resistance and 30–50% lower thermal conductivity than comparable RE-stabilized  $t$ - $ZrO_2$  [55, 83, 84]. Pyrochlore and  $\delta$ -phase are derived from the fluorite structure and are defined by distinct ordering of the oxygen vacancies that are introduced as  $RE_2O_3$  is dissolved into  $ZrO_2$ . Both phases revert to the disordered defect-fluorite structure at high temperatures



**Fig. 16.5** Stability of binary RE zirconate, hafnate, aluminate and silicate compounds relevant to the design of TBCs and EBCs. Filled symbols indicate that there is general agreement that the compound is stable. Open symbols indicate incomplete or inconsistent data in the literature

(Fig. 16.4). However, the order-disorder reactions tend to be sluggish and occur without significant changes in the unit cell volume or thermal properties and therefore do not represent a significant challenge for TBC performance. In addition, partial ordering (i.e., within discrete nano domains in the material) can occur over a range of compositions on either side of the nominal stoichiometry [56, 85]. These characteristics relax the coating design constraints near the center of the REO<sub>1.5</sub>-ZrO<sub>2</sub> systems, enabling selection of materials that deviate from the nominal stoichiometries and allowing for modest processing-related variations in coating composition without significant changes in properties.

Models suggest that the RE<sup>3+</sup> size influences the thermal conductivity for the pyrochlore and  $\delta$ -phase zirconates, with the lowest thermal conductivity at intermediate RE<sup>3+</sup> size. However, experimental measurements have not revealed meaningful differences among this family of materials [13, 55, 83, 84, 86]. Likewise, while the RE<sup>3+</sup> identity would likely influence the CTE, available evidence suggests that this variation is limited to 1 to 2  $\times 10^{-6}$ /K across the period, and that the CTE for the zirconates is generally slightly less than 7YSZ [13, 59]. Thus, the choice of RE<sup>3+</sup> is driven as much by practical considerations such as cost and processibility as by these functional thermal properties. Initial efforts to develop RE zirconate TBCs

focused on  $\text{La}_2\text{Zr}_2\text{O}_7$  which is advantageous, in part, due to its lower cost compared to other materials. Tests showed promising coating performance but also revealed challenges controlling the composition during processing due to the high  $\text{La}_2\text{O}_3$  vapor pressure as compared to  $\text{ZrO}_2$  [22, 87]. Additionally, it proved more difficult to achieve consistent columnar morphology in EB-PVD  $\text{La}_2\text{Zr}_2\text{O}_7$  compared to conventional 7YSZ coatings [22]. There have been successful lab-scale demonstrations of a variety of pyrochlore and  $\delta$ -phase coatings including  $\text{Nd}_2\text{Zr}_2\text{O}_7$  [88],  $\text{Sm}_2\text{Zr}_2\text{O}_7$  [89], a  $\text{YO}_{1.5}$ - $\text{ZrO}_2$  solid solution adjacent  $\text{Y}_4\text{Zr}_3\text{O}_{12}$  [90, 91] and  $\text{Yb}_4\text{Hf}_3\text{O}_{12}$  [92]. However, coatings based on  $\text{Gd}_2\text{Zr}_2\text{O}_7$  have received the most attention and shown the most potential in terms of their collective performance, leading to their commercial adoption [24, 30, 93–97].

Although the development of RE zirconate materials was originally driven by their improved thermal properties and high-temperature stability, it was soon recognized that they also provide improved performance to mitigate CMAS-induced coating failure [30, 98]. CMAS resistance has subsequently become a major driver in the development and implementation of RE zirconate materials, and concomitant increase in RE oxide utilization in TBCs. The dissolution of these materials into silicate melts rapidly saturates the melt with RE oxide, leading to concomitant precipitation of a calcium-RE-silicate phase, nominally  $\text{Ca}_2\text{RE}_8(\text{SiO}_4)_6\text{O}_2$ , with the apatite crystal structure. In conjunction with other crystalline reaction products, the apatite blocks open infiltration channels in the coating microstructure thereby limiting the degree of infiltration. Research has shown that the effectiveness of this mitigation strategy, which depends on the solubility of the  $\text{RE}^{3+}$  in the silicate melt and the driving force for apatite precipitation, increases with the  $\text{RE}^{3+}$  size [31]. This behavior favors either selecting coatings with the larger  $\text{RE}^{3+}$  (e.g., gadolinium (Gd) rather than Y or Yb) or increasing the concentration of the  $\text{RE}^{3+}$  in the coating material.

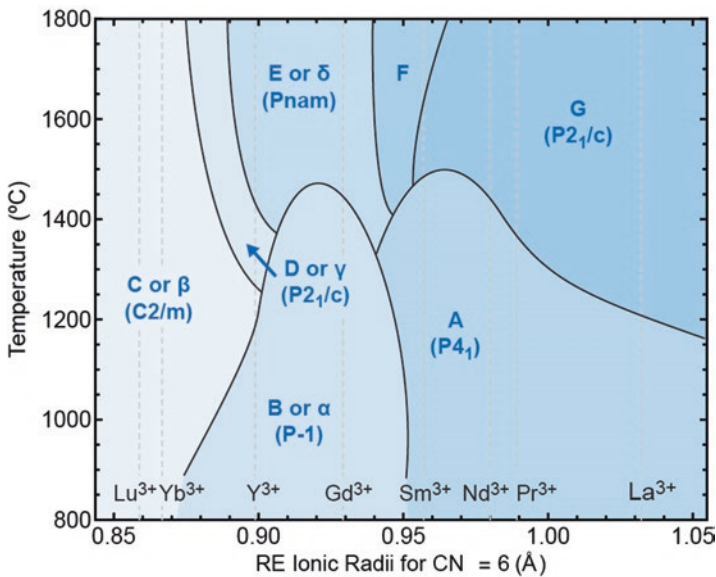
### 16.2.3 Rare Earth Silicate Coating Materials

RE silicate compounds have received considerable attention for use as EBC materials on SiC- and  $\text{Si}_3\text{N}_4$ -based ceramics. Their desirable properties include low thermal conductivity, relatively high melting temperatures, resistance to volatilization in the combustion environment and, for some polymorphs, a low CTE compared to other refractory oxides. Unlike the RE-stabilized zirconia materials, the absence of structural oxygen vacancies also significantly lowers the rate of oxidant transport. There are three binary RE silicate stoichiometries. All trivalent RE cations are reported to form a monosilicate ( $\text{RE}_2\text{SiO}_5$ , REMS) and a disilicate ( $\text{RE}_2\text{Si}_2\text{O}_7$ , REDS) compound. The larger  $\text{RE}^{3+}$  ( $\text{Gd}^{3+}$  to  $\text{La}^{3+}$ ) form a third compound with intermediate  $\text{SiO}_2$  content ( $\text{RE}_{9.33}(\text{SiO}_4)_6\text{O}_2$ ) with the apatite crystal structure. EBC development has focused more on the disilicate and monosilicate compounds.

The crystal structure for the RE monosilicates depends primarily on the  $\text{RE}^{3+}$  size [99, 100]. From La to Gd, the compound crystallizes with the monoclinic X1 structure with space group  $\text{P}2_1/c$ , and for Dy to Lu the compound forms a different

monoclinic structure (X2) with space group C2/m. Tb and Y form the X1 structure at low temperatures and the X2 structure at higher temperature. However, the reconstructive reversion from X2 to X1 upon cooling is sluggish and therefore the existence of this transformation does not preclude the use of the more cost-effective  $\text{Y}_2\text{SiO}_5$  as a coating material. Both structures exhibit CTEs in the range of  $5 \times 10^{-6}/\text{K}$  to  $7 \times 10^{-6}/\text{K}$  over the relevant temperature range. The modest positive  $\Delta\alpha$  relative to Si-based ceramics leads to the formation of penetration cracks during thermal cycling, which limits the coating lifetime if the REMS is used as the predominant material in an EBC architecture [101–103].

The RE disilicates exhibit seven distinct crystal structures depending on the  $\text{RE}^{3+}$  size and temperature (Fig. 16.6) [104]. This polymorphism has important implications for the selection of EBC materials. First, there are significant differences in the CTE between the polymorphs [105]. The  $\beta$  and  $\gamma$  structures formed by the smaller  $\text{RE}^{3+}$  exhibit CTEs in the range of  $4 \times 10^{-6}/\text{K}$  to  $5 \times 10^{-6}/\text{K}$ , resulting in a near-zero  $\Delta\alpha$  relative to  $\text{SiC}$  and  $\text{Si}_3\text{N}_4$ . The  $\alpha$ ,  $\delta$  and G structures exhibit higher CTEs in the range of  $7 \times 10^{-6}/\text{K}$  to  $9 \times 10^{-6}/\text{K}$ , and the A structures exhibit CTEs greater than  $10 \times 10^{-6}/\text{K}$ . Second, volume changes associated with polymorphic transformations can cause the coatings to crack, so it is desirable to prevent transformations during processing or in service use. Only  $\text{Lu}_2\text{Si}_2\text{O}_7$  and  $\text{Yb}_2\text{Si}_2\text{O}_7$  exhibit a single stable polymorph spanning from room temperature to the anticipated service temperatures of  $1400^\circ\text{C}$  or greater. These constraints, along with considerations of RE oxide cost and availability make  $\text{Yb}_2\text{Si}_2\text{O}_7$  a preferred choice for EBC applications. Solid solution disilicates containing several RE cations have been used to tune the thermal



**Fig. 16.6** Stability of RE disilicates ( $\text{RE}_2\text{Si}_2\text{O}_7$ ) as a function of cationic radius and temperature. (Stability data adapted from Felsche [104] using ionic radii from Shannon et al. [49])

expansion behavior or to reduce the thermal conductivity for applications where the coating must also provide thermal protection [106–108]. To reduce cost while maintaining performance, investigations have shown that solid solutions comprising two or more  $\text{RE}^{3+}$ , including the less expensive  $\text{Y}^{3+}$ , maintain the desired  $\beta$  polymorph [109, 110].

Based on minimizing CTE mismatch and achieving oxygen permeability [111], the RE disilicates provide better performance than the monosilicate as EBCs. Their low silica chemical activity also effectively reduces the rate of silicon hydroxide formation (and silica volatilization) by approximately two orders of magnitude relative to a pure  $\text{SiO}_2$  TGO [112, 113]. However, selective  $\text{SiO}_2$  volatilization from the RE disilicates leads the formation of an outer layer of porous RE monosilicate after extended exposure to high velocity water vapor [114]. Combustion gases can readily permeate through the open porosity structure and the friable structure tends to detach under thermo-cyclic stresses. Thus, the RE disilicates are generally not suitable for use as a single-phase monolayer EBC.

## 16.2.4 Rare Earth Aluminate Coating Materials

RE aluminates have been investigated for use as both TBCs and EBCs owing to their low thermal conductivity, high thermal stability, sintering resistance and reduced oxygen permeability compared to zirconia-based materials [51, 115–119]. These investigations have focused on determining thermophysical properties, developing suitable processing strategies and lab-scale testing of coating performance. However, there is less data on these materials compared to the RE zirconates and silicates, and coatings based on these materials are not in widespread commercial use.

There are four relevant aluminate stoichiometries:  $\text{RE}_4\text{Al}_2\text{O}_9$ ,  $\text{REAlO}_3$ ,  $\text{RE}_3\text{Al}_5\text{O}_{12}$  and  $\text{REAl}_{11}\text{O}_{18}$  (Fig. 16.5). The compound  $\text{RE}_4\text{Al}_2\text{O}_9$  is stable for the smaller RE cations ranging from  $\text{Lu}^{3+}$  to  $\text{Nd}^{3+}$ . At room temperature, it exhibits a monoclinic structure ( $\text{P2}_1/\text{c}$ ) and is often denoted REAM, where RE would be replaced by the symbol for the RE cation such as YAM for  $\text{Y}_4\text{Al}_2\text{O}_9$ . It transforms to an orthorhombic, cuspidine-type structure ( $\text{Pnma}$ ) at higher temperatures [120, 121]. The transformation temperatures increase with decreasing size, ranging from approximately 1000 °C to 1400 °C. There is presently insufficient information to know whether the small (approximately 0.5%) volume change associated with this polymorphic transformation would have a negative impact on coating durability. The compound  $\text{REAlO}_3$  belongs to the perovskite family (REAP, thus YAP for  $\text{YAlO}_3$ ). It is more stable for the larger RE cations. The aluminate garnets,  $\text{RE}_3\text{Al}_5\text{O}_{12}$  (Ia3d, REAG, or YAG for  $\text{Y}_3\text{Al}_5\text{O}_{12}$ ), are only stable for the smaller RE cations including LuAG, YbAG and YAG. The cation-size-dependent stability limit is likely around GdAG.  $\text{REAl}_{11}\text{O}_{18}$  represents the aluminate endmember of the magnetoplumbite family. As a pure aluminate it is only stable for the largest  $\text{RE}^{3+}$ , but the addition of an alkali earth oxide (e.g.,  $\text{REMGAl}_6\text{O}_{19}$ ) increases its stability.



The monoclinic, perovskite and garnet aluminates possess CTEs generally in the range of  $8 \times 10^{-6}/\text{K}$  to  $9 \times 10^{-6}/\text{K}$ . This makes them well-suited for application on alumina-based composites, and also of interest as coatings for niobium-based refractory alloys [122]. However, the aluminates would produce higher thermal stresses compared to the use of RE silicates as EBCs on Si-based ceramics, or compared to the zirconia-based materials as TBCs on superalloys. YAP and YAM are highly resistant to hydroxide-induced volatilization, with material loss rates comparable to the RE monosilicates and 7YSZ [52]. The higher alumina content of YbAG and YAG increases their volatilization rates into a range comparable to the RE disilicates [52]. The higher CTE of the magnetoplumbite structure, approximately  $10 \times 10^{-6}/\text{K}$  for all RE cations, makes it better-suited for use as a TBC on Ni-based alloys compared to the other aluminates [117, 118]. However, the high alumina content and moisture sensitivity of  $\text{La}_2\text{O}_3$ -containing materials lead to increased volatilization rates that complicate their use in a combustion environment. Additionally, none of the aluminates possess the high intrinsic toughness characteristics of  $t'$ - $\text{ZrO}_2$ , there are some that report that multiphase materials including the RE aluminates could exhibit modestly increased toughness [123].

### 16.2.5 Other Material Families

A variety of other RE-containing materials have been studied for prospective use in TBCs and EBCs. Despite promising individual properties, these materials have not yet demonstrated the requisite combination of collective performance characteristics and processability to displace the current commercial materials.

#### Rare Earth Phosphates

RE monophosphates ( $\text{REPO}_4$ ) of the larger  $\text{RE}^{3+}$  crystallize with the monazite structure ( $\text{P}_2/\text{n}$ ), while those based on the smaller  $\text{RE}^{3+}$  form the xenotime structure ( $\text{I}_4/\text{a}$ ). Monazite compounds have been considered for use as TBCs given their improved high temperature stability compared to 7YSZ, as well as desirable combination high CTE, low thermal conductivity and compatibility with an alumina TGO [124, 125]. Likewise, xenotime compounds have been considered for use as EBCs owing to their high thermal stability, moderate elastic modulus and CTE falling between that of the  $\beta$ - $\text{RE}_2\text{Si}_2\text{O}_7$  and  $\text{RE}_2\text{SiO}_5$  [126]. These materials show a strong tendency to form mixed RE-phosphate-apatite compounds upon reaction with molten silicate (CMAS) deposits, which enables the materials to resist infiltration by these corrosive melts [127].  $\text{GdPO}_4$  and  $\text{LaPO}_4$  TBCs deposited by APS showed reasonable performance in short-term thermo-cyclic and CMAS-resistance testing [128, 129].

Longer-term testing is necessary to benchmark performance against current state-of-the-art zirconate materials. However, several potential challenges are

evident. First, efforts to develop monazite-based interphase for ceramic composites has shown it forms a weak bond with alumina [130]. This suggests that achieving good adherence to an alumina TGO would be difficult. Second, while the  $\text{REPO}_4$  compounds possess high melting temperatures, deep eutectics on both sides of the line compound present challenges in the inevitable case of segregation or composition fluctuations during processing. Finally, preliminary volatilization studies suggest that  $\text{REPO}_4$  compounds exhibit similar or higher volatilization rates than the RE disilicates, which would further limit their durability in a combustion environment [52].

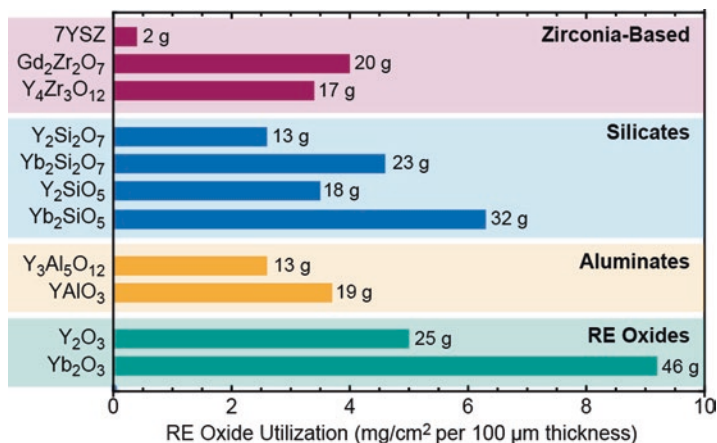
### Rare Earth Tantalates

Investigations of  $\text{Ta}_2\text{O}_5$  co-doping with RE oxides-stabilized tetragonal  $\text{ZrO}_2$  led to the identification of several RE tantalate phases with promising properties. There are several stable compounds in the  $\text{REO}_{1.5}\text{-TaO}_{2.5}$  systems, including  $\text{RE}_3\text{TaO}_7$ ,  $\text{RETaO}_4$ ,  $\text{RETa}_3\text{O}_9$  and  $\text{RETa}_7\text{O}_{19}$  [131]. Each of these can exhibit multiple polymorphs, which are distinguished either by differences in cation or defect ordering, or by martensitic or shear-type displacements of the unit cell. The most effort has been focused on the region around  $\text{YTaO}_4$  which represents complete, equiatomic substitution of  $\text{Y}_2\text{O}_3$  and  $\text{Ta}_2\text{O}_5$  into the Y- and Ta-stabilized t- $\text{ZrO}_2$  [81, 132–134].  $\text{YTaO}_4$  forms several stable and metastable monoclinic and tetragonal phases and, when doped with  $\text{ZrO}_2$ , exhibits significantly lower thermal conductivity than conventional 7YSZ while also remaining stable upon thermal aging. However, due to the early stage of development there are, to date, no reports in the open literature of the performance of these materials as coatings.

## 16.3 Coating Architecture Design Trends and Rare Earth Oxide Utilization

Over the past two decades, TBC and EBC architecture development has favored a wider range of coating materials in more diverse configurations. These architectures have progressively increased in the utilization of RE oxides by adopting materials with a higher mole fraction of the RE element (e.g.,  $\text{RE}_2\text{Zr}_2\text{O}_7$  or  $\text{RE}_2\text{Si}_2\text{O}_7$  vs. 7YSZ). Additionally, trading  $\text{Y}_2\text{O}_3$  in favor of the heavier  $\text{Yb}_2\text{O}_3$  and  $\text{Gd}_2\text{O}_3$  oxides has a compounding effect on the mass utilization and cost of the coating materials. The following sections describe specific developments in the context of TBCs for Ni-alloys and EBCs for ceramic composites.

To provide context for the relative utilization of RE oxides in various coating materials and architectures, it is useful to first make comparisons based on an equivalent coating geometry. Figure 16.7 shows the RE oxide mass requirements for



**Fig. 16.7** Relative utilization of RE oxides in various TBC and EBC materials illustrating that the trend toward architectures based on materials other than 7YSZ significantly increases. The abscissa scale is based on a normalized unit area of dense coating. The masses listed illustrate the utilization to coat a notional 200 cm<sup>2</sup> turbine blade with a 250-µm thick coating

various coating materials, normalized per square centimeter of area coated to a thickness of a 100 µm with a dense coating layer, calculated based on the theoretical density of each material. The values can then be scaled to account for various coating thicknesses and relative densities for different coating architectures. Figure 16.7 also lists the total mass of oxide required to deposit a 250-µm thick coating over an area of 200 cm<sup>2</sup>, a geometry intended to represent a single turbine blade or vane in a modern engine design. (The actual material utilization would be considerably higher due to the inefficiency of the coating deposition processes, but the overspray or material condensed on deposition chamber walls can be recovered for recycling.)

Several important trends emerge. First, the transition from yttria-stabilized zirconia (YSZ) to a RE zirconate (i.e., pyrochlore or δ-phase) results in approximately an order-of-magnitude increase in the mass of RE oxide required for an equivalent coating. Similarly, the RE silicates and aluminates used as EBCs require considerably more RE oxide than 7YSZ. For a given RE<sup>3+</sup>, the monosilicates and perovskite aluminates require approximately 40% more RE oxide than the disilicates and garnet aluminates. Accounting for the combined effects of the difference in molar mass and REO price, the material cost for a Yb-silicate coating would be nearly eight times higher than an equivalent yttrium-silicate coating. For this reason, there is a strong driver to use Y-containing phases except in instances where the performance advantage of a heavier RE element outweighs the added cost.

### 16.3.1 Thermal Barrier Coatings

#### Single Layer Top Coat Architectures

The first ceramic thermal barrier coatings comprised single layers of YSZ applied to metallic components first by APS and then using a combination of EB-PVD and APS based in the requirements for a given component [135]. These remained the predominate commercial coating architecture for several decades following introduction. The development of alternative TBCs was driven by the desire for lower thermal conductivity, improved temperature capability (to overcome limitations associated with the destabilization of the metastable  $t'$ -ZrO<sub>2</sub>) and, later, resistance to degradation by CMAS deposits [3, 136]. Early research into the application of RE zirconate compounds (i.e., La<sub>2</sub>Zr<sub>2</sub>O<sub>7</sub> and Gd<sub>2</sub>Zr<sub>2</sub>O<sub>7</sub>) adopted a similar single layer structure [22, 56, 87]. Although the coatings were initially adherent, extended testing resulted in premature delamination. This behavior was later attributed to a combination of deleterious reactions between the TBC material and the Al<sub>2</sub>O<sub>3</sub> TGO, and the presence of the low-toughness zirconate in the inner regions of the coating that are subject to the highest thermal stresses [56, 89].

#### Bilayer Top Coat Architectures

Bilayer coating architectures were first developed to combine the desirable attributes of 7YSZ and the RE zirconates [56, 89, 95, 137]. These architectures typically comprise a layer of 7YSZ adjacent the TGO, where the lower temperature reduces the rate of  $t'$ -ZrO<sub>2</sub> decomposition. This layer also provides higher toughness in the regions with the highest thermal stresses and ensures thermochemical compatibility with the Al<sub>2</sub>O<sub>3</sub>. The RE zirconate is then applied as an outer layer which experiences higher in-service temperatures and direct exposure to corrosive species in the gas stream. Diffusion of the RE<sup>3+</sup> from the zirconate into the YSZ converts the later to fluorite but the layers are typically thick enough to always maintain a significant fraction of  $t'$ -YSZ in the relevant regions. Single-material, bilayer coating architectures have also been developed to combine higher porosity, more insulating microstructures at the coating surface with more dense, higher toughness layers closer to the substrate [138]. Bilayer architectures combining YSZ and a RE zirconate with deliberate microstructure control to tune thermal conductivity and toughness lead to further performance enhancement [24, 93]. By enabling the use of RE zirconates, these bilayer architectures are one of the primary drivers for increased RE oxide consumption in TBCs over the past decade.

## Multilayer and Multiphase Top Coat Architectures

A variety of alternative multilayer TBC architectures have been explored to further increase or monitor coating performance. These approaches fall into several categories:

- (1) Architectures based on thin, alternating layers of YSZ and a RE zirconate aiming to leverage the higher toughness of YSZ for improved erosion resistance and the reduced thermal conductivity and CMAS resistance of the RE zirconate [139, 140]. These approaches are effective if the surface temperature is low enough to prevent decomposition of the  $t'$ -ZrO<sub>2</sub> phase, and the layers are thick enough to prevent complete dissolution of the zirconate into the stabilized ZrO<sub>2</sub>.
- (2) Implementation of materials with reduced transmittance for infrared radiation, or alternating layers of high- and low-refractive index materials to reduce radiative heat transfer through semitransparent oxide phases [136, 141, 142]. Here no single architecture has yet been identified to optimize performance, but many of the materials of interest contain significant RE oxide content.
- (3) Selective doping of luminescent RE<sup>3+</sup> such as dysprosium (Dy), terbium (Tb) or europium (Eu) into specific layers the zirconia-based TBC to enable luminescence thermometry [136, 143]. This approach can be used in laboratory settings to understand the performance of novel coating architectures, and prospective in-service implementation would enable coating health monitoring. This is one of the primary applications for these less common RE oxides in TBCs.
- (4) Thin, dense surface layers of a reactive material such Gd<sub>2</sub>Zr<sub>2</sub>O<sub>7</sub>, Al<sub>2</sub>O<sub>3</sub> or a pure RE oxide atop the traditional bilayer coating architecture to act as barriers against molten deposit infiltration [144–147].

### 16.3.2 Environmental Barrier Coatings for Ceramic Composites

#### Rare Earth Silicate Architectures for SiC and Si<sub>3</sub>N<sub>4</sub>-Based Ceramics

Early EBC architectures for Si-based CMCs were based on aluminosilicates such as mullite (3Al<sub>2</sub>O<sub>3</sub>·2SiO<sub>2</sub>) and barium-strontium-aluminosilicate (BSAS) [5, 148]. However, performance limitations dictated by high SiO<sub>2</sub> volatility from mullite and incompatibility between BSAS and the SiO<sub>2</sub> TGO above 1300 °C led to the adoption of coating architectures based on RE silicates [6]. As described in Sect. 16.2.3, the near-zero  $\Delta\alpha$  relative to the Si-based ceramics (i.e., SiC and Si<sub>3</sub>N<sub>4</sub>) and moderate cost make Yb<sub>2</sub>Si<sub>2</sub>O<sub>7</sub> a preferred choice for the bulk of the EBC. Lu<sub>2</sub>Si<sub>2</sub>O<sub>7</sub> does not appear to offer sufficient performance benefit to justify its much higher cost. Y<sub>2</sub>Si<sub>2</sub>O<sub>7</sub> could offer comparable performance at significantly lower material cost than Yb<sub>2</sub>Si<sub>2</sub>O<sub>7</sub> if the coating deposition process could be designed to suppress transformations involving the  $\delta$ -Y<sub>2</sub>Si<sub>2</sub>O<sub>7</sub> polymorph. However, if Yb<sub>2</sub>Si<sub>2</sub>O<sub>7</sub> (or another

disilicate) is used in a single layer architecture, selective  $\text{SiO}_2$  volatilization results in a friable, non-protective surface layer [149]. Coatings based primarily on a RE monosilicate ( $\text{RE}_2\text{SiO}_5$ ) are much more resistant to volatilization, but suffer from cracking and spallation due to the higher CTE mismatch between the silicate and ceramic substrate [6, 101, 150].

### Coatings for $\text{Al}_2\text{O}_3$ -Based Ceramics

Coating architectures for  $\text{Al}_2\text{O}_3$ -based ceramic composites are typically based on relatively thick, single layer coatings of  $\text{Y}_2\text{O}_3$ ,  $\text{YAlO}_3$  or  $\text{Y}_3\text{Al}_5\text{O}_{12}$  [42, 43, 52]. Of these,  $\text{YAlO}_3$  exhibits the lowest volatility in the combustion environment. However, preliminary efforts to process both aluminates by APS have revealed challenges in achieving a high degree of crystallinity and suggests that residual stresses from the coating process and those generated during annealing can weaken the underlying composite [52, 116]. This implies the need for careful processing development for the utilization of aluminate coatings. APS  $\text{Y}_2\text{O}_3$  coatings have shown better performance, including good cyclic lifetimes. It appears that the adhesion of these coatings benefits from reactions between the composite and the  $\text{Y}_2\text{O}_3$  coating leading to the formation of thin aluminate layers across the coating-substrate interface [43].

### Multilayer Thermal-Environmental Architectures

As with TBCs, multilayer architectures provide benefits for the performance of EBC systems. For Si-based ceramics, the benefits derive from managing thermal stresses while also meeting the requirements for substrate compatibility and volatilization resistance. For instance, it is advantageous to apply an outer layer of a monosilicate to provide additional surface protection. The thickness of this layer must be tuned to provide the desired protection against water vapor volatilization while minimizing the thermal stresses associated with the increased  $\Delta\alpha$  [102]. Given the reduced sensitivity of the RE monosilicate properties on the identity of the  $\text{RE}^{3+}$  employed, the selection of the material for this outer silicate layer can be driven more by cost (i.e., favoring  $\text{Y}_2\text{SiO}_5$ ) and processibility. There have also been investigations into the use of porous or segmented YSZ, zirconate or hafnate layers applied atop of the silicate EBCs to provide additional thermal insulation or CMAS resistance [6, 40, 92]. Although these coatings initially exhibit promising characteristics, their lifetime is limited by stress-induced delamination as the top coat sinters. Ongoing efforts seek to develop material and microstructure combinations that combine the desired functional performance with suitable durability. There are limited reports of the development of multilayer coating architectures for use of aluminum oxide-based CMCs, although these composites would likely benefit from similar architecture designs.

## 16.4 Rare Earth Containing Coating Feedstocks, Opportunities for Efficient Material Designs and Utilization and Outlook

The feedstock materials used for coating deposition are designed in terms of composition and physical form to produce coatings with the desired chemistry and microstructure. There is a significant industry associated with the formulation of these feedstocks from the raw materials comprising refined RE oxides and other constituents. In many cases, the vendors supplying these feedstocks have close relationships with companies supplying the equipment used to produce the coatings, and the engine manufacturers who use the coatings leading to integrated development of the coating architecture, material feedstocks and processing technique.

The typical feedstock for EB-PVD processing comprises cylindrical ceramic ingots enabling continuous feeding as the ingot is consumed during processing. These ingots can be produced either from mixed powders of the constituent oxides, which may partially react during sintering before fully mixing in the melt pool during evaporation, or can be produced from powders that have been pre-reacted to produce a uniform composition in the ingot. The two approaches offer trade-offs between cost and the thermal stability of the ingot during processing and use. Regardless of the production approach, the materials used for EB-PVD processing are typically very high purity, with the concentration of any single impurity oxide maintained below 100 ppm (parts per million). The powders used for thermal spray deposition processes must be able to flow freely through powder feeders, and to melt in a uniform and predictable manner. This requires particles of intermediate size (typically tens to hundreds of  $\mu\text{m}$ ) and narrow particle-size distribution. Several methods are commonly used to produce these powders. In the simplest case, the raw materials can be melted or otherwise fused, mechanically crushed, and separated to extract the desired size range. However, this method produces angular particles that are less free flowing than spherical particles. Alternatively, powders produced by spray-drying slurries of fine particles or other spheroidization techniques flow better, but in some cases are more costly to produce. Powders produced for thermal spray techniques typically have higher impurity content (e.g., hundreds of ppm of  $\text{CaO}$ ,  $\text{Fe}_2\text{O}_3$  and  $\text{Al}_2\text{O}_3$ , and over 1000 ppm  $\text{TiO}_2$  and  $\text{SiO}_2$ ). However, because these impurities can negatively impact the phase stability and sintering resistance of the coating, many suppliers now offer higher-purity powders with impurity contents comparable to the EB-PVD feedstocks.

Two important observations related to materials design and RE oxide utilization emerge from the preceding discussion. First is that the trajectory of coating materials development has led to increased utilization of RE oxides to achieve the functional property requirements. Current materials also favor the use of the less abundant, and more expensive, RE oxides such as  $\text{Yb}_2\text{O}_3$  and  $\text{Gd}_2\text{O}_3$ , in place of the  $\text{Y}_2\text{O}_3$  used historically to stabilize YSZ. Increased adoption of these new materials for a larger number of components and engine designs will continue to drive RE oxide demand for ceramic coatings. For instance, replacing a 7YSZ coating with a

Gd<sub>2</sub>Zr<sub>2</sub>O<sub>7</sub> coating of equivalent thickness increases the RE mass utilization by a factor of ten, and uses a RE that is nearly ten times more expensive. Thus, the material cost could increase by as much as two orders of magnitude. This trend motivates the development of processing techniques to improve the yield, and by improving reclaim and recycling processes.

The second observation is that the stability and properties of the coating materials are determined by the size of the RE<sup>3+</sup> cation, rather than specific or distinct details of the electronic structure. Therefore, while materials development has traditionally focused on single-RE materials or defined combinations of RE cations, there are likely opportunities to achieve equivalent performance by selecting feedstocks to achieve the same “average” RE cation size in solid solutions. As the case study for the RE silicates illustrates [109], this approach can likely provide economic and environmental benefits by reducing the need for chemical separation, and by more efficiently utilizing waste streams generated from other RE oxide refining processes. Implementing this material design approach provides opportunity for closer collaboration between RE oxide processors, coating producers and materials designers in the future.

## References

1. U.S. Energy Information Administration, *Annual Energy Outlook 2021* (AEO 2021, 2021)
2. C.G. Levi, Emerging materials and processes for thermal barrier systems. *Curr. Opinion Solid State Mater. Sci.* **8**(1), 77–91 (2004)
3. A.G. Evans, D.R. Clarke, C.G. Levi, The influence of oxides on the performance of advanced gas turbines. *J. Eur. Ceram. Soc.* **28**(7), 1405–1419 (2008)
4. D.R. Clarke, M. Oechsner, N.P. Padture, Thermal barrier coatings for more efficient gas turbine engines. *MRS Bull.* **37**(10), 891–898 (2012)
5. K.N. Lee, Current status of environmental barrier coatings for Si-based ceramics. *Surf Coat Technol* **133–134**, 1–7 (2000)
6. K.N. Lee, D.S. Fox, N.P. Bansal, Rare earth silicate environmental barrier coatings for SiC/SiC composites and Si<sub>3</sub>N<sub>4</sub> ceramics. *J. Eur. Ceram. Soc.* **25**(10), 1705–1715 (2005)
7. D. Tejero-Martin, C. Bennett, T. Hussain, A review on environmental barrier coatings: history, current state of the art and future developments. *J. Eur. Ceram. Soc.* **41**(3), 1747–1768 (2021)
8. D.L. Poerschke, R.W. Jackson, C.G. Levi, Silicate deposit degradation of engineered coatings in gas turbines: Progress toward models and materials solutions. *Ann. Rev. Mater. Res.* **47**, 297–330 (2017)
9. T. Gheno, B. Gleeson, Modes of deposit-induced accelerated attack of MCrAlY systems at 1100 °C. *Oxid. Met.* **87**(1–2), 249–270 (2017)
10. M.S.A. Karunaratne, S. Kyaw, A. Jones, R. Morrell, R.C. Thomson, Modelling the coefficient of thermal expansion in Ni-based superalloys and bond coatings. *J. Mater. Sci.* **51**(9), 4213–4226 (2016)
11. R.W. Jackson, M.S. Titus, M.R. Begley, T.M. Pollock, Thermal expansion behavior of new Co-based alloys and implications for coatings. *Surf. Coat. Technol.* **289**, 61–68 (2016)
12. T.H. Nielsen, M.H. Leipold, Thermal expansion of yttria-stabilized zirconia. *J Am Ceram Soc* **47**(3), 155 (1964)



13. H. Lehmann, D. Pitzer, G. Pracht, R. Vassen, D. Stover, Thermal conductivity and thermal expansion coefficients of the lanthanum rare-earth-element zirconate system. *J. Am. Ceram. Soc.* **86**(8), 1338–1344 (2003)
14. H. Hayashi, T. Saitou, N. Maruyama, H. Inaba, K. Kawamura, M. Mori, Thermal expansion coefficient of yttria stabilized zirconia for various yttria contents. *Solid State Ionics* **176**(5–6), 613–619 (2005)
15. S. Sampath, U. Schulz, M.O. Jarligo, S. Kuroda, Processing science of advanced thermal-barrier systems. *MRS Bull.* **37**(10), 903–910 (2012)
16. E. Bakan, R. Vassen, Ceramic top coats of plasma-sprayed thermal barrier coatings: materials, processes, and properties. *J. Therm. Spray Technol.* **26**(6), 992–1010 (2017)
17. J. Singh, D.E. Wolfe, J. Singh, Architecture of thermal barrier coatings produced by electron beam-physical vapor deposition (EB-PVD). *J. Mater. Sci.* **37**(15), 3261–3267 (2002)
18. R. Naraparaju, M. Huttermann, U. Schulz, P. Mechnich, Tailoring the EB-PVD columnar microstructure to mitigate the infiltration of CMAS in 7YSZ thermal barrier coatings. *J. Eur. Ceram. Soc.* **37**(1), 261–270 (2017)
19. J.R. Nicholls, K.J. Lawson, A. Johnstone, D.S. Rickerby, Methods to reduce the thermal conductivity of EB-PVD TBCs. *Surf. Coat. Technol.* **151**, 383–391 (2002)
20. S.G. Terry, J.R. Litty, C.G. Levi, *Evolution of Porosity and Texture in Thermal Barrier Coatings Grown by EB-PVD* (Elevated Temperature Coatings: Science and Technology III Proceedings of Symposium 1999 TMS Annual Meeting, 1999), pp. 13–25
21. J.S. Van Sluytman, S. Krämer, V.K. Tolpygo, C.G. Levi, Microstructure evolution of ZrO<sub>2</sub>-YbTaO<sub>4</sub> thermal barrier coatings. *Acta Mater.* **96**, 133–142 (2015)
22. B. Saruhan, P. Francois, K. Fritscher, U. Schulz, EB-PVD processing of pyrochlore-structured La<sub>2</sub>Zr<sub>2</sub>O<sub>7</sub>-based TBCs. *Surf. Coat. Technol.* **182**(2–3), 175–183 (2004)
23. G.M. Smith, A. Smith, S. Sampath, Fracture toughness of thermal spray ceramics: Measurement techniques and processing dependence. *J. Therm. Spray Technol.* **27**(7), 1076–1089 (2018)
24. V. Viswanathan, G. Dwivedi, S. Sampath, Multilayer, multimaterial thermal barrier coating systems: Design, synthesis, and performance assessment. *J. Am. Ceram. Soc.* **98**(6), 1769–1777 (2015)
25. S. Rezanka, D.E. Mack, G. Mauer, D. Sebold, O. Guillon, R. Vassen, Investigation of the resistance of open-column-structured PS-PVD TBCs to erosive and high-temperature corrosive attack. *Surf. Coat. Technol.* **324**, 222–235 (2017)
26. M.P. Schmitt, B.J. Harder, D.E. Wolfe, Process-structure-property relations for the erosion durability of plasma spray-physical vapor deposition (PS-PVD) thermal barrier coatings. *Surf. Coat. Technol.* **297**, 11–18 (2016)
27. S. Krämer, J. Yang, C.G. Levi, C.A. Johnson, Thermochemical interaction of thermal barrier coatings with molten CaO–MgO–Al<sub>2</sub>O<sub>3</sub>–SiO<sub>2</sub> (CMAS) deposits. *J. Am. Ceram. Soc.* **89**(10), 3167–3175 (2006)
28. R.W. Jackson, E.M. Zaleski, D.L. Poerschke, B.T. Hazel, M.R. Begley, C.G. Levi, Interaction of molten silicates with thermal barrier coatings under temperature gradients. *Acta Mater.* **89**, 396–407 (2015)
29. S. Krämer, S. Faulhaber, M. Chambers, D.R. Clarke, C.G. Levi, J.W. Hutchinson, A.G. Evans, Mechanisms of cracking and delamination within thick thermal barrier systems in aero-engines subject to calcium-magnesium-alumino-silicate (CMAS) penetration. *Mater. Sci. Eng. A* **490**(1–2), 26–35 (2008)
30. S. Krämer, J. Yang, C.G. Levi, Infiltration-inhibiting reaction of gadolinium zirconate thermal barrier coatings with CMAS melts. *J. Am. Ceram. Soc.* **91**(2), 576–583 (2008)
31. D.L. Poerschke, C.G. Levi, Effects of cation substitution and temperature on the interaction between thermal barrier oxides and molten CMAS. *J. Eur. Ceram. Soc.* **35**(2), 681–691 (2015)
32. F. Zok, Ceramic-matrix composites enable revolutionary gains in turbine engine efficiency. *Am. Ceram. Soc. Bull.* **95**(5), 22–28 (2016)

33. E.J. Opila, R.E. Hann, Paralineer oxidation of CVD SiC in water vapor. *J. Am. Ceram. Soc.* **80**(1), 197–205 (1997)
34. K.A. Terrani, B.A. Pint, C.M. Parish, C.M. Silva, L.L. Snead, Y. Katoh, Silicon carbide oxidation in steam up to 2 MPa. *J. Am. Ceram. Soc.* **97**(8), 2331–2352 (2014)
35. P.J. Meschter, E.J. Opila, N.S. Jacobson, Water vapor-mediated volatilization of high-temperature materials. *Ann. Rev. Mater. Res.* **43**, 559–588 (2013)
36. H.E. Eaton, G.D. Linsey, Accelerated oxidation of SiC CMC's by water vapor and protection via environmental barrier coating approach. *J. Eur. Ceram. Soc.* **22**(14–15), 2741–2747 (2002)
37. C.J. Armani, M.B. Ruggles-Wrenn, R.S. Hay, G.E. Fair, Creep and microstructure of nextel™ 720 fiber at elevated temperature in air and in steam. *Acta Mater.* **61**(16), 6114–6124 (2013)
38. R.S. Hay, C.J. Armani, M.B. Ruggles-Wrenn, G.E. Fair, Creep mechanisms and microstructure evolution of nextel (TM) 610 fiber in air and steam. *J. Eur. Ceram. Soc.* **34**(10), 2413–2426 (2014)
39. M. Fritsch, H. Klemm, M. Herrmann, B. Schenk, Corrosion of selected ceramic materials in hot gas environment. *J. Eur. Ceram. Soc.* **26**(16), 3557–3565 (2006)
40. I. Spitsberg, J. Steibel, Thermal and environmental barrier coatings for SiC/SiC CMCs in aircraft engine applications. *Int. J. Appl. Ceramic Technol.* **1**(4), 291–301 (2004)
41. H.E. Eaton, G.D. Linsey, Accelerated oxidation of SiC CMCs by water vapor and protection via environmental barrier coating approach. *J. Eur. Ceram. Soc.* **22**(14–15), 2741–2747 (2002)
42. P. Mechnich, W. Braue, Air plasma-sprayed Y<sub>2</sub>O<sub>3</sub> coatings for Al<sub>2</sub>O<sub>3</sub>/Al<sub>2</sub>O<sub>3</sub> ceramic. *J. Eur. Ceram. Soc.* **33**(13–14), 2645–2653 (2013)
43. W. Braue, P. Mechnich, Tailoring protective coatings for all-oxide ceramic matrix composites in high temperature/high heat flux environments and corrosive media. *Mater. Werkst.* **38**(9), 690–697 (2007)
44. B.T. Richards, H.N.G. Wadley, Plasma spray deposition of tri-layer environmental barrier coatings. *J. Eur. Ceram. Soc.* **34**(12), 3069–3083 (2014)
45. E. Garcia, H.F. Garces, L.R. Turcer, H. Bale, N.P. Padture, S. Sampath, Crystallization behavior of air-plasma-sprayed ytterbium-silicate-based environmental barrier coatings. *J. Eur. Ceram. Soc.* **41**(6), 3696–3705 (2021)
46. K.N. Lee, D.L. Waters, B.J. Puleo, A. Garg, W.D. Jennings, G. Costa, D.E. Sacksteder, Development of oxide-based High temperature environmental barrier coatings for ceramic matrix composites via the slurry process. *J. Eur. Ceram. Soc.* **41**(2), 1639–1653 (2021)
47. A. Navrotsky, W. Lee, A. Mielewczyk-Gryn, S.V. Ushakov, A. Anderko, H.H. Wu, R.E. Rimann, Thermodynamics of solid phases containing rare earth oxides. *J. Chem. Thermodyn.* **88**, 126–141 (2015)
48. M. Zinkevich, Thermodynamics of rare earth sesquioxides. *Prog. Mater. Sci.* **52**(4), 597–647 (2007)
49. R.D. Shannon, C.T. Prewitt, Effective ionic radii in oxides and fluorides. *Acta Crystall B-Stru.* **25**, 925 (1969)
50. CRC Handbook of Chemistry and Physics. 102nd (2021)
51. Shanghai Metal Market Trading Price, Retrieved from [Metals.com](https://www.metals.com), July 15, 2021
52. C. Gatzert, D.E. Mack, O. Guillon, R. Vassen, YAlO<sub>3</sub> – A novel environmental barrier coating for Al<sub>2</sub>O<sub>3</sub>/Al<sub>2</sub>O<sub>3</sub> – Ceramic matrix composites. *Coatings* **9**(10) (2019)
53. S. Deville, G. Guenin, K. Chevalier, Martensitic transformation in zirconia – Part I. Nanometer scale prediction and measurement of transformation induced relief. *Acta Mater.* **52**(19), 5697–5707 (2004)
54. J. Chevalier, L. Gremillard, A.V. Virkar, D.R. Clarke, The tetragonal-monoclinic transformation in zirconia: Lessons learned and future trends. *J. Am. Ceram. Soc.* **92**(9), 1901–1920 (2009)
55. M.R. Winter, D.R. Clarke, Oxide materials with low thermal conductivity. *J. Am. Ceram. Soc.* **90**(2), 533–540 (2007)
56. R.M. Leckie, S. Krämer, M. Rühle, C.G. Levi, Thermochemical compatibility between alumina and ZrO<sub>2</sub>-GdO<sub>3/2</sub> thermal barrier coatings. *Acta Mater.* **53**(11), 3281–3292 (2005)

57. O. Fabrichnaya, F. Aldinger, Assessment of thermodynamic parameters in the system  $ZrO_2$ - $Y_2O_3$ - $Al_2O_3$ , *Z Metallkd.* **95**(1), 27–39 (2004)
58. M.R. Winter, D.R. Clarke, Thermal conductivity of yttria-stabilized zirconia-hafnia solid solutions. *Acta Mater.* **54**(19), 5051–5059 (2006)
59. K.V.G. Kutty, S. Rajagopalan, C.K. Mathews, U.V. Varadaraju, Thermal-expansion behavior of some rare-earth-oxide pyrochlores. *Mater. Res. Bull.* **29**(7), 759–766 (1994)
60. R.P. Haggerty, P. Sarin, Z.D. Apostolov, P.E. Driemeyer, W.M. Kriven, Thermal expansion of  $HfO_2$  and  $ZrO_2$ . *J. Am. Ceram. Soc.* **97**(7), 2213–2222 (2014)
61. W.S. Denzil, D.R. Wilder, Thermal expansion in the system  $Y_2O_3$ - $HfO_2$ . *J. Am. Ceram. Soc.* **56**(4), 224 (1973)
62. S.J. Stecura, *Effects of compositional changes on the performance of a thermal barrier coating system* (NASA TM-78976, NASA Lewis Research Center, Cleveland, 1978)
63. S. Nichani, K. Pillai, J. Varma, *Thermal Barrier Coatings Market Report* (Grandview Research, 2018)
64. R.A. Miller, Phase Stability in Plasma Sprayed, Partially Stabilized Zirconia-Yttria, in *Science and Technology of Zirconia*, ed. by A. Heuer, L.W. Hobbs, vol. I, (The American Ceramics Society Inc, Columbus, 1981), pp. 241–253
65. J.R. Brandon, R. Taylor, Phase-stability of zirconia-based thermal barrier coatings Part 1. Zirconia yttria alloys. *Surf Coat Technol.* **46**(1), 75–90 (1991)
66. A.V. Virkar, R.L.K. Matsumoto, Ferroelastic domain switching as a toughening mechanism in tetragonal zirconia. *J. Am. Ceram. Soc.* **69**(10), C224–C2C6 (1986)
67. R.H.J. Hannink, P.M. Kelly, B.C. Muddle, Transformation toughening in zirconia-containing ceramics. *J. Am. Ceram. Soc.* **83**(3), 461–487 (2000)
68. A.G. Evans, D.R. Mumm, J.W. Hutchinson, G.H. Meier, F.S. Pettit, Mechanisms controlling the durability of thermal barrier coatings. *Prog. Mater. Sci.* **46**(5), 505–553 (2001)
69. A.G. Evans, R.M. Cannon, Toughening of brittle solids by martensitic transformations. *Acta Metall.* **34**(5), 761–800 (1986)
70. D.L. Porter, A.G. Evans, A.H. Heuer, Transformation-toughening in partially-stabilized zirconia (Psz). *Acta Metall.* **27**(10), 1649–1654 (1979)
71. D.M. Lipkin, J.A. Krogstad, Y. Gao, C.A. Johnson, W.A. Nelson, C.G. Levi, Phase evolution upon aging of air-plasma sprayed  $t'$ -zirconia coatings: I synchrotron X-ray diffraction. *J. Am. Ceram. Soc.* **96**(1), 290–298 (2013)
72. J.A. Krogstad, R.M. Leckie, S. Krämer, J.M. Cairney, D.M. Lipkin, C.A. Johnson, C.G. Levi, Phase evolution upon aging of air plasma sprayed  $t'$ -zirconia coatings: II-microstructure evolution. *J. Am. Ceram. Soc.* **96**(1), 299–307 (2013)
73. J.A. Krogstad, S. Krämer, D.M. Lipkin, C.A. Johnson, D.R.G. Mitchell, J.M. Cairney, C.G. Levi, Phase stability of  $t'$ -zirconia-based thermal barrier coatings: Mechanistic insights. *J. Am. Ceram. Soc.* **94**, s168–ss77 (2011)
74. N.R. Rebollo, A.S. Gandhi, C.G. Levi, Phase stability issues in emerging TBC systems. *Elec Soc S.* **2003**(16), 431–442 (2003)
75. N.R. Rebollo, *Phase stability of thermal barrier oxides based on  $t$ -zirconia with trivalent oxide additions* (PhD Dissertation, University of California Santa Barbara, 2005)
76. J.M. Cairney, N.R. Rebollo, M. Ruhle, C.G. Levi, Phase stability of thermal barrier oxides: A comparative study of Y and Yb additions. *Int. J. Mater. Res.* **98**(12), 1177–1187 (2007)
77. M. Matsumoto, N. Yamaguchi, H. Matsubara, Low thermal conductivity and high temperature stability of  $ZrO_2$ - $Y_2O_3$ - $La_2O_3$  coatings produced by electron beam PVD. *Scr. Mater.* **50**(6), 867–871 (2004)
78. J.S. Wang, J.B. Sun, Q.S. Jing, B. Liu, H. Zhang, Y.S. Yu, J.Y. Yuan, S.J. Dong, X. Zhou, X.Q. Cao, Phase stability and thermo-physical properties of  $ZrO_2$ - $CeO_2$ - $TiO_2$  ceramics for thermal barrier coatings. *J. Eur. Ceram. Soc.* **38**(7), 2841–2850 (2018)
79. J.A. Krogstad, M. Lepple, C.G. Levi, Opportunities for improved TBC durability in the  $CeO_2$ - $TiO_2$ - $ZrO_2$  system. *Surf. Coat. Technol.* **221**, 44–52 (2013)

80. F.M. Pitek, C.G. Levi, Opportunities for TBCs in the  $\text{ZrO}_2\text{-YO}_{1.5}\text{-TaO}_{2.5}$  system. *Surf. Coat. Technol.* **201**(12), 6044–6050 (2007)
81. Y. Shen, R.M. Leckie, C.G. Levi, D.R. Clarke, Low thermal conductivity without oxygen vacancies in equimolar  $\text{YO}_{1.5} + \text{TaO}_{2.5}$ - and  $\text{YbO}_{1.5} + \text{TaO}_{2.5}$ -stabilized tetragonal zirconia ceramics. *Acta Mater.* **58**(13), 4424–4431 (2010)
82. C.A. Macauley, A.N. Fernandez, C.G. Levi, Phase equilibria in the  $\text{ZrO}_2\text{-YO}_{1.5}\text{-TaO}_{2.5}$  system at 1500 °C. *J. Eur. Ceram. Soc.* **37**(15), 4888–4901 (2017)
83. R. Vassen, X.Q. Cao, F. Tietz, D. Basu, D. Stover, Zirconates as new materials for thermal barrier coatings. *J. Am. Ceram. Soc.* **83**(8), 2023–2028 (2000)
84. J. Wu, X.Z. Wei, N.P. Padture, P.G. Klemens, M. Gell, E. Garcia, P. Miranzo, M.I. Osendi, Low-thermal-conductivity rare-earth zirconates for potential thermal-barrier-coating applications. *J. Am. Ceram. Soc.* **85**(12), 3031–3035 (2002)
85. A.V. Shlyakhtina, D.A. Belov, S.Y. Stefanovich, I.V. Kolbanov, O.K. Karyagina, A.V. Egorov, S.V. Saviylov, L.G. Shcherbakova,  $\delta$ -phase-to-defect fluorite (order disorder) transition in the  $\text{R}_2\text{O}_3\text{-MO}_2$  (R = Sc, Tm, Lu; M = Zr, Hf) systems. *Mater. Res. Bull.* **46**(4), 512–517 (2011)
86. W. Pan, S.R. Phillpot, C.L. Wan, A. Chernatynskiy, Z.X. Qu, Low thermal conductivity oxides. *MRS Bull.* **37**(10), 917–922 (2012)
87. X.Q. Cao, R. Vassen, W. Jungen, S. Schwartz, F. Tietz, D. Stover, Thermal stability of lanthanum zirconate plasma-sprayed coating. *J. Am. Ceram. Soc.* **84**(9), 2086–2090 (2001)
88. G. Moskal, L. Swadzba, M. Hetmanczyk, B. Witala, B. Mendala, J. Mendala, P. Sosnowy, Characterisation of the microstructure and thermal properties of  $\text{Nd}_2\text{Zr}_2\text{O}_7$  and  $\text{Nd}_2\text{Zr}_2\text{O}_7/\text{YSZ}$  thermal barrier coatings. *J. Eur. Ceram. Soc.* **32**(9), 2035–2042 (2012)
89. H.B. Zhao, M.R. Begley, A. Heuer, R. Sharghi-Moshtaghin, H.N.G. Wadley, Reaction, transformation and delamination of samarium zirconate thermal barrier coatings. *Surf. Coat. Technol.* **205**(19), 4355–4365 (2011)
90. A.R. Krause, B.S. Senturk, H.F. Garces, G. Dwivedi, A.L. Ortiz, S. Sampath, N.P. Padture,  $2\text{ZrO}_2\text{-Y}_2\text{O}_3$  thermal barrier coatings resistant to degradation by molten CMAS: Part I, optical basicity considerations and processing. *J. Am. Ceram. Soc.* **97**(12), 3943–3949 (2014)
91. A.R. Krause, H.F. Garces, B.S. Senturk, N.P. Padture,  $2\text{ZrO}_2\text{-Y}_2\text{O}_3$  thermal barrier coatings resistant to degradation by molten CMAS: Part II, interactions with sand and fly ash. *J. Am. Ceram. Soc.* **97**(12), 3950–3957 (2014)
92. D.L. Poerschke, D.D. Hass, S. Eustis, G.G.E. Seward, J.S. Van Sluytman, C.G. Levi, Stability and CMAS resistance of ytterbium-silicate/hafnate EBCs/TBC for SiC composites. *J. Am. Ceram. Soc.* **98**(1), 278–286 (2015)
93. S. Mahade, N. Curry, S. Bjorklund, N. Markocsan, P. Nylen, R. Vassen, Functional performance of  $\text{Gd}_2\text{Zr}_2\text{O}_7/\text{YSZ}$  multi-layered thermal barrier coatings deposited by suspension plasma spray. *Surf. Coat. Technol.* **318**, 208–216 (2017)
94. R.W. Jackson, E.M. Zaleski, B.T. Hazel, M.R. Begley, C.G. Levi, Response of molten silicate infiltrated  $\text{Gd}_2\text{Zr}_2\text{O}_7$  thermal barrier coatings to temperature gradients. *Acta Mater.* **132**, 538–549 (2017)
95. R. Vassen, E. Traeger, D. Stover, New thermal barrier coatings based on pyrochlore/YSZ double-layer systems. *Int. J. Appl. Ceram. Technol.* **1**(4), 351–361 (2004)
96. P. Mechnich, W. Braue, Volcanic ash-induced decomposition of EB-PVD  $\text{Gd}_2\text{Zr}_2\text{O}_7$  thermal barrier coatings to Gd-oxypatite, zircon, and Gd, Fe-zirconolite. *J. Am. Ceram. Soc.* **96**(6), 1958–1965 (2013)
97. Oerlikon Metco, Material Product Data Sheet *Gadolinia-Containing Zirconium Oxide and Gadolinium Zirconate Powders for Thermal Spray* (2021)
98. C.G. Levi, J.W. Hutchinson, M.-H. Vidal-Setif, C.A. Johnson, Environmental degradation of TBCs by molten deposits. *MRS Bull.* **37**(10), 932–941 (2012)
99. J. Felsche, *The Crystal Chemistry of the Rare-Earth Silicates* (Rare Earths, 1973), pp. 99–197
100. J.G. Wang, S.J. Tian, G.B. Li, F.H. Liao, X.P. Jing, Preparation and X-ray characterization of Low-Temperature Phases of  $\text{R}_2\text{SiO}_5$  (R = Rare Earth Elements). *Mater. Res. Bull.* **36**(10), 1855–1861 (2001)

101. B.T. Richards, S. Sehr, F. de Franqueville, M.R. Begley, H.N.G. Wadley, Fracture mechanisms of ytterbium monosilicate environmental barrier coatings during cyclic thermal exposure. *Acta Mater.* **103**, 448–460 (2016)
102. B.T. Richards, M.R. Begley, H.N.G. Wadley, Mechanisms of ytterbium monosilicate/mullite/silicon coating failure during thermal cycling in water vapor. *J. Am. Ceram. Soc.* **98**(12), 4066–4075 (2015)
103. W.D. Summers, M.R. Begley, F.W. Zok, Transition from penetration cracking to spallation in environmental barrier coatings on ceramic composites. *Surf. Coat. Technol.* **378**, 125083 (2019)
104. J. Felsche, Polymorphism and crystal data of the rare-earth disilicates of type  $RE_2Si_2O_7$ . *J. Less Common. Metals.* **21**(1), 1–14 (1970)
105. A.J. Fernández-Carrión, M. Allix, A.I. Becerro, M. White, Thermal expansion of rare-earth pyrosilicates. *J. Am. Ceram. Soc.* **96**(7), 2298–2305 (2013)
106. Y.X. Luo, L.C. Sun, J.M. Wang, Z. Wu, X.R. Lv, J.Y. Wang, Material-genome perspective towards tunable thermal expansion of rare-earth di-silicates. *J. Eur. Ceram. Soc.* **38**(10), 3547–3554 (2018)
107. M.V. Ayyasamy, J.A. Deijkers, H.N.G. Wadley, P.V. Balachandran, Density functional theory and machine learning guided search for  $RE_2Si_2O_7$  with targeted coefficient of thermal expansion. *J. Am. Ceram. Soc.* **103**(8), 4489–4497 (2020)
108. L.R. Turcer, N.P. Padture, Rare-earth pyrosilicate solid-solution environmental-barrier coating ceramics for resistance against attack by molten calcia-magnesia-aluminosilicate (CMAS) glass. *J. Mater. Res.* **35**(17), 2373–2384 (2020)
109. A.Y. Ku, C. Dosch, T.R. Grossman, J.L. Herzog, A.F. Maricocchi, D. Polli, D.M. Lipkin, Addressing rare-earth element criticality: An example from the aviation industry. *JOM-US.* **66**(11), 2355–2359 (2014)
110. A.J. Fernandez-Carrion, M.D. Alba, A. Escudero, A.I. Becerro, Solid solubility of  $Yb_2Si_2O_7$  in beta, gamma- and delta- $Y_2Si_2O_7$ . *J. Solid State Chem.* **184**(7), 1882–1889 (2011)
111. T. Matsudaira, M. Wada, N. Kawashima, M. Takeuchi, D. Yokoe, T. Kato, M. Takat, S. Kitaoka, Mass transfer in polycrystalline ytterbium monosilicate under oxygen potential gradients at high temperatures. *J. Eur. Ceram. Soc.* **41**(5), 3150–3160 (2021)
112. N.S. Jacobson, Silica activity measurements in the  $Y_2O_3$ - $SiO_2$  system and applications to modeling of coating volatility. *J. Am. Ceram. Soc.* **97**(6), 1959–1965 (2014)
113. G.C.C. Costa, N.S. Jacobson, Mass spectrometric measurements of the silica activity in the  $Yb_2O_3$ - $SiO_2$  system and implications to assess the degradation of silicate-based coatings in combustion environments. *J. Eur. Ceram. Soc.* **35**(15), 4259–4267 (2015)
114. R.A. Golden, K. Mueller, E.J. Opila, Thermochemical stability of  $Y_2Si_2O_7$  in high-temperature water vapor. *J. Am. Ceram. Soc.* **103**(8), 4517–4535 (2020)
115. N.P. Padture, P.G. Klemens, Low thermal conductivity in garnets. *J. Am. Ceram. Soc.* **80**(4), 1018–1020 (1997)
116. C.M. Weyant, K.T. Faber, Processing-microstructure relationships for plasma-sprayed yttrium aluminum garnet. *Surf. Coat. Technol.* **202**(24), 6081–6089 (2008)
117. R. Gadow, M. Lischka, Lanthanum hexaaluminate – Novel thermal barrier coatings for gas turbine applications – Materials and process development. *Surf. Coat. Technol.* **151**, 392–399 (2002)
118. N.P. Bansal, D.M. Zhu, Thermal properties of oxides with magnetoplumbite structure for advanced thermal barrier coatings. *Surf. Coat. Technol.* **202**(12), 2698–2703 (2008)
119. L.R. Turcer, A.R. Krause, H.F. Garces, L. Zhang, N.P. Padture, Environmental-barrier coating ceramics for resistance against attack by molten calcia-magnesia-aluminosilicate (CMAS) glass: Part I,  $YAlO_3$  and  $\gamma$ - $Y_2Si_2O_7$ . *J. Eur. Ceram. Soc.* **38**, 3905 (2018)
120. H. Yamane, K. Ogawara, M. Omori, T. Hirai, Phase-Transition of rare-earth aluminates ( $RE_4Al_2O_9$ ) and rare-earth gallates ( $RE_4Ga_2O_9$ ). *J. Am. Ceram. Soc.* **78**(9), 2385–2390 (1995)
121. H. Yamane, K. Ogawara, M. Omori, T. Hirai, Thermal expansion and athermal phase transition of  $Y_4Al_2O_9$  ceramics. *J. Am. Ceram. Soc.* **78**(5), 1230–1232 (1995)

122. Y.-C. Yu, D.L. Poerschke, Design of thermal and environmental barrier coatings for Nb-based alloys for high-temperature operation. *Surf Coat Technol* **431**, 128007 (2022)
123. M.P. Schmitt, J.L. Stokes, A.K. Rai, A.J. Schwartz, D.E. Wolfe, Durable aluminate toughened zirconate composite thermal barrier coating (TBC) materials for high temperature operation. *J. Am. Ceram. Soc.* **102**(8), 4781–4793 (2019)
124. X.Q. Cao, R. Vassen, D. Stoeber, Ceramic materials for thermal barrier coatings. *J. Eur. Ceram. Soc.* **24**(1), 1–10 (2004)
125. A.B. Du, C.L. Wan, Z.X. Qu, W. Pan, Thermal conductivity of monazite-type REPO<sub>4</sub> (RE=La, Ce, Nd, Sm, Eu, Gd). *J. Am. Ceram. Soc.* **92**(11), 2687–2692 (2009)
126. J. Han, Y.F. Wang, R.J. Liu, F. Wan, Theoretical and experimental investigation of xenotime-type rare earth phosphate REPO<sub>4</sub>, (RE = Lu, Yb, Er, Y and Sc) for potential environmental barrier coating applications. *Sci. Rep-Uk* **10**(1) (2020)
127. F. Wang, L. Guo, C.M. Wang, F.X. Ye, Calcium-magnesium-alumina-silicate (CMAS) resistance characteristics of LnPO<sub>4</sub> (Ln = Nd, Sm, Gd) thermal barrier oxides. *J. Eur. Ceram. Soc.* **37**(1), 289–296 (2017)
128. L. Guo, Z. Yan, Z.H. Li, J.X. Yu, Q. Wang, M.Z. Li, F.X. Ye, GdPO<sub>4</sub> as a novel candidate for thermal barrier coating applications at elevated temperatures. *Surf. Coat. Technol.* **349**, 400–406 (2018)
129. L. Guo, Z. Yan, Y. Yu, J. Yang, M.Z. Li, CMAS resistance characteristics of LaPO<sub>4</sub>/YSZ thermal barrier coatings at 1250 °C – 1350 °C. *Corros. Sci.* **154**, 111–122 (2019)
130. P.E.D. Morgan, D.B. Marshall, Ceramic composites of monazite and alumina. *J. Am. Ceram. Soc.* **78**(9), 2574 (1995)
131. A.N. Fernandez, C.A. Macauley, D. Park, C.G. Levi, Sub-solidus phase equilibria in the YO<sub>1.5</sub>-TaO<sub>2.5</sub> system. *J. Eur. Ceram. Soc.* **38**(14), 4786–4798 (2018)
132. M. Gurak, Q. Flamant, L. Laversenne, D.R. Clarke, On the yttrium tantalate – zirconia phase diagram. *J. Eur. Ceram. Soc.* **38**(9), 3317–3324 (2018)
133. Q. Flamant, M. Gurak, D.R. Clarke, The effect of zirconia substitution on the high-temperature transformation of the monoclinic-prime phase in yttrium tantalate. *J. Eur. Ceram. Soc.* **38**(11), 3925–3931 (2018)
134. A.M. Limarga, S. Shian, R.M. Leckie, C.G. Levi, D.R. Clarke, Thermal conductivity of single- and multi-phase compositions in the ZrO<sub>2</sub>-Y<sub>2</sub>O<sub>3</sub>-Ta<sub>2</sub>O<sub>5</sub> system. *J. Eur. Ceram. Soc.* **34**(12), 3085–3094 (2014)
135. T.E. Strangman, Thermal barrier coatings for turbine airfoils. *Thin Solid Films* **127**(1–2), 93–106 (1985)
136. D.R. Clarke, C.G. Levi, Materials design for the next generation thermal barrier coatings. *Annu. Rev. Mater. Res.* **33**, 383–417 (2003)
137. Z.H. Xu, L.M. He, R.D. Mu, X.H. Zhong, Y.F. Zhang, J.F. Zhang, X.Q. Cao, Double-ceramic-layer thermal barrier coatings of La<sub>2</sub>Zr<sub>2</sub>O<sub>7</sub>/YSZ deposited by electron beam-physical vapor deposition. *J. Alloys Compd.* **473**(1–2), 509–515 (2009)
138. V. Viswanathan, G. Dwivedi, S. Sampath, Engineered multilayer thermal barrier coatings for enhanced durability and functional performance. *J. Am. Ceram. Soc.* **97**(9), 2770–2778 (2014)
139. M.P. Schmitt, A.K. Rai, R. Bhattacharya, D.M. Zhu, D.E. Wolfe, Multilayer thermal barrier coating (TBC) architectures utilizing rare earth doped YSZ and rare earth pyrochlores. *Surf. Coat. Technol.* **251**, 56–63 (2014)
140. A.K. Rai, M.P. Schmitt, R.S. Bhattacharya, D.M. Zhu, D.E. Wolfe, Thermal conductivity and stability of multilayered thermal barrier coatings under high temperature annealing conditions. *J. Eur. Ceram. Soc.* **35**(5), 1605–1612 (2015)
141. Q. Flamant, D.R. Clarke, Opportunities for minimizing radiative heat transfer in future thermal and environmental barrier coatings. *Scr. Mater.* **173**, 26–31 (2019)
142. D.M. Wang, X. Huang, P. Patnaik, Design and modeling of multiple layered TBC system with high reflectance. *J. Mater. Sci.* **41**(19), 6245–6255 (2006)
143. M.D. Chambers, D.R. Clarke, Doped oxides for high-temperature luminescence and lifetime thermometry. *Annu. Rev. Mater. Res.* **39**, 325–359 (2009)

144. N.K. Eils, P. Mechnich, W. Braue, Effect of CMAS deposits on MOCVD coatings in the system  $Y_2O_3$ - $ZrO_2$ : Phase relationships. *J. Am. Ceram. Soc.* **96**(10), 3333–3340 (2013)
145. A. Nieto, M. Walock, A. Ghoshal, D.M. Zhu, W. Gamble, B. Barnett, M. Murugan, M. Pepi, C. Rowe, R. Pegg, Layered, composite, and doped thermal barrier coatings exposed to sand laden flows within a gas turbine engine: microstructural evolution, mechanical properties, and CMAS deposition. *Surf. Coat. Technol.* **349**, 1107–1116 (2018)
146. Y.Q. Guo, L.L. Wei, Q. He, Y.P. Deng, W.T. He, H.B. Guo, PS-PVD alumina overlayer on thermal barrier coatings against CMAS attack. *J. Therm. Spray Technol.* **30**(4), 864–872 (2021)
147. C. Mikulla, R. Naraparaju, U. Schulz, F.L. Toma, M. Barbosa, L. Steinberg, C. Leyens, Investigation of CMAS resistance of sacrificial suspension sprayed alumina topcoats on EB-PVD 7YSZ layers. *J. Therm. Spray Technol.* (2019)
148. K.N. Lee, D.S. Fox, J.I. Eldridge, D. Zhu, R.C. Robinson, N.P. Bansal, R.A. Miller, Upper temperature limit of environmental barrier coatings based on mullite and BSAS. *J. Am. Ceram. Soc.* **86**(8), 1299–1306 (2003)
149. B.T. Richards, K.A. Young, F. de Francqueville, S. Sehr, M.R. Begley, H.N.G. Wadley, Response of ytterbium disilicate-silicon environmental barrier coatings to thermal cycling in water vapor. *Acta Mater.* **106**, 1–14 (2016)
150. K.N. Lee, J.I. Eldridge, R.C. Robinson, Residual stresses and their effects on the durability of environmental barrier coatings for SiC ceramics. *J. Am. Ceram. Soc.* **88**(12), 3483–3488 (2005)

# **Part IV**

## **Recycling**



# Chapter 17

## Value Recovery Pathways for Rare Earth Elements and Nd-Fe-B Magnets from End-of-Life Products



Nighat Afroz Chowdhury, Ikenna C. Nlebedim, Daniel M. Ginosar, Carol Handwerker, and Hongyue Jin

### 17.1 Introduction

Rare earth elements (REEs) used in neodymium-iron-boron (Nd-Fe-B) permanent magnets are classified as critical materials by various nations including the United States (U.S.), European Union (EU), Canada and Australia due to their contribution to clean energy-related technologies and potential for a significant supply risk [1–4]. With the growing interests in renewable energy and decarbonization technologies, the market for electric vehicles (EVs) and wind turbines have become vulnerable to REE availability. For example, it was projected that the demand for dysprosium (Dy) for EV magnets could exceed the supply by 2025 [5]. The global deficiencies of Nd-Fe-B alloys are expected to reach around 48,000 metric tons by 2030 which is equivalent to the amount needed to produce 25–30 million units of EV traction motors [6]. Moreover, geographically concentrated REE production could pose a significant supply risk associated with geopolitical conflicts (e.g., trade war, export quota and tariffs) and other disruptive events (e.g., COVID-19 pandemic) [7, 8]. This risk can be averted by the abundant secondary sources of REEs contained in end-of-life (EOL) products, especially in electronics including hard disk drives (HDDs).

---

N. A. Chowdhury · H. Jin (✉)

Critical Materials Institute, University of Arizona, Tucson, AZ, USA

e-mail: [hjin@arizona.edu](mailto:hjin@arizona.edu)

I. C. Nlebedim

Critical Materials Institute, Ames National Laboratory, Ames, IA, USA

D. M. Ginosar

Critical Materials Institute, Idaho National Laboratory, Idaho Falls, ID, USA

C. Handwerker

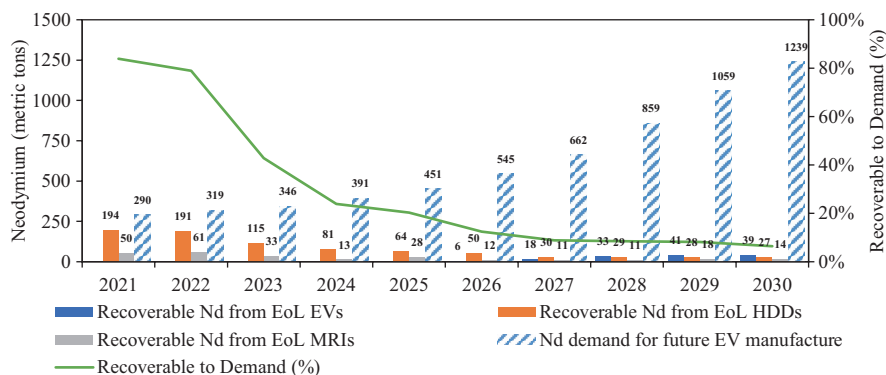
Purdue University, West Lafayette, IN, USA

© The Editor(s) (if applicable) and The Author(s), under exclusive license to Springer Nature Switzerland AG 2024

Y. V. Murty et al. (eds.), *Rare Earth Metals and Minerals Industries*,  
[https://doi.org/10.1007/978-3-031-31867-2\\_17](https://doi.org/10.1007/978-3-031-31867-2_17)

Research indicated that EOL products such as HDDs, EVs and MRIs could be the promising feedstock to recover REEs in the next 10 years [9]. Figure 17.1 shows the Nd recovery potential from these products to meet the EV demand. In 2021, the recoverable amount of Nd was projected to be the highest for HDDs, capable of supplying over 80% of Nd demand for new EV production. This is because there is a large number of HDDs reaching EOL—over 46 million units available for value recovery per year in North America alone [10]. HDDs have a relatively short lifetime (i.e., 3–5 years), which increases their turnover rate and thus availability at EOL [11]. The collection rate of EOL HDDs is also high, especially from hyper-scale data centers (i.e., approximately 95%) [12] due to data security reasons that mandate data wiping of enterprise drives [11, 13]. Therefore, various HDD value recovery pathways have been developed in collaboration with the industry [13]. For example, Dell partnered with an IT asset disposition company, Reconext (formerly Teleplan), and a major HDD manufacturer, Seagate, to produce 25,000 new HDDs from closed-loop recycled REEs in 2019 [14]. Such circular economy approaches could facilitate the secondary supply of critical materials.

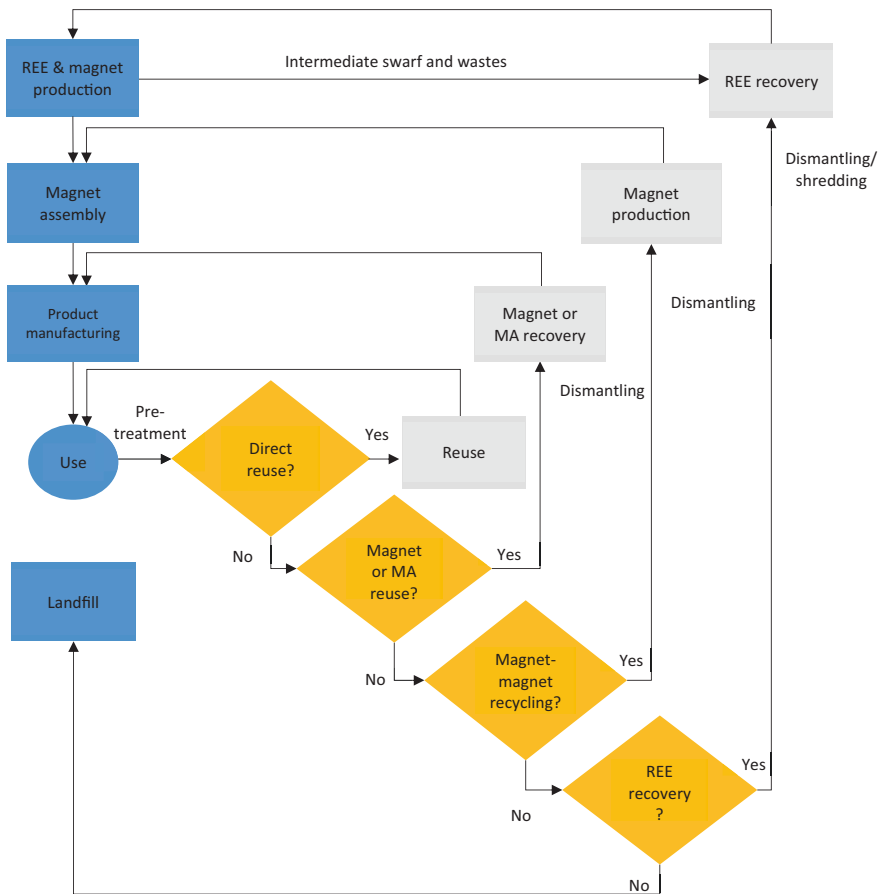
However, the importance of HDDs for REE recovery will decline progressively, while that of EVs will increase substantially [9]. EVs are projected to be the most abundant source of Nd for recycling in the late 2020s because of the growing market—EV registrations increased by 41% in 2020 according to the International Energy Agency (IEA) [15], and Nd supply from EOL EVs is expected to rise from 5.84 metric tons in 2026 to 110 metric tons in 2034 [9]. The collection rate of EOL EVs is also high, reaching approximately 95%, higher than many other secondary sources of REEs [16–18]. On the contrary, the number of EOL HDDs will decrease due to the increasing data storage capacity per drive and demand for solid-state drives. Similarly, recoverable REE from MRIs is also projected to decrease with superconducting magnets replacing the Nd-Fe-B permanent magnets in MRIs [16, 18]. Other products such as refrigerators, e-bikes, acoustic transducers, air



**Fig. 17.1** Potential secondary supply of Nd from three major EOL products: EVs, HDDs and MRIs. (“Recoverable to demand (%)” shows the ratio of recoverable EOL Nd divided by the Nd demand in EV production. The figure is adapted from Maani et al. [9] and reused with permission)

conditioners and laundry machines also represent potential for REE recovery; however, their collection rate is low (approximately 11–47%) [16]. As such, REE recovery potential differs across products over time, and knowledge gained from the existing recovery process such as that for HDDs should be conveyed to the emerging applications of Nd-Fe-B magnets, especially EVs, for sustainable long-term REE recovery.

The cascaded value recovery pathways for REEs and Nd-Fe-B magnets are depicted in Fig. 17.2. Value recovery processes preserve the highest value through prioritizing reuse over recycling. However, the specific value recovery options depend on company policies, economics and functionalities and conditions of EOL products and components which may lead to lower-value recovery resorts. The



**Fig. 17.2** Schematic diagram illustrating different value recovery options for REE and Nd-Fe-B magnets. (The figure is adapted from circular economy infographics from Jin et al. [20], INEMI value recovery project [13] and Ellen MacArthur Foundation [22]. MA stands for magnet assembly—a combination of permanent magnets with other nonmagnetic materials)

practice of reusing EOL products generally offers the highest value among all the options due to the extended product life.

Before implementing direct reuse, stakeholders should consider the operating conditions of the products, policy constraints (e.g., end users' data security mandates for HDDs) and EOL product handling logistics. Moving toward lower-value recovery options, direct reuse of magnets and magnet assemblies (MAs) from EOL products represents a viable solution when product reuse is not possible [13]. Based on the component quality, recovery costs and transboundary shipment for reintroducing EOL components into new products, a thorough evaluation of recovery processes and reverse logistics is the key for sustainable execution of this value recovery pathway.

Next is magnet-to-magnet recycling that employs hydrogen ( $H_2$ ) to recover magnet powders and produce new magnets in a closed-loop fashion. Such recycled magnets can be reinserted into the original supply chain much faster than metal recycling processes that return the products as metals or oxides [19].

Lastly, REE recovery from EOL products allows for both open-loop recycling where the recovered REEs may be used for magnets or nonmagnet applications as well as closed-loop recycling within Nd-Fe-B magnets. Nonetheless, REE recycling is often more costly and offers less value compared to the other options [20, 21]. Therefore, REE recovery from Nd-Fe-B magnets and EOL products should be considered as the last resort when the other reuse and remanufacturing options are not viable.

## 17.2 Value Recovery Pathways

### 17.2.1 Direct Reuse of EOL Products

Various pathways are being explored to ensure the direct reuse of EOL products such as HDDs and smartphones. Fully functional HDDs retire from data storage systems for a variety of reasons including age, technology and IT upgrades. Peeters et al. [23] examined 149 units of discarded laptop HDDs and found 38% of them reusable. Most data centers periodically remove their fully operational, under warranty [20] HDDs from the system and insert new ones to increase the data storage capacity without having to expand the data center infrastructure. These drives represent a significant reuse opportunity.

In order to reuse HDDs, they are first extracted from the system (e.g., computers and servers) and tested by SMART (Self-Monitoring, Analysis and Reporting Technology) to evaluate the functionality. If the extracted HDDs are deemed reusable, they can be wiped of data according to the National Institute of Standards and Technology (NIST), Department of Defense (DOD) or National Security Agency (NSA) standards and verified for complete data erasure. The recovered HDDs can be used internally or sold to the secondary market in the form of original equipment

manufacturers (OEM) labeled recertified HDDs, white-label HDDs and other out-of-warranty HDDs [10, 13].

Although reusing HDDs has an order of magnitude higher value than shredding [13], millions of fully functional HDDs are shredded, constituting the most common practices of EOL HDDs. The major bottleneck for HDD reuse is the perceived data security concern, even though the existing technologies are capable of erasing data securely. Human and logistics-related errors during HDD handling, transportation and storage are a major source of data breach so that many data centers employ on-site data wiping and physical destruction processes. Regulated data disposal commands significant legal and financial penalties to data breach organizations, promoting physical shredding of EOL HDDs which became a significant barrier for reuse [24].

To help protect data privacy and reuse HDDs, self-encrypting drives with crypto-erase capability have emerged [25]. Data are encrypted when writing to the drives, and users can change the encryption key with a simple command that instantly transforms the prior encrypted data to unreadable forms. Crypto-erase reduces data wiping time and protects data from human and logistics-related errors to facilitate HDD reuse.

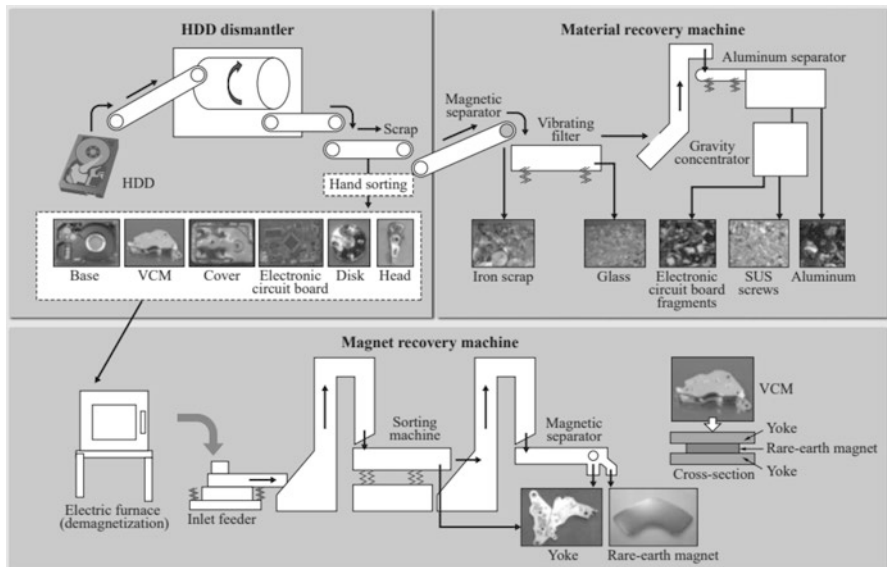
Besides technological development, it is crucial to change HDD user policies to move away from physical destruction and prioritize reuse. It requires a more stringent EOL HDD handling process and infrastructure to assure data security. The specific measures include [1] following the NIST 800-88 R1 standards [26] for secure data sanitization; [2] working with trusted, certified IT asset disposition companies that effectively manage EOL HDDs and [3] enhancing inventory control and monitoring to keep track of EOL HDDs and ensure no loss of sight.

Although reuse strategies and policies are quite established for HDDs, the literature on direct reuse for other EOL products is limited. In the United States and the United Kingdom, 50–65% of collected EOL cell phones are reused than going through recycling options [16]. Reuse of cell phones is ensured by third-party enterprises rather than the OEMs. Such organizations collect, inspect and sort the EOL handsets for their reuse opportunities based on their functionality, aesthetic conditions and demand in the secondary market. Cell phones that cannot be resold are sent for recycling to recover valuable materials. Repurposing or refurbishing cell phones for other applications is another strategy for cell phones to make use of their computational capacity [16]. EOL cell phones can be an excellent fit for primary school education, according to one research on an educational software running on smartphones [16]. Li et al. [16] demonstrated that the lifetime of EOL smartphones can be extended for additional 5 years with the remaining resources left with the devices. Zink et al. [27] demonstrated repurposing and refurbishing cell phones for use as in-vehicle parking meters. Apple also highlighted the importance of refurbishing discarded phones through their “Reuse and Recycle” trade-in program [28]. The cell phones collected through this program could be sold into the secondary market [28]. However, the operating conditions, age of the phones and compatibility with recent software could be the limiting factors for this pathway [28].

### 17.2.2 Dismantling EOL Products for Magnets and Magnet Assemblies

When reusing the entire EOL product is not possible, the next pathway is to extract magnets and MAs through dismantling. Dismantling or shredding operations are often applied to EOL products to recover components containing critical materials such as REEs. Preservative dismantling guarantees that magnets are recovered in their entirety which results in a higher economic value. Due to less complexity in design specifications, large REE magnets in EVs and turbines can be removed and these big magnets could also be repurposed after refurbishment [28]. Small- to medium-sized recycling enterprises often use manual dismantling; nonetheless, cost and time may be two major constraints for such a process. Manual disassembly to retrieve the MAs, for example, might take several minutes to hours on average depending on the EOL products. Therefore, automatic dismantling is being explored as an alternative to manual dismantling so that the magnets and MAs could be recovered more efficiently with less processing time.

Hitachi developed an automatic dismantling process to extract Nd-Fe-B magnets and MAs from HDDs and air conditioners on a commercial scale [29]. The upper-left section of Fig. 17.3 shows their HDD dismantling process, where HDDs are loaded into a dismantling machine via an in-feed conveyor and the dismantled



**Fig. 17.3** A process developed by Hitachi to extract REE magnets from HDDs. (The upper-left block shows HDD dismantling operations to sort and separate MAs. The upper-right section shows the base metal recovery process and the lower section represents the working principles of the magnet recovery machine to recover REE magnets through demagnetization. The figure is from Baba et al. [29] and reused with permission)

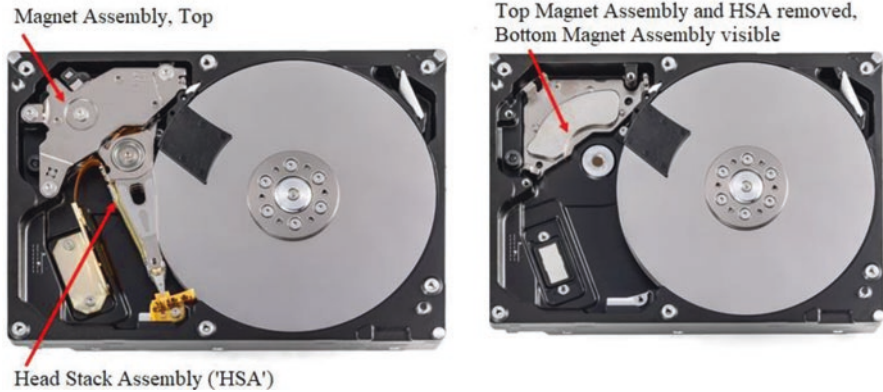
components are hand-sorted on a sorting conveyor to recover magnets (same as MAs defined earlier) from voice coil motors (VCM), printed circuit board and other components. The extracted MAs are demagnetized in an electric furnace, and the bond between REE magnets and yokes is loosened in a magnet recovery machine to liberate the magnets as shown in the lower section of Fig. 17.3. The other HDD components go through magnetic separation for ferrous-component recovery, vibrating filtration for glass recovery, aluminum separation/recovery and gravity concentration for printed circuit board and screw recovery as shown in the upper-right section of Fig. 17.3. Such a co-recovery process maximizes the value recovered from HDDs. The system was reported to be capable of processing 200 HDDs per h, which could vary based on the HDD design.

Apple also developed dismantling robots, Daisy and Dave, to mechanically disassemble iPhones and reclaim critical minerals preserving the original function and quality of the dismantled components [28]. Daisy, with an hourly dismantling rate of 200 iPhones, uses a four-stage mechanical process to dismantle the iPhones [30, 31]. It first separates the body from the screen by pressing a series of prongs into the seam [30]. In the next step, Daisy utilizes a blasting procedure that uses freezing air ( $-80\text{ }^{\circ}\text{C}$ ) to provide enough force to release the battery from the body which is bonded together with glue [30, 31]. The screws that hold the logic board in place on the phones are then removed. Identifying the phone model and the angle at which it is mounted, Daisy ensures positioning accuracy for this process [30]. Finally, Daisy retrieves various components such as cameras, speakers and modules, including the haptics, which controls the phone's vibratory activities [30]. After collecting all the components, the aluminum case of the phone remains which may be recycled.

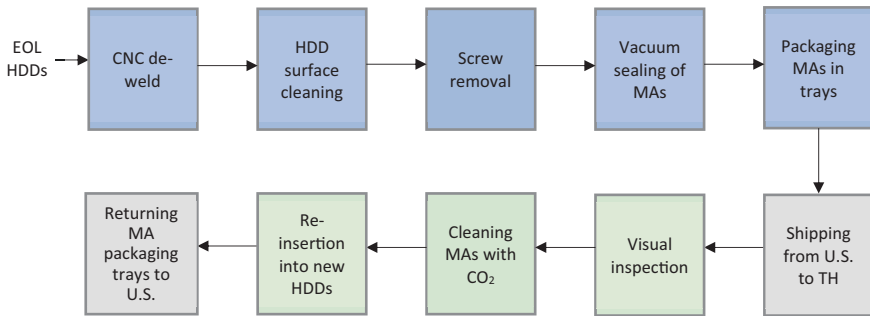
Oak Ridge National Laboratory (ORNL), as part of the DOE Critical Materials Institute (CMI), developed a HDD dismantling process for magnet reuse in gap motors [32]. They developed a mapping station including a barcode scanner with a 3D coordinate measuring machine to generate an inventory database containing information such as HDD make, model, data storage capacity, serial number and fastener locations. The information was used to identify the incoming HDD types and plan for an automated disassembly (e.g., alignment for robotic disassembly). Then REE magnet assemblies were separated from HDDs by high-speed robots mechanized for drilling. The process also liberated other HDD components such as circuit boards and disk platters.

### ***17.2.3 Nd-Fe-B Magnet and Magnet Assembly Reuse***

After dismantling of HDDs, two Nd-Fe-B magnets can be recovered from the top and bottom of the MAs, as shown in Fig. 17.4. The MA set weighs about 100 g per drive and contains approximately 27 g of Nd-Fe-B magnets that are attached to yokes [20, 33]. Properly recovered MAs preserve the function and reliability even after HDDs retire allowing almost 100% of reuse in new HDDs [34].



**Fig. 17.4** Rare earth magnet assemblies inside an HDD. (The figure is from Handwerker et al. [43] and reused with permission)

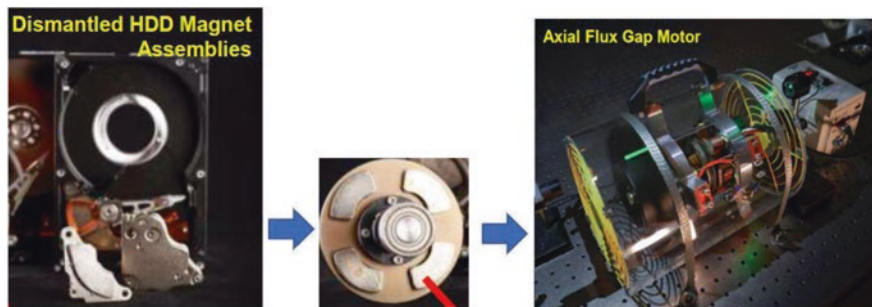


**Fig. 17.5** Magnet assembly recovery process for reuse in new HDDs [34]. (TH stands for Thailand, the largest HDD manufacturing country. Blue and green boxes represent the clean-room operations in the US and TH, respectively. Gray boxes show the shipping between the two countries)

More than 90% of EVs use Nd-Fe-B magnets in different motors such as traction motors, brushed and brushless DC, axial flux and synchronous motors, consuming 2–5 kg of REE-containing magnets per EV depending on the geometric requirements [35–37]. Smartphones also use up to 14 Nd-Fe-B magnets in the speaker, receiver, VCMs in cameras and vibration motors that account for approximately 1.03 g per cell phone [38–40]. Reusing the magnets from these products as they reach EOL could reduce virgin REE production, Nd-Fe-B magnet manufacturing and MA assembly processes, avoiding the environmental life cycle impacts (e.g., global warming) and fostering a more sustainable circular economy [41, 42].

Frost et al. [34] demonstrated a pilot-scale MA recovery and reuse process (Fig. 17.5) in collaboration with major HDD industry stakeholders. Over 6000 units of EOL HDDs were disassembled within a U.S. data center to minimize transportation distance and data breach risks. The process started with de-welding by a computer numerical control (CNC) machine to remove HDD top covers in a cleanroom





**Fig. 17.6** Reuse of HDD magnets in axial flux gap motors. (The figure was from Handwerker et al. [43] and reused with permission)

environment. Torque drivers were employed to remove screws and liberate MAs which were then vacuum-sealed and packaged into a specialized shipping tray. As Thailand manufactures over 80% of global HDDs [44], MAs were shipped to Thailand, cleaned with pressurized CO<sub>2</sub> “air knives” and placed back into new HDDs for reuse. The process was estimated to reduce the embodied carbon footprint of MAs by 67–86% compared to the business-as-usual of shredding EOL HDDs for base metals recovery and producing MAs from virgin materials.

The harvested Nd-Fe-B magnets from the dismantling process developed by ORNL could be reused by conceptual motor manufacturers in applications such as axial, radial and linear gap motor designs and manufacturing. ORNL and Ames National Laboratory, as part of CMI, demonstrated a successful implementation of EOL HDDs magnet reuse in axial gap flux motor [13] as shown in Fig. 17.6.

The major limitations of magnets and MA reuse include the high-quality requirement of the recovered components and the changing product designs. HDDs are extremely sensitive to minute particle contaminations, so MA recovery processes (e.g., dismantling, MA retrieval and reassembly) need to be performed in a clean-room environment preserving the original component quality for direct reuse in new HDDs. In addition, product designs change constantly over time resulting in magnet design modifications. By the time magnets and MAs are recovered after their first life cycle, the products may become obsolete and thus component reuse may not be feasible. Therefore, design for “X” (e.g., disassembly, remanufacturing and reuse) and keeping the magnet/product design consistent through multiple generations will allow the reuse process to scale [45].

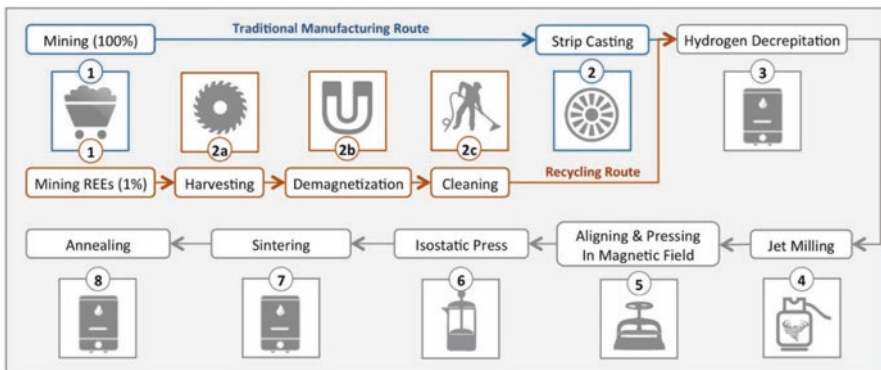
## 17.2.4 Nd-Fe-B Magnet Remanufacturing

### Full-Density Magnet Remanufacturing

When MAs and magnets cannot be reused directly, magnet-to-magnet recycling could be the next best option to reproduce sintered magnets from EOL magnets. The process aims to preserve all the magnet materials without extracting REEs and

separating them down to the individual element level. It is considered beneficial because it is a faster route for returning recycled products back to the supply chain with significant economic and environmental advantages over traditional REE recovery and the subsequent magnet production.

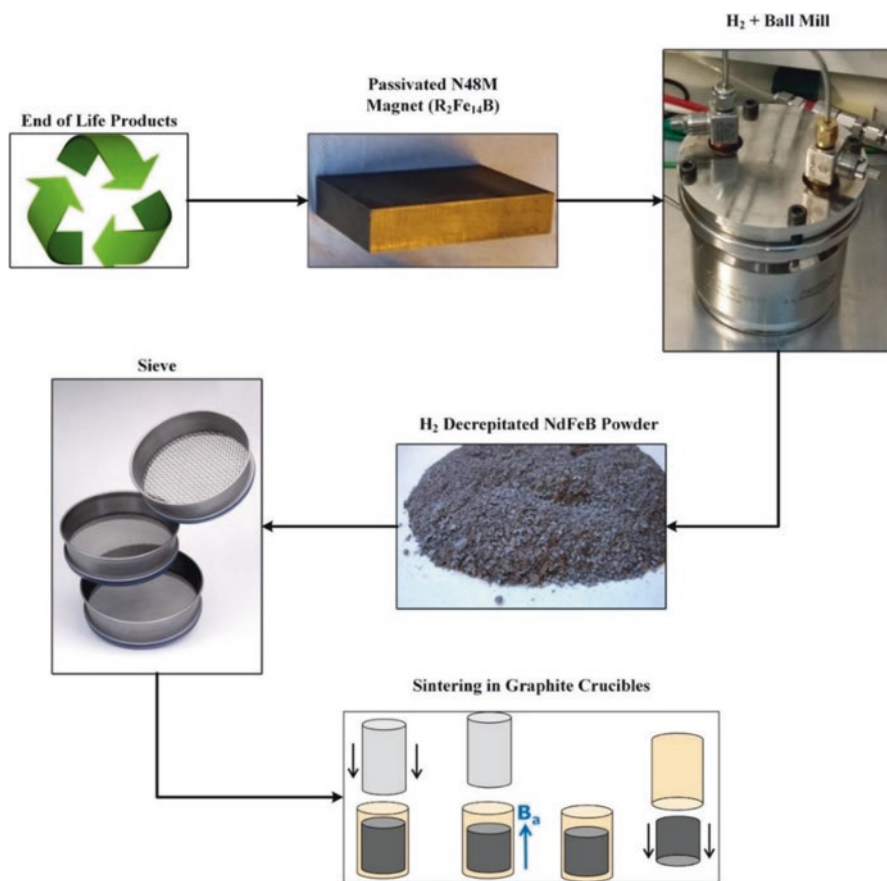
Figure 17.7 illustrates the processes for virgin magnet manufacturing versus magnet-to-magnet recycling commercialized by Urban Mining Company [46, 47]. In the virgin magnet production route, REEs, Fe, B and other additives are produced from their respective ores [47, 48]. Rare earth oxide (REO) production from Bayan Obo, the largest REE mine on the globe, entails mining, Fe separation, REE concentration, acid roasting, water leaching, solvent extraction and calcination, which are notorious for the environment due to the chemical- and energy-intensive processes [42]. The REOs are further reduced to RE metals through electrorefining and alloyed with other virgin materials (e.g., Fe, B and copper (Cu)) at an elevated temperature (approximately 1400 °C), which are then strip-casted for virgin Nd-Fe-B magnet manufacturing. In the case of magnet-to-magnet recycling, it reduces the virgin materials requirement by utilizing almost all the materials from Nd-Fe-B magnets harvested from EOL products. The harvested magnets are demagnetized at a temperature around 400 °C and cleaned to remove the surface coating (e.g., galvanized nickel). The de-coated magnets are then treated with H<sub>2</sub>, in addition to a grain boundary modifier alloy that consists of a small amount of REEs (e.g., Nd and Dy; less than 5% of the initial feedstock) to enhance the magnetic properties of recycled magnets [47]. The latter processes of jet milling, magnetic alignment, pressing, sintering and annealing are common with the virgin magnet production route. As REE production constitutes the single largest environmental hot spot for Nd-Fe-B manufacturing, magnet-to-magnet recycling has a significant environmental benefit over virgin magnet production [47]. Nevertheless, it is not suitable for all types of EOL magnets, especially small magnets, such as those in cell phones or those that are significantly fractured. This is because the surface coating removal also removes a



**Fig. 17.7** Comparison of virgin Nd-Fe-B magnet manufacturing processes with magnet-to-magnet recycling. (The figure is from Zakotnik et al. [47] and reused with permission)

small layer of the magnet which, for small magnets, yields product that are not suitable for treatment with  $H_2$  and are unprofitable to further process.

A similar version of magnet-to-magnet recycling was proposed by Xia et al. [49] in which a press-less process (PLP) was coupled with  $H_2$  decrepitation (Fig. 17.8). In this process, the authors first applied  $H_2$  decrepitation and ball milling to EOL Nd-Fe-B magnets in an inert atmosphere (i.e., argon (Ar) glovebox) to obtain Nd-Fe-B powder of proper sizes (less than  $100\ \mu\text{m}$ ), similar to traditional magnet manufacturing. Then the Nd-Fe-B powder was sieved and PLP was applied where the powder was sintered in a graphite mold as previously reported by Popov et al. [50] The PLP has some advantages over the traditional press-and-sinter process in that it requires less tooling which saves costs. In addition, elimination of tooling also makes it easier to handle fine magnet powders and can potentially result in magnets with higher performance and a process with a higher yield.



**Fig. 17.8** Schematic diagram of  $H_2$  decrepitated PLP method to recycle anisotropic magnets. (The figure is from Xia et al. [49] and reused with permission)

A key benefit of magnet-to-magnet recycling is the possibility for the recycled magnets to outperform the original magnets by adjusting the material composition and other parameters during recycling [46]. For example, a small amount of Dy (0.2–1.3 at.%) can be added to enhance temperature performance parameters of the magnet such as the thermal coefficients of remanence ( $\alpha$ ) and coercivity ( $\beta$ ). Some intermetallic alloys of rare earth (e.g., Nd and Pr) and transition metal elements (Cu, Ga and Al) can be added to enhance coercivity.

Perhaps one of the most significant benefits of the magnet-to-magnet recycling method is that it opens a new avenue for creating sintered magnets which has been severely limited by various Hitachi patents [51–54]. Those patents, which have been the subject of different lawsuits, have made it challenging for new players to enter the market. Nevertheless, some of these patents are soon expiring. Until then, magnet-to-magnet recycling provides an opportunity for other companies to produce sintered magnets for clean energy technologies and defense security.

### **Bonded Magnet Remanufacturing**

Isotropic and anisotropic powders derived from different EOL Nd-Fe-B magnets can be reintroduced into the supply chain as bonded magnets. Bonded magnets comprise magnet powders in a suitable binder (i.e., nylon, polyphenylene sulfide; Teflon and thermoset epoxies) prepared with methods like calendaring, compression, injection and extrusion molding [55, 56]. Recycling HDD magnets into bonded magnets requires that the sintered magnets be first converted to powders. This creates a great challenge because any pulverization method that is adopted must retain the hard magnetic properties (e.g., maximum energy product and coercivity) of the resulting powders for subsequent permanent magnet production. However, it is easier to recycle bonded magnets back into bonded magnets [57] than converting sintered magnets into bonded magnets. Commercial powders for bonded permanent magnets are produced mainly by hot-deformation (or die-upsetting) or the hydrogenation-disproportionation-desorption-recombination (HDDR) process [58].

Although sintered magnets can be converted to powder by  $H_2$  decrepitation, powders obtained via such an approach lose their magnetic properties because they can consist of multiple phases including  $Nd_2Fe_{14}BH_x$ ,  $NdH_2$ , RE-rich phases,  $\alpha$ -Fe and  $Fe_2B$  depending on the decrepitation parameters such as temperature and pressure [49, 59, 60]. Consequently, it is unlikely that  $H_2$ -decrepitated magnet powders can be directly recycled into bonded magnets as suggested by Walton et al. [61]. Nevertheless, the hard-magnetic properties can be recovered with some added thermal treatments [62].

An alternative method reported by Itoh et al. [63] recycled EOL anisotropic nickel-coated sintered HDD magnets into isotropic powder for bonded magnets. In their method, the authors subjected the scrap HDD magnets to the melt-spinning process. The process includes ejecting a molten magnet alloy onto a rotating Cu wheel to rapidly solidify it into ribbons. The ribbons were grounded into powders for bonded magnet production. The recycled magnet powder was reported to have

magnetic properties comparable with commercial powders for bonded magnet manufacturing. Although the authors reported using Ni-coated samples, it is unclear whether the coatings were removed prior to melt-spinning. Moreover, this process yields isotropic, instead of anisotropic magnets.

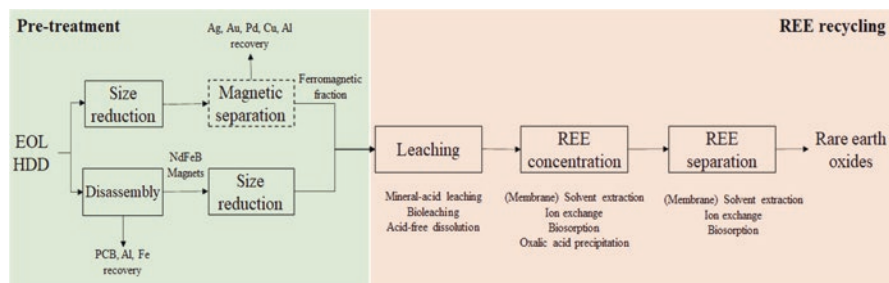
Gutfleisch et al. [64] demonstrated that anisotropic Nd-Fe-B sintered magnets can be recycled into anisotropic bonded magnets that have properties comparable to non-recycled bonded magnets produced with the same powder as the sintered magnet. The method combined the traditional H<sub>2</sub> decrepitation method with the dynamic HDDR process. The former produced single-crystal powders from the sintered magnets, while the latter enabled the development of textured particles for magnetically anisotropic powders.

Poskovic et al. [65] reported on recycling sintered Nd-Fe-B magnets into powder for bonded magnets based on mechanical treatments. The authors compared three different mechanical treatments namely ball milling, impact milling and lamination to demonstrate their effects on retaining properties suitable for bonded magnets. It was found that impact milling is more effective than ball milling and lamination and milling in an Ar environment is more effective than in a nitrogen (N<sub>2</sub>) environment for particle sizes between 250–500 μm. They also compared the properties of recycled powders with commercial powders used in conventional bonded magnet production. The method for assessing the performance of the resulting powder is, however, questionable as HDD magnets are anisotropic and commercial magnet powders are isotropic. In addition, the isotropic powder outperformed the recycled powder indicating substantial degradation of magnetic properties due to the mechanical grinding methods used.

### 17.2.5 REE Recycling

REE recycling technologies such as hydrometallurgical, pyrometallurgical and gas-phase extraction methods aim to break down products and components into the individual constituent elements which entails significant materials and energy consumption [66]. The final products from REE recycling are reinserted further up in the supply chain than the prior options discussed in Sects. 17.2.1, 17.2.2, 17.2.3 and 17.2.4, which requires additional resources, efforts and costs to reprocess them for the final products (e.g., HDDs) [67]. However, REE recycling is necessary for shredded e-wastes, magnet grinding swarfs or magnets that cannot be recovered via *other approaches*. The technologies also make it possible to recycle REEs for both open- and closed-loop applications.

As REEs are concentrated in Nd-Fe-B magnets, pretreatments such as disassembly (not as preservative as for the reusing scenario), size reduction (e.g., shredding and milling) and magnetic separation are typically employed to mechanically remove other materials (e.g., printed circuit boards that contain precious metals in electronics). A typical hydrometallurgical process (Fig. 17.9) employs leaching to dissolve REEs and then further concentrates and separates REEs through

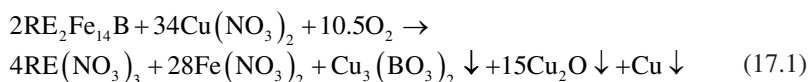


**Fig. 17.9** A general process flow diagram of hydrometallurgical REE extraction and recovery from EOL HDDs. (The dashed box indicates an optional process. PCB is an abbreviation for printed circuit board)

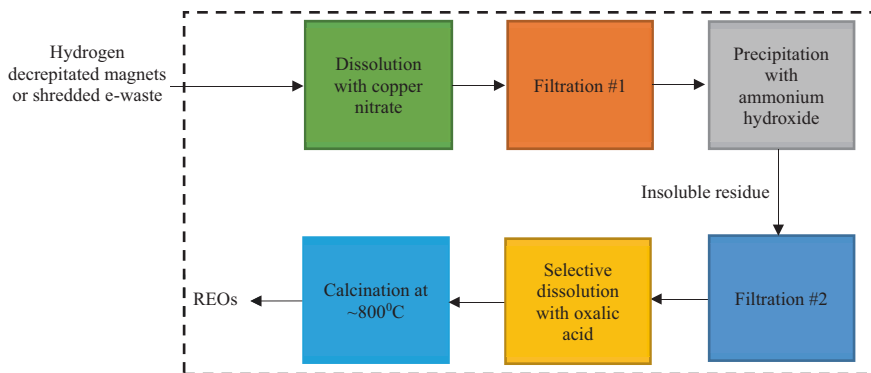
(membrane) solvent extraction, ion exchange, biosorption and other competing technologies to produce high-purity REOs.

Diaz and Lister [68] and Li et al. [69] emphasized the significance of co-recovery of REEs and precious metals from electronic waste for economic and environmental sustainability. The technology utilized hydrochloric acid leaching of the ferromagnetic fraction of shredded e-waste, followed by rare earth precipitation using sodium sulfate [70]. Although REE recovery efficiency was over 80%, REE contributed less than 1% of the total revenue. Precious metals—gold and silver contributed 80–97% of the total revenue for all three options of hydrometallurgical-, pyrometallurgical- and a comprehensive recovery that included electrochemical processing. The global warming potential of the comprehensive recovery process was 1–10% of the relevant REE production impact from ion adsorption clays, depending on the allocation assumptions (i.e., how to allocate the environmental impacts of recycling multiple products (e.g., precious metals and rare earth elements) that share the same processing steps (e.g., size reduction)).

Prodius et al. [71] reported a novel acid-free dissolution process for extracting REEs from H<sub>2</sub>-decrepitated Nd-Fe-B magnets and shredded e-wastes. The process flows are shown in Fig. 17.10. The key chemical reaction is shown in Eq. (17.1) which utilizes a copper (II) nitrate hemi(pentahydrate) solution to dissolve REEs.



These chemical activities produced an insoluble solid deposit of Cu salt, oxide and metallic powder of which more than 98.5% was filtered away. Then a solution of oxalic acid (H<sub>2</sub>C<sub>2</sub>O<sub>4</sub>) was added to generate rare earth oxalates (RE<sub>2</sub>(C<sub>2</sub>O<sub>4</sub>)<sub>3</sub>·10H<sub>2</sub>O). They were precipitated, filtered and calcined to generate a mixture of REOs that has a purity greater than 99.5%. The recycled REOs could be used directly to produce magnets without separating into individual REOs and thus forgoing solvent

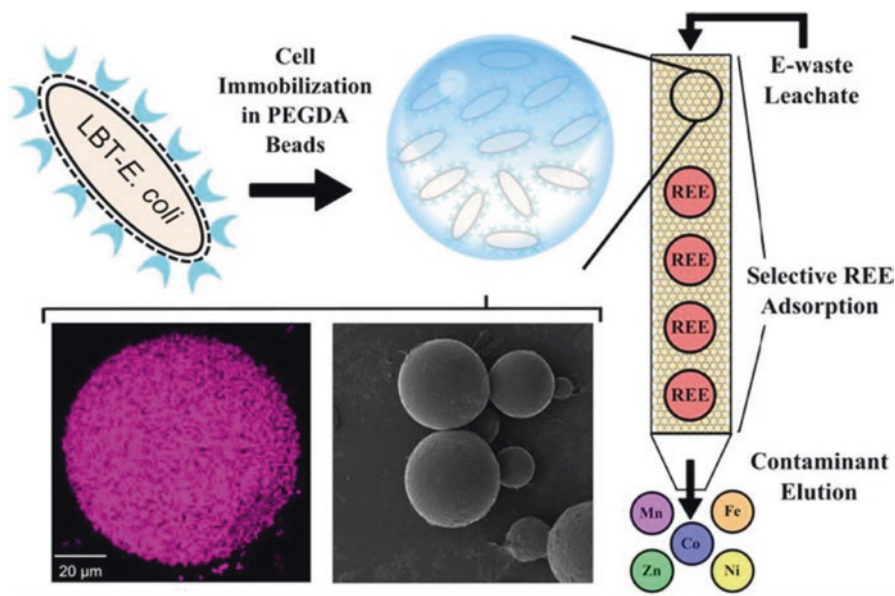


**Fig. 17.10** Process flow diagram for REO recycling from Nd-Fe-B magnet waste through acid-free dissolution

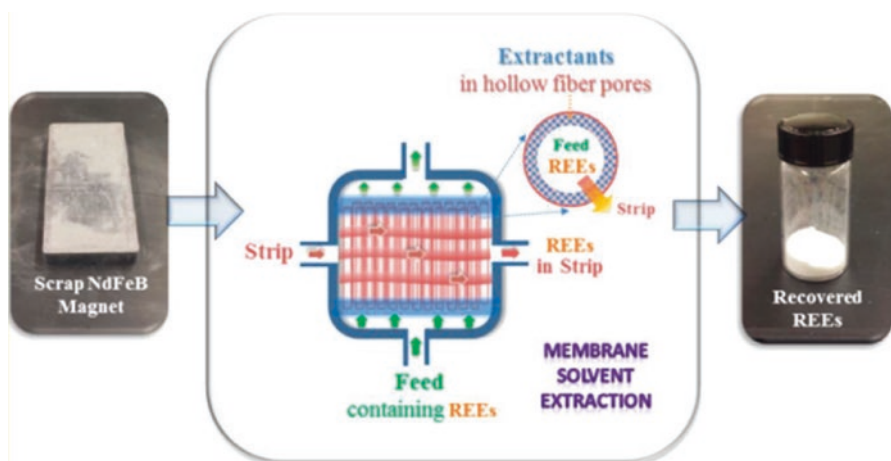
extraction. The authors demonstrated that Nd-Fe-B magnets produced from these recycled REOs had comparable coercivity, remanence and energy product as commercially available magnets.

Brewer et al. [72] developed biosorption technology for REE recovery from electronic waste leachate (Fig. 17.11). *E. coli* microbes were genetically modified to display lanthanide-binding tags (LBT) on the cell surface to selectively adsorb rare earth elements from the leachate solution. The microbes were encapsulated in permeable polyethylene glycol diacrylate (PEGDA,  $C_5H_{10}O_4$ ) bead, and the resulting bio-sorbent material was packed into a flow-through column that the leachate was fed into to remove unwanted contaminants (e.g., Fe, Ni and Co). To desorb REEs from the bio-sorbent, sodium citrate ( $Na_2C_6H_5O_7$ ) was pumped into the column, recovering 91% of REEs with a purity of 95%. The process could be more sustainable than solvent extraction which uses harsher chemicals (e.g.,  $P_2O_4$ ). However, the process required pH adjustment of the leachate up to 6 which may precipitate REEs before applying biosorption. In addition, REE adsorption capacity (2.6 mg/g) was lower than unencapsulated microbes, resulting in a high materials cost [72, 73].

Deshmane et al. [74] developed a membrane-assisted solvent extraction technology to recover  $\geq 99.5$  wt.% pure REEs in a single-step continuous process (Fig. 17.12). REE-containing feed solution was prepared by leaching Nd-Fe-B magnet scraps from a variety of sources including HDDs and hybrid EVs with nitric acid (8 M  $HNO_3$ ). Tetraoctyl diglycolamide (TODGA, N, N, N', N' -tetra-n-octyldiglycolamide) was used as an extractant (Eq. 17.2) along with Isopar-L L as a solvent and tributyl phosphate (TBP,  $C_{12}H_{27}O_4P$ ) as a phase modifier at a volume ratio of 30%, 40% and 30%, respectively. The organic phase was immobilized by a polypropylene ( $(C_3H_6)_n$ ) hollow fiber membrane and over 95% of REEs were selectively extracted from the starting feedstock. To lower the extractant cost, technical grade TODGA of 90+% purity was tested which showed a similar performance to refined TODGA of 97+% purity. REE was recovered in the stripping solution containing 0.02 M  $HNO_3$ . Finally,  $C_2H_2O_4$  precipitation, filtration and oven-drying were

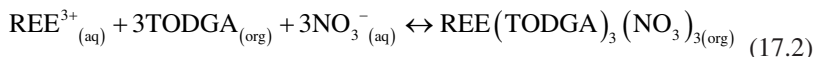


**Fig. 17.11** Process flow diagram of a biosorption process for REE recovery from e-waste leachate. (This figure is from Brewer et al. [72] and reused with permission)



**Fig. 17.12** Process flow diagram of a membrane solvent extraction process for REE recovery from scrap Nd-Fe-B magnets. (This figure is from Kim et al. [75] and reused with permission)

applied to recover  $\geq 99.5$  wt.% pure REOs. REE extraction rate was highly dependent on the REE feed concentration as a lower REE concentration ( $\sim 23,000$  mg/L) resulted in a much lower extraction rate ( $1\text{--}2$  g/(h m<sup>2</sup>)).

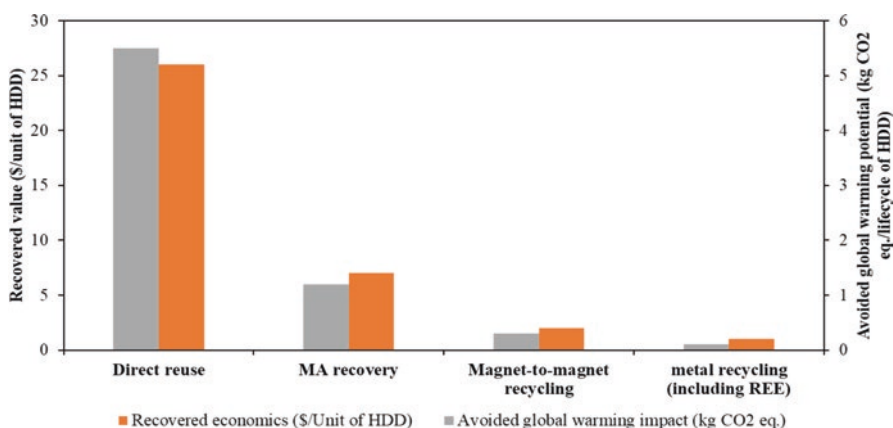




### 17.2.6 Economic and Environmental Implications of Value Recovery Pathways

Conventional operations from REE mining to magnet manufacturing pose a significant environmental challenge due to harsh chemical usage, energy-intensive processes and artisanal mining not being compliant with environmental regulations in the developing countries [76, 77]. As a remedy, value recovery pathways for REEs and Nd-Fe-B magnets could enable waste valorization of critical materials with a lower environmental footprint. While the specific economic and environmental impacts vary from case to case, Fig. 17.13 shows a general trend of value recovery options for HDDs in terms of recovered value and avoided global warming potential (GWP) [78] which could also be applicable for other EOL products. The economic and environmental benefits follow a decreasing trend from reuse to metal recycling.

1. As the first option in the value recovery cascade, EOL product reuse may have the highest economic and environmental potential due to their extended lifetime of entire functional products [20]. The process requires a minimum amount of energy (e.g., HDD data wiping and reconditioning) and materials cost compared to the other recovery options [79, 80]. For example, reusing cell phones could cost \$1.76–\$3.37 per unit, while the resulting resale value ranges between \$17 and \$23 per phone and the avoided GWP is about 4.04 kg of CO<sub>2</sub> equivalent [79, 80].
2. The second option involves magnet or MA reuse which may result in less economic and GWP benefits than reusing the entire product due to additional processing steps such as disassembly of MAs and reassembly into new products. The mode of transportation is a crucial aspect that influences the GWP of MA reuse in HDDs. If entire HDDs are transported by air from the United States to Malaysia for MA disassembly and reuse, the global warming potential will be



**Fig. 17.13** A representative scheme of economic value and environmental benefit from four circular economy pathways of HDDs [10, 13, 20, 78].

higher than new MA production [20]. Transportation via air is faster, easier and reliable than transportation via sea; however, it generates significant environmental impacts that outweigh the benefits from avoided virgin MA production.

3. Magnet-to-magnet recycling employs powder metallurgical processes to recover magnet materials from EOL magnets and recycles them into sintered or bonded magnets. The energy consumption and magnet material loss during cutting, grinding and shaping processes or out-of-spec magnets are the key drivers of costs and environmental impacts. The overall economic and environmental benefits are expected to be greater than those of virgin magnet production because it avoids over 99% of new REE production which is considered as the most environmentally harmful process of Nd-Fe-B magnet manufacturing [81].
4. For the last option of REE recycling, the expected economic and environmental benefits are the lowest due to the employment of chemical- and/or energy-intensive processes to break down EOL products and components to the elemental materials. The benefits of metal recycling are its [1] flexibility in processing EOL products of different conditions; [2] versatile applications of recovered metals, oxides or salts and [3] potentially more suitable for large-scale applications. The prior three options, in particular, reuse, require intact EOL products (e.g., MA or magnets) which will eventually retire from the product system and may not be reused further. These feedstocks can be recovered for multiple materials (e.g., precious metals from e-waste, REEs and base metals) through recycling.

### 17.3 Future Outlook and Recommendations

Value recovery technologies for REEs and Nd-Fe-B magnets from different EOL products have captured a lot of attention in the fields of research, education and innovation that are considered the key drivers of a knowledge triangle. To fully comprehend and integrate the emerging technologies into the existing product and REE supply chain, the following perspectives are presented:

1. *Reuse than recycling*: Existing studies indicated that the major cost and environmental footprint in Nd-Fe-B magnet manufacturing are driven by mining, extraction and separation of REEs [82–84]. While REE recycling from EOL products also contributes to the circular economy, the process is generally more complex, costly and environmentally challenging than reuse. Therefore, direct reuse of REE-containing products, magnet assemblies and magnets should be encouraged rather than going through various recycling steps [85]. However, there are limited studies on direct reuse, and in particular, on design for reuse and remanufacturing, warranting future research [86].
2. *Compliance toward OEM requirements*: Different methods to recycle Nd-Fe-B magnets and a comparison of several performance characteristics with the virgin

magnets were presented. However, OEM requirements on the product specification may not be available in the open market and recovered products may lack quality to be directly reinserted into the existing supply chain. For example, recycled REOs shall be of  $\geq 99.5\%$  purity in order to be compatible with the existing REE production facility operations. Therefore, it is of crucial importance to identify OEM requirements and industry standards to ensure the maximum utility from value recovery technologies.

3. *Future dominance of electric vehicles*: Although this chapter focused on the circular economy of HDDs, the future available EOL Nd-Fe-B magnets are projected to be largely driven by EVs in the next 10–20 years [9]. This is because the number of HDDs will decrease gradually due to the increasing adoption of solid-state drives (SDDs) and increasing data storage capacity per drive. EV demand, on the other hand, has been growing exponentially. In 2020, the global EV registration increased by 41% [15], and the trend is expected to continue with substantial governmental support and industry follow-up [87]. Therefore, knowledge gained from HDD value recovery shall be transferred to EV recovery to prepare for such a transition [20].
4. *Collaboration among stakeholders*: As HDD and REE recovery technologies and supply chains are complex, there should be close collaborations among the key stakeholders in the industry as well as academia and National Laboratories for technology development, commercialization and integration. Frost et al. [34, 88] highlighted the importance of micro-, macro- and even meso-level collaboration in transitioning the economy model from a linear to a circular one. Such collaborations shall promote and establish joint ventures among stakeholders and business entities at various stages of accomplishing the pathways to REE value recovery [87].
5. *Policy incentives*: The U.S. government recognized the importance of government data center HDDs for REE recovery [45, 87]. If governmental policies could be developed on a scale similar to the plan to electrify the federal fleet, the REE recovery processes could serve thousands of government-run data centers [45, 87]. Currently, Subpart 23.7 of the Federal Acquisition Regulation (FAR) requires federal agencies to procure environmentally sustainable electronic products, according to the US Environmental Protection Agency (EPA) [89]. Global Electronics Council (GEC) grants two points for the HDDs containing 5% or more postconsumer recycled Nd or Dy in the actuators or VCMs through EPEAT (Electronic Product Environmental Assessment Tool) Ecolabel [90]. More of such policy incentives will accelerate value recovery technologies and their commercialization for REEs and REE-containing magnets from EOL products.

**Acknowledgments** We thank Dan McFarland Park for providing valuable feedback on biosorption. This work is supported by CMI, an Energy Innovation Hub funded by the U.S. Department of Energy (DOE), Office of Energy Efficiency and Renewable Energy (EERE), Advanced Manufacturing Office (AMO).

## References

1. U. S. Department of the Interior, Final list of critical minerals 2018. Fed. Regist. **83**, 23295–23296 (2018)
2. European Commission, *Communication from the Commission to the European Parliament, the Council, the European Economic, and Social Committee and the Committee of the Regions Critical Raw Materials Resilience: Charting a Path towards Greater Security and Sustainability*. 1–24 (2020)
3. Government of Canada. Critical Minerals, *Natural Resources Canada* 1, (2021). <https://www.nrcan.gc.ca/our-natural-resources/minerals-mining/critical-minerals/23414>. <https://doi.org/10.1126/science.212.4492.306>
4. Australian Trade and Investment Commission, *Australian Critical Minerals Prospectus 2020* (2020)
5. B. Ballinger, D. Schmeda-Lopez, B. Kefford, B. Parkinson, M. Stringer, C. Greig, S. Smart, The vulnerability of electric-vehicle and wind-turbine supply chains to the supply of Eare earth elements in a 2-degree scenario. *Sustain. Prod. Consum.* **22**, 68–76 (2020)
6. UBS Rare Earth Forecasts Only Tell Half the Story. *Adamas Intelligence* (2021). <https://www.adamasintel.com/ubs-ndpr-forecasts-miss-mark/>
7. R. Eggert, C. Wadia, C. Anderson, D. Bauer, F. Fields, L. Meinert, P. Taylor, Rare earths: Market disruption, innovation, and global supply chains. *Annu. Rev. Environ. Resour.* **41**, 199–222 (2016)
8. R. Chadha, *Skewed Critical Minerals Global Supply Chains Post COVID-19* (2020). <https://www.brookings.edu/research/skewed-critical-minerals-global-supply-chains-post-covid-19/>
9. T. Maani, N. Mathur, S. Singh, C. Rong, J.W. Sutherland, Potential for Nd and Dy recovery from end-of-life products to meet future electric vehicle demand in the U.S. *Procedia CIRP* **98**, 109–114 (2021)
10. C. Handwerker, B. Olson, I. Lovell, Value recovery from used electronics. INEMI Final Project Report- Phase 1 (2017). <https://doi.org/10.13140/RG.2.2.14511.94885>
11. M. Sabbaghi, W. Cade, W. Olson, S. Behdad, The global flow of hard disk drives: Quantifying the concept of value leakage in E-waste recovery systems. *J. Ind. Ecol.* **23**, 560–573 (2019)
12. R.T. Nguyen, L.A. Diaz, D.D. Imholte, T.E. Lister, Economic assessment for recycling critical metals from hard disk drives using a comprehensive recovery process. *J. Miner. Met. Mater. Soc.* **69**, 1546–1552 (2017)
13. C. Handwerker, B. Olson, *Value Recovery from Used Electronics, INEMI Final Project Report-Phase 2* (2019). <https://www.inemi.org/value-recovery-2-final-report>
14. Responsible Business Alliance, *CASE STUDIES ON LEADERSHIP, INNOVATION AND IMPLEMENTATION* (2019). <http://www.responsiblebusiness.org/media/docs/RBACompassAwardsCaseStudies2019.pdf>
15. International Energy Agency (IEA), *Electric Vehicles Initiatives and Clean Energy Ministerial. Global EV Outlook 2021: Accelerating Ambitions Despite the Pandemic*. 1–101 (2021).
16. R. Schulze, M. Buchert, Estimates of global REE recycling potentials from NdFeB magnet material. *Resour. Conserv. Recycl.* **113**, 12–27 (2016)
17. European Commission. Eurostat. <https://ec.europa.eu/eurostat>
18. L. Ciacci, I. Vassura, Z. Cao, G. Liu, F. Passarini, Recovering the “new twin”: Analysis of secondary neodymium sources and recycling potentials in Europe. *Resour. Conserv. Recycl.* **142**, 143–152 (2019)
19. L. Hayes-Labruto, S.J.D. Schillebeeckx, M. Workman, N. Shah, Contrasting perspectives on China’s rare earths policies: Reframing the debate through a stakeholder lens. *Energy Policy* **63**, 55–68 (2013)
20. H. Jin, K. Frost, I. Sousa, H. Ghaderi, A. Bevan, M. Zakotnik, C. Handwerker, Life cycle assessment of emerging technologies on value recovery from hard disk drives. *Resour. Conserv. Recycl.* **157**, 104781 (2020)

21. J. Walzberg, F. Zhao, K. Frost, A. Carpenter, G.A. Heath, Exploring social dynamics of hard-disk drives circularity with an agent-based approach, in *2021 IEEE Conference on Technologies for Sustainability (SusTech)*, (IEEE, 2021), pp. 1–6. <https://doi.org/10.1109/SusTech51236.2021.9467439>
22. Ellen MacArthur Foundation: Circular Economy System Diagram (2019). <https://www.ellen-macarthurfoundation.org/circular-economy/concept/infographic>
23. J.R. Peeters, E. Bracquene, D. Nelen, M. Ueberschaar, K. Van Acker, J.R. Duflou, Forecasting the recycling potential based on waste analysis: A case study for recycling Nd-Fe-B magnets from hard disk drives. *J. Clean. Prod.* **175**, 96–108 (2018)
24. G. Hughes, T. Coughlin, Tutorial on disk drive data sanitization. *Nist Spec. Publ.*, 1–15 (2006)
25. Seagate. *Seagate Instant Secure Erase Deployment Options*. [https://www.seagate.com/files/www-content/product-content/\\_cross-product/en-gb/docs/ise-deployment-technology-paper-tp627-1-1203gb.pdf](https://www.seagate.com/files/www-content/product-content/_cross-product/en-gb/docs/ise-deployment-technology-paper-tp627-1-1203gb.pdf)
26. R. Kissel, A. Regenscheid, M. Scholl, K. Stine, *Guidelines for Media Sanitization* (2014). <https://nvlpubs.nist.gov/nistpubs/SpecialPublications/NIST.SP.800-88r1.pdf>. <https://doi.org/10.6028/NIST.SP.800-88r1>
27. T. Zink, F. Maker, R. Geyer, R. Amirtharajah, V. Akella, Comparative life cycle assessment of smartphone reuse: Repurposing vs. refurbishment. *Int. J. Life Cycle Assess.* **19**, 1099–1109 (2014)
28. Apple. *Product Environmental Report* (2020). [https://www.apple.com/environment/pdf/products/iphone/iPhone\\_12\\_PER\\_Oct2020.pdf](https://www.apple.com/environment/pdf/products/iphone/iPhone_12_PER_Oct2020.pdf)
29. K. Baba, Y. Hiroshige, T. Nemoto, Rare-earth magnet recycling. *Hitachi Rev* **62**, 1–4 (2013)
30. J. Martin, I. Sherr, How Apple’s Daisy iPhone Recycling Robot Works. *CNet Tech.* (2019). <https://www.cnet.com/tech/mobile/how-apples-daisy-iphone-recycling-robot-works/>
31. G. Barbosa, Here’s what happens to your old iPhone under Apple’s ‘reuse and recycle’ program. *9to5Mac* (2016) <https://9to5mac.com/2016/02/17/recycled-iphone-what-happens/>
32. T.J. McIntyre, J.J. Harter, T.A. Roberts, *Development and Operation of a High Throughput Computer Hard Drive Recycling Enterprise* (2019). <https://info.ornl.gov/sites/publications/Files/Pub133587.pdf>
33. Oak Ridge National Laboratory, *ORNL Licenses Rare Earth Magnet Recycling Process to Momentum Technologies* (Department of Energy (DoE), 2016). <https://www.energy.gov/technologytransitions/articles/ornl-licenses-rare-earth-magnet-recycling-process-momentum>
34. K. Frost, I. Sousa, J. Larson, H. Jin, I. Hua, Environmental impacts of a circular recovery process for hard disk drive rare earth magnets. *Resour. Conserv. Recycl.* **173**, 105694 (2021)
35. F. Un-Noor, S. Padmanaban, L. Mihet-Popa, M. Mollah, E. Hossain, A comprehensive study of key electric vehicle (EV) components, technologies, challenges, impacts, and future direction of development. *Energies* **10**, 1217 (2017)
36. P. Fears, Rare Earth Magnets in Electric Vehicle Motors. *Bunting: Global Magnetic Force* (2021) <https://www.bunting-berkhamsted.com/rare-earth-magnets-in-electric-vehicle-motors/>
37. Roskill. Rare Earths: Tesla Extends EV Range Using Permanent Magnets. *Industry News* (2019). <https://roskill.com/news/rare-earths-tesla-extends-ev-range-using-permanent-magnets/#:~:text=Over90%25%20of%20EV%20models,permanent%20magnet%20switched%20reluctance%20motor>
38. I.M. Solutions, *Small NdFeB Magnets in Smartphones and Personal Electronics*. <https://idealmagnetsolutions.com/knowledge-base/small-ndfeb-magnets-in-smartphones-and-personal-electronics/>
39. N.F. Nissen, J. Reinhold, K. Schischke, Klaus-Dieter-Lang, Recyclability of tungsten, tantalum and neodymium from smartphones. *EcoDesign and Sustainability*, 365–381 (2021). [https://doi.org/10.1007/978-981-15-6779-7\\_26](https://doi.org/10.1007/978-981-15-6779-7_26)
40. B. Bookhagen, D. Bastian, P. Buchholz, M. Faulstich, C. Opper, J. Irrgeher, T. Prohaska, C. Koeberl, Metallic resources in smartphones. *Resour. Policy* **68**, 101750 (2020)
41. J. Marx, A. Schreiber, P. Zapp, F. Walachowicz, Comparative life cycle assessment of NdFeB permanent magnet production from different rare earth deposits. *ACS Sustain. Chem. Eng.* **6**, 5858–5867 (2018)

42. P.S. Arshi, E. Vahidi, F. Zhao, Behind the scenes of clean energy: The environmental footprint of rare earth products. *ACS Sustain. Chem. Eng.* **6**, 3311–3320 (2018)
43. C. Handwerker, B. Olson, M. Schaffer, *Creating a Circular Economy for Hard Disk Drives – A Shared Vision* (2018). [https://community.inemi.org/value\\_recovery\\_2](https://community.inemi.org/value_recovery_2)
44. Thailand's HDD Industry Outlook 2019, *AEC+ Business Advisory*. (2019). [https://kasikornbank.com/international-business/en/Thailand/IndustryBusiness/Pages/201902\\_Thailand\\_HDD\\_outlook2019.aspx](https://kasikornbank.com/international-business/en/Thailand/IndustryBusiness/Pages/201902_Thailand_HDD_outlook2019.aspx)
45. Grist. Can You Recycle a Hard Drive? Google Is Quietly Trying to Find Out (2021). <https://grist.org/technology/can-you-recycle-a-hard-drive-google-is-quietly-trying-to-find-out/>
46. M. Zakotnik, C.O. Tudor, Commercial-scale recycling of NdFeB-type magnets with grain boundary modification yields products with 'designer properties' that exceed those of starting materials. *Waste Manag.* **44**, 48–54 (2015)
47. M. Zakotnik, C.O. Tudor, L.T. Peiró, P. Afiuny, R. Skomski, G.P. Hatch, Analysis of energy usage in Nd–Fe–B magnet to magnet recycling. *Environ. Technol. Innov.* **5**, 117–126 (2016)
48. M. Zakotnik, P. Afiuny, S. Dunn, C.O. Tudor, Magnet Recycling to Create Nd–Fe–B Magnets with Improved or Restored Magnetic Performance. (2015)
49. M. Xia, A.B. Abrahamsen, C.R. Bahl, B. Veluri, A.I. Søgaard, P. Bøjsøe, Hydrogen decrepitation press-less process recycling of NdFeB sintered magnets. *J. Magn. Magn. Mater.* **441**, 55–61 (2017)
50. A.G. Popov, A.V. Shitov, E.G. Gerasimov, D.Y. Vasilenko, M.Y. Govorkov, D.Y. Bratushev, V.P. Vyatkin, K.Y. Shunyaev, T.L. Mikhailova, Preparation of sintered Nd-Fe-B magnets by pressless process. *Phys. Met. Metallogr.* **113**, 331–340 (2012)
51. K. Tokuhara, S. Okumura, A. Oota, Sumitomo Special Metals Co Ltd. Method of Pressing Rare Earth Alloy Magnetic Powder. U.S. Patent 6,461,565 (2002)
52. K. Okayama, N. Ishigaki, S. Okumura, Sumitomo Special Metals Co Ltd. Rare Earth Magnet and Method for Manufacturing the Same. U.S. Patent 6,491,765 (2002)
53. G Li, Sumitomo Special Metals Co Ltd. Rare Earth Magnet and Method for Making Same. U.S. Patent 6,527,874 (2003)
54. K. Okayama, N. Ishigaki, S. Okumura, Sumitomo Special Metals Co Ltd. Rare Earth Magnet and Method for Manufacturing the Same. U.S. Patent 6,537,385 (2003)
55. I.C. Nlebedim, H. Ucar, C.B. Hatter, R.W. McCallum, S.K. McCall, M.J. Kramer, M.P. Paranthaman, Studies on *in situ* magnetic alignment of bonded anisotropic Nd-Fe-B alloy powders. *J. Magn. Magn. Mater.* **422**, 168–173 (2017)
56. J. Ormerod, Bonded magnets: A versatile class of permanent magnets. *Magn. Bus. Technol.* (2015) <https://magneticsmag.com/bonded-magnets-a-versatile-class-of-permanent-magnets/>
57. K. Gandha, G. Ouyang, S. Gupta, V. Kunc, M.P. Paranthaman, I.C. Nlebedim, Recycling of additively printed rare-earth bonded magnets. *Waste Manag.* **90**, 94–99 (2019)
58. P.J. McGuinness, C. Short, A.F. Wilson, I.R. Harris, The production and characterization of bonded, hot-pressed and die-upset HDDR magnets. *J. Alloys Compd.* **184**, 243–255 (1992)
59. M. Awais, F. Coelho, M. Degri, E. Herraiz, A. Walton, N. Rowson, Hydrocyclone separation of hydrogen decrepitated NdFeB. *Recycling* **2**, 22 (2017)
60. J. Luo, *Development of Anisotropic Nd-Fe-B Powders from Sintered Magnets by Hydrogen Decrepitation/Desorption Process* (Université Joseph-Fourier - Grenoble I, 2009)
61. A. Walton, H. Yi, N.A. Rowson, J.D. Speight, V.S.J. Mann, R.S. Sheridan, A. Bradshaw, I.R. Harris, A.J. Williams, The use of hydrogen to separate and recycle neodymium–iron–boron-type magnets from electronic waste. *J. Clean. Prod.* **104**, 236–241 (2015)
62. A.S. Kim, D.H. Kim, S. Namkung, T.S. Jang, D.H. Lee, H.W. Kwon, D.H. Hwang, Development of high coercive powder from the Nd-Fe-B sintered magnet scrap. *IEEE Trans. Magn.* **40**(4), 2877–2879 (2004)
63. M. Itoh, M. Masuda, S. Suzuki, K. Machida, Recycling of rare earth sintered magnets as isotropic bonded magnets by mMelt-spinning. *J. Alloys Compd.* **374**, 393–396 (2004)
64. O. Gutfleisch, K. Güth, T.G. Woodcock, L. Schultz, Recycling used Nd-Fe-B sintered magnets via a hydrogen-based route to produce anisotropic, resin bonded magnets. *Adv. Energy Mater.* **3**, 151–155 (2013)

65. E. Poskovic, L. Ferraris, F. Franchini, M.A. Grande, E. Pallavicini, A different approach to rare-earth magnet recycling, in *2018 IEEE International Conference on Environment and Electrical Engineering and 2018 IEEE Industrial and Commercial Power Systems Europe (EEEIC / I&CPS Europe)*, (IEEE, 2018), pp. 1–6. <https://doi.org/10.1109/EEEIC.2018.8494531>
66. K. Binnemans, P.T. Jones, B. Blanpain, T. Van Gerven, Y. Yang, A. Walton, M. Buchert, Recycling of rare earths: A critical review. *J. Clean. Prod.* **51**, 1–22 (2013)
67. I.C. Nlebedim, A.H. King, Addressing criticality in rare earth elements via permanent magnets recycling. *JOM* **70**, 115–123 (2018)
68. L.A. Diaz, T.E. Lister, Economic evaluation of an electrochemical process for the recovery of metals from electronic waste. *Waste Manag.* **74**, 384–392 (2018)
69. Z. Li, L.A. Diaz, Z. Yang, H. Jin, T.E. Lister, E. Vahidi, F. Zhao, Comparative life cycle analysis for value recovery of precious metals and rare earth elements from electronic waste. *Resour. Conserv. Recycl.* **149**, 20–30 (2019)
70. T.E. Lister, M. Meagher, M.L. Strauss, L.A. Diaz, H.W. Rollins, G. Das, M.M. Lencka, A. Anderko, R.E. Riman, A. Navrotsky, Recovery of rare earth elements from recycled hard disk drive mixed steel and magnet scrap. *Rare Metal Technol.*, 139–154 (2021). [https://doi.org/10.1007/978-3-030-65489-4\\_15](https://doi.org/10.1007/978-3-030-65489-4_15)
71. D. Prodius, K. Gandha, A.-V. Mudring, I.C. Nlebedim, Sustainable Urban Mining of critical elements from magnet and electronic wastes. *ACS Sustain. Chem. Eng.* **8**, 1455–1463 (2020)
72. A. Brewer, A. Dohnalkova, V. Shutthanandan, L. Kovarik, E. Chang, A.M. Sawvel, H.E. Mason, D. Reed, C. Ye, W.F. Hynes, L.N. Lammers, Microbe encapsulation for selective rare-earth recovery from electronic waste leachates. *Environ. Sci. Technol.* **53**, 13888–13897 (2019)
73. M. Alipanah, D.M. Park, A. Middleton, Z. Dong, H. Hsu-Kim, Y. Jiao, H. Jin, Techno-economic and life cycle assessments for sustainable rare earth recovery from coal byproducts using biosorption. *ACS Sustain. Chem. Eng.* **8**, 17914–17922 (2020)
74. V.G. Deshmane, S.Z. Islam, R.R. Bhawe, Selective recovery of rare earth elements from a wide range of e-waste and process scalability of membrane solvent extraction. *Environ. Sci. Technol.* **54**, 550–558 (2019)
75. D. Kim, L.E. Powell, L.H. Delmau, E.S. Peterson, J. Herchenroeder, R.R. Bhawe, Selective extraction of rare earth elements from permanent magnet scraps with membrane solvent extraction. *Environ. Sci. Technol.* **49**, 9452–9459 (2015)
76. R.T. Nguyen, D.D. Imholte, China's rare earth supply chain: Illegal production, and response to new cerium demand. *JOM* **68**, 1948–1956 (2016)
77. J. Navarro, F. Zhao, Life-cycle assessment of the production of rare-earth elements for energy applications: A review. *Front. Energy Res.* **2** (2014)
78. K. Frost, H. Jin, W. Olson, M. Schaffer, G. Spencer, C. Handwerker, The use of decision support tools to accelerate the development of circular economic business models for hard disk drives and rare-earth magnets. *MRS Energy Sustain.* **7** (2020)
79. P. He, H. Feng, G. Hu, K. Hewage, G. Achari, C. Wang, R. Sadiq, Life cycle cost analysis for recycling high-tech minerals from waste Mobile phones in China. *J. Clean. Prod.* **251**, 119498 (2020)
80. R. Hischier, H.W. Böni, Combining environmental and economic factors to evaluate the reuse of eElectrical and electronic equipment – A Swiss case study. *Resour. Conserv. Recycl.* **166**, 105307 (2021)
81. H. Jin, P. Afunoy, S. Dove, G. Furlan, M. Zakotnik, Y. Yih, J.W. Sutherland, Life cycle assessment of neodymium-iron-boron magnet-to-magnet recycling for electric vehicle motors. *Environ. Sci. Technol.* **52**, 3796–3802 (2018)
82. Y. Yang, A. Walton, R. Sheridan, K. Güth, R. Gauß, O. Gutfleisch, M. Buchert, B.M. Steenari, T. Van Gerven, P.T. Jones, K. Binnemans, REE recovery from end-of-life Nd-Fe-B permanent magnet scrap: A critical review. *J. Sustain. Metall.* **3**, 122–149 (2017)
83. N.A. Mancheri, B. Sprecher, G. Bailey, J. Ge, A. Tukker, Effect of Chinese policies on rare earth supply chain resilience. *Resour. Conserv. Recycl.* **142**, 101–112 (2019)

84. J.C.K. Lee, Z. Wen, Pathways for greening the supply of rare earth elements in China. *Nat. Sustain.* **1**, 598–605 (2018)
85. L. Cong, F. Zhao, J.W. Sutherland, Integration of dismantling operations into a value recovery plan for circular economy. *J. Clean. Prod.* **149**, 378–386 (2017)
86. C.W. Babbitt, S. Althaf, F. Cruz Rios, M.M. Bilec, T.E. Graedel, The role of design in circular economy solutions for critical materials. *One Earth* **4**, 353–362 (2021)
87. The White House, *Building Resilient Supply Chains, Revitalizing American Manufacturing, and Fostering Broad-Based Growth. 100-Day Reviews Under Executive Order 14017* (2021). <https://www.whitehouse.gov/wp-content/uploads/2021/06/100-day-supply-chain-review-report.pdf>
88. I.E. Nikolaou, N. Jones, A. Stefanakis, Circular economy and sustainability: The past, the present and the future directions. *Circ. Econ. Sustain.* **1**, 1–20 (2021)
89. United States Environmental Protection Agency. Electronic Product Environmental Assessment Tool (EPEAT). <https://www.epa.gov/greenerproducts/electronic-product-environmental-assessment-tool-epeat>
90. TÜV Rheinland and Global Electronics Council, *Criteria for the Sustainability Assessment of Network Equipment for the Global Electronics Council EPEAT® Ecolabel and the TÜV Rheinland Green Product Mark* (2021). [https://globalelectronicscouncil.org/wp-content/uploads/EPEAT-Network-Equipment-Criteria\\_FINAL-April-2021.pdf](https://globalelectronicscouncil.org/wp-content/uploads/EPEAT-Network-Equipment-Criteria_FINAL-April-2021.pdf)



# Chapter 18

## Recovery of Rare Earth Metals from Waste Fluorescent Lights



Brajendra Mishra, Mark Strauss, and Manish Kumar Sinha

### 18.1 Background

In Japan, it has been said that “oil is the *blood*, steel is the *body* and rare earths are the *vitamins* of a modern economy.” [1] In recent years, technological advances have resulted in multiple applications using rare earths which has increased their demand as they are considered to rapidly becoming “*the next oil*.” [2] A global drive toward the introduction of emerging technologies or *green technologies* or *low-carbon technology* has been motivated by growing concerns about the environment and our decreased reliance on the fossil fuels. Wind turbines, electric cars and energy-saving lighting are among the low-carbon technologies that require rare earth metals (REM) for their manufacture and/or production.

To date, China alone accounts for 80% of the total REE production. Moreover, after decades of development and use, REE resources are becoming rapidly depleted limiting the availability of these critical materials. As a result, scarcity of these materials may arise in many countries in the coming years leading to price volatility and vulnerabilities in the supply chain. It is estimated that the demand will reach 210,000 metric tons by 2025 [3, 4]. In 2021, the United States imported \$160 M of REE-compounds and metals, a significant increase from \$109 M in 2020 [5]. To meet this demand, alternative sources of REEs are needed. One potential secondary resource of REEs is the phosphor powder from waste fluorescent lamps (FLs).

End-of-life or waste FLs contain over ten times the REE content of industrial-grade primary ores (1.5–2%). The contained REEs account for up to 28% of the total weight of FL phosphors. Triband phosphors generally consist of several REE-containing compounds [6] including.

---

B. Mishra (✉) · M. Strauss · M. K. Sinha  
Material Science and Engineering, Worcester Polytechnic Institute, Worcester, MA, USA  
e-mail: [bmishra@wpi.edu](mailto:bmishra@wpi.edu)

- Red phosphors ( $YOX - Y_2O_3; Eu^{3+}$ ).
- Blue phosphors ( $BAM - BaMgAl_{10}O_{17}; Eu^{2+}$ ).
- Green phosphors ( $LAP - LaPO_4; Ce^{3+}, Tb^{3+}$ ;  $CAT - CeMgAl_{11}O_{19}; Tb^{3+}$ ;  $CBT - (Ce, Gd)MgB_5O_{10}; Tb^{3+}$ ); Halophosphate Phosphors ( $HALO - ((Ca, Sr)_{10}(PO_4)_6Cl; Eu^{2+})$ ;  $(Sr, Ca)_{10}(PO_4)_6(Cl, F)_2; Sb^{3+}, Mn^{2+}$ ).

Among all REEs present in the FL phosphor powder, Eu is one of the most expensive and rarest element accounting for only 0.05–0.10 wt.% of the total REE content in the primary ores found in China, India, Brazil and Australia [7]. According to the list of U.S. critical minerals [8], fourteen individual REEs, including Eu, are critical for the country because of their global shortages and importance as raw materials. Typically, FLs contain three times the amount of Y, two times the amount of terbium (Tb) and 1.5 times the amount of Eu compared to REE ores [9]. The quantity of phosphor and rare earth oxide (REO) concentrations in various FLs are presented in Table 18.1.

It was reported that in 2020, the stockpiled lamp phosphor waste contained around 25,000 metric tons of rare earths [11]. Globally, 1.5 billion fluorescent lamps are produced each year. More than 600 million fluorescent lamps are discarded each year in the United States which is equivalent to approximately 1300 metric tons of rare earth elements [12]. In the United States, recycling rates remain at 23% [13] due primarily to the lack of advanced separations technology, and with non-cost-effective, manual sorting, only a limited quantity of material is available for recycle processing [14].

Red phosphors exist as an oxide and are easily leached in acid solution. In contrast, blue phosphors and green phosphors are difficult to be leached directly due to their stable spinel structures. Since, red phosphors are the major fraction of phosphor powder, most previous research studies have focused on the hydrometallurgical recovery of Y and Eu from waste phosphor because of their high economic value and ease of extraction [15]. The process is mostly limited to dissolution of the phosphor using acids such as hydrochloric acid (HCl), nitric acid (HNO<sub>3</sub>) and sulfuric acid (H<sub>2</sub>SO<sub>4</sub>) followed by recovery of REEs from the leached solution by oxalate precipitation [7, 16]. Separation is often directed toward recovery of all REEs contained in the starting material or manufactured product (e.g., CFL or LFL), and not to the separation and recovery of specific, individual, phosphor REEs [17–19].

**Table 18.1** Quantity of phosphors and REOs in various fluorescent lamps [10]

Lighting	Phosphors (g/unit)	Y <sub>2</sub> O <sub>3</sub>	Eu <sub>2</sub> O <sub>3</sub>	Tb <sub>4</sub> O <sub>7</sub>	CeO <sub>2</sub>	La <sub>2</sub> O <sub>3</sub>
		g/unit (% phosphor)				
CFL	1.3	0.61 (46.9)	0.04 (3.07)	0.05 (3.8)	0.19 (14.6)	0.08 (6.15)
LFL (T5)	2.4	0.75 (31.2)	0.05 (2.08)	0.06 (2.5)	0.08 (3.33)	0.25 (10.4)
LFL (T8)	5.8	1.79 (30.8)	0.12 (2.06)	0.13 (2.2)	0.18 (3.10)	0.59 (10.2)

Compact Fluorescent Lamp/Light (CFL); Linear Fluorescent Lamp/Light (LFL)

T5 and T8 = Tubular lamps with 1.59 cm and 2.54 cm diameter

Tb Terbium, Ce Cerium, La Lanthanum

There are only a few studies that report the separation of Y and Eu from leached phosphor powder solutions. For example, the recovery of REEs was investigated using supercritical carbon dioxide (SF-CO<sub>2</sub>) containing tri-*n*-butyl phosphate (TBP) complexes with HNO<sub>3</sub> and H<sub>2</sub>O [20]. During experimental testing, aqueous droplets were generated when the leached metal oxides were vigorously mixed with a TBP: 1.8HNO<sub>3</sub>: 0.6H<sub>2</sub>O complex. More than 99% co-extraction of Y and Eu was observed after static extraction for 120 min at 15 MPa and 60 °C.

Rabah [21] studied the selective extraction of Eu and Y from the thiocyanate solution using trimethyl-benzylammonium chloride (C<sub>10</sub>H<sub>16</sub>ClN) as an extractant. In the process, the mixed sulphate salt of Y and Eu obtained after H<sub>2</sub>SO<sub>4</sub> leaching of phosphor was converted into thiocyanate at low temperature. After extraction, the metal loaded in the extractant was recovered by *N*-tributylphosphate (TBP, C<sub>12</sub>H<sub>27</sub>O<sub>4</sub>P) in 1 M HNO<sub>3</sub> at 125 °C to produce nitrate salts of Eu and Y. Subsequently, europium(III) nitrate (Eu(NO<sub>3</sub>)<sub>3</sub>) was separated from yttrium(III) nitrate (Y(NO<sub>3</sub>)<sub>3</sub>) by dissolving in ethyl alcohol (C<sub>2</sub>H<sub>6</sub>O).

Separation of Y and Eu using Cyanex 572, a commercial extractant for separation of REEs by solvent extraction, was addressed by Tunsu et al. [22] Yttrium was selectively extracted at pH<sub>eq</sub> = 0, whereas complete Eu recovery was observed at pH<sub>eq</sub> = ~1 with 1 M Cyanex 572 in 12.5 min. Stripping with 3 M HCl solutions led to complete recovery of the extracted Y and Eu. Finally, from the individually purified stripped solutions, Y and Eu oxides were prepared by oxalate precipitation and calcination.

Separation of Y(III) and Eu(III) by undiluted quaternary phosphonium thiocyanate ionic liquid [C101][SCN] was investigated [23]. Selective extraction of Y was carried out with undiluted ionic liquids with an organic to aqueous ratio (O/A) = 1:10 in four countercurrent steps. High-purity (e.g., 98.7%) Eu<sub>2</sub>O<sub>3</sub> was prepared from the raffinate containing Eu(III), by precipitation with ammonia (NH<sub>3</sub>) solution, followed by calcinations at 400–450 °C.

Recently, the solvent extraction and separation of Y and Eu from chloride leach liquor using D2EHPA was studied by Mishra et al. [24] The complete and selective extraction of Y from the leach liquor was achieved in two countercurrent stages at an O/A ratio of 1:1.5 at pH 2.56 with minor Eu co-extraction. In an alternative method, the chemical reduction of Eu(III) to Eu(II) using zinc (Zn) metal was also tried in order to separate Y and Eu from leached solution. It was observed that 78.1% Eu(III) was reduced in 1 h. However, 16% Y was also coprecipitated along with EuSO<sub>4</sub>.

Despite being a multistep process, solvent extraction is the accepted method for producing high-purity REE salts. The selective reduction-precipitation process presents a promising innovative one-step separation technique for the separation of Eu from Eu-containing solutions. The reduction of Eu(III) can be realized in a chemical, electrochemical or photochemical way. The various reductive separation methods for Eu were reviewed in detail by Kumari et al. [7] The recovery of Eu as EuSO<sub>4</sub> from monazite, bastnäsite and Eu-rich REE concentrate leached solution using Zn-amalgam has been previously reported [25, 26]. In contrast, very few attempts have been made to separate Eu from phosphor powder leached solution by

reduction-precipitation. In view of this, an advanced process for efficient Eu recovery as a value-added product from waste phosphor powder using the reduction-precipitation method has been developed and is presented in Sect. 18.2.

## 18.2 Europium Recovery from Waste Fluorescent Phosphor Dust

Figure 18.1 shows the process flow sheet for recycling REEs from waste phosphors. Waste FL phosphors collected from Veolia North America, LLC, were used to demonstrate the proposed recovery process. The as-received phosphor dust was sieved to separate glass and aluminum (Al) particles, and the <math><74\ \mu\text{m}</math> fraction was used.

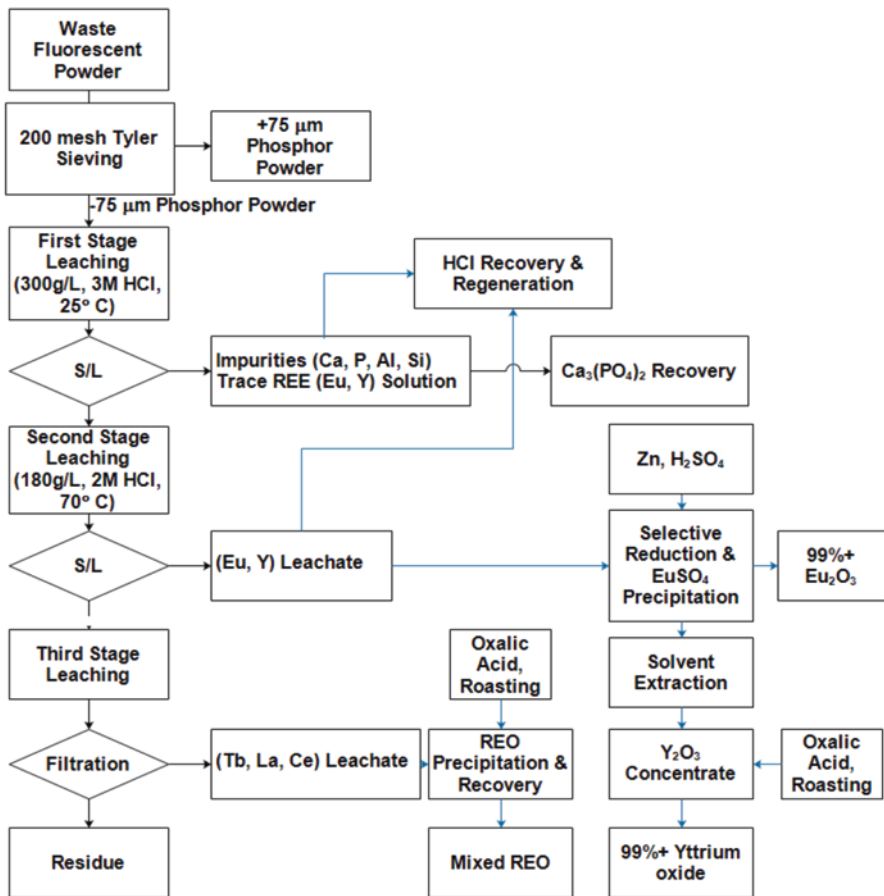
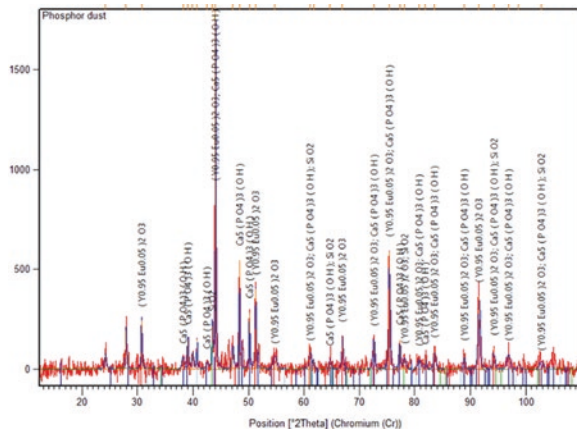


Fig. 18.1 Complete flow sheet for REE recovery from waste phosphor dust

Oxides	Wt.%
Y <sub>2</sub> O <sub>3</sub>	31.47
La <sub>2</sub> O <sub>3</sub>	2.97
Ce <sub>2</sub> O <sub>3</sub>	2.82
Eu <sub>2</sub> O <sub>3</sub>	1.96
Tb <sub>2</sub> O <sub>3</sub>	1.14
Fe <sub>2</sub> O <sub>3</sub>	0.10
CaO	22.81
Al <sub>2</sub> O <sub>3</sub>	10.74
Na <sub>2</sub> O	1.58
K <sub>2</sub> O	0.53
MgO	0.25
P <sub>2</sub> O <sub>5</sub>	14.38
SiO <sub>2</sub>	9.30



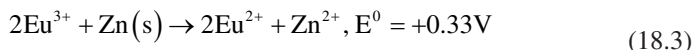
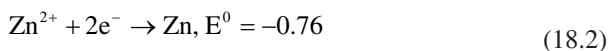
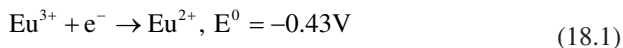
**Fig. 18.2** Composition of phosphor dust as determined by ICP-OES analysis and XRD spectrum

Figure 18.2 shows the chemical composition of the waste phosphor as analyzed by ICP-OES (inductively coupled plasma optical emission spectrometry). The major phases determined from X-ray analysis (XRD) were YOX (Y<sub>2</sub>O<sub>3</sub>:Eu<sup>3+</sup>), calcite (CaCO<sub>3</sub>) and apatite (Ca<sub>10</sub>(PO<sub>4</sub>)<sub>6</sub>(OH)<sub>2</sub>).

Compared to other phosphors, HALO dissolves very easily, but its dissolution consumes considerable amount of acid and introduces metallic contaminants into the leach solution. Therefore, in the first stage HALO phase was selectively leached at below room temperature in dilute HCl using a pulp density of 150 g/L for 15 min. The temperature was regulated by surrounding the leaching reactor with an ice water bath. More than 80% calcium (Ca) from the HALO phase selectively dissolved in the solution while Y and Eu was retained in the leach residue. The YOX phase was selectively leached from the REE-rich leached residue using 2 M HCl at 70 °C for 60 min while maintaining the pulp density of 180 g/L. The as-obtained leach liquor was further used for recovery of Eu as EuSO<sub>4</sub> via reduction-precipitation. A variety of factors affect the final grade and recovery of EuSO<sub>4</sub>, including pH, sulfate concentration, selective reduction time and the precipitation time.

### 18.2.1 Eu(III) Reduction Chemistry

Eu(III) has the highest standard redox potential of all rare earth salts (RES) that can be reduced to their divalent oxidation state, making its selective reduction and recovery from a solution containing rare earth mixture possible. Since, Eu<sup>3+</sup> easily oxidizes to Eu<sup>2+</sup> in presence of oxygen (O<sub>2</sub>), Eu reduction-precipitation is always carried out in an inert or nonoxidizing environment [27]. As Zn metal or Zn amalgam has a more negative reduction potential than Eu(III), it has traditionally been used to reduce Eu(III) to Eu(II). This can be shown by the following reduction potential equations:

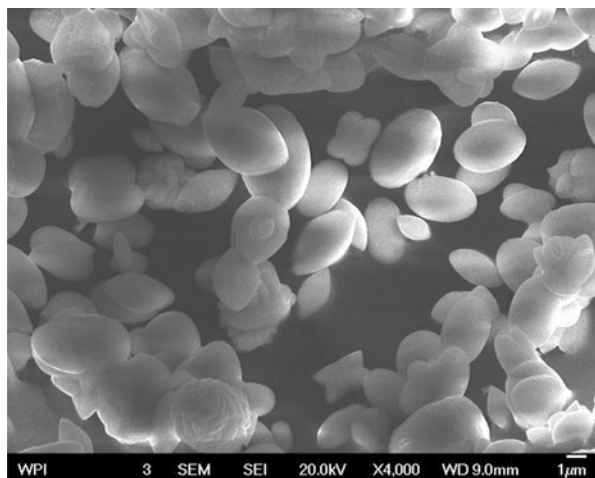


In order to avoid the difficulty of separating unreacted excess Zn-dust from the  $\text{EuSO}_4$  product, reduction and precipitation was performed in a different reaction vessel. Europium(II) sulphate of 92.77% purity was obtained at the following optimal processing conditions: Initial Eu(III) solution pH = 3, 30 min reduction time, 3 M  $\text{H}_2\text{SO}_4$  and 2 h precipitation time.

The major impurities are Ca and other alkali/alkaline metals from the HALO phosphor which remain undissolved in the first stage of leaching. The inclusion of other metallic impurities in Y-Eu leach liquor can be controlled by better optimization of the first stage leaching of the phosphor dust. The  $\text{EuSO}_4$  powder produced was then characterized by scanning electron microscopy (SEM). The SEM image presented in Fig. 18.3 shows the formation of agglomerated, oval-shaped,  $\text{EuSO}_4$  particles that range between 5 and 10  $\mu\text{m}$  in size.

Yttrium was further recovered from the filtrate by solvent extraction. Using the leached residue obtained after selective removal of Y and Eu, mixed rare earth oxides of La, Ce and Tb can be recovered after acid leaching followed by oxalate precipitation and calcination. As an alternate method, alkali roasting could be used, followed by water leaching, acid leaching and oxalate precipitation. Solvent extraction can be performed directly on the leach solution for the recovery of individual rare earths.

**Fig. 18.3** SEM image of the precipitated  $\text{EuSO}_4$



## 18.3 Conclusions

The end-of-life FLs are considered as an alternate source of REEs. A combined acid-leaching and reduction-precipitation method was developed to recover Eu as  $\text{EuSO}_4$  from the waste phosphor dust of spent FLs. The FL phosphor waste is treated with dilute HCl solution in an ice-cooled bath to initially dissolve the HALO phosphor. After removal of HALO from the phosphor dust, selective leaching of the YOx phase was carried out in 2 M HCl at 70 °C for 60 min. Europium in the Y-Eu leach solution was effectively separated and recovered via a reduction-precipitation method using Zn as a reductant. Under the optimal conditions of pH 3 with 3 M  $\text{H}_2\text{SO}_4$ , 92.77% pure  $\text{EuSO}_4$  could be obtained by reduction-precipitation in inert environment. This process has the potential for larger scale production of  $\text{EuSO}_4$  salt from waste phosphor dust.

## References

1. P.C. Dent, Rare earth elements and permanent magnets. *J. Appl. Phys.* **111**, 07A721 (2012)
2. E. Brennan, *The Next Oil?: Rare Earth Metals* (The Diplomat, 2013)
3. T. Liu, J. Chen, Extraction and separation of heavy rare earth elements: A review. *Sep. Purif. Technol.* **276**, 119263 (2021)
4. B. Mwewa, M. Tadie, S. Ndlovu, G.S. Simate, E. Matinde, Recovery of rare earth elements from acid mine drainage: A review of the extraction methods. *J. Environ. Chem. Eng.* **10**, 107704 (2022)
5. U.S. Geological Survey, *Mineral Commodity Summaries* (January, 2022). <https://pubs.usgs.gov/periodicals/mcs2022/mcs2022-rare-earths.pdf>
6. J. Zhang, J. Anawati, G. Azimi, Urban Mining of terbium, europium, and yttrium from real fluorescent lamp waste using supercritical fluid extraction: Process development and mechanistic investigation. *Waste Manag.* **139**, 168–178 (2022)
7. A. Kumari, M.K. Jha, D.D. Pathak, S. Chakravarty, J.C. Lee, Processes developed for the separation of europium (Eu) from various resources. *Sep. Purif. Rev.* **48**(2), 91–121 (2019)
8. <https://www.usgs.gov/news/national-news-release/us-geological-survey-releases-2022-list-critical-minerals>
9. G. Gaustad, E. Williams, A. Leader, Rare earth metals from secondary sources: Review of potential supply from waste and Byproducts. *Resour. Conserv. Recycl.* **167**, 105213 (2021)
10. Y. Qiu, S. Suh, Economic feasibility of recycling rare earth oxides from end-of-life lighting technologies. *Resour. Conserv. Recycl.* **150**, 104432 (2019)
11. N.R. Rodriguez, B. Grymonprez, K. Binnemans, Integrated process for recovery of rare-earth elements from lamp phosphor waste using Methanesulfonic acid. *Ind. Eng. Chem. Res.* **60**(28), 10319–10326 (2021)
12. T. Jiang, S. Singh, K.A. Dunn, Y. Liang, Optimizing leaching of rare earth elements from red mud and spent fluorescent lamp phosphors using Levulinic acid. *Sustainability* **14**(15), 9682 (2022)
13. L.N. Viana, A.P.S. Soares, D.L. Guimarães, W.J.S. Rojano, T.D. Saint’Pierre, Fluorescent lamps: A review on environmental concerns and current recycling perspectives highlighting hg and rare earth elements. *J. Environ. Chem. Eng.* **10**, 108915 (2022)
14. A.T. Lima, G.M. Kirkelund, F. Ntuli, L.M. Ottosen, Screening dilute sources of rare earth elements for their circular recovery. *J. Geochem. Explor.* **238**, 107000 (2022)

15. N.M. Ippolito, A. Amato, V. Innocenzi, F. Ferella, S. Zueva, F. Beolchini, F. Vegliò, Integrating life cycle assessment and life cycle costing of fluorescent spent lamps recycling by hydro-metallurgical processes aimed at the rare earths recovery. *J. Environ. Chem. Eng.* **10**(1), 107064 (2022)
16. N. Dhawan, H. Tanvar, A critical review of end-of-life fluorescent lamps recycling for recovery of rare earth values. *Sustain. Mater. Technol.* **32**, e00401 (2022)
17. S. Pavón, A. Fortuny, M.T. Coll, A.M. Sastre, Rare earths separation from fluorescent lamp wastes using ionic liquids as extractant agents. *Waste Manag.* **82**, 241–248 (2018)
18. H. Yang, W. Wang, H. Cui, D. Zhang, Y. Liu, J. Chen, Recovery of rare earth elements from simulated fluorescent powder using bifunctional ionic liquid Extractants (Bif-ILEs). *J. Chem. Technol. Biotechnol.* **87**(2), 198–205 (2012)
19. F. Yang, F. Kubota, Y. Baba, N. Kamiya, M. Goto, Selective extraction and recovery of rare earth metals from phosphor powders in waste fluorescent lamps using an ionic liquid system. *J. Hazard. Mater.* **254**, 79–88 (2013)
20. R. Shimizu, K. Sawada, Y. Enokida, I. Yamamoto, Supercritical fluid extraction of rare earth elements from luminescent material in waste fluorescent lamps. *J. Supercrit. Fluids* **33**(3), 235–241 (2005)
21. M.A. Rabah, Recyclables recovery of europium and yttrium metals and some salts from spent fluorescent lamps. *Waste Manag.* **28**(2), 318–325 (2008)
22. C. Tunsu, J.B. Lapp, C. Ekberg, T. Retegan, Selective separation of yttrium and europium using Cyanex 572 for applications in fluorescent lamp waste processing. *Hydrometallurgy* **166**, 98–106 (2016)
23. R. Banda, F. Forte, B. Onghena, K. Binnemans, Yttrium and europium separation by solvent extraction with undiluted thiocyanate ionic liquids. *RSC Adv.* **9**(9), 4876–4883 (2019)
24. B.B. Mishra, N. Devi, K. Sarangi, Yttrium and europium recycling from phosphor powder of waste tube light by combined route of hydrometallurgy and chemical reduction. *Miner. Eng.* **136**, 43–49 (2019)
25. C.K. Gupta, N. Krishnamurthy, *Extractive Metallurgy of Rare Earths* (CRC Press, Boca Raton, 2005)
26. K.A. Rabie, S.A. Sayed, T.A. Lasheen, I.E. Salama, Europium separation from a middle rare Earth concentrate derived from Egyptian black sand monazite. *Hydrometallurgy* **86**(3–4), 121–130 (2007)
27. S.A. Sayed, K.A. Rabie, I.E. Salama, Studies on europium separation from a middle rare earth concentrate by in situ zinc reduction technique. *Sep. Purif. Technol.* **46**(3), 145–154 (2005)



**Part V**  
**Economics and Regulatory Issues**

# Chapter 19

## Fundamental Perspectives on the Economic Analysis of Rare Earth Processing from Various Feedstocks



Aaron Noble

### 19.1 Introduction and Objectives

#### 19.1.1 Background

The economic analysis of REE mineral resources is fundamentally similar to that of other mined commodities. Initial estimates of economic feasibility are conducted early in the project development cycle and include rough estimates of the capital costs, fixed and variable operating costs, tax and royalty payments and sales revenue. From these estimates, pro forma cash flow statements can be derived, and ultimately, indicators of economic viability (e.g., net present value and internal rate of return (IRR)) can be calculated. If the economic indicators are sufficient to warrant further investment, the project will progress through the preliminary and detailed feasibility studies where further delineation of the reserve size, mine design and extraction process lead to refined accuracy in the economic projections.

While this overall economic evaluation process is identical for any mineral development project, REE projects have some unique attributes, which warrant specific attention. The most notable of these is the lack of a well-developed and transparent downstream supply chain. Unlike most base metals, which can be bought and sold on an open metal exchange, REEs are sold through bilateral private contracts. Individual REE prices are not quoted on the open market and must instead be obtained through consultancies or industrial trade journals, which often report prices for high grade, individually separated oxide products, free-on-board China. The lack of a clear and consistent pricing structure should prompt caution when analyzing reported economic projections at face value. The REE pricing used in

---

A. Noble (✉)  
Virginia Tech, Blacksburg, VA, USA  
e-mail: [aaron.noble@vt.edu](mailto:aaron.noble@vt.edu)

individual economic studies may vary considerably depending on the data source and the year of the study. In addition, the actual REE prices used in the pro forma cash flow may or may not be discounted from their standard prices to account for deviations in product quality and market entry barriers [1]. These issues and other inconsistencies between reporting entities have been described by various authors [2, 3].

The challenge of price transparency is further compounded when one also considers the potential number of independent products that must be considered in the economic analysis. While most modern base metal operations rely on revenue from multiple coproducts or by-products, REE resources usually contain all 16 REEs to some degree in addition to potential non-REE by-products. The distribution of REEs in naturally occurring ore material rarely matches the distribution of market demand, which naturally causes some elements to be perpetually oversupplied. This challenge has been noted as the REE *balance problem*, and it has been well-reported [4–6].

While the two aforementioned issues on REE price transparency and supply-demand imbalance are market-side challenge, they do often have technical implications, particularly with respect to the separation process design and the extent of processing included in the project. The economic analysis included with REE development projects may include varying degrees of processing and refining, with some stopping at the production of mineral concentrates, mixed rare earth oxides (MREO) or salts (MRES), partial elemental separation of target elements or full elemental separation of all REEs. The degree of separation is used to justify the REE price deck utilized for economic projections.

### ***19.1.2 Objectives and Organization***

The objective of this chapter is to provide fundamental perspectives on the economic evaluation of both conventional and unconventional REE resources. Section 19.1 has provided an overview of the process used for economic evaluation of mineral deposits and described some of the unique challenges associated with comparative evaluation of REE resources. Section 19.2 further defines standard terminology used in REE project valuation and describes typical procedures for project cost and revenue estimation. Section 19.3 provides a comparative case study of several notable REE deposits using data from various public disclosures and National Instrument (NI) 43-101 documents. Section 19.4 provides a similar, albeit abbreviated discussion on several unconventional resources, namely monazite sands, coal by-products, acid mine drainage and seafloor sediments. Finally, Sect. 19.5 provides conclusions and recommendations. Altogether, this chapter provides economic benchmarks, which can be used to evaluate the economic merits of new projects and processes.

## 19.2 Definitions and Valuation Methodologies

### 19.2.1 Value Indicators

#### REE Prices

One of the most critical elements in the economic evaluation of any mineral development project is the selection of an appropriate mineral price forecast. Choosing a price that is lower than the eventual market value may lead to abandoning an otherwise profitable project, while choosing a price that is higher than the eventual market value may lead to perpetual and irreconcilable operating losses. While global supply and demand dictate long-term prices for any commodity, short- and medium-term price volatility may be influenced by speculation, current inventory levels and other global market trends. In addition, REE prices are also affected by locked-in supply contracts and market manipulation by state actors. Academic efforts to forecast general commodity prices and REE-specific prices [7] are abundant; however, Rudenno [8] points out that the pragmatic success rate for commodity price forecasting is very poor and instead suggests an intensified focus on low cost production as a means of natural protection against falling commodity prices.

Given the market-side challenges described above, the issues associated with price forecasting are intensified for REE development projects. Compounding the pricing transparency issues, production quotas from China have also proven to have a dramatic influence on REE prices. This issue was most pronounced in 2011–2012 when the Chinese cut production, leading to a dramatic and rapid increase in REE prices, which was subsequently followed by a similarly rapid decrease. Current REE prices, shown in Table 19.1, are among the lowest over the last decade. Note that scandium (Sc), which is included with the other REEs in some publications is not included in the analyses presented in this assessment.

**Table 19.1** Indicative REE oxide prices, FOB China, January 2020 [9]

Rare earth oxide	Nominal purity (%)	Price (\$/kg REO)
Lanthanum oxide	99.5	\$2.00
Cerium oxide	99.5	\$2.00
Praseodymium oxide	99.5	\$50
Neodymium oxide	99.5	\$42
Samarium oxide	–	–
Europium oxide	99.99	\$30
Gadolinium oxide	99.5	\$23
Terbium oxide	99.5	\$500
Dysprosium oxide	99.5	\$250
Holmium oxide	–	–
Erbium oxide	99.5	\$22
Thulium oxide	–	–
Ytterbium oxide	–	–
Lutetium oxide	–	–
Yttrium oxide	99.99	\$6.00

## Basket Price

REE ore deposits may contain as many as 15 marketable elements, each with its own feed grade and market price (notwithstanding scandium and other non-REE by-products). The high dimensionality of this problem often complicates preliminary assessments where one may seek to compare just one or two indicative metrics that assess the ore feedstock. One approach to reduce this dimensionality is through the calculation of an REE *basket price*. The basket price is simply the weighted average price of rare earth oxides (REOs) in a particular material (expressed as \$/kg REO). When referencing an orebody, the basket price calculation typically uses the market price of individually separated REOs, which are then weighted by the mass proportion of REOs in the unprocessed ore. The use of separated REO prices occurs irrespective of the specific company's plan to produce separated oxides, as the separated oxide prices are the product prices that are most readily available. Goode [10] shows that the basket price for nine selected REE deposits ranges from \$12.3 to \$32.6/kg REO when using 2016 REE prices adjusted for inflation to 2020. Furthermore, to reduce the complexity and required capital of their project, many REE juniors will report a discounted REE basket price, assuming their mixed REE concentrate can be sold to existing separation facilities, albeit at a discount.

While the basket price is frequently reported in REE economic assessments, use of the basket price as a relative economic indicator can be problematic. First, the reader should take note whether the reported basket price refers to the feed/orebody REE distribution or to the product REE distribution as differential recovery between individual REEs through the concentration process may lead to variations. For preliminary assessments where the final process route is not yet defined, authors will often report (without qualification) the basket price as based on the distribution of REEs in the orebody. This calculation thus assumes that all elements included in the calculation will be recovered at the same rate and that all elements will be individually separated and marketed. This assumption is rarely valid, as recovery processes will tend to preferentially recover specific elements, either by design or by convention. Second, the basket price is not directly influenced by the REE feed grade but rather only by the relative distribution of REEs. Since the calculation is merely a weighted average, a rich ore with a 20% REE grade can have a basket price identical to that of a background rock material with a 100 ppm REE grade, even though the two may have drastically different economic outcomes. Third, the basket price calculation does not consider the mining and processing costs associated with a specific deposit. Thus, two deposits with the same basket price and the same feed grade may still show varying levels of economic viability based on the process amenability of the ore and other technical factors.

## Contained Value

*Contained value*, also denoted as in situ value, in-place value or inherent value, is a common mining and mineral processing term that describes the value of a particular commodity contained within a unit mass of raw ore (usually expressed as \$/tonne). Contained value is readily calculated from the raw ore grade and the commodity price (or the basket price when referencing REE projects). The contained value is useful for preliminary economic analyses as it represents the maximum cost threshold for economic viability. For example, to be economically viable, an ore with a contained value of \$20/tonne must have mining and processing costs significantly less than \$20/tonne, as the contained value must not only cover the costs, but it must also account for any processing losses as well as the profits required to obtain investment. Rudenno [8] shows that across many mined commodities, contained values for economically viable deposits typically range from \$50 to \$150/tonne, with aluminum being the highest (\$771/tonne) and silver being the lowest (\$16/tonne).

Contained value can be a useful indicator of economic merit for REE projects; however, this comparison must be made with caution. Contained value is a better metric than basket price, as it is influenced by the overall feed grade; however, the contained value does not consider the process amenability and thus the processing costs of the specific ore. As alluded to above, two ore deposits with identical contained values may have drastically different economic outcomes due to differences in ore mineralogy and subsequently the processing intensity required to produce an enriched product. Moreover, like the basket price, the contained value assumes that all elements will be equally recovered and marketed, which may be not optimal or even tenable for all projects.

### 19.2.2 Cost Indicators

For REE projects, production costs include the mining, processing and refining costs needed to deliver the marketable REE product from the ore body to the consumer. Depending on case assumptions for each project, the final process stages could range from production of mineral concentrates to the full elemental separation of individual REEs or even the production of rare earth metals and alloys. As mentioned above, if the final process step does not include production of individually separated REOs, economic assessments will typically employ a flat toll refining cost or use a discounted REE price deck to account for the cost of separations. For the REE development projects assessed over the last decade, these price discounts have ranged from 19% [11] to 43% [12]; however, most utilize a value between 25% and 30%. Dahlberg [13] includes a discussion justifying the use of 25% to fully account for the cost of separation.

## Estimation Accuracy and Standards

Standard practices for reporting the mineral reserves and projected economic merit of mine development projects have been developed in many jurisdictions. Larsen [14] provides a detailed review of these standards as well as the engineering studies that must accompany the public disclosures. The two most common standards for REE projects and for mining projects in general, include the Canadian National Instrument (NI) 43-101 [14] and the Australasian Code for Reporting of Exploration Results, Mineral Resources and Ore Reserves (or the JORC Code [15]). Other notable standards include the South African Code for the Reporting of Exploration Results, Mineral Resources and Mineral Reserves (SAMREC) [16] and the recently updated US SEC Regulation S-K [17].

Common to all reporting standards is the use of staged engineering studies to describe the extent of the orebody and the economic merits of the project. Typical studies included as part of the mine development and financing process include a conceptual study or resource estimate (RES), a preliminary economic assessment (PEA) or scoping study, a prefeasibility study (PFS) and a feasibility study (FS). The feasibility study can also be referred to as definitive feasibility study (DFS), bankable feasibility study (BFS) and/or front-end engineering design (FEED). The study name implies the degree of accuracy in the cost estimates, and the various reporting codes provide definitions for the level of engineering detail to be included in each stage. While different engineering firms may apply different minimum standards, the level of accuracy in the cost estimates may vary from  $\pm 50\%$  at the PEA stage (Association for the Advancement of Cost Engineering (AACE) Class V) to  $\pm 25\text{--}40\%$  at the PFS stage (AACE Class IV) to  $\pm 15\text{--}25\%$  at the FS study stage (AACE Class III) [18].

Technical reports prepared as part of the NI 43-101 or JORC process may be found on company websites or through database services such as the SEDAR filing system [19].

## Capital Cost Estimation

Capital costs for mining and processing operations include both fixed capital (i.e., equipment, installations, buildings, services and the required engineering and construction costs) as well as working capital (e.g., the capital needed to finance plant startup prior to revenue generation). For mining projects, fixed capital often represents 90% of the total capital costs and entails a significant investment. Fixed capital costs generally follow a power law equation of the form:

$$\text{CAPEX} = \left[ \frac{\text{CI}_c}{\text{CI}_R} \right] [K] [aX^b] \quad (19.1)$$

where  $CI_C$  and  $CI_R$  are the cost indices for the construction year and the reference year, respectively,  $K$  is the equipment cost ratio (or Lang) factor,  $X$  is the unit capacity and  $a$  and  $b$  are fitting constants unique to each equipment item [20]. The  $a$  and  $b$  fitting constants can be found in (or derived from) a number of resources and texts [8, 20, 21] and indicative values for a number of common process operations found in mineral processing and hydrometallurgical plants [22].

In addition to the cost-capacity relationship, Eq. (19.1) also accounts for changes in time from the data's reference year to the year of construction. This conversion is a simple ratio of the cost indices between the 2 years. Several cost indexing sources are available with one of the more popular being the Chemical Engineering Plant Cost Index (CEPCI) [23]. Lastly, Eq. (19.1) accounts for installation and ancillary costs through an installation or Lang factor. Lang factors for mining and mineral processing operations are specified by Gentry and O'Neil [20] and typically range from 3.0 to 6.0 depending on the specific equipment and the installation conditions.

Use of the cost-capacity relationships and Lang factors are common in PEA and PFS stages. As the project advances to more detailed design phases, the use of cost-capacity relationships and Lang factors should be offset by budgetary quotes, firm vendor quotes and detailed line-item estimates. Nevertheless, these cost-capacity relationships can be useful in evaluating process alternatives and optimizing process scale.

## Operating Cost Estimation

Operating costs generally include variable costs (e.g., process chemicals, energy, waste disposal and direct labor), fixed costs (e.g., indirect labor, maintenance, administrative, insurance, interest, property taxes and intellectual property costs), and overhead (e.g., marketing and sales, accounting, legal, research and development, environmental, social and governance). Variable operating costs are typically estimated by direct calculation based on process requirements, mass and energy balances, and personnel tables. Alternatively, for early stage estimates, indirect and overhead costs are often estimated by ratio methods using other known costs as the basis. For REE projects, operating costs are often presented as \$/kg REO produced to provide a comparable metric to the basket price, which has the same units.

### 19.2.3 Economic Modeling and Worth Indicators

An economic (or fiscal) model for a project is generated by combining the capital cost estimate, operating cost estimate, revenue projection, production schedule and tax/deduction structure. The economic model assimilates these inputs and provides the cash flow projections on an annual basis for the life of the project. These cash-flow projections are then in turn used to generate life cycle economic indicators, including net present value (NPV), IRR and PP (discounted or undiscounted). Less



common indicators include return on equity, debt service coverage ratio, present value ratio, present worth index, benefit-cost ratio and others.

By definition, NPV is the sum of all future cash flows after applying a discount rate to future cash flows to account for the time value of money. NPV may be calculated from the following formula:

$$NPV = \sum_{t=0}^N \frac{ACF}{(1+i)^t} \quad (19.2)$$

where  $t$  is the project year,  $N$  is the total project life, ACF is the annual cash flow, and  $i$  is the discount rate. For mineral development projects, a discount rate of 10% is often used; however, sensitivity analyses may also include values from 6% to 15%.

With respect to the other standard indicators, the IRR is the annual interest rate that causes the NPV to be zero and is representative of an equivalent annual growth rate anticipated from the capital investment. Lastly, the PP is the time needed for the project revenues to recoup the initial capital investment. Payback period is often presented using discounted future cash flows; however, undiscounted (i.e., cash basis) PP may also be found in some studies.

## 19.3 Assessment of Conventional Resources

### 19.3.1 Methodology and Limitations

Using the principles described above, a fundamental economic assessment of most of the world's major REE development projects was conducted. The initial list of REE projects was adapted from Goode [10] and included 42 distinct projects from 14 countries on 6 continents. After identifying the list of deposits, various publicly available resources, including company websites, annual investor presentations, public databases (i.e., SEDAR) and other academic literature were assessed to build a database of various technical and economic parameters for each project. Fields included in the database are as follows:

- Deposit location (country)
- Study level (PEA vs. PFS vs. FS/DFS/BFS)
- Year of study (date)
- Mineral resource (million metric tonnes, mt) and TREO grade (%)
- Individual REO resource grade (%)
- Cutoff grade (%)
- Annual REO production (tonne/year)
- Mine life (years)
- Reported REE basket price (\$/kg TREO)
- Reported REE price discount, if applicable (%)

- Reported preproduction capital costs (\$)
- Operating costs (\$/kg TREO)
- Reported net present value and discount rate (\$ and %)
- Reported internal rate of return (%)
- Reported payback period
- Calculated gross margin, reported basket price – reported operating cost (\$/kg REO)
- Calculated capital intensity, reported preproduction capital/annual REO production (\$/(kg/year) REO)
- Calculated present worth index, reported NPV/reported preproduction capital (\$/\$).

For project reporting financial indicators in currencies other than USD, fixed exchange rates of 1.00 CAD = 0.80 USD and 1.00 AUS = 0.77 USD were applied regardless of the original exchange rate listed for the project. These rates are reflective of May 2021 rates when this analysis was conducted. Moreover, when some database values were not explicitly reported (e.g., basket price, REE price discount and payback period), reasonable efforts were made to estimate the values from the other information included in the publicly available documentation. Lastly, some modifications were needed to account for variations in infrastructure and other large capital costs. While most projects included the infrastructure needed to produce a MREO product, some projects also included major REE separation and refining facilities in their capital cost estimation. To form the best comparison with the other projects in the dataset, these refinery costs and other major infrastructure costs (e.g., ports, large access roads) were excluded from the analysis. Only two projects (i.e., Strange Lake [24] and Nechalacho [25]) required such adjustments.

The intent of this assessment is to broadly show the range and distribution of various financial parameters reported in public financial disclosures for REE projects. This data may provide a quantitative basis for benchmarking and evaluating future conventional and unconventional projects; however, direct comparison between the projects included in the study should be taken only with extreme care. Specific limitations of the current assessment are as follows:

- Notwithstanding the minor adjustments described above (e.g., currency conversions), all of the database values were directly taken from the source documents as is. To eliminate any opportunity for bias or subjectivity, no effort was made to verify the veracity or reliability of the reported values.
- The various projects represent a range of study levels from the PEA/scoping study level to the DFS level. Thus, the reported indicators reflect a large range of accuracy levels and corresponding engineering detail. As reflected in most of the reporting codes, analyses at the PEA level are often very preliminary, utilize many assumptions and are typically not valid for economic decision making beyond a go/no-go decision. While similar, many other assumptions like REE cutoff grade and REE price discount are not consistent between the projects and may lead to significant discrepancy in the final outcomes.

- The reported financial indicators (NPV, IRR and PP) are often very sensitive to the REE price deck, which varies considerably between projects. Depending on the study year and pricing methodology employed, some projects have incorporated pricing scenarios that were partially or fully influenced by the REE crisis prices in 2011–2012.

### 19.3.2 *Metadata*

Table 19.2 shows a list of all 42 projects as well as the associated metadata (i.e., deposit location, study level, study year and references). Technical details for these projects can be found in the respective project documents, and Goode [10] also provides geologic information and technical data for many of the projects included in this table. As shown, the projects have been split into two groups – one dataset that includes economic data suitable for comparison and analysis and a second dataset that only includes information on the resource size and grade. As indicated above, the projects span 6 continents and 14 countries and include representation from most of the world’s major mining districts.

Figure 19.1 shows the distribution of projects by study year from 2011 to 2019. The majority of the reports (57%) were published in a 3-year span from 2013 to 2015 in the immediate period after the REE pricing crisis. As described by Cox and Kynicky [61], junior REE mining companies raised approximately \$4.2 billion between 2010 and 2012; however, by 2015, most of the investment had subsided as the market found other solutions, such as substitution or offshoring of the manufacturing processes. In recent years, though, interest in REE projects has once again increased, as indicated by the growing number of updated studies published in 2019 [1, 36, 38, 40, 49].

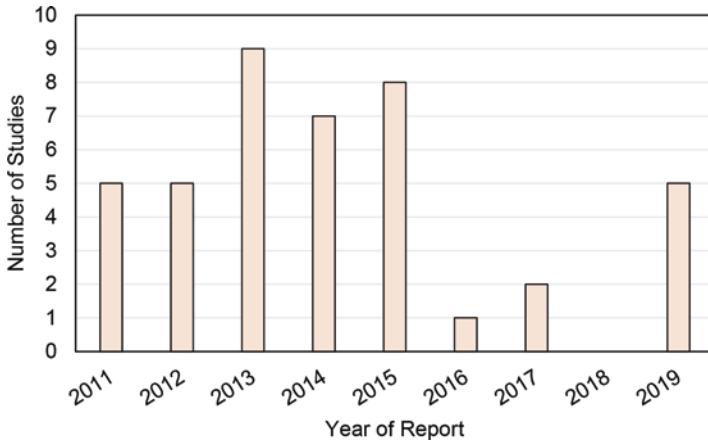
### 19.3.3 *Project Resource Data*

Prior to analyzing the economic data, the mineral resource data from all 42 projects were initially assessed to identify the extent and grade of the orebodies under consideration for development. Figure 19.2 shows the results of this analysis as box and whisker plots for the resource tonnage, average grade and REO tonnage from all 42 projects. The data presented here represents the total of the measured, indicated and inferred resource, as not all projects provided data in the measured and indicated categories.

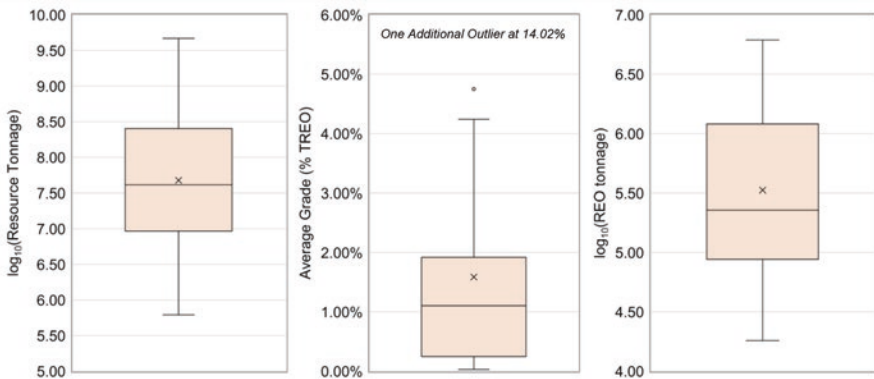
The cutoff grades used to delineate the ore resource varied with respect to formulation (% total REE (TREE) vs. %NdPr vs. \$/ton net smelter return). Of the 42 projects, 26 provided a resource cutoff grade as a %TREE, with values varying from 300 ppm TREE (Tantalus and Milo [53, 58]) to 3.5% TREE (Kanganunde [49]). For projects at the PEA stage or higher, 1.00% REO was the most common cutoff grade utilized. For the remaining projects, cutoff grade was typically specified by a

**Table 19.2** REE development projects

Deposit name	Study level	Country	Year of latest update	References
<i>Included in economic dataset and the resource dataset</i>				
Araxa	PEA	Brazil	2012	[26]
Ashram	PEA	Canada	2015	[27]
Bear lodge	PFS	USA	2014	[13]
Bokan	PEA	USA	2013, 2015	[28]
Browns range	PFS	Australia	2015	[29]
Charley Creek	Scoping	Australia	2013	[30]
Eco ridge	PEA	Canada	2012	[31]
Foxtrot	PEA	Canada	2016	[32]
Glenover	PEA	South Africa	2012, 2013	[33]
Kipawa	FS	Canada	2013	[34]
Lofdal	PEA	Namibia	2014	[11]
Nechalacho	FS	Canada	2013	[25]
Ngualla	BFS	Tanzania	2017	[35]
Nolans	DFS	Australia	2019	[36]
Norra Karr	PFS	Sweden	2015	[37]
Sarfartoq	PEA	Greenland	2013	[12]
Songwe Hill	PFS	Malawi	2015, 2019	[38]
Steenkampskraal	PFS	South Africa	2014	[39]
Strange Lake	PEA	Canada	2014	[24]
Yangibana	DFS	Australia	2019	[40]
Zandkopsdrift	PFS	South Africa	2015	[41]
<i>Economics available but excluded from analysis. Included in resource dataset only</i>				
Buckton	PEA	Canada	2013	[42]
Round top	PEA	USA	2019	[1]
<i>Included only in the resource dataset</i>				
Aksu Diamas	RES	Turkey	2011, 2013	[43]
Brockmans	RES	Australia	2015	[44]
Clay-Howells	RES	Canada	2011	[45]
Cummins range	RES	Australia	2019	[46]
Elliot Lake Teasdale	RES	Canada	2013	[47]
Hoidas Lake	RES	Canada	2014	[48]
Kangankunde	RES	Malawi	2019	[49]
Kutessay II	RES	Kyrgyzstan	2011	[50]
Kvanefjeld	RES	Greenland	2014	[51]
Lavergne-Springer	RES	Canada	2012	[52]
Milo	RES	Australia	2012	[53]
Montviel	RES	Canada	2015	[54]
Mrima Hill	RES	Kenya	2013	[55]
Olserum	RES	Sweden	2013	[56]
Serra Verde	RES	Brazil	2012	[57]
Sorensen	RES	Greenland	2014	[51]
Tantalus	RES	Madagascar	2016, 2017	[58]
Two tom	RES	Canada	2011	[59]
Wigu Hill Twiga	RES	Tanzania	2011	[60]



**Fig. 19.1** Distribution of study year for the projects included in this analysis



**Fig. 19.2** Mineral resource data for all project ( $n = 42$ ). Values presented herein reflect measured, indicated and inferred resources

minimum net smelter return (e.g., \$16/tonne, Round Top [1]) or by a minimum contained value (e.g., \$100/tonne, Eco Ridge [31]).

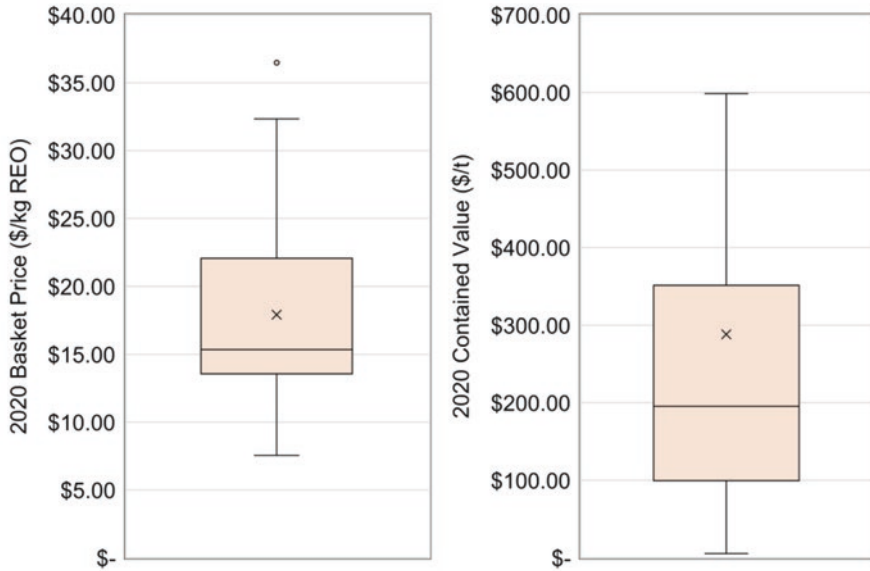
Results show that the resource tonnage and the contained REO tonnage span several orders of magnitude. For example, the REO tonnage varies from 18,000 tonnes (Lofdal [11]) to more than 6.1 million tonnes (Mrima Hill [55]); however, most of the projects fall between 100,000 and 1000,000 tonnes. Likewise, average resource grade varied from 300 ppm (Buckton and Charley Creek [30, 42]) to the anomalously high 14.02% (Steenkampskraal [9]). For studies at the PEA stage or higher, the median grade was slightly higher than that of the full dataset, 1.36% vs. 1.10%. In total, the 42 projects described herein accounted for over 45.6 million tonnes of REO resource, a number nearly 200 times the global REO production in

2019, 210,000 metric tonnes [62]. For more information on the resource characters of various projects, the reader is directed to Goode [10] who has provided detailed data and interesting visualizations.

With respect to the economic benchmarks, Table 19.3 shows a summary of the resource data, basket price and contained value for most of the resource deposits (13 entries were excluded due to lack of readily available individual REE data). In addition, Fig. 19.3 graphically depicts these data as box and whisker plots. Rather than using the reported basket price and the reported REE price deck, this analysis

**Table 19.3** Summary of resource economic indicators for conventional REE resources

Deposit name	Measured + indicated + inferred resource			2020 basket price (\$/kg REO)	2020 contained value (\$/tonne)
	Tonnage (tonnes)	Average grade (% REO)	REO tonnage (kt REO)		
Araxa	28.3	4.22	1193.0	\$11.02	\$550.67
Ashram	249.1	1.88	4688.4	\$13.23	\$250.86
Glenover	10.4	2.13	221.0	\$17.57	\$386.53
Sarfartoq	8.3	1.72	143.2	\$13.37	\$236.63
Songwe Hill	48.6	1.36	662.8	\$13.99	\$197.86
Yangibana	20.9	1.17	245.5	\$21.53	\$240.80
Bear lodge	45.2	2.75	1242.8	\$13.84	\$383.75
Lofdal	6.2	0.29	18.1	\$32.34	\$106.22
Nolans	55.9	2.59	1449.8	\$14.51	\$402.34
Steenkampskraal	0.6	14.02	86.8	\$15.74	\$2352.97
Kipawa	27.1	0.40	107.9	\$22.60	\$92.78
Charley Creek	805.0	0.03	235.0	\$18.41	\$5.43
Norra Karr	31.1	0.61	189.8	\$26.18	\$146.81
Bokan	5.8	0.60	35.2	\$25.30	\$152.29
Browns range	9.0	0.63	56.8	\$36.48	\$255.37
Ngualla	21.3	4.75	1012.1	\$11.50	\$549.11
Eco ridge	86.6	0.11	98.0	\$14.42	\$20.88
Foxtrot	9.4	1.11	103.5	\$17.72	\$195.95
Two tom	40.6	1.18	479.5	\$13.67	\$161.59
Wigu Hill Twiga	3.3	2.60	85.8	\$7.54	\$195.40
Tantalus	627.7	0.09	561.8	\$17.87	\$16.04
Milo	187.0	0.06	114.1	\$14.91	\$9.15
Clay-Howells	8.5	0.73	62.1	\$15.95	\$116.27
Montviel	266.6	1.45	3876.6	\$11.85	\$178.80
Olserum	7.8	0.61	47.8	\$23.40	\$141.79
Brockmans	41.4	0.21	87.9	\$32.25	\$68.37
Elliot Lake Teasdale	51.6	0.16	82.1	\$13.55	\$26.82
Hoidas Lake	2.8	2.00	57.0	\$15.35	\$318.56
Mrima Hill	159.4	3.85	6139.1	\$13.58	\$598.58

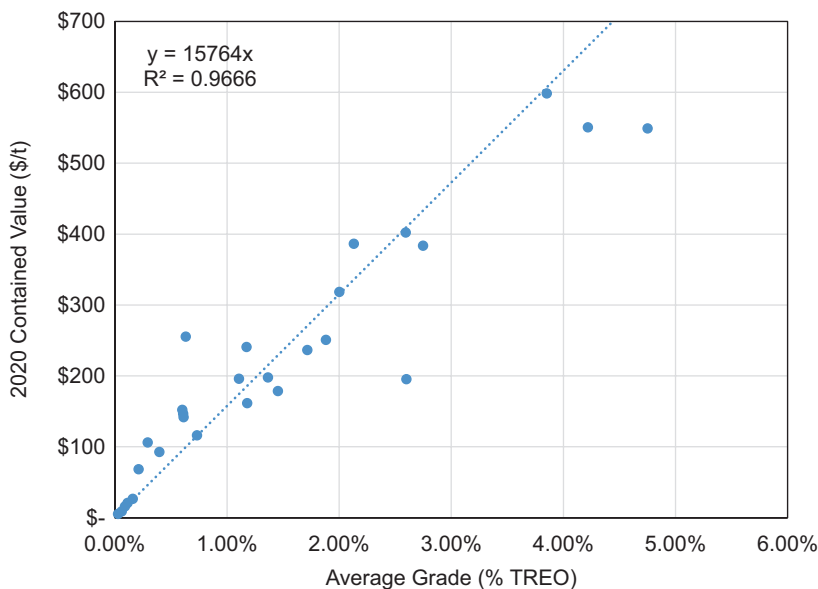


**Fig. 19.3** Basket price and contained value for several projects included in the overall dataset ( $n = 29$ ). Values calculated using 2020 REE prices

normalizes all of the deposits to a common price deck, namely, the 2020 REE prices shown in Table 19.1. As indicated in Fig. 19.3, the contained value, like the REE grade spans several orders of magnitude ranging from \$5.43/tonne (Charlie Creek [30]) to \$2353/tonne (Steenkampskraal [39]). A plot of contained value versus average grade (Fig. 19.4) shows a strong forced-zero intercept linear trend ( $R^2 = 0.96$ ) with slight deviations indicative of over or under enrichment of more valuable REEs.

### 19.3.4 Project Economic Data

Of the 42 projects included in the study, 19 were not yet at the PEA stage and thus did not have publicly available economic data. In addition, two other projects were also excluded from the economic dataset due to confounding factors that may complicate the comparisons. For example, the Buckton project [42] PEA showed an IRR less than 10%, which would prompt a negative NPV at a 10% discount rate and thus anomalous findings when compared to the other projects with much higher IRRs. Moreover, the Round Top deposit [1], while being a significant REE deposit, also includes considerable economic contributions from other technology metals and industrial mineral products. As indicated in their 2019 PEA, <30% of the project revenue is derived from REEs. As such, the capital requirements and revenue projects are not anticipated to follow the same pattern as that of primary REE projects, and as a result, it has been omitted from the forgoing statistical distributions.

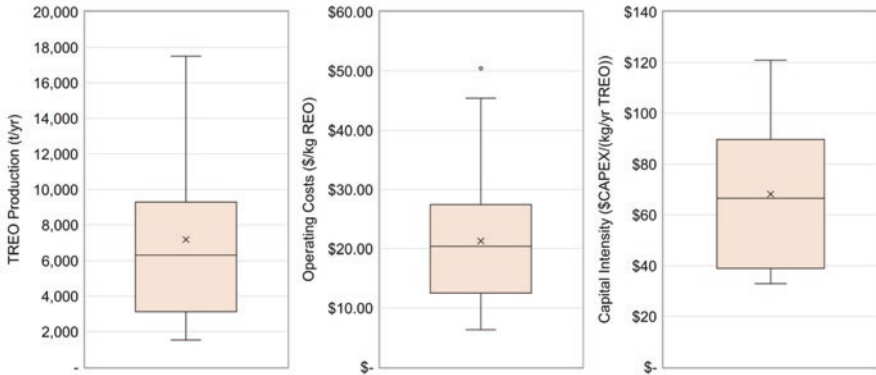


**Fig. 19.4** Relationship between contained value and REE grade for several projects included in the overall dataset ( $n = 29$ ). Contained value calculated using 2020 REE prices; Average REE grade reflective of measured, indicated, and inferred mineral resources. One anomalous point (14.02% grade, \$2353/tonne contained value) not shown in plot but included in linear regression

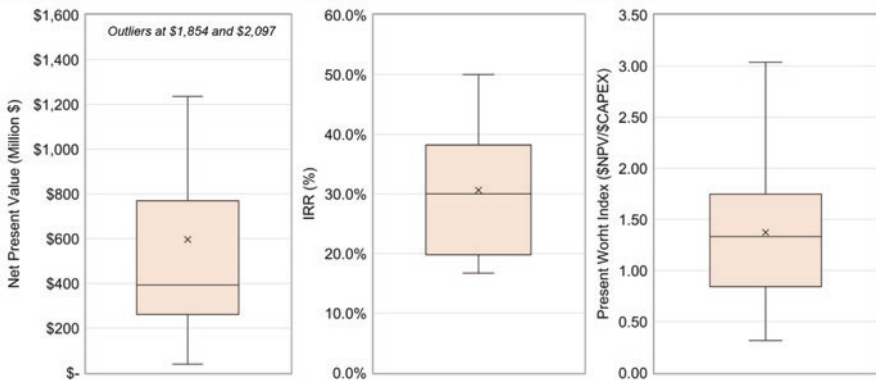
After accounting for these factors, the 21 remaining projects were included in the economic dataset and analyzed to identify the statistical distributions and trends. Figure 19.5 shows box and whisker plots for three key fiscal model inputs, namely, annual TREO production, operating costs and capital intensity (herein defined as the total preproduction capital cost divided by the annual TREO production). Likewise, Fig. 19.6 shows box and whisker plots for key fiscal model outputs, namely, the reported NPV (at a 10% discount rate), the IRR and the present worth index (herein defined as the net present value divided by the preproduction capital).

The anticipated TREO production from the 21 projects in the economic dataset varies from approximately 1500 tonnes/year (Lofdal and Steenkampskraal [11, 39]) to more than 17,000 tonnes/year (Araxa and Strange Lake [24, 26]). For reference, the apparent TREE consumption in the United States is approximately 10,000 tonnes/year based on average of the last 5 years [62]. In total, these 21 projects account for over 150,000 tonnes/year of production, which is on the same order of magnitude of the total global mine production from conventional sources (i.e., estimated to be 240,000 tonnes in 2020). It should be noted that in both of these comparisons that the elemental distribution of the REEs included in the production total may not be properly balanced with the demand-side consumption requirements, as discussed in the introduction.





**Fig. 19.5** Production and cost data for projects at the PEA stage or higher ( $n = 21$ )



**Fig. 19.6** Reported economic indicators for projects at the PEA stage or higher ( $n = 21$ ). Net present value shown in the left panels are reflective of a 10% discount rate

With respect to costs, when normalized to \$/kg REO produced, the operating costs vary from \$6.33/kg REO (Ashram [27]) to \$50.45/kg (Lofdal [11]). Likewise, the capital intensity values vary from \$32.95/(kg/year) (Charley Creek [30]) to \$120.92/(kg/year) (Bokan [28]).

All projects included in the economic dataset showed robust economics with NPVs (10% discount) ranging from \$38 million (Foxtrot [32]) to more than \$2 billion (Zandkopsdrift [41]). When normalized to the level of capital investment through the PWI calculation, the data showed a much smaller relative range, varying from 0.32 (Foxtrot [32]) to 3.04 (Ashram [27]).

### 19.3.5 Analysis and Assessment

The data from the economic dataset was further analyzed to show trends with respect to the costs and other economic indicators. Figure 19.7 shows the relationship between capital cost and TREO production. While there is some deviation, particularly at high production rates, these data follow a power law trend similar to Eq. (19.1), with an exponent of approximately 0.70 and regression coefficient ( $R^2$ ) of 0.68. Interestingly, this regression coefficient is slightly higher than the values reported by Rudenno [8], which span from 0.61 to 0.66 and include more than 200 mineral development projects from various commodity sectors.

Figure 19.8 is a similar plot showing the relationship between operating cost and production capacity. The data show that operating cost (presented as \$/kg REO produced) follows a power law with a negative exponent, indicative of increase economy of scale at higher throughputs. Since operating costs are driven by numerous confounding factors (e.g., mining method, ore mineralogy and processing intensity), the regression coefficient is notably lower than that of the capital cost (0.45 vs. 0.68) and commensurate with values reported (0.33–0.48) by Rudenno [8]. The exponents in both fitting equations are very similar to those reported by Rudenno.

For mineral commodities with a robust supply chain and a large set of publicly available production/cost data, an industry-wide cost curve is typically used to show the relative position of various producers. In a conventional cost curve, the

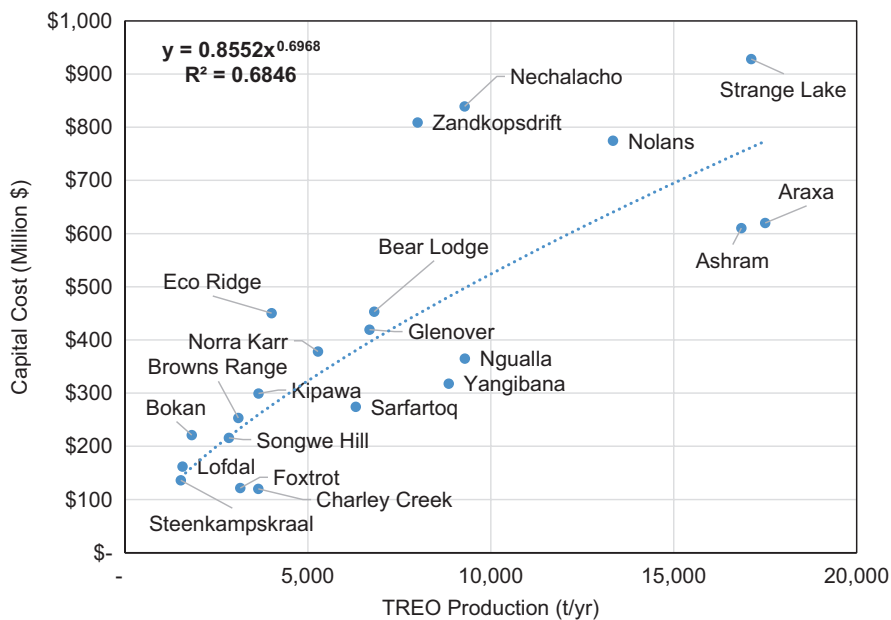
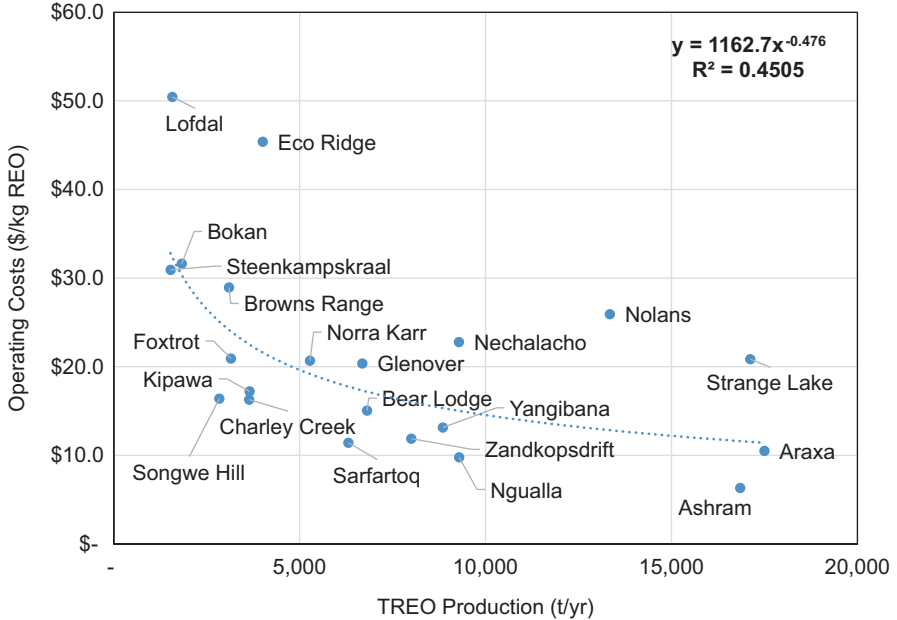


Fig. 19.7 Relationship between capital cost and TREO production rate for REE development projects ( $n = 21$ )

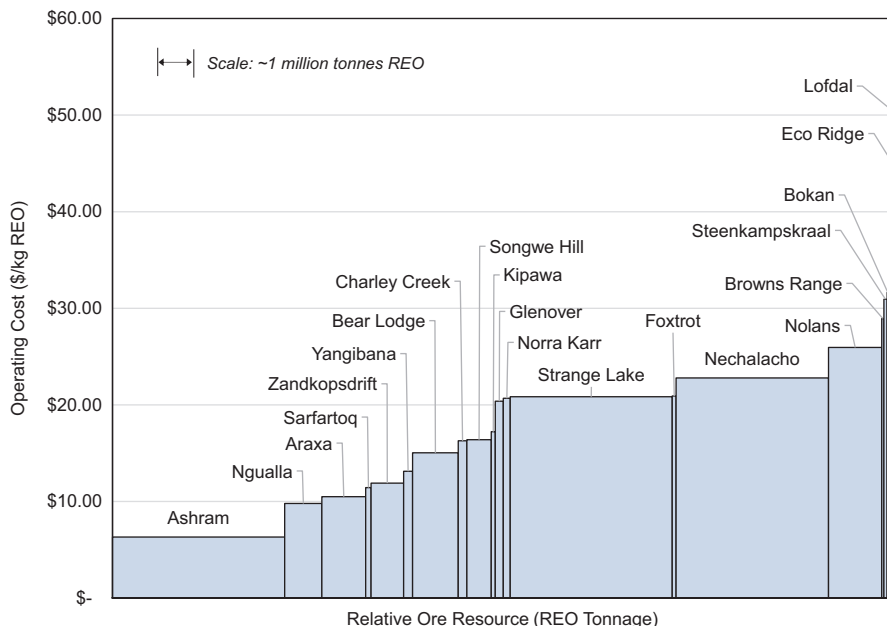


**Fig. 19.8** Relationship between operating cost and TREO production for REE development projects ( $n = 21$ )

production cost is plotted against the cumulative production for a given time period, typically 1 year. Individual producers are shown as bars, with the width of the bar being proportional to the volume of production. For the current dataset, a similar cost curve was generated; however, since all projects are in the development phase, the typical  $x$ -axis was replaced with the total REO tonnage included in the measured, indicated and inferred resource category. Figure 19.9 shows this plot for the 21 REE development projects. While direct comparisons between projects are problematic for the reasons given above, this plot does provide a clear visualization of low and high cost producers as well as the large and small REO resources. Moreover, this plot provides benchmarks that can be used to assess and guide technology development and alternative resources.

While most of the analyses have focused on cost components, Fig. 19.10a shows a relationship between the reported basket price and the reported operating cost, both in units of \$/kg REO. The breakeven line as well as parallel lines of constant gross margin (defined as basket price less production costs) are also shown for convenience. Interestingly, this data follows a very clear power law trend ( $R^2 = 0.73$ ), potentially indicating that lower basket prices demand lower cost processing options. Nevertheless, most of the data falls within the \$25 to \$30/kg REO margin limits.

Figure 19.10b shows a similar plot; however, in this case, the reported basket prices have been replaced with an updated basket price using the January 2020 price deck shown in Table 19.1. Note that some projects were removed from this updated

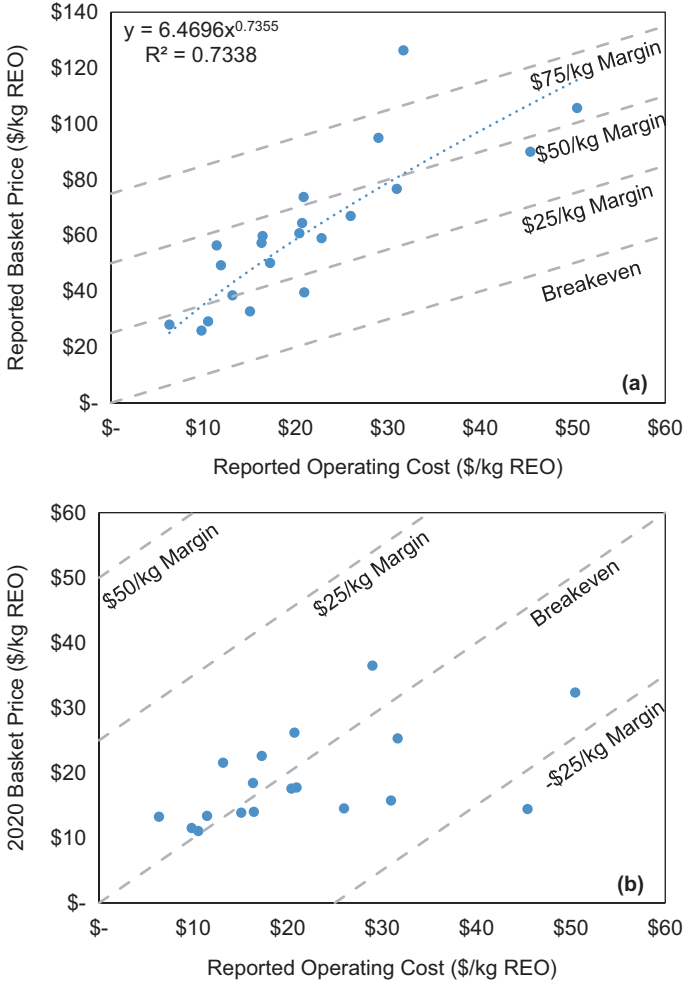


**Fig. 19.9** Cost-resource curve for the REE development projects included in the economic dataset ( $n = 21$ ). The  $x$ -axis shows cumulative REO resources contained in the measured, indicated and inferred resource categories, and the width of each bar is proportional to the total resource

analysis in cases where element-by-element concentration data were not readily available. For most elements, the 2020 prices include some of the lowest over the last decade and are considerably lower than the prices from the mid-2010s, which were utilized in many of the original technical reports. This trend is clearly depicted in these two plots, as basket prices have been reduced from \$25–\$120 to \$10–\$35/kg REO, a reduction of nearly 71% on average. After adjusting the basket price to reflect updated pricing, fewer than half (9 of 21) of the original projects meet the breakeven threshold, and many that do provide only marginal benefits above the breakeven point. Of the 9 projects that meet the breakeven point, all but one have a reported operating cost less than approximately \$20/kg REO, emphasizing the impetus for low cost production.

### 19.4 Unconventional Resources

The REO basket price, production cost, resource size and contained value data presented above provide suitable benchmarks upon which unconventional resources can be assessed at a fundamental level. To this end, salient points for some of the more prominent and well-studied unconventional resources are presented below. The reader is encouraged to review the papers and review articles in the reference list for further detail.



**Fig. 19.10** Relationship between basket price and operating cost for REE development projects included in the economic dataset. (a) shows basket price as initially reported in the economic disclosure ( $n = 21$ ) while (b) shows an updated basket price using 2020 REE pricing ( $n = 18$ )

### 19.4.1 Monazite Sand

Monazite is one of the principle REE-bearing minerals and one of only three minerals commonly exploited in commercial production [63]. Historically, monazite placer deposits were dominant source of REEs in the United States; however, the Mountain Pass mine and subsequent competition from foreign sources reduced the importance of this resource [64]. Monazite often occurs as an accessory mineral in commercial heavy mineral sand operations, which produce titanium (Ti) minerals

and zircon as saleable products. According to the USGS [62], monazite is currently being commercially produced in the United States, and a 2017 application for a Nuclear Regulatory Commission (NRC) export license describes the composition and quantity of a monazite product to be exported to China [65]. According to the documents in the license application, the sand product includes 60% monazite, 5% xenotime and 35% other minerals, with assays of approximately 23% REO.

Using the 2020 pricing deck and the elemental assay in the NRC permit application documents, the monazite sand was found to have a 2020 basket price of \$16.60/kg REO, approximately equal to the median of the data for conventional resources shown in Fig. 19.3. However, owing to the high grade, the material was found to have a contained value of nearly \$3900/tonne, greatly exceeding all other conventional resources, even the high-grade Steenkampstraal deposit [39]. Lastly, while the total volume of REEs in placer monazite resources is difficult to estimate, the NRC license application does indicate an ongoing production of 2900 metric tonnes of sand per year or approximately 650 tonne/year on an REO basis. While this value alone is much smaller than that of the conventional projects, other undeveloped coastal sediment resources occur from Virginia to Florida in the United States as well as in many other coastal regions around the world [64]. For example, monazite reserves in India total nearly five million tonnes of REO equivalent [64, 66].

### 19.4.2 Coal and Coal Ash

Since 2014, the U.S. Department of Energy (DOE) has supported research and development investigating the technical and economic feasibility of recovering REEs from coal and coal by-products, which include preparation plant rejects, underclays, partings, tailings, combustion residuals and other related materials. Over the last decade, hundreds of papers have been written on this topic and the reader is encouraged to consult a seminal paper by Seredin and Dai [67], a 2015 review article by Zhang [68] and more recent 2020 review article by the same lead author [69].

With respect to economic potential, coal and coal by-products tend to have low concentrations (often 300–500 ppm in the raw coal and to 1000–1500 in the ash) and by extension low contained values. Noble and Luttrell [70] showed that contained values for the lanthanides and yttrium in raw coal varied from \$10 to \$15/tonne when using REE prices from 2015 [71] and average concentrations from a large sample database [72]. While this value is low relative to conventional REE deposits, Zhang [69] notes several advantages for coal-based materials including a higher concentration of heavy and critical REEs, little or no mining costs, lower concentrations of radionuclides and the potential to mitigate or eliminate legacy environmental issues. Moreover, coal has the potential to synergistically produce other critical by-products (e.g., lithium (Li) [73, 74]). Most of the economic analyses include scandium (Sc), which is typically not assessed in conventional REE deposits and considerably improves the contained value. Work by Honaker [22] as

well as other researcher groups has shown that extraction and recovery of high-purity mixed rare earth products from coal is technically feasible and with proper optimization, processing costs can be reduced substantially. While a comprehensive assessment of the REE resource in coal is not available, Luttrell [75] indicated that the refuse in 20 coal preparation plants may contain more than 10,000 tonnes/year of REE, a value commensurate with U.S. demand.

### 19.4.3 Acid Mine Drainage

Acid mine drainage (AMD) is a longstanding environmental issue whereby pyrite-bearing rocks are liberated during the mining process and subsequently exposed to air and water. The subsequent oxidation of the pyrite produces sulfuric acid, which leaches major metals and can contaminate waterways if not captured and treated. In 2019, Vass published two studies on the occurrence and concentration of REEs in the Northern and Central Appalachian Coal Basins in the United States [76, 77]. The first study showed data from a small prospect survey ( $n = 9$ ) and indicated that the concentration of REEs in AMD can vary from the ppb to low ppm levels. However, the study also showed that the conventional approach to capturing and treating AMD can enrich the concentration value several thousand times, producing precipitates with concentrations as high as 1200 ppm (dry weight basis). Following up in the second study, a larger regional survey was conducted, and more than 140 AMD sites were directly sampled and analyzed. The data showed that average concentration in the treatment by-products was approximately 700 ppm; however, values as high as 2500 ppm were also observed.

Comparative economic assessment of AMD versus conventional REE deposits is difficult for many factors. First, AMD is not a fixed in place resource with a limited life. Instead, it is a distributed, perpetually producing resource with an indefinite or hard-to-define life. Regional flow estimates for the Appalachian Basin have been provided by Vass [77] and Stewart [78], which range from 771 to 3400 tonnes/year REE. Using an average oxide ratio of 1.12, these values correlate to a range of 864–3800 tonnes/year REO. The upper bound estimate for annual production in this case (3800 tonnes/year REO) exceeds that of approximately 30% of the conventional resources, as shown in Fig. 19.5.

Second, simple contained value calculation of solid AMD treatment products may not account for technology advances that can simultaneously treat and concentrate REEs at little to no added cost. Vass [76] showed the relative basket price and contained value for a 500 ppm AMD treatment by-product relative to that of conventional resources. When using a fixed price deck, the contained value of the AMD treatment by-product exceeds that of approximately 25% of the other conventional deposits. However, upstream technologies, such as a recent patent by Ziemkiewicz [79] shows that an REE-enriched preconcentrate of 0.1–5% TREE can be produced while treating raw AMD. This grade rivals that of many of the notable conventional deposits. Moreover, the REE distribution in AMD tends to favor heavy and critical

REEs, with yttrium (Y) and neodymium (Nd) concentrations often exceeding that of lanthanum (La) and cerium (Ce). Assuming a preconcentrate grade of 1% and using the 2020 REE price deck, a basket price of \$30.84 and a contained value of \$308/tonne were determined. The basket price represents one of the highest analyzed of all conventional and unconventional materials, while the contained value is greater than that of 70% of the conventional resources (Fig. 19.3).

Lastly, AMD and the associated treatment by-products represent current environmental liabilities, which in many cases are funded by state reclamation funds. The economic merits of valorizing a perpetual pollution source are evident but can be hard to define in a manner that is consistent with traditional ore deposit valuation.

#### 19.4.4 *Seafloor Sediments*

The ocean seafloor has been a speculative target for mineral resources for several decades. According to the USGS, exploration for REEs in seafloor sediments was conducted as early as 2011 by Japanese researchers, [64] and a review article by Milinovic [80] includes technical details from a number of direct studies that have analyzed samples of seafloor material. This chapter shows that REE concentrations vary considerably between the ocean settings, with Atlantic deposits having the lowest concentrations (up to 130 ppm) and Pacific deposits having the highest (up to 22,000 ppm).

In a 2018 article, Takaya [81] conducted a detailed geospatial and mineral processing study to evaluate potential of Pacific seafloor sediments as an REE resource. The results show that the resource potential in a 105-km<sup>2</sup> target area may be as high as 1.2 million tonnes of REO, a value that would be greater than 75% of the conventional projects. Takaya's study isolated three categories of seafloor mud: a normally REY-rich (795 ppm TREE), a highly rich mud (3950 ppm REE) and an extremely rich mud (7226 ppm TREE). By applying the 2020 price deck to the extremely rich mud assay, the basket price was determined to be extremely high, \$31.04/kg REO; however, the contained value was found to be only \$26.98 per metric tonne.

#### 19.4.5 *Summary*

Table 19.4 summarizes the resource value indicators for the four unconventional resources, namely, monazite sand, coal ash, AMD sludge and seafloor sediments. These values should be compared against those in Table 19.3 for the conventional deposits, which utilize the same REE price deck. In addition, the overall attractiveness of these resources as REE feedstocks should also consider the environmental, social, geopolitical and other intangible or difficult-to-quantify benefits described in the earlier sections.



**Table 19.4** Summary of resource economic indicators for unconventional REE resources

Unconventional resource	Nominal grade %REO	Resource potential	2020 basket price (\$/kg REO)	2020 contained value (\$/tonne)
Monazite sand	23	Vast, millions of tonnes	\$16	\$3900
Coal ash	0.1	Moderate, more than 10,000 tonnes per year	\$18	\$18
Pre-concentrated AMD sludge	1.0	Moderate, hundreds to thousands of tonnes per year	\$31	\$310
Seafloor sediment	0.9	Vast, millions of tonnes	\$31	\$27

## 19.5 Summary and Conclusions

A fundamental economic assessment of conventional and unconventional REE resources was conducted to provide a holistic view of the economic indicators and provide benchmarks for future comparative analysis. In this analysis, 42 global REE development projects with publicly disclosed resource data were analyzed to identify resource indicators including size and grade. Most of these studies were published from 2011 to 2015 in the immediate aftermath of the REE pricing crisis of 2011, though several projects also had recent updates since 2019. From that master list, a subset of 21 projects at the PEA stage or higher were further assessed to identify production and life cycle economic data, including reported capital and operating costs, production capacity, net present value, internal rate of return and payback period. These data were analyzed to identify the distribution and range of the various output values as well as industry-wide cost-capacity relationships. These data were then evaluated against several unconventional resources using a fixed REE price deck for comparative purposes.

The findings show that REE ore deposits vary in grade from approximately 300 ppm to nearly 15% TREO; however, the majority of the deposits with viable economic outcomes are between 0.5% and 2% TREO. The REO mass in the measured, indicated and inferred resource categories typically varies from 0.1 to 1.0 million tonnes; however, some outliers do fall considerably outside of this range. Relative to today, the elevated REE pricing used in the disclosures generally supported robust economic outcomes, with the 21 projects all having payback periods of 7 years or less and NPVs (10% discount rate) in the hundreds of millions to billions of dollars. Analysis of unconventional resources showed that while the REE resource is vast in most cases (e.g., seafloor sediment and monazite sand), the contained values of some can be quite low, but still within the range of the conventional deposits.

When current (2020) REE prices [9] were applied to the conventional deposits, many projects do not show the same robust economic viability, with only 9 of the 21 having a positive gross margin (defined here as basket price – reported production cost, \$/kg REO). Of those 9, all but one initially reported an operating cost lower than \$10/kg REO, emphasizing the need for low cost production for robust economic viability.

**Acknowledgments** The author would like to acknowledge Tommee Laroche and Alice Noble for their help in the database development and in their thoughtful contributions to the narrative discussion.

## References

1. D.E. Hulse, D. Malhotra, T. Matthews, C. Emanuel, *NI 43-101 Preliminary Economic Assessment Round Top Project Sierra Blanca, Texas: USA Rare Earth LLC and Texas Mineral Resources Corp* (Gustavson Associates, 2019), p. 230
2. G. Barakos, H. Mischo, A review of misleading methods and biased practices in evaluating the feasibility of rare earth mining projects, in *28th SOMP Annual Meeting and Conference*, (GEAM – Associazione Georisorse e Ambiente, Torino, 2017)
3. M.S. Jaroni, B. Friedrich, P. Letmathe, Economical feasibility of rare earth mining outside China. *Fortschr. Mineral.* **9**(10), 576 (2019)
4. K. Binnemans, P.T. Jones, K. Van Acker, B. Blanpain, B. Misra, D. Apelian, Rare earth economics: the balance problem. *JOM* **65**(7), 846–848 (2013)
5. K. Binnemans, P.T. Jones, Rare earths and the balance problem. *J. Sustain. Metall.* **1**(1), 29–38 (2015)
6. K. Binnemans, P.T. Jones, T. Müller, L. Yurramendi, Rare earths and the balance problem: how to deal with changing markets? *J. Sustain. Metall.* **4**(1), 126–146 (2018)
7. M.V.R. Garcia, A. Krzemień, M.Á.M. del Campo, C.E. Garcia-Miranda, F.S. Lasheras, Rare earth elements price forecasting by means of transgenic time series developed with ARIMA models. *Resour. Policy* **59**, 95–102 (2018)
8. V. Rudenno, *The Mining Valuation Handbook 4e: Mining and Energy Valuation for Investors and Management* (Wiley, 2012)
9. FedConnect, Opportunity: production of mixed rare earth oxides (REOs) from coal-based resources. Solicitation number: 89243320RFE000032 (2021). Retrieved 2021.05.02. Accessed <https://www.fedconnect.net/FedConnect/default.aspx?ReturnUrl=/fedconnect%3Fdoc%3D89243320RFE000032%26agency%3DDOE&doc=89243320RFE000032&agency=DOE>
10. J.R. Goode, Rare earth elements, in *SME Mineral Processing and Extractive Metallurgy Handbook*, ed. by R.C. Dunne, S.K. Kawatra, C.A. Young, (Society for Mining, Metallurgy and Exploration, Englewood, 2019), pp. 2049–2075
11. D.S. Dodd, P.J.F. Hannon, W.D. Roy, P.R. Siegfried, M.R. Hall, *Preliminary Economic Assessment on the Lofdal Rare Earths Project, Namibia: Namibia Rare Earths Inc.* (MDM Engineering, 2014), p. 363
12. P. Broad, J. Robinson, D. Coley, R.G. Simpson, D. Ramsey, *Preliminary Economic Assessment on the Sarfartoq Rare Earth Element Project, Greenland: Hudson Resources Inc.* (Tetra Tech Wardrop, 2011), p. 230
13. P.S. Dahlberg, A. Noble, J.T. Pickarts, W.L. Rose, J. Jaacks, *Bear Lodge Project Canadian NI 43-101 Pre-Feasibility Study Report on the Reserves and Development of the Bull Hill Mine, Wyoming* (Rare Element Resources, Ltd, Vancouver, 2014), pp. 1–516
14. National Instrument 43-101, Standards of disclosure for mineral projects (2022). Retrieved 2022.07.07. Accessed [https://www.osc.ca/sites/default/files/pdfs/irps/ni\\_20160509\\_43-101\\_mineral-projects.pdf](https://www.osc.ca/sites/default/files/pdfs/irps/ni_20160509_43-101_mineral-projects.pdf)
15. JORC, Australasian code for reporting of exploration results, mineral resources and ore reserves. The JORC code (2022). Retrieved 2022.07.07. Accessed [http://www.jorc.org/docs/JORC\\_code\\_2012.pdf](http://www.jorc.org/docs/JORC_code_2012.pdf)
16. SAMCODES, The South African code for the reporting of exploration results, mineral resources and mineral reserves (The SAMREC code) (2022). Retrieved 2022.07.07. Accessed [https://www.crisco.com/docs/SAMREC\\_2016.pdf](https://www.crisco.com/docs/SAMREC_2016.pdf)

17. U.S. Securities and Exchange Commission, Modernization of property disclosures for mining registrants (2022). Retrieved 2022.07.07. Accessed <https://www.sec.gov/corpfin/secg-modernization-property-disclosures-mining-registrants>
18. D. Larsen, R. Addison, R. Kehmeier, T. Swendsheid, T. Brown, J. Uhrle, Minimum engineering requirements for assessing mining projects. *Miner. Metall. Process.* **33**(4), 214–225 (2016)
19. SEDAR, Alberta Securities Commission (2022). Retrieved 2022.07.07. Accessed <https://www.sedar.com/>
20. D.W. Gentry, T.J. O’Neil, *Mine Investment Analysis* (Society of Mining Engineers of American Institute of Mining, Metallurgical, and Petroleum Engineers, New York, 1984)
21. D.E. Garrett, *Chemical Engineering Economics* (Springer Science and Business Media, Dordrecht, 2012)
22. R.Q. Honaker, W. Zhang, J. Werner, A. Noble, G.H. Luttrell, R.H. Yoon, Enhancement of a process flowsheet for recovering and concentrating critical materials from bituminous coal sources. *Min. Metall. Explor.* **37**(1), 3–20 (2020)
23. The Chemical Engineering Plant Cost Index (CEPCI) (2022). Retrieved 2022.07.07. Accessed <https://www.chemengonline.com/pci-home>
24. R.M. Gowans, W.J. Lewis, S. Shoemaker Jr., J. Spooner, R.V. Zalnieriunas, *NI 43-101 Technical Report on the Preliminary Economic Assessment (PEA) for the Strange Lake Property Quebec, Canada: Quest Rare Minerals Ltd* (Micon International Ltd, 2014), p. 258
25. T. Ciuculescu, B. Foo, R. Gowans, K. Hawton, C. Jacobs, J. Spooner, *Technical Report Disclosing the Results of the Feasibility Study on the Nechalacho Rare Earth Elements Project: Avalon Rare Metals Inc.* (Micon International Ltd, 2013), p. 307
26. A.N. Clay, B.A. Ackroyd, *A Preliminary Economic Assessment in the Form of an Independent Technical Report on MBAC Fertilizer Corp. Araxá Project* (Venmyn Rand (Pty) Ltd, 2012), p. 113
27. G. Gagon, G. Rousseau, Y. Camus, J. Gagné, *Preliminary Economic Assessment Ashram Rare Earth Deposit for Commerce Resources Corp* (SGS Canada Inc., 2015), p. 219
28. E.H. Bentzen, H. Ghaffari, L. Galbraith, R.F. Hammen, R.J. Robinson, S.A. Hafez, S. Annavarapu, *Preliminary Economic Assessment—Bokan Mountain Rare Earth Element Project, Near Ketchikan, Alaska: Ucore Rare Metals* (Tetra Tech, 2013), p. 244
29. Northern Minerals, *DFS Positions Browns Range Project as Next Dysprosium Supplier* (Northern Minerals Ltd, 2015), p. 71
30. G.S. Eupene, N.M. O’Brien, *Charley Creek Rare Earth Project Scoping Study Results: Crossland Uranium Mines Ltd* (MSP Engineering Pty Ltd, 2013), p. 54
31. J.J. Cox, T. Ciuculescu, K. Altman, L. Hwozdyk, *Technical Report on the Eco Ridge Mine Project, Elliot Lake, Ontario, Canada: Pele Mountain Resources Inc.* (Roscoe Postle Associates Inc., 2012), p. 259
32. K. Masun, I.C. Weir, J.R. Goode, *Technical Report on the Foxtrot Project, Newfoundland and Labrador, Canada* (Roscoe Postle Associates Inc., 2016), p. 219
33. I. Fairhall, I. Jackson, C. Bailey, *Preliminary Economic Assessment-Executive Summary on Glenover Rare Earth Project PEA to Glenover Phosphate (PTY) Ltd* (GBM Minerals Engineering Consultants, 2012), p. 22
34. G. Saucier, C. Noreau, P. Casgrain, P. Cote, E. Larochelle, M. Bilodeau, A. Hayden, E. Poirier, M. Garon, V. Bertrand, M. Kissiova, M. Mailloux, M. Rougier, Y. Camus, G. Gagnon, *Feasibility Study for the Kipawa Project Temiscamingue Area, Québec, Canada: Matamec Explorations, Inc.* (Roche Ltd, EHA Engineering Genivar, Golder Associates SGS Canada Inc., 2013), p. 768
35. Peak Resources Ltd, *Bankable Feasibility Study Executive Summary Ngualla Rare Earth Project* (Peak Resources Ltd, 2017), p. 59
36. Arafura Resources Ltd, *Nolans Project Definitive Feasibility Study Summary Report* (Arafura Resources Ltd, 2019), p. 157
37. T. Davidson, J. Thompson, *Amended and Restated Prefeasibility Study – NI 43-101 – Technical Report for the Norra Kärr Rare Earth Element Deposit: Tasman Metals Ltd* (GBM Minerals Engineering Consultants Ltd, 2015), p. 378

38. J.C. Witley, S. Swinden, G. Trusler, N. Dempers, *Songwe Hill Rare Earth Element (REE) Project Phalombe District, Republic of Malawi: Mkango Resources Ltd* (MSA Group Ltd, 2019), p. 199
39. A.N. Clay, R. Machowski, G.L. Marra, F. Harper, I. Jones, V. Duke, A.J. de Klerk, *National Instrument 43-101 Independent Technical Report on the Results of a Feasibility Study for the Steenkampskraal Rare Earth Element Project in the Western Cape, South Africa for Great Western Minerals Group Ltd* (Venmyn Deloitte, 2014), p. 264
40. Hastings Technology Metals Ltd, *Yangibana Project Definitive Feasibility Study Executive Summary* (Hastings Technology Metals Ltd, 2017), p. 66
41. F. Harper, G. Wild, P. Siegfried, J. Brown, M. Hall, G. Njowa, J. Vivier, R. Zietsman, V. Duke, *National Instrument 43-101 Independent Technical Report on the Results of a Preliminary Feasibility Study on the Zandkopsdrift Rare Earth Element and Manganese By-Product Project in the Northern Cape Province of South Africa for Frontier Rare Earths Limit* (Venmyn Deloitte, 2015), p. 245
42. E. Puritch, R. Eccles, M. Dufresne, S. Nicholls, K. Kuchling, G. Watts, K. Rogers, B. Cron, *Preliminary Economic Assessment for the Buckton Deposit SBH Property, North-East Alberta: DNI Metals Inc.* (P&E Mining Consultants Inc., 2014), p. 237
43. J.J. Cox, K.M. Masun, T. Fayram, *Technical Report on the Aksu Diamas Rare Earth Element and Minor Metals, Isparta District, Southwest Turkey NI-43-101 Report* (Roscoe Postle Associates Inc., 2013)
44. Hastings Technology Metals Ltd, *Brockman JORC Resource* (Hastings Technology Metals Ltd, 2015)
45. P. Daigle, *Technical Report on the Clay-Howells Fe-REE Project, Ontario, Canada: Rare Earth Metals Inc.* (Tetra Tech Wardrop, 2011), p. 145
46. RareX Ltd, *Cummins Range Rare Earths Project* (RareX Ltd, 2019)
47. A. Workman, K. Breede, J. Goode, *Update Report on the Appia Energy Corp. Uranium-Rare Earth Property, Elliot Lake District, North-Central Ontario, Canada* (Watts, Griffiss and McOuat Ltd, 2013), p. 394
48. B. Dunn, *Update to Resource Estimate on the Hoidas Lake Property, Saskatchewan Canada: Star Minerals Group Ltd* (Barr Engineering Co., 2014), p. 121
49. Lindian Resources Ltd, *December Quarterly Activity Report* (Lindian Resources Ltd, 2019), p. 4
50. V. Danilov, O. Rozjivin, *Technical Report on the Kutessay II Rare Earth Property, Kemin District, Kyrgyzstan, with Rare Earth Resource Estimate: Kutisay Mining OJSC* (Kazakhstan Mineral Co., 2011), p. 151
51. Greenland Minerals and Energy Ltd, *Presentation on Kvanefeld Development Strategy for European Investor Updates* (Greenland Minerals and Energy Ltd, 2014), p. 29
52. P. Daigle, *Technical Report and Resource Estimate of the Lavergne-Springer REE Project, Ontario, Canada: Rare Earth Metals Inc.* (Tetra Tech Wardrop, 2012), p. 174
53. GBM Resources Ltd, *Scoping Study Confirms Strong Commercial Opportunity at GBM's Milo IOCG-REE Project* (GBM Resources Ltd, 2012), p. 24
54. E. Belzile, R. Marchand, A. Bouajila, *NI 43-101 Technical Report Montviel Rare Earth Project Québec, Canada: GéoMégA Resources Inc.* (Belzile Solutions Inc, 2015), p. 186
55. B. Pollard, D. Mapleson, *NI 43-101 Technical Report for the Mrima Hill Niobium and Rare Earth Project Kwale District, Kenya: Pacific Wildcat Resources Corp* (BMGS Perth, 2013), p. 179
56. G.C. Reed, *Amended and Restated Technical Report for Olserum REE Deposit, Southern Sweden: Tasman Metals Ltd* (Reed Leyton Consulting, 2013), p. 85
57. *Mineração Serra Verde, Serra Verde*, 2018
58. G. Desharnais, Y. Camus, C. Bisailion, *Updated NI 43-101 Technical Report – Resources for the Tantalus Rare Earth Ionic Clay Project Northern Madagascar* (SGS Canada Inc, 2016), p. 165
59. P. Daigle, *Resource Estimate and Technical Report for the Two Tom REE Deposit of the Red Wine Complex Labrador, Canada: Rare Earth Metals Inc.* (Tetra Tech Wardrop, 2012), p. 163
60. T. Eggleston, E. Sides, *Wigu Hill Rare Earth Element Project, Eastern Tanzania NI 43-101 Technical Report: Montero Mining and Exploration Ltd* (AMEC Earth & Environmental UK Ltd, 2011), p. 169

61. C. Cox, J. Kynicky, The rapid evolution of speculative investment in the REE market before, during and after the rare earth crisis of 2010-2012. *Extr. Ind. Soc.* **5**(1), 8–17 (2018)
62. J. Gambogi, Mineral commodity summaries, rare earths. *US Geol. Surv.* **132**, 1–2 (2020)
63. A. Jordens, Y.P. Cheng, K.E. Waters, A review of the beneficiation of rare earth element bearing minerals. *Miner. Eng.* **41**, 97–114 (2013)
64. B.S. Van Gosen, P.L. Verplanck, R.R. Seal, K.R. Long, J. Gambobi, Rare-earth elements, in *Critical Mineral Resources of the United States: Economic and Environmental Geology and Prospects for Future Supply*, ed. by K.J. Schulz, J.H. DeYoung, R.R. Seal, D.C. Bradley, (US Geological Survey, Reston, 2018)
65. U.S. Nuclear Regulatory Commission, Application for NRC export or import license, amendment, renewal, or consent request. Southern Ionics Minerals, dated 2017.08.03 (2022). Retrieved 2022.07.07. Accessed <https://www.nrc.gov/docs/ML1721/ML17215A492.pdf>
66. Government of India, Department of Atomic Energy, *Lok Sabha Unstarred Question No. 300—Deposits of Rare Earths* (Government of India, Department of Atomic Energy, 2011)
67. V.V. Seredin, S. Dai, Coal deposits as potential alternative sources for lanthanides and yttrium. *Int. J. Coal Geol.* **94**, 67–93 (2012)
68. W. Zhang, M. Rezaee, A. Bhagavatula, Y. Li, J. Groppo, R.Q. Honaker, A review of the occurrence and promising recovery methods of rare earth elements from coal and coal by-products. *Int. J. Coal Prep. Util.* **35**(6), 281–294 (2015)
69. W. Zhang, A. Noble, X. Yang, R.Q. Honaker, A comprehensive review of rare earth elements recovery from coal-related materials. *Fortschr. Mineral.* **10**(5), 451 (2020)
70. A. Noble, G.H. Luttrell, Micro-pricing: the value of trace rare earth elements in coal and coal by-products, in *2016 SME Annual Conference and Expo: The Future for Mining in a Data-Driven World*, (Society for Mining, Metallurgy & Exploration, Englewood, 2016)
71. Asian Metal, AM rare earth oxide prices, FOB China (2015). Retrieved 2015.07.10. Accessed <http://www.asianmetal.com/price>
72. U.S. Department of Energy, NETL rare earth element database (2015). Retrieved 2015.11.05. Accessed <https://edx.netl.doe.gov/ree/>
73. S. Qin, C. Zhao, Y. Li, Y. Zhang, Review of coal as a promising source of lithium. *Int. J. Oil Gas Coal Technol.* **9**(2), 215–229 (2015)
74. W. Zhang, A. Noble, X. Yang, R.Q. Honaker, Lithium leaching recovery and mechanisms from density fractions of an Illinois Basin bituminous coal. *Fuel* **268**, 117319 (2020)
75. G.H. Luttrell, M.J. Kiser, R.H. Yoon, A. Noble, M. Rezaee, A. Bhagavatula, R.Q. Honaker, A field survey of rare earth element concentrations in process streams produced by coal preparation plants in the eastern USA. *Min. Metall. Explor.* **36**(5), 889–902 (2019)
76. C.R. Vass, A. Noble, P.F. Ziemkiewicz, The occurrence and concentration of rare earth elements in acid mine drainage and treatment by-products: Part 1 – Initial survey of the Northern Appalachian Coal Basin. *Min. Eng.* **71**(11), 49–50 (2019)
77. C.R. Vass, A. Noble, P.F. Ziemkiewicz, The occurrence and concentration of rare earth elements in acid mine drainage and treatment by-products. Part 2: Regional survey of Northern and Central Appalachian Coal Basins. *Min. Metall. Explor.* **36**(5), 917–929 (2019)
78. B.W. Stewart, R.C. Capo, B.C. Hedin, R.S. Hedin, Rare earth element resources in coal mine drainage and treatment precipitates in the Appalachian Basin, USA. *Int. J. Coal Geol.* **169**, 28–39 (2017)
79. P. Ziemkiewicz, A. Noble, C. Vass, Systems and processes for recovery of high-grade rare earth concentrate from acid mine drainage. U.S. Patent No. 10,954,582, 23 Mar 2021
80. J. Milinovic, F.J.L. Rodrigues, F.J.A.S. Barriga, B.J. Murton, Ocean-floor sediments as a resource of rare earth elements: an overview of recently studied sites. *Fortschr. Mineral.* **11**(2), 142 (2021)
81. Y. Takaya, K. Yasukawa, T. Kawasaki, K. Fujinaga, J. Ohta, Y. Usui, K. Nakamura, J.I. Kimura, Q. Chang, M. Hamada, G. Dodbiba, T. Nozaki, K. Iijima, T. Morisawa, T. Kuwahara, Y. Ishida, T. Ichimura, M. Kitazume, T. Fujita, Y. Kato, The tremendous potential of deep-sea mud as a source of rare earth elements. *Sci. Rep.* **8**(1), 1–8 (2018)

# Chapter 20

## Rare Earth Element Mining and Recovery: A Regulatory Overview



Larry Long

### 20.1 Introduction: Current Regulatory Environment

Rare earth elements, also called rare earth metals (REM), are elements that are critical materials used in the production of electronics, magnets, and computer chips, as well as in other applications. The U.S. environmental regulations for production of these materials and their applications are the focus of this section [1]. The U.S. Environmental Protection Agency (EPA) considers these materials to be critical due to their national and global strategic importance. Other nonenvironmental regulations, such as mine safety and state, local ordinances may also apply but will not be discussed in this section. All terms related to rare earths referred to herein (i.e., REE, REM, and CM) will be called critical rare earth metals (CREM).

Not all countries regulate the CREM recovery using the same level of legal authority. A brief overview follows illustrating how the regulatory structure influences potential impacts from the recovery of CREM globally. While the global perspective differs greatly from country to country, most regulatory programs have the same objectives and goals for the protection of human health and the environment. This section addresses some of the current CREM policy, and the consequences of that policy by discussing the environmental regulatory approach. Not all recovery or mining, recycling, and recovery operations will require the same level of regulatory oversight. It should be noted that regulatory requirements vary based on the type of discharge(s), and how it affects the environment, human health, country policy as well as, state, tribal and local laws, and ordinances, within the continental United States. Country-specific regulations are beyond the scope of this chapter.

In 2011, it was estimated that less than 1% of CREM was recycled [2]. This may be due in part to the vast number of products that contain CREM, the difficulty of

---

L. Long (✉)  
Environmental Protection Agency, Washington, DC, USA  
e-mail: [Long.larry@epa.gov](mailto:Long.larry@epa.gov)

recovering CREM from a variety of different products, the lack of incentives and regulatory oversight, and the lack of investment in recycling CREM. The main global perspective for obtaining CREM is from mining operations.

## 20.2 China

China's policy toward CREM is one of strategic dominance [3]. China's current approach to obtaining CREM is predominantly from mining. China is believed to be the world's largest producer of CREM. Some estimate that China provides as much as 90% of the world's supply of CREM and is home to some of the largest open pit mines in the world. The recovery of CREM in China is illustrated by its impacts [4] in association with the benefits [5]. Although China's policies have not been based on strong environment regulation, China is proposing new policy documents to gather public comments on future proposed regulations.

CREM mining processes in China provide a stark example for the need for environmental regulatory oversight. The Bayan Obo mine located in the inner Mongolia region of China is the world's largest, rare earth mine (Fig. 20.1). Figure 20.2 shows discharge waters from this mine loaded with chemicals in streams north of the town of Baotou in inner Mongolia which is 120 km south of the Bayan Obo mine.

Whereas past regulations focused on the technical aspects of mining such as the physical recovery of ore, separation and smelting, the new proposed regulations seek to manage the overall industrial process chain. The proposed regulation also provides a structure to impose penalties for violations of the regulation and has the potential to regulate exports as well [8]. China currently dominates the *green energy technology* due to their Made in China 2025 strategy [8]. It is unknown how or if the proposed new regulations will affect global supply chain markets.



Fig. 20.1 Rare earth mine at Bayan Obo [6]

**Fig. 20.2** Discharge waters from the Bayan Obo mine [7]



### 20.3 European Union Regulatory Overview

The European Union (EU) has one of the most extensive CREM programs in the world today. The European Commission (EC) realized their dependence on CREM imports presented both obstacles and opportunities. They therefore set out to develop a legislative framework in 2008 which provides for (1) single market standards, (2) entrepreneurship, (3) finance access, (4) industry and market sector analysis, and (5) research tools and databases [9]. This framework was created to provide the foundation for which legislation could be based. The EC was the first to provide an in-depth understanding of the circular economics of CREM which refers to the recycling and reuse of materials. The 2019 Circularity GAP Report [10] was subsequently prepared which states that only 9% of our world supply chain is circular and suggests that a greater opportunity may be had from the recycling of existing sources of CREM, rather than the creation of new mining operations.

### 20.4 Australia

Australia is a global leader in the mining technology of CREM. Although administered differently than the U.S. regulatory process, the goals and objectives of the Australian regulatory system seek to achieve a high level of environmental compliance. The Australian regulatory process is a system based on checks and balances, much like U.S. processes. Australia's Critical Minerals Strategy [11] promotes an open and innovative approach governed by separate authorities. It is focused mainly on mining with limited focus on recycling. Australia is estimated to be the second largest producers with and estimated to have the sixth largest concentration of CREM reserves in the world [12].

Western Australia is known to have significant deposits of precious metals, including CREM. CREM resources are known to exist in all states in the Northern



Territory except for Tasmania. The Northern Territory is estimated to contain one of the world's largest deposits of CREM. Other CREM deposits have been identified in New South Wales.

The Government of Western Australia's Department of Mines, Industry Regulations and Safety regulates mining activities in Western Australia under The Mining Act [13] which outlines the law for mining in Western Australia. The Government of South Australia's Department of Energy and Mining regulates mining in South Australia following the Mining Act of 1971 [14], Mines and Works Inspection Act of 1920 [15] and Opal Act of 1995 [16], and associated regulations. Together, mining regulations coupled with national and local environmental regulations provide the foundation for the Australian regulatory process. The Australian regulatory agencies websites provide in-depth information for new and existing CREM recovery operations [17].

## 20.5 United Nations Charter

The United Nations Environmental Assembly (UNEA) consists of several member nations around the world on all continents. The assembly is currently working with the International Resource Panel to create assessment reports for the financing of mineral production, sustainable production, equitable distribution, and the social benefits of CREM throughout the global commons. The global commons describe international, supranational, and global resource domains where common sources of CREM resources are found. This includes the earth's shared natural resources such as the air, ocean, and minerals as well as imports of commerce such as electronics and transportation routes required for CREM imports. A key challenge of the global commons is the design of governance structures and management systems capable of addressing the complexity of multiple governmental and corporate interests, often subject to unpredictable changes, ranging from the domestic to the international level. It should be noted that more developed countries export their technological mining expertise to less-developed countries where environmental regulations provide less environmental regulatory oversight.

As with global public goods, management of the global commons requires pluralistic legal entities – usually international and supranational, public, and private – structured to match the diversity of interests and the type of resource to be managed, and sufficiently stringent guidelines with adequate incentives to ensure compliance. Without such management systems, common resources are often overexploited.

To ensure that the governances passed by the United Nations (UN) fulfill their stated obligations, the UN includes enforcement mechanisms. The enforcement mechanism will generally fall into four categories: (1) charter-based, (2) convention or treaty-based, (3) oversight by a UN specialized agency such as the World Health Organization, and (4) rapporteurs appointed by the General Assembly. The United Nations Environmental Assembly (UNEA) has created working groups to assess the international economic and environmental impact associated with CREM within

member nations and the world's oceans. For over 70 years, the UN is the only international forum where nations can meet to discuss security issues and to resolve problems. When nations become members, they agree to accept UN charters. One such charter is the United Nations Convention on the Law of the Sea (UNCLOS) which covers many issues with a focus on deep sea mining of rare earth minerals.

The recovery of CREM from deep sea can provide certain obstacles such as structural features. The structural features of the oceans are divided into the near-shore, continental shelf, continental slope and rise, basin (or abyssal plain), and mid-oceanic ridges (National Oceanic and Atmospheric Administration (NOAA) Ocean Floor Features) [18]. The shore region is that portion of the land mass that extends beneath coastline and has been modified by oceanic processes. Providing some of the richest fisheries known, the continental shelf extends seaward from the near-shore and is characterized by a gentle slope of about 1:500 m. At the seaward extent of the shelf, the steepness of the slope first increases to about 1:20 m (the continental slope), and then flattens (the continental rise). The ocean basin constitutes about 75% of the ocean bottom, ranging in depth from about 9840 feet to 19,700 feet (3000–6000 m). The deepest areas of the ocean basins are the deep-sea trenches, contrasted by the mid-oceanic ridges, which provide relatively high points on the ocean bottom [19].

The existence of mineral deposits in the abyssal plains in some of the deepest parts of the ocean has been known since the 1860s [20]. Because these mineral deposits are found in great depths, at great pressure they form into crust and nodules. Fe-Mn crusts and nodules are potential CREM sources, along with phosphorites which concentrated CREM (i.e., heavy rare earths and yttrium (Y)) during early diagenetic formation [21]. These deposits are of sufficiently high grade to be of economic interest [21]. Mining of the ocean is governed by the 1982 UNCLOS [22] which includes 168 ratified member parties and governs 60% of the world's seabed that lie beyond national jurisdiction (i.e., over 50% of the entire seabed). UNCLOS's primary function is to regulate exploration and exploitation of deep seabed minerals, where the seabed and subsoil are defined as the area beyond the limits of national jurisdiction, or beyond the outer limits of the continental shelf. UNCLOS has established three international institutions: (1) the Commission on the Limits of the Continental Shelf, (2) the International Tribunal for the Law of the Sea, (3) and the International Seabed Authority (ISA). The ISA was established to regulate member states for the exploration and exploitation of mineral resources with a key principle to protect the marine environment from harmful effects [23]. Currently, the United States is not a member of UNCLOS.

## 20.6 U.S. Regulatory Overview

Natural resources obtained from the earth are used to produce raw materials to produce goods. Humans cannot create natural resources, rather they use and modify existing resources for beneficial use. In the United States, regulatory review and

permitting is broken down into federal, state, tribal and local regulations, and ordinances. Environmental Regulatory Permitting (ERP) is dependent on the ore/source material, the recovery processes, chemical storage, and the types of potential discharges to the natural environment. The objective of environmental regulations is the protection of human health and the environment. To achieve this objective, the permitting agency will follow a systematic process of evaluating the potential discharges from a facility or mining operation and the cumulative impacts from those discharges on the affected environments.

### ***20.6.1 Presidential Executive Order***

U.S. Presidential Executive Order (EO) 13,817 – *A Federal Strategy to Ensure Secure and Reliable Supplies of Critical Minerals* [24] – directed the Secretary of the Interior to identify which minerals are critical to the national defense an economy and declare that it is the policy of the Federal Government to reduce the Nation’s vulnerability to disruptions in the supply of CM. Critical minerals in EO 13817 were (1) identified to be a nonfuel mineral or mineral material essential to the economy and national security of the United States; (2) from a supply chain that is vulnerable to disruptions; and (3) that serves an essential function in the manufacturing of a product, the absence of which would have substantial consequences for the U.S. economy or national security.

### ***20.6.2 The Administrative Procedure Act***

The Administrative Procedure Act (APA) governs the process by which federal agencies develop and issue regulations (APA Act., 1946) [25]. It includes requirements for publishing notices of proposed and final rulemaking in the *Federal Register* and provides opportunities for the public to comment on notices of proposed rulemaking. The APA requires most rules to have a 30-day delayed effective date. The APA helps to provide a foundation of checks and balances for all federal agencies. In addition to setting forth rulemaking procedures, the APA addresses other agency actions such as issuance of policy statements, licenses, and permits. It also provides standards for judicial review if a person has been adversely affected or aggrieved by an agency action. The APA may not directly affect CREM mining and recovery actions but does so by regulating the rulemaking process.

### ***20.6.3 National Environmental Policy Act***

The National Environmental Policy Act (NEPA) was one of the first environmental laws written that established a broad framework for the protection of the environment. The purpose of NEPA documents is to provide an understanding of the

subject purpose and need by evaluating alternatives that address environmental impact to the surrounding environment.

The overall purpose of NEPA is to ensure that federal agencies evaluate the potential environmental impacts of their proposed actions and consider the consequences when determining whether to proceed with the action by evaluating project specific alternatives including the *No Action Alternative*. NEPA (NEPA Act, 1970) [25] requires development and consideration of a reasonable range of management alternatives. Alternatives must be (1) viable and reasonable; (2) meet the stated purpose and need for the plan; (3) provide a mix of resource protections, management use, and development; (4) be responsive to issues identified during scoping; (5) and meet established planning criteria, as well as federal laws, including state and tribal regulations. Each management alternative evaluated in the NEPA document needs to represent a reasonable approach in evaluating the selected CREM recovery methods and processes, and for managing resources and activities of facilities operations. NEPA authority may be delegated to other federal and state regulatory agencies, defined as the *Lead Agency* (LA). The LA has the discretion to select an alternative in its entirety or to combine aspects of the various alternatives presented in a draft NEPA document. It should be noted that NEPA documents are planning documents and that permits are issued in the NEPA evaluative process.

The life-cycle stages include but are not limited to (1) exploration or collection in the case of recycling; (2) development (i.e., planning, permitting, construction, and remediation); and (3) closure (i.e., monitoring both pre and post, and reclamation). The NEPA documents evaluate each of the stages and discuss alternatives that can be used by the permitting agency for the protection of human health and the environment. NEPA may be applied to CREM mining and recovery operations when there is a (1) federal permit, (2) federal land and money, and (3) controversy related to a project.

#### **20.6.4 Clean Water Act**

The Clean Water Act (CWA) establishes the basic structure for regulating discharges of pollutants into the waters of the United States (WOTUS) and regulating quality standards for surface waters (CWA 1972) [26]. The basis of the CWA was enacted in 1948 and was called the Federal Water Pollution Control Act. The Act was significantly reorganized and expanded in 1972. *Clean Water Act* became the Act's common name with amendments in 1972. Congress established the CWA with the goal of *restor[ing] and maintain[ing] the chemical, physical, and biological integrity of the Nation's waters* (CWA 1972) [27]. To achieve that objective, the CWA prohibits the discharge of pollutants from point sources into waters of the United States, unless consistent with the requirements of the act (CWA 1972, 1983) [27]. The CWA allows for the discharge of pollutants into waters of the United States under two permitting programs – Section 402 governs the discharge of pollutants

other than dredged or fill material (CWA, 1972, 33 U.S.C. §1251, 1983) [28] and Section 404 governs the discharge of dredged or fill material (CWA 1972, 33 U.S.C. §1311, 2006) [29]. Congress charged EPA with oversight authority of delegated state-authorized permit programs (CWA Section 404, 1972) [30] and provided EPA with other authorities in connection with Section 404 permits issued by the United States Army Corps of Engineers (USACE) (33 USC 1342, 2018) [30]. Pursuant to the CWA, the EPA implemented pollution control programs including establishing wastewater standards for industry. The EPA also developed national water quality criteria recommendations for pollutants in surface waters. The CWA made it unlawful to discharge any pollutant from a point source into navigable waters without a permit. EPA's National Pollutant Discharge Elimination System (NPDES) permit program regulates discharges. Point sources include discrete conveyances such as pipes or man-made ditches. Industrial, municipal, and other facilities must obtain permits if their discharges go directly to surface waters. EPA enforces federal clean water and safe drinking water laws, provides support for municipal wastewater treatment plants, and takes part in pollution prevention efforts aimed at protecting watersheds and sources of drinking water. The CWA could apply to CREM mining and recovery operation where there are potential discharges to WOTUS.

### **CWA Section 303 Water Quality Standards**

Section 303 of the CWA requires states and tribes to adopt water quality standards applicable to their intrastate and interstate waters (33 U.S.C.1344, 2006) [31]. Water quality standards (WQS) assist in maintaining the physical, chemical, and biological integrity of a waterbody by designating uses, setting criteria to protect those uses, and establishing provisions to protect water quality from degradation. Water quality standards established by states are subject to EPA review (33 USC 1313, 2000) [32]. The EPA may object to state-adopted water quality standards and may require changes to the state-adopted water quality standards and, if the state does not respond to EPA's objections, EPA may promulgate federal standards (40 CFR 131.5, 1972) [33].

WQS are the foundation of the water quality-based pollution control program mandated by the CWA. They define the goals for a water body by designating its highest attainable uses, setting criteria that reflect the current and evolving body of scientific information to protect those uses, and establishing provisions to protect water bodies from further degradation. WQS developed specifically for wetlands help ensure that the provisions of the CWA are consistently applied to wetlands. WQS for wetlands are developed by states, territories, and authorized tribes in accordance with EPA's regulations (33 USC 1313(C)(3), 1981) [34].

## CWA Section 401 Water Quality Certification

State water quality standards are incorporated into all federal CWA permits through Section 401, which requires each applicant to submit a certification from the affected state that the discharge will be consistent with state water quality requirements (40 CFR Part 131, 2021) [35]. Thus, Section 401 provides states and tribes with veto authority over federal CWA permits that may allow exceedances of state water quality standards and empowers states to impose and enforce water quality standards that are more stringent than those required by federal law (33 USC 1341(a)(1), 2018) [36].

## CWA Section 402 Permits

Section 402 of the CWA (33USC 1370, 1972) [37] governs discharges of pollutants other than dredged or fill material. Permits issued under the authority of Section 402 are known as NPDES permits, and typically contain numerical limits called *effluent limitations* that restrict the amounts of specified pollutants that may be discharged. NPDES permits must contain technology-based effluent limits, and any more stringent water quality-based effluent limits necessary to meet applicable state water quality standards (33 USC 1342, 2018) [38]. Water quality-based effluent limitations are required for all pollutants that the permitting authority determines *are or may be discharged at a level [that] will cause, have the reasonable potential to cause, or contribute an excursion above any [applicable] water quality standard, including State narrative criteria for water quality* (33 USC 1311(b)(1)(a) &(c), 2018) [39]. The procedure for determining the need for water quality-based effluent limits is called a *reasonable potential analysis*.

## CWA Section 404 Wetlands

The USACE is the permitting agency for Section 404 permits (40 CFR 122.44, 2000) [40], with state regulatory agencies providing Section 401 Water Quality Standards (WQS) permits. The USACE 404 permits are required for any work within the WOTUS in cooperation the U.S. EPA. The USACE 404 permitting process balances the reasonably foreseeable benefits and determinants of proposed projects. The USACE evaluates applications under a public interest review, as well as the environmental criteria set forth in the CWA Section 404 guidelines (40 CFR 122.44(d)(1)(i), 2022) [41], regulation promulgated by the U.S. EPA. The Section 404 CWA regulates the discharge of dredged or fill materials into WOTUS. The basic premise of the program is that no discharge of dredged or fill materials may be permitted if (1) a practicable alternative exists that is less damaging to the aquatic environment, and (2) steps have been taken to avoid impacts to wetlands, streams, and other aquatic resources; those potential impacts have been minimized; and that

compensation will be provided for all remaining unavoidable impacts. Some states have assumed permitting authority and regulate the 404 programs in their state. Applicants should check with their state and federal regulatory authority for application for the discharge of dredged and fill materials.

Wetlands (CWA Section 404, 2022) [42] are areas where water covers the soil or is present either at or near the surface of the soil all year or for varying periods of time during the year, including during the growing season. Water saturation largely determines how the soil develops and the types of plant and animal communities living in and on the soil. Wetlands may support both aquatic and terrestrial species. The prolonged presence of water creates conditions that favor the growth of specially adapted plants (hydrophytes) and promotes the development of characteristic wetland (hydric) soils. Wetlands vary widely because of regional and local differences in soils, topography, climate, hydrology, water chemistry, vegetation, and other factors, including human disturbance. Indeed, wetlands are found from the tundra to the tropics and on every continent except Antarctica. Two general categories of wetlands are recognized. These are coastal or tidal wetlands and inland or nontidal wetlands.

WQS are the foundation of the water quality-based pollution control program mandated by the CWA. They define the goals for a water body by designating its highest attainable uses, setting criteria that reflect the current and evolving body of scientific information to protect those uses, and establishing provisions to protect water bodies from further degradation. WQS developed specifically for wetlands help ensure that the provisions of the CWA are consistently applied to wetlands. WQS for wetlands are developed by states, territories, and authorized tribes in accordance with EPA's regulations (CWA Part 230, 2008) [43].

### **20.6.5 Clean Air Act**

The Air Pollution Prevention and Control or Clean Air Act (CAA) is an oversight/preventative type regulation (CAA 101 (c)) [44]. The CAA is the comprehensive federal law that regulates air emissions from stationary and mobile sources. Among other things, this law authorizes the U.S. EPA to establish National Ambient Air Quality Standards (NAAQS) to protect public health and public welfare and to regulate emissions of hazardous air pollutants. The CAA could apply to CREM mining and recovery operations based on the type of air emission from the chemical, physical processing and storage of chemicals and reagents at the facility. The Chemical Safety Information, Site Security and Fuels Regulatory Relief Act establishes amended provisions for reporting and disseminating information under Section 112(r) of the CAA. The law has two distinct parts that pertain to (1) flammable fuels and (2) public access to Off-Site Consequence Analysis data (CAA amend, 2000) [45].

### **20.6.6 Resource Conservation Recovery Act**

The Resource Conservation Recovery Act (RCRA) (42 U.S.C. 6901, 1976) [46] is the primary federal law used to regulate hazardous and solid waste. RCRA provides the authority to control hazardous waste from cradle to grave, including the generation, transportation, storage, and disposal. States that have federally delegated programs provide state regulatory agencies the authority and responsibility for oversight and enforcement of this program. The U.S. EPA has state oversight responsibility for this program. RCRA will apply in the recovery of CREM facilities where hazardous chemical and solid waste are present.

#### **Brownfields**

The Brownfield Utilization, Investment and Local Development (BUILD) Act [47] within RCRA is an incentive program that promotes the cleanup of contaminated sites. The Brownfield program has the potential to provide incentives for the public and communities sector to clean up sites that have demonstrated the existence of CREM in economically viable qualities.

### **20.6.7 CERCLA/Superfund**

The Comprehensive Environmental Response, Compensation, and Liability Act (CERCLA) (CERCLA, 1980) [48] or Superfund provides a federal trust fund to finance the cleanup of uncontrolled or abandoned hazardous-waste sites and to respond to accidents, spills, and other emergency releases of pollutants and contaminants into the environment. CERCLA established requirements for addressing closed and abandoned hazardous waste sites, funding to cover the cost of cleanup when no responsible party can be identified and creates liabilities for those that are responsible for releases. CERCLA also provided guidelines from the National Contingency Plan (NCP, 1982) [49] to establish the National Priorities List (NPL, 2022) [50] which is a list of sites eligible for investigation and remediation under the long-term cleanup program.

The Superfund program ensures long-term protection when conducting hazardous waste removal and enforcement actions. Both the Superfund and Brownfield programs have significant community outreach programs that may have potential to be used in the recovery of CREM from contaminated sites. Superfund Amendments and Reauthorization Act (SARA) (SARA, 1986) [51], the Emergency Planning & Community Right-to-Know Act (EPCRA), was enacted by Congress as the national legislation on community safety. This law is designed to help local communities protect public health, safety, and the environment from chemical hazards.



### **Emergency Planning and Community Right-To-Know Hazardous Chemical Inventory Reporting Requirements Section 311, 312, 313**

To implement EPCRA (Part 370, 2008) [52], Congress requires each state to appoint a State Emergency Response Commission (SERC). The SERCs are required to divide their states into Emergency Planning Districts and to name a Local Emergency Planning Committee (LEPC) for each district. EPCRA was created to help communities plan for chemical emergencies (Title III, 2018) [53], provides important protections and information to communities near facilities with potentially significant environmental releases. Under Section 311, EPCRA facilities must submit material data safety sheets for hazardous chemicals present on site. Under Section 312, facilities need to submit an annual inventory for their 311 chemicals by March 1 of each year to the state regulatory agencies and local fire department. EPCRA Section 313 expands the 311 and 312 reporting requirements to mining operations. Facilities are required to report the recovery and beneficiation of ore, as *processing* on the grounds that the Toxics Release Inventory (TRI) chemicals contained in the ores had been manufactured prior to their recovery and beneficiation.

#### **20.6.8 Atomic Energy Act**

The Atomic Energy Act (AEA) (AEA, 1954) [54] established the Atomic Energy Commission (AEC) to promote the *utilization of atomic energy for peaceful purposes to the maximum extent consistent with the common defense and security and with the health and safety of the public*. Since the abolition of the AEC, much of the AEA has been carried out by the Nuclear Regulatory Commission (NRC) (NRC, 2020) [55] and the U.S Department of Energy (DOE, 2022) [56]. When EPA was formed, however, the AEC's authority to issue generally applicable environmental radiation standards was transferred to EPA. Other federal and state organizations must follow these standards when developing requirements for their areas of radiation protection. The requirements of the AEA (and associated regulations) could apply where there are potential releases of radiation to the environment.

Rare earth elements, numbered 57–71 in the Periodic Table are called the lanthanide elements [57]. Lanthanides and Y that are primarily recovered from ores contain low concentrations of uranium (U) and thorium (Th); however, some level of radioactive material can be found in association with many REE [58]. Waste rock and sludges that result from the recovery process for REE are technologically enhanced naturally occurring radioactive materials (TENORM) [59]. The EPA estimates naturally occurring radioactive material (e.g., monazite, xenotime, and bastnäsité) range from 5.7 to 3224 picocuries per gram (pCi/g) [60]. The USGS has also estimated the U and Th content of REE [61]. These elements are not rare but were thought to be rare at the time of their discovery. Due to REEs' or CREMs' high

affinity for heavy metals with which they tend to co-occur, it is difficult to discern the effects of individual lanthanides, both in human cases and animal studies. In addition, the co-occurrence of the lanthanides, Th isotopes, and silica dust has complicated the interpretation of toxicity especially about human occupational exposures [62]. REE are conventionally processed primarily from ores and minerals that naturally contain U and Th. Processing rare earth minerals involves the separation and removal of U and Th which results in technologically enhanced naturally occurring radioactive material (TENORM) wastes. Tighter regulation on the use of radioactive minerals has been identified as the primary factor that pressured many sources of monazite out of the REE market during the 1980s (CCR Regs., 2022) [63].

Coal by-products such as coal combustion residuals (CCR) and boiler slags consist of course, hard, black, angular, glassy material formed when bottom ash melts during combustion (CCR Guidance, 2022) [64]. Literature does indicate the potential for marketable volumes of CREM in coal by-products which may contain regulated levels of radioactive material [65].

REE recovery methods accumulate waste materials to varying degrees. Some of these wastes from conventional feedstock resources may be hazardous and/or radioactive [66]. Handling these wastes has the potential to increase the overall operational cost of CREM recovery from the selected waste stream (SWS). Depending on the source material, recovery process and associated discharges, federal and state regulations for the handling, processing and transportation could apply. The Occupational Safety and Health Administration (OSHA) regulations (OSHA 1977) [67] may also apply and should be consulted prior to the operation of any new or existing CREM recovery operation.

## 20.7 Other Federal Environmental Regulations

The regulatory review section is an overview of the more common federal regulations. State and tribal regulatory agencies may have their own stricter regulations. All state, tribal, and local environmental regulatory agencies should be consulted prior to the operation of any new or existing CREM recovery operations.

### 20.7.1 *National Marine Sanctuaries Act*

The National Marine Sanctuaries Act (NMSA) in 2020 [68] authorizes the Secretary of Commerce to designate and protect areas of the marine environment with special national or international significance due to their conservation, recreational, ecological, historical, scientific, cultural, archeological, educational, or aesthetic qualities as national marine sanctuaries [69].

### **20.7.2 *Marine Mammal Protection Act***

The Marine Mammal Protection Act (MMPA) [70] was enacted in 1972 to protect marine mammals and ensure that population stocks and essential habitats of marine mammals are maintained at, or restored to, healthy population levels. Jurisdiction over marine mammals under the MMPA is shared between U.S. Fish and Wildlife Service (USFWS) and NOAA National Marine Fisheries Service (NOAA Fisheries). USFWS has jurisdiction over sea and marine otters, polar bears, manatees, dugongs, and walruses, while NOAA Fisheries has jurisdiction over all other marine mammals (i.e., all cetaceans and pinnipeds, except walruses).

### **20.7.3 *Farmland Protection Act***

The Farmland Protection Policy Act (FPPA) (USDA, 1981) [70] provides for preservation of prime farmland, which is defined as having the availability and best combination of physical and chemical characteristics for producing food, feed, forage, fiber, and oilseed crops. The optimal soil quality, growing season, and moisture supply of prime farmland can produce economically sustained high yields of crops when treated and managed according to acceptable farming methods, including water management. Some soils within a CREM recovery facility planning area could be identified as prime farmland. FPPA requires identification of proposed actions that may affect lands classified as prime farmlands. This is a potential issue on split-estate agricultural lands overlying federal mineral ownership. The U.S. Department of Agriculture (USDA) classifies acreage as prime farmland on a statewide basis. The management plan for CREM recovery should evaluate facilities within or near farmland.

### **20.7.4 *Migratory Bird Treaty Act***

The Migratory Bird Treaty Act (MBTA) (FWS, 1918) [71] implements a series of treaties the United States has entered with Canada, Mexico, Japan, and Russia for the conservation of migratory birds. The USFWS has statutory authority and responsibility of enforcing the MBTA.

### **20.7.5 *Endangered Species Act***

The Endangered Species Act (ESA) [72] provides a program for the conservation of threatened and endangered plants and animals and the habitats in which they are found. The lead federal agency for implementing ESA is the USFWS. The ESA of

1973 (FWS, 1973) [72] establishes policy to protect, and conserve threatened and endangered species and the habitats in which they are found and on which they depend. The ESA is administered by the USFWS and the NOAA Fisheries. Section 7 of the ESA requires federal agencies to consult with USFWS, NOAA Fisheries, and the appropriate state agencies to determine if a proposed action might affect listed or candidate species or designated critical habitat.

### ***20.7.6 Surface Mining Control and Reclamation Act of 1977***

The Surface Mining Control and Reclamation Act (SMCRA) establishes the Office of Surface Mining Reclamation and Enforcement (OSMRE) within the Department of the Interior (DOI). The Surface Mining Control and Reclamation Act (DOI, 1977) [73] was the first federal environmental statute to regulate a specific industry, which in this case is coal mining. SMCRA created two major programs: (1) an abandoned mine land (AML) reclamation program, to reclaim land and water resources adversely affected by coal mines abandoned before August 3, 1977 and (2) a regulatory program to ensure that surface coal mining operations are conducted and reclaimed in an environmentally sound manner. SMCRA relies on other environmental authority such as the CWA in support of the agency's reclamation process. For this reason, reclamation of a coal facility has the potential to trigger other environmental regulations. OSMRE must comply with NEPA whenever the bureau proposes to take an action, or authorizes any other entity to take an action, that could possibly affect environmental resources.

### ***20.7.7 The Marine Protection Research and Sanctuaries Act***

The Marine Protection, Research and Sanctuaries Act (MPRSA) (EPA, 1972) [74] prohibits the dumping of material into the ocean. Titles I and II of MPRSA, also referred to as the Ocean Dumping Act, generally prohibits (1) transportation of material from the United States for the purpose of ocean dumping, (2) transportation of material from anywhere for the purpose of ocean dumping by U.S. agencies or U.S.-flagged vessels, and (3) dumping of material transported from outside the United States into the U.S. territorial sea. A permit is required to deviate from these prohibitions. Under MPRSA, the standard for permit issuance is whether the dumping will *unreasonably degrade or endanger* human health, welfare, or the marine environment.

## 20.8 State Regulatory Environmental Overview

Federal environmental regulation forms the basis for many states' regulatory programs through the process of delegation of certain environmental acts. State regulatory programs have the option to use the federal regulations as minimum standards and can make their regulations stricter but cannot make their regulations less strict than the federal regulations. Many states have adopted environmental regulations that parallel federal programs where there are no current federal regulations. An example would be for mining and dams where the state has dedicated mining and dam inspector programs. It is always advisable for applicants to check with the state environmental authorities prior to conducting any CREM mining or recovery operations.

## 20.9 Potential Regulatory Roadblocks

Environmental regulatory roadblocks occur when state and local regulations conflict with federal regulations. Where state and local regulations are founded on federal regulations but are stricter, they are not considered roadblocks. When there is a conflict between federal regulations and less strict state and local regulations or when state and local regulations provide a different remedy in conflict with federal law, these types of regulations can be considered a roadblock. Regulatory roadblocks confuse the process for the applicant. They may also present duplications for the applicant to apply for a permit. Where facilities cross state lines, and these states have different levels of compliance, this circumstance can also be a roadblock for prospective CREM recovery facilities.

## 20.10 Conclusions

The purpose of this overview is to serve as an information resource guide for current regulations which may apply to the vast number of chemical, physical, and biological recovery processes for CM and REE. The vast majority of information is current, but it should be noted that the recovery of CM and REE is dynamic. New sources and recovery process are being introduced at a very rapid pace. Therefore, these new recovery processes will need to be evaluated on a case-by-case basis. The recovery of CM and REE processes have the potential to create several environmental risks to human health and the environment. The current economic conditions along with Presidential Executive Orders have heightened the importance for the need for a sustainable domestic supply of CREM (EOs, 2017) [75]. The increase in demand will greatly increase the need for environmental and human health oversight.

Applicable regulations for CREM recovery operations are dependent upon their location, type of source material, processing chemicals, type of discharges to the environment, local and state regulations and ordinances, exposure to human health and the environment, and transportation of the final product. All these issues should be considered for new, and existing, critical minerals recovery operations. All federal, state, and tribal regulatory agencies should also be consulted as to those entities' regulations, codes, and requirements. This section may not be all inclusive of state, tribal, and local governances. It is recommended that any applications for the recovery of CREM consult their federal, state, and local environmental regulatory agencies.

## References

1. Federal Register/Vol. 86, No. 214/Tuesday, November 9, 2021/Notices, <https://www.regulations.gov/documents/DOI-2021-0013-002>
2. Marshall, J., *Why Rare Earth Recycling is Rare-And What We Can Do About It*, April 7, 2012., [Ensia.com/features/rare-earth-recycling/](https://www.ensia.com/features/rare-earth-recycling/)
3. China to Form Two Rare Earth Giants to Strengthen Pricing Power, Bloomberg News September 24, 2021, updated [www.bloomberg.com/news/articles/2021-9-247](https://www.bloomberg.com/news/articles/2021-9-247)
4. China “Watch” Canada: Rare-Earth Mining in China Comes at a Heavy Cost for Local Villages, [www.theguardian.com/environment/2012/aug/07/china-rare-earth-village-pollution](https://www.theguardian.com/environment/2012/aug/07/china-rare-earth-village-pollution), [www.china-briefing.com/news/china-tighens-control-over-management-of-rare-earth](https://www.china-briefing.com/news/china-tighens-control-over-management-of-rare-earth)
5. Rare Element Security-Air Force Magazine, November 1, 2020, [www.airforcemag.com/article/rare-elements-of-security](https://www.airforcemag.com/article/rare-elements-of-security)
6. China “Watch” Canada: Rare-Earth Mining in China Comes at a Heavy Cost for Local Villages, [www.theguardian.com/environment/2012/aug/07/china-rare-earth-village-pollution](https://www.theguardian.com/environment/2012/aug/07/china-rare-earth-village-pollution)
7. China and The Rare Earth Supply Chain Policy Brief August 4, 2020, Institute For Energy Research.org, <https://intituteforenergyresearch.org/renewable/china-and-the-rare-earth-policy-brief/>
8. China and The Rare Earth Supply Chain Policy Brief February 23, 2021, Institute For Energy Research.org, <https://intituteforenergyresearch.org/renewable/china-and-the-rare-earth-policy-brief/>
9. International Market, Industry, Entrepreneurship and SMEs, European Commission, [https://ec.europa.eu/growth/sectors/raw-materials/areas-specific-interest/critical-raw-materials\\_en](https://ec.europa.eu/growth/sectors/raw-materials/areas-specific-interest/critical-raw-materials_en)
10. The Circularity Gap Report, 2019., <https://legacy.circularity-gap.world/2019>
11. Australian Government Department of Industry, Science, Energy and Resources, Regulations and Standards, <https://www.industry.gov.au>
12. Australian Government, Geoscience Australia Applying Geoscience to Australia’s Most Important Challenges, <https://www.ga.gov.au/scientific-topics/mineralsresources-reviews/rare>
13. Government of Western Australia Department of Mines, Industry Regulation and Safety, Legislation and Compliance, <https://www.dmp.wa.gov.au/Minerals/Legislation-Compliance-1531.aspx>
14. South Australia Mining Act of 1971, Version: 25.2.2021, <https://www.legislation.sa.gov.au/legislation/lz/c/a/mining%201971/current/1971.109.auth.pdf>
15. South Australia Mines and Works Inspection Act of 1920, Historical Version: 4.10.2018 to 30.9.2019, <https://www.legislation.sa.gov.au>
16. South Australia Opal Act of 1995, Version:1.1.2021, <https://legislation.sa.gov>
17. Australia Minerals Legislation, regulations, and guidelines, <https://australianminerals.gov.au/legislation-regulations-and-guidelines>

18. Deep-Sea Mining Interest and Activities in the Western Pacific, <https://oceanexplorer.noaa.gov.gov>
19. The International Seabed Authority and Deep-Sea Mining, May 2017, Nos.1 & 2 Volume LIV, Our Ocean, Our World. Un Chronicle, <https://www.un.org/en/chronicle/article/international-seabed-authority-and-deep-seabed-mining>
20. Hein et al., 2016, Fuimoto et al., 2016
21. J. Hein, A. Koschinsky, M. Mikesell, K. Mizell, R. Glenn, Marine Phosphorites as potential resources for heavy rare earth elements and yttrium. *Fortschr. Mineral.* **6**, 88 (2016). <https://doi.org/10.3390/min6030088>
22. Convention on the Law of the Sea, Dec. 10, 1982, 1833 U.N.T.S.
23. International Seabed Authority, 1994., [www.unclosuk.org/international-seabed-authority-isa](http://www.unclosuk.org/international-seabed-authority-isa)
24. U.S. Presidential Executive Order (EO) 13817 – A Federal Strategy to Ensure Secure and Reliable Supplies of Critical Minerals, December 20, 2017 82FR 60835, <https://www.federal-register.gov/documents/2017/12/26/2017>
25. The Administrative Procedure Act Pub. L. 79-404, 60 Stat. 237, June 1946, 5U.S.C §§551-559, [https://www.law.cornell.edu.wex/administrative\\_procedure\\_act](https://www.law.cornell.edu.wex/administrative_procedure_act)
26. National Environmental Protection Act (NEPA) 40 CFR 1500-1508, <https://epa.gov/nepa/>
27. Clean Water Act 1972, 33U.S.C §§ 125-1387, Water of the United States (WOTUS) Title 40 Code of Federal Regulations 40 CFR 230.3
28. 33 USC § 1251(a)
29. 33 USC § 1311(a)
30. Section 404 of the Clean Water Act: Permitting Discharges of Dredge or Fill Materials, <https://epa.gov/cwa-404>
31. 33 USC §§ 1342(b)-(e); §§ 1344(g)(l), (n)
32. 33 USC §§ 1344(b)-(c), (q), (n))
33. 33 USC § 1313(a)(c)
34. 40 CFR § 131.5; 33 USC § 1313(c)
35. 33 USC §§ 1313(c)(3)-(4); 40 CFR §§ 131.5 and 131.21
36. 40 CFR Part 131
37. 33 USC § 1341(a)(1)
38. 33 USC § 1370
39. 33 USC § 1342
40. 33 USC §§ 1311(b)(1)(A) & (C) and 1342(a)
41. CWA Section 404, 2022, 40 CFR §§ 122.44(a)(1) and (d)(1)
42. CWA Part 230, 2008, 40 CFR § 122.44(d)(1)
43. USC Title 42 Chapter 85, 1990, CAA 101 (c)
44. CAA amend 74 U.S.C. 7412 (r)(4)(b) and 7412(r)(h)(7), 2000
45. 42 U.S.C. §6901 et seq (1976)
46. Pub.L.No.107-118,115 stat,2356, 2018 BUILD Act
47. 42 U.S.C. §9601 et seq. (1980)
48. Section 105 of CERCLA, 42 U.S.C 1905 codified at 40 C.F.R. Part 300, National Contingency Plan March 12, 1982., <https://archive.epa.gov/epa/aboutepa/national-contingency-plan-superfund-announcement.html>
49. National Priorities List Section 105(a)(8)(B) of CERCLA, 2022., <http://www.epa.gov/superfund/basic-npl-information>
50. SARA 42 U.S.C. §11001 et seq. (1986)
51. EPCRA 40CFR part 370, 2008
52. SARA Sections 311,312,313, 2018
53. Atomic Energy Act, 1954, 42 U.S.C. §2011 et seq. (1946)
54. Nuclear Regulatory Commission (NRC) [www.nrc.gov/about-nrc.html](http://www.nrc.gov/about-nrc.html)
55. U.S Department of Energy (DOE), 2022., [www.energy.gov](http://www.energy.gov)
56. Rare Earth Elements: A Review of Production, Processing, Recycling, and Associated Environmental Issue, EPA 600R-12/572, December 2012., [www.epa.gov/ord](http://www.epa.gov/ord)

57. EPA 600R-12/572, December 2012., [www.epa.gov/ord](http://www.epa.gov/ord)
58. Palmer et al., 1987; as cited by EPA, 2009b, 2009c, 2009d
59. Long, K.R., Bradley, S., et al., The Principal Rare Earth Element Deposits of the United States, A Summary of Domestic Deposits, and a Global Perspective. 2010
60. USGS scientific Investigation Report 2010-5220, Reston, Virginia. <http://pubs.usgs.gov/sir/2010/5220/>
61. 40 CFR Part 257, CCR guidance 2022., [www.epa.gov/coalash/coal-ash-basics](http://www.epa.gov/coalash/coal-ash-basics)
62. CCR Rule, [www.epa.gov/coalash/coal-ash-rule](http://www.epa.gov/coalash/coal-ash-rule)
63. CCR, [www.epa.gov/coalash](http://www.epa.gov/coalash)
64. EPA 2021., [www.epa.gov/radtown/radioactive-wastes-coal-fire-power-plants](http://www.epa.gov/radtown/radioactive-wastes-coal-fire-power-plants)
65. TENORM: Coal Combustion Residuals | US EPA, <https://epa.gov/radiation/tenorm-coal-combustion-residual>
66. Federal Mine Safety and Health Act 1977., [www.oshaeducationcenter.com/articles/msha/](http://www.oshaeducationcenter.com/articles/msha/) 29 CFR Parts 1910 – 2205
67. P.L. 106-513 2000, E.O. 13178 20000, 16 U.S.C. 1431
68. 16 U.S.C. 1361 et seq, <https://sanctuaries.noaa.gov/about/legislation/welcome.html>
69. P.L. 97-98 Title XV, Section 1539-1549, 1994, 16 U.S.C. 703 et seq
70. Fish and Wildlife, 16 U.S.C. 1531 et seq
71. Endangered species Act 1973. <https://fws.gov/law/migratory-bird-treaty-act-1918>, Public Law 95-87, 33 U.S.C. §1401 et seq. and Endangered Species Act 1973, 16 U.S.C. § 1431 et seq
72. Surface Control and Reclamation Act, 1977, P.L. 95-87
73. Marine Protection, Research, and sanctuaries Act 1972, 16 USC 1431et. seq. 33 USC 1401 et. seq (1988), <https://epa.gov/enforcement/marine-protection-research-and-sanctuaries-act%2D%2Dmprsa-and-federal-facilities>
74. EO-13817 – A Federal Strategy to Ensure Secure and Reliable Supplies of Critical Minerals. 2017 EO-13953 addressing the Threat to Domestic Supply Chain from Reliance on Critical Minerals (CM) from Foreign Adversaries and Supporting the Domestic Mining and Processing Industries. 2020, EO-14017 America’s Supply Chain, 2021, EO-14008 Tackling the Climate Crisis at Home and Abroad, 2021
75. <https://www.epa.gov/radiation/technologically-enhanced-naturally-occurring-radioactive-material-tenorm>



# Index

## A

Absorbents, 128  
Acid extraction, 191  
Acid mine drainage (AMD), 4, 13, 58, 59,  
71–81, 83–87, 458, 478–480  
Additive manufacturing (AM), 353, 354, 360  
Administrative Procedure Act (APA), 13, 490  
Al-Ce-Mg alloys, 347, 352  
Alkaline igneous deposits, 17  
Al-Sc alloys, 10, 359, 362, 363, 379, 381, 382  
Al-Si casting alloys, 351, 355  
Al-Si-Cu-Mg alloys, 343  
Aluminates, 395, 401, 404–405, 407, 410  
Aluminum chloride-based ILs, 218  
Anisotropic bonded magnets, 435  
Annual cash flow (ACF), 464  
Apatite deposit, 43, 46  
Aqueous two phase systems (ATPS), 196,  
202, 210–211  
Atomic Energy Act (AEA), 496–497

## B

Basic extraction, 151–152  
Basket price, 460, 461, 463–465, 469,  
470, 474–480  
Bastnasite, 4, 19, 22, 23, 27, 29, 33, 35, 37,  
38, 59, 75, 275, 278, 281, 449, 496  
Blue phosphors, 448  
Bonded magnets, 250, 301–303, 305, 314,  
315, 434–435, 440  
Brownfield Utilization, Investment and Local  
Development (BUILD) Act, 495

## C

Calcination, 432, 449, 452  
Calciothermic reduction, 260, 261  
CaO, MgO, Al<sub>2</sub>O<sub>3</sub> and SiO<sub>3</sub> (CMAS), 394,  
402, 405, 408–410  
Capital expenditure (CAPEX), 5, 149, 159,  
169, 172, 174–176  
Carbothermic reduction, 259–261  
Carboxylate Reduction Process (CRP), 6, 264,  
265, 267  
Castings, 10, 296, 298, 300, 301, 343–355,  
361, 373, 374, 376  
Catalysts, 6, 9, 13, 17, 18, 29, 30, 80, 215,  
278, 319–337  
Catalytic applications, 321  
Catalytic converters, 9, 18, 319, 329, 331–333  
Cation based ILs, 197  
Chelating agents, 143, 144, 146, 191  
Circular economy (CE), 82, 84, 86, 424,  
425, 439–441  
Clean air act (CAA), 494  
Clean water act (CWA), 84, 491–494, 499  
CMAS deposits, 394, 408  
Coal sourced rare earth elements, 123–146  
Collectors, 4, 103–120, 134, 212  
Colum separation, 172–174  
Comminution, 104, 107, 398  
Complexing agents, 25, 127, 145,  
184, 187–190  
Comprehensive Environmental Response,  
Compensation, and Liability Act  
(CERCLA), 495–496  
Contained ore deposit, 461

Continuous Counter Current Ion Exchange (CCIX), 180–184, 190  
 Continuous ion chromatography (CIC), 5, 179–191, 463  
 Continuous ion exchange (CIX), 5, 180–185, 190  
 Coordination chemistry, 336, 337  
 Corrosion, 7, 8, 10, 218, 245, 248, 257, 258, 300, 343, 348, 352, 355, 359, 360, 363, 365, 373, 374, 384  
 Cost and revenue projection, 463

**D**

D2EHPA, 202, 205–209, 449  
 Depressants, 4, 103–120

**E**

Economic projections, 457, 458  
 Electrical potential, 237  
 Electrochemical reduction, 154, 212, 261, 265  
 Electrolysis in ionic liquid medium, 212, 213  
 Electrometallurgy, 196, 212–218, 246, 247  
 Electrowinning, 4, 248–254, 261, 383, 384  
 Elevated temperature properties, 343, 353  
 Endangered Species Act (ESA), 498–499  
 End-of-life (EOL), 5, 11–12, 156, 163, 313, 423–441, 447, 453  
 Environmental barrier coatings (EBCs), 10, 11, 391, 393–395, 397–399, 401–407, 409–410  
 Environmental protection, 332–335  
 Environmental Protection Agency (EPA), 485, 492–496, 499  
 2-Ethylhexyl phosphonic acid mono-2-ethylhexyl ester (EHEHPA), 197, 202, 206–209  
 Eu and Y recycling, 449  
 European Commission (EC), 13, 198, 209, 215, 487  
 E-waste, 435, 436, 438, 440  
 Extrusions, 300, 301, 303, 352–354, 374, 376, 434

**F**

Farmland Protection Policy Act (FPPA), 498  
 FCC Process (Fray, Farthing and Chen), 253, 263–264  
 Flotation of REEs, 108  
 Flow sheets, 240–243, 450  
 Fluid anode molten salt electrolysis, 258, 264

Fluid catalytic cracking (FCC) process, 9, 320–328, 333, 337, 362  
 Fluorescent lights (FL), 11, 447–453  
 Fluorocarbons, 253, 254  
 Fly ash, 4, 13, 58, 59, 61–64, 67, 70, 82, 83, 85–87, 124, 382–383  
 Formability, 10, 359, 360, 363, 365, 384  
 Frothers, 4, 105, 106, 108, 110

**G**

Gadolinite, 3, 19, 22, 37, 45, 104, 140, 274, 275  
 Gibbs energy of formation, 238, 239  
 Global mineral landscape, 17–51  
 Grain refining, 344, 360–361  
 Green phosphors, 448

**H**

Hafnates, 399–402, 410  
 Halloysite, 20, 25, 43, 104, 123, 127–129, 142  
 Hard disk drives (HDDs), 283, 286, 288, 423–431, 434–437, 439, 441  
 Heavy mineral placer deposits, 39  
 Heavy REEs (HREEs), 2, 4, 11, 13, 19, 21, 22, 25–27, 29, 30, 32, 37, 38, 41, 43, 44, 48, 50, 51, 59, 60, 63, 76, 77, 80, 103, 104, 123, 124, 128, 129, 131, 132, 134, 135, 137, 138, 141, 144–146, 188, 191, 204–206, 284, 285, 378  
 High performance aluminum alloys, 343–355  
 H<sub>2</sub>SO<sub>4</sub> cracking, 132  
 Hydrogen decrepitation (HD) process, 302  
 Hydrogen decrepitation disproportionation and recombination (HDDR), 302, 434, 435  
 Hydro metallurgical operations, 4, 5  
 Hydrophobicity, 109

**I**

Imidazolium-based ILs, 196, 213  
 Industrial production of REEs, 150, 245  
 Ion adsorption clay (IAC), 4, 17, 19, 25, 27, 31, 32, 41–45, 50, 123–129, 131–135, 137–140, 143–146, 285, 378, 436  
 Ion chromatography, 5, 179–191  
 Ion exchange (IX), 29, 77, 123, 124, 126, 128, 129, 132–134, 138, 143, 144, 146, 179–184, 190, 191, 239, 278, 327, 333, 436  
 Ion-exchange leaching, 128, 146

Ionic liquids (ILs), 5, 62, 76, 153, 195–200, 202–218, 251, 265–266, 449

## K

Kaolinite, 20, 25–27, 29, 41, 43, 64, 67, 104, 123, 124, 126–129, 132, 142, 143

## L

Lanthanides (REEs), 1–3, 6, 20–26, 43, 59, 60, 62–64, 75, 77, 103, 106, 123, 124, 129, 134, 143, 149–151, 154, 156, 160, 163, 169, 182, 196, 210–213, 215–218, 259–266, 277, 278, 319, 359, 370, 396, 400, 477, 496, 497

Leaching, 4, 5, 29, 66, 123, 126, 129, 132, 133, 135, 138, 141–145, 167, 191, 239, 240, 432, 449, 451–453

Light REEs (LREEs), 2, 4, 10, 11, 19–22, 25–27, 29, 30, 33, 34, 37, 40, 41, 59–61, 63, 69, 76, 77, 103, 104, 129, 131, 136, 141, 164, 188, 191, 204, 258, 264, 285, 380

Loparite, 4, 22, 24, 25, 27, 32, 37, 104

## M

Magnet applications, 8, 167, 257, 304, 314, 315

Magnetic refrigeration, 288, 289

Magnetocaloric effect (MCE), 288

Magnets, 295, 329, 423

Marine Mammal Protection Act (MMPA), 498

Marine Protection, Research and Sanctuaries Act (MPRSA), 499

Mechanical agitation, 105

Medium REEs (MREEs), 2, 21, 22, 50, 60, 63, 76, 77, 103, 206

Metallothermic reduction, 6, 212, 236, 239–245, 248, 251, 253, 258–261, 264, 265, 267, 355

Metallurgy of Al-Sc system, 359–384

Methanol synthesis, 335–337

Migratory Bird Treaty Act (MBTA), 498

Mineral deposits, 2, 19, 29, 32, 47, 50, 51, 104, 458, 489

Minerology of REEs, 17–51

Mischmetal, 6, 9, 10, 245–247, 251, 258, 274–278

Mixer-settlers (MSs), 163, 169, 171–176, 180, 315

Molecular organic solvents, 198–200, 202, 219

Molten salt electrolysis (MSE), 4, 212, 213, 245–247, 251, 258, 259, 261–265, 267

Monazite, 4, 5, 12, 20, 22, 23, 25, 27, 32, 35, 37–40, 43, 44, 46, 47, 59, 63, 64, 66, 70, 76, 104, 108, 111–119, 123, 126, 132, 135, 137, 140, 144, 145, 212, 246, 275, 277, 278, 281, 283, 380, 405, 449, 458, 476–477, 479, 480, 496, 497

## N

National Marine Sanctuaries Act (NMSA), 497

NdFeB Permanent magnets, 423–441

Neochem process, 251–252

Neodymium iron boron (NdFeB), 8, 11, 12, 29, 196, 216, 217, 257, 258, 261, 264, 283–288, 296–303, 305, 308, 310, 312–314, 423–441

Net present value (NPV), 457, 463–466, 470–472, 480

Neutral extraction, 151–152

Neutral ligand based ILs, 217

Ni-based alloys, 392–394, 405

## O

Organic molecules (extractants, ligands), 151

## P

Payback period (PP), 463–466, 480

Perfluorocarbon emissions, 213

Permanent magnets, 6, 8, 18, 21, 29, 30, 156, 196, 254, 257, 274, 281–284, 286–288, 295–297, 304, 305, 309–312, 315, 319, 397, 423–425, 434

Petroleum refining, 9, 319

Phosphonium-based ILs, 209–211, 216, 218, 266

Phosphorite deposits, 48

Phosphors, 5, 6, 11–13, 17, 18, 29, 30, 149, 274, 278–281, 289, 319, 320, 334, 447–453

Phosphor thermochemistry, 278–281

Pressurized annular chromatography, 180

Protective ceramic coating, 391–395

Purity of REEs (99.9 or 3N; 99.99 or 4N), 149

Pyrrolidinium-based ILs, 213, 266

**R**

- Rare earth elements (REEs), 1, 17, 57, 123, 149, 179, 257, 273, 319, 344, 359, 423, 485
- Rare earth magnets, 282, 295–315, 330, 331, 430
- Rare earth markets, 273–290
- Rare earth metals (REMs), 1, 30, 104–106, 108, 111–115, 117, 118, 120, 179, 212, 235, 236, 240, 243–247, 254, 258, 259, 261, 265–267, 278, 283, 315, 323, 329, 333, 335, 402, 403, 447–453, 461, 485
- Rare earth minerals and materials (REMMs), 2
- Rare earth mineral systems, 30–33
- Rare earth oxides (REOs), 1, 4–7, 10, 12, 13, 17, 28–30, 35, 43, 46, 78, 81, 82, 84, 85, 104, 106, 108, 123, 132, 134, 138, 145, 236–238, 240–242, 244, 249, 251, 276–280, 283–286, 290, 321, 326, 391–412, 432, 436–438, 441, 448, 452, 458–461, 463–466, 468, 469, 472–475, 477–480
- RE phosphate, 395, 405
- RE tantalates, 395, 406
- Recrystallization temperature, 359, 362–363, 384
- Recycling, 11–14, 86, 156, 163, 187, 189, 191, 219, 315, 337, 407, 412, 424–428, 431–440, 448, 450, 485–487, 491
- Red phosphors, 280, 448
- REE applications, 9, 278, 289
- REE distribution in coal related sources, 59–61
- REE enriched coals, 66–69
- REE refining, 5
- REE separation, 5, 11, 150, 154, 160, 164, 167, 169, 172, 173, 180, 184, 187–191, 465
- REEs from coal byproducts, 123–146, 477
- REEs in AMD, 75, 84, 85, 478
- Regolith-hosted deposit, 139–142
- Regulatory oversight, 485, 486, 488
- Remediation of coal related liabilities, 86
- REO concentrate, 4
- REO production trends, 472, 473
- Resource and reserve estimation, 462
- Resource Conservation Recovery Act (RCRA), 495
- Reuse, remanufacture and recycle, 426–427, 429–438
- Run-of-mine (ROM), 104

**S**

- Samarium Cobalt (SmCo), 6, 8, 281–283, 311–313

- Scandium raw materials sources, 359–384
- Silicates, 3, 22, 25, 35, 43, 46, 63, 104–106, 108, 119, 120, 126, 395, 401–405, 407, 409–410, 412
- Sintered magnets, 250, 264, 265, 283, 297, 299, 300, 302, 305, 309, 315, 431, 434, 435
- Solid Phase Extraction (SPE), 174–176
- Solvent extraction (SX), 5, 149–176, 179, 180, 191, 195–211, 218, 239, 432, 436–438, 449, 452
- Solvometallurgy, 196, 197, 219
- Supply chain, 2, 7, 12–14, 176, 219, 257, 266, 267, 284, 309, 311, 314–315, 376, 379, 426, 432, 434, 435, 440, 441, 447, 457, 473, 486, 487, 490
- Surface Mining Control and Reclamation Act (SMCRA), 499
- Suspension Plasma Spray (SPS), 313, 394
- SX circuit (SX battery), 155–158, 164

**T**

- Thermal barrier coatings (TBCs), 10, 11, 391–395, 397–402, 404–410
- Thermal stability, 9, 195, 321, 323, 327, 331, 332, 335, 348, 374, 400, 404, 405, 411
- Total rare earth oxide (TREO) content, 81

**U**

- United Nations Convention on the Law of the Sea (UNCLOS), 13, 489
- United Nations Environmental Assembly (UNEA), 13, 488
- U.S. Presidential Executive Order (EO), 13, 490

**V**

- Value recovery pathways, 423–441

**W**

- Weldability, 10, 360, 367, 376, 384
- Wrought alloys, 10, 366–379, 383

**X**

- Xenotime, 4, 20, 22, 32, 38, 39, 46, 47, 50, 59, 63, 70, 104, 123, 126, 132, 140, 405, 477, 496

**Z**

- Zirconates, 393, 395, 399–402, 404, 405, 407–410